# Imaging the craniofacial skeleton:

# Is MRI a viable alternative to ionising radiation?

Dr Karen A Eley

*Nuffield Department of Surgical Sciences*




*A thesis in fulfilment of the degree of Doctor of Philosophy*

*Trinity Term 2012*

## Abstract

The potential deleterious effects of ionising radiation continue to be highlighted, with radiation reduction largely consisting of low dose techniques rather than a shift to non-ionising methods. The craniofacial region is a key anatomical area for radiation protection in view of the radiosensitive lens and thyroid gland. CT scanning is routinely employed to image this region in view of its superior imaging of bone and ability to create 3D rendered images and anatomical models for diagnosis and surgical planning. Standard MRI sequences make 3D rendering of bone a challenging problem. The objectives of the thesis were to explore the potential of MRI as an alternative to CT in three key patient groups: children with premature fusion of the cranial sutures (craniosynostosis), adolescents with facial disproportion, and adults with malignancy of the facial skeleton. Investigation was undertaken with routine MRI sequences, and a new low flip-angle gradient echo sequence "Black Bone."

Overall, the potential of "Black Bone" far exceeded that of routine MRI sequences. In children with craniosynostosis, the cranial sutures were clearly delineated on "Black Bone" with accurate distinction between normal and prematurely fused sutures. In adolescents with facial disproportion "Black Bone" offered a reliable method of 2D-cephalometric assessment with potential for development of 3D cephalometry. In adults with malignancy of the craniofacial skeleton the "Black Bone" sequence was useful in detecting bony erosion and tumours contained within the facial skeleton. However it was of limited value in tumour volume measurements where the tumour involved surrounding soft tissues, and routine sequences offered a reliable solution. A positive correlation was seen with tumour volume and clinical outcome, surpassing the accuracy of the current TNM staging system.

The clear soft-tissue-bone boundary of the "Black Bone" sequence was successfully utilised for the first time to produce 3D rendered images and anatomical models of the craniofacial skeleton from MRI datasets. This novel application demonstrated comparable accuracy of "Black Bone" and CT rendered datasets.

This work has made a significant contribution to radiation protection and is likely to change clinical practice in the near future.

**To my Mum and Dad, for their never ending support and love in everything that I do.**

**In loving memory of my Nan and Grandad, who continue to inspire me every day.**

# Contents


Abstract ..... i
List of Figures ..... vii
List of Tables ..... x
Abbreviations and Acronyms ..... xii
Manufacturer details ..... xiv
Acknowledgements ..... xv
**1. Introduction ..... 16**
1.1 Introduction ..... 17
1.2 Thesis Objectives and Structure ..... 18
**2. Background ..... 20**
2.0. Background ..... 21
2.1 Medical Imaging: A technical Review ..... 21
2.1.1 Radiography ..... 21
2.1.2 Computed Tomography (CT) ..... 22
2.1.3 Magnetic Resonance Imaging (MRI) ..... 24
2.2 Ionising Radiation Concerns ..... 30
2.2.1 Quantifying Exposure ..... 30
2.2.2 Problems with Measuring Dose ..... 31
2.2.3 Risk of Radiation Exposure Related to Dose ..... 31
2.2.4 The Increasing Use of CT ..... 34
2.3 Craniofacial Anatomy ..... 38
2.4 Pathology Affecting the Craniofacial Skeleton ..... 39
2.4.1 Cranial Sutures and Craniosynostosis ..... 39
2.4.2 Facial Disproportion ..... 43
2.4.3 Mandibular and maxillary squamous cell carcinoma ..... 50
2.5 3D Imaging and Anatomical Models ..... 55
2.6 Imaging the Craniofacial Skeleton with MRI ..... 57
**3. Preliminary Work ..... 63**
3.0 Preliminary Work ..... 64
3.1 "Black Bone" MRI Optimisation & Accuracy ..... 65
3.2 "Black Bone" MRI Optimisation ..... 65
3.2.1 Materials and Method ..... 65
3.2.2 Results ..... 67
3.2.3 Discussion ..... 69
3.3 Biometric Accuracy ..... 70
3.3.1 Materials and Methods ..... 70
3.3.2 Results ..... 72
3.3.3 Discussion ..... 74
Chapter Conclusion ..... 74
**4. Children ..... 75**
4.0 Children ..... 76
4.1 Cranial Sutures on Routine MRI ..... 77
4.1.1 Unblinded Cranial Suture Review ..... 77
4.1.1.1 Materials and Method ..... 77
4.1.1.2 Results ..... 79
4.1.1.3 Discussion ..... 83
4.1.2 Blinded cranial suture review ..... 84
4.1.2.1 Materials and Method ..... 84
4.1.2.2 Results ..... 85
4.1.2.3 Discussion ..... 88
4.2 Cranial Sutures on MRI: Suture width ..... 89
4.2.1 Materials and Methods ..... 89
4.2.2 Results ..... 90
4.2.3 Discussion ..... 91

4.3 Cranial Sutures & "Black Bone" MRI ..... 92
4.3.1 Animal Work ..... 92
4.3.1.1 Materials and Methods ..... 92
4.3.1.2 Results ..... 93
4.3.1.3 Discussion ..... 99
4.4 Alternative MRI Sequences ..... 100
4.4.1 FIESTA ..... 100
4.4.2 Ultra short Time to Echo ..... 101
4.4.3 BRAVO & Cube ..... 103
4.4.4 Discussion ..... 103
4.5 "Black Bone" MRI in Children ..... 104
4.5.1 Materials and Methods ..... 104
4.5.2 Results ..... 105
4.5.3 Discussion ..... 107
4.6 "Black Bone" MRI in craniosynostosis ..... 108
4.6.1 Materials and Methods ..... 108
4.6.2 Results ..... 110
4.6.3 Discussion ..... 122
4.7 Cranial Suture Widths on "Black Bone" ..... 124
4.7.1 Materials and Methods ..... 124
4.7.2 Results ..... 124
4.7.3 Discussion ..... 125
Chapter Conclusion ..... 125
**5. Adolescents ..... 126**
5.0 Adolescents ..... 127
5.1 Two Dimensional Cephalometric Analysis ..... 127
5.1.1 Materials & Methods ..... 127
5.1.1.1 Adult Volunteers ..... 127
5.1.1.2 Patients with Facial Disproportion ..... 128
5.1.1.3 Cephalometric Landmarks ..... 129
5.1.1.4 Cephalometric Analysis - AWW ..... 130
5.1.1.5 Cephalometric analysis - Dolphin cephalometric software ..... 131
5.1.2 Results ..... 135
5.1.2.1 Advantage Windows ..... 135
5.1.2.1.1 Measuring device ..... 135
5.1.2.1.2 Repeatability - Lateral Cephalogram ..... 135
5.1.2.1.3 Repeatability - "Black Bone" ..... 136
5.1.2.1.4 Repeatability - T1 ..... 137
5.1.2.1.5 Confidence of Point Selection ..... 138
5.1.2.1.6 Comparison of Lateral Cephalogram and "Black Bone"- Volunteers ..... 138
5.1.2.1.7 Comparison of Lateral Cephalogram and "Black Bone" - Patients ..... 139
5.1.2.2 Dolphin Cephalometric Software ..... 141
5.1.2.2.1 Repeatability ..... 141
5.1.2.2.2 Comparison of MRI and Lateral Cephalogram - Volunteers ..... 145
5.1.2.2.3 Comparison of "Black Bone" and Lateral Cephalogram - Patients ..... 146
5.1.3 Discussion ..... 147
5.2 Development of 3D "Black Bone" Cephalometry ..... 148
5.2.1 Dolphin cephalometric software ..... 148
5.2.2 3D Landmarks ..... 149
5.2.3 Discussion ..... 150
Chapter Conclusion ..... 150
**6. Adults ..... 151**
6.0 Adults ..... 152
6.1 Tumour Volume Analysis in Maxillary Complex SCC ..... 152
6.1.1 Materials and Methods ..... 152
6.1.2 Results ..... 158
6.1.3 Discussion ..... 162
6.2 Tumour Volume Analysis in Mandibular SCC ..... 163
6.2.1 Materials and Methods ..... 163

6.2.2 Results ..... 164
6.2.3 Discussion ..... 168
6.3 Potential of "Black Bone" MRI in Tumour Assessment ..... 169
6.3.1 Maxillary Complex Tumours ..... 169
6.3.2 Mandibular Region Tumours ..... 170
6.3.3 Discussion ..... 171
6.4 "Black Bone" MRI & Craniofacial Pathology ..... 172
6.4.1 "Black Bone" MRI in the Diagnosis of Craniofacial Pathology ..... 172
6.4.1.1 Materials and Methods ..... 172
6.4.1.2 Results ..... 173
6.4.1.3 Discussion ..... 175
6.5 "Black Bone" MRI instead of CT imaging ..... 176
6.5.1 Materials & Methods ..... 176
6.5.2 Results ..... 176
6.5.3 Report of Cases ..... 177
6.5.4 Discussion ..... 183
Chapter Conclusion ..... 184
**7. 3D MRI & Anatomical Models ..... 185**
7.0. 3D Reconstruction & Anatomical Models ..... 186
7.1 3D Rendering Techniques ..... 187
7.1.1. Advantage Windows Workstation ..... 188
7.1.1.1 Phantom and Animal Models ..... 189
7.1.1.2 Adult Volunteer and Children Datasets ..... 190
7.1.2 BrainLab ..... 191
7.1.3 InVesalius ..... 194
7.1.3.1 Phantom Datasets ..... 194
7.1.4 MITK-3M3 ..... 195
7.1.4.1 Phantom Datasets ..... 195
7.1.4.2 Adult Volunteer Datasets ..... 197
7.1.5 Mimics ..... 198
7.1.5.1 Phantom and Animal Models ..... 198
7.1.5.2 Adult Dataset ..... 199
7.1.5.3 "Black Bone" Datasets from Children ..... 200
7.1.5.4 Mimics and Craniosynostosis ..... 202
7.1.6 Osirix ..... 204
7.1.6.1 Phantom ..... 204
7.1.6.2 Adult Datasets ..... 204
7.1.6.3 Datasets from Children ..... 205
7.1.6.4 Children with Craniosynostosis ..... 206
7.1.6.5 Comparison between Mimics and Osirix ..... 207
7.1.7 Fovia ..... 209
7.1.7.1 Phantoms and Animal Models ..... 210
7.1.7.2 Adult Volunteers ..... 212
7.1.7.3 Adult Patients ..... 213
7.1.7.4 Children with Normal Cranial Sutures ..... 215
7.1.7.5 Children with Craniosynostosis ..... 218
7.1.7.6 Alternative MRI Sequences ..... 226
7.1.8 3D Doctor ..... 228
7.1.8.1 Phantom Datasets ..... 228
7.1.8.2 Adult Volunteer Datasets ..... 229
7.1.8.3 Children with Craniosynostosis ..... 231
7.1.9 Image J ..... 232
7.1.9.1 Phantom Datasets ..... 232
7.1.9.2 Adult Volunteer Datasets ..... 234
7.1.10 Mirada ..... 235
7.1.10.1 Phantom Datasets ..... 235
7.1.10.2 Adult Volunteer Datasets ..... 235
7.1.11 ZIBAmira ..... 237
7.1.12 Matlab ..... 239

7.1.13 Discussion ..... 239
7.2 3D Accuracy of "Black Bone" MRI ..... 241
7.2.1 Direct Measurements ..... 241
7.2.1.1 Fovia ..... 242
7.2.1.2 Mimics ..... 244
7.2.1.3 Osirix ..... 245
7.2.1.4 Discussion ..... 247
7.2.2 Volume Measurements ..... 247
7.2.2.1 Direct Volume Measurements of Cube Phantom ..... 247
7.2.2.2 Osirix ..... 248
7.2.2.3 Mirada ..... 249
7.2.3 Mathematical Modelling ..... 250
7.2.4 ZIBAmira ..... 250
7.2.5 Discussion ..... 252
7.3 Smoothing Effects ..... 253
7.3.1 Discussion ..... 255
7.4 Imaging the Orbits ..... 256
7.4.1 Discussion ..... 258
7.5 Anatomical Models ..... 259
7.5.1 Accuracy of the Model Process with CT data ..... 260
7.5.1.1 Materials and Methods ..... 260
7.5.1.2 Results ..... 260
7.5.2 Anatomical Models from "Black Bone" MRI ..... 262
7.5.2.1 Anatomical Models using Adult "Black Bone" Datasets ..... 262
7.5.3 Accuracy of the Model Process with "Black Bone" ..... 264
7.5.3.1 Between Phantom and Model ..... 265
7.5.3.2 Between Model from CT and Model from "Black Bone" ..... 266
7.5.4 Application of Techniques to Children with Craniosynostosis ..... 267
7.5.5 Discussion ..... 268
7.6 Future Applications ..... 269
7.6.1 Cervical Fractures ..... 269
7.6.2 Imaging of the Hip ..... 271
7.6.3 Imaging of the Tibia & Fibula ..... 273
7.6.4 Imaging of the Hand and Wrist ..... 274
7.6.5 Discussion ..... 276
Chapter Conclusion ..... 276
**8. General Discussion & Conclusion ..... 277**
8.1 Discussion ..... 278
8.2 Scope for Further Work ..... 283
8.3 Conclusion ..... 284
References ..... 285
Appendices ..... 293
Appendix A: Optimal "Black Bone" flip angle ..... 296
Appendix B: Biometric Accuracy of "Black Bone" MRI ..... 299
Appendix C: Cranial Sutures on MRI ..... 302
Appendix D: "Black Bone" MRI in Craniosynostosis ..... 305
Appendix E: Cephalometrics ..... 315
Appendix F: Tumour Volume ..... 338
Appendix G: "Black Bone" MRI & Pathology ..... 349
Appendix H: 3D "Black Bone" ..... 352
Appendix I: "Black Bone" & Anatomical Models ..... 430

# List of Figures

Figure 1: Basic design of an x-ray tube. ..... 21
Figure 2: Simplified diagram of CT scanners ..... 23
Figure 3: Cone beam and fan beam geometry ..... 23
Figure 4: Spin and precession. ..... 24
Figure 5: T1 Recovery and T2 Decay ..... 25
Figure 6: T1 and T2 weighting ..... 28
Figure 7: Spin echo and gradient echo sequence ..... 28
Figure 8: Number of imaging examinations, England ..... 34
Figure 9: The craniofacial skeleton. ..... 38
Figure 10: Characteristic skull shape anomalies as a result of single suture synostosis ..... 40
Figure 11: Skeletal relationships ..... 44
Figure 12: LeFort I osteotomy and bilateral sagittal split osteotomy ..... 45
Figure 13: The oral cavity and maxillary sinus ..... 50
Figure 14: Cervical lymph node levels. ..... 54
Figure 15: Mandibulectomy and classification of maxillary defects ..... 54
Figure 16: “Black Bone” and a more conventional MRI appearance of the thigh ..... 64
Figure 17: x, y, z and RF gating signal of “Black Bone” sequence. ..... 64
Figure 18: Selection of ROI in mandible and brain. ..... 66
Figure 19: Axial “Black Bone” image demonstrating the path for measuring pixel values ..... 66
Figure 20: The effect of varying the flip angle on the “Black Bone” MRI sequence. ..... 67
Figure 21: Graphs of pixel values for “Black Bone” with a flip angle of 1, 5, 10 and 60° ..... 68
Figure 22: Measurements completed on “Black Bone” images ..... 72
Figure 23: The cranial sutures viewed from the vertex of the skull ..... 76
Figure 24: Bar chart of percentage of each suture identified ..... 82
Figure 25: Percentage of each suture identified for each MRI sequence ..... 82
Figure 26: Bar chart of the appearance of the cranial sutures ..... 82
Figure 27: Box plot of combined assessor score for cranial suture identification ..... 86
Figure 28: Appearance of cranial sutures on axial STIR and axial T2 ..... 87
Figure 29: Cranial suture width measurements ..... 89
Figure 30: Location of cranial sutures on piglet ..... 93
Figure 31: Effect on suture identification with variation in flip angle ..... 95
Figure 32: Effect on “Black Bone” sequence of decreasing the receive bandwidth ..... 96
Figure 33: The identification of the cranial sutures ..... 96
Figure 34: Cranial suture appearance on FIESTA sequence. ..... 97
Figure 35: Confirmation of the appearance of the cranial sutures on CT. ..... 97
Figure 36: Comparable “Black Bone” and CT images. ..... 98
Figure 37: Images of dissected piglet ..... 98
Figure 38: FIESTA imaging on adult volunteer ..... 100
Figure 39: Attempt to reproduce “Black Bone” sequence on AVIC Siemens MR scanner. ..... 102
Figure 40: UTE scanning & resultant subtraction ..... 102
Figure 41: Axial FSPGR BRAVO and Sagittal CUBE T2 images of adult volunteer ..... 103
Figure 42: Appearance of cranial sutures in Patient 1 and Patient 2 ..... 105
Figure 43: Appearance of the cranial sutures in Patient 3 and Patient 4 ..... 106
Figure 44: Comparable axial “Black Bone” images demonstrating contrast settings ..... 111
Figure 45: Patient 1 and Patient 2 both with a diagnosis of sagittal synostosis ..... 112
Figure 46: Patient 2 and 3 both with a diagnosis of sagittal synostosis ..... 113
Figure 47: Patient 5 and Patient 6 ..... 114
Figure 48: Patient 7 with right unicoronal synostosis, and Patient 8 with metopic synostosis ..... 115
Figure 49: Patient 9 and Patient 10 both with a diagnosis of sagittal synostosis ..... 116
Figure 50: Patient 11 and Patient 12 both with a diagnosis of sagittal synostosis. ..... 117
Figure 51: Patient 13 with a diagnosis of Apert Syndrome, with bilateral coronal synostosis ..... 118
Figure 52: Appearance of chemical shift artefact, with close-up view. ..... 119
Figure 53: Effect of fat shift selection and water shift selection ..... 120
Figure 54: “Black Bone” acquisition in the coronal plane. ..... 120
Figure 55: Cephalometric points used for analysis of lateral cephalogram and “Black Bone” ..... 129
Figure 56: Measuring device used on sagittal “Black Bone” imaging ..... 130

Figure 57: Lateral cephalogram and mid-sagittal “Black Bone” image with landmarks identified.....131
Figure 58: Dolphin workspace with measurements on lateral cephalogram .....133
Figure 59: Images for the three volunteers used for cephalometric analysis. .....133
Figure 60: Images for the five patients included for cephalometric analysis. .....134
Figure 61: Superimposed images of “Black Bone” and lateral cephalogram. .....140
Figure 62: Tracings for 10 repeated attempts at digitising lateral cephalogram of one volunteer. ...142
Figure 63: Digitisation of mid-sagittal “Black Bone” image and subsequent tracing .....143
Figure 64: Tracing of mid-sagittal “Black Bone” images on ten occasions using Dolphin .....143
Figure 65: Repeated digitisatons for T1 .....145
Figure 66: 3D rendering in Dolphin software for cephalometric assessment .....148
Figure 67: Tumour volume measurement of a maxillary SCC on coronal MRI .....154
Figure 68: Screenshot of “Plan Content” view of Brainlab software. .....155
Figure 69: Kaplan meier plots of ACS, DFS, Tv, resection margins, and pT staging .....161
Figure 70: Tumour volume measurement of a mandibular SCC. .....163
Figure 71: Kaplan meier plots of ACS, DFS for Tv, resection margins, and pT staging. .....166
Figure 72: Kaplan meier plots for ACS, DFS and stratification of tumour volume .....167
Figure 73: Appearance of maxillary complex tumours on the “Black Bone” sequence .....169
Figure 74: Appearance of mandibular region tumours on the “Black Bone” sequence. .....170
Figure 75: Vascular malformation in cheek tissues in 1 year old child .....174
Figure 76: Patient 35 - all reviewers identified the radiological diagnosis of right mandibular SCC ..175
Figure 77: Axial “Black Bone” imaging of Patient 1 demonstrating normal zygomatic bodies .....181
Figure 78: Coronal “Black Bone” images of Patient 2 withvdisplacement of the left orbital floor ....181
Figure 79: Axial “Black Bone” images of Patient 3, with left mandibular keratocyst. .....181
Figure 80: Axial “Black Bone” images of Patient 4, with granuloma in the right maxillary sinus. .....182
Figure 81: Axial “Black Bone” images of Patient 5, with no evidence of bony expansion .....182
Figure 82: Axial “Black Bone” images of Patient 6, with normal cortical morphology. .....182
Figure 83: Axial “Black Bone” images of Patient 7, with a lesion within the left maxillary alveolus. .183
Figure 84: Axial “Black Bone” images of Patient 8, with normal appearances of the orbital bones. .183
Figure 85: Phantoms used for CT and MRI imaging .....188
Figure 86: Initial attempt at 3D rendering using AWW .....189
Figure 87: Volume rendering of adult volunteer and child.....190
Figure 88: Independent segmentation of the mandible on a CT dataset .....191
Figure 89: Axial “Black Bone” MRI demonstrating ROI set at the limit of the soft tissue envelope. ..192
Figure 90: Segmentation of the skull cap using the magic brush tool .....192
Figure 91: 3D rendered images of adult volunteer “Black Bone” datasets using BrainLab. .....193
Figure 92: Workflow in InVesalius .....194
Figure 93: Screen layout in MITK-3M3 .....195
Figure 94: Polygon model of the phantom cube .....196
Figure 95: Volume rendering with CT dataset and “Black Bone” phantom cube dataset. .....196
Figure 96: Using the region growing tool to remove the outer shell on the phantom skull. .....196
Figure 97: Volume rendered image of “Black Bone” with polygon overlay of model .....197
Figure 98: Threshold selection and mask editing in 3D in Mimics. .....198
Figure 99: 3D rendered images of the phantom in Mimics, and application of a smoothing factor..198
Figure 100: 3D rendered “Black Bone” MRI dataset of piglet using Mimics. .....199
Figure 101: Region growing tool to create second mask from first and resultant 3D image. .....200
Figure 102: Segmentation of the skull and brain using region growing tool. .....200
Figure 103: 3D reconstructed images of children with normal cranial sutures using Mimics .....201
Figure 104: Using the 3D live wire tool and volume rendering functions in Mimics .....202
Figure 105: 3D rendered images of “Black Bone” datasets in children with craniosynostosis.....203
Figure 106: Surface rendering of phantom using Osirix .....204
Figure 107: Final ROI of cranial bone, surface and volume rendering results. .....205
Figure 108: 3D surface and volume rendered images from child with normal cranial sutures .....206
Figure 109: 3D surfac and volume rendered images of children with craniosynostosis using Osirix .207
Figure 110: Comparison between STL files created in Mimics and Osirix .....208
Figure 111: Fovia workspace containing the 3D CT dataset for the skull phantom .....209
Figure 112: TF adjusted to visualise the skull phantom through the perpex shell .....210
Figure 113 Segmentation of the skull phantom using Fovia and 2TF. .....210
Figure 114: Skull phantom, 3D rendered CT data using Fovia & 3D rendered “Black Bone”. .....211
Figure 115: 3D rendered images of phantom using “Black Bone” and CT.....211

Figure 116: 3D rendering process with “Black Bone” piglet dataset. ....212
Figure 117: Fovia window showing TF and resultant 3D image ....212
Figure 118: Fovia workflow demonstrating TF selection and segmentation. ....213
Figure 119: 3D rendered “Black Bone” images from ....214
Figure 120: Initial attempts at rendering of “Black Bone” MR images in a 3 year old child ....215
Figure 121: 3D rendered Fovia images for Patients 1 and 2. ....216
Figure 122: 3D rendered images from children with normal sutures using Fovia. ....217
Figure 123: Fovia Results and comparable CT images for Patient 1. ....218
Figure 124: Fovia results & comparable CT images for Patients’ 2 & 3. ....219
Figure 125: Fovia results and comparable CT images for Patients’ 4 & 5. ....220
Figure 126: Fovia results and comparable CT images for Patients’ 6 & 7. ....221
Figure 127: Fovia results and comparable CT images for Patients’ 8 & 9. ....222
Figure 128: Fovia results and comparable CT images for Patients’ 10 & 11. ....223
Figure 129: Fovia results and comparable CT images for Patients’ 12 & 13 ....224
Figure 130: Fovia results with T1, T2 and FIESTA sequences. ....227
Figure 131: 3D rendered images of the phantom cube with 3D doctor ....228
Figure 132: Initial attempt at rendering adult “Black Bone” dataset. ....229
Figure 133: 3D rendering of adult volunteer “Black Bone” datasets with 3D-Doctor ....229
Figure 134: Axial “Black Bone” images demonstrating artificial boundary ....230
Figure 135: Automatic detection of boundaries on axial “Black Bone” image ....231
Figure 136: Subtracting the background of the phantom cube dataset in Image J. ....232
Figure 137: Utilising the flood fill and paint tools in Image J to remove the air ....233
Figure 138: Edge detection function after segmentation in Image J. ....233
Figure 139: Applying a freehand ROI to permit removal of everything outside of the ROI ....233
Figure 140: Attempt to 3D render the phantom skull “Black Bone” dataset with Image J. ....234
Figure 141: Attempts to segment and render adult “Black Bone” dataset in Image J. ....234
Figure 142: Identifiying the cube boundaries in Mirada software. ....235
Figure 143: Edge detection with adult “Black Bone” dataset ....236
Figure 144: Initial results obtained by ZIBAmira research team using adult volunteer ....238
Figure 145: Screen layout for ZIBAmira ....238
Figure 146: Axial “Black Bone” and CT image on which investigation was conducted ....240
Figure 147: Measurements on cube phantom. ....242
Figure 148: Volume rendering of “Black Bone” phantom cube dataset ....242
Figure 149: Phantom cube 3D rendered with Mimics. ....244
Figure 150: Phantom cube 3D rendered with Osirix ....246
Figure 151: ZIBAmira workflow to compare “Black Bone” and CT phantom cube datasets ....251
Figure 152: Graphical display of difference between 3D rendered “Black Bone” and CT phantom ....251
Figure 153: Effect of varying the smoothing factor and number of iterations. ....254
Figure 154: 3D rendering of the orbits using Mimics, Osirix, and Fovia. ....256
Figure 155: Coronal, axial and sagittal “Black Bone” image of a normal orbit ....257
Figure 156: Coronal “Black Bone” image, and 3D reconstructions in orbital floor fracture. ....258
Figure 157: Z-printer 650. ....259
Figure 158: The cue phantom, and the measurements used to determine accuracy ....260
Figure 159: Model of cube phantom created from CT dataset on z-corp printer ....261
Figure 160: 3D rendered image of mandible produced in Mimics ....263
Figure 161: Images of the finished anatomical model of the mandible from adult volunteer ....263
Figure 162: Processes involved in finishing the model ....263
Figure 163: The eleven measurements completed directly on phantom cube and models ....264
Figure 164: Frontal and superior views of anatomical model from of infant with synostosis. ....268
Figure 165: Axial “Black Bone” MRI with orthogonal reconstructions of Patient 1 ....269
Figure 166: Axial “Black Bone” MRI with orthogonal reconstructions of Patient 2 ....270
Figure 167: 3D rendered cervical spine images of Patient 1 and patient 2 ....271
Figure 168: Axial “Black Bone” imaging of the pelvis at the level of the femoral heads ....272
Figure 169: Coronal “Black Bone” MRI of hip joint demonstrating the femoral head ....272
Figure 170: 3D rendered images from axial imaging and coronal imaging ....273
Figure 171: Axial imaging of the tibia and fibula with orthogonal reconstructions. ....273
Figure 172: 3D rendered images of tibia and fibula using Fovia and Mimics. ....274
Figure 173: Axial “Black Bone” MRI of the hand with orthogonal reconstructions ....275
Figure 174: 3D rendered images of the hand ....275

# List of Tables

Table 1: Typical patient doses from x-ray examinations of the head ..... 30
Table 2: Approximate mean T2 times of some short T2 tissues and tissue components ..... 61
Table 3: "Black Bone" MRI Scanning parameters ..... 66
Table 4: Anatomical measurements completed on phantom, CT and MRI. ..... 71
Table 5: Mann-Whitney U Test results for anatomical, CT and "Black Bone" measurements on skull 73
Table 6: Mean and Standard Error results for distances measured on phantom ..... 73
Table 7: Clinical indication for imaging and radiological diagnosis for 121 patients reviewed ..... 78
Table 8: Scoring system for review of cranial sutures on routine MRI sequences ..... 78
Table 9: Number of patients with each sequence of available for review ..... 79
Table 10: Frequency of cranial suture identification and appearance for each MRI sequence ..... 80
Table 11: Comparison of patient age for those in whom any cranial suture was identified. ..... 81
Table 12: Identification of cranial sutures on each MRI sequence ..... 81
Table 13: MRI imaging parameters for the datasets included for review ..... 84
Table 14: Stratified results by age group ..... 86
Table 15: Cranial suture widths ..... 90
Table 16: Cranial suture widths stratified for age ..... 90
Table 17: Paediatric patients undergoing "Black Bone" imaging of the head ..... 104
Table 18: Children recruited to craniosynostosis study ..... 111
Table 19: "Black Bone" MRI parameters for Philips 1.5T scanner. ..... 118
Table 20: "Black Bone" data sets included for anonymised independent review ..... 121
Table 21: Diagnosis made for 12 "Black Bone" datasets by 3 reviewers. ..... 122
Table 22: Mean score assigned by the 3 reviewers for each of the cranial sutures ..... 122
Table 23: Mean±SD cranial suture widths on "Black Bone." ..... 124
Table 24: Distance and angle measurements used for cephalometric analysis. ..... 129
Table 25: Repeated cephalometric measurements for the 3 volunteers on lateral cephalogram. ..... 135
Table 26: Repeated cephalometric measurements for the 2 patients on lateral cephalogram. ..... 136
Table 27:Repeated cephalometric measurements for the 3 volunteers on "Black Bone" ..... 136
Table 28: Repeated cephalometric measurements for 2 patients on "Black Bone." ..... 137
Table 29: Repeated cephalometric measurements for the 3 volunteers on T1 MRI. ..... 137
Table 30:Confidence scores for cephalometric point identification. ..... 138
Table 31:Discrepancy between lateral cephalogram and "Black Bone" angles and distances ..... 139
Table 32: Discrepancy between lateral cephalogram and "Black Bone" angles and distance ..... 140
Table 33: Repeated digitisation of lateral cephalogram, sagittal "Black Bone" and sagittal T1 MRI. 142
Table 34: Difference in x and y co-ordinates. ..... 142
Table 35: Difference in x and y co-ordinates compared to the first digitisation ..... 144
Table 36: Difference in x and y co-ordinates ..... 145
Table 37: Difference between measurements on lateral cephalogram, "Black Bone" or T1 images. 146
Table 38: Difference between measurements on lateral cephalogram, "Black Bone" for patients ... 147
Table 39: Available imaging sequences and those used for tumour volume measurements ..... 156
Table 40: Data collection parameters ..... 157
Table 41: ACE-27 scoring distribution ..... 158
Table 42: Tumour resection and reconstruction methods ..... 158
Table 43: Tumour volume measurements for review of intra-observer variability. ..... 159
Table 44: Distribution of tumour volume according to T stage as per the AJCC TNM classification .. 159
Table 45: Fisher's exact test for nodal involvement at or within 1 year of surgery ..... 160
Table 46: Tumour volume cut-off to correlate with TNM staging system ..... 162
Table 47: Effect of Tv on pT staging ..... 162
Table 48: Available MRI sequences and those suitable for tumour volume measurements ..... 163
Table 49: Correlation of pT stage with tumour volume ..... 165
Table 50: Univariate analysis of factor effect on DFS ..... 165
Table 51: Cox regression analysis of DFS and ACS using Tv stratification ..... 167
Table 52: Stratification of tumour volume measurements for correlation with current TNM ..... 168
Table 53: Frequency and inter-rater agreement for pathological diagnosis on "Black Bone" MRI .... 174
Table 54: Summary of presented patients undergoing "Black Bone" MRI ..... 177
Table 55: "Black Bone" MRI ±CT in patients with varying pathologies of the head & neck ..... 177
Table 56: Children with normal cranial sutures undergoing "Black Bone" MRI ..... 187

Table 57: Children with craniosynostosis .....187
Table 58: Slice thickness of CT and “Black Bone” MRI used for phantom cube. .....241
Table 59: Overall mean difference in measurements between phantom and imaging dataset .....243
Table 60: Overall mean difference in measurements between phantom and imaging dataset .....245
Table 61: Overall mean difference in measurements between direct measurement and imaging ...246
Table 62: Measurement of phantom cube volume from the amount of displaced water. .....248
Table 63: Volume measurements of phantom cube using Osirix with “Black Bone”& CT datasets ...248
Table 64: Volume calculations of the phantom cube obtained on “Black Bone” and CT .....249
Table 65: Independent samples t-test for comparison between volume measurements. .....249
Table 66: Smoothing factor and number of iterations applied to the phantom cube 3D dataset. ....253
Table 67: Mean discrepancy between measurements obtained with various smoothing factors. ....255
Table 68: Measurements obtained on phantom and resultant model .....261
Table 69: Discrepancy between distances on phantom and CT model .....262
Table 70: Direct measurements of phantom cube .....265
Table 71: Mean±SD difference between Phantom and model using CT and “Black Bone” .....266
Table 72: Mean±SD discrepancy between models created with CT and “Black Bone” .....267

## CD Attachment

"Black Bone" MRI:

- Movie Clip 1: Mimics Rendered Craniofacial Skeleton from Adult Volunteer
- Movie Clip 2: Mimics Rendered Mandible from Adult Volunteer
- Movie Clip 3: Mimics Rendered Craniofacial Skeleton of Child with Unicoronal Synostosis
- Movie Clip 4: Mimis Rendered Craniofacial Skeleton of Child with Sagittal Synostosis
- Movie Clip 5: Osirix Rendered Craniofacial Skeleton of Adult Volunteer
- Movie Clip 6: Osirix Rendered Skull Cap of Child with Normal Cranial Sutures
- Movie Clip 7: Osirix Rendered Craniofacial Skeleton of Child with Unicoronal Synostosis
- Movie Clip 8: Osiric Rendered Craniofacial Skeleton of Child with Sagittal Synostosis
- Movie Clip 9: Fovia Rendered Craniofacial Skeleton of Adult Volunteer
- Movie Clip 10: Fovia Segmentation Process of Child with Metopic Synostosis
- Movie Clip 11: Fovia Rendered with Soft Tissues in Child with Sagittal Synostosis
- Movie Clip 12: Fovia Rendered Craniofacial Skeleton in Child with Unicoronal Synostosis
- Movie Clip 13: Fovia Rendered Craniofacial Skeleton in Child with Sagittal Synostosis
- Movie Clip 14: 3D-Doctor Rendered Craniofacial Skeleton in Adult Volunteer
- Movie Clip 15: Resultant Anatomical Model of Adult Volunteer Mandible

# Abbreviations and Acronyms

| | |
|---|---|
| 2D | Two-Dimensional |
| 3D | Three-Dimensional |
| ACE-27 | Adult Co morbidity Evaluation 27 |
| ACS | All Cause Survival |
| AJCC | American Joint Committee on Cancer |
| AP | Anterior-Posterior |
| AWW | Advantage Windows Workstation |
| BW | Bandwidth |
| CCD | Charged Coupled Device |
| Ceph | Cephalogram |
| CH | Churchill Hospital |
| CBCT | Cone Beam CT |
| CoV | Covariance |
| CT | Computed Tomography |
| cTNM | Clinical TNM Stage |
| CV | Coefficient of Variation |
| DFS | Disease Free Survival |
| DICOM | Digital Imaging and Communications in Medicine |
| DNA | Deoxyribonucleic acid |
| ECS | Extracapsular spread |
| ETL | Echo Train Length |
| FLAIR | Fluid Attenuation Inversion Recovery |
| FOV | Field of View |
| FPD | Flat Panel Detector |
| FSE | Fast Spin Echo |
| GA | General Anaesthesia |
| GRE | Gradient Echo |
| Gy | Gray |
| HPV | Human Papilloma Virus |
| HR | Hazard Ratio |
| HU | Hounsfield Unit |
| IR | Inversion Recovery |
| J | Joules |
| JPEG | Joint Photographic Experts Group |
| JR | John Radcliffe Hospital |
| KE | Dr Karen A Eley |
| Kg | Kilograms |
| kVp | Peak kilovoltage |
| mA | Milliampers |
| mAS | Milliampere-seconds |
| MDCT | Multi-detector CT |
| MDT | Multidisciplinary Team |
| MRI | Magnetic Resonance Imaging |
| NEX | Number of Excitations |
| NHS | National Health Service |
| Mths | Months |
| OCU | Oxford Craniofacial Unit |
| OMRI | Oxford Magnetic Resonance Imaging |
| OPG | Orthopantogram |
| OUH | Oxford University Hospitals NHS Trust |
| PA | Posteroanterior |
| PACS | Picture Archiving and Communications Service |
| PAS | Patient Archiving Service |
| PC | Personal Computer |
| PET | Positron Emission Tomography |
| Pixel | Picture Element |

| | |
|---|---|
| pTNM | Pathological TNM Stage |
| RF | Radiofrequency |
| RIS | Radiology Information System |
| ROI | Region of Interest |
| SCC | Squamous Cell Carcinoma |
| SD | Standard Deviation |
| SE | Spin Echo |
| SJG | Dr Stephen J Golding |
| SNR | Signal-to-noise Ratio |
| SPSS | Statistics Package for Social Scientists |
| STIR | Short Tau Inversion Recovery |
| STL | Stereolithography (file type for rapid prototyping) |
| Sv | Sievert |
| TE | Time to Echo |
| TF | Transfer Function |
| TI | Time to Inversion |
| TNM | Tumour, Nodes, Metastases |
| TR | Time to Repetition |
| UK | United Kingdom |
| UNSCEAR | United Nations Scientific Committee |
| USA | United States of America |
| UTE | Ultrashort TE |
| Voxel | Volume element |
| Yrs | Years |

# Manufacturer details

The following software and hardware are utilised throughout the thesis:

- 3D-doctor Version 4.0 20110710, Able Software Corp, Lexington, Massachusetts, USA
- Adobe Photoshop CS5 Extended v. 12.0.3x64, Adobe Systems Incorporated, San Jose, California, USA
- Advantage Windows Workstation, GE Medical Systems, Buckinghamshire, UK
- BrainLab iPlan CMF Version 3.0, BrainLab, Feldkirchen, Germany
- CaseNotes Version 5, Build B268R0, OHIS, Oxford, UK
- Centricity© Enterprise Version 3.0, GE Medical Systems, Buckinghamshire, UK
- ClearCanvas Workstation Version 2.0 (open source), Clear Canvas Inc, Toronto, Canada
- Dolphin Cephalometric Software, Version 11.5.04.23 Premium, Dolphin Imaging, Chatsworth, CA, USA
- Fovia High Definition Volume Rendering, Fovia Medical Inc, Palo Alto, California, USA
- Efilm Workstation Version 1.8.3, Merge Healthcare, Chicago, Illinois, USA
- GE Medical Systems, Buckinghamshire, UK
- Osirix (opensource), Pixmeo, Bernex, Switzerland
- Matlab, Version 7.11.0.584, Mathworks, Natick, Massachusetts, USA
- Microsoft Access 2007, Microsoft, Redmond, Washington, USA
- Microsoft Excel 2007, Microsoft, Redmond, Washington, USA
- Mimics Version 14.01, Materialise, Leuven, Belgium
- Philips Healthcare, Andover, MA, USA
- Siemens Healthcare, Camberley, Surrey, UK
- Statistical Package for the Social Sciences, SPSS Version 18.0, IBM Corp, Somers, NY, USA
- Tektronix TPS 2024 4 Channel Digital Oscilloscope, Tektronix Inc, Beaverton, Oregon, USA
- Z-printer 650, Z-Corporation , Burlington, MA, USA
- Z-Print 7.6, Z-Corporation, Burlington, MA, USA

# Acknowledgements

First and foremost, I would like to thank my supervisor Dr Stephen Golding, who has provided guidance and encouragement from beginning to end.

Secondly, I would like to thank the person who first inspired me to embark on an academic career, correctly identifying a passion for research that I never knew that I had: Mr Stephen Watt-Smith; without that recognition I would never have embarked on an MSc or DPhil.

Thank you to Dr Fintan Sheerin, Dr Russ Evans, Mr Steve Wall, Mr David Johnson, and Dr Jo Byren without whom the "Black Bone" cranial suture study would never have been possible. Nor would any of the MRI work been possible without all of the radiographers, volunteers, patients and their families who have all kindly given up their free time to assist with this work; special thanks go to Anthony McIntyre, Marianne Turnbull, Jane Andrews, Sally Ogg, Kim Nelson, Fiona McMillan, and Alex Eves.

Thank you also to Dermot Dobson, and my collaborators (including software developers), whose technical assistance has been invaluable.

Finally, thank you to my family and my friends – Alex Phillips, Simon Harvey and Jeff Fearon for their never ending support and to the Newlife Foundation and AO Foundation who funded this research.

# 1. Introduction

## 1.1 Introduction

Roentgen's discovery of the penetrating x-ray in 1896 heralded a revolution in medicine. Today, over one hundred years later, x-radiation remains the cornerstone of medical imaging. Hounsfield in his 1973 paper on Computed Tomography (CT) stated that "the exposure of the patient to x-rays must be restricted."[1] The potential deleterious effects of ionising radiation are well documented; however we continue to fall somewhat short of Hounsfield's advice.

Despite the considerable benefit of x-rays in clinical practice the consensus amongst radiology professionals is that steps should be taken to reverse, or at least arrest radiation exposure. However, the significant applications, particularly of CT, have made this somewhat of a difficult task.[2]

For the cranium and facial skeleton (craniofacial skeleton) CT with three-dimensional (3D) reconstruction has become the "gold standard" both as a diagnostic and surgical planning tool.

This thesis explores the potential of MRI as a non-ionising alternative to CT for imaging the craniofacial skeleton. This work has made original contributions to the field in three key patient groups:

1. Children with premature fusion of the skull sutures (craniosynostosis) who are routinely investigated and followed up with CT.
2. Adolescents with facial disproportion who often require repeated plain film examinations and in whom 3D imaging would confer a significant advantage in terms of treatment planning.
3. Adults with malignancy affecting the facial skeleton in whom multimodal imaging for diagnosis and surveillance is frequently necessary.

This work was completed at the Oxford University Hospitals NHS Trust, encompassing the John Radcliffe Hospital (JR), including the Oxford MRI Centre (OMRI) and West Wing (WW), and the Churchill Hospital.

## 1.2 Thesis Objectives and Structure

The thesis builds upon preliminary work on "Black Bone" MRI submitted in partial fulfilment of the degree of Master of Science in Diagnostic Imaging.[3]

The primary objectives of the thesis were:

1. To determine the potential advantages of MRI when imaging the craniofacial skeleton.
2. To determine the potential of "Black Bone" MRI as a diagnostic and surgical planning tool.

To fulfil these objectives, the thesis has been sub-divided (albeit with some overlap) into the following chapters:

**Chapter 3:** Preliminary work

- Optimisation of the "Black Bone" sequence.
- Determination of the biometric accuracy of "Black Bone" MRI.

**Chapter 4:** Children

- Investigation of cranial suture appearance and width on routine MRI sequences in infants.
- Investigation of cranial suture appearance and width on "Black Bone" and other non-routine MRI sequences
- Determination of the accuracy of "Black Bone" MRI in the diagnosis of craniosynostosis.

**Chapter 5:** Adolescents

- Determination of the cephalometric accuracy of "Black Bone" MRI in pre-treatment orthognathic patients, with comparison to standard lateral cephalograms.

**Chapter 6:** Adults

- Correlation of tumour volume on routine MRI with patient clinical outcome.
- Investigation of the potential of "Black Bone" MRI in tumour visualisation and volume measurements in maxillary complex and mandibular tumours.
- Determination of the accuracy of "Black Bone" MRI in the radiological diagnosis of pathology affecting the cranio-maxillofacial region.

**Chapter 7:** 3D imaging and anatomical models

- Development of 3D rendering techniques to create 3D reconstructed "Black Bone" images of the craniofacial skeleton.
- Investigation of the accuracy of the 3D imaging techniques.
- Development of techniques to create 3D anatomical models of the craniofacial skeleton using "Black Bone" datasets.
- Investigation of the accuracy of the resultant 3D anatomical models.
- Investigation into the potential wider applications of "Black Bone" MRI.

A brief overview and discussion of findings are provided at the end of each chapter with a more comprehensive discussion in the concluding section of the thesis.

# 2. Background

# 2.0. Background

This chapter provides a brief overview and literature review of the imaging techniques, anatomy and pathology on which this thesis focuses. As the primary motivation for the thesis is to determine if MRI could be utilised as a non-ionising alternative to CT when imaging the craniofacial skeleton, it is pertinent to commence with a review of these imaging techniques and the associated risks of ionising radiation, prior to reviewing the anatomy and pathology relevant to the three patient groups.

## 2.1 Medical Imaging: A technical Review

### 2.1.1 Radiography

X-radiation is the fundamental principle of diagnostic imaging most frequently employed worldwide. The key components of an x-ray tube *(Figure 1)* include the cathode electron source and a positively charged rotating anode target, housed within an evacuated glass envelope. Electrons are produced by the process of thermionic emission, and are accelerated by a potential difference across a vacuum toward the anode target. The interaction of electrons with the atoms of the target material results in the release of heat energy (99%) and x-ray photons. As x-rays are passed through tissues they are attenuated to an extent dependent upon the penetrating characteristics of the beam and the physical characteristics of the tissues.

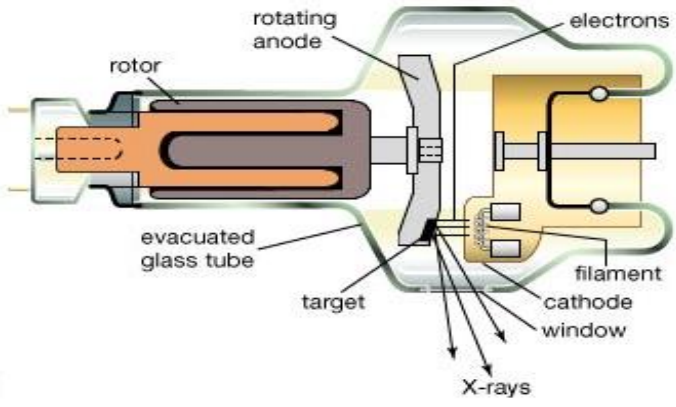



***Figure 1: Basic design of an x-ray tube. Electrons are accelerated by a potential difference across a vacuum toward the anode target, where they result in heat and x-ray photons***

### 2.1.2 Computed Tomography (CT)

Computed tomography (CT) utilises the basic principles of radiography by means of a rotating gantry. The gantry consists of an x-ray tube, a collimator and detector array, with the underlying principle to reconstruct large numbers of one-dimensional views of a transverse axial slice from multiple directions.[4-7] The processes are subdivided into: data acquisition, image reconstruction, and image display.[8] To acquire the images, the x-ray beam passes through the body in either a pencil or fan beam and is recorded by Xenon gas or solid state crystal detectors *(Figure 2)*.[8-9] The resultant image consists of a matrix of picture elements (pixels (2D), voxels (3D)), each representing the degree of attenuation of x-rays at a particular point in the body.[10] The value stored in each pixel, the Hounsfield Unit (HU) (or CT number), represents the average linear attenuation coefficient, $\mu_t$, of the tissues within the voxel and is given by:

$$HU = 1000\, x\, \frac{\mu_t - \mu_w}{\mu_w}$$

*where $\mu_w$ is the linear attenuation coefficient of water*.[9]

Water has a HU of zero, and air -1000. Since the HU reflects the average attenuation of a voxel of tissue, it is susceptible to error associated with the averaging process, a phenomenon termed **partial voluming**. This effect is reduced by utilising a smaller slice thickness, which decreases the voxel size and improves image resolution. The greyscale range contained within a typical image is between -1000 to +3000 HU. Since the human eye is unable to distinguish such an extensive distribution the technique of windowing is used to set an upper and lower threshold; all voxels falling outside of the defined range are set to white or black, respectively. Predefined values e.g. lung or bone windows, optimise the viewing of these structures.

The key development in CT came with slip-ring technology. This resulted in the ability for continuous rotation of the gantry unrestricted by wires. The combination of improvements in tube cooling efficiency, an increased milliamperage (mA) capability, more efficient detectors and uninterrupted table movement, has led to dramatic reductions in CT scanning time, the virtual elimination of movement artefact, and helical and multislice scanning.

The risks in terms of ionising radiation exposure of CT are considered in Section 2.2.

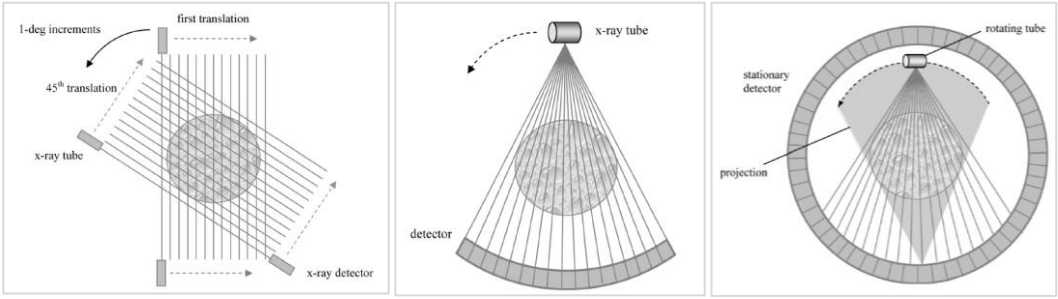



*Figure 2: Simplified diagram of "first" (left), "third" (centre) and "fourth" generation CT scanners.*[5,7]

### 2.1.2.1 Cone Beam CT

The first dedicated cone beam CT (CBCT) scanners for use in the dental and maxillofacial specialities were pioneered in the late 1990's.[11-13] The main impetus for their introduction was an increased demand for 3D imaging in these specialities. The physical size of the machines, and their reduced cost (approximately ¼ that of conventional CT) led to widespread incorporation both in primary and secondary care. The fundamental difference to CT is that CBCT utilises a conical shaped x-ray beam with a flat panel detector (FPD) or a charge-coupled device (CCD) *(Figure 3)*. The cone beam produces a more focused beam with reduced scatter when compared to conventional fan shaped or spiral-scan CT devices.[14-15] The tube and detector complete one rotation around the **region of interest** (ROI), during which multiple (150 - >600) sequential planar projection images of the **field of view** (FOV) are acquired.[15] The voxel dimensions primarily depend on the pixel size on the area detector, unlike those in conventional CT which depend on slice thickness.[15] Therefore, voxels are typically isotropic, and as small as 0.076mm, which is of particular value in 3D reconstruction.

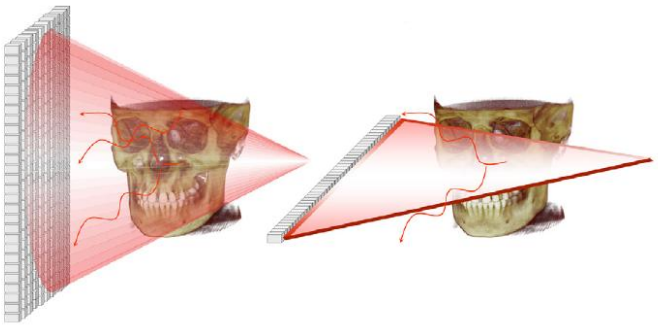


*Figure 3: Cone beam geometry, left, compared to Fan beam, right.*[15] *A cone beam produces a more focused beam with reduced scatter than conventional fan-shaped beam. The voxel size in CBCT is dependent upon the detector size rather than slice thickness.*

### 2.1.3 Magnetic Resonance Imaging (MRI)

Magnetic Resonance Imaging (MRI) utilises the principle that atomic nuclei with an unbalanced number of protons when placed in a magnetic field and stimulated by radio waves of a particular frequency re-emit some of the absorbed energy in the form of radio signals.[9,16]

Within the nucleus of atoms, protons and neutrons spin about their own axes.[17] This is an intrinsic phenomenon which remains constant. As protons have mass and charge (+1), they induce a magnetic moment, behaving like tiny bar magnets.[18-20] Those nuclei which contain an odd number of protons are considered "MR active." Hydrogen, with its single proton induces a large magnetic moment, making it particularly valuable in MRI. Usually the net magnetic effect is zero, since the individual dipoles are randomly aligned, with an equal number in each direction. When placed in an external magnetic field ($B_0$) the alignment constantly changes, however at any moment there are a small excess of protons aligned parallel (spin up) to the magnetic field compared to those antiparallel (spin down), producing the **net magnetisation vector** (NMV). With increasing strength of $B_0$ increasing numbers of protons align parallel, since more energy is required to align against the field. When placed in an external magnetic field, the spinning protons "wobble" or precess *(Figure 4)*. The frequency of precession is defined by the Larmor equation:

$$\omega_0 = \gamma B_0$$

*where $\omega_0$ is the precessional frequency, $B_0$ is the external magnetic field strength and $\gamma$ is the gyromagnetic ratio.*

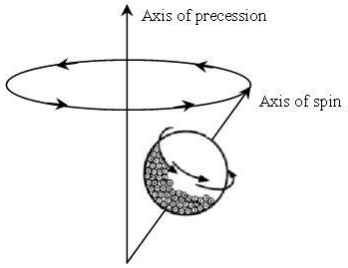



***Figure 4: The concept of proton spin and precession.***

Precessional frequency will therefore increase with increasing external magnetic field strength. When placed in $B_0$, the magnetic moments of the nuclei are on different positions on their precessional paths and considered out of phase. Resonance is an energy transition that occurs when a nucleus is exposed to electromagnetic radiation delivered at its precessional frequency and perpendicular to the main magnetic field.[19] This is achieved by a radiofrequency (RF) pulse of the same frequency as the Larmor frequency, produced by RF coils surrounding the patient. The protons absorb the energy from the RF pulse, increasing the number of protons that are aligned

antiparallel (spin up) and equalling those that are parallel. As a result the NMV in the $M_z$ plane, will flip through 90$^o$ to lie within the transverse $M_{xy}$ plane, as the net magnetisation lies between the two energy states. In addition the protons will move into phase with each other (align on their precessional paths). The required RF pulse to cause resonance is specific to each nuclei i.e. that required for hydrogen is different to carbon-13. For hydrogen nuclei in a 1.5T magnet, the required RF pulse is 63.86MHz at 90 degrees to $B_0$. As the NMV rotates around the transverse plane it passes across the receiver coil inducing a voltage in it, and constituting the MRI signal. When the RF pulse stops, the signal induced in the receiver coil begins to fall, due to the decreasing NMV. This process is termed **free induction decay**. The nuceli emit the energy they absorbed from the RF pulse, and revert to the low energy (parallel) state, and the NMV realigns to $B_0$. In addition, there is a loss of phase coherence (dephasing). T1 is defined as the time taken for 63% of the longitudinal magnetisation to recover *(Figure 5)*. It is dependent on the strength of the external magnetic field and the internal motion of the molecules. Energy transfer between nuclei produces a loss of phase coherence, resulting in an exponential decay of the transverse magnetic vector, dependent upon the tissue type.[9] T2 is defined as the time taken for 63% of the transverse magnetisation to be lost *(Figure 5)*. In the presence of external magnetic field inhomogeneities there is slight difference in the phase and dephasing of the spins that pass through these areas. The transverse magnetisation decay that occurs does so exponentially, and is referred to as T2*. It occurs before T2, and its effects need to be eliminated to observe true T2 dephasing. This is achieved through rephasing, by the application of a 180$^o$ RF pulse which flips the dephased nuclei through 180$^o$.

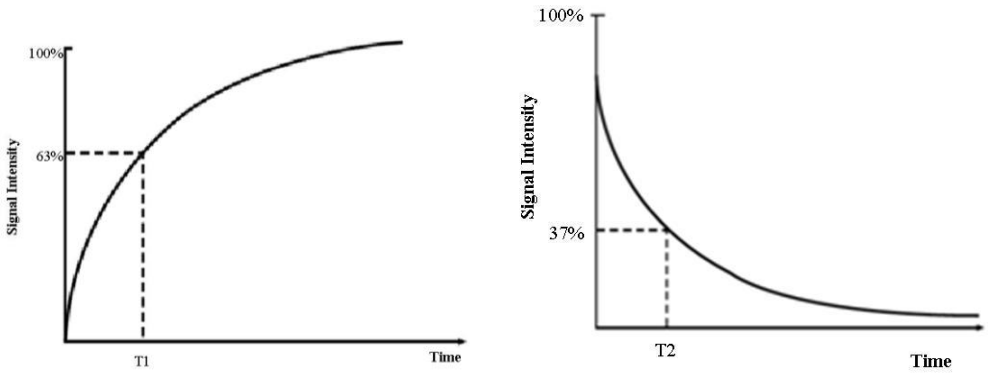



***Figure 5: T1 Recovery (left) and T2 Decay (right) plotted as signal intensity against time. T1 is defined as the time taken for 63% of the longitudinal magnetisation to recover. T2 is the time taken for 63% of the transverse magnetisation to be lost.***

The **repetition time** (TR), is the time from the application of one RF pulse to the application of the next. The TR affects the length of the relaxation period after the application of one RF excitation pulse to the beginning of the next. It determines the amount of T1 relaxation that occurs. With a long TR, there is more time for excited spins to rotate back to the z-plane and contribute to the regrowth of longitudinal magnetisation. The interval between the application of the excitation pulse and collection of the MR signal is termed the **time to echo** (TE). The TE controls the amount of T2 relaxation that occurs.

Gradients alter the magnetic field strength of the bore magnet in a predictable linear manner by the passage of current, resulting in unique precessional frequency of the tissue along its line. Three orthogonal gradients are used to permit spatial resolution: x, y and z. At the isocentre, the magnetic field strength will equal that of the bore magnet. The three main gradients are defined as:

1. **Slice selection gradient** – this is switched on during the delivery of the RF excitation pulse, and also during the $180^{o}$ pulse so that the rephasing pulse can be delivered specifically to the slice selected.
2. **Frequency encoding gradient** – this is switched on during the echo. It is often referred to as the readout gradient.
3. **Phase encoding gradient** – this is switched on after the RF excitation pulse has been switched off.

In order to obtain slice thickness, a range of frequencies are transmitted (**transmit bandwidth**) to produce resonance across the whole slice.

The system maps the individual signals from the encoding process onto a two dimensional matrix. By the mathematical process of Fast Fourier transformation (FFT) the raw data is converted to the signal amplitude measured relative to its frequency. K space is where raw data is stored until the acquisition process is complete. It consists of an x and y axis representing the phase and frequency encoding, respectively. The data within each line in k-space represents data acquired from the whole image during each TR. The number of lines that are filled is dependent upon the size of the matrix selected. Each line may be filled more than once by applying the same phase encoding gradient slope repeatedly, and is referred to as the **number of signal averages or excitations** (NEX). Whilst this increases the signal to noise ratio (SNR) it also increases scan time. Since k-

space is symmetrical about its axes, not all of k-space needs to be filled, and data can be interpolated to reduce scan times.

Image quality is dependent upon the optimal balance of three key factors:

1. Signal to noise ratio, which in turn is dependent upon:
    a. Voxel volume (dependent upon matrix size, FOV and slice thickness)
    b. NEX
    c. TR & TE
    d. Receive bandwidth
    e. Proton density of the area being imaged
2. Spatial resolution, which in turn is dependent upon:
    a. Matrix size
    b. FOV
3. Scan time, which is in turn dependent upon:
    a. NEX
    b. Phase encode
    c. TR

By increasing spatial resolution, there will be a resultant decrease in SNR and increase in scan time. The development of MRI scanners with higher field strength was stimulated by promise of increased SNR, decreased scan times and improved spatial resolution.[21] However, there are disadvantages, including decreased contrast due to lengthening of T1 and increased susceptibility effects.[21]

#### 2.1.3.1. Image Contrast

Image contrast on MRI is the result of signal intensity due to three main factors within the tissues:

1. Proton density – the number of excitable spins per unit volume; this can be optimised by minimising T1 and T2
2. T1 weighting
3. T2 weighting

In a T1 weighted image, variations in the T1 recovery times of the tissues are predominantly responsible for the variations in signal intensities of the image *(Figure 6)*. T1 relaxation occurs as a result of energy exchange of the nuclei to the surrounding environment. Fat can do this much faster than water, and therefore has a short T1. Variations in the T2 dephasing of the tissues are predominantly responsible for the variations in contrast in a T2 weighted image *(Figure 6)*. In proton density weighted images it is necessary to minimise the effects of both T1 and T2.

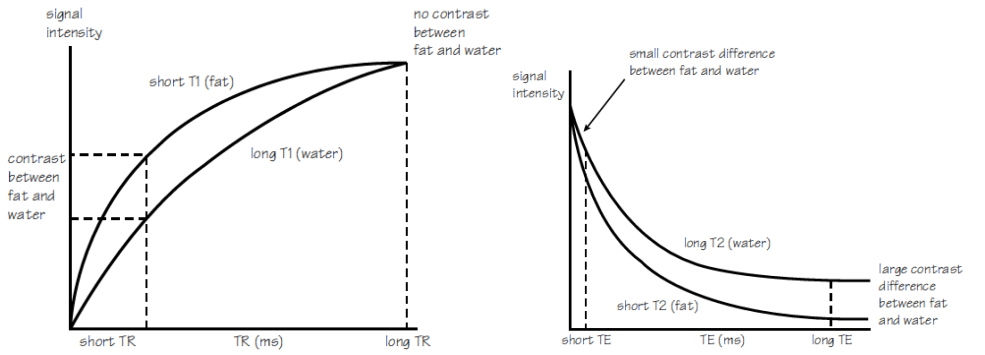



*Figure 6: T1 weighting (left) and T2 weighting (right) plotted as signal intensity against TR and TE, respectively.[17] The maximal contrast between fat and water is seen with a short TR and long TE.*

### 2.1.3.2. MRI Sequences

Every year, new MRI sequences are introduced in an attempt to improve imaging of particular tissue types in terms of spatial resolution and signal contrast and/or decrease examination times.[22] The most basic sequence structure include the spin echo and gradient echo techniques.

#### *Spin Echo Pulse Sequence*

The spin echo pulse sequence is the most frequently utilised sequence in MRI. It is used to produce T1, T2 or proton density weighted images. The basic principles are a 90$^{o}$ excitation pulse followed by a 180$^{o}$ rephasing pulse followed by an echo *(Figure 7)*.

#### *Fast Spin Echo*

To reduce scan time, fast spin echo techniques incorporate more than one phase encoding per TR. This is achieved by using an echo train which consists of several 180$^{o}$ rephasing pulses. At each rephasing, a phase encoding step is performed and data from the resultant echo stored. The number of echoes used is termed the **echo train length** (ETL).

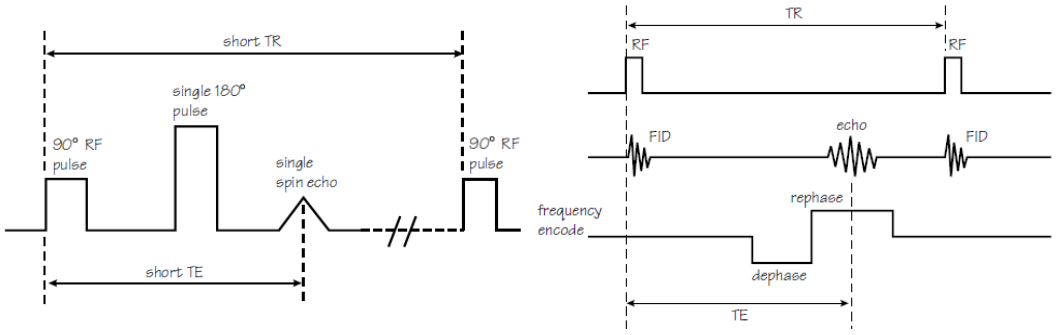



*Figure 7: Spin echo sequence (left) and gradient echo sequence (right).[17] The spin echo sequence consists of a 90° excitation pulse followed by a 180° rephasing pulse followed by an echo. The gradient echo sequence consists of a RF excitation pulse followed by a relaxation period and a gradient reversal to produce rephrasing of the spins.*

### *Gradient Echo Sequences*

The gradient echo sequence consists of a RF excitation pulse followed by a relaxation period and a gradient reversal to produce rephasing of the spins *(Figure 7)*. Since the gradient reversal is not as effective as the $180^{o}$ RF pulse utilised in spin echo sequences, gradient echo images contain some residual T2* effects. The magnitude and duration of the RF excitation pulse selected determines the flip angle, i.e. the angle through which the NMV moves away from $B_0$ during resonance.[17] The TR and flip angle control the T1 and proton density weighting. The TE determines T2*. The gradient echo sequence is particularly relevant to the thesis.

### *STIR & FLAIR*

Short TI (**time to inversion**) inversion recovery (STIR) is an inversion recovery pulse sequence with specific timing to suppress signal from fat. The TI controls the degree of saturation and therefore the contrast. With short TI the 90 degree detection pulse is at the time that the NMV of fat is passing exactly into the transverse plane. When the $90^{o}$ pulse is applied the fat vector is flipped to $180^{o}$ resulting in a signal void, and thus suppression of fat on the image. Suppression of any tissue is possible by selecting a TI that results in the $90^{o}$ pulse occurring at the null point of the tissue. With a long TI, the result is suppression of signal from fluid, and the sequence termed FLAIR (fluid attenuated inversion recovery).

### *Ultra Fast Techniques*

Besides image contrast, imaging speed is probably the most important consideration in clinical MRI.[23] Methods to reduce imaging time include echo-planar imaging (EPI),[24] fast low-angle shot (FLASH), and turbo spin echo (TSE). EPI collects all of the data required to fill K space from a single echo train by generating multiple echoes which are encoded by a different slope of gradient.

Having reviewed the principal techniques of CT and MRI the next step is to consider the risks associated with ionising radiation and thus why consideration should be given to MRI as an alternative to CT when imaging the craniofacial skeleton.

## 2.2 Ionising Radiation Concerns

The associated risks of ionising radiation were recognised at the first introduction of x-rays into medicine, with reports of erythema, dermatitis and alopecia noted in both operators and patients.[5] However, it was a further twenty years before the first radiation protection recommendations by the British Roentgen Society were announced.

### 2.2.1 Quantifying Exposure

To accurately quantify patient exposure to ionising radiation it is necessary to define dose. **Absorbed dose** is defined as the energy deposited per unit mass of the stated material ($JKg^{-1}$ or Gy).[9] It is commonly used to define the quantity of radiation delivered at a specific point within the radiation field. The typical absorbed dose for a chest radiograph is 0.15mGy, and for a CT scan 10-30mGy.[9] However, it was noted that organs have differing sensitivities to ionising radiation. The concept of "**effective**" dose was introduced in 1975 to provide a mechanism for assessing the radiation detriment from partial body irradiations.[25] This method takes into account both the radiation dose and the relative radiosensitivity of the exposed organs, measured in sieverts (Sv).

$$\textbf{Effective dose} = \sum_T W_T D_T$$

*where $D_T$ is organ-specific dose, $W_T$ is the tissue weighting factor for organ or tissue T.*

Typical effective doses from x-ray examinations of the head are shown in *Table 1*.

For CT scanning, more practical measures of dose are **CT dose index** (CTDI), and **dose length product** (DLP). CTDI is a measure of dose from a single rotation of the gantry, and can be calculated for the imaged volume. DLP is defined as the product of CTDI for the volume and total scan length.

| Examination | Effective dose (µSv) | Dose as a multiple of the dose from a typical panoramic exam |
|---|---|---|
| **Panoramic radiograph** | 24 | 1 |
| **Small FOV CBCT** | 48 - 652 | 2 - 27 |
| **Large FOV CBCT** | 68 - 1073 | 3 - 45 |
| **CT scan (dental)** | 534 - 2100 | 22 - 88 |

***Table 1: Typical patient doses from x-ray examinations of the head in reference to a panoramic radiograph (OPG).*** [26]

### 2.2.2 Problems with Measuring Dose

Whilst used as an indicator of patient risk there are some intrinsic problems with the methods of radiation dose calculation. Measurement of dose is largely reliant upon custom built phantoms or cadavers, which may not truly represent the anatomy of the patient. For example, cylindrical acrylic phantoms are often used to simulate the head (16 cm diameter) or body (32 cm).[27] The fundamental problem with effective dose is related to the tissue weighting factors. These are decided by a committee based upon cancer risk, taking into account a balance between the risk of malignant transformation, associated mortality and hereditary risk.[28] The weighting factors can therefore be considered to be arbitrarily set, and vary between different groups of experts.[28] In addition, effective dose is calculated independently of age, yet radiation risks are often highly age-dependent. Brenner recommended a new measure of dose with reference to cancer risk alone, which is both age dependent and based upon the best-available organ-specific lifetime cancer risks.[28] Whilst Brenner, concluded that this measure would be easier to interpret, it has failed to be incorporated into routine practice.

### 2.2.3 Risk of Radiation Exposure Related to Dose

The effects of radiation exposure can be defined as deterministic or stochastic. Deterministic effects are characterised as those having a threshold dose below which the effect will not occur.[9] These are rarely encountered in medical imaging, but may occur as a result of equipment or operator error. Deterministic effects include erythema, hair loss and cataracts. In the USA, the Food and Drug Administration (FDA) have recently been investigating reports of patients exposed to excess radiation whilst undergoing brain perfusion scans.[29] However, ordinarily the main concerns related to medical radiation exposure are stochastic effects, where the probability of an adverse event increases with increasing dose, yet its severity is unrelated and therefore unpredictable.

Ionising radiation causes damage or death to living cells directly, or indirectly, through the creation of free radicals. Modifications within the DNA structure, if not repaired, may be transmitted to further cells, potentially resulting in malignancy.[30-31] Early evidence supporting the theory that radiation exposure is implicated in malignancy include the increased incidence of leukaemia in radiologists compared to the general population, increased incidence of carcinoma of the thyroid and leukaemia in children who received radiation for thymic enlargement, adenoid hypertrophy or

cervical adenitis, and patients receiving prolonged radiation therapy for spondylitis.[32] The United Nations Scientific Committee on the Effects of Atomic Radiation (UNSCEAR) in their year 2000 report derived risk estimates for radiation-induced cancer.[30] For a population of all ages with an acute dose of 1 Sv, they estimated a lifetime risk of mortality from solid cancer of 9% for men and 13% for women, and a lifetime risk of death from leukaemia of 1%.

The risk associated with ionising radiation in the range that is used for diagnostic purposes has been the subject of much debate. Brenner et al[33] questioned the epidemiological basis for adverse outcome following radiation exposure. They stated that whilst there was little question that intermediate and high doses of ionising radiation (>100mSv), acutely or over a prolonged period, resulted in deleterious consequences, the effect of low dose exposure was less clear. With the large sample size and lifetime follow-up required for investigation into such exposures exploration is unfeasible. The fact that risks cannot be directly estimated at low dose, does not imply any conclusion as to whether risks actually exist at these lower doses.[33]

Studies into the effects of radiation exposure are largely limited to the epidemiological studies of atomic bomb survivors. This cohort of patients is both large, and with complete long-term follow up. Approximately 50% of the cohort was exposed to doses less than 50mSv. Individuals exposed to 5-100mSv had a significant ($p=0.05$) increase in solid cancer.[33] However, a number of limitations need to be considered. Many of the atomic bomb survivors were exposed to acute radiation exposure, with doses dependent upon their distance from the blast. They were exposed to both $\beta$ and $\gamma$ radiation rather than simple x-radiation, with internal and external exposure from contaminated food and water source, with the dose being fairly uniform.[34] In general, protracted exposures to x-radiation are associated with lower risk than those of acute exposure to the same total dose.[33]

Alternative studies have utilised patient groups exposed to repeated radiological investigations. Doody et al[35] evaluated the patterns in breast cancer mortality in women with scoliosis with regard to diagnostic radiography exposure. The average number of examinations per patient was 24.7, with a mean estimated cumulative dose to the breast of 10.8cGy. In total, 77 breast cancer deaths were observed, against an expected 45.6. Risk was significantly increased with increasing number

of radiograph exposures. However, the authors noted potential confounding factors, such as severity of disease and reproductive history.

Exposure to ionising radiation at a young age is of greatest concern. Children are more susceptible to the effects of radiation because of the higher proportion of dividing cells and the longer life expectancy in which complications may develop.[33,36] Polhemus et al[32] reviewed the radiation histories of 251 children with leukaemia and compared these to matched controls. They found that exposure to radiation was significantly more frequent among those children with leukaemia, with thymic radiation being statistically significant ($p<0.01$) as a contributing factor for development of leukaemia. Similar findings were found by Bartley et al[37] who conducted a case-control study of children aged under 14 years with a diagnosis of leukaemia. However this study was subject to the bias associated with self-reporting of x-ray exposure. In contrast, Meinert et al[31] in their case-control study found no association between the number of x-rays during childhood and cancer. However, again the study was reliant upon accurate parental recall during postal and telephone interviews. Hammer et al[38] examined the incidence of childhood cancer in a cohort of 100,000 children exposed to diagnostic x-rays at one hospital, with cancer diagnosis from the national cancer registry. The median radiation dose was 7μSv. However, no quantification was made for x-ray exposure at different hospitals. They found no increase in the risk of solid tumours or leukaemia in childhood.

The risk of intrauterine x-ray exposure is well recognised.[39-40] It was found that children exposed in utero to pelvimetry or to another similar procedure, had approximately double the normal risk of dying from cancer before the age of 10 years.[41] Many similar studies have attempted to associate death from leukaemia with intrauterine exposure to radiation. Court Brown et al[41] however, identified all pregnant women exposed to abdominal or pelvic radiation and correlated this with the number of associated deaths from leukaemia. They found no increase in the rate of leukaemia however, few had been exposed to radiation during the first trimester of pregnancy. Following the publication of the Oxford Survey of Childhood Cancer, highlighting the risk of intrauterine radiation exposure, there was an abrupt reduction in radiography requests for a period of 10-12 years.[42]

The effects of radiation exposure are likely to be multi-factorial, with age at exposure, and genetic susceptibility being contributory factors. An important consideration is that whilst a specific area of the body may be targeted in a radiologic study, even organs distant to the site of interest are exposed to small amounts of radiation due to scatter.[43] The extrapolation of risks from high to low doses may both under- and over-estimate the risks of radiation exposure. However, even a small increased risk when applied to the population, can reflect a significant public health problem.

### 2.2.4 The Increasing Use of CT

The greatest concern for radiation exposure arises from the increasing use of CT. In his 1973 paper describing CT, Hounsfield stated that "the exposure of the patient to x-rays must be restricted." [1] However, with further advances in technology, the number of CT exposures have consistently increased. A study conducted in the USA found that whilst CT scanning constituted 11% of diagnostic radiological procedures, they accounted for 70% of effective dose.[44] Similar findings have been reported in the UK. During the year 2002-3 the NHS in England reported 1.7 million CT examinations, representing 8% of all x-ray examinations, and 6% of all imaging investigations.[45] By 2009-10 this had risen to over 3.7 million, 13% and 10% respectively (*Figure 8*). Worldwide, UNSCEAR estimated that CT constitutes about 5% of all x-ray examinations whilst accounting for 34% of the resultant collective dose.[46] The radiation dose received by patients undergoing CT examination are estimated to be 1-24 mSv[30] for adults, and 2-6.5 mSv[47] per examination in children. Placing this into context, natural background radiation results in an annual exposure of 2.4mSv.[30]

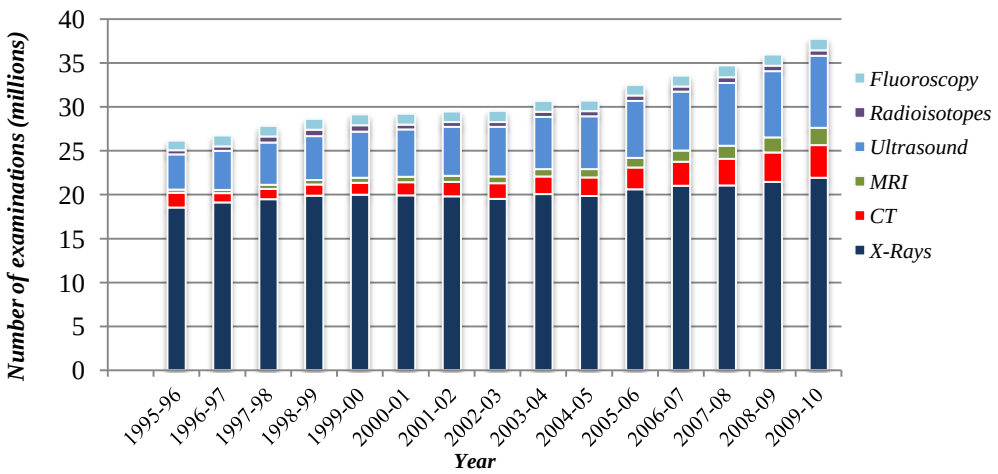



*Figure 8: Total Number of imaging and radiodiagnostic examinations or tests, by imaging modality, England, 1995-96 to 2009-10.*[45]

The radiation dose to organs from any given CT scan depend upon a number of factors; the most important are the number of scans, the product of tube current and scan time (the "mAs"), patient size, the axial scan range, the scan pitch (the degree of overlap between adjacent CT "slices"), the maximum tube voltage (the $kV_p$) and the particular scanner design.[48] The speed at which images can be obtained facilities wide-range scanning, with incidental exposure of non-target organs. It is widely recognised that variability exists among manufacturers and local protocols with regard to x-ray based imaging systems. Since the dose associated with CT is much larger than with plain radiography, the effects of this variability can be significant. Most operators follow the recommended settings of the manufacturer, but these may not be the most appropriate settings.[49] The ALARA principle states that all exposures for diagnostic imaging purposes should be kept "as low as reasonably achievable." However, geographical variation exists in the setting of CT parameters – in the USA exposure is typically set to achieve lower image noise, resulting in higher exposure, whilst in Europe radiation protection is seen to be more important.[50] It is widely accepted that unoptimised CT protocols are a significant contributor of unnecessary radiation dose.[46] Recently, the American Association of Physicists in Medicine (AAPM) began posting scan protocols (outlining the CT settings and parameters) on its website. In 2001, the US FDA issued a health notification with guidelines stating that radiologists and health-care providers should attempt to minimise radiation exposure in children and more recently a national paediatric CT dose registry has been introduced across North America.[51] In the UK, the use of ionising radiation for medical exposures is subject to the Ionising Radiation Regulations 1999 (IR99) and the Ionising Radiation (Medical Exposure) Regulations 2000 (IR(ME)R). IR(ME)R requires the employer to establish diagnostic reference levels (DRLs) for standard radiodiagnostic examinations.

The trend in technology is generally towards more dose efficient equipment, with solid-state detectors, an emphasis on high geometric dose efficiency and dose-saving and dose-awareness features.[2] However, it is ultimately the responsibility of the referrer, radiologist and radiographer to further decrease radiation exposure.

It is recognised that advancements in CT technology (e.g. multislice CT) have also brought increases in patient dose. Yates et al[52] audited the impact of the introduction of multislice CT in

East Anglia on dose. They obtained 550 sets of patient data, and calculated effective dose using the results of Monte Carlo simulations published by the National Radiological Protection Board. They found that the multislice scanners resulted in, on average, 35% more effective dose than single-slice scanners. Feng et al[36] investigated the radiation associated with 64-slice multidetector row computed tomography (MDCT) using a 5-year-old paediatric phantom with common CT protocols. They found that the effective dose for head CT was 0.7mSv, with the thyroid, brain and salivary gland receiving relatively higher organ doses of 2.52mGy, 17.91mGy and 22.33mGy, respectively. The dose to the lens was 25.88mGy. Nishizawa et al[53] investigated the radiation exposure associated with six types of MDCT in common use. They found that the effective dose for a child head examination was 1.4-4.8mSv with variability in results across scanners.

The growth of CT use in children has been driven by the decreased time required to perform the examination, largely eliminating the need for anaesthesia.[34] Mettler et al[54] estimated that 30% of all paediatric and adult patients who undergo CT evaluation of any body part have at least three scans, 7% have at least five, and 4% have at least nine. They also found that children aged under 15 years accounted for 11.2% of all scans with head examinations being the most frequent procedure performed.[53] Organ doses for children are larger than for adults[55] as a result of reduced partial shielding from the rotating x-ray source. Huda et al[56] compared the radiation doses of infant patients (under 2 years of age) to adults undergoing routine non contrast CT examinations of the head. They obtained data on 23 infants, and 23 adults, including kVp, mAs, and slice thickness. To determine dose they used a uniform cylinder of water corresponding to the patient size data. The energy imparted to infants correlated with patient weight much more than it did with adults. The average effective dose to the infants (7.6 +/- 3.1mSv), was approximately six times higher than that for adults (1.3 +/- 0.1mSv).

Whilst it is recognised that the dose associated with cranial imaging is considerably less than that associated with chest or abdominal imaging, in view of the frequency with which cranial CTs are performed, their contribution to total collective effective dose to the population is significant.[46,57] Smyth et al[58] reported two cases to highlight the concern of repeated radiation exposure in children. Stein et al[59] constructed a mathematical model to predict radiation-induced tumours, and concluded

that the risks of a single head CT were so small in older children as to be barely measureable. It can be expected to shorten the lifespan of an average 15-year old by approximately 2 days and have almost no impact on quality of life. For a 2 year old the lifetime risk of a neoplasm induced by a single head CT is 0.15, and 40% of these children will die of their tumours.

Chan et al[49] investigated the impact on image quality of reducing radiation dose in paediatric cranial CT. They compared the images of 53 children undergoing CT using manufacturers default settings of 200-250mAs, to 47 children using 125-150mAs, finding no statistical difference and providing further scope for dose reduction.

In many cases, the risk of increased radiation exposure is overshadowed by the potential sequelae of the condition being imaged. However, the frequency with which benign conditions, particularly in children, are being imaged with CT is causing significant concern. The investigation should be justified, alternative techniques considered (e.g. MRI and ultrasound), and the examination optimised.

The next section reviews the pathology, justification for imaging and methods used to currently optimise radiological investigations in the three patient groups on which this thesis focuses: children with craniosynostosis, adolescents with facial disproportion, and adults with malignancy involving the facial skeleton.

## 2.3 Craniofacial Anatomy

The craniofacial skeleton comprises the neurocranium (cranium) and the viscerocranium (facial skeleton). The cranium is sub-divided into the cranial vault and base of skull and comprises eight bones: occipital, paired parietal, frontal, two temporal, sphenoid and ethmoids, which articulate via intervening fibrous sutures. Of relevance in terms of the thesis are the sagittal suture (between the paired parietal bones), the metopic suture (between the paired frontal bones), the paired coronal sutures (between the frontal and parietal bones) and the paired lambdoid sutures (between the occipital and parietal bones) *(Figure 9)*.

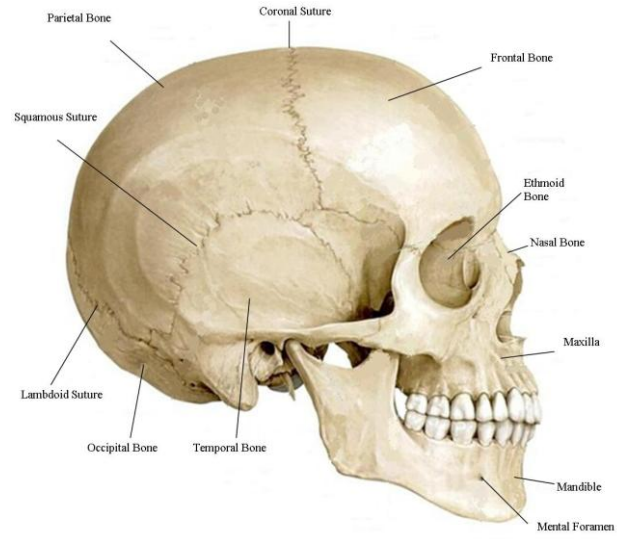



***Figure 9: The craniofacial skeleton consists of the cranium and facial skeleton. The intervening cranial sutures of the cranium can be seen.***

The facial skeleton primarily comprises of the mandible, maxilla, nasal bones and zygoma. The paired maxillae have multiple functions; they bare the upper teeth within the alveolar process, form the roof of the oral cavity, house the maxillary sinus and contribute to the floor of the orbit. Within the body of the maxilla lies the maxillary sinus (or antrum), one of four such bilateral paranasal sinuses communicating with the nasal cavity and being lined with respiratory epithelium. The mandible articulates with the cranium at the temporomandibular joints. The body of the mandible consists of alveolar bone forming the walls of the tooth sockets. This is covered by mucoperiosteum to form the gingivae.

Further anatomical considerations are included in the pathological and radiological review of the three patient groups.

## 2.4 Pathology Affecting the Craniofacial Skeleton

The thesis explores both benign pathology (craniosynostosis and abnormal growth of the facial skeleton), and malignant pathology (squamous cell carcinoma affecting the mandible and maxilla). This section focuses on the pathology and required radiological investigations to confirm diagnosis and aid surgical planning.

### 2.4.1 Cranial Sutures and Craniosynostosis

The cranial sutures consist of two bone ends with an intervening fibrous tissue which differentiates from embryonic mesenchyme.[60] The main functions of the sutures are to act as: (1) sites of bone growth, (2) articulations, holding the constituent elements of the skull together while allowing deformation of the skull during child birth and thereafter minor movements, and (3) mechanical stress absorbers, thus protecting the sutural osteogenic tissue.[60] Bone growth occurs by intramembranous osteogenesis at the bone margins of sutures, and continued growth is dependent on maintaining the space between the opposing bone margins so that they do not unite. Except for the metopic suture, which starts to close after the first year, after a period of major broadening of the forehead, and is obliterated by 7 years of age, most calvarial sutures start to fuse in adult life between the ages of 25 and 30 years.[60] Most facial sutures remain patent until late adulthood.

The premature fusion of the cranial sutures (craniosynostosis) results in characteristic abnormalities in terms of skull shape resulting from overgrowth at the remaining patent sutures *(Figure 10)*. A single suture may fuse in isolation (single suture synostosis) or multiple synostoses may occur as the result of one of the craniofacial syndromes (e.g. Apert, Pfeiffer, Crouzon syndrome) which have associated facial and limb anomalies. Clinical presentation of single suture synostosis is typically during infancy with abnormal head shape; a ridge may be palpable along the fused suture. Occasionally presentation is with visual impairment, signs of neurological deficit or developmental delay.[61-62]

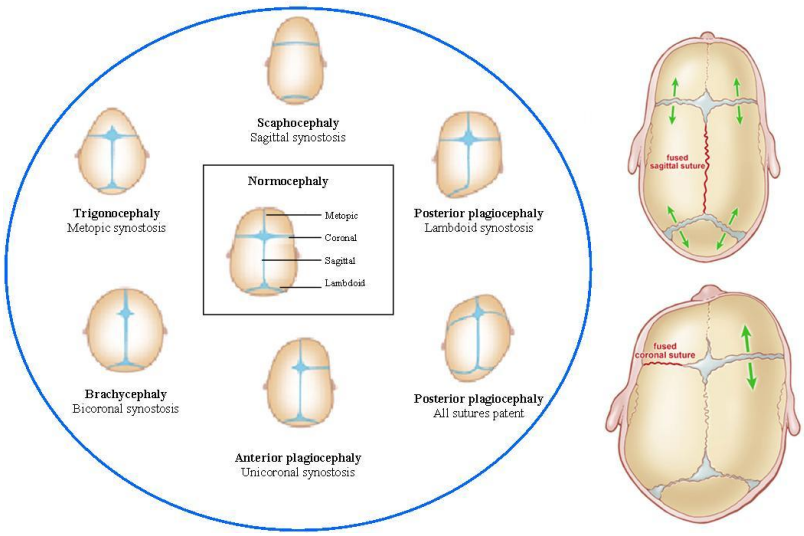



*Figure 10: Characteristic skull shape anomalies as a result of single suture synostosis (left) and the result of sagittal synostosis (top right) and unicoronal synostosis (bottom right).*[62,72]

Advances in human molecular genetics during the last decade have had a significant impact on the understanding of craniosynostosis.[63] The identification of mutations in the genes encoding the fibroblast growth factor receptors 1, 2 and 3 (FGFR1, FGFR2, FGFR3), MSX2, TWIST, and EFNB1 has enabled the molecular basis for the majority of syndromic craniosynostosis to be elucidated.[63] The majority of craniosynostoses are not syndromic, rather, isolated, sporadic single suture synostoses. In the majority of these cases, no molecular abnormality is detected, and it is therefore postulated that the aetiology is not primarily genetic.

Estimates of the incidence of craniosynostosis vary between 34.3/100,000 and 47.6/100,000 live births.[64] Syndromic cases are rare, with an incidence of about 1.5/100,000.[65] Sagittal synostosis is most common (40-55%), followed by coronal (20-25%), metopic (5-15%), multiple suture synostosis (5-15%) and lambdoid (0-5%).[66]

Surgical correction is generally advocated in view of the progressive deformity, and associated risk of raised intracranial pressure (ICP).[61,67-68] This is typically performed prior to 12 months of age with fronto-orbital advancement and/or calvarial remodelling.[69-72]

### *Imaging in Craniosynostosis*

Traditionally, the diagnosis of craniosynostosis has relied on standard radiography; the diagnosis being made by the absence of the suture, perisutural sclerosis, and/or bony bridging. Only part of the suture may be involved. Modern CT imaging techniques have revealed numerous details of clinical importance not visible on a plain x-ray, with soft tissue abnormalities potentially having a considerable influence on the treatment. [65,69] Findings on CT may vary. Thickened bony ridges predominate at the sagittal suture, focal bone thickening and erosions are more likely to be found at the metopic suture, and perisutural sclerosis is the prevalent finding on one side of the lambdoid suture.[69] The development of 3D CT resulted in improved visualisation of the cranial sutures and Tartaro et al[73] reported the diagnostic accuracy on 3D CT of 90.7-100% compared to 83.7-95.5% on axial CT.

It should be noted that craniosynostoses are often associated with changes not only in the calvarium but also in the cranial base, mandibular joints and other structures, and inclusion of the entire head in imaging is justified. Additional information provided by CT examination includes the estimation of cranial suture widths. Mitchell et al[74] established normal sutural width measurements for the coronal and sagittal sutures in infants on CT. In total, they evaluated 483 patients, with an age range of 1 day to 395 days. They found that the proximal suture widths for the sagittal and coronal sutures at zero months of age were 5.0 ± 0.2 and 2.5 ± 0.1mm, respectively. As anticipated, the sutures narrowed significantly with advancing age. Similar results have been reported by authors using ultrasound. Soboleski et al[75] examined the sonographic appearance and cranial suture width of the coronal, sagittal and lambdoid sutures. The study group consisted of 50 infants aged 0-5 months of age undergoing brain sonography. The mean width was 0.89 ±0.35 mm for coronal sutures, 0.93 ± 0.28 mm for sagittal sutures, and 0.96 ±0.39 mm for lambdoid sutures. However, unlike Mitchell et al, Soboleski et al found no correlation with age. These normative measurements provide useful information in the distinction between the normal and prematurely fused suture.

Typically, many craniofacial surgeons base their practice on the model developed and implemented by Paul Tessier (the “father” of craniofacial surgery). This includes obtaining 3D CT scans to aid diagnosis, plan surgery and evaluate post-operative outcome; resulting in potentially significant

cumulative ionising radiation exposure. Jaffurs and Denny[76] reviewed the radiation exposure of their craniofacial patients over a 7 year period. Dosage data were available for 77 patients. On average, patients with newly diagnosed craniosynostosis underwent 1.74 CT scans per year at an average dose of 1.39mSv per scan (range 0.48-3.36mSv). They concluded that the evidence was insufficient to support the theory that low-dose radiation exposure as in their practice had adverse consequences. There is no doubt that 3D CT scans permit excellent visualisation of the bony architecture and the ability to produce 3D anatomical models, improving both diagnosis and surgical planning. However, it has been questioned by Fearon et al[77] if CT imaging is necessary in the diagnosis of single suture synostosis. They prospectively analysed the diagnostic accuracy of clinical examination compared to CT imaging and surgical findings. In the 67 children studied, all but one, were diagnosed correctly on clinical examination alone. The incorrect diagnosis was made in a child presenting with posterior plagiocephaly but shown to have patent sutures on CT imaging. Without imaging this child may potentially have undergone unnecessary surgery; however, conversely the remaining 66 children potentially could have avoided CT examination. It is likely, in view of the significant risks of surgery, that the majority of surgeons would be reluctant to proceed without pre-operative imaging. Minimising post-operative CT has been more widely accepted. Binning et al[78] examined the necessity of routine post-operative imaging following craniosynostosis surgery. In their practice at the time of the study it was routine to obtain a head CT in the immediate post-operative period (day 1). This was justified by the difficulty of neurological examination with analgesia, intubation, swelling and surgical dressings. However, on review of the imaging findings, they concluded that routine imaging was of little benefit, with CT not altering patient management.

In all cases, CT should be optimised, using the lowest exposure possible. Harshbarger et al[79] presented methods of radiation reduction in patients with craniosynostosis. Their pilot study reduced average radiation dose from 26.1mGy to 2.85mGy without a significant reduction in bone image quality. However, MRI was additionally required to assess for structural brain anomalies.

The ability to diagnose craniosynostosis accurately on MRI would eliminate (or at least reduce) radiation exposure in these young patients.

### 2.4.2 Facial Disproportion

Growth of the face is closely related to growth of the body as a whole, and therefore accelerates considerably during adolescence.[80] Normal variations in skeletal and dental relationships arise as a result of ethnicity, and race. **Malocclusion** is the term used to describe misalignment of teeth or an incorrect relationship between the teeth of the maxillary and mandibular dental arches. Malocclusion is a common finding (approximately 60% of the population)[81] which usually requires no intervention. In more severe cases orthodontic treatment is often sought by the patient. When malocclusion is coupled with skeletal disharmony of the maxilla and mandible orthodontics is frequently used in conjunction with orthognathic surgery to achieve a satisfactory functional and aesthetic result. Surgical intervention is justified in approximately 5% of the population. The aetiology in only a small proportion of these patients is known, such as facial syndromes and congenital anomalies.[81] Surgery is usually deferred until growth is complete to obtain a predictable outcome and reduce the risk of relapse.

Clinical presentation is most frequently with aesthetic concerns; severe malocclusion may result in the primary complaint being difficulties with speech and eating. The three important tissue groups in orthognathic surgery and orthodontics can be referred to as a triad – facial soft tissues, facial skeleton, and dentition.[82] Successful management requires a careful balance of these components and necessitates close co-operation between surgeon and orthodontist.

Assessment of patients with malocclusion includes accurate documentation of the skeletal and dental relationships *(Figure 11)*. This is enhanced with the use of dental models cast in plaster of Paris from impressions of the teeth and dental arches. Surgical correction of skeletal discrepancy is completed with osteotomy, most frequently a Le Fort I and/or bilateral sagittal split osteotomy *(Figure 12)*.[83]

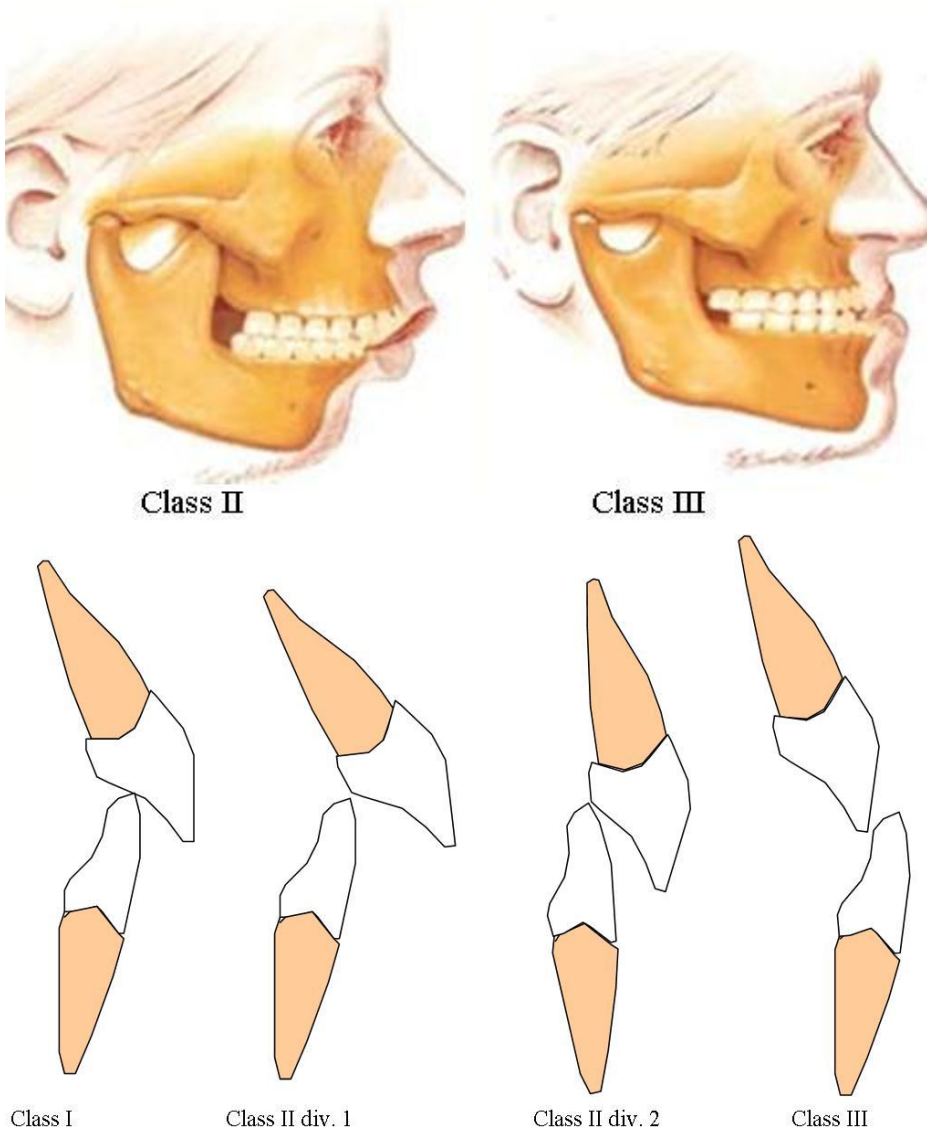



***Figure 11: The classification of skeletal and dental relationships [83]:***
***Skeletal relationships (top)***
***Class I - There is normal alignment between the mandible and maxilla***
***Class II - The mandible is positioned too far posteriorly in relation to the maxilla***
***Class II - May be due to either the maxilla being too far posteriorly or the mandible too far anteriorly.***
***Dental relationships (bottom):***
***Class I - The lower incisors bite 2-4 mm behind the upper incisors (normal)***
***Class II div 1 - The lower incisors bite further behind the upper incisors than normal and the upper incisors are normally inclined or proclined.***
***Class II div 2 - The lower incisors bite further behind the upper incisors than normal and the upper incisors are retroclined.***
***Class III - The lower incisors bite further forwards of the upper incisors than normal.***

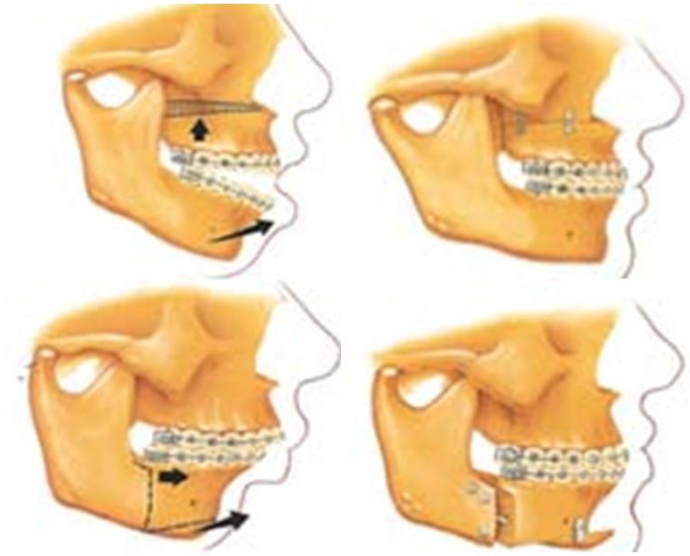


*Figure 12: LeFort I osteotomy (top) and bilateral sagittal split osteotomy (bottom) (this diagram also includes a genioplasty, which may be performed in addition to provide improved chin definition).*[83]

### *Imaging in Facial Disproportion*

The radiological investigation of patients with facial disproportion is conducted with plain radiographs in the form of an orthopantogram (OPG) to visualise the teeth, a lateral cephalogram to assess skeletal relationships, and a posteroanterior (PA) skull radiograph to assess for asymmetry. Often, serial radiographs are necessary.[84] These radiographs are utilised for cephalometric analysis and for surgical planning. **Cephalometrics** is an essential clinical and research tool in orthodontics, to obtain absolute and relative measures of the craniofacial skeleton.[85] It is a valuable tool for assessing growth, response to treatment and long-term stability. Since the first introduction of the craniostat in 1931 by Broadbent[86] the cephalogram has been accepted as the "gold standard" for planning orthodontic treatment and orthognathic surgery. This is enhanced by large collections of normative data permitting clinicians to monitor and predict outcome.[87] This normative data dates back to as early as 1901 when equipment was largely confined to callipers and data collected at social gatherings or by hat makers as a result of an interest in the correlation of head shape with intelligence.[88-89] It was the subsequent interest in deformity of the jaw by Schwarz[90] and Franke that resulted in collection of measurements on dry skulls, with the definition of cephalometric points arising from anthropologists and anatomists at the time. However, in 1931, Broadbent[86] recognised the inherent discrepancy between data collected on dry skulls and living children,

remarking “a dead child is usually a defective one.” He sought a reliable method of cephalometric analysis publishing a landmark paper introducing the lateral radiographic cephalogram. A system was developed to standardise the position with which the patient was placed, and the distance of the x-ray source and film. Using a piece of lead of known size on one of the supports permitted calibration of the measurements. During an 18 month period, 1700 children between the ages of 6 months and 20 years were x-rayed at 3 or 6 monthly intervals to provide large quantities of normative data.

In the 80 years that have passed since Broadbent first introduced the cephalogram very little has changed; the lateral radiograph is acquired in much the same way albeit now with digital radiography techniques. Digital cephalometry brought many advantages, including the ability to enhance images, manipulate image size and contrast, superimpose images, and archive results.[91-92] Many clinicians, however, still prefer the traditional method of cephalometrics, placing a sheet of acetate over the radiograph, tracing salient features, identifying landmarks, and measuring distances and angles between landmark locations with a ruler and protractor.[93-94] Whilst this technique is time consuming, and prone to error, even computerised methods of cephalometry are based upon these basic methods with manual identification of the cephalometric points. Landmark identification is dependent upon training and experience, with some landmarks being located with more precision than others.[92] The distribution of error for many landmarks is systematic and follows a typical pattern (non-circular envelope), making the landmarks more reliable in either the horizontal or vertical plane depending on the topographic orientation of the anatomical structures along which they are defined.[92] Geelen et al[92] evaluated the reproducibility of cephalometric landmarks. They defined reproducibility as an observer’s deviation (in mm) from the mean between all observers. They found a statistically significant difference for all methods in 11 of 21 landmarks. Baumrind et al investigated the reliability of point identification using 20 randomly selected lateral cephalograms and 16 cephalometric points. They found large differences in reliability of estimation among the landmarks. They concluded that even with the same radiograph, the errors in landmark identification were too great to be ignored, with the magnitude of error varying from landmark to landmark. [95-96]

In 1979, Moyers and Bookstein questioned the appropriateness of modern day cephalometrics.[97] They highlighted the inaccuracy associated with a lateral film which relies upon points and anatomic shadows, indeed with some points being derived rather than being actual physical points on the skull.[97-98] Change on sequential imaging is assessed from a central point of the skull (usually the sella), and all location measures are beset by the measurement error of the standard location and orientation in addition to their own.[97] The assumption is that the fixed point (sella) has not moved between the two time points, yet there is a level of inaccuracy associated with defining the midpoint of the pituitary fossa. Further problems arise as the result of the need to average bilateral structures in 2D analysis, such as the right and left inferior borders of the mandible to create the mandibular plane, resulting in a loss of any asymmetry (such as those associated with craniofacial syndromes) that may exist in the patient.[99-100]

Attempts to increase the accuracy and speed of cephalometric analysis have included digital cephalometric software such as Dolphin. Huja et al[101] compared hand-traced cephalograms with those obtained using Dolphin software. The discrepancy between the two methods was less than 1mm in all cases. Uysal et al[93] evaluated intra-examiner repeatability and inter-examiner reproducibility of landmarks between two manual and computerised analyses, with comparison for speed. Intra-examiner repeatability of landmarks with manual and Dolphin techniques showed high correlation, however, inter-examiner reproducibility was unacceptable for both methods. The tracing time for Dolphin was significantly less than the manual technique (2 minutes 41 seconds versus 6 minutes 51 seconds). Power et al[102] compared the reproducibility and reliability of digitisation using Dolphin. Notable errors were found with the Dolphin software and the authors concluded that the software at that time was not as reliable as traditional techniques. Subsequent papers in 2007 by Sayinsu et al,[103] and in 2009 by Uysal et al[93] demonstrated improved correlation between Dolphin and manual techniques.

Even the earliest investigators were aware of the inaccuracies associated with cephalometry, and the continued reliance of a 2D representation of 3D anatomy, which also fails to appreciate the contribution of the soft tissues, is somewhat surprising.[84,95-96,104]

### *Three Dimensional Cephalometrics*

The shortcomings of 2D analysis resulted in attempts to obtain 3D visualisation and measurements. This included facial surface laser scanning, 3D stereophotogrammetry (3D photography) and 3D video imaging, in recognition that 3D analysis is essential for precisely assessing craniofacial morphology.[82,105] CT and CBCT have been seen as potentially revolutionary for cephalometry however the fundamental difficulty lies in the lack of comparative norms. Databases of normal and treated patient populations for lateral and frontal cephalograms were established prior to the recognition of radiation exposure. Such awareness today would result in an unethical exposure of patients to obtain the required normative data.

In a preliminary study evaluating the potential of CT, Waitzman et al[106] used five dry skulls impregnated with small pieces of metal to standardise measurement points to perform eight measurements on both CT and directly on the skulls. They reported a percentage difference between CT and direct measurement of 0.1 to 3% concluding that craniofacial measurements from CT scans were accurate and reproducible. Similar findings have been reported by a number of authors.[105,107-108] Periago et al[109] investigated the accuracy of 3D images acquired using CBCT reporting a discrepancy between anatomical and CBCT measurements of less than 2mm in all but two (10%) measurements. In their paper, they suggested that the dose associated with CBCT was the same magnitude as that obtained from dental radiographs – however, more recently it has been demonstrated that such assumptions are a gross underestimate. Kumar et al[85] investigated whether CBCT synthesised cephalograms using Dolphin provided the same accuracy as conventional cephalograms. In total, 31 patients treated in the dentofacial deformities program were recruited and underwent CBCT in addition to routine cephalogram. In total, twelve linear and five angular measurements were assessed, and in the majority of cases no statistical difference found between the two modalities.

Cavalcanti et al[110] examined the precision and accuracy of anthropometric measurements using 3D volume rendered CT. Using 13 cadaver heads, they reviewed ten linear measurements based upon eight craniometric anatomical landmarks, which were identified both on the 2D and 3D images,

and subsequently directly measured on the cadavers. The standard error was between 0.45% and 1.44%, with no statistically significant difference between imaging and physical measurements.

Kitaura et al[111] attempted to establish a new 3D cephalometry protocol with helical CT by introducing the matrix transformation of the 3D coordinate system. They used the sella as the reference point, having determined this using the axial and sagittal imaging. Helical CT was performed on 44 patients aged 5 to 26 years. The accuracy for length measurements was less than 3% of standard error of means.

The majority of studies have utilised the lateral cephalogram as the "gold standard" for comparison. With many inherent inaccuracies associated with the cephalogram the results should be interpreted with caution. Whilst considered as the ideal, 3D cephalometry is not as straight forward as 2D analyses and requires the definition of 3D landmarks on complex curving structures.[112] [104]

### *Alternatives to Ionising Radiation*

One attempt to remove ionising radiation exposure in cephalometry was the development of the DigiGraph™ Workstation (Dolphin Imaging Systems). The system utilises direct sonic digitisation of patients to obtain cephalometric landmarks by placing a sonic digitising probe on each facial or intra-oral cephalometric landmark. The spatial location is determined in three dimensions by the systems overhead microphones. However, certain points are determined geometrically and mathematically from other landmarks, with resultant compounded error. Tsang et al[84] compared the validity and reproducibility of the system to conventional cephalometric radiographs on 30 dry human skulls and found significant differences between the two methods for all cephalometric measurements except the gonial angle. The standard deviations (SD) of the differences between measurement values for both methods were large. These findings were similar to those of other authors[113] suggesting that the DigiGraph should be used with caution.

The potential of a 3D MRI method of cephalometry that would permit landmark identification in orthogonal planes and on 3D reconstructed images may potentially revolutionise the management of patients with facial disproportion.

### 2.4.3 Mandibular and Maxillary Squamous Cell Carcinoma

Squamous cell carcinomas (SCC) of the maxilla and mandible are the most common tumours affecting the bone of the craniofacial skeleton. In view of the close proximity of these bony structures to the soft tissues of the oral cavity, tumours arising from the gingivae, floor of mouth, retromolar trigone and maxillary sinus frequently invade the underlying bone *(Figure 13)*.[114-116]

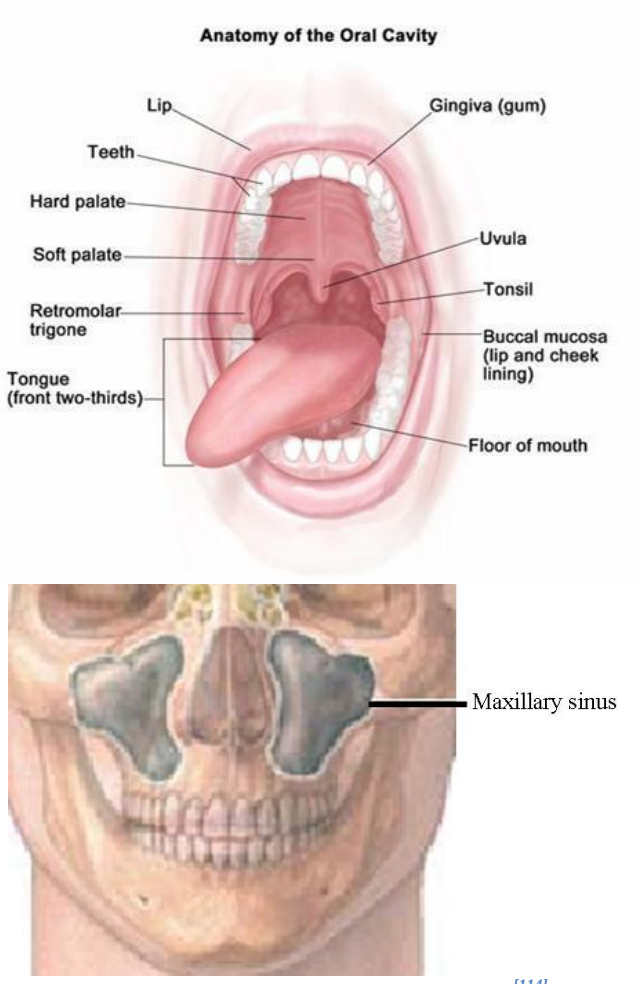



***Figure 13: The oral cavity (top) and maxillary sinus (bottom).[114] The close proximity of bone to the overlying soft tissues tumours frequently results in bone involvement.***

The incidence of head and neck cancer, particularly oral cancer continues to rise and is currently the 15th most common form of cancer in the UK.[117] Head and neck cancer is more common in advanced age, and is strongly associated with alcohol and tobacco use. In approximately 25% of cases the aetiological factor is demonstrated to be the human papillomavirus (HPV), with the most common subtypes being HPV-16 and HPV-18.[118-119]

Oral cavity tumours involving the gingivae, floor of mouth and retromolar trigone most typically present with a non-healing ulcer, tooth mobility, or a mass. With lymphatic drainage to the cervical lymph nodes in the neck, these nodes are a common site for metastases. Tumours affecting the maxillary complex (maxilla, hard palate and paranasal sinuses), are less frequently encountered when compared to other sub sites in the head and neck region and typically present late, resulting in locally advanced disease and metastatic nodal involvement.[120-121]

Pre-operative imaging is performed to assess local, regional and distant spread. The accurate identification of bony invasion is particularly important to determine whether bony resection is required, and provide accurate tumour staging.[122] Multi-modal imaging with CT and MRI in addition to OPG have become standard pre-operative practice in head and neck malignancy. This is particularly useful in examination of the maxilla and paranasal sinuses, which form a complex system of soft tissue, bone and air. The accurate radiological site of the primary lesion may be difficult to find in some patients as they may have superficial disease.[123] Ariyoshi et al[124] reviewed the MRI findings in 14 patients with SCC of the maxillary region, including the maxillary gingiva, alveolar bone and maxillary antrum. T1- and T2-weighted MRI imaging prior- and following gadolinium contrast with simultaneous CT examination were compared to OPG. They found that CT could detect bone destruction not visible on plain radiographs, and MRI could detect bone destruction as equally as conventional radiography.

Clinical tumour staging is completed using the TNM system (Tumour Nodes Metastasis) (clinical stage cTNM), first developed in 1977 by the American Joint Committee on Cancer (AJCC).[125] The TNM criteria for oral cavity and parasinus tumours are included in *Appendix F*.

TNM staging and grading are mostly seen as very important factors in terms of prognosis and have a strong influence on the management decision process; however, the prognostic value has been variably reported.[120-121,125-133] Lenz et al and Boland et al found that clinical T stage (cT) of oral cancer predicted the pathological T stage (pT) less than 47% of the time.[134-135] The TNM system is based almost exclusively on uni-dimensional measurements; tumours greater than 40mm usually invade surrounding structures resulting in their upstaging to T4.[136] The presence of tumour invasion into bone in the third edition of the Staging Manual (1988)[137] classified these tumours into the T4

group, resulting in much debate. Tumours of the hard palate and upper and lower gingivae are so anatomically close to the underlying bone, that tumours at these sites are frequently upstaged. However despite this, the criterion has largely remained, albeit with the more recent caveat that superficial erosion is inadequate to reclassify gingival primaries as T4.[130] This upstaging inevitably results in a paucity of T2 and T3 tumours and many authors have demonstrated that invasion of the mandible does not influence outcome.[115,138]Mucke et al[138] evaluated the prognostic impact of bone invasion in patients undergoing mandibulectomy for SCC. Of the 334 patients treated surgically, 74 patients were upstaged to T4 tumours because of bony invasion, resulting in 223 (67%) being classified as pT4 tumours. The authors found no correlation between survival and tumour location, tumour grade, sex of patient, or bone invasion. A method to enhance the TNM staging criteria for oral tumours and thus removing the reliance on anatomical invasion is desperately needed.

Attempts to provide an alternative classification system include Yokoo et al[139] who presented the maxillary sinus floor (MSF) with the defining boundary between T1-T3 and T4 being the maxillary sinus floor and the nasal floor. Thus, T4 is extensive invasion of the maxillary sinus, nasal cavity or external skin that is revealed by various diagnostic imaging techniques. They found that there was no significant difference in the survival rate under the TNM classification; however, the survival of patients with T4 tumours was significantly lower than that of those with T1 tumours when classified according to MSF. Sasaki et al[140] proposed the sinus and nasal floor (SNF) criteria for tumours arising in the upper alveolus and gingiva and hard palate. Their study group consisted of 53 patients; 41 with carcinoma of the upper alveolus and gingivae and 12 with carcinoma of the hard palate. The majority of tumours were classified as T4 using the TNM criteria, however, the SNF criteria resulted in redistribution with increased numbers in the T2 and T3 categories. Using the SNF criteria, the survival rate decreased with advancing T stage, however no significant difference in survival was seen with the TNM criteria.

Appropriate surgical and adjuvant therapy is largely dependent upon accurate pre-treatment tumour staging. Surgical management primarily involves enbloc resection of the tumour, with or without neck dissection to remove the draining lymph nodes either ipsilaterally or bilaterally *(Figure 14)*. The management of patients without nodal disease in the neck (N0) has been questioned. Le et al[141] explored lymph node metastases in maxillary sinus carcinoma, the overall risk of neck relapse was

12% at 5 years. None of the patients presenting with SCC and N0 necks had nodal recurrence after elective neck dissection. Waldron et al[131] found that the presence of nodal disease in the neck at presentation was an independent predictor of cause-specific survival. It is likely that nodal disease at presentation is a marker of a biologically aggressive and therapy-resistant tumour. Since nodal disease has a powerful impact upon overall survival, it is unsurprising that treatment of the clinically node negative neck has been the subject of some debate. Untreated occult metastases manifest themselves as delayed regional recurrence despite control of the primary.[142] Elective neck dissection reduces the incidence of cervical node recurrence, reduces the need for salvage therapy, and is associated with modest improvement in survival.[132,142-144]

Maxillectomy and subsequent reconstructive options have been classified by Brown et al[145] *(Figure 15)*. The extent of mandibular resection has been debated, but segmental resection is frequently necessitated in tumours arising from the retromolar trigone, gingiva, floor of mouth and mandible.[146-147] Both mandibular and maxillary resection has functional and aesthetic consequences.

Surgical reconstruction aims to restore form and function. This may involve simply a prosthesis in the form of an obturator following maxillary resections, or require free tissue microvascular techniques where extensive resection of bone and/or soft tissue is required. Formal pathological staging (pTNM) of the resected specimen provides information on likely prognosis and guides the decision on adjuvant therapy in the form of chemo-radiotherapy.[148]

The ability to accurately identify bony ingress and stage tumours on MRI may potentially avoid multi-modal imaging and yield further prognostic information in this patient group. In the next section the methods and benefits of 3D rendered images and anatomical models are considered.

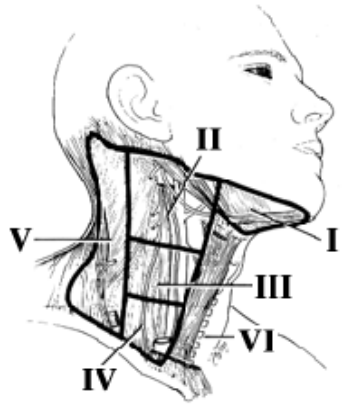



*Figure 15: Cervical lymph node levels. Tumours involving the head and neck tissues drain to these lymph nodes, and surgical resection of the nodes in levels I-III is most frequently completed in head and neck cancers to improve survival rates.*

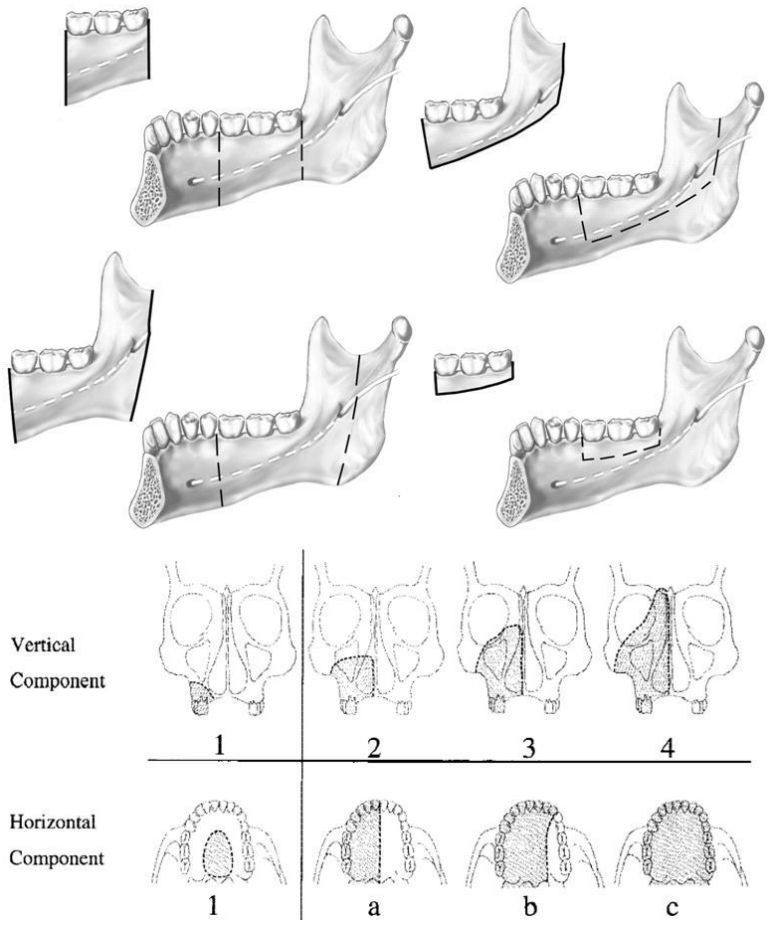



*Figure 14: The surgical principles of mandibular resection (top). Mandibulectomy may be possible without sacrificing the inferior alveolar nerve. The nerve has been highlighted as it travels through the bony canal. Classification of maxillary defects (bottom).[145,148] Resection of tumours involving the maxillary region are classified according to both their vertical extent and palatal resection.*

## 2.5 3D Imaging and Anatomical Models

In all three patient groups, 3D imaging provides the optimal method to visualise pathology and plan surgery, offering significant advantages over axial imaging and plain radiographs.[149]

### *Segmentation*

To create a 3D reconstruction of the dataset, segmentation needs to be completed. **Segmentation** is the process in which contents of the dataset are grouped into various structures present in the image.

The simplest method of image segmentation is thresholding. This is useful when the structure of interest lies within a threshold range which is unique to its surroundings. This can be successfully utilised in CT imaging of the craniofacial skeleton, since bone has unique HU values compared to the soft tissues and air. Other methods of segmentation include edge detection, region growing and model based segmentation techniques.

### *Anatomical Models*

3D CT data has the added advantage of being amenable to conversion to stereolithographic (STL) files to produce anatomical models. **Rapid prototyping** (RP) is a phrase coined in the 1980's to describe new technologies that produced physical models directly from a 3D computer-aided design of an object.[150]

RP technologies produce models using layered methods, in contrast to previous technologies such as milling. Medical modelling has developed enormously in the past 10 years to encompass a range of applications including diagnosis, teaching, surgical planning, and prosthetic design.[150] The utilisation of this technology has been largely within the cranio-maxillofacial and neurosurgical specialities. Erickson et al[151] sought the opinions of surgeons on the use of stereolithographic models in diagnosis, and treatment planning. They found that 65% of respondents reported that a model changed the way in which they approached surgery, and resulted in a significant time saving at surgery. Fruhwald et al[152] examined the accuracy of models from nine children with craniofacial

asymmetry. Stereolithographic models were produced from CT data. Fourteen landmarks were identified with a digitiser on the models, and corresponding measurements made on the planar CT reformats, and 3D reconstruction. There was no significant difference between model and 3D CT. With continuing technological advancements, today many RP machines are capable of producing models at higher resolution than current medical scanners are capable of generating.[150]

The ability to produce such images and models from MRI would be of particular value in the three patient groups on which this thesis focuses. This would enable MRI to fully fulfil all of the pre-operative imaging requirements in cranio-maxillofacial surgery which are currently achieved with CT.

In the next section a comprehensive review of the literature was undertaken to determine what was already achievable with MRI in children with craniosynostosis, adolescents with facial disproportion and adults with malignancy of the craniofacial skeleton. Attention is also given to the ability to create 3D rendered MRI images and anatomical models.

## 2.6 Imaging the Craniofacial Skeleton with MRI

A comprehensive review of the literature was conducted to determine what was already achievable with MRI when imaging the craniofacial skeleton in the three patient groups of interest. This was completed using NCBI Pubmed with the following MeSH terms:

*("MRI" [All fields]) and ("craniofacial abnormalities" or "craniosynostosis" or "synostoses" or "cranial sutures" or "facial asymmetry" or "bone" or "facial bones" or "facial neoplasms" or "malocclusion" or "dentition" or "mandibular advancement" or cephalometry or "models, anatomic" or "imaging, three dimensional" or "skull" or "tumour volume" or "oral cancer" or "mouth neoplasms")*

The titles and abstracts were reviewed to identify those papers with clinical relevance.

### *MRI in Craniosynostosis*

The utilisation of MRI in patients with craniosynostosis has largely been confined to studies exploring co-existing intracranial pathology. Haywood et al[153] highlighted the benefit of MRI in 30 patients with craniosynostosis in their 1992 paper. Of the 30 children, 19 had evidence of hindbrain herniation on MRI and 12 of these had hydrocephalus. No information is provided regarding the MRI sequences performed and the authors do not discuss the appearance of the cranial bone or sutures. Engel et al[154] retrospectively reviewed the pre-operative MRI images of 42 children with sagittal synostosis. T1 and T2-weighted spin echo imaging were available in the axial and sagittal planes. The authors found that MRI confirmed the clinical diagnosis, revealed the typical skull deformities, and identified brain anomalies in a small number of children. However, they did not document the appearance of the cranial sutures on MRI. Fjortoft et al[155] reviewed the potential of MRI in prenatal diagnosis of craniosynostosis in 15 patients. They found that the calvarial sutures could not be visualised directly on MRI, and diagnosis was based mainly on skull deformity.

The only paper located in the literature which specifically aimed to determine the appearance of cranial sutures and craniometric points on MRI was by Cotton et al.[156 157] The authors evaluated the appearance of cranial sutures and craniometric points on MRI in 150 patients aged 20-49 years. The imaging protocol consisted of 5mm sagittal spin echo T1-weighted images, axial transverse

5mm spin echo T2-weighted images and gradient echo T2*-weighted images, and gadolinium enhanced T1-weighted images with a 1mm isotropic voxel size. The authors identified the coronal and lambdoid sutures in all cases, noted as an area of signal void. The sutures were increasingly identified with a slice thickness of 5mm rather than 1mm.

No studies were identified in the literature that have specifically explored the appearance of cranial sutures in infants with normal sutures or craniosynostosis. This may be the result of the increased difficulty of MRI examination in infants compared to CT. In young children, sedation or general anaesthesia (GA) is generally required to obtain good quality MRI images. The magnetic fields create unique problems with the use of physiologic monitors, standard anaesthesia machines and ventilators.[158] Malviya et al[159] retrospectively reviewed all children undergoing sedation or general anaesthesia for MRI/CT scanning. They found a 2.9% incidence of hypoxaemia and a failure rate of 7% in children who received sedation for these procedures. Additionally, the scans were not optimal in 29% of sedated cases. In contrast, the procedure was successful in all children who received GA, with one incident (0.7%) of laryngospasm, despite these children having higher American Society of Anaesthesiologists (ASA)[160] scores.

### *MRI and Cephalometrics*

The majority of work utilising MRI in cephalometry has been in the evaluation of the airway, particularly in obstructive sleep apnoea.[161-163] As previously discussed, Cotton et al[156] reviewed the craniometric points on MRI. Cevidanes et al[164] evaluated the repeatability, measurement error and validity of locating anatomical landmarks on high resolution MRI with 1mm isotropic voxel resolution. In total, ten anatomical landmarks were identified in the coronal, axial and sagittal plane of four head MRI's. Information regarding the sequence used was not included, and to date this work has not been published. The authors concluded that landmark data collected from MRI images was consistent and precise. However in contrast, Plooji et al[82] in their review article concluded that MRI was unsuitable for image fusion for monitoring and follow up in view of the horizontal position of the patient, and long acquisition time with risk of facial movement.

### *Mandibular and Maxillary SCC*

Attempts to image the mandible with MRI have long been investigated. In 1989 Christianson et al[165] published their work correlating the results from MRI, CT and plain x-rays of 18 patients with abnormalities of the mandible. Using a spin echo sequence the authors reported the bone marrow of the mandible as high signal, surrounded by low signal of the cortex. Invasion of the mandible by tumour resulted in replacement of the high signal bone marrow by lower signal tumour. The extent of marrow involvement seen on MRI and confirmed at surgery was significantly underestimated on CT.

Brown et al[147] compared the predictability of OPG, bone scans, CT, MRI and periosteal stripping with direct inspection in predicting both the presence and extent of tumour invasion of the mandible. They included 35 consecutive patients requiring mandibular resection for SCC. Extent of invasion was determined from the pathological specimen. MRI over predicted the width and depth of invasion by 19mm and 10mm with one false positive. Whilst CT over predicted invasion to a lesser extent, there were more false negatives.

Brown and Lewis-Jones[122] in their 2001 review evaluated the evidence for pre-operative imaging of mandibular invasion. They identified 5 papers, all published between 1994-8, evaluating between 11 and 29 patients. The sensitivity of MRI in detecting tumour invasion ranged between 39-100% and the specificity 40-100%. The authors concluded that there was no single investigation that could reliably predict whether tumour has invaded the mandible. However, Bolzoni et al[166] reported the results of 43 patients investigated at their unit with MRI alone. They reported a sensitivity of 93%, and specificity of 93%, in detecting mandibular involvement.

The other main advantage of MRI over CT in head and neck malignancy is the ability to perform tumour volume measurements which may improve the prognostic information of the current TNM system. Whilst MRI and CT imaging are routinely employed to guide management, the data is not incorporated in the resultant TNM stage. Tumour volume (Tv) measurements, as obtained from pre-treatment CT and MRI are increasingly demonstrated to be more reliable predictors of outcome than TNM stage. [135,167]

Tv has been accepted as a sensitive predictor of treatment outcome after radiation therapy in cervical cancer.[168] Similar predictive responses have been seen with Tv measurements of breast tumours in response to neoadjuvant chemotherapy and recurrence-free survival, with initial MRI volume being the strongest predictor of recurrence-free survival.[169] In the head and neck CT tumour volumes have been used as a predictor for laryngeal cancer treated surgically, and in response to radiotherapy for a range of head and neck tumours.[168] Been et al[126] evaluated Tv on CT imaging in 79 patients with primary SCC of the oropharynx. The study failed to demonstrate a significant relationship between Tv and locoregional failure treated with primary radiotherapy. Wang et al[170] retrospectively reviewed Tv measured on CT in 88 patients diagnosed with SCC of the hard palate, of whom 55 underwent primary treatment with surgery. Those with a Tv over 10ml, or ulcerative tumours had poorer outcomes. Studer et al[171] evaluated the effect of Tv on disease outcome in IMRT treated head and neck cancer. They found that gross tumour volume predicted local outcome, nodal and distant outcome and disease free survival.

MRI does not involve ionising radiation and the soft tissue contrast permits accurate Tv measurements and is ideally suited to the long term observation of tumour recurrence.[172-174] Baghi et al[168] evaluated the efficacy of Tv measured on MRI in head and neck cancers treated with chemotherapy. In the 50 patients studied, the pre-treatment Tv was related to remission after treatment in all patients ($p<0.001$). The authors noted that the key limitation of their study was the patient population with different disease stages and sites. Kimura et al[174] studied 66 patients with a range of oral, maxillary sinus and oropharyngeal tumours. They found that the volumes for oropharyngeal cancers were significantly greater for patients with metastatic nodes as compared with those without metastasis. However, no significant correlation was observed for Tv and nodal metastasis for patients with oral or maxillary sinus cancer. This is most likely a result of the small number of tumours located at these sites.

Boland et al[135] reported the benefit of MRI volume measurements in lingual SCC. In a study of 40 patients, significant differences in disease related survival (DRS) and disease free survival (DFS) were found at 2 years with a Tv of $8cm^3$. Similarly, a significant relationship was seen with occult lymph node metastasis with a $3cm^3$ cut-off.

Oral and oropharyngeal anatomy is extremely varied and complex, comprising many different tissues, both hard and soft. It would be optimistic that a simple staging system reliant on a single linear measurement would be sensitive enough to predict disease survival and spread to local lymph nodes with any accuracy. Modification of the TNM system to incorporate Tv analysis appears a useful adjuvant making use of MRI data which is routinely obtained for pre-operative staging of head and neck malignancy. As commented upon by Kimura et al[174] measurement of Tv is a laborious process, with unavoidable intra- and inter-observer errors. However, MR imaging based Tv measurements have been demonstrated to be reliably reproducible.[175]

### *Other Attempts at Bony Imaging with MRI*

With conventional clinical MRI pulse sequences many tissues have such short T2s that they produce little or no detectable signal.[176] The MRI signal from these tissues characteristically decades very rapidly, so that, with the conventional TE used with pulse sequences, little or no signal is detectable. As a result, these tissues appear dark *(Table 2)*.[177] Ultrashort echo time (UTE) pulse sequences use TEs 20-50 times shorter than conventional sequences, which may permit signal from these short T2 components to be detected. Whilst the potential of UTE sequences have been apparent since their introduction in 1991, it is only in the last few years that the majority of papers examining the clinical applications have been published.[176-179] With UTE, cortical bone can be visualised with a high signal in spite of its very short T2 of 0.42-0.50ms. UTE techniques have not yet been utilised to visualise the craniofacial skeleton.

| Tissue or tissue component | Mean T2 |
|---|---|
| **Periosteum** | 5 – 11 ms |
| **Cortical bone** | 7 ms |
| **Dentine** | 0.4 – 0.5 ms |
| **Dental enamel** | 70 µs |

*Table 2: Approximate mean T2 times of some short T2 tissues and tissue components.[177]*

### *Segmentation of the Craniofacial Skeleton*

Although numerous MRI segmentation techniques are described in the literature, there is little research dedicated to the problem of segmenting the skull on MRI as CT has typically been used for this purpose.[180] Attempts to segment the craniofacial skeleton from MRI data have largely been restricted to the skull cap, often as a by-product of attempts to segment the underlying brain. Daliri et al[181] successfully segmented the neonatal skull (gestational age 39 to 42 weeks) on T1 weighted MRI. Wang et al[182] utilised the statistical anatomy extracted from CT data from a group of subjects to construct a shape model of the skull surface. This was successfully utilised to segment the cranial vault on T1 weighted MRI. The images in their paper included the resultant MRI segmentation in the axial plane; however, 3D reconstructed MRI images were not. Other attempts to achieve this have utilised mathematical morphology.[180]

Goto et al successfully segmented the mandible from adult volunteer MRI datasets.[183] They found that the optimal sequence was the 3D vibe sequence (volumetric interpolated breath hold examination); however, MRI segmentation was subjective because it was reliant upon manual techniques.

No studies exploring segmentation of the entire craniofacial skeleton with MRI or their subsequent use to create anatomical models could be located in the literature.

Having reviewed the pathology and routine imaging conducted in the three key patient groups on which this thesis focuses the next chapter marks the commencement of the preliminary exploratory work, focusing on the "Black Bone" MRI sequence.

# 3. Preliminary Work

## 3.0 Preliminary Work

The starting point for the thesis was the "Black Bone" MRI sequence. This gradient echo sequence first evolved when the imaging parameters were entered incorrectly whilst imaging the thigh at OUH *(Figure 16).* Whilst recognised as being an error of future potential benefit, its incorporation into clinical practice was limited. Preliminary investigation of "Black Bone" failed to explore the full potential of the sequence as a non-ionising alternative when imaging the craniofacial skeleton.[3,184] The key benefit of the technique, as seen in *Figure 16*, is the clear soft-tissue – bone boundary. This arises as a result of the exploitation of the susceptibility of bone and minimisation of soft tissue contrast. The bone appears densely black, and the soft tissues are almost uniform in their appearance. As mentioned, the fundamental basis of the sequence is a gradient echo technique. Shown in *Figure 17* is a representation of the gradients, obtained by connecting an oscilloscope to voltage output points on the scanner.

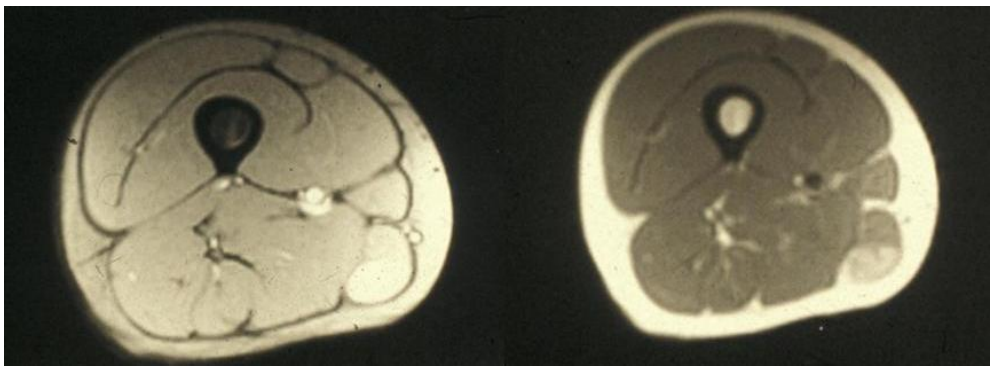


***Figure 16: "Black Bone" image (left), and a more conventional MRI appearance of the thigh.***




***Figure 17: x, y, z and RF gating signal captured on oscilloscope of "Black Bone" sequence.***

## 3.1 "Black Bone" MRI Optimisation & Accuracy

The first step in exploring the "Black Bone" sequence was to fully appraise the technique in terms of biometric accuracy and optimal soft tissue-bone boundary prior to further exploration. This aspect of the thesis is divided into two aspects:

1. Optimisation of the "Black Bone" sequence
2. Confirmation of the biometric accuracy of the technique

## 3.2 "Black Bone" MRI Optimisation

This phase of the study commenced with the "Black Bone" sequence already in limited clinical use. Experimentation with each of the MRI parameters was undertaken to determine if further optimisation was possible in terms of soft tissue signal suppression to enhance the visualisation of bony structures.

### 3.2.1 Materials and Method

The ideal parameters to suppress signal from both fat and water to provide a uniform soft tissue contrast and thereby improving bony definition were investigated with a human volunteer (KE). This was completed at Churchill Hospital (CH), on a 1.5T magnet. Imaging was performed using the neurovascular array head coil with the volunteer positioned supine. Images were acquired in the axial plane using the gradient echo sequence with 3D volume acquisition as per the original "Black Bone" parameters *(Table 3).* Initial investigation focused on the flip angle, which was decreased incrementally from 60 to 1 degree whilst all other scanning parameters remained constant. Sequential adjustment was subsequently made to the TE, TR, bandwidth, and slice thickness. The images were reviewed by three assessors in an unblinded fashion on an Advantage Windows workstation (AWW) to determine which parameters provided the optimal result in terms of soft tissue signal suppression and clear bone boundary. In an attempt to quantitatively assess the optimal result investigation was completed in three ways; firstly, using Osirix (an open source DICOM viewer for Apple Mac) a region of interest (ROI) was defined and saved for application to each dataset in turn *(Figure 18)*. The mean and variance for the pixels within the ROI was recorded. This was completed for a number of corresponding areas on each dataset. It would be

anticipated that an optimal bone appearance in terms of being densely black, would be represented by a low mean pixel value, and uniform soft tissue contrast demonstrated mathematically with a low variance. Secondly, the mean and variance of pixel values within a number of ROI were determined using an AWW. Experimentation was conducted with a further software package (Adobe Photoshop) to obtain mean and variance results, utilising the DICOM import functionality. However, there was no method to enable standardisation of the ROI; with high levels of selection error this method was limited. Finally, using Mimics (a medical imaging processing software) a graph was obtained for the pixel values across a soft-tissue – bone – soft-tissue path *(Figure 19)*. The results were standardised using the orthogonal line in Mimics to ensure that the same region on each dataset was sampled. A rapid change in pixel value on either side of the bone would be anticipated to signify a clear bone boundary.

| Parameter | Value |
|---|---|
| **TR** | 8.6 ms |
| **TE** | 4.2 ms |
| **Slice thickness** | 2.4 mm |
| **Slice Spacing** | 1.2 mm |
| **Scan FOV** | 240 mm |
| **Phase Encode** | 256 |
| **Frequency Encode** | 256 |
| **Receive Bandwidth** | 31.25 |
| **ZIP** | 2, 512 |

*Table 3: "Black Bone" MRI Scanning parameters.*

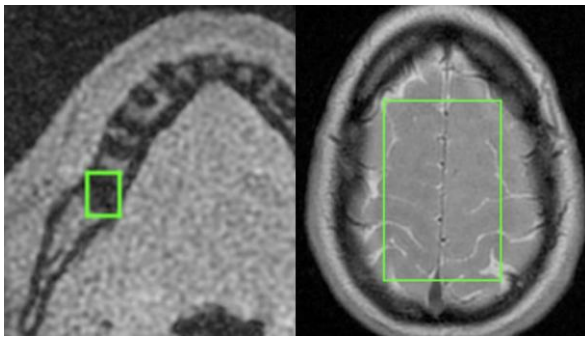


*Figure 18: Selection of ROI in mandible and brain used to determine mean and variance of containing pixel values.*

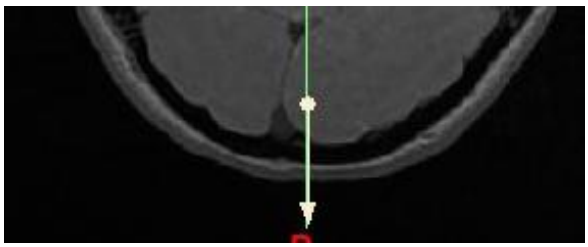


*Figure 19: Axial "Black Bone" image demonstrating the path of transection (white arrow) for measuring pixel values of the tissues from brain, to bone to soft tissue.*

### 3.2.2 Results

The effect of varying the flip angle on the "Black Bone" sequence is shown in *Figure 20*. With increasing flip angles, as anticipated, the signal from the soft tissues increased, and with a flip angle of 1° the image quality was significantly degraded. Degradation of the image quality occurred to a less significant effect with a flip angle of 3°. There was minimal change seen when varying the flip angle between 5° and 7°.

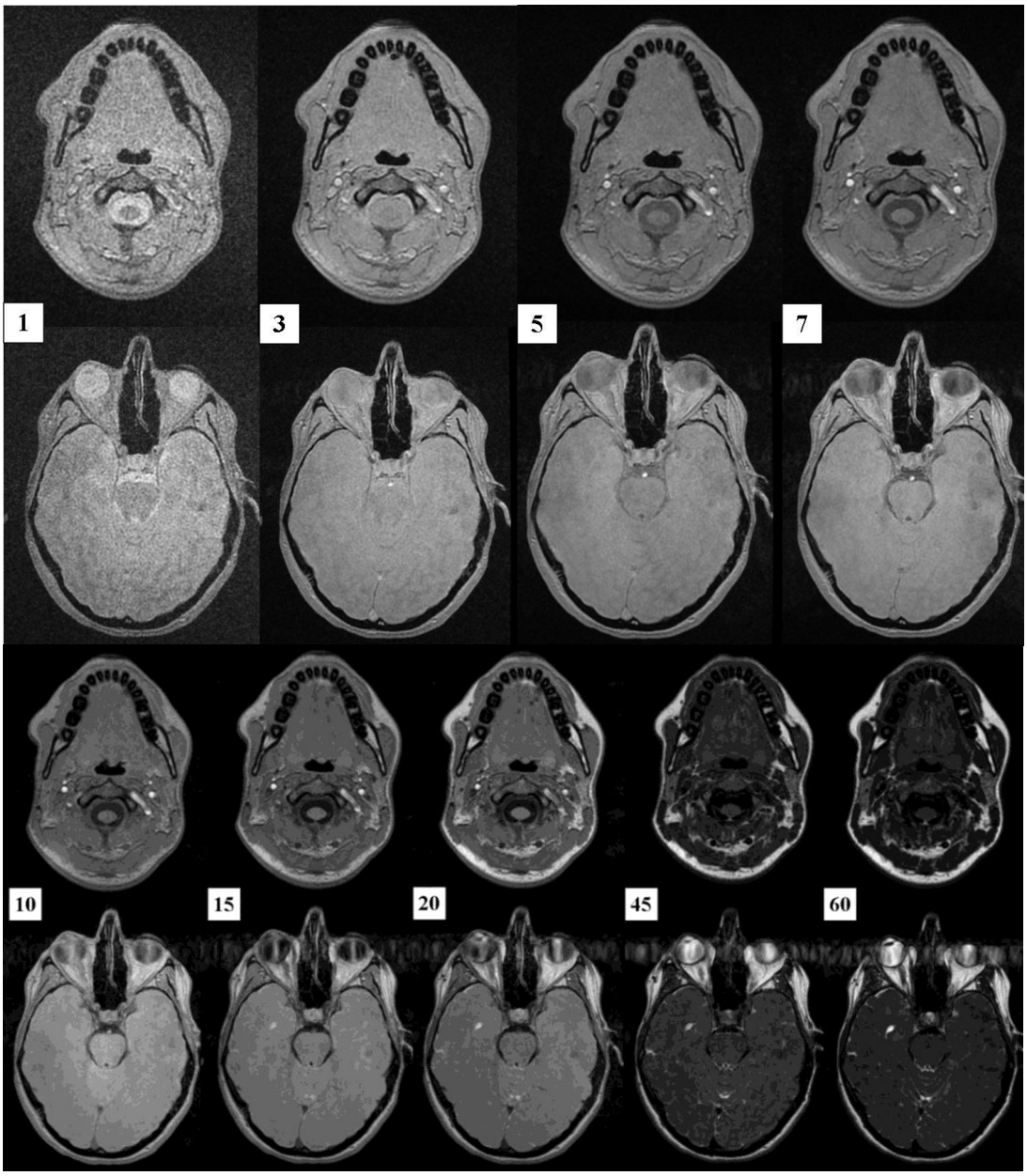



***Figure 20: The effect of varying the flip angle on the "Black Bone" MRI sequence. With increasing flip angles, the signal from the soft tissues increased making the bone-soft-tissue boundaries less well defined. Degredation of the image occurred with a flip angle below 3°. Miminal change was noted between flip angles of 5° and 7°***

On review of the imaging, all three assessors selected the dataset corresponding to a flip angle of 5° as representing the most optimal appearance. Sequential adjustment of the TE, TR, bandwidth and slice thickness identified that the sequence parameters could not be further optimised.

### *Quantifying an Optimal Result*

The mean and variance results for the ROIs tested with Osirix are shown in *Appendix A*. For the ROIs centred on the soft tissues a smaller variance was obtained with decreasing flip angles. For bone, a lower mean pixel value was seen with lower flip angles. Similar results were found with measurements on AWW *(Appendix A).* The results using Adobe Photoshop are shown in *Appendix A*. It must be noted that with an inability to control the FOV across all datasets these results contain an element of inaccuracy. The graphs in *Figure 21* demonstrate the change in pixel values as the transecting line passes from soft tissue through bone and into soft tissue using Mimics. The most rapid change in pixel values either side of bone was seen when the flip angle was 5, correlating with a distinct soft-tissue – bone boundary.

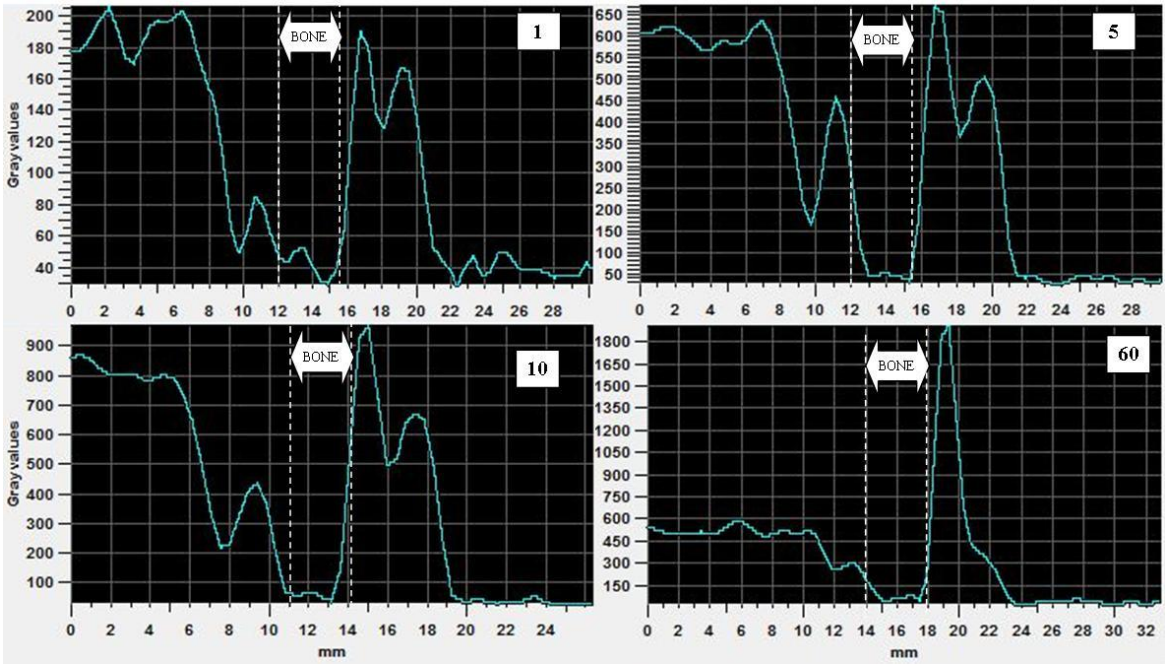



*Figure 21: Graphs of pixel values on traversing from soft tissue to bone to soft tissue for "Black Bone" with a flip angle of 1, 5, 10 and 60°. The most rapid change in pixel value either side of the bone occurs with a flip angle of 5°.*

### 3.2.3 Discussion

Starting with the original “Black Bone” sequence, investigation was undertaken into the effects of the various sequence parameters in an attempt to determine if the sequence could be further optimised. On visual inspection the optimal flip angle was confirmed as 5° providing the least soft tissue contrast, and clearest bone-soft tissue boundary. However, this could not be demonstrated mathematically to be the most optimal result. The main problem in attempting to calculate mean and variance results for the pixel values on each image, was the inability to calibrate the results, thus accurate comparison between datasets could not be guaranteed. On the graphs produced in Mimics it was apparent that a flip angle of 5° provided the most rapid change in pixel values when passing from bone to soft tissue and vice versa. This pattern suggested a distinct bony boundary. Adjustment of the remaining parameters failed to improve the “Black Bone” image quality, and therefore the original parameters were maintained.

Having optimised the “Black Bone” sequence the next step was to confirm that this was biometrically accurate.

## 3.3 Biometric Accuracy

Accurate measurements of anatomy or anomalies are frequently required in all aspects of radiological imaging. Having optimised the imaging parameters for the "Black Bone" sequence the next step was confirm that the sequence was biometrically accurate.

### 3.3.1 Materials and Methods

The biometric accuracy of the "Black Bone" sequence was investigated with a custom made phantom. This consisted of a disarticulated skull confined within a water-tight Perspex anthromorphic shell filled with copper sulphate solution (concentration =10mMolar). The phantom provided the opportunity for direct anatomical measurements in addition to "Black Bone" imaging free of movement artefact. The "Black Bone" sequence was compared to the current gold standard imaging technique for the craniofacial skeleton, CT. Measurements were made between anatomical points that were directly visible on the phantom and imaging datasets *(Table 4, Figure 22).* These included the distance between paired foramina, and maximum heights and widths of bony structures. To minimise discrepancy due to drying of the skull (noted to be up to 2mm), the skull was kept in the copper sulphate solution until the time measurements were made. Using vernier callipers (resolution 0.01mm; accuracy: <100mm ±0.02mm; 100-200mm ±0.03mm) each measurement was made twenty times on two separate occasions.

#### *"Black Bone" MRI*

The phantom was supported to maintain it in the supine position consistent with standard positioning for head/brain examinations. Using the pre-determined "Black Bone" sequence images were acquired in the axial, sagittal and coronal planes. Using an AWW the images were reviewed to determine the image on which the anatomical points were most clearly identifiable, and the image number recorded to permit correlation with subsequent measurement attempts. Each measurement was made using the integral cursor function, and each repeated twenty times on two separate occasions. To minimise any potential bias distance results were removed from the image prior to attempting the next series of measurements.

### *CT*

Comparable CT images of the phantom were obtained with a slice thickness of 0.625mm on a 64 slice spiral CT scanner with the phantom positioned in the same manner as for MRI. Axial images were acquired with no gantry tilt and reconstructed in the sagittal and coronal planes. The images were reviewed on an AWW and the measurements repeated twenty times on two separate occasions.

Mann Whitney U Test and Kruskal-Wallis tests were performed using SPSS with the null hypothesis that there was no significant difference between the groups ($p<0.05$).

| Anatomical Measurement | Imaging Plane |
|---|---|
| 1. Maximum cranial-caudal aperture of the right orbit | Sagittal |
| 2. Maximum cranial-caudal aperture of the left orbit | Sagittal |
| 3. Maximum height of the mandible from chin point in the midline | Sagittal |
| 4. Maximum coronal dimension of the skull at the disarticulation point | Coronal |
| 5. Maximum coronal dimension of the skull cap at the disarticulation point | Coronal |
| 6. Distance between the lateral most aspect of the paired infraorbital foramen | Coronal |
| 7. Maximum cranial-caudal aperture of the piriform aperture | Coronal |
| 8. Maximum coronal aperture of the piriform aperture | Coronal |
| 9. Distance between the lateral most aspect of the paired mental foramen | Cor & Ax |
| 10. Distance between the lateral most aspect of the paired mandibular condyles | Axial |
| 11. Maximum dimension of posterior hard palate between most posterior identifiable molar teeth | Axial |
| 12. Maximum distance between lateral surfaces of the paired posterior upper molar teeth | Axial |

*Table 4: Anatomical measurements completed on phantom, CT and MRI.*

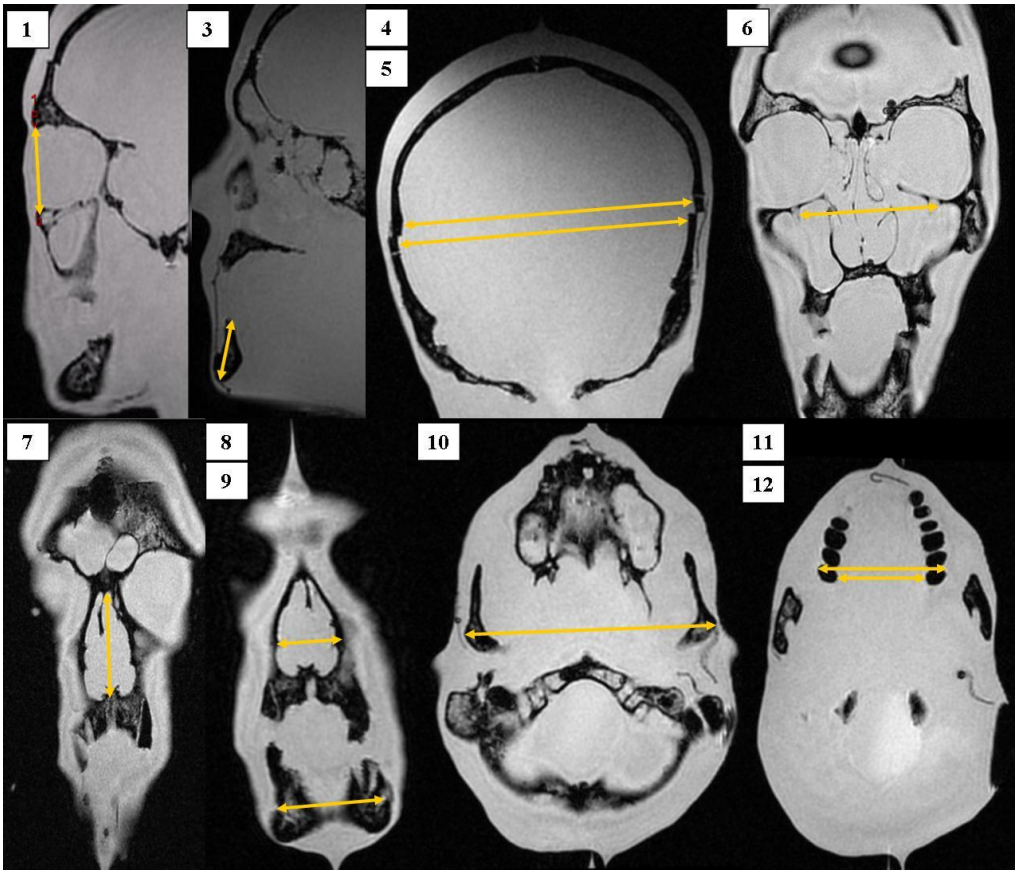



*Figure 22: Measurements completed on "Black Bone" images of the skull phantom; Numbers correspond to Table 4.*

### 3.3.2 Results

The individual measurements obtained directly on the phantom, CT and "Black Bone" are included in *Appendix B*. For the repeated measurements, intra-observer concordance was high, with no statistical significance ($p>0.05$) between the two groups of results for CT, MRI or direct measurements. The repeated measurements were therefore combined and analysed collectively for each modality.

Using the direct anatomical measurements as the reference group, no statistical difference was found for three of the twelve distances on "Black Bone," and two of the twelve distances on CT *(Table 5)*. Whilst statistically different, the difference between the measurements for each group was less than 1mm for all measurements *(Table 6)*. The average discrepancy between "Black Bone" and anatomical mean values for each group was 0.32mm (0.76%), and for CT 0.40mm (0.76%). The mean difference between "Black Bone" and CT was 0.38mm.

| | Anatomical v MRI | Anatomical v CT | CT v MRI |
|---|---|---|---|
| **1. Right Orbit** | <0.05 | <0.05 | <0.05 |
| **2. Left Orbit** | ***0.11*** | ***0.48*** | ***0.22*** |
| **3. Mandible Height** | <0.05 | <0.05 | ***0.42*** |
| **4. Coronal Skull Base** | <0.05 | <0.05 | ***0.11*** |
| **5. Coronal Skull Cap** | <0.05 | <0.05 | <0.05 |
| **6. Infraorbital Foramina** | <0.05 | <0.05 | <0.05 |
| **7. Piriform fossa height** | <0.05 | ***0.27*** | <0.05 |
| **8. Piriform fossa width** | <0.05 | <0.05 | <0.05 |
| **9. Mental Foramina** | <0.05 | <0.05 | <0.05 |
| **10. Intercondylar Distance** | <0.05 | <0.05 | <0.05 |
| **11. Maxilla with teeth** | ***0.50*** | ***0.48*** | ***0.22*** |
| **12. Maxilla without teeth** | ***0.28*** | <0.05 | <0.05 |

*Table 5: Mann-Whitney U Test results for anatomical, CT and "Black Bone" measurements on skull phantom. Results where there was no significant difference are shown in bold.*

| | | Mean (mm) | SE | Percentage difference compared to anatomical (%) |
|---|---|---|---|---|
| **1. Right Orbit** | Anatomical | 32.74 | 0.038 | |
| | MRI | 32.97 | 0.044 | 0.70 |
| | CT | 32.49 | 0.058 | 0.76 |
| **2. Left Orbit** | Anatomical | 32.89 | 0.020 | |
| | MRI | 32.87 | 0.031 | 0.06 |
| | CT | 32.80 | 0.051 | 0.27 |
| **3. Mandible Height** | Anatomical | 27.69 | 0.040 | |
| | MRI | 27.99 | 0.053 | 1.08 |
| | CT | 27.93 | 0.054 | 0.87 |
| **4. Coronal Skull Base** | Anatomical | 139.48 | 0.040 | |
| | MRI | 139.95 | 0.034 | 0.33 |
| | CT | 140.04 | 0.055 | 0.40 |
| **5. Coronal Skull Cap** | Anatomical | 140.62 | 0.045 | |
| | MRI | 140.28 | 0.042 | 0.24 |
| | CT | 140.08 | 0.041 | 0.38 |
| **6. Infraorbital Foramina** | Anatomical | 55.81 | 0.008 | |
| | MRI | 56.19 | 0.042 | 0.68 |
| | CT | 56.83 | 0.534 | 1.82 |
| **7. Piriform aperture height** | Anatomical | 32.35 | 0.024 | |
| | MRI | 32.39 | 0.038 | 0.12 |
| | CT | 32.96 | 0.042 | 1.89 |
| **8. Piriform aperture width** | Anatomical | 21.54 | 0.041 | |
| | MRI | 22.25 | 0.038 | 3.30 |
| | CT | 21.75 | 0.039 | 0.97 |
| **9. Mental Foramina** | Anatomical | 44.47 | 0.042 | |
| | MRI | 43.61 | 0.032 | 1.93 |
| | CT | 44.78 | 0.050 | 0.70 |
| **10. Condylar Distance** | Anatomical | 110.13 | 0.073 | |
| | MRI | 110.40 | 0.086 | 0.25 |
| | CT | 110.93 | 0.037 | 0.73 |
| **11. Maxilla with teeth** | Anatomical | 58.11 | 0.061 | |
| | MRI | 58.07 | 0.050 | 0.07 |
| | CT | 58.24 | 0.073 | 0.22 |
| **12. Maxilla without teeth** | Anatomical | 40.54 | 0.025 | |
| | MRI | 40.70 | 0.051 | 0.39 |
| | CT | 40.57 | 0.033 | 0.07 |

*Table 6: Mean and Standard Error results for distances measured on phantom.*

### 3.3.3 Discussion

The "Black Bone" sequence has been demonstrated to be reliable, with good correlation to measurements obtained both from CT and direct anatomical dimensions. Whilst a statistically significant difference was identified between the direct anatomical measurements and those on the "Black Bone" and CT sequences, these differences correlated to a discrepancy of less than 0.5 mm in all cases. This corresponds to an average error of 0.76% (range 0.06 – 3.30%), similar to results obtained in other studies on accuracy in CT analysis.[106,110,185] Errors are likely to have been compounded by the difficulties in obtaining perfectly correlated measurements on direct anatomical, CT and MRI imaging. The greatest discrepancies were seen for distances between transected foramina resulting from the oblique path of the canal on imaging, and for the piriform fossa as a result of sectioning at differing points through the steep nasal bones.

## Chapter Conclusion

The "Black Bone" MRI sequence has been optimised, and confirmed as biometrically accurate, demonstrated by comparison with direct measurements on a phantom skull, and on imaging with CT.

Having demonstrated the accuracy of the technique, exploration progressed to the potential of "Black Bone" in imaging the craniofacial skeleton.

# 4. Children

## 4.0 Children

This section of the thesis explores the appearance of normal cranial sutures on routine MRI sequences and on “Black Bone” MRI. Attention is subsequently turned to the potential of “Black Bone” in the diagnosis of craniosynostosis.

The cranial sutures on which this work focuses are the metopic, coronal, sagittal and lambdoid sutures *(Figure 23).*

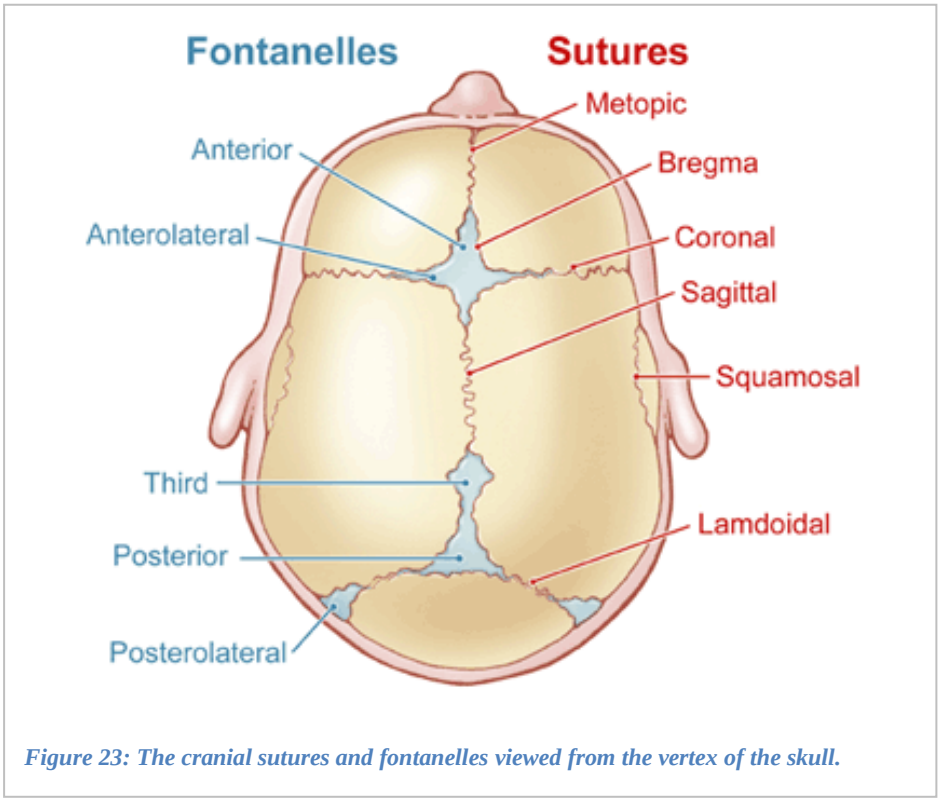



***Figure 23: The cranial sutures and fontanelles viewed from the vertex of the skull.***

## 4.1 Cranial Sutures on Routine MRI

To determine the potential of routine MRI sequences as an alternative to CT, in the identification of cranial sutures, in infants, four phases were completed:

1. An unblinded preliminary study of the cranial sutures in infants
2. Blinded independent review of the cranial sutures on routine MRI sequences in infants
3. Measurement of cranial suture width on routine MRI

This section of the thesis is subdivided into these three phases.

### 4.1.1 Unblinded Cranial Suture Review

This unblinded review of MRI scans formed the preliminary study prior to blinding of images and independent review. This provided preliminary data on the most frequently requested MRI sequences in infants, their availability and the appearance of the sutures.

#### 4.1.1.1 Materials and Method

To identify infants with available MRI examinations of the head the hospital Picture Archiving and Communications (PACS) service (Centricity©) was utilised. The PACs system contains no inherent search facility, and infants under 12 months of age were identified by sequential date review, named consultant paediatrician, and "MRI" in the identification parameters. The radiology reports were reviewed to exclude any infant that had undergone surgery to the skull, had a known syndrome or any condition likely to impact upon cranial suture identification. In total, 121 patients with available MRI sequences were available for review. These were distributed across eight sequences: Axial EPI, Axial STIR, Axial T1, Axial T2, Axial T2*, Sagittal T1, Sagittal T2, and Coronal FLAIR. Not all patients had all of the sequences available for review. The indication for imaging and diagnosis for the patients reviewed are shown in *Table 7*. For each patient, the MRI sequences that were available were recorded, to permit generation of a list of available sequences. If a child had undergone multiple MRI examinations prior to the age of 1 year, inclusion was limited to one of each of the relevant sequences. In each case, age at the time of imaging was recorded. Each imaging data set was reviewed independently using a scoring system to assess each of the cranial sutures including the ease of identification and the suture appearance *(Table 8).*

| Clinical Indication | Frequency |
|---|---|
| Seizures/Spasms/Abnormal Tone | 45 |
| Trauma | 8 |
| Ear or eye abnormalities | 10 |
| Developmental delay or abnormal features | 19 |
| Prematurity | 5 |
| Infection | 4 |
| Respiratory problems | 9 |
| Other | 21 |
| **Radiological Diagnosis** | |
| Normal | 65 |
| Bleed/Ischaemia | 36 |
| Structural anomaly | 20 |
| **MRI Sequence Available** | |
| Axial EPI | 32 |
| Axial STIR | 52 |
| Axial T2* | 83 |
| Axial T2 | 77 |
| Axial T1 | 41 |
| Sagittal T1 | 64 |
| Sagittal T2 | 54 |
| Coronal FLAIR | 119 |

*Table 7: Clinical indication for imaging and radiological diagnosis for 121 patients reviewed and sequences available.*

| | Score | Description |
|---|---|---|
| **Suture Identification** | **N** | Not Possible due to poor image quality e.g. movement artefact |
| | **0** | Unable to identify suture |
| | **1** | Suture identifiable for part of the course |
| | **2** | Suture clearly identifiable throughout course |
| **Suture Appearance** | **B** | Black void |
| | **W** | White/Contrast |
| | **O** | Other (Specify) |

*Table 8: Scoring system for review of cranial sutures on routine MRI sequences.*

To minimise potential bias, the MRI datasets were reviewed in groups of sequence type, so that suture identification on one sequence did not influence its identification on another, in the same patient. All imaging was reviewed on an AWW; magnification and window levels were adjusted, where appropriate, to optimise the image. The coronal, sagittal, lambdoid and metopic sutures were assessed independently.

#### 4.1.1.2 Results

In total, 121 infants under 12 months of age with MRI scans available were identified on PACS. Of these, 67 were male and 54 female, with a mean age at the time of imaging of 131 days (4 months) (0 – 361 days). Each patient had a mean of 3 sequences available (1 – 6 sequences). A number of datasets were not of sufficient quality for review of the cranial sutures, mainly because of significant movement artefact, and were excluded. The sequences included for review are shown in *Table 9*, and the results corresponding to the data collection sheet (including those which were excluded) are shown in *Table 10*.

| Sequence | Number of patients |
|---|---|
| **Coronal FLAIR** | 72 |
| **Sagittal T1** | 56 |
| **Sagittal T2** | 43 |
| **Axial STIR** | 28 |
| **Axial T1** | 38 |
| **Axial T2** | 59 |
| **Axial T2*** | 52 |

***Table 9: Number of patients with each sequence available for review, following exclusion of those which were of non-diagnostic quality as a result of insufficient field of view and significant movement artefact.***

On the axial EPI datasets, the cranial bone and sutures were not identifiable as a result of high signal from the brain. This sequence was therefore excluded from subsequent analysis.

For the remaining sequences, at least one set of cranial sutures were identifiable on at least one MRI sequence in 69% of the infants (n=83). Only 2 infants had all cranial sutures identifiable on at least one MRI sequence reviewed.

| | Coronal | | | | Sagittal | | | | Lambdoids | | | | Metopic | | | |
|---|---|---|---|---|---|---|---|---|---|---|---|---|---|---|---|---|
| App ID | U | B | W | O | U | B | W | O | U | B | W | O | U | B | W | O |
| **Coronal FLAIR** | | | | | | | | | | | | | | | | |
| **N** | 47 | | | | 47 | | | | 47 | | | | 47 | | | |
| **0** | 70 | | | | 70 | | | | 57 | | | | 72 | | | |
| **1** | | 2 | | | | | | | | 15 | | | | | | |
| **2** | | | | | | 2 | | | | | | | | | | |
| **Sagittal T1** | | | | | | | | | | | | | | | | |
| **N** | 8 | | | | 8 | | | | 8 | | | | 8 | | | |
| **0** | 52 | | | | 56 | | | | 55 | | | | 56 | | | |
| **1** | | 3 | | | | | | | | 1 | | | | | | |
| **2** | | 1 | | | | | | | | | | | | | | |
| **Sagittal T2** | | | | | | | | | | | | | | | | |
| **N** | 11 | | | | 11 | | | | 11 | | | | 11 | | | |
| **0** | 36 | | | | 43 | | | | 34 | | | | 43 | | | |
| **1** | | 7 | | | | | | | | 9 | | | | | | |
| **2** | | | | | | | | | | | | | | | | |
| **Axial STIR** | | | | | | | | | | | | | | | | |
| **N** | 24 | | | | 24 | | | | 24 | | | | 24 | | | |
| **0** | 8 | | | | 23 | | | | 19 | | | | 22 | | | |
| **1** | | 19 | 1 | | | 4 | 1 | | | 8 | 1 | | | 6 | | |
| **2** | | | | | | | | | | | | | | | | |
| **Axial T1** | | | | | | | | | | | | | | | | |
| **N** | 3 | | | | 3 | | | | 3 | | | | 3 | | | |
| **0** | 38 | | | | 38 | | | | 38 | | | | 38 | | | |
| **1** | | | | | | | | | | | | | | | | |
| **2** | | | | | | | | | | | | | | | | |
| **Axial T2** | | | | | | | | | | | | | | | | |
| **N** | 18 | | | | 18 | | | | 18 | | | | 18 | | | |
| **0** | 22 | | | | 47 | | | | 22 | | | | 59 | | | |
| **1** | | 35 | | | | 12 | | | | 29 | 6 | 2 | | | | |
| **2** | | 2 | | | | | | | | | | | | | | |
| **Sagittal T2*** | | | | | | | | | | | | | | | | |
| **N** | 30 | | | | 30 | | | | 30 | | | | 30 | | | |
| **0** | 46 | | | | 50 | | | | 32 | | | | 51 | | | |
| **1** | | 1 | 4 | | | | 1 | | | 4 | 15 | | | | | |
| **2** | | | | | | | | | | | | | | | | |
| **Axial EPI** | | | | | | | | | | | | | | | | |
| **N** | | | | | | | | | | | | | | | | |
| **0** | 32 | | | | 32 | | | | 32 | | | | 32 | | | |
| **1** | | | | | | | | | | | | | | | | |
| **2** | | | | | | | | | | | | | | | | |

*Table 10: Frequency of cranial suture identification and appearance for each MRI sequence; (App=appearance; ID=identification; Appearance classification: B=Black void, W=White/contrast, O=Other; Identification classification: 0=Unable to identify suture, 1=Suture identifiable for part of its course, 2=Suture clearly identifiable throughout its course).*

To determine if age was a potential contributing factor in cranial suture identification, analysis was completed in a binary fashion inclusive across all of the available sequences for each patient *(Table 11)*. The distribution was not normal, and non-parametric analysis (Mann Whitney U-Test) identified a significant difference (p=0.007) for age between the two groups (suture identified or not-identified). The cranial sutures were more likely to be identified in patients who were older, with the difference in mean age being 56 days (1.9 months).

Subsequent analysis was performed per sequence. The distribution for cranial suture appearance on each imaging sequence reviewed is shown in *Table 12.*

Axial T2 images appeared to be the optimal sequence studied, identifying at least one cranial suture in 88% of cases.

| | Any cranial suture identified for patient? | |
|---|---|---|
| | **No** | **Yes** |
| **Mean** | 93 | 149 |
| **95% CI for mean** | 54 - 133 | 123-174 |
| **Median** | 32 | 146 |
| **Minimum** | 0 | 0 |
| **Maximum** | 353 | 361 |
| **SD** | 120 | 118 |

***Table 11: Comparison of patient age for those in whom any cranial suture was identified, with those with no visible cranial sutures. Age is in days.***

| Sequence | Number of patients | Any suture identified | Coronal | Sagittal | Lambdoid | Metopic |
|---|---|---|---|---|---|---|
| **Coronal FLAIR** | 72 | 17 (24%) | 2 (12%) | 2 (12%) | 15 (88%) | 0 |
| **Sagittal T1** | 56 | 5 (9%) | 5 (100%) | 0 | 1 (20%) | 0 |
| **Sagittal T2** | 43 | 12 (28%) | 7 (58%) | 0 | 9 (75%) | 0 |
| **Axial STIR** | 28 | 20 (71%) | 20 (100%) | 5 (25%) | 9 (45%) | 6 (30%) |
| **Axial T1** | 38 | 0 | 0 | 0 | 0 | 0 |
| **Axial T2** | 59 | 52 (88%) | 37 (71%) | 12 (23%) | 37 (71%) | 0 |
| **Axial T2*** | 52 | 19 (37%) | 5 (26%) | 1 (5%) | 19 (100%) | 0 |

***Table 12: Identification of cranial sutures on each MRI sequence.***

*Figure 24* displays graphically those cases where at least one cranial suture was identifiable on the sequence, demonstrating that the coronal and lambdoid sutures were the most frequently identified sutures, with axial STIR being the only useful sequence in visualisation of the metopic suture.

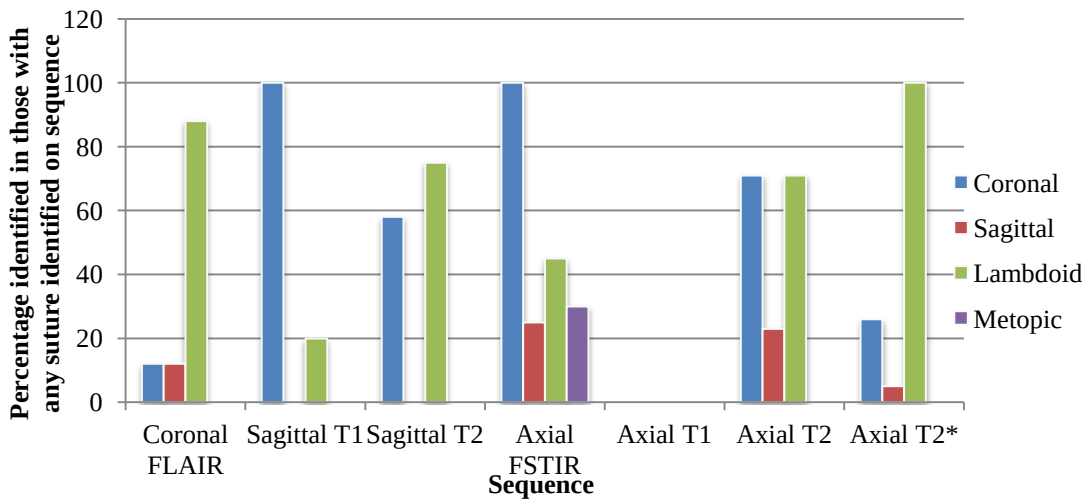



*Figure 24: Bar chart of percentage of each suture identified, only on imaging where at least one suture was visualised.*

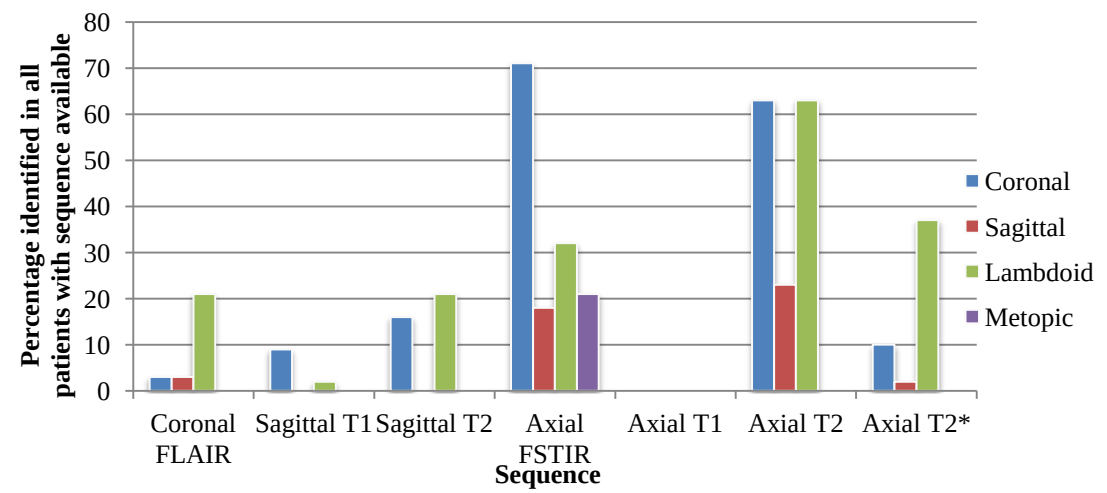



*Figure 25: Percentage of each suture identified for each MRI sequence across all available datasets.*

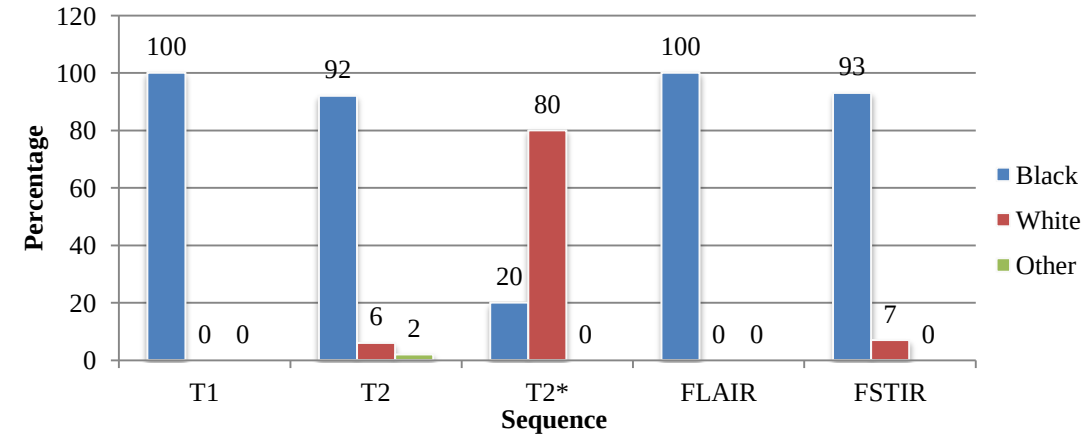



*Figure 26: Bar chart of the appearance of the cranial sutures as either areas of signal void (appearing black), increased signal (appearing white) or an alternative appearance. For most sequences reviewed the cranial sutures appeared as areas of signal void.*

Analysis per patient for each sequence revealed that the coronal suture was optimally identified on axial STIR followed by axial T2 weighted images *(Figure 25).* The axial T2 sequence was also optimal for the lambdoid suture, although only seen in 63% of patients. The metopic and sagittal sutures were least frequently identified, with their optimal sequence being axial STIR and axial T2 respectively.

In the majority of cases, the cranial sutures appeared as areas of signal void (black) *(Figure 26).* However, on T2* sequences, the suture appeared with increased signal compared to the surrounding bone. In a number of cases, it was noted that whilst the suture appeared as a signal void, the surrounding bone appeared to have increased signal.

#### 4.1.1.3 Discussion

The axial T2 and STIR sequences were most optimal at identifying the cranial sutures of the datasets reviewed. The coronal and lambdoid sutures were the sutures most frequently identified.

Two factors influenced suture identification – the MRI sequence, and slice orientation. It has previously been stated that the optimal orientation for suture visualisation is perpendicular to its path. Therefore, the coronal suture would best be seen on sagittal slices at the crown, and axial images inferiorly. The sagittal suture should be optimally visualised on coronal slices, lambdoids on axials, and metopic on axials.

Axial imaging transects both the lambdoid and coronal sutures perpendicular to their path at some point, enhancing visualisation. Whilst the metopic suture was also transected at 90 degrees in the axial plane, it was only seen in 21% of axial STIR images. This may relate to the age of the patients studied and timing of metopic suture closure. Surprisingly, the sagittal suture was rarely identified. The difficulty in this area relates to the path of the sagittal sinus making distinction potentially difficult. In those cases where the cranial sutures were visualised, very few could be identified throughout the entire length of their course. This would make the reviewed sequences unreliable in the accurate distinction of normal and prematurely fused cranial sutures.

However, prior to concluding this, these preliminary findings required further investigation in the form of anonymised independent assessment by experts in the field.

### 4.1.2 Blinded Cranial Suture Review

This fully anonymised blinded review of the cranial sutures on MRI by experts in the field provided the opportunity to fully assess the potential of routinely used MRI sequences when visualising the cranial sutures.

#### 4.1.2.1 Materials and Method

Again utilising the hospital PACs system, infants under the age of 12 months were identified by sequential date review and "MRI" in the identification parameters over the preceding 5 years (2006-2011), without limitation to referring clinician. To minimise any potential bias patients whose imaging had been included in the unblinded review were excluded. For each patient identified on PACS, their radiological imaging folders and reports were reviewed and any patient with evidence of a condition likely to impact upon the cranial sutures was excluded. The MRI sequences that had been completed for each infant were documented, and five routinely used sequences were selected for inclusion in the study: axial T1, axial T2, coronal FLAIR, axial STIR, and sagittal T1. The sequences were reviewed to ensure they were free of significant movement artefact. The imaging parameters are shown in *Table 13*. In total, 53 infants of which 25 were female and 28 male, each provided 1-3 of the required sequences, resulting in 100 data sets (twenty each of the 5 selected sequences). All MRI examinations had been completed on a GE or Philips 1.5 Tesla MRI scanner, with slice thickness set to 3, 3.5, 4 or 5mm.

| Sequence | TR | TE | ET | Matrix |
|---|---|---|---|---|
| **Axial STIR** | 5660 | 29 | 12 | 512 x 512 |
| **Axial T2** | 5400 | 100 | 11 | 288 x 288 |
| **Axial T1** | 625 | 16 | 1 | 240 x 240 |
| **Coronal FLAIR** | 11000 | 140 | 53 | 288 x 288 |
| **Sagittal T1** | 677 | 16 | 1 | 288 x 288 |

***Table 13: MRI imaging parameters for the datasets included for review.***

Age was calculated from the scan date minus date of birth, both in terms of number of days and number of months. The mean age of those included in the study was 142 days (1 - 361). Age was subsequently stratified into five groups: <1 month, 1-3 months, 3-6 months, 6-9 months, and 9-12 months.

The image datasets were fully anonymised using Clear Canvas (Clear Canvas Inc, Toronto, Canada), and assigned a number in random order from 1 to 100.

The images were reviewed by 5 assessors and scored with regard to cranial suture identification. A score of 0 was assigned where the suture could not be identified, 1 where it was partially identifiable and 2 where it was clearly identifiable and the assessor confident of its presence. Scores were independently assigned for the coronal, sagittal and lambdoid sutures. The assessors included three certified and experienced head and neck and/or neuroradiologists, a head and neck surgeon, and myself. To minimise potential bias from the anonymising process a period of three months prior to review was awaited. Review of the imaging took place independently with assessors free to manipulate the image on screen as required to optimise interpretation.

Statistical analysis was performed on SPSS. Descriptive analysis was first performed with histograms, boxplots and scatterplots to view the distribution of assessor score and cranial suture identification with patient age. Inter-rater agreement was calculated using Randolph's free marginal kappa.[186] A Kruskal Wallis test was used to determine statistical correlation of assessor score and patient age.

#### 4.1.2.2 Results

The mean age of those included in the study was 142 days (1 - 361). Of the 100 image sets reviewed, at least one pair of cranial sutures was identified by at least one assessor in 69 cases. The coronal sutures were most frequently identified. Overall inter-rater agreement was moderate, with a Kappa score of 0.6. The radiologists identified a greater frequency of sutures; however, the highest agreement was between the two non-radiologists (Kappa 0.9).

Of the sutures, there was greatest concordance between raters for the sagittal suture, although this was the suture identified least frequently. Confidence at suture identification was low, with scores of 2 being assigned in only 9 cases (coronal n=2; sagittal n=1; lambdoid n=6), with agreement between at least two raters, in only one case. No scores of 2 were assigned by the non-radiologists.

All further statistical correlations were performed using binary categories of suture identified or not (0 or 1), with a maximum total score of 15 for the 5 assessors and 3 sutures in each case *(Table 14).* A Kruskal Wallis test identified an increasing total score with increasing patient age ($p<0.05$).

| Age (months) | Cranial suture identification | |
|---|---|---|
| | n | Mean Score |
| <0 | 37 | 1.9±2.5 |
| 1-3 | 15 | 3.2±3.7 |
| 3-6 | 4 | 7.8±5.3 |
| 6-9 | 22 | 3.7±3.4 |
| 9-12 | 22 | 4.0±4.1 |

***Table 14: Stratified results by age group, demonstrating number of data sets per group, age, identification score (based upon binary score of 0 or 1 for suture identification, with maximum total score of 15 – 5 assessors, 3 sutures).***

The slice thickness for the reviewed scans ranged between 3 to 5mm (3mm n=1, 3.5mm n=1, 4mm n=79, 5mm n=19). The mean total cranial suture score was 3.0 for a slice thickness of 4mm sequences, and 4.6 for a slice thickness of 5mm.

Overall, axial T2 images were most optimal for viewing the cranial sutures of the sequences studied consistently obtaining the highest reviewer scores *(Figure 27).* The appearance of the cranial sutures on axial T2 images was of an area of signal void *(Figure 28).* This was consistent in all cases where the suture was identifiable. Review of those patients with more than one imaging sequence available demonstrated that failure to identify the cranial sutures on one sequence did not preclude identification on another. Whilst the cranial sutures could often be followed throughout all or part of their course, on close inspection their true limits were frequently difficult to determine.

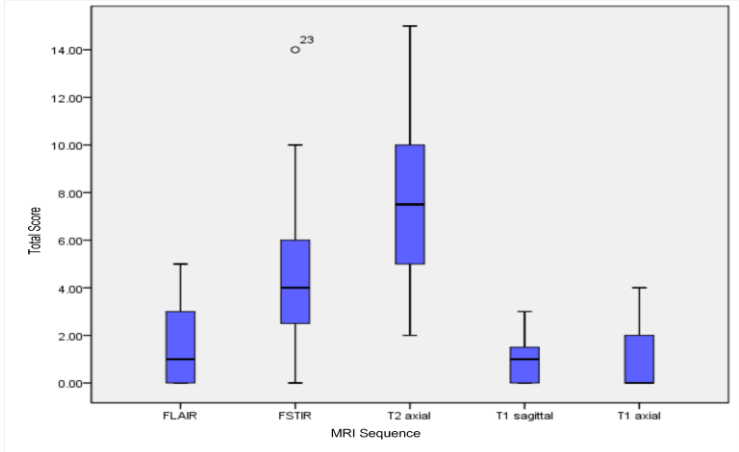



***Figure 27: Box plot of combined assessor score for cranial suture identification for each imaging sequence reviewed.***

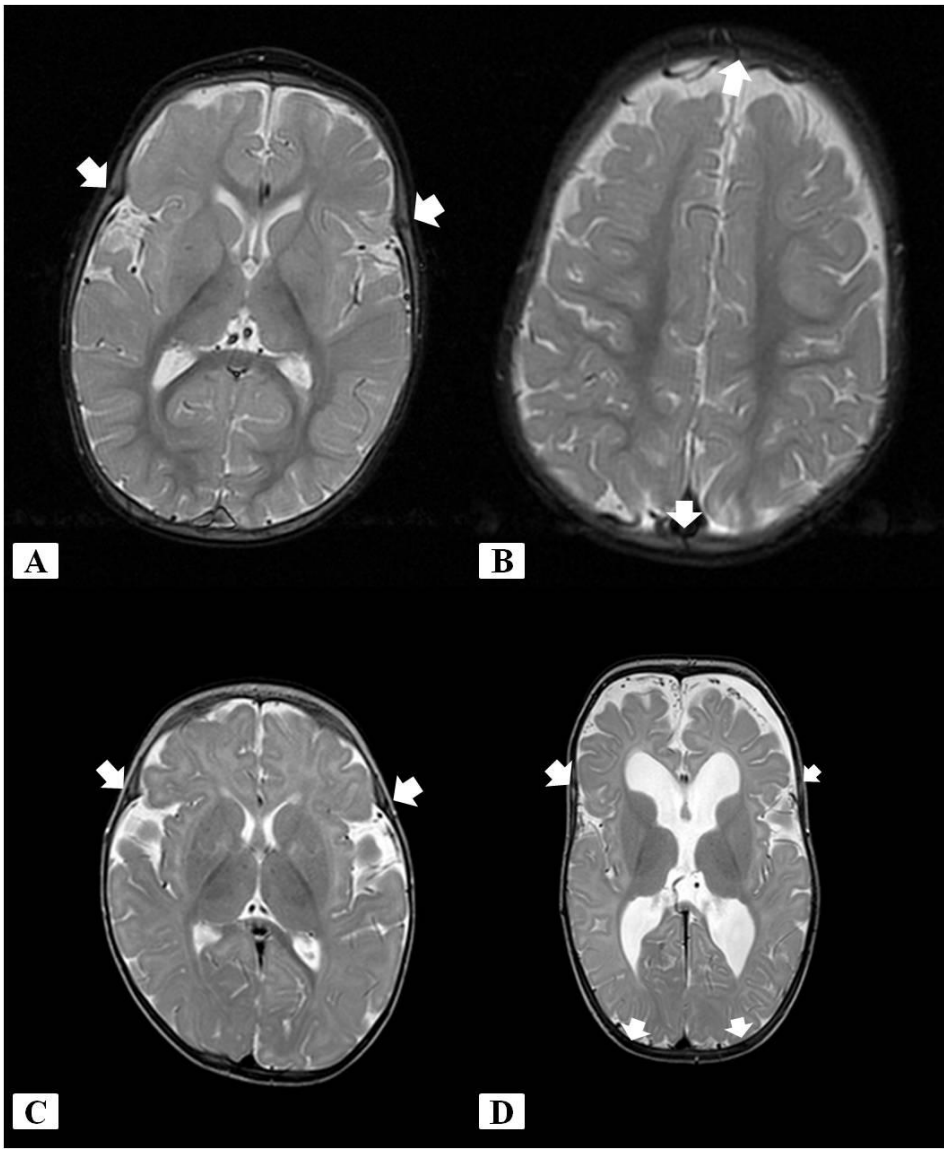



*Figure 28: Appearance of cranial sutures on (a & b) axial STIR demonstrating coronal and sagittal sutures, and axial T2 (c & d) demonstrating coronal and lambdoid sutures.*

#### 4.1.2.3 Discussion

Overall, the cranial sutures were infrequently identified and inter-rater agreement lower than anticipated. The radiologists identified more cranial sutures, and were more likely to score 2 indicating their increased confidence. In some cases, the presence of cranial moulding may have resulted in a higher identification rate of the sutures; however this was an inevitable consequence of the dependent head shape in the young infants reviewed.

As expected, the cranial sutures were increasingly identified with advancing age. The increasing cranial thickness with advancing age provides improved contrast between the suture and bone aiding suture identification. It was assumed that significant prematurity would have been documented on the radiology report; since medical records were not reviewed it was not possible to perform accurate age correction. The inability to correct for those cases of unidentified prematurity may have further contributed to the significant finding of increased cranial suture identification with advancing age.

One of the key challenges in identifying cranial sutures on MRI was the confident interpretation of an area of signal void, when there were many other structures, such as blood vessels, within a small area all giving rise to a similar appearance. Whilst all of the readers were familiar with MRI interpretation, MRI is rarely used to review bone and its intervening sutures, and clinical familiarity with these appearances is required.

Cranial MRI is relatively infrequently requested in the age group studied; being utilised in cases of structural anomaly, trauma, and intracranial pathology, which in many cases precluded them from the study. In many cases imaging was acquired without GA resulting in a number of sequences being unsuitable due to movement artefact.

Whilst the cranial sutures could be identified on routine MRI imaging, the inconsistency would make the five sequences studied unreliable in the radiological diagnosis of craniosynostosis; however, MRI may yield useful data on sutural widths, and this is explored in the next section.

## 4.2 Cranial Sutures on MRI: Suture width

In assessment of the cranial sutures, the variation in width from normal may provide useful information regarding abnormal potential. Normative values have been obtained on both CT and ultrasound.[74-75,187] The purpose of this aspect of the study was to determine the cranial width measurements of the cranial sutures on MRI and to compare these to the normative values available in the literature.

### 4.2.1 Materials and Methods

Utilising the imaging and results from Section 4.1 the MRI data sets where at least two reviewers had identified the cranial sutures were used to obtain measurements of the cranial suture widths. The images were viewed on an AWW. Only those images where the cranial suture (sagittal, coronals or lambdoids) were visible on two consecutive image slices were used for analysis. For each suture the same region was utilised for width assessment, aided by standard acquisition protocols. For the coronal sutures the region approximately 1cm above the most superior aspect of the orbits was selected. The region of the suture was magnified to maximum so that the suture edges could be clearly identified. Measurements were made perpendicular to the direction of the suture at its cross-sectional centre using the integrated callipers on the workstation *(Figure 29).* Each measurement was repeated three times for both left and right (or anterior and posterior for the sagittal) sutures on two consecutive image slices.

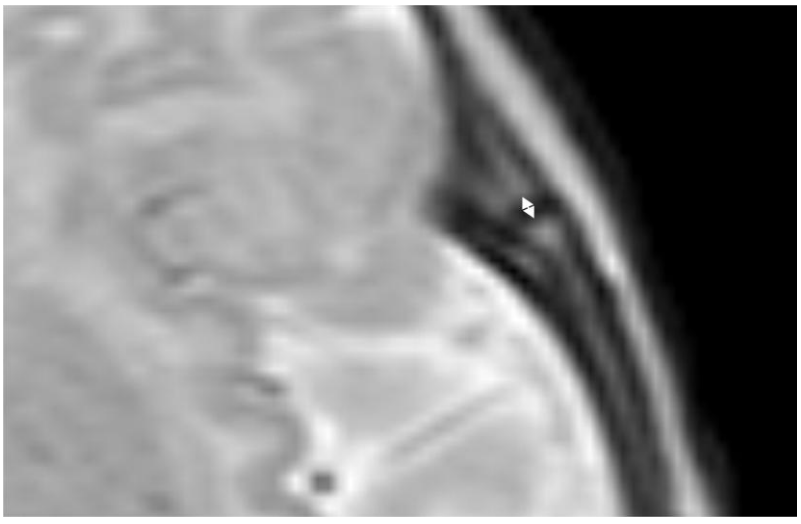


***Figure 29: Cranial suture width measurements were made by magnifying the image and measuring perpendicular to the path of the suture.***

Analysis was performed for results obtained for the two consecutive image slices, and a mean result ultimately calculated for each suture. A paired t-test was used to determine significant differences between left and right (or anterior and posterior) cranial sutures. A Kruskal Wallis test was used to determine significance of stratified age upon cranial suture width. The significance level for all comparisons was set to 0.05.

### 4.2.2 Results

Of the 100 scans available, 38 (29 patients) were suitable for cranial suture width measurement. This included 26 for the coronal sutures, 6 for the sagittal sutures, and 6 for the lambdoids. The mean age at the time of these images was 200 days (3 – 361 days). Of the 38 scans, 13 were STIR, 22 axial T2, and 3 coronal FLAIR sequences. The cranial suture width measurements are shown in *Table 15*. There was no significant difference between right or left (anterior or posterior) cranial sutures, nor suture width with age (p=0.141; Kruskall Wallis) *(Table 16).*

| | Coronals | | Sagittal | | Lambdoids | |
|---|---|---|---|---|---|---|
| | Mean (mm) | Range (mm) | Mean (mm) | Range (mm) | Mean (mm) | Range (mm) |
| **Right / Anterior** | 1.2 ± 0.4 | 0.6-2.6 | 1.4 ± 2.0 | 0.3-0.9 | 1.4 ± 0.6 | 0.9-2.7 |
| **Left / Posterior** | 1.2 ± 0.5 | 0.5-3.3 | 1.4 ± 2.8 | 0.6-0.9 | 1.3 ± 0.2 | 0.8-1.7 |
| **Combined** | 1.2 ± 0.4 | 0.5-3.3 | 1.4 ± 0.4 | 0.3-0.9 | 1.3 ± 0.3 | 0.8-2.7 |

*Table 15: Cranial suture widths (results are displayed as mean±SD).*

| Age (months) | Cranial suture width | | | | | |
|---|---|---|---|---|---|---|
| | Coronal | | Sagittal | | Lambdoid | |
| | n | Width (mm) | n | Width (mm) | n | Width (mm) |
| **<0** | 5 | 1.2±0.6 | 0 | - | 0 | - |
| **1-3** | 6 | 1.0±0.3 | 0 | - | 0 | - |
| **3-6** | 2 | 1.0±0.1 | 1 | 1.1 | 1 | 1.1 |
| **6-9** | 6 | 1.4±0.4 | 2 | 1.1±0.0 | 1 | 1.6 |
| **9-12** | 7 | 1.3±0.3 | 3 | 1.4±0.1 | 4 | 1.4±0.4 |

*Table 16: Cranial suture widths stratified for age.*

### 4.2.3 Discussion

Of those sequences included in the first aspect of the study, only a small percentage (38%) was suitable for cranial suture width measurements. Whilst a greater proportion of these were of a slice thickness of 5mm, the difference between 4 and 5 mm slice thickness is unlikely to be significant. There were no scans with a slice thickness less than 4mm suitable for width analysis; however, there were only 2 datasets in this group.

The mean suture width was 1.2±0.4mm, 1.4±0.4mm, and 1.3±0.3mm for the coronal, sagittal and lambdoid sutures respectively. Whilst measurements were only obtained for two consecutive images slices for each of the data sets, there were no significant discrepancies between imaging slices; the inability to clearly visualise the suture throughout its course restricted the number of available images on which measurements could be made.

The greatest challenge in utilising these sequences for sutural width measurement was the infrequency with which the sutures could clearly be identified. The next phase of the thesis focuses upon whether “Black Bone” MRI provides a reliable solution to these problems.

## 4.3 Cranial Sutures & "Black Bone" MRI

To determine the benefit of "Black Bone" MRI in the identification of the cranial sutures, and distinction between the normal suture and craniosynostosis, three phases were completed:

1. Animal work to optimise the sequence, and further experimentation with alternative MRI sequences
2. Completion of "Black Bone" MRI in children undergoing MRI of the head in whom the cranial sutures would be anticipated to be normal
3. "Black Bone" imaging in infants with craniosynostosis

This section of the thesis is subdivided into these three phases.

### 4.3.1 Animal Work

To eliminate movement artefact whilst undertaking multiple sequences and to enable dissection of the sutures to confirm patency, an animal model was required. Determining an appropriate animal model for any experimental manipulation is fundamental to successful experimental design.[188] The most frequently used animal models for craniofacial research include mice, sheep and pigs. Piglets were deemed most appropriate in view of their availability and size.

#### 4.3.1.1 Materials and Methods

Five piglets, which were runt of the litter, and therefore had died shortly after birth were obtained from the University Farm (Gloucester Old Spot and Tamworth breeds). MRI imaging was completed on a 1.5T magnet at the CH. The piglet was placed supine and imaged using a General Purpose (GP) Flex Coil. Sequential imaging was completed, to determine the optimal parameters of the "Black Bone" sequence in terms of cranial suture identification, with variation of one parameter (TE, TR, Flip angle, and 3D volume or 2D slice acquisition).

"Black Bone" was compared to other available MRI sequences, including fast spin echo (FSE) with T1, T2 and PD weighting, Gradient Recalled Acquisition in Steady State (GRASS), Fast Imaging Employing Steady State Acquisition (FIESTA), FLAIR, and STIR. Where possible CT imaging was obtained to permit comparison of MRI with the current "gold standard." Images were reviewed by one assessor (KE) on an AWW, with regard to the coronal, sagittal, lambdoid and snout sutures

and mandibular symphysis *(Figure 30).* Once imaging had been completed, the piglet was dissected to confirm patency of the cranial sutures and to permit direct comparison to the imaging findings.

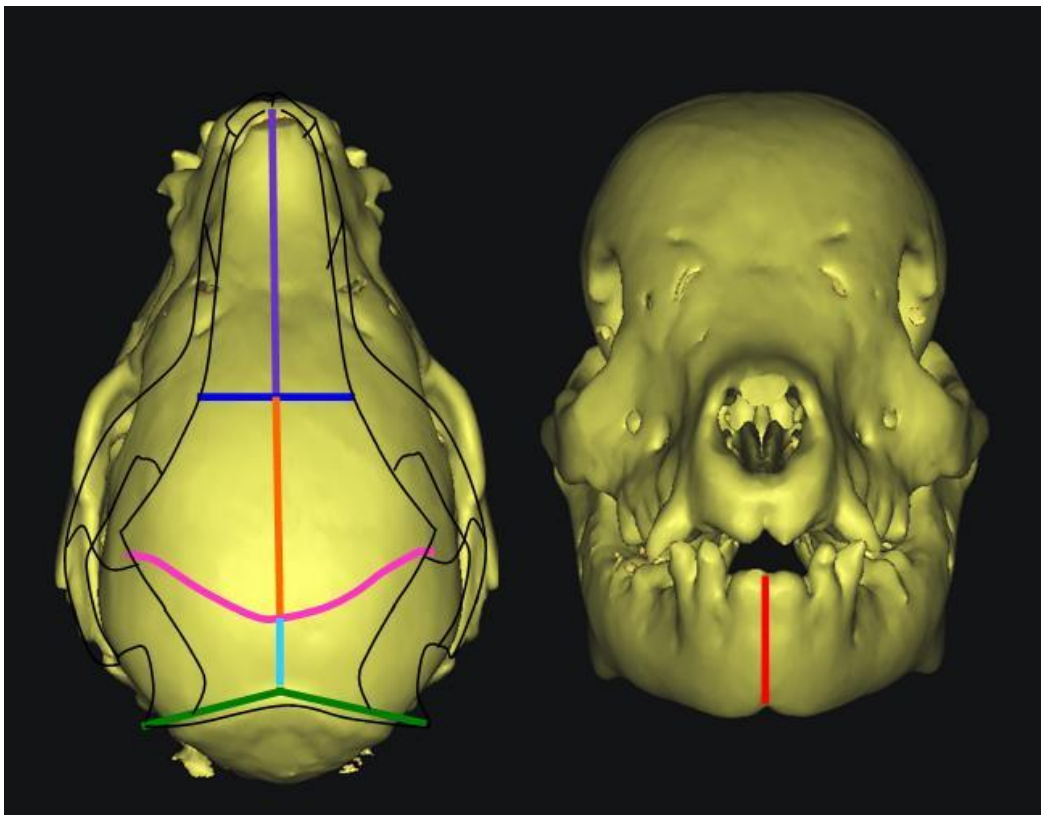


***Figure 30: Location of cranial sutures on piglet; internasal suture (purple), nasofrontal suture (blue), interfrontal or sagittal suture (orange), coronal suture (pink), interparietal suture (cyan), lambdoid sutures (green), mandibular symphysis (red).***

#### 4.3.1.2 Results

The most reliable breed of piglet in terms of suture patency was the Tamworth pig. Identification of the cranial sutures on "Black Bone" was superior to the sequences reviewed in Sections 4.1 and 4.2. The appearance of the mandibular symphysis and lambdoid sutures, with variation in the flip angle of the "Black Bone" sequence, are shown in *Figure 31.* As the flip angle was increased, the signal from the soft tissues increased making suture identification increasingly challenging. A flip angle of $<10^{\circ}$ permitted identification of the lambdoid sutures in addition to the mandibular symphysis.

Adjustment of the receive bandwidth had negligible effect on the appearance of the sutures on the "Black Bone" sequence *(Figure 32).* Minimal effects were also seen with further reduction of the TE and TR. Acquisition as a 3D volume (as per the "Black Bone" sequence) associated with a small slice thickness and FOV enhanced identification of the sutures, and this was further optimised when imaging was available in multiple planes. This was achievable post-processing with the "Black Bone" sequence, however, some loss of quality was noted compared to images that were acquired in that plane *(Figure 33).*

As previously noted, the majority of routinely used sequences were unhelpful in the identification of the cranial sutures. However, it was found that the cranial sutures could be distinguished on the FIESTA sequence *(Figure 34).* In comparison to "Black Bone," FIESTA results in a greater soft-tissue signal, making the distinction of cranial bone and soft tissue more challenging. Overall, the appearance of the sutures at the skull vertex was superior on "Black Bone" compared to FIESTA.

The cranial sutures were confirmed to be patent on CT imaging and on anatomical dissection, consistent with the areas identified on MRI *(Figure 35-37).*

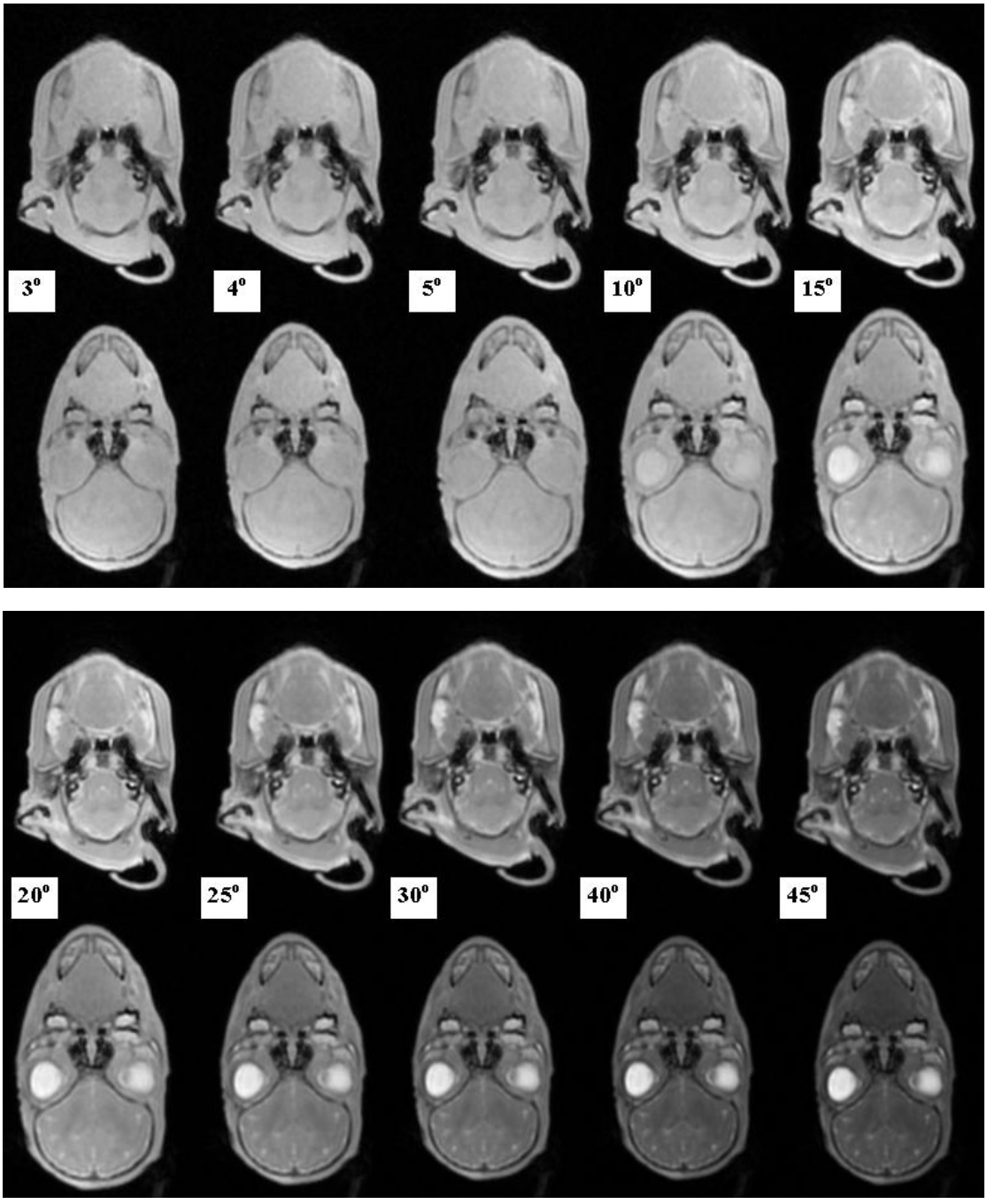



*Figure 31: Effect on suture identification with variation in flip angle on comparable imaging slices.*

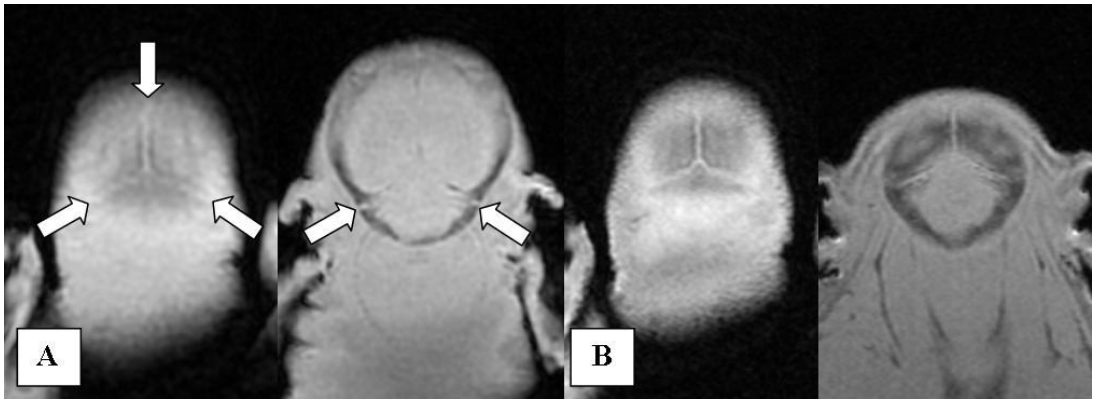



*Figure 33: Effect on "Black Bone" sequence (A) of decreasing the receive bandwidth (B).*

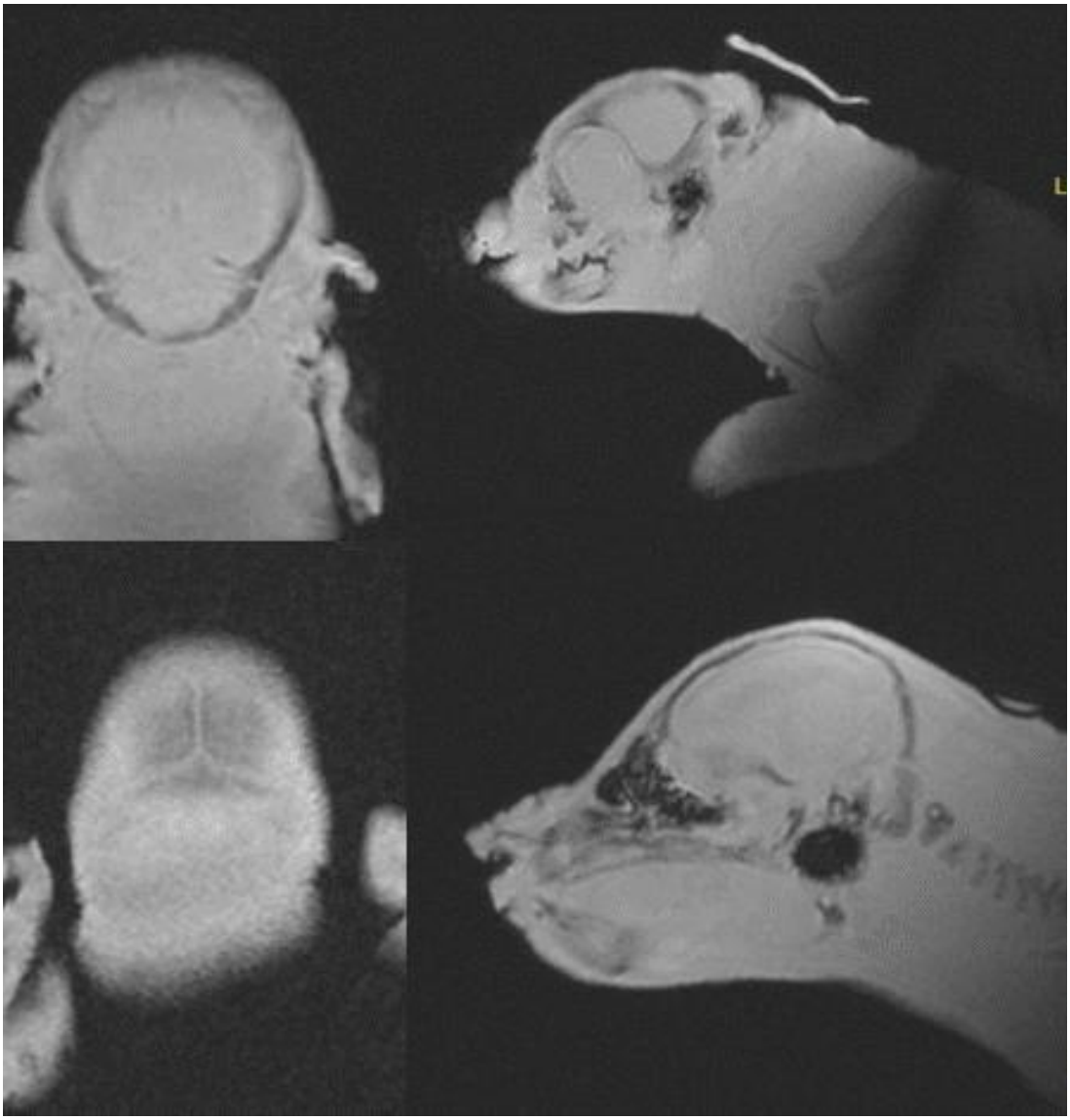


*Figure 32: The identification of the cranial sutures was aided by having imaging in multiple planes. Also note on the sagittal views that the epiphyses of the femur can be visualised.*

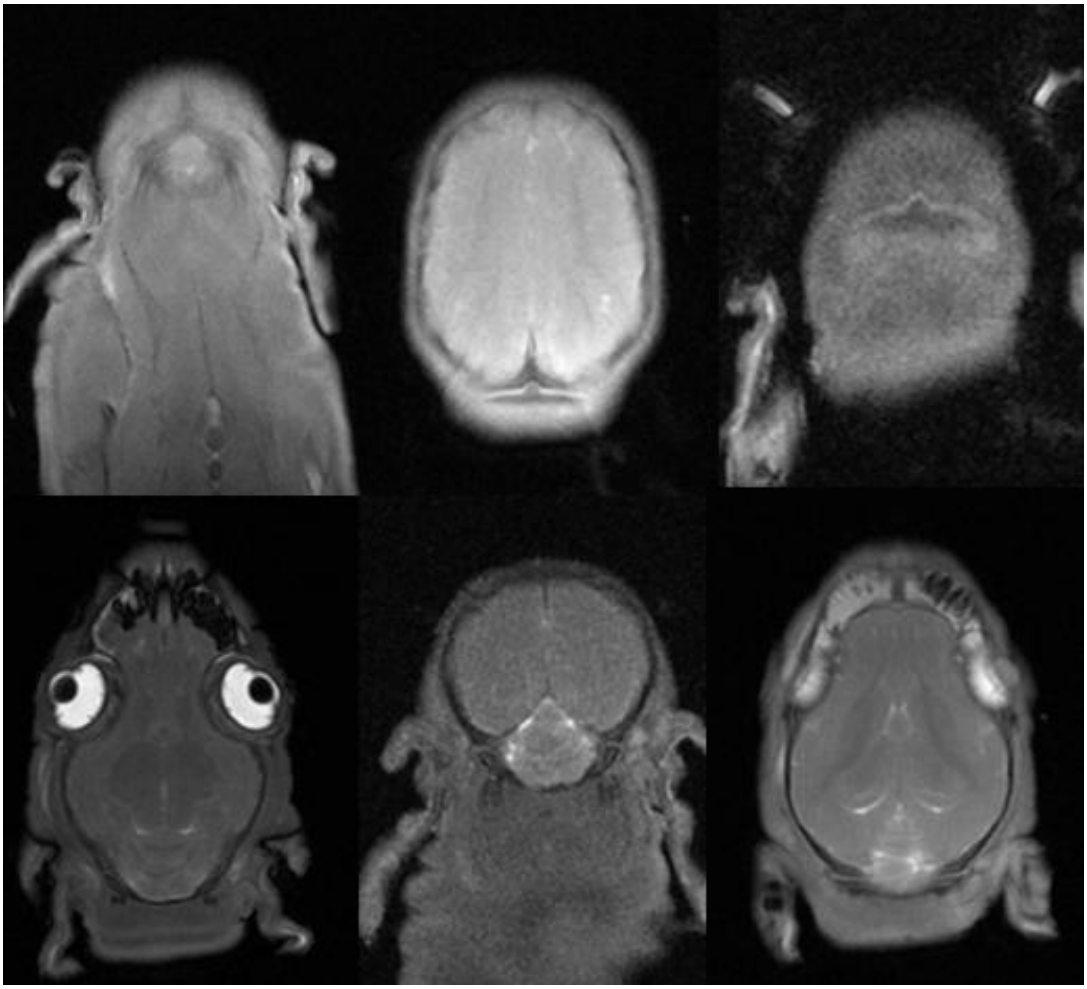


*Figure 34: Cranial suture appearance on FIESTA sequence.*

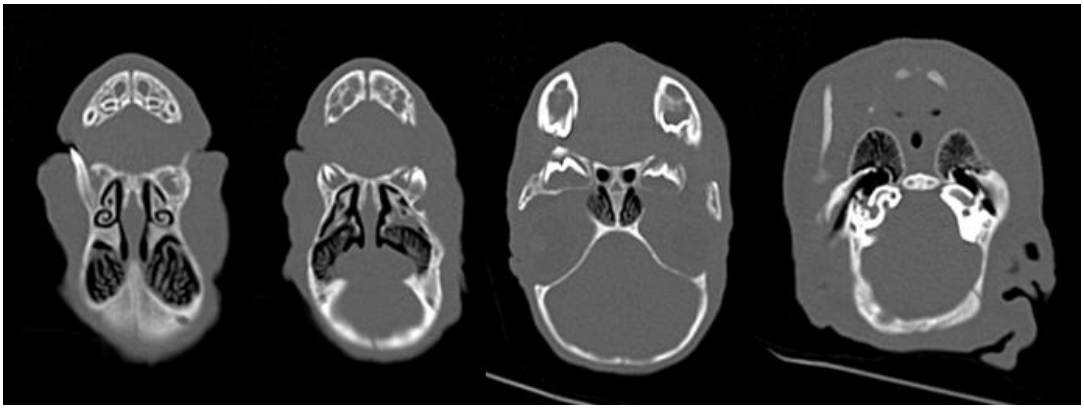


*Figure 35: Confirmation of the appearance of the cranial sutures and mandibular symphysis on axial CT imaging.*

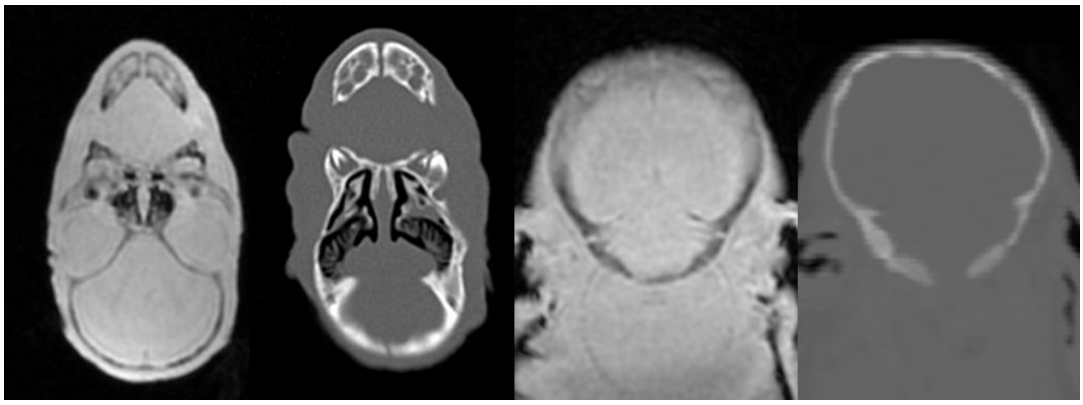


*Figure 36: Comparable "Black Bone" and CT images.*

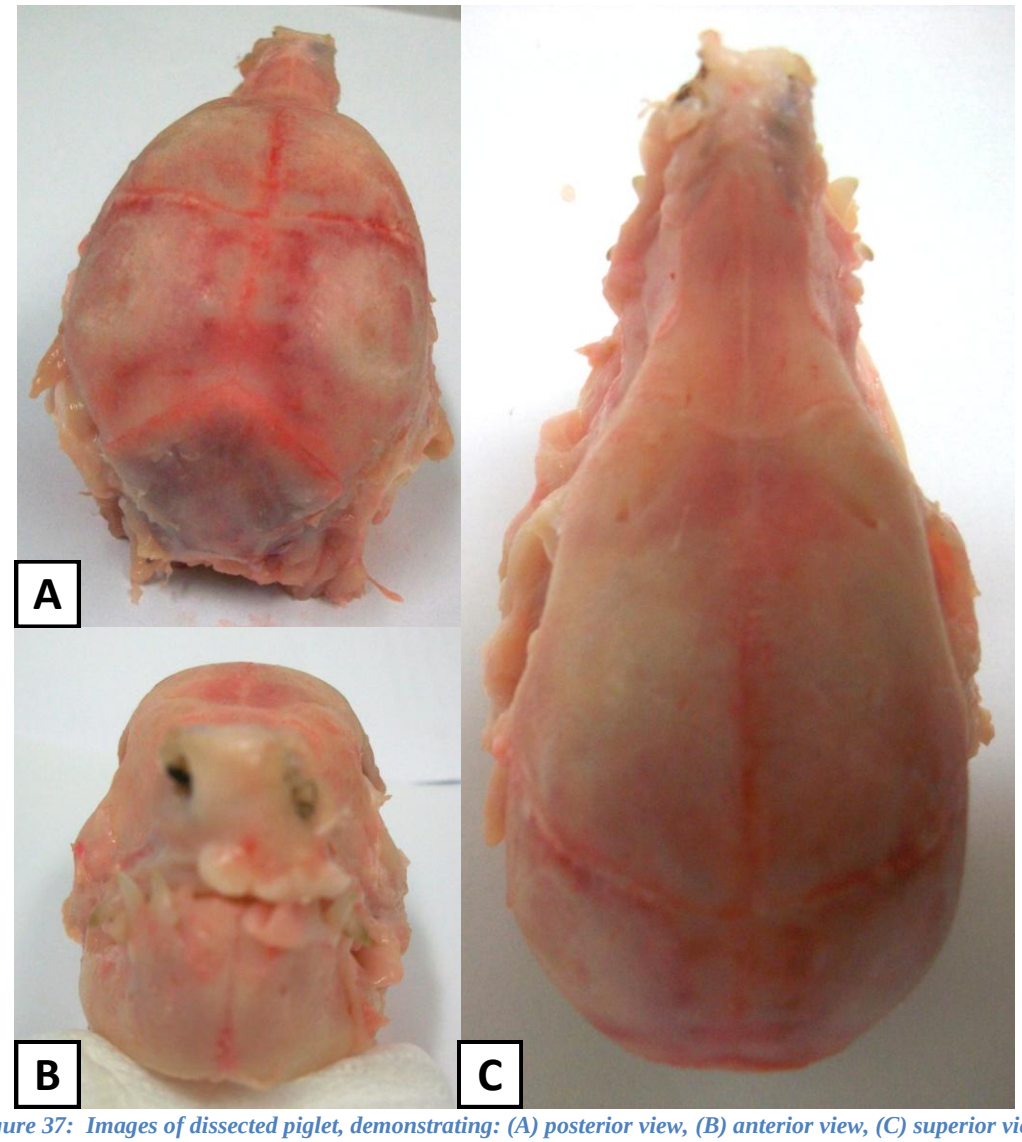



*Figure 37: Images of dissected piglet, demonstrating: (A) posterior view, (B) anterior view, (C) superior view.*

#### 4.3.1.3 Discussion

"Black Bone" demonstrated good potential in the identification of the cranial sutures; the sutures being visualised as areas of increased signal and correlating with CT and dissection findings. One of the important observations noted was the need for the correct slice orientation to aid suture identification. As has previously been noted, the cranial sutures were optimally identified when the image slice was perpendicular to the path of the cranial suture. This was aided with 3D volume acquisition rather than 2D slice data, with the "Black Bone" sequence amenable to post-process formatting in any plane. However, it was noted that there is some loss of image quality during this process.

Manipulation of the "Black Bone" imaging parameters failed to improve visualisation of the sutures. The shortest available TE of 2.112ms was compared to the TE parameter in use in the "Black Bone" sequence (TE=4.2ms). As would be anticipated, this had no noticeable effect on the final image result.

Previous work in the literature that has investigated the potential of ultra short TE in bony imaging have utilised TE's in the range 0.05-0.20ms, far shorter than the available range on the MRI scanners on which this work was completed.

With short TR and TE the FIESTA sequence had comparable imaging times to the "Black Bone" sequence and being acquired as a 3D volume it also conferred many of the imaging advantages of "Black Bone." However, whilst it demonstrated potential in the identification of the cranial sutures, the increased signal from the soft tissues made some areas of bone more challenging to distinguish when compared to the "Black Bone" sequence. The FIESTA sequence, however, warranted further investigation.

## 4.4 Alternative MRI Sequences

Investigation of cranial sutures on routine MRI in infants and an animal model identified further potential sequences in the identification of cranial sutures which warranted further investigation.

### 4.4.1 FIESTA

The animal work demonstrated that the FIESTA sequence permitted clear identification of the cranial sutures in the piglets. To further explore this sequence, imaging was acquired of the craniofacial skeleton on an adult volunteer (KE) at the CH *(Figure 38)*. This demonstrated that in living patients, the increased MR signal associated with fluid containing regions had a significant negative impact on the visualisation of the cranial bone and intervening sutures. In addition, the increased soft tissue contrast resulted in the bone – soft-tissue being less clearly defined than with the "Black Bone" sequence. It was therefore concluded that the FIESTA sequence would be of limited value in this work.

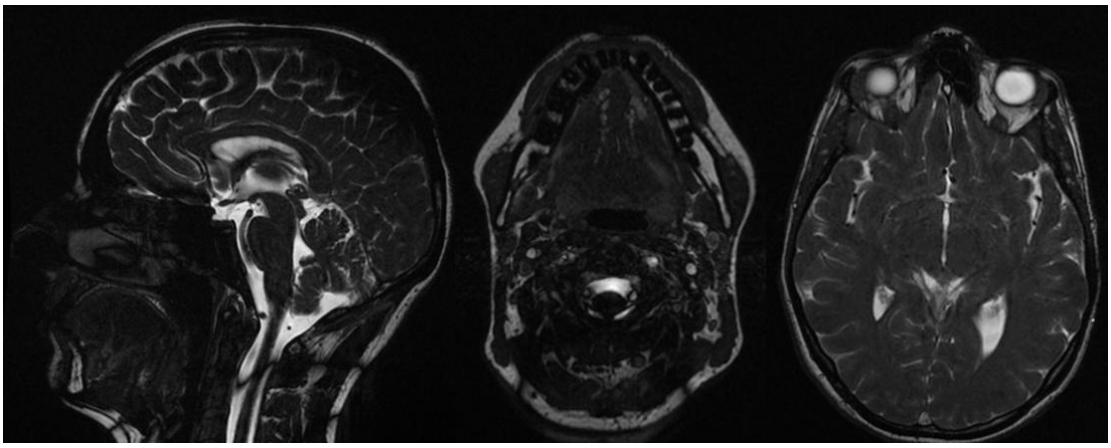


*Figure 38: FIESTA imaging on adult volunteer.*

### 4.4.2 Ultra short Time to Echo

In collaboration with Dr Mathew Robson, at the department of cardiovascular medicine, University of Oxford, investigation of the potential for ultrashort TE (UTE) in imaging the craniofacial skeleton was undertaken. UTE imaging was completed on a 3T magnet (Siemens) at the Acute Vascular Imaging (AVIC) Centre at the JR, with an adult volunteer (KE).

In an attempt to provide an artificial barrier between outside air and air within the ear canal and outside of the body, fluid filled bags were placed against each ear. UTE imaging was acquired as both 2D and 3D volume acquisition. To permit the potential subtraction of one image set from another, to enhance the appearance of bone, two echoes were utilised. In addition, to allow direct comparison to the "Black Bone" sequence, "Black Bone" imaging was also completed.

"Black Bone" *(Figure 39)* images demonstrated increased soft tissue contrast compared to images acquired at the John Radcliffe MRI Centre (OMRI) and CH. It was apparent that with almost identical parameters, there was some variability in the resultant sequences. Optimisation of the sequence would be required on scanners from a range of manufacturers before full incorporation into routine clinical practice.

Overall UTE images *(Figure 40)* did not demonstrate significant potential in imaging the craniofacial skeleton. Whilst on some of the subtraction images the bone appeared as regions of increased signal (thus appearing white and comparable to CT), this was inconsistent. As many of the soft tissues had a similar appearance to bone, UTE did not appear to confer any advantage over "Black Bone."

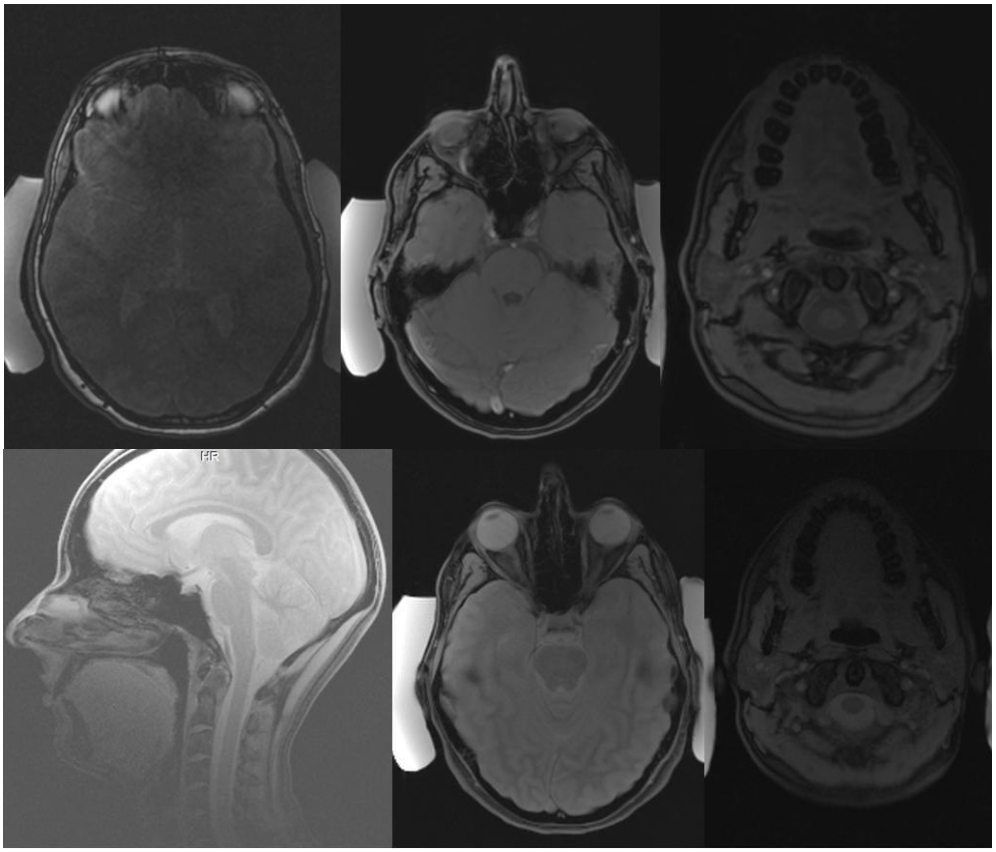


*Figure 39: Attempt to reproduce "Black Bone" sequence on AVIC Siemens MR scanner; 3D acquisition (top), and 2D acquisition (bottom).*

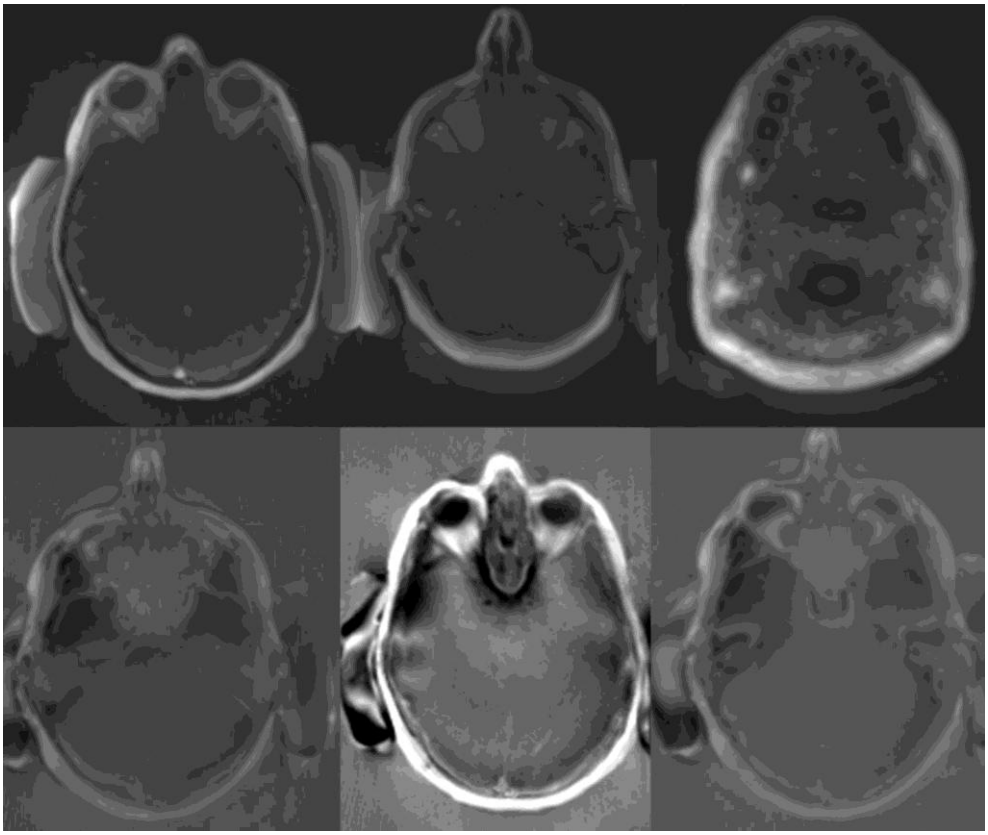


*Figure 40: UTE scanning; resultant subtraction images bottom row.*

### 4.4.3 BRAVO & Cube

A 3T magnet became available during the research period. This provided the opportunity to work with representatives from GE to explore alternative sequences to visualise the craniofacial skeleton. These were investigated on an adult volunteer (KE). The parameters were sequentially adjusted within two sequences: FSPGR BRAVO (Fast Spoiled Gradient Echo BRAinVOlume - a rapid 3D volume acquisition high-resolution T1-weighted sequence) and Cube T2 (a FSE based pulse sequence that allows isotropic imaging and reformatting in any plane) *(Figure 41).* Whilst the cranial sutures could be visualised as regions of signal void in some instances, the increased soft tissue contrast, particularly in fluid containing regions, resulted in these sequences offering no advantage over "Black Bone" for the craniofacial skeleton.

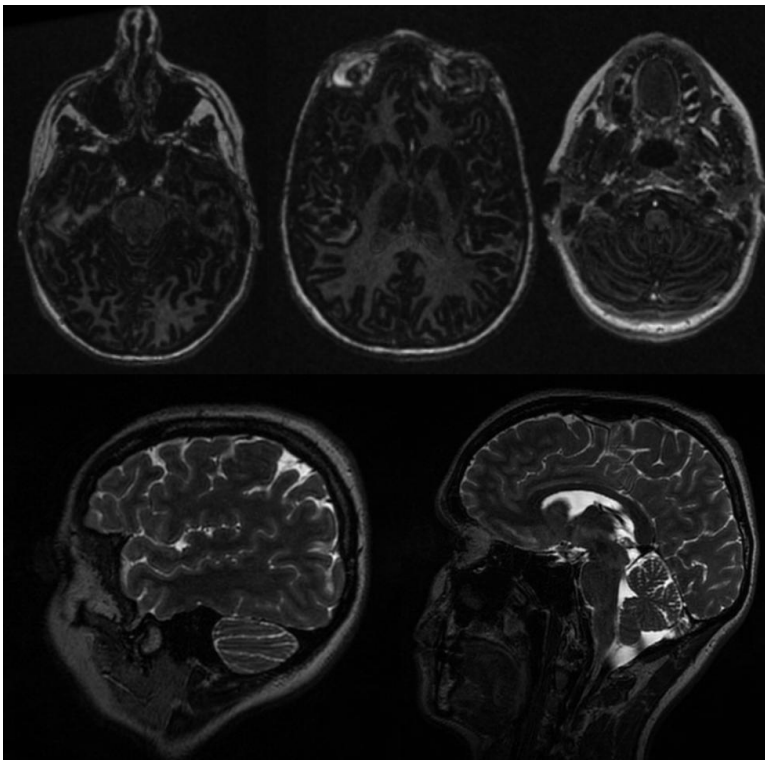


***Figure 41: Axial FSPGR BRAVO (top row) and Sagittal CUBE T2 (bottom row) images of adult volunteer.***

### 4.4.4 Discussion

Of the additional MRI sequences explored in this section none provided a similar clarity of the bone-soft tissue boundary or visualisation of the sutures as seen with "Black Bone." The next phase was to determine if the results obtained with the animal model on "Black Bone" were transferable to patients with craniosynostosis.

## 4.5 "Black Bone" MRI in Children

Prior to evaluating the "Black Bone" sequence in infants with craniosynostosis, it was necessary to confirm that the sequence adequately delineated the normal suture in children in whom the cranial sutures were deemed to be patent.

### 4.5.1 Materials and Methods

The "Black Bone" sequence was obtained in children undergoing imaging of the head and/or neck region at the Oxford MRI Centre (OMRI). During the course of the study there was one paediatric general anaesthetic list per week in OMRI, with most paediatric imaging completed in the West Wing (WW). Following discussion with the paediatric radiologists it was deemed that "Black Bone" may confer potential clinical benefit to children undergoing MRI of the head/face. As the "Black Bone" sequence forms part of the routine protocol of imaging in OMRI, and it was deemed that this may yield additional clinical information, ethical approval for this aspect of the study was not required. With agreement from the paediatric radiologist, anaesthetist, and radiographers, it was possible to obtain the "Black Bone" sequence in 4 children whilst under general anaesthesia *(Table 17)*.

| Patient | Age | Sex | Diagnosis |
|---|---|---|---|
| 1 | 3 years | Female | Langerhans Histiocytosis |
| 2 | 5 years | Male | Posterior fossa anaplastic ependymoma |
| 3 | 9 months | Female | Haemangioma of cheek |
| 4 | 13 months | Male | Metastatic Neuroblastoma |

*Table 17: Paediatric patients undergoing "Black Bone" imaging of the head.*

In all cases, imaging was completed on a 1.5T magnet using an 8 channel head coil. Where possible, the FOV was set to include from above the skull vertex to below the mandible. Imaging was acquired in the axial plane and where time permitted coronal and/or sagittal imaging was additionally obtained.

### 4.5.2 Results

The “Black Bone” imaging findings for each of the 4 children imaged are shown in *Figure 42 & 43.*

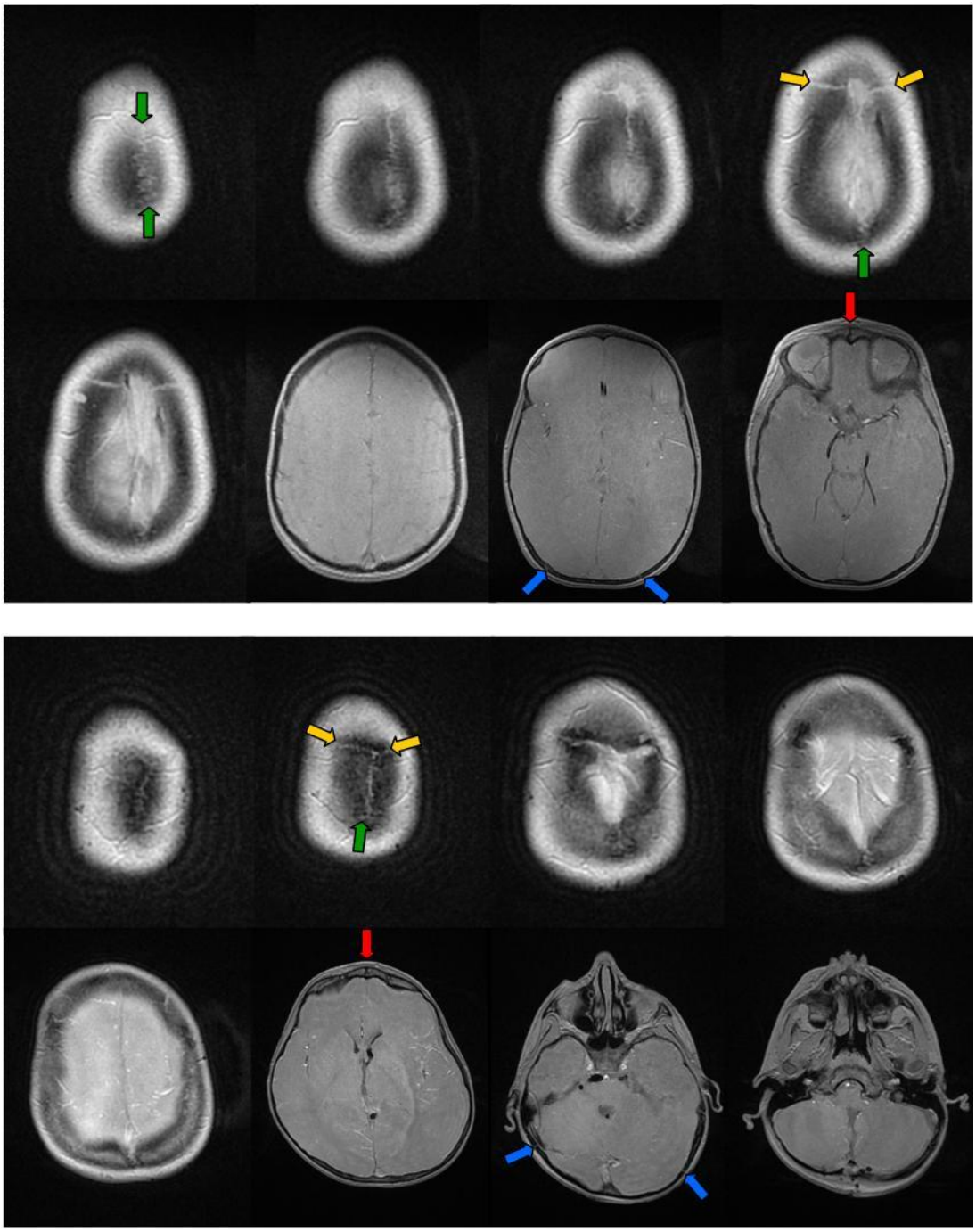


*Figure 42: Appearance of cranial sutures in Patient 1 (Top) and Patient 2 (Bottom). At the vertex, the tortuous path of the sagittal and coronal sutures can clearly be delineated as areas of increased signal on the dense bone. In Patient 1, the anterior fontanelle is additionally identified. (Arrows - Yellow=Coronal Suture; Green=Sagittal Suture; Blue=Lambdoid Suture; Red=Metopic Suture).*

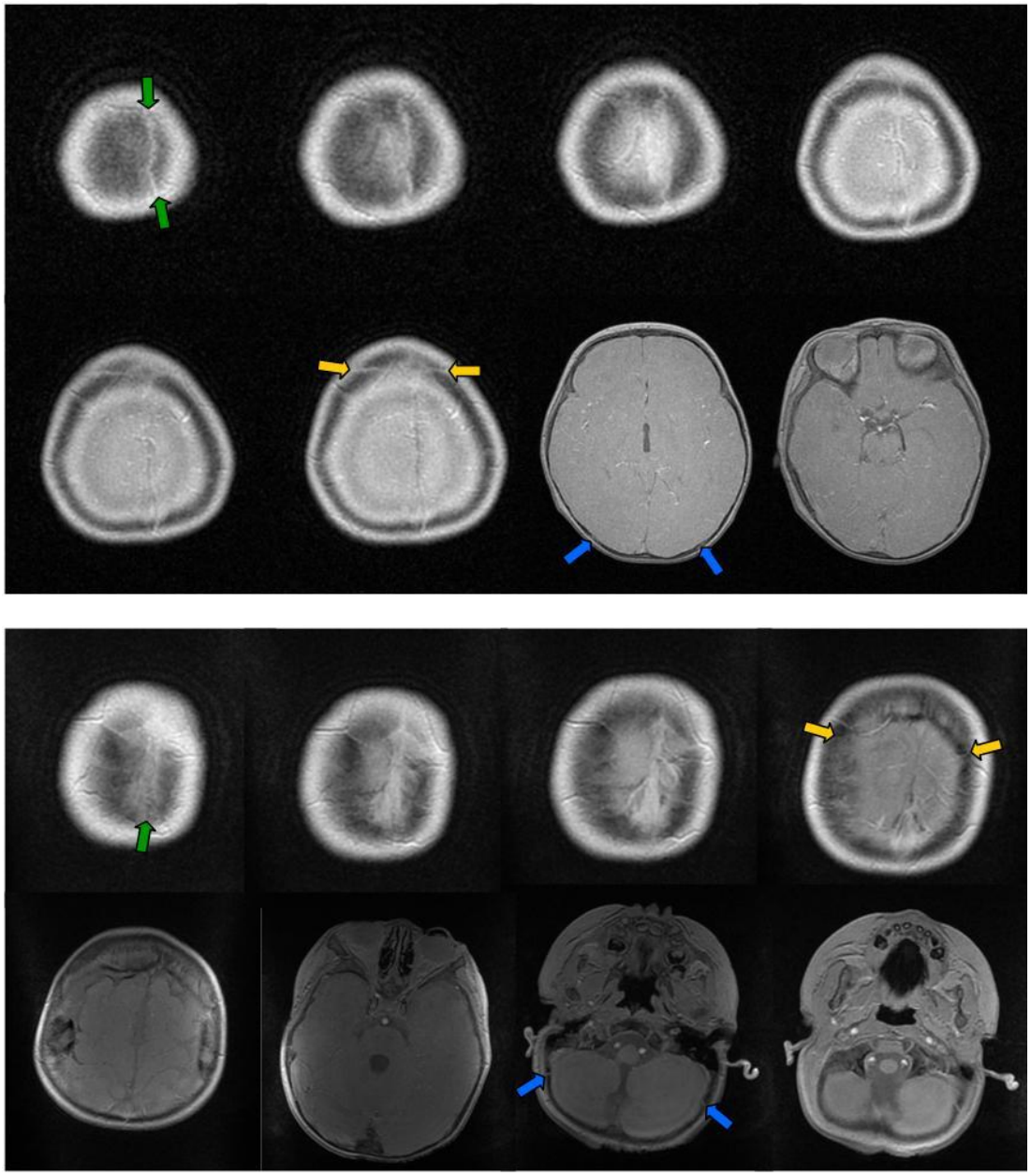


*Figure 43: Appearance of the cranial sutures in Patient 3 (Top) and Patient 4 (Bottom). The cranial sutures are again seen as areas of increased signal. The extensive intracranial pathology seen in Patient 4 results in added difficulty in identifying the sutures throughout their course. (Arrows - Yellow=Coronal Suture; Green=Sagittal Suture; Blue=Lambdoid Suture; Red=Metopic Suture).*

The cranial sutures were consistently identified on the “Black Bone” datasets in the four children as areas of increased signal, thus appearing white against the signal void of the cranial bone. The sutures could be followed throughout their course in all cases, except Patient 4 where there was significant intracranial pathology. The cranial bone appeared less densely black when compared to that obtained in adults. However, the bone was distinct from the surrounding soft tissues.

### 4.5.3 Discussion

In all of the children studied, the cranial sutures appeared as areas of increased signal, which could easily be distinguished from the cranial bone and soft tissues. This was further aided by the characteristic tortuosity of the sutures, and in some cases the identification of the anterior fontanelle. In the eldest child imaged (Patient 2), the cranial bone surrounding the suture appeared particularly dense, and this acted as a further localiser for the intervening sutures. The cranial sutures could be followed throughout their course when there was no significant associated pathology. When compared to the routinely used MRI sequences studied in this chapter, where the cranial sutures were seen as areas of signal void and thus being indistinguishable from the cranial bone, the “Black Bone” sequence demonstrates significant advantage. This preliminary work provided justification for “Black Bone” imaging in infants with a clinical diagnosis of craniosynostosis.

## 4.6 "Black Bone" MRI in Craniosynostosis

Having demonstrated that the "Black Bone" sequence was able to identify the normal cranial suture, the next phase was to determine if the sequence could reliably distinguish the normal from the abnormally fused suture. This would make the "Black Bone" sequence clinically valuable as an alternative to CT in the radiological diagnosis of craniosynostosis.

### 4.6.1 Materials and Methods

In collaboration with the Oxford Craniofacial Unit (OCU), children with a clinical diagnosis of craniosynostosis were considered for inclusion in the study. 3D CT is routinely obtained in all children where synostosis is suspected clinically, with the majority of children requiring GA. Ethical approval was granted from the Oxford Research Ethics Committee to obtain an MRI in addition to CT whilst under GA in children with a clinical diagnosis of synostosis. The safest environment to complete back-to-back CT/MRI under GA was the WW neuroradiology suite. The craniofacial co-ordinator identified potential patients and parents were contacted by telephone to explain the study. An information sheet *(Appendix D)* further outlining the study was sent to the families and this was followed up with a further telephone call to answer any residual questions. Families agreeing to participate in the study were provided with hospital admission details. Imaging lists were arranged "out of hours" with dedicated staff provision. In total, nine patients were identified during the study period as suitable for inclusion in the study. All nine families provided informed consent and were recruited. To minimise any potential difficulties associated with anaesthetising children with syndromic synostosis the study was limited to children with single suture synostosis; however, two syndromic children had clinical requirements for MRI and were recruited.

Imaging was completed on a 1.5T MRI (Philips) with imaging completed in the axial plane from above the skull vertex to below the mandible. The "Black Bone" sequence required further adjustment on the Philips scanner to try and match the imaging results as closely as possible to those obtained on GE scanners. In view of the potential for intracranial pathology in this patient group, axial T2 imaging was also completed of the brain. In cases where an MRI of the brain was clinically indicated, a full brain imaging protocol was completed.

It was identified that the OCU had a small number of patients with craniosynostosis who had not undergone surgical intervention. This provided a small cohort of patients who were potentially suitable to undergo MRI examination without the need for GA.

A search of the comprehensive craniofacial database identified 133 patients with single suture synostosis in whom there was no record of surgery. On review of the medical records, 12 of these had undergone surgical correction at another craniofacial unit, and were excluded. A further search was conducted to include those patients with single suture synostosis who had undergone intracranial pressure monitoring (ICPM), since this is routinely performed at the unit when a non-operative path is to be followed in patients with single suture synostosis. In this group, 33 patients were identified. Of the 154 patients identified from both search criteria, 42 were awaiting surgical intervention and were excluded, since these children were under 1 year of age and would require GA for an MRI. It was deemed unlikely that patients under 6 years of age would tolerate MRI without sedation, and that the cranial sutures were unlikely to be identified in patients post skeletal maturity. The medical records of patients between the ages of 6 and 16 were reviewed to confirm the diagnosis and identify the date of next follow up. Since outpatient appointments for these patients were not within the research period recruitment to the study would necessitate the patient travelling to Oxford solely for research purposes. Patients living outside of a 1 hour travelling time to Oxford were therefore excluded. Of the 112 remaining patients, nine met these additional criteria and their parents contacted by telephone. In one case the parents felt that with a coexisting diagnosis of autism MRI would not be possible without sedation. In three cases, despite multiple attempts, the families could not be reached. Information sheets *(Appendix D)* were forwarded to the remaining five families and followed up with a further telephone call to address any residual questions. All five patients agree to participate. However, two children were unable to attend on any of the dates available for imaging. Imaging was completed "out of hours" in OMRI on a 1.5T magnet (GE). The "Black Bone" sequence was obtained from above the skull vertex to below the mandible, and axial T2 imaging was obtained of the brain.

In addition, a 2 month old infant with a clinical diagnosis of Apert's syndrome was identified by the craniofacial team as a potential candidate for the study since MRI was clinically indicated. In

view of the young age of the patient it was anticipated that imaging could be completed without the need for GA. MRI including "Black Bone" was completed on a 3T magnet (GE) at the CH.

Review of the imaging was completed on an AWW and compared to CT.

### *Independent Review of Imaging*

To explore the accuracy of the technique, 12 "Black Bone" MRI datasets from both children with normal cranial sutures and those with a diagnosis of craniosynostosis that were considered representative of the sequence were selected for independent review. In cases of craniosynostosis, only single suture synostoses were included. The data sets were imported into Clear Canvas anonymised, numbered in random order from 1 to 12, and saved in efilm. All identifying information, including the series descriptions were removed. Three of the assessors (neuroradiologist, head & neck radiologist and head & neck surgeon) previously used in the review of the routine MRI sequences, were asked to grade each cranial suture on a scale of 0 to 2 for its identification, and to conclude whether there was evidence of synostosis for any of the sutures. Assessors were informed that the 12 data sets had all been obtained from children with either normal sutures or craniosynostosis. They were asked to disregard any co-existent pathology and to concentrate only on the cranial sutures. The scoring sheet is included in *Appendix D*. Review of imaging was undertaken on efilm, with the assessors free to manipulate images on screen.

## 4.6.2 Results

A summary of the children recruited the study is shown in *Table 18*. Patient number 1-9 underwent imaging under GA, whilst Patients 10-13 were imaged without the need for anaesthesia.

The "Black Bone" imaging parameters on the Philips scanner resulted in too much soft tissue contrast, requiring the additional Philips contrast parameter to be set to "no contrast" rather than the default "T1" or "T2." The effect of this with Patient 1 is shown in *Figure 44*. The "Black Bone" images were not as optimal as those obtained on GE scanners, and the NEX was increased from 2 to 4. This increased the time for image acquisition but produced marginally improved images. Adjustment of the flip angle between 3-6° did not confer any improvement.

| Patient | Age | Syndromic? | Diagnosis |
|---|---|---|---|
| **1** | 5mths | No | Sagittal synostosis |
| **2** | 12mths | No | Sagittal synostosis |
| **3** | 22mths | No | Sagittal synostosis |
| **4** | 5mths | No | Sagittal synostosis |
| **5** | 10mths | No | Right unicoronal synostosis |
| **6** | 19mths | Yes - Crouzons | Sagittal & lambdoid synostosis |
| **7** | 9mths | No | Right unicoronal synostosis |
| **8** | 17mths | No | Metopic synostosis |
| **9** | 8mths | ?Yes | Sagittal synostosis |
| **10** | 9yrs | No | Sagittal synostosis |
| **11** | 12yrs | No | Sagittal synostosis |
| **12** | 12yrs | No | Sagittal synostosis |
| **13** | 2mths | Yes - Aperts | Bilateral coronal synostosis |

*Table 18: Children recruited to craniosynostosis study.*

The "Black Bone" images for the 13 patients are shown in *Figures 45-51*, with comparable CT images. In all cases the patent cranial sutures were visualised as areas of increased signal and the suture was absent in cases of craniosynostosis. The findings were consistent with CT; for some of the children CT acquisition was not in the true axial plane, making accurate comparison with "Black Bone" more challenging. This was overcome with 3D reconstruction explored in Chapter 7.

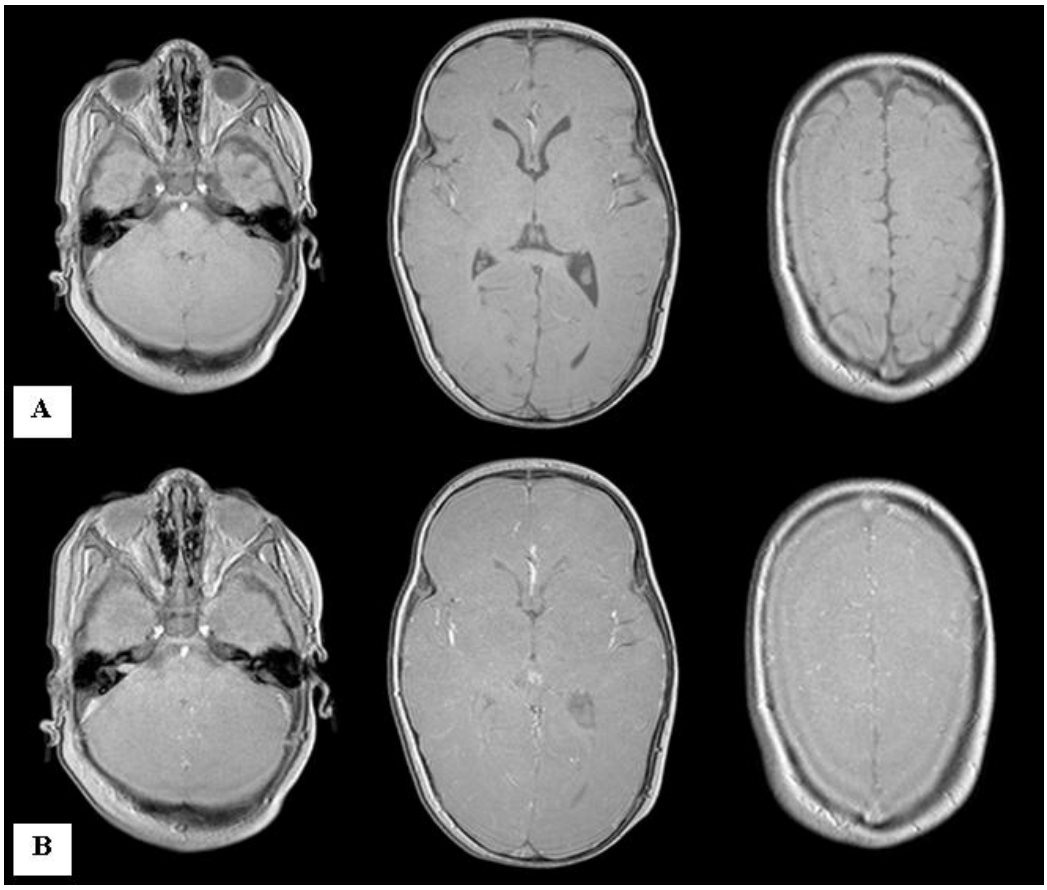



*Figure 44: Comparable axial "Black Bone" images of Patient 1, demonstrating differing soft tissue contrast on Philips scanner with initial settings (A), and with selection of "no contrast" (B).*

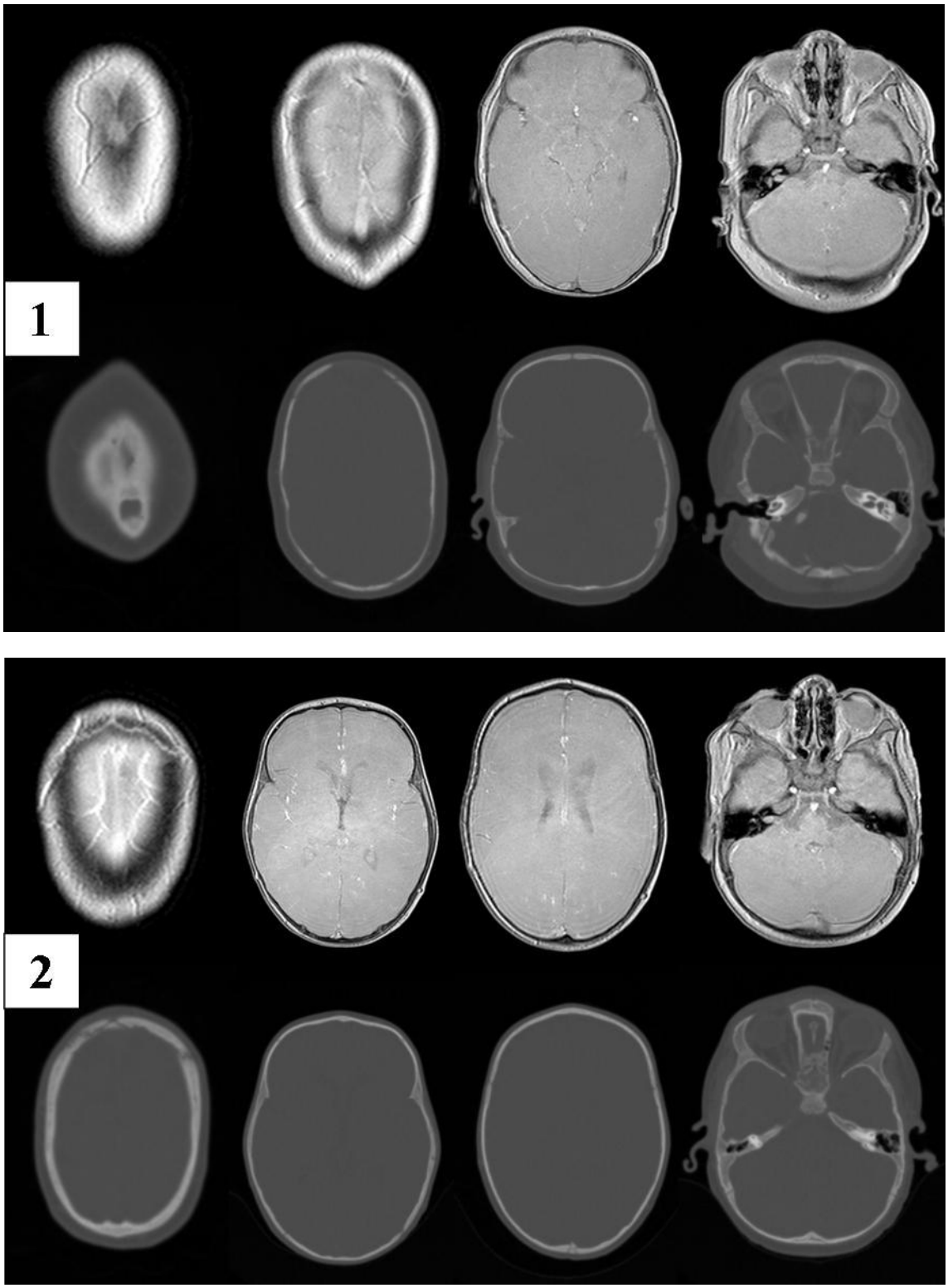
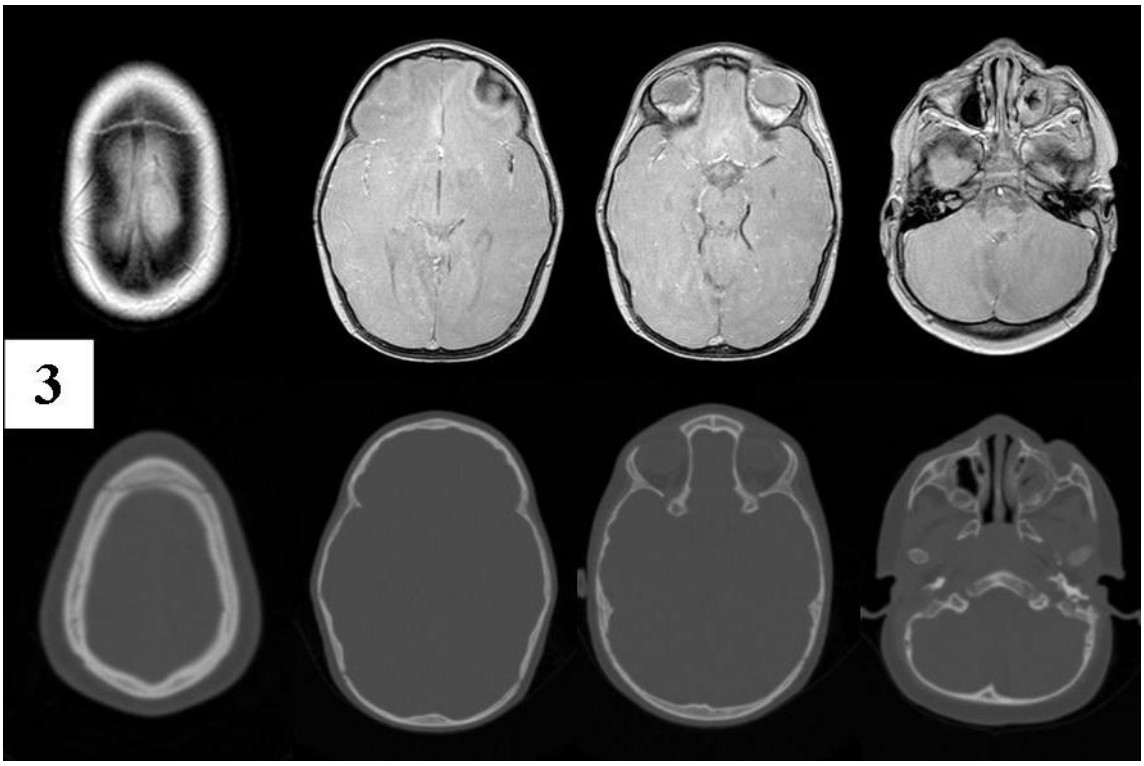



*Figure 45: Patient 1 (top) and Patient 2 (bottom) both with a diagnosis of sagittal synostosis. The anterior fontanelle can be visualised in Patient 1 in the first image.*



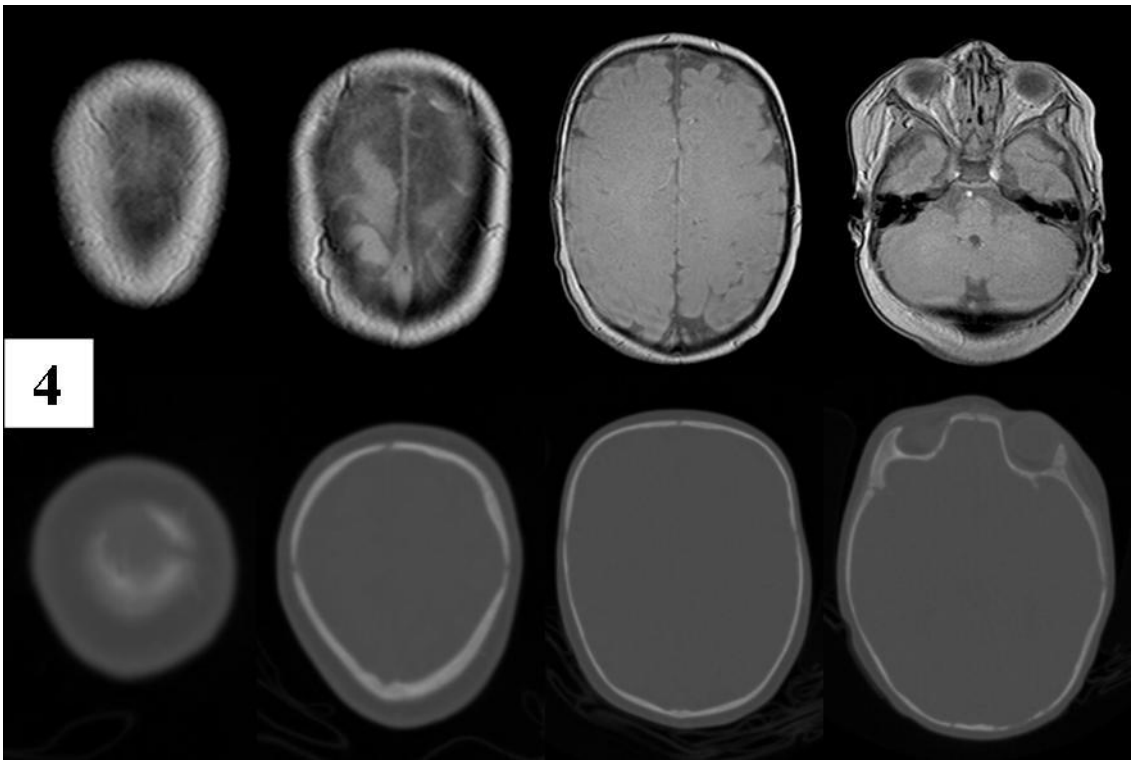




*Figure 46: Patient 2 (top) and 3 (bottom) both with a diagnosis of sagittal synostosis. In Patient 4 there is too much contrast within the brain, which results in difficulty in distinguishing the sagittal sinus from the sagittal suture (which in this case is absent). It later became apparent that this was the result of the contrast setting not being set to "no."*

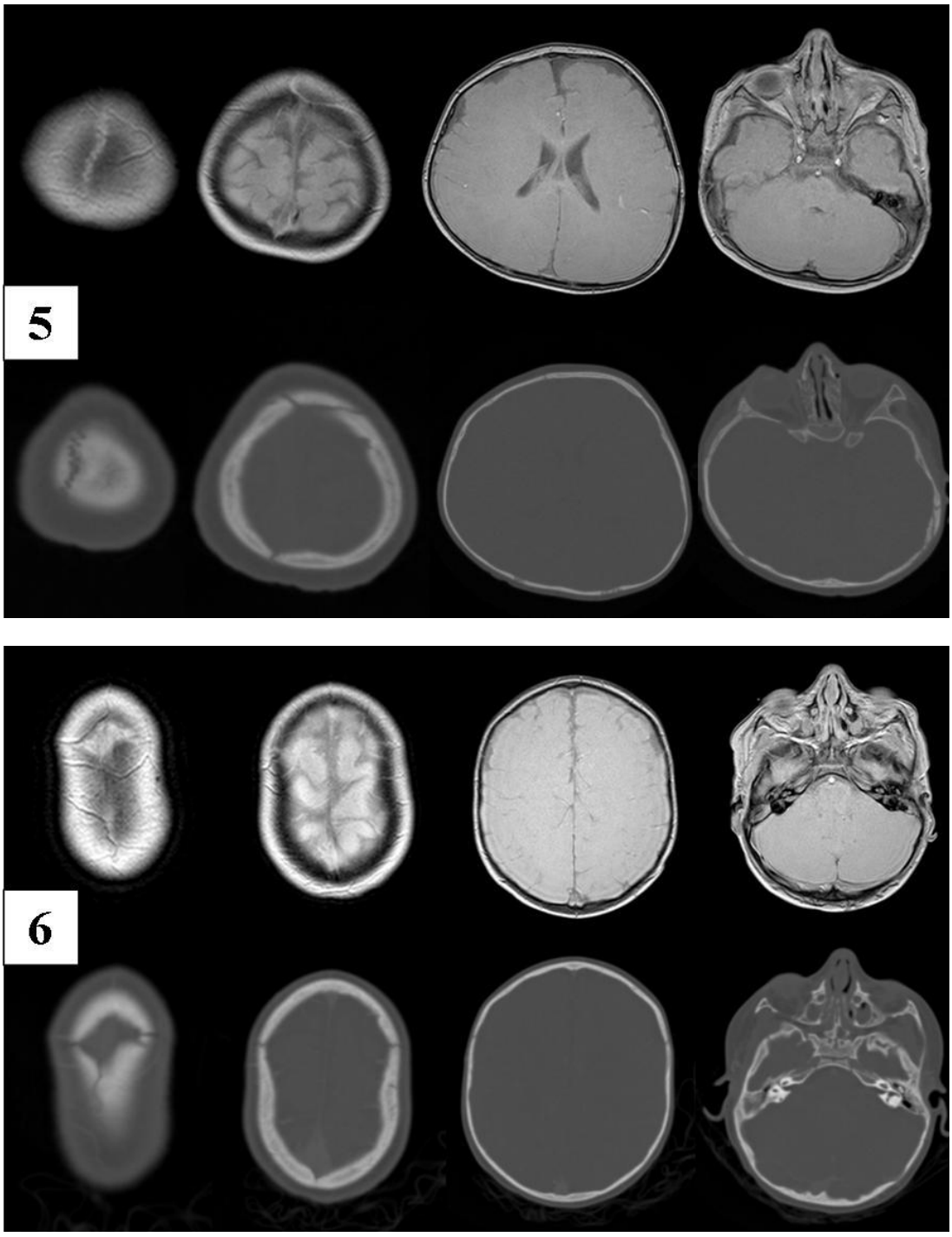



*Figure 47: Patient 5 (top) with a diagnosis of right unicoronal synostosis, and Patient 6 (bottom) with a diagnosis of sagittal and lambdoid synostosis.*

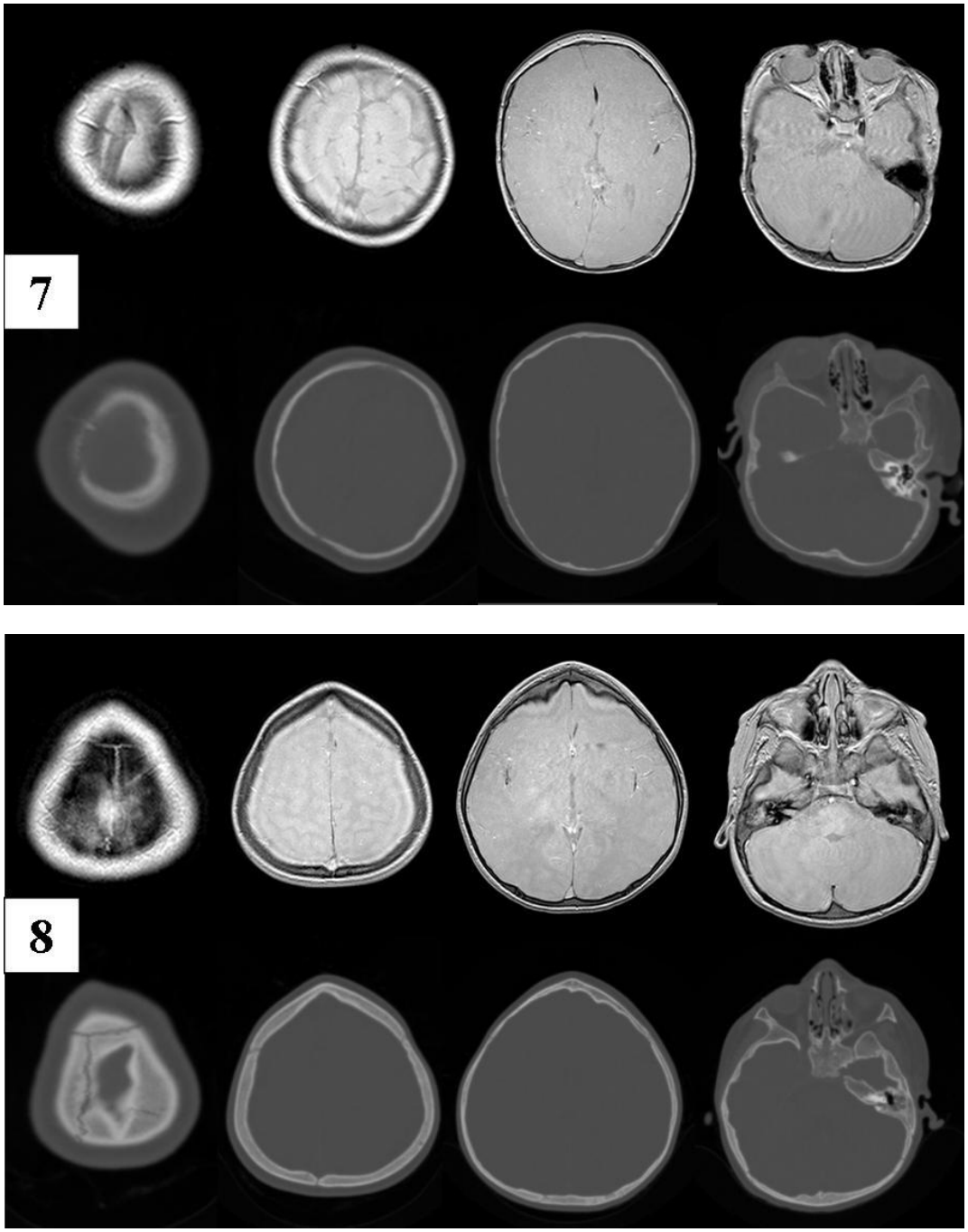



*Figure 48: Patient 7 (top) with a diagnosis of right unicoronal synostosis, and Patient 8 (bottom) with a diagnosis of metopic synostosis. The soft tissue and bone appearance in Patient 8 most closely represents those obtained when imaging with a GE scanner.*

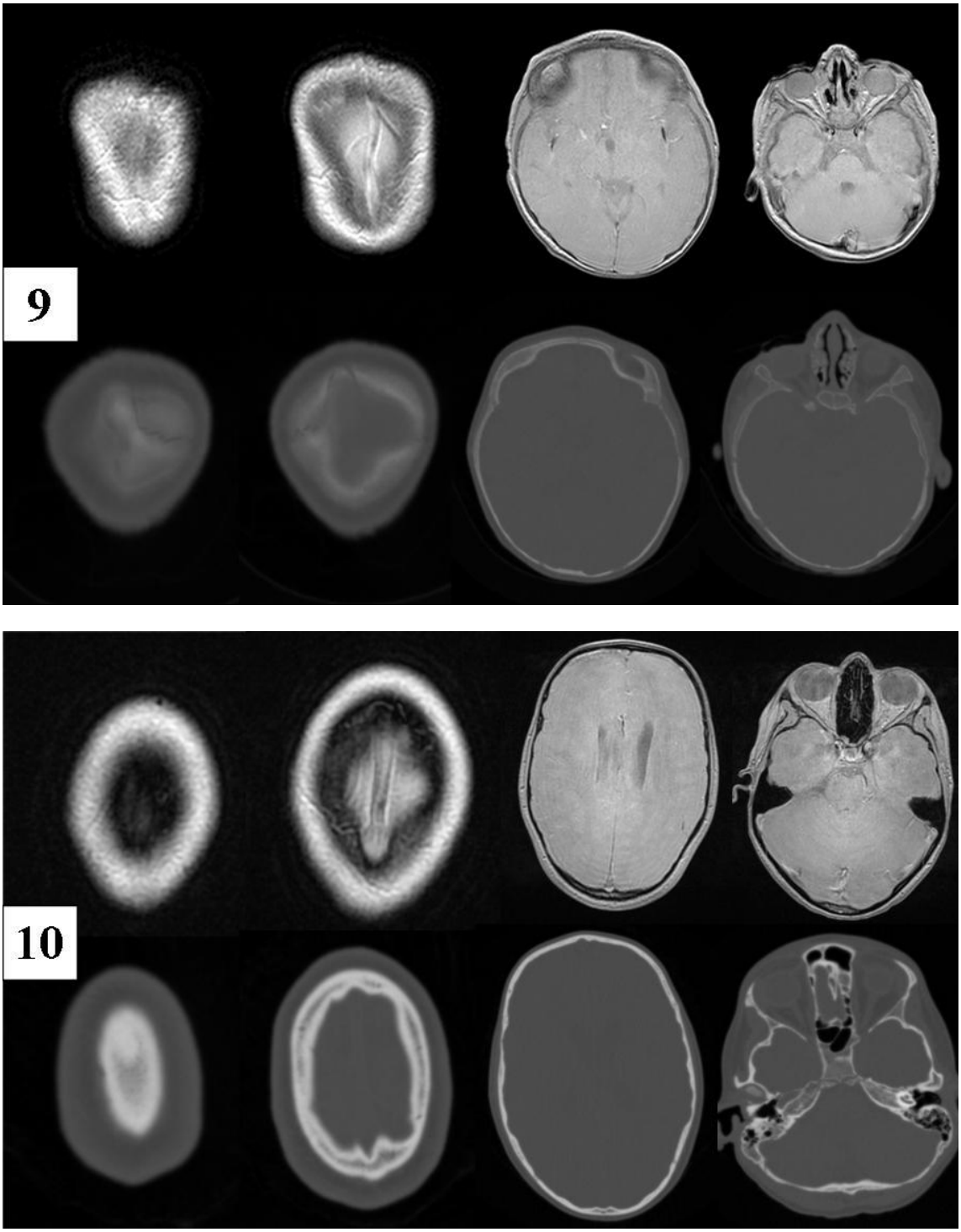



*Figure 49: Patient 9 (top) and Patient 10 (bottom) both with a diagnosis of sagittal synostosis. Patient 10 was imaged in OMRI on a GE scanner, and the effect of this and patient age can be readily seen with more dense cranial bone.*

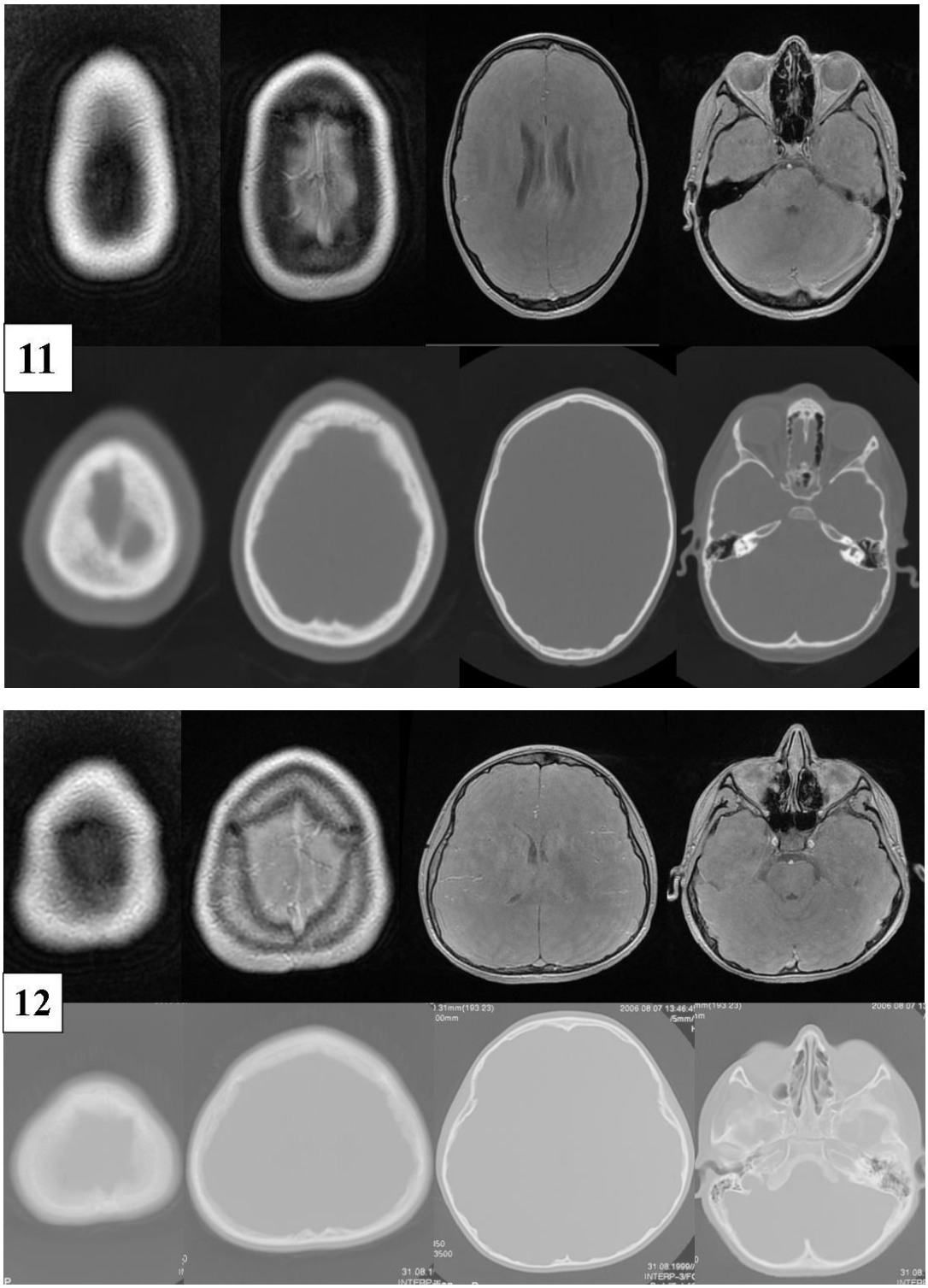



*Figure 50: Patient 11 (top) and Patient 12 (bottom) both with a diagnosis of sagittal synostosis. Both of these children were imaged in OMRI. At aged 12 years, we can see that the bone surrounding the cranial sutures appears increasingly dense compared to that seen in younger children. NB. The CT images for Patient 12 were only available as a digitised sheet.*

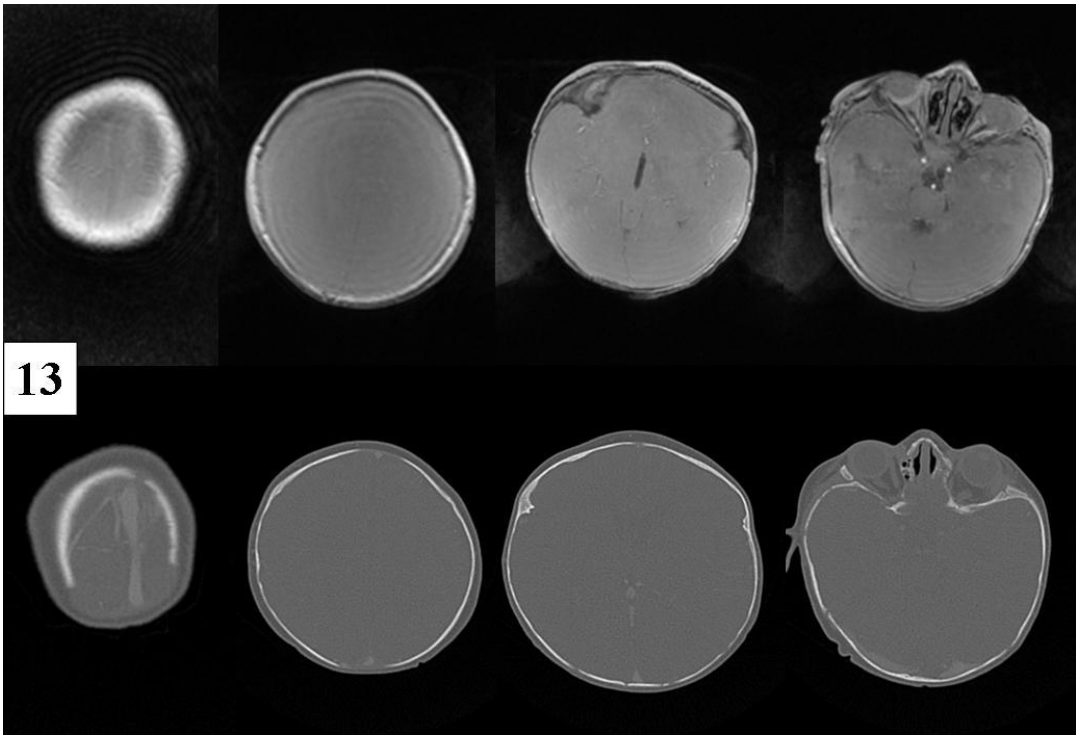



*Figure 51: Patient 13 with a diagnosis of Apert Syndrome, with bilateral coronal synostosis. This 2 month old child was imaged at the CH on a 3T magnet. With movement artefact, and particularly thin cranial bone the cranial sutures are difficult to identify. However, the regions of bone do correlate on "Black Bone" and CT.*

In Patient 13 the cranial sutures and bone were difficult to identify on the "Black Bone" sequence as a result of the particularly thin bone and raised intracranial pressure in this infant with Apert syndrome. These findings correlated with those seen on CT albeit with bone on the "Black Bone" images being less well defined.

The optimised imaging parameters for the Philips scanner are shown in *Table 19*. The closest TR and TE values to those used on GE scanners permissible on the Philips scanner were selected.

| Parameter | Value |
|---|---|
| **Acquisition** | 3D |
| **TR** | 8.19 |
| **TE** | 4.008 |
| **Flip Angle** | 5 |
| **Slice Thickness** | 2.4 |
| **Spacing** | 1.2 |
| **Number of Averages** | 4 |
| **Matrix** | 512 x 512 |
| **Echo Train Length** | 1 |
| **Contrast** | None |

*Table 19: "Black Bone" MRI parameters for Philips 1.5T scanner.*

One of the problems encountered on datasets acquired in the WW was image artefact resulting in an additional outline adjacent to the cranial bone *(Figure 52).* The artefact could be transposed by switching the phase and frequency directions, confirming that this was a chemical shift artefact. Chemical shift artefact is the result of the difference in resonance frequency between fat and water. Methods to reduce this effect include a higher bandwidth, a higher matrix, an in phase TE, a spin echo technique and fat suppression techniques. With the close relationship to the bone this resulted in particular difficulties with 3D rendering, discussed in Chapter 7. Investigation into attempts to minimise the artefact were therefore conducted. On Philips scanners, the bandwidth is controlled by the water fat shift selection. This was both increased and decreased, however the resultant images had more significant artefact *(Figure 53).*The next option was to apply a fat saturation pulse, in an attempt to null all signal from fat and therefore eliminate the chemical shift. This was unsuccessful in eliminating the problem.

Acquisition in an alternative plane frequently offered a compromise by moving the artefact out of the ROI as much as possible *(Figure 54).* This was possible as a post-processing option for the "Black Bone" sequence but as previously noted this resulted in some loss of image quality and primary acquisition in the desired plane was considered optimal.

An additional advantage of MRI acquisition in the patient group studied was the identification of prominent optic nerve sheaths in Patient 6, suggesting raised intracranial pressure (ICP). Evidence suggests that a retrobulbar optic nerve sheath diameter above 5.82mm predicts raised ICP in 90% of cases.[189] T2 weighted MRI therefore confers a significant advantage over CT in children with a clinical diagnosis of craniosynostosis who are at increased risk of raised ICP

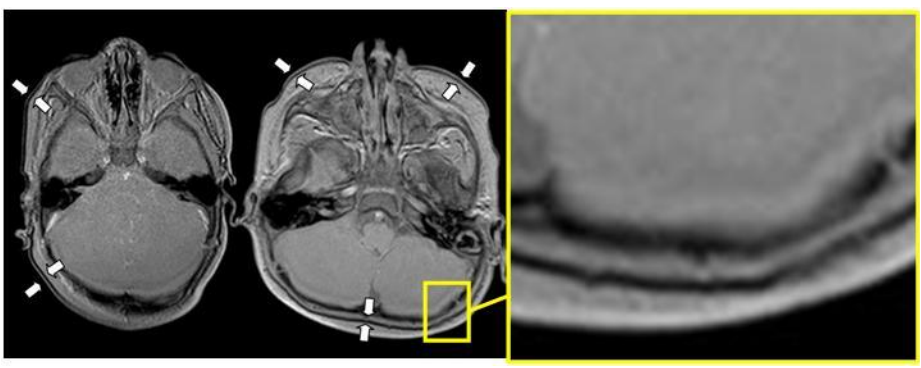


***Figure 52: Appearance of chemical shift artefact, with close-up view. The artefact could be moved by switching the phase-frequency direction.***

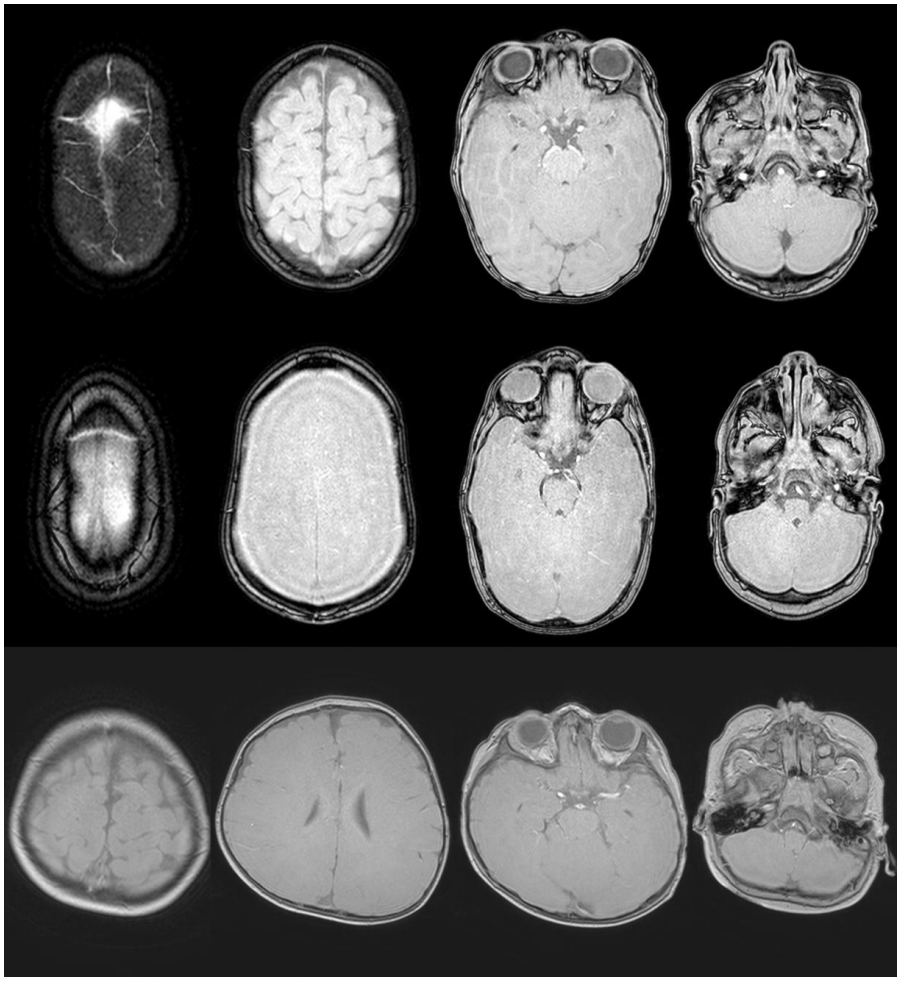


*Figure 53: Effect of fat shift selection (top and middle) and water shift selection (bottom) on the "Black Bone" sequence.*

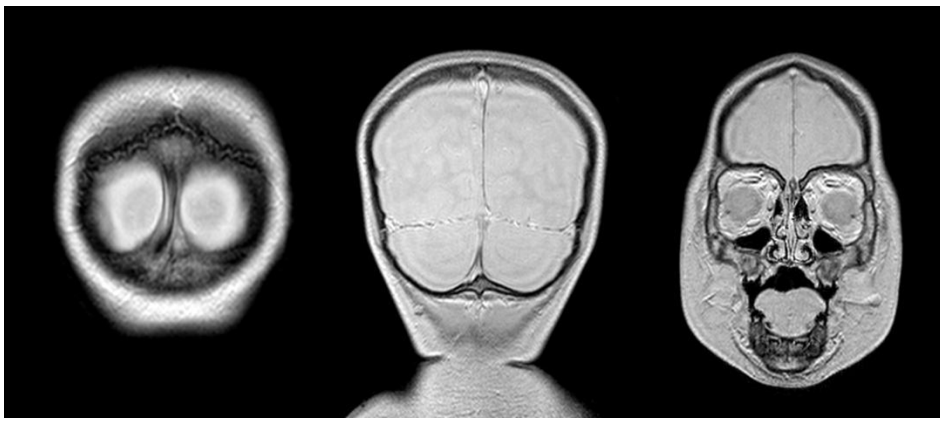


*Figure 54: "Black Bone" acquisition in the coronal plane. In this example, the lambdoid and sagittal sutures are clearly seen.*

### *Independent Review of Imaging*

The anonymised "Black Bone" data sets included for independent review are shown in *Table 20.* The results from each of the three assessors are included in *Appendix D.*

| Patient | Age | Diagnosis |
|---|---|---|
| **1** | 12 mths | Sagittal synostosis |
| **2** | 12 yrs | Sagittal synostosis |
| **3** | 9 mths | Right unicoronal synostosis |
| **4** | 3 yrs | Normal sutures |
| **5** | 17 mths | Metopic synostosis |
| **6** | 22 mths | Sagittal synostosis |
| **7** | 5 yrs | Normal sutures |
| **8** | 10 mths | Right unicoronal synostosis |
| **9** | 9 yrs | Sagittal synostosis |
| **10** | 12 yrs | Sagittal synostosis |
| **11** | 5 mths | Sagittal synostosis |
| **12** | 9 mths | Normal sutures |

*Table 20: "Black Bone" data sets included for anonymised independent review.*

The metopic suture was the least frequently identified suture consistent with the age of the patients studied. A score of 2 (suture fully identified, and confident of its presence) was often selected, and this was of somewhat contrast to the scores seen with the routine MRI sequences. The diagnosis of craniosynostosis assigned by each of the assessors is shown in *Table 21*.

The neuroradiologist made the correct diagnosis in all 12 cases. In the absence of synostosis, a score of 2 was assigned for all sutures, apart from the metopic suture, which could only be visualised in two cases.

The correct diagnosis was made in eight of the twelve cases by the head and neck radiologist, with scores of 1 being more frequently assigned, particularly for the coronal and lambdoid sutures. Eleven of the twelve cases were correctly diagnosed by the head and neck surgeon, again with increasing assignment of a score of 1 for the lambdoid sutures.

The mean scores assigned by the reviewers for each of the cranial sutures on the "Black Bone" datasets are shown in *Table 22.* Cases of synostosis received the lowest mean scores, despite this not always being identified by the reviewer as the diagnosis.

| Patient | Diagnosis | Craniofacial Radiologist | Head & Neck Radiologist | Head & Neck Surgeon |
|---|---|---|---|---|
| 1 | Sagittal synostosis | Sagittal | Normal | Sagittal |
| 2 | Sagittal synostosis | Sagittal | Normal | Sagittal |
| 3 | Right unicoronal | Right unicoronal | Right unicoronal | Normal |
| 4 | Normal sutures | Normal | Normal | Normal |
| 5 | Metopic synostosis | Metopic | Metopic | Metopic |
| 6 | Sagittal synostosis | Sagittal | Sagittal | Sagittal |
| 7 | Normal sutures | Normal | Normal | Normal |
| 8 | Right unicoronal | Right unicoronal | Left unicoronal | Right unicoronal |
| 9 | Sagittal synostosis | Sagittal | Sagittal | Sagittal |
| 10 | Sagittal synostosis | Sagittal | Normal | Sagittal |
| 11 | Sagittal synostosis | Sagittal | Sagittal | Sagittal |
| 12 | Normal sutures | Normal | Normal | Normal |

*Table 21: Diagnosis made for 12 "Black Bone" datasets by 3 reviewers.*

| Patient | Metopic | Right coronal | Left coronal | Sagittal | Right Lambdoid | Left Lambdoid |
|---|---|---|---|---|---|---|
| 1 | 0.7 | 1.7 | 1.7 | 0.0* | 1.7 | 1.7 |
| 2 | 0.3 | 1.3 | 1.3 | 0.0* | 2.0 | 2.0 |
| 3 | 0.0 | 0.3* | 1.0 | 1.3 | 1.0 | 1.0 |
| 4 | 0.7 | 2.0 | 2.0 | 2.0 | 1.7 | 1.7 |
| 5 | 0.3* | 2.0 | 2.0 | 2.0 | 2.0 | 2.0 |
| 6 | 1.0 | 1.7 | 1.7 | 0.0* | 1.7 | 1.7 |
| 7 | 0.7 | 2.0 | 2.0 | 2.0 | 1.7 | 1.7 |
| 8 | 1.7 | 0.0* | 1.3 | 2.0 | 2.0 | 2.0 |
| 9 | 0.0 | 1.7 | 1.7 | 0.0* | 1.7 | 1.7 |
| 10 | 0.0 | 1.7 | 1.7 | 0.0* | 2.0 | 2.0 |
| 11 | 1.3 | 1.7 | 1.7 | 0.0* | 1.7 | 1.7 |
| 12 | 0.0 | 2.0 | 2.0 | 1.7 | 2.0 | 2.0 |

*Table 22: Mean score assigned by the 3 reviewers for each of the cranial sutures on the 12 "Black Bone" datasets. (Cases of synostosis are shown with *).*

### 4.6.3 Discussion

The findings on "Black Bone" correlated with CT in all patients with craniosynostosis. Independent blinded review demonstrated that "Black Bone" was accurate in the distinction between normal and prematurely fused sutures. Inaccuracies arose mainly where the sequence did not truly represent "Black Bone." In the children who were imaged in OMRI where the "Black Bone" sequence is well-established, the cranial sutures could clearly be distinguished from those which were prematurely fused (in all cases, this was sagittal synostosis). All of these children were older, and were imaged without the need for general anaesthesia. As has been the case when imaging older patients with normal sutures, the surrounding cranial bone appeared more densely black.

The main difficulty associated with this phase of the study was the transfer of the "Black Bone" sequence to the WW since Philips scanners require the user to consider the output rather than the input parameters as with GE. It was not possible to optimise the sequence prior to commencing the

study in infants due to unavailability of the scanner. In view of the need for GA it was important to minimise the imaging time to reduce any potential associated risks. This limited the opportunities for sequence manipulation in each child with the optimal parameters being identified after imaging had been acquired in multiple patients. It was not possible to fully eliminate the chemical shift artefact, despite discussion with the Philips applications team, and this provides further scope for investigation.

In the one infant imaged at the CH on a 3T magnet, there was considerable movement artefact which made cranial suture identification particularly challenging. This was made more difficult by the very thin bone, as a result of the young age of the infant, and the syndromic diagnosis of Apert syndrome.

With a small number of available datasets of sufficient quality to permit independent review, it was not possible to provide datasets on which the assessors could become familiar with the identification of the cranial sutures on the "Black Bone" sequence. Whilst two of the assessors are not actively involved in the assessment of the cranial sutures in their normal roles, all had been involved in previous review of the routine MRI sequences, and were therefore familiar with the course of the sutures. The sagittal suture can be difficult to distinguish from the sagittal sinus, particularly when this suture is absent. This resulted in some difficulty in a small number of cases of sagittal synostosis on blinded review. In most cases, the diagnosis assigned was correct, and in all cases by the neuroradiologist. In the majority of cases, the cranial sutures were identified with confidence, and the "Black Bone" sequence was therefore far superior to the routine MRI sequences reviewed.

Overall, the "Black Bone" sequence appears useful in the identification of cranial sutures and appears accurate in the diagnosis of craniosynostosis. The main limitation appears to be syndromic cases, particularly in young infants where the cranial bone is very thin. However, further datasets from syndromic patients are required to fully explore the limitations of the sequence. The clear visualisation of the cranial sutures provided the opportunity to obtain width measurements, explored in the next section.

## 4.7 Cranial Suture Widths on "Black Bone"

As has previously been noted the assessment of cranial suture widths may provide further information regarding abnormal potential. To quantitatively compare the appearance of the cranial sutures on "Black Bone," with routine MRI sequences and CT this section explores the measurements of cranial sutures on "Black Bone."

### 4.7.1 Materials and Methods

Utilising two of the "Black Bone" datasets from infants with normal cranial sutures (Patient 1 & 3), the imaging was reviewed on an AWW. Each image was magnified on screen, and measurements were completed with the integral measuring device perpendicular to the path of the suture. This was completed on every imaging slice on which the suture could be identified. As imaging had been acquired in the axial plane, and the extent of the lambdoid sutures was not always clear, only the sagittal and coronal sutures were studied. Measurements were obtained for two sites on the suture – anterior and posterior for the sagittal suture, and right and left for the coronal suture, with two measurements completed for each. Measurements were subsequently combined to obtain mean sutural widths for the two cranial sutures.

### 4.7.2 Results

The mean sutural width measurements for Patient 1 and 3 are shown in *Table 23*. The overall mean width for the sagittal suture was 1.02±0.18mm and for the coronal suture 0.99±0.21mm.

| | Sagittal | | Coronal | |
|---|---|---|---|---|
| **Patient** | Anterior | Posterior | Right | Left |
| **1** | 0.93±0.13 | 0.93±0.14 | 0.98±0.23 | 0.88±0.17 |
| **3** | 1.09±0.14 | 1.05±0.19 | 0.98±0.19 | 1.13±0.16 |
| **Overall** | 1.03±0.16 | 1.02±0.19 | 0.98±0.21 | 0.99±0.21 |

*Table 23: Mean±SD cranial suture widths on "Black Bone."*

### 4.7.3 Discussion

Only two "Black Bone" datasets were suitable for cranial suture width measurement in view of artefact in one case, and a history of neurosurgery in the second case having potential impact upon the cranial sutures. Datasets from patients with craniosynostosis were not deemed suitable for cranial suture width measurements, as overgrowth at the patent sutures may impact upon their width. Despite measurements being made in only two children, the results were comparable to findings on CT in the literature, and the findings on routine MRI sequences. Further work is necessary to validate these findings in a larger patient group; however, this work demonstrates the feasibility of such measurements on "Black Bone."

## Chapter Conclusion

The appearance of cranial sutures on routine MRI sequences is frequently as an area of signal void which can be difficult to confidently identify from surrounding structures. With "Black Bone" MRI the sutures appear as areas of increased signal, clearly distinguishing them from the cranial bone. The sequence accurately differentiates the normal suture from the prematurely fused, demonstrating considerable clinical potential as an alternative to CT.

# 5. Adolescents

# 5.0 Adolescents

In adolescents with facial disproportion the ability to perform accurate cephalometric analysis with "Black Bone" images would offer a non-ionising alternative to conventional plain radiographs. The combined distance and angle measurements which make up standard cephalometry provide a further method to critically assess the accuracy of the "Black Bone" sequence. The utilisation of the entire 3D "Black Bone" dataset could provide a method of assessing the skeletal and dental relationships in three-dimensions, thereby enhancing surgical planning.

This aspect of the thesis is subdivided into two phases:

1. Two dimensional cephalometric analysis
2. Development of three-dimensional cephalometry techniques

## 5.1 Two Dimensional Cephalometric Analysis

Prior to developing methods of 3D cephalometry with "Black Bone," it was necessary to confirm the two-dimensional accuracy of the technique. The "gold standard" in conventional cephalometrics is the lateral cephalogram, which incorporates a measuring device for standardisation of measurements. The lateral cephalogram was therefore utilised as the comparator for this aspect of the study. Comparison was also made with T1 and T2 weighted images, having demonstrated some potential in cephalometry in previous studies.[164]

### 5.1.1 Materials & Methods

#### 5.1.1.1 Adult Volunteers

Initial investigation was completed with three adult volunteers who had lateral cephalograms available on PACs. All volunteers were members of Oxford University Hospital (OUH) staff freely providing consent for MRI. Imaging was completed at CH on a 1.5T magnet. Sagittal T1, T2 and "Black Bone" images were obtained ensuring that the alignment for image acquisition would pass precisely through the mid-sagittal structures to permit comparison with the lateral radiographs. Methods to incorporate a measuring device onto the "Black Bone" datasets in a similar fashion to

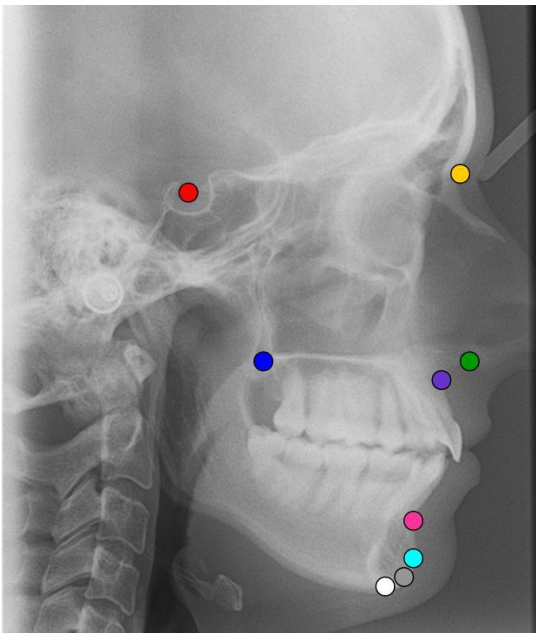
those used on lateral cephalograms was investigated; this included placing fluid filled capsules a known distance apart and using a ruler with gadolinium filled capillary tubes placed at one centimetre intervals within the FOV. Investigation with these measuring devices was completed at OMRI on both a 1.5T and 3.0T magnet with one of the volunteers (KE). The three volunteers provided "Black Bone" datasets from healthy adults without history of orthognathic surgery. However, in one case, orthodontic treatment had been completed between the period of the radiograph being completed and recruitment for MRI, with impact upon dental based cephalometric measurements.

#### 5.1.1.2 Patients with Facial Disproportion

Following preliminary investigation with the volunteer group, datasets from patients with facial disproportion were required. Ethical approval was granted from the Berkshire Research Ethics Committee to recruit patients over the age of 14 years undergoing routine orthodontic treatment and/or prior to orthognathic surgery in whom lateral cephalograms were required as part of routine management, for MRI examination. Suitable patients were identified by combined review of orthodontic clinic lists and sequential date review of PACs for patients having undergone recent lateral cephalogram. Patients who had previously undergone surgery, had completed orthodontic treatment or had fixed orthodontic appliances were excluded. Patients were contacted by telephone to discuss the study, confirm their suitability for MRI and potential availability. For those patients demonstrating an initial willingness to participate, an information sheet *(Appendix E)* was provided. Patients were subsequently contacted again by telephone to answer any further questions, and to ascertain preliminary consent to participate in the study. Formal written consent was obtained prior to imaging. In total, 6 patients agreed to participate in the study, however, one failed to attend their allocated MRI session, resulting in 5 datasets. Imaging in the first two cases was completed at the CH on a 1.5T magnet, and the remaining patients were imaged at OMRI also on a 1.5T magnet. Sagittal "Black Bone" imaging was obtained in all patients, and where possible, axial "Black Bone," coronal "Black Bone," Sagittal T1 and Sagittal T1 sequences were also acquired. Patients were asked to bite on their molar teeth to maintain their normal dental occlusion which would enhance alignment of the "Black Bone" and lateral cephalogram images.

### 5.1.1.3 Cephalometric Landmarks

Many of the landmarks utilised in standard cephalometry are those which arise from projection of overlying bony anatomy, rather than representing true anatomical points in the midline. It was therefore necessary to identify the true mid-sagittal landmarks, which were identifiable on both mid-sagittal MRI and lateral cephalogram. In total 17 measurements – 6 angles and 11 distances, representing a combination of aspects of Steiner, Bell and Burstone cephalometric analyses were deemed suitable for analysis *(Figure 55, Table 24).*[190-194]



- ***Sella*** *– Centre of the pituitary fossa of the sphenoid bone*
- ***Nasion*** *– Intersection of the internasal suture with the nasofrontal suture in the midsagittal plane*
- ***ANS*** *– The tip of the anterior nasal spine*
- ***PNS*** *– Tip of the posterior nasal spine*
- ***A Point*** *– Deepest point of the curve of the maxilla, between anterior nasal spine (ANS) and the dental alveolus*
- ***B Point*** *- Most posterior point in the concavity along the anterior border of the symphysis*
- ***Pogonion*** *- Most anterior point on the mid-sagittal symphysis*
- ***Menton*** *– Most inferior point of the symphysis*
- ***Gonion*** *– Midpoint between Pogonion and Menton*

*Figure 55: Cephalometric points used for analysis of lateral cephalogram and "Black Bone" datasets.*

| Angles | Distance |
|---|---|
| SNA | S-N |
| SNB | S-PNS |
| ANB | S-ANS |
| Interincisal Angle | S-Gn |
| 1-NA Angle | Me-ANS |
| 1-NB Angle | N-A |
| | N-B |
| | N-Pog |
| | 1-NA |
| | 1-NB |
| | PNS-ANS |

*Table 24: Distance and angle measurements used for cephalometric analysis; S=Sella; N=Nasion; A=A point; B=B point; 1=Incisor; ANS=Anterior nasal spine; PNS=Posterior nasal spine; Gn=Gonion; Me=Menton; Pog=Pogonion.*

#### 5.1.1.4 Cephalometric Analysis - AWW

The lateral cephalogram was imported into an AWW, and the magnification factor determined by measurement of the integral measuring device. This was completed by magnifying the image on screen, and measuring a 10mm distance on the device. This was repeated 10 times and a mean result obtained for each image. This provided the multiplication factor to standardise all subsequent measurements obtained on the plane radiograph. To determine if a similar process was required for the MRI datasets, measurements were completed between the liquid filled capsules and gadolinium filled capillary tubes on the "Black Bone" datasets. Imaging was obtained on both 1.5T and 3.0T magnet with a measuring device within the FOV. The image slice where the measuring device was most clearly seen was selected for measurement. Using the measuring device of a known 10mm distance, measurements were repeated ten times on both the 1.5T and 3.0T "Black Bone" sagittal images on two occasions *(Figure 56).*

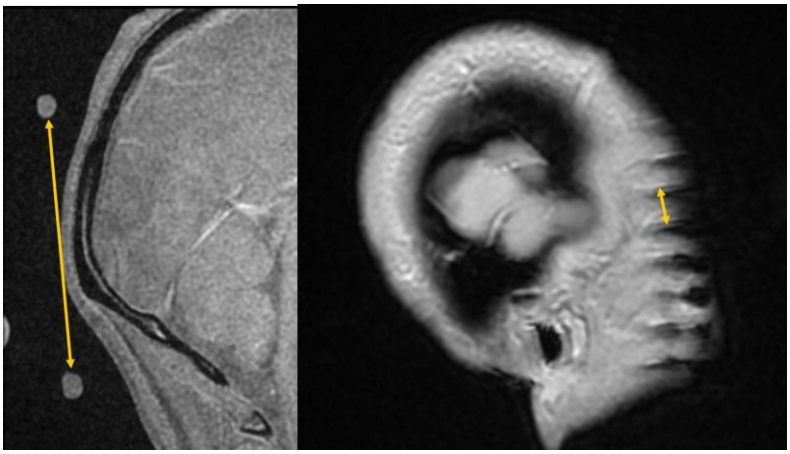


***Figure 56: Measuring device used on sagittal "Black Bone" imaging. Two fluid filled capsules placed 10cm apart (left), and capillary tubes filled with gadolinium placed at 1cm intervals (right).***

For MRI, the sagittal images were reviewed, and the slice corresponding to the mid-sagittal image determined. For both lateral cephalogram and sagittal MRI image, cephalometric analysis was completed in a standardised manner. Images were manipulated on screen so that the image represented a right lateral view *(Figure 57).* The cephalometric points were identified on a magnified view and a marker placed; for the midpoint of the pituitary fossa an oval drawing object was used to correlate with the inferior aspect of fossa, and the centre of the object marker used to

define the centre of the fossa. The distances and angles between these points were each measured 10 times.

For the volunteer datasets, the confidence with which the cephalometric points could be identified was recorded on a ten point scale from 0 (no confidence) to 10 (maximal confidence). A score was recorded for each of the 10 cephalometric points, and these were subsequently combined to provide an overall score for the image. For those datasets where there was little confidence in point identification, a greater variability in measurements would be anticipated making such modality unsuitable for accurate cephalometric analysis. All measurements were entered into Microsoft Excel and analysed using SPSS.

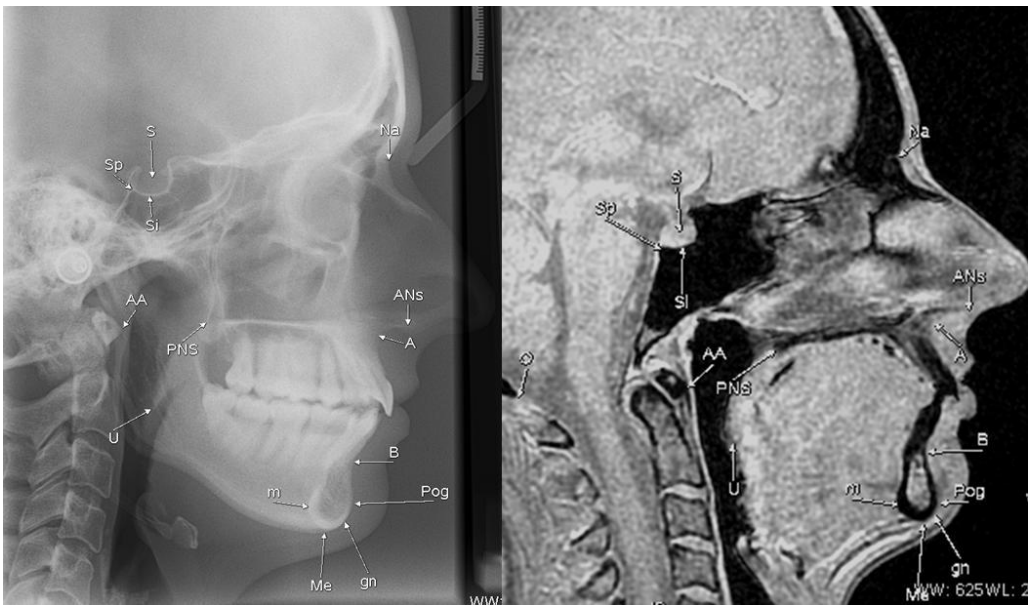



*Figure 57: Lateral cephalogram (left) and mid-sagittal "Black Bone" image (right) with cephalometric landmarks identified.*

#### 5.1.1.5 Cephalometric analysis - Dolphin cephalometric software

Dolphin cephalometric software is a semi-automated program for digitisation of lateral cephalograms. The software was developed for orthodontists to maintain electronic patient records including pre-and post-treatment digitised lateral radiographs for analysis of intervention and outcome. Additional developments, with the increasing use of CT and CBCT have included the ability to create a standard cephalogram from the 3D DICOM data, merge soft-tissue and bone images, and perform airway measurements. An educational research licence for Dolphin was

purchased for the purpose of this aspect of the study. Analysis of lateral cephalograms and sagittal "Black Bone" images was completed in a similar manner to that conducted on the AWW. Since the cephalometric points and measurements utilised did not correspond to a standard cephalometric analysis method, the measurements were identified on Dolphin and combined to produce a new analysis protocol *(Figure 58).* To avoid loss of image quality, the relevant DICOM image was directly imported into Dolphin; for the MRI datasets the same mid-sagittal image used on the AWW was utilised *(Figure 59 & 60).* The software package incorporates a method of calibration prior to point identification. The option to identify two points on the image of a known distance apart was selected. For the lateral cephalogram a 10mm distance on the integral measuring device was utilised. For the MRI images, the known FOV was used by marking the horizontal extremes of the image. This was confirmed as an accurate method with both Clear Canvas and Osirix by adjusting the window level and identifying the extremes of the image, and then measuring the image size. This corresponded to the FOV. Importing the image into Adobe Photoshop, the size of the DICOM image was confirmed in pixels. Further confirmation was provided by the DICOM header. A matrix of 256 by 256 with pixel spacing of 0.9375 corresponded to a FOV of 240mm. Review of imported images in Dolphin demonstrated that the full FOV was included on screen.

The repeatability of the digitisation process was examined by performing each cephalometric analysis ten times. This was performed for "Black Bone" and lateral cephalogram from one patient.

Measurements were automatically calculated from the identified cephalometric points by the software. These were exported to Microsoft Excel and analysed using SPSS. Repeatability was assessed using the coefficient of variation expressed as a percentage (CV=$\frac{SD}{mean}$x100).

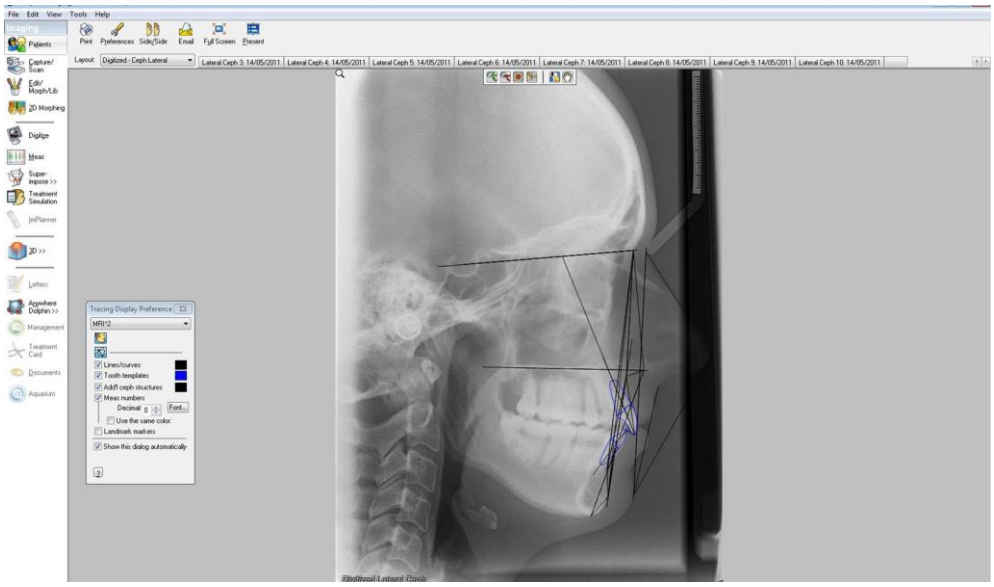


*Figure 58 Dolphin workspace with measurements on lateral cephalogram.*

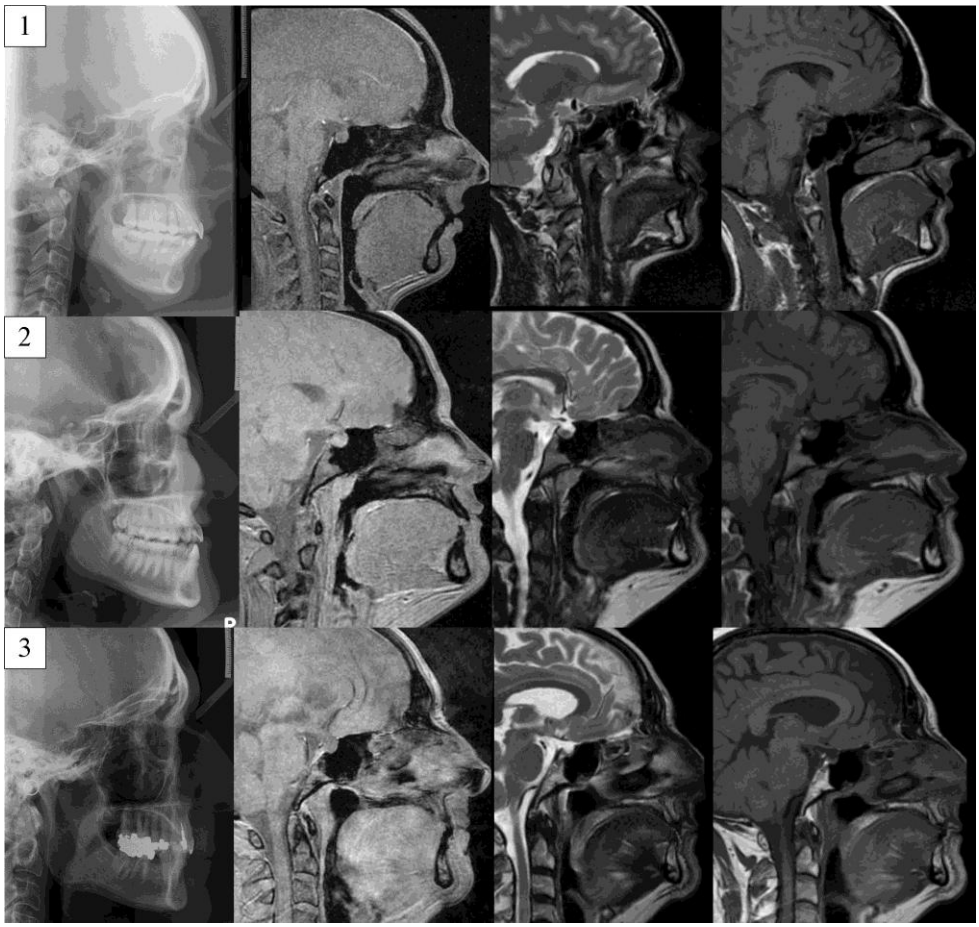



*Figure 59: Lateral cephalogram (left), sagittal "Black Bone" (2nd from left), sagittal T2 weighted (2nd from right), and sagittal T1 weighted MRI images of the three volunteers used for cephalometric analysis.*

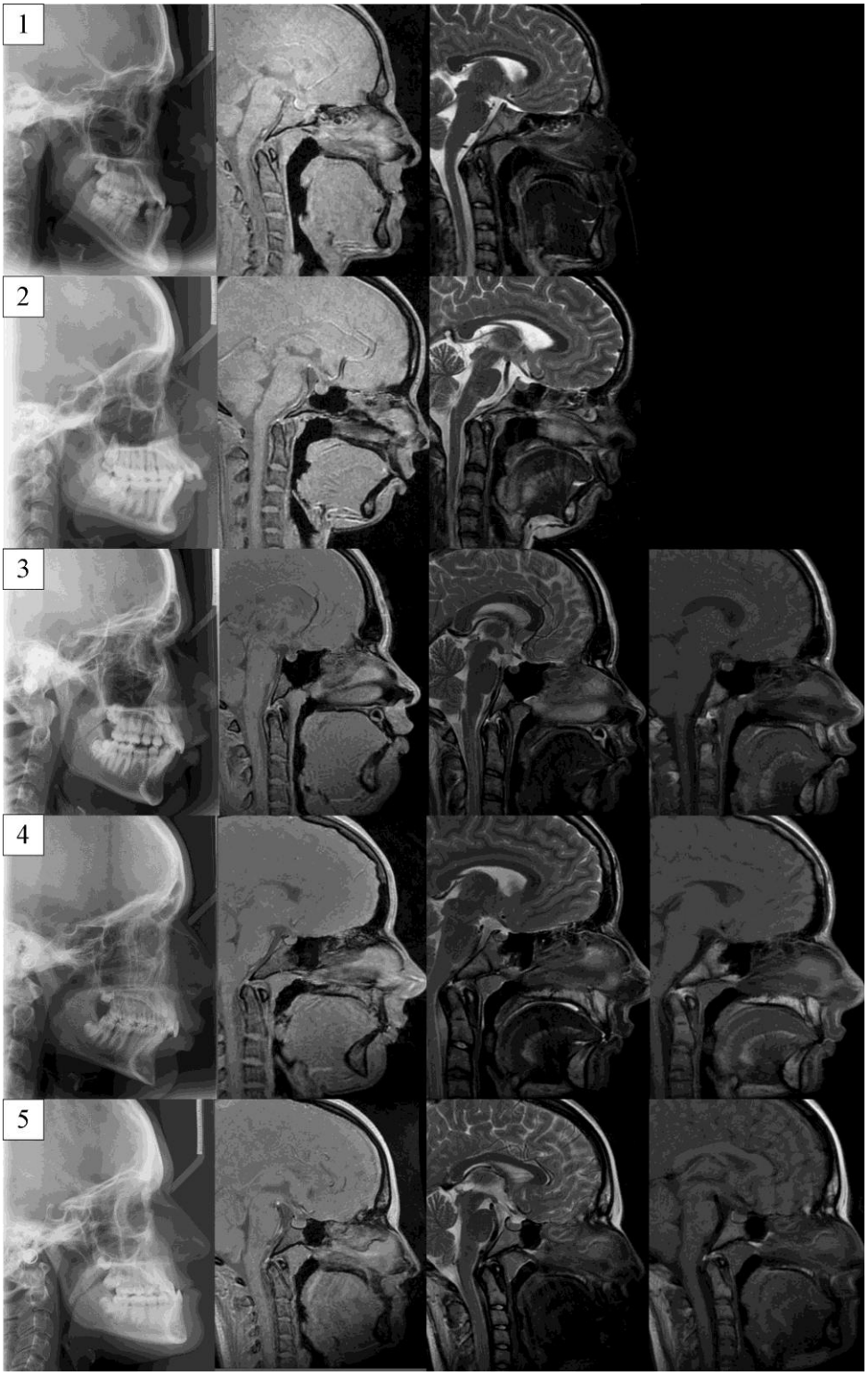



*Figure 60: Lateral cephalogram (left), sagittal "Black Bone" (2nd from left), Sagittal T2 weighted (2nd from right), and sagittal T1 weighted MRI images of the five patients included for cephalometric analysis. Sagittal T1 imaging was not acquired in Patients 1 & 2.*

### 5.1.2 Results

#### 5.1.2.1 Advantage Windows

##### 5.1.2.1.1 Measuring Device

For the 1.5T "Black Bone" dataset the mean measurement for the 10mm device was 10.0±0.4mm with a coefficient of variation of 4.2%; for the 3.0T dataset the mean was 10.2±0.5mm and coefficient of variation 4.4%. There was no significant difference between results for the measuring device on 1.5T and 3.0T datasets (p=0.22, Independent samples t-test). A scaling factor was therefore not required for the "Black Bone" datasets.

##### 5.1.2.1.2 Repeatability - Lateral Cephalogram

For the three volunteers measurements were completed ten times on five separate occasions for each lateral cephalogram. Comparisons were made using the coefficient of variation across the groups. *Table 25* demonstrates that for the angles, those involving the teeth and ANB demonstrated the highest variability. The distance measurements involving the central incisor teeth also demonstrated the highest variability.

| | 1 | | | 2 | | | 3 | | |
|---|---|---|---|---|---|---|---|---|---|
| | Mean | SD | CoV | Mean | SD | CoV | Mean | SD | CoV |
| **Angles** | | | | | | | | | |
| **SNA** | 83.2 | 0.4 | 0.5 | 89.0 | 0.0 | 0.0 | 85.8 | 0.8 | 0.9 |
| **SNB** | 78.8 | 0.4 | 0.5 | 90.8 | 0.4 | 0.5 | 81.8 | 0.8 | 0.9 |
| **ANB** | 4.3 | 0.5 | 10.8 | 1.8 | 0.4 | 22.5 | 4.0 | 0.0 | 0.0 |
| **Interincisal** | 114.0 | 7.2 | 6.3 | 136.4 | 1.4 | 1.0 | 157.2 | 1.6 | 1.0 |
| **1-NA** | 29.6 | 3.9 | 13.2 | 28.4 | 0.8 | 2.9 | 7.6 | 0.5 | 6.5 |
| **1-NB** | 32.2 | 4.6 | 14.2 | 16.4 | 1.4 | 8.4 | 13.0 | 1.4 | 11.0 |
| **Distances** | | | | | | | | | |
| **1-NA** | 3.7 | 0.3 | 7.4 | 5.8 | 0.4 | 6.9 | 1.4 | 0.3 | 24.7 |
| **1-NB** | 5.6 | 0.3 | 4.5 | 0.9 | 0.2 | 24.8 | 2.0 | 0.3 | 14.0 |
| **S-N** | 68.0 | 0.3 | 0.4 | 63.2 | 0.3 | 0.4 | 68.5 | 0.5 | 0.7 |
| **PNS-ANS** | 52.9 | 1.2 | 2.2 | 49.2 | 0.8 | 1.6 | 50.5 | 0.6 | 1.2 |
| **S-ANS** | 84.8 | 1.7 | 2.0 | 79.8 | 0.4 | 0.4 | 87.3 | 0.4 | 0.5 |
| **Me-ANS** | 62.9 | 0.2 | 0.4 | 62.1 | 0.2 | 0.4 | 62.6 | 0.7 | 1.1 |
| **N-Pog** | 99.7 | 0.6 | 0.6 | 98.7 | 0.7 | 0.7 | 105.9 | 1.6 | 1.5 |

***Table 25: Mean, SD and Coefficient of variation results for repeated cephalometric measurements for the 3 volunteers on lateral cephalogram.***

To confirm that these findings were consistent with patients with facial disproportion, the cephalometric measurements were each repeated ten times on five separate occasions for two of the patients *(Table 26).* The coefficient of variation results for these two patients was in keeping with those from the volunteers, and again highlighted the inconsistencies associated with measurements involving the incisor teeth.

| | 1 | | | 2 | | |
|---|---|---|---|---|---|---|
| | Mean | SD | CoV | Mean | SD | CoV |
| **Angles** | | | | | | |
| **SNA** | 80 | 2.3 | 2.9 | 79.4 | 0.8 | 1.0 |
| **SNB** | 75.2 | 1.6 | 2.1 | 87.6 | 0.5 | 0.6 |
| **ANB** | 4.8 | 0.8 | 15.7 | 8.2 | 0.8 | 9.2 |
| **Interincisal** | 111.6 | 1.9 | 1.7 | 136.4 | 4.5 | 3.3 |
| **1-NA** | 36.6 | 2.5 | 6.9 | 32.2 | 3 | 9.4 |
| **1-NB** | 27.2 | 1.5 | 5.5 | 19.6 | 1.4 | 7.0 |
| **Distances** | | | | | | |
| **1-NA** | 10 | 1.6 | 15.9 | 11.5 | 1.4 | 11.8 |
| **1-NB** | 5.7 | 0.3 | 5.8 | 3.5 | 0.4 | 11.5 |
| **S-N** | 62.7 | 1.3 | 2.1 | 67.9 | 1.3 | 1.9 |
| **PNS-ANS** | 41.5 | 0.9 | 2.2 | 46.9 | 2 | 4.3 |
| **S-ANS** | 71.9 | 0.4 | 0.6 | 82.4 | 1.2 | 1.5 |
| **Me-ANS** | 59.5 | 0.3 | 0.5 | 70.8 | 0.4 | 0.6 |
| **N-Pog** | 93.9 | 1.2 | 1.3 | 117.8 | 0.6 | 0.5 |

*Table 26: Mean, SD and Coefficient of variation results for repeated cephalometric measurements for the 2 patients on lateral cephalogram.*

#### 5.1.2.1.3 Repeatability - "Black Bone"

The repeatability of measurements obtained on the mid-sagittal "Black Bone" images for the three volunteers was assessed in the same manner as for the lateral cephalogram. The coefficient of variation results are shown in *Table 27*. This demonstrated similar findings to the lateral cephalogram, with the greatest variability seen for those measurements incorporating the incisor teeth. Overall, the coefficient of variation results was similar for "Black Bone" and lateral cephalogram.

Repeatability was again confirmed on two of the patients with facial disproportion *(Table 28).* Measurements were obtained ten times on five separate occasions for Patient 2 and on ten occasions for Patient 1.

| | 1 | | | 2 | | | 3 | | |
|---|---|---|---|---|---|---|---|---|---|
| | Mean | SD | CoV | Mean | SD | CoV | Mean | SD | CoV |
| **Angles** | | | | | | | | | |
| **SNA** | 83.8 | 1.0 | 1.2 | 91.8 | 0.4 | 0.4 | 84.4 | 0.5 | 0.6 |
| **SNB** | 79.2 | 0.8 | 1.0 | 88.6 | 0.5 | 0.6 | 80.4 | 0.5 | 0.6 |
| **ANB** | 4.8 | 0.4 | 8.4 | 3.2 | 0.4 | 12.6 | 4.0 | 0.0 | 0.0 |
| **Interincisal** | 123.6 | 2.4 | 2.0 | 131.6 | 3.0 | 2.3 | 137.4 | 4.8 | 3.5 |
| **1-NA** | 21.8 | 2.1 | 9.5 | 21.2 | 0.8 | 3.6 | 18.4 | 3.8 | 20.4 |
| **1-NB** | 31.0 | 2.6 | 8.5 | 24.6 | 3.6 | 14.8 | 21.4 | 2.1 | 9.7 |
| **Distances** | | | | | | | | | |
| **1-NA** | 4.6 | 0.6 | 12.3 | 4.7 | 0.3 | 5.8 | 1.3 | 0.3 | 22.2 |
| **1-NB** | 6.6 | 0.9 | 13.1 | 1.2 | 0.3 | 27.5 | 4.3 | 0.6 | 13.5 |
| **S-N** | 70.2 | 0.3 | 0.4 | 56.7 | 0.3 | 0.6 | 67.6 | 0.3 | 0.5 |
| **PNS-ANS** | 56.1 | 3.5 | 6.3 | 48.8 | 2.4 | 4.9 | 57.4 | 0.3 | 0.6 |
| **S-ANS** | 86.3 | 2.2 | 2.6 | 78.8 | 0.3 | 0.4 | 86.8 | 0.5 | 0.5 |
| **Me-ANS** | 64.7 | 0.9 | 1.4 | 60.8 | 0.4 | 0.6 | 63.7 | 0.4 | 0.6 |
| **N-Pog** | 99.9 | 1.4 | 1.4 | 102.6 | 0.7 | 0.7 | 109.1 | 0.7 | 0.7 |

*Table 27: Mean, SD and Coefficient of variation results for repeated cephalometric measurements for the 3 volunteers on "Black Bone."*

| | 1 | | | 2 | | |
|---|---|---|---|---|---|---|
| | Mean | SD | CoV | Mean | SD | CoV |
| | **Angles** | | | | | |
| **SNA** | 80.5 | 0.5 | 0.6 | 81.4 | 0.5 | 0.6 |
| **SNB** | 75 | 0.6 | 0.8 | 87.8 | 0.4 | 0.5 |
| **ANB** | 5.5 | 0.5 | 9.1 | 6.4 | 0.5 | 7.7 |
| **Interincisal** | 112.6 | 1.8 | 1.6 | 136.8 | 2.5 | 1.8 |
| **1-NA** | 36.6 | 1.8 | 4.9 | 31.8 | 1.2 | 3.7 |
| **1-NB** | 25.9 | 1.6 | 6.4 | 19.2 | 2.3 | 12.2 |
| | **Distances** | | | | | |
| **1-NA** | 11 | 0.4 | 3.9 | 9.8 | 1.0 | 9.8 |
| **1-NB** | 7.7 | 0.4 | 4.9 | 4.5 | 0.6 | 13.3 |
| **S-N** | 64.3 | 0.3 | 0.4 | 68.0 | 0.4 | 0.6 |
| **PNS-ANS** | 51 | 0.8 | 1.6 | 52.5 | 2.1 | 4.1 |
| **S-ANS** | 75 | 0.4 | 0.5 | 86.5 | 2.1 | 2.5 |
| **Me-ANS** | 59.2 | 0.4 | 0.7 | 68.9 | 0.4 | 0.6 |
| **N-Pog** | 92.9 | 1.2 | 1.3 | 117.5 | 1.4 | 1.2 |

*Table 28: Mean, SD and Coefficient of variation results for repeated cephalometric measurements for 2 patients on "Black Bone."*

#### 5.1.2.1.4 Repeatability - T1

The repeatability of measurements obtained on the volunteer T1 datasets was assessed in a similar manner *(Table 29).* For the majority of measurements T1 imaging demonstrated a higher coefficient of variation than "Black Bone" or the lateral cephalogram.

| | 1 | | | 2 | | | 3 | | |
|---|---|---|---|---|---|---|---|---|---|
| | Mean | SD | CoV | Mean | SD | CoV | Mean | SD | CoV |
| | **Angles** | | | | | | | | |
| **SNA** | 83.4 | 2.4 | 2.9 | 93.0 | 0.0 | 0.0 | 90.0 | 0.8 | 0.9 |
| **SNB** | 80.3 | 1.1 | 1.4 | 90.3 | 0.5 | 0.5 | 84.7 | 1.0 | 1.1 |
| **ANB** | 4.2 | 1.8 | 44.5 | 2.7 | 0.5 | 18.0 | 5.3 | 0.5 | 9.0 |
| **Interincisal** | 121.7 | 5.4 | 4.4 | 128.7 | 2.5 | 2.0 | 142.7 | 1.3 | 0.9 |
| **1-NA** | 29.3 | 3.8 | 12.8 | 24.7 | 1.7 | 7.0 | 9.7 | 0.5 | 5.0 |
| **1-NB** | 26.7 | 6.0 | 22.3 | 24.3 | 2.5 | 10.4 | 24.0 | 1.7 | 6.9 |
| | **Distances** | | | | | | | | |
| **1-NA** | 7.9 | 5.0 | 62.4 | 3.2 | 0.6 | 18.5 | 1.4 | 0.4 | 31.4 |
| **1-NB** | 6.1 | 0.6 | 9.7 | 2.2 | 0.7 | 33.1 | 3.0 | 0.3 | 10.5 |
| **S-N** | 69.7 | 2.0 | 2.8 | 59.1 | 0.5 | 0.8 | 65.5 | 0.2 | 0.3 |
| **PNS-ANS** | 56.6 | 3.8 | 6.8 | 48.6 | 1.5 | 3.1 | 49.7 | 1.9 | 3.9 |
| **S-ANS** | 87.0 | 3.3 | 3.8 | 80.3 | 1.0 | 1.2 | 86.9 | 0.5 | 0.6 |
| **Me-ANS** | 66.1 | 1.5 | 2.2 | 61.6 | 0.6 | 0.9 | 65.0 | 0.4 | 0.6 |
| **N-Pog** | 98.6 | 1.4 | 1.4 | 100.4 | 0.3 | 0.3 | 106.6 | 0.3 | 0.3 |

*Table 29: Mean, SD and Coefficient of variation results for repeated cephalometric measurements for the 3 volunteers on T1 MRI.*

It was apparent that the variability encountered in the measurements on all images examined was the result of a combination in factors. To explore if uncertainty regarding the location of the cephalometric landmarks was a major contributing factor, the confidence scores applied during the measuring process were analysed.

#### 5.1.2.1.5 Confidence of Point Selection

Utilising a scoring system of 1 to 10 for each of the nine bony landmarks, a mean result was obtained for each imaging modality *(Table 30).* It was apparent that there was greater difficulty in identifying landmarks on T1 and T2 imaging, with lower confidence scores. In addition, it was noted that whilst the lateral cephalogram was considered the "gold standard," there were some landmarks that were particularly challenging to identify, such as the PNS in cases of partially erupted wisdom teeth.

Overall, the confidence of cephalometric point identification on "Black Bone" was comparable to the lateral cephalogram.

The poor reliability of dental measurements identified in work to this point led to the decision to exclude these measurements from subsequent analysis, and to incorporate some additional distance measurements to compare MRI and lateral cephalogram images.

| | T1 | T2 | BB | Lat ceph |
|---|---|---|---|---|
| **S** | 7.4±0.9 | 6.3±2.3 | 8.6±0.5 | 8.3±1.0 |
| **N** | 4.1±2.7 | 1.6±2.2 | 6.7±2.8 | 6.8±2.2 |
| **A** | 3.6±2.5 | 1.3±1.8 | 7.4±0.7 | 6.5±1.7 |
| **B** | 6.9±1.6 | 6.4±0.9 | 8.2±0.4 | 8.3±0.5 |
| **PNS** | 2.4±2.2 | 0.0±0.0 | 6.1±1.4 | 5.0±2.7 |
| **ANS** | 2.4±2.2 | 0.4±0.7 | 6.9±0.8 | 4.5±2.6 |
| **Gn** | 6.8±0.7 | 6.5±1.3 | 8.2±0.8 | 8.5±0.6 |
| **Pog** | 7.6±0.7 | 7.0±0.9 | 8.7±0.5 | 8.8±0.5 |
| **Me** | 7.6±0.7 | 7.4±0.7 | 8.7±0.5 | 8.8±0.5 |
| **S** | 7.4±0.9 | 36.8±2.6 | 8.6±0.5 | 8.3±1.0 |
| **Overall score** | 48.8±9.9 | 36.8±2.6 | 69.4±5.3 | 65.3±8.7 |

*Table 30: Mean±SD confidence scores for cephalometric point identification on T1, T2, "Black Bone" and lateral cephalogram.*

#### 5.1.2.1.6 Comparison between Lateral Cephalogram and "Black Bone" - Volunteers

Exploration of the data revealed that the majority of measurements were not normally distributed, therefore non-parametric tests including an independent samples Mann Whitney U test were used to identify significant differences in measurements obtained on lateral cephalogram and "Black Bone." In volunteer 1, all measurements except N-Pog were significantly different; for volunteer 2 all but PNS-ANS were significant, and in volunteer 3, all but ANB angle, NA-1 and N-A were significant.

To determine the extent of discrepancy between measurements obtained from "Black Bone" and the lateral cephalogram, a mean value was calculated for each measurement across all repeated measures for each image type per patient. The difference in mean values between lateral cephalogram and "Black Bone" was calculated for each measurement and subsequently combined to obtain an overall mean for angular and distance measurements *(Table 31)*. The overall discrepancy between "Black Bone" and lateral cephalogram results was 1.2±0.9° for the angles, and 2.1±1.8mm for the distances.

| | 1 | 2 | 3 | mean | SD |
|---|---|---|---|---|---|
| | | | **Angles** | | |
| **SNA** | 0.6 | 2.8 | 1.4 | 1.6 | 1.1 |
| **SNB** | 0.4 | 2.2 | 1.4 | 1.3 | 0.9 |
| **ANB** | 0.5 | 1.4 | 0.0 | 0.6 | 0.7 |
| | | | | 1.2 | 0.9 |
| | | | **Distances** | | |
| **S-N** | 2.2 | 6.5 | 0.8 | 3.2 | 3.0 |
| **PNS-ANS** | 3.2 | 0.4 | 6.9 | 3.5 | 3.3 |
| **S-PNS** | 0.8 | 1.6 | 3.1 | 1.8 | 1.2 |
| **S-ANS** | 1.5 | 1.1 | 0.4 | 1.0 | 0.5 |
| **S-Gn** | 2.1 | 3.9 | 0.8 | 2.2 | 1.6 |
| **Me-ANS** | 1.8 | 1.3 | 1.0 | 1.4 | 0.4 |
| **N-A** | 3.2 | 3.3 | 0.6 | 2.4 | 1.5 |
| **N-B** | 2.5 | 1.0 | 0.2 | 1.2 | 1.2 |
| **N-Pog** | 0.2 | 3.9 | 3.2 | 2.4 | 2.0 |
| | | | | 2.1 | 1.8 |

*Table 31: Mean & SD results for discrepancy between lateral cephalogram and "Black Bone" angles and distance measurements for the three volunteers.*

#### 5.1.2.1.7 Comparison between Lateral Cephalogram and "Black Bone" - Patients

Comparisons between measurements on lateral cephalogram and "Black Bone" images were made in the same manner as for the volunteers *(Table 32)*. A Mann Whitney U test identified no significant difference between lateral cephalogram and "Black Bone" for S-N, N-Pog, and N-B in Patient 1, SNB angle and N-B in Patient 2, ANB angle in patient 4, and SNB angle and S-N in patient 5. All other measurements were significantly different.

The overall discrepancy was 1.5±1.6° for the angles, and 3.0±2.9mm for the distances. The greatest discrepancy occurred with the measurement between PNS and ANS, most likely as a result of difficulty in confidently identifying the PNS.

| | 1 | 2 | 3 | 4 | 5 | Mean | SD |
|---|---|---|---|---|---|---|---|
| | | | **Angles** | | | | |
| **SNA** | 2.0 | 0.5 | 5.6 | 2.6 | 0.7 | 2.3 | 2.1 |
| **SNB** | 0.2 | 0.2 | 3.7 | 2.6 | 0.0 | 1.3 | 1.7 |
| **ANB** | 1.8 | 0.7 | 1.7 | 0.0 | 0.9 | 1.0 | 0.7 |
| | | | | | | 1.5 | 1.6 |
| | | | **Distances** | | | | |
| **S-N** | 0.1 | 1.7 | 0.6 | 1.2 | 0.2 | 0.7 | 0.7 |
| **PNS-ANS** | 5.6 | 9.5 | 5.0 | 8.4 | 2.1 | 6.1 | 2.9 |
| **S-PNS** | 1.9 | 6.7 | 2.5 | 3.4 | 0.6 | 3.0 | 2.3 |
| **S-ANS** | 4.1 | 3.1 | 0.8 | 1.8 | 1.7 | 2.3 | 1.3 |
| **S-Gn** | 0.7 | 9.3 | 4.6 | 4.6 | 0.2 | 3.9 | 3.7 |
| **Me-ANS** | 2.0 | 0.3 | 5.6 | 5.0 | 0.5 | 2.7 | 2.5 |
| **N-A** | 0.8 | 2.6 | 0.3 | 4.1 | 2.8 | 2.1 | 1.6 |
| **N-B** | 0.3 | 0.3 | 10.4 | 1.1 | 1.6 | 2.7 | 4.3 |
| **N-Pog** | 0.4 | 1.0 | 9.1 | 1.8 | 4.4 | 3.3 | 3.6 |
| | | | | | | 3.0 | 2.9 |

*Table 32: Mean & SD results for discrepancy between lateral cephalogram and "Black Bone" angles and distance measurements for the five patients.*

One of the contributing factors to the discrepancy seen between "Black Bone" and lateral cephalogram was the inability to standardise positioning of the patient between MRI and lateral cephalogram – one being performed with the patient upright and the other when supine. This is demonstrated in *Figure 61* where the two images have been superimposed, and the differences in the soft tissues are particularly noticeable.

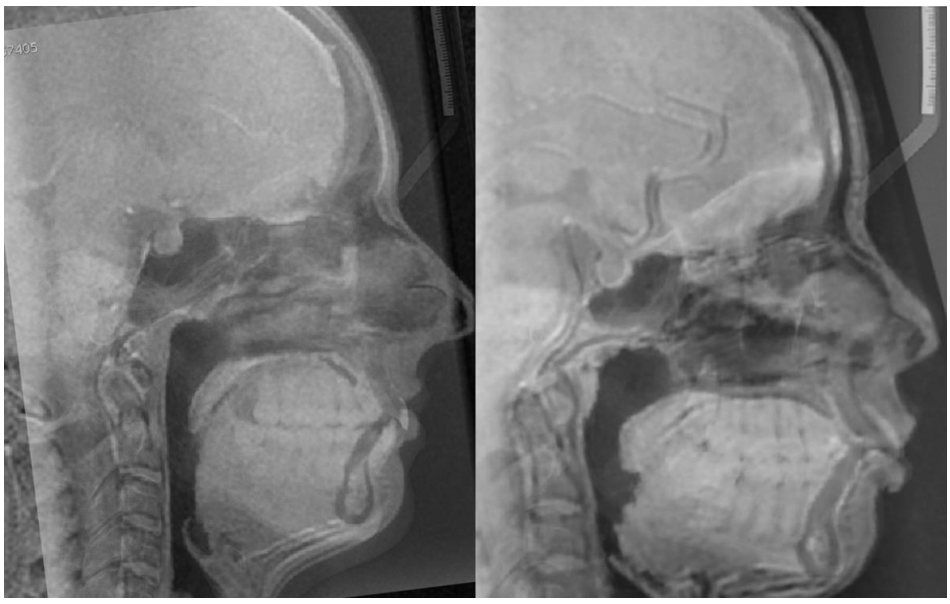


*Figure 61: Superimposed images of "Black Bone" and lateral cephalogram in a volunteer and patient to demonstrate the discrepancies caused by inability to standardise patient position.*

Overall, it was noted that the level of discrepancy between "Black Bone" and lateral cephalogram was within an acceptable range in cases where the cephalometric points were confidently identified. However, inaccuracy was compounded by error associated with measurement between the identified points; Dolphin Cephalometric software was considered to offer a potential solution.

#### 5.1.2.2 Dolphin Cephalometric Software

To ensure familiarity with the software, digitisation was completed on 50 occasions prior to completing any formal measurements. This provided the opportunity to review the workflow, and enhance accuracy in cephalometric point identification on the software.

##### 5.1.2.2.1 Repeatability

The repeatability of cephalometric point identification was assessed on Dolphin for lateral cephalogram, sagittal "Black Bone," and sagittal T1 imaging from one of the volunteers. Digitisation was completed on ten occasions for each image. The repeatability was assessed using the coefficient of variation based upon the co-ordinates of each landmark from the sella, with alignment along a line between the sella and nasion, using the first digitisation as the reference trace to which the remaining 9 digitisations were compared. In addition, comparison was made between the resultant cephalometric measurements.

###### Lateral Cephalogram

The co-efficient of variation demonstrated a wide range of results for the repeated digitisations of the lateral cephalogram *(Table 33).* This is demonstrated graphically in *Figure 62*, in which all 10 tracings have been combined, with alignment along the line between sella and nasion, at the sella. For the distances the greatest variability was in the measurements associated with the central incisor teeth. This was also the case for the angular measurements, however, the greatest variability was seen with ANB. In terms of the bony landmarks *(Table 34)* the coefficient of variation for the direct distance between landmark and sella varied between 31-68%. These results highlight the inherent inaccuracies in point identification on the lateral cephalogram, and provide a bench mark on which to compare "Black Bone."

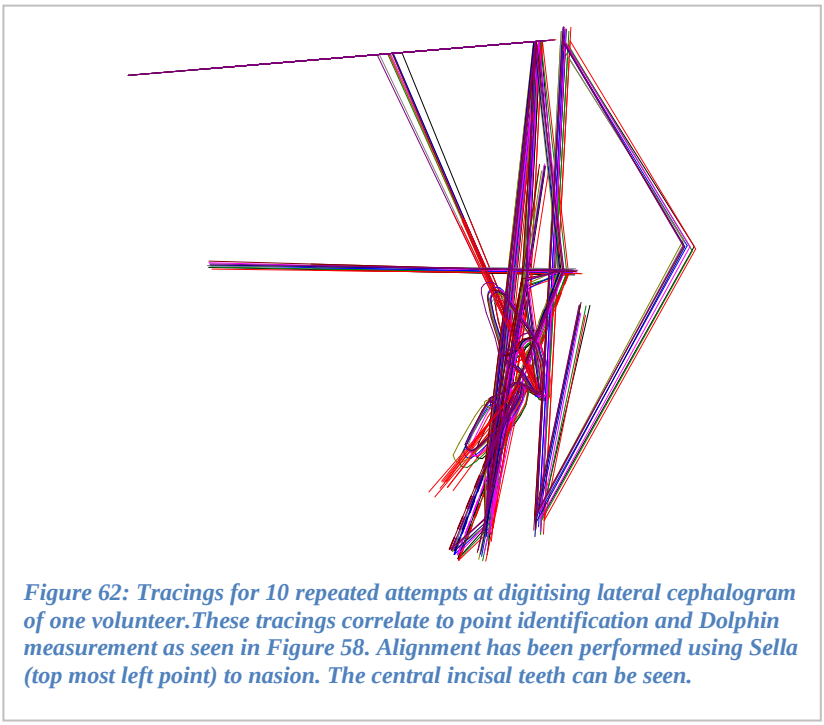


*Figure 62: Tracings for 10 repeated attempts at digitising lateral cephalogram of one volunteer.These tracings correlate to point identification and Dolphin measurement as seen in Figure 58. Alignment has been performed using Sella (top most left point) to nasion. The central incisal teeth can be seen.*

| | Lateral Ceph | | | "Black Bone" | | | T1 | | |
|---|---|---|---|---|---|---|---|---|---|
| | Mean | SD | CoVar | Mean | SD | CoV | Mean | SD | CoVar |
| **Angles (°)** | | | | | | | | | |
| **SNA** | 82.45 | 0.72 | 0.88 | 82.22 | 0.88 | 1.06 | 75.39 | 2.35 | 3.12 |
| **SNB** | 78.69 | 0.25 | 0.32 | 77.66 | 0.63 | 0.81 | 79.53 | 0.90 | 1.13 |
| **ANB** | 3.74 | 0.55 | 14.76 | 4.54 | 0.38 | 8.32 | -4.15 | 1.99 | -47.91 |
| **Interincisal** | 117.75 | 2.08 | 1.77 | 123.33 | 2.38 | 1.93 | 116.19 | 3.01 | 2.59 |
| **1 - NA** | 26.72 | 1.06 | 3.98 | 22.28 | 1.69 | 7.59 | 32.35 | 2.69 | 8.30 |
| **1 - NB** | 31.80 | 1.74 | 5.47 | 29.83 | 1.47 | 4.94 | 35.59 | 2.57 | 7.22 |
| **Distances (mm)** | | | | | | | | | |
| **S-N** | 69.42 | 0.66 | 0.95 | 70.19 | 0.33 | 0.47 | 69.95 | 0.46 | 0.66 |
| **S - ANS** | 85.93 | 0.71 | 0.82 | 88.20 | 0.39 | 0.44 | 78.13 | 2.68 | 3.42 |
| **ANS - Me** | 63.78 | 0.45 | 0.71 | 65.12 | 0.36 | 0.55 | 63.31 | 0.54 | 0.85 |
| **N - Pog** | 100.44 | 0.88 | 0.88 | 94.62 | 1.75 | 1.85 | 96.86 | 1.05 | 1.09 |
| **U1 - NA** | 4.41 | 0.75 | 17.02 | 4.27 | 0.68 | 15.81 | 15.95 | 2.41 | 15.10 |
| **L1 - NB** | 5.28 | 0.34 | 6.49 | 7.37 | 0.67 | 9.05 | 8.41 | 0.48 | 5.70 |
| **ANS - PNS** | 52.99 | 0.54 | 1.02 | 60.15 | 2.22 | 3.70 | 44.23 | 3.65 | 8.24 |

*Table 33: Mean, SD and Coefficient of variation (%) results for repeated digitisation attempts on lateral cephalogram, sagittal "Black Bone" and sagittal T1 MRI.*

| | Dx (mm) | | | Dy (mm) | | | Direct Distance (mm) | | |
|---|---|---|---|---|---|---|---|---|---|
| | Mean | SD | CoV | Mean | SD | CoV | Mean | SD | CoV |
| **A Point** | 0.54 | 0.37 | 68.18 | 0.89 | 0.62 | 69.91 | 1.20 | 0.38 | 31.46 |
| **ANS** | 0.63 | 0.47 | 74.48 | 0.73 | 0.37 | 50.10 | 1.08 | 0.29 | 26.56 |
| **B Point** | 0.47 | 0.39 | 82.99 | 1.07 | 0.85 | 79.55 | 1.22 | 0.83 | 68.18 |
| **Menton** | 0.82 | 0.59 | 71.90 | 1.27 | 0.74 | 58.42 | 1.53 | 0.89 | 58.24 |
| **Nasion** | 0.83 | 0.55 | 65.45 | 0.06 | 0.05 | 94.87 | 0.83 | 0.55 | 65.45 |
| **PNS** | 0.27 | 0.21 | 77.31 | 0.60 | 0.34 | 57.13 | 0.71 | 0.25 | 34.76 |
| **Pogonion** | 0.71 | 0.45 | 62.67 | 0.74 | 0.51 | 68.53 | 1.19 | 0.41 | 34.79 |
| **Overall** | 0.61 | 0.47 | 76.14 | 0.77 | 0.64 | 83.60 | 1.11 | 0.60 | 53.63 |

*Table 34: Difference in x and y co-ordinates and direct distance between the reference lateral cephalogram (1st digitisation) and each of nine digitisations of the same image.*

### "Black Bone"

The "Black Bone" image used for repeated digitisation is shown in *Figure 63*, with the cephalometric landmarks identified manually shown in red, and the subsequent tracing completed by the software package to provide the required cephalometric measurements.

The co-efficient of variation was calculated as a measure of repeatability for the repeated measures across the ten digitisations of the "Black Bone" sagittal images *(Table 33)*. The effects of each digitisation are shown graphically in *Figure 64* in terms of the tracings performed between the cephalometric points.

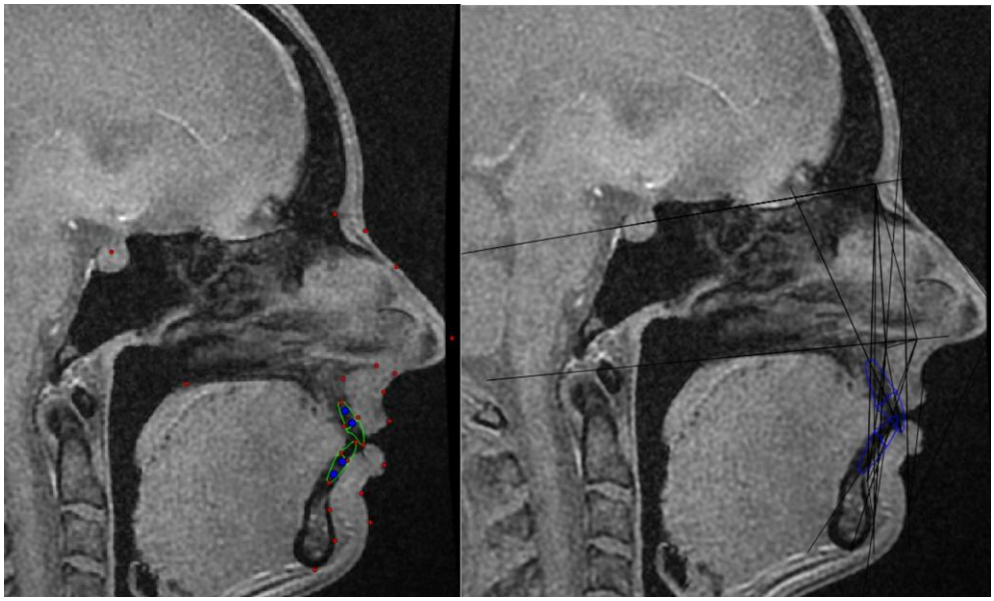


***Figure 63: Digitisation of mid-sagittal "Black Bone" image (left) and subsequent tracing (right) in Dolphin cephalometric software.***

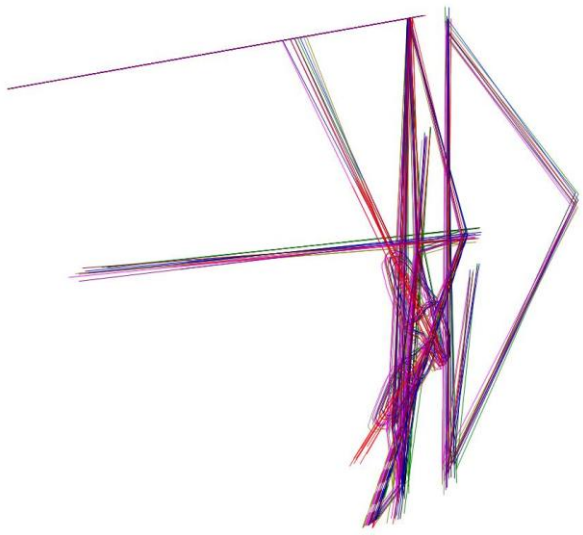


***Figure 64: Tracing of mid-sagittal "Black Bone" images on ten occasions using Dolphin cephalometric software. The line from sella to nasion, at the sella was used as the reference point for alignment of tracings.***

The reference point used for both the calculations and diagrams was the sella along the line from sella to nasion. This was selected as the reference point in view of the importance of this landmark in the majority of cephalometric work, despite the inherent discrepancies associated with finding the centre of a circular structure. The greatest variability occurred with the measurements associated with the teeth as a result of the difficulty in clearly identifying the central incisor outline on one sagittal image. In addition to comparing the difference in measurements obtained on each digitisation, the identification of the landmarks were compared in terms of co-ordinates using the first digitisation as the reference *(Appendix E).* This provided results for the change in x and y co-ordinates and the direct distance for each measurement *(Table 35).* Overall the PNS and A point demonstrated the least variability for the bony landmarks, whilst the boundaries of the incisor teeth demonstrated the greatest variability. This would be anticipated in view of the limited tooth outline obtained on one mid-sagittal image. Despite the nasion often being a bony landmark easily identified on "Black Bone" it demonstrated high variability in this investigation. It must be remembered that the sella was used as the reference point, and the variability associated with the identification of this landmark would result in associated secondary variability with the other landmarks. Overall, the variability associated with cephalometric digitisation on "Black Bone" images were comparable to those on lateral cephalogram.

| Landmark | Dx | | | Dy | | | Direct distance | | |
|---|---|---|---|---|---|---|---|---|---|
| | Mean | SD | CoV % | Mean | SD | CoV % | Mean | SD | CoV % |
| **A Point** | 1.1 | 0.5 | 49.2 | 1.9 | 0.9 | 46.3 | 2.2 | 1.0 | 43.9 |
| **ANS** | 0.6 | 0.4 | 66.0 | 1.7 | 0.8 | 46.7 | 1.9 | 0.9 | 47.4 |
| **B Point** | 1.3 | 0.7 | 51.2 | 1.1 | 0.8 | 69.9 | 1.7 | 1.0 | 57.1 |
| **Menton** | 1.3 | 0.9 | 70.2 | 0.9 | 0.5 | 54.1 | 1.6 | 1.0 | 60.2 |
| **Nasion** | 0.3 | 0.2 | 76.3 | 0.0 | 0.1 | 100 | 0.3 | 0.2 | 76.3 |
| **PNS** | 5.3 | 2.0 | 37.4 | 1.5 | 0.8 | 54.2 | 5.6 | 2.1 | 38.0 |
| **Pogonion** | 1.3 | 0.7 | 52.4 | 0.5 | 0.5 | 88.1 | 1.4 | 0.7 | 46.3 |
| **Overall** | 1.6 | 1.8 | 100 | 1.1 | 0.9 | 80.9 | 2.1 | 1.9 | 88.9 |

***Table 35: Mean, SD and Coefficient of variance results for the difference in x and y co-ordinates and direct distance for each of the cephalometric points compared to the first digitisation, with alignment at sella.***

### T1 MRI

Digitisation was attempted on a sagittal T1 weighted MRI image, and as shown graphically in *Figure 65* greater variability in cephalometric point selection on repeated attempts was noted. This was confirmed with higher coefficient of variation for the distance and angle measurements *(Table 33)*, when compared to both lateral cephalogram and "Black Bone." However, this was not the case for all landmarks *(Table 36).*

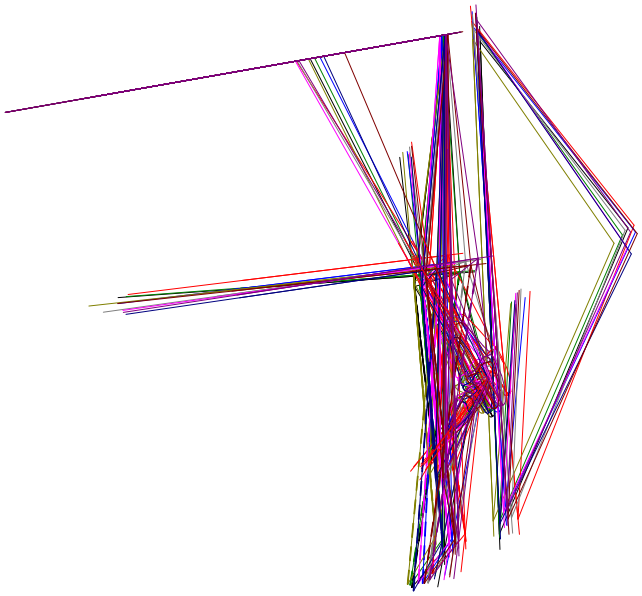


*Figure 65: Repeated digitisations for T1 images. Tracing performed using mid-sagittal images using Dolphin cephalometric software. The line from sella to nasion, at the sella was used as the reference point for alignment of tracings.*

| | Dx | | | Dy | | | Direct distance | | |
|---|---|---|---|---|---|---|---|---|---|
| **Landmark** | Mean | SD | CoV % | Mean | SD | CoV % | Mean | SD | CoV % |
| **A Point** | 2.23 | 2.05 | 91.82 | 1.37 | 0.96 | 69.99 | 2.76 | 2.04 | 73.86 |
| **ANS** | 2.93 | 1.58 | 53.93 | 1.71 | 1.04 | 60.55 | 3.56 | 1.50 | 42.17 |
| **B Point** | 1.32 | 0.94 | 71.03 | 1.19 | 0.86 | 72.04 | 1.88 | 1.13 | 59.94 |
| **Menton** | 2.01 | 1.42 | 70.47 | 1.04 | 0.72 | 68.56 | 2.31 | 1.52 | 65.64 |
| **Nasion** | 0.37 | 0.31 | 84.06 | 0.06 | 0.07 | 130.77 | 0.38 | 0.31 | 81.35 |
| **PNS** | 1.74 | 1.78 | 101.99 | 0.94 | 0.63 | 66.57 | 2.10 | 1.76 | 83.60 |
| **Pogonion** | 1.78 | 1.18 | 66.36 | 2.11 | 0.52 | 24.55 | 2.84 | 1.05 | 36.96 |
| **Overall** | 1.77 | 1.55 | 87.35 | 1.20 | 0.93 | 77.49 | 2.26 | 1.64 | 72.78 |

*Table 36: Mean, SD and Coefficient of variance results for the difference in x and y co-ordinates and direct distance for each of the cephalometric points compared to the first digitisation, with alignment at sella.*

#### 5.1.2.2.2 Comparison between MRI and Lateral Cephalogram - Volunteers

The results obtained on "Black Bone" and T1 images were compared to the lateral cephalogram for the three volunteers by calculating the difference in result for each measurement *(Table 37).* A greater discrepancy between MRI and lateral cephalogram measurements was seen for Volunteer 2

compared to Volunteers 1 & 3. Overall the discrepancy between "Black Bone" and lateral cephalogram was 2.1±1.7° for the angles, and 2.8±2.7mm for the distances. A greater discrepancy was seen for T1 results when compared to the lateral cephalogram.

The work with the volunteer group identified that T1 weighted MRI demonstrated a greater degree of inaccuracy when compared to the lateral cephalogram than "Black Bone." This would make T1 MRI unsuitable in the clinical setting for cephalometric analysis, and was therefore excluded from further analysis.

| | "Black Bone"- Lateral Cephalogram | | | | | T1- Lateral Cephalogram | | | | |
|---|---|---|---|---|---|---|---|---|---|---|
| | 1 | 2 | 3 | Mean | SD | 1 | 2 | 3 | Mean | SD |
| | | | | | **Angles** | | | | | |
| **SNA** | 0.50 | 6.80 | 2.00 | 3.10 | 3.29 | 9.60 | 5.80 | 5.60 | 7.00 | 2.25 |
| **SNB** | 0.00 | 3.10 | 2.60 | 1.90 | 1.66 | 0.90 | 2.90 | 3.20 | 2.33 | 1.25 |
| **ANB** | 0.50 | 3.70 | 0.70 | 1.63 | 1.79 | 8.60 | 2.90 | 2.50 | 4.67 | 3.41 |
| **Interincisal** | 1.30 | 1.90 | 1.50 | 1.57 | 0.31 | 5.00 | 5.30 | 7.20 | 5.83 | 1.19 |
| **U1 - NA** | 1.80 | 1.80 | 2.40 | 2.00 | 0.35 | 5.80 | 1.80 | 10.00 | 5.87 | 4.10 |
| **L1 - NB** | 3.70 | 3.60 | 0.30 | 2.53 | 1.93 | 7.90 | 4.20 | 0.40 | 4.17 | 3.75 |
| **Overall** | | | | 2.12 | 1.66 | | | | 4.98 | 2.88 |
| | | | | | **Distances** | | | | | |
| **U1 - NA** | 2.10 | 1.00 | 0.70 | 1.27 | 0.74 | 12.60 | 0.90 | 1.50 | 5.00 | 6.59 |
| **L1 - NB** | 3.00 | 0.10 | 1.90 | 1.67 | 1.46 | 3.60 | 1.20 | 1.10 | 1.97 | 1.42 |
| **S-N** | 0.90 | 4.30 | 0.10 | 1.77 | 2.23 | 2.20 | 1.90 | 2.40 | 2.17 | 0.25 |
| **ANS-PNS** | 4.00 | 8.10 | 9.50 | 7.20 | 2.86 | 8.50 | 1.50 | 1.80 | 3.93 | 3.96 |
| **S - ANS** | 0.80 | 0.00 | 1.60 | 0.80 | 0.80 | 6.80 | 0.10 | 0.90 | 2.60 | 3.66 |
| **ANS-Me** | 0.70 | 1.60 | 1.50 | 1.27 | 0.49 | 1.60 | 1.30 | 1.30 | 1.40 | 0.17 |
| **N- Pog** | 5.10 | 6.00 | 4.80 | 5.30 | 0.62 | 4.50 | 8.30 | 4.80 | 5.87 | 2.11 |
| **Overall** | | | | 2.75 | 2.68 | | | | 3.28 | 3.23 |

*Table 37: Difference & mean±SD, between measurements obtained on lateral cephalogram and "Black Bone" or T1 images.*

#### 5.1.2.2.3 Comparison between "Black Bone" and Lateral Cephalogram - Patients

Comparison between cephalometric measurements obtained on "Black Bone" and the lateral cephalogram were completed in a similar manner to the volunteer group. As shown in *Table 38*, the greatest discrepancies occurred for measurements involving the incisal teeth which have previously been noted to be particularly difficult on a single sagittal "Black Bone" image. Other problems encountered on the patient images were the accurate identification of the PNS, which was obscured on the lateral cephalogram in some patients by unerrupted wisdom teeth.

| | 1 | 2 | 3 | 4 | 5 | Mean | SD |
|---|---|---|---|---|---|---|---|
| | | | **Angles** | | | | |
| **SNA** | 5.0 | 2.4 | 5.4 | 4.1 | 0.2 | 3.42 | 2.14 |
| **SNB** | 2.4 | 1.8 | 5.5 | 1.8 | 1.0 | 2.50 | 1.75 |
| **ANB** | 2.6 | 0.5 | 0.1 | 2.3 | 1.2 | 1.34 | 1.09 |
| **Interincisal** | 0.3 | 10.7 | 14.3 | 3.3 | 18.8 | 9.48 | 7.65 |
| **U1 - NA** | 2.2 | 5.0 | 3.0 | 8.2 | 12.8 | 6.24 | 4.34 |
| **L1 - NB** | 4.5 | 5.2 | 11.2 | 2.6 | 7.4 | 6.18 | 3.29 |
| **Overall** | | | | | | 4.86 | 4.60 |
| | | | **Distances** | | | | |
| **U1 – NA** | 2.2 | 0.5 | 2.6 | 1.7 | 5.3 | 2.46 | 1.77 |
| **L1 - NB** | 0.1 | 1.8 | 3.5 | 1.7 | 0.0 | 1.42 | 1.44 |
| **S-N** | 0.3 | 1.2 | 5.0 | 5.0 | 1.6 | 2.62 | 2.22 |
| **ANS-PNS** | 6.0 | 12.4 | 3.3 | 3.1 | 12.1 | 7.38 | 4.59 |
| **S - ANS** | 3.3 | 5.4 | 3.8 | 4.8 | 1.4 | 3.74 | 1.55 |
| **ANS-Me** | 1.5 | 1.4 | 0.3 | 0.4 | 0.0 | 0.72 | 0.68 |
| **N - Pog** | 6.2 | 6.0 | 7.6 | 5.1 | 13.5 | 7.68 | 3.37 |
| **Overall** | | | | | | 3.72 | 3.48 |

*Table 38: Difference between measurements on lateral cephalogram and "Black Bone" for the patient group.*

### 5.1.3 Discussion

It has been demonstrated that there are some inherent difficulties when attempting to compare sagittal MRI images to the "gold standard" lateral cephalogram. Some of the cephalometric landmarks incorporated into traditional analysis are based upon projection of bony landmarks rather than representing true anatomy, which resulted in fewer landmarks being available in the true mid-sagittal plane for comparison. The central incisor teeth are poorly defined on a single mid-sagittal MRI image making measurements here inaccurate. Overall discrepancies between MRI and lateral cephalogram measurements were in the range of 2-4mm, compounded by difficulties associated with performing cephalometric measurements on the lateral cephalogram itself. Frequent difficulties with the lateral cephalogram include identification of the PNS in the presence of unerrupted wisdom teeth, a problem not encountered on mid-sagittal MRI images. In addition, the lateral cephalogram has inherent projection inaccuracies both because of its 2D nature and the requirement for interpolation in cases where there is even the most minor of facial skeletal asymmetry. The discrepancies found between "Black Bone" and lateral cephalogram results may therefore reflect the problems associated with using the lateral cephalogram as a "gold standard." In orthognathic surgery, movement of the mandible and maxilla is often in the range of <10mm, and thus a discrepancy in the range seen between lateral cephalogram and MRI would be of significance clinically. It is noted, however, that in total, only 8 datasets from patients and volunteers were included in this aspect of the study, and a larger study would be required to fully assess the significance between results.

## 5.2 Development of 3D "Black Bone" Cephalometry

"Black Bone" offers the potential advantage of being utilised for three-dimensional cephalometry. This would enhance surgical planning, but would require the development of new cephalometric measurements to incorporate those anatomical landmarks that are clearly identifiable on the "Black Bone" datasets.

### 5.2.1 Dolphin cephalometric software

Initial investigation into the potential of 3D cephalometry with "Black Bone" was with the 3D function available within the Dolphin cephalometric software. This included the option to import an entire DICOM dataset, some limited volume rendering functionality and the ability to plot the cephalometric points on the resultant 3D image *(Figure 10).* However, since there was no ability to remove the outer soft tissues, the cephalometric points could not be placed directly on the bone, thus making analysis inaccurate.

The other feature available in Dolphin is the option to convert 3D datasets into a 2D image equivalent to a lateral cephalogram. The results obtained with "Black Bone" datasets were poor *(Figure 66)*, and indeed would not confer any advantage to 2D cephalometry.

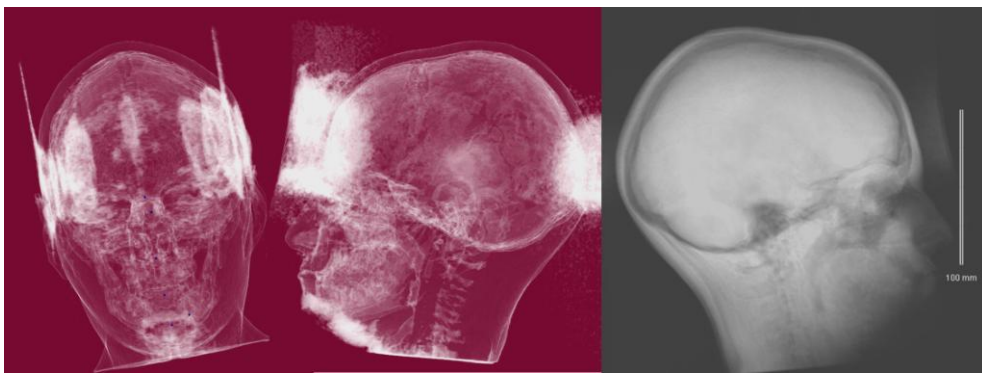



***Figure 66: 3D rendering in Dolphin software for cephalometric assessment (left & centre), and attempt to convert "Black Bone" dataset into a 2D cephalogram.***

### 5.2.2 3D Landmarks

The "Black Bone" datasets were reviewed in orthogonal planes for identifiable bony landmarks which would provide useful information on craniofacial proportions. The starting point for this was previous work completed on 3D cephalometry using CT datasets available in the literature.[195-197] The majority of landmarks that have been utilised in this published work have originated from 2D cephalometry rather than defining de novo landmarks.[198-199]

Of the software available, Mimics provides the option to measure angles and distances on orthogonal views. However, these are limited to being performed on one plane, rather than permitting identification in complementary planes or slices which would enhance identification. Mathematically this would be a simple process incorporating Pythagoras theory. Mimics provides the option to measure distances across the surface of a three-dimensionally reconstructed image, however it is straight-line distances that are important in cephalometric work.

It was determined that reliable anatomical points which could be identified in multiple planes, and also visualised on 3D reconstructed images included:

- Nasion – intersection of the internasal suture with the nasofrontal suture
- Menton – lowest point of the mandibular symphysis
- Upper and lower incisors
- ANS – most anterior point of the maxillary process
- Sella – although this has inherent inaccuracy associated with finding the centre of the pituitary fossa
- Basion – most anterior point of the foramen magnum
- Pogonion – most anterior point of the mandibular symphysis
- Gnathion – most anterereoinferior point of the mandibular symphysis

As was noted in the 2D cephalometry work, there were a number of inherent inaccuracies in performing cephalometric analysis, and these inaccuracies may be reduced by identifying landmarks in three orthogonal planes and on 3D reconstructed images. An additional module for

Mimics has recently become available to permit such cephalometric measurements, and this would provide further scope for investigation with "Black Bone" datasets.

### 5.2.3 Discussion

The lateral cephalogram has remained the "gold standard" as a result of the vast database of normal values built up over many years. Attempts to utilise CT and CBCT for 3D cephalometry have failed as a result of the unethical exposure of healthy patients to ionising radiation, to achieve a comparable database. This would, however, be feasible with "Black Bone," albeit a somewhat costly process, both in terms of image acquisition and interpretation. As with any measurement process inaccuracies arise as a result of operator error and intrinsic errors of the measuring device. The optimal method of 3D cephalometry with "Black Bone" would be a combination of landmark identification in orthogonal planes, and directly onto 3D rendered images of the facial skeleton. A fully automated process could be feasible with the incorporation of an atlas-based technique, and would minimise operator error. This was beyond the scope of this work, however, 3D rendering is explored in Chapter 7.

The main limitation with "Black Bone" based cephalometry is the restriction of its use to pre-operative planning, since "fixed" orthodontic appliances result in image degradation due to the metal components, as is the case with all MRI sequences.

## Chapter Conclusion

"Black Bone" MRI has been demonstrated to provide comparable cephalometric results to the lateral cephalogram, which itself has some inherent inaccuracies. "Black Bone" offers the advantage of 3D cephalometry without exposing patients to ionising radiation, and may be of particular value as a surgical planning tool in this patient group.

# 6. Adults

## 6.0 Adults

The third and final group of patients who undergo repeated CT examination throughout diagnosis and follow-up, and in whom MRI may yield additional information, are those with head and neck malignancy. With the focus of this thesis being on the craniofacial skeleton, the most common sites of malignant involvement are the maxilla and mandible. This section is sub-divided into three key sections to evaluate the pre-treatment predictive value of MRI-based tumour volume (Tv) assessment and the potential of "Black Bone" MRI in this patient group:

1. Tumour volume analysis in maxillary complex tumours
2. Tumour volume analysis in mandibular tumours
3. "Black Bone" MRI in maxillary complex and mandibular tumours

## 6.1 Tumour Volume Analysis in Maxillary Complex SCC

The first phase of this aspect of the study was to determine the value of pre-treatment tumour volume in maxillary complex squamous cell carcinoma. The maxilla and maxillary sinus provided a good starting point in view with the relative ease in which tumours can be identified on MRI in this region.

### 6.1.1 Materials and Methods

A retrospective study of all patients presenting with tumours involving the maxillary sinus, maxilla, hard palate and maxillary alveolus between February 2001 and August 2011 to the head and neck cancer unit at the OUH was completed. The inclusion criteria were: (1) a histological diagnosis of SCC affecting the maxillary complex; (2) primary surgical management of the tumour with or without post-operative adjuvant chemo-radiation; (3) negative past history for head and neck malignancy or radiation therapy to the head and neck; and (4) availability of pre-treatment MRI of diagnostic quality. Consent is routinely obtained from patients for case note review for audit and research purposes; ethical approval was not required for this aspect of the study.

Using a combination of the departmental database, department diaries, operating theatre lists, and a search of the pathology system, a comprehensive and combined list of all patients having undergone excision of tumours of the maxillary complex was created. The list was subsequently confirmed for accuracy by review of the electronic patient record system (CaseNotes®) to include only those tumours which were confirmed as involving bone, and/or the maxillary sinus. Any identified tumours which were classified as tumour recurrence, or second primary head and neck tumours were excluded, after confirming if the initial primary tumour was suitable for inclusion in the study. The date of primary surgery was cross-referenced with the theatre lists and pathology reports. Using the hospital PACS system, the corresponding imaging available for the patient was identified. Both CT and MRI imaging reports were reviewed to further verify the patient list as being accurate. For the patients identified in the departmental logbook dating back to 1998, in many instances full patient identifiers were not documented, and in some instances the hand written details, illegible. The majority of these patients were identified using "wild card" searches of the hospital electronic systems; however, some were ultimately excluded as the patient untraceable, and it was deemed likely that these patients followed a non-surgical management pathway. All MRI sequences and CT images for the patient were retrieved from the PACs server, where available, using efilm and the images saved to disc. For those patients whose images pre-dated the PACS system, the radiology reports were located on the Radiology Information system (RIS), and the date of imaging confirmed. Using the hand-written logbooks held within OMRI, the corresponding optical disc numbers were identified, and the discs located. For those scans performed at the CH, an electronic database was available, and the optical disc numbers identified by patient name. Once the optical discs had been located, the scans were uploaded to the server using the reader on the MRI 1.5T scanner at the CH. This was performed manually for each disc. The scans were subsequently obtained from the server and saved to disc. There was one patient whose images could not be located on optical disc, despite the details being located in the logbook. Review of the pre-and pro-ceding optical discs failed to locate the data, and it was considered most likely that the images had not been stored at the time of image acquisition

### *Tumour Volume Measurement*

BrainLab iPLAN® CMF was obtained on loan from BrainLab Ltd, and used for completion of all tumour volume calculations. BrainLab was developed initially for neurosurgery, and now has applications spanning image-guided surgery and stereotactic surgery in neurosurgery, oncology, orthopaedics, otolaryngology and cranio-maxillofacial surgery.[200]

Image sets were loaded into BrainLab, and all available MRI sequences for the patient were reviewed to identify the limits of the tumour prior to volume calculations. Where CT imaging was available, these were utilised to provide further clarification of the tumour extent. For each available dataset the image was magnified on screen, and the tumour outline manually defined *(Figure 67).*

Semi-automated tumour segmentation was possible with interpolation between two non-adjacent image slices. However, the interpolation function was found to be of limited value in view of the subsequent fine adjustment required. The tumour limits were therefore manually defined on each image slice to enhance accuracy. The images were re-reviewed on a second occasion to confirm that the tumour had been accurately outlined. Each Tv measurement was repeated 3 times on each available sequence on which the tumour could be clearly identified. Initial attempts were made to identify and outline the tumours on CT, however, it was noted that the tumour outline was frequently difficult to clearly identify and a decision to use only MRI was made. The Tv measurement was automatically calculated by the software, and the result viewed in the "Plan Content" *(Figure 68).* The measurements were transferred to Microsoft Excel for analysis.

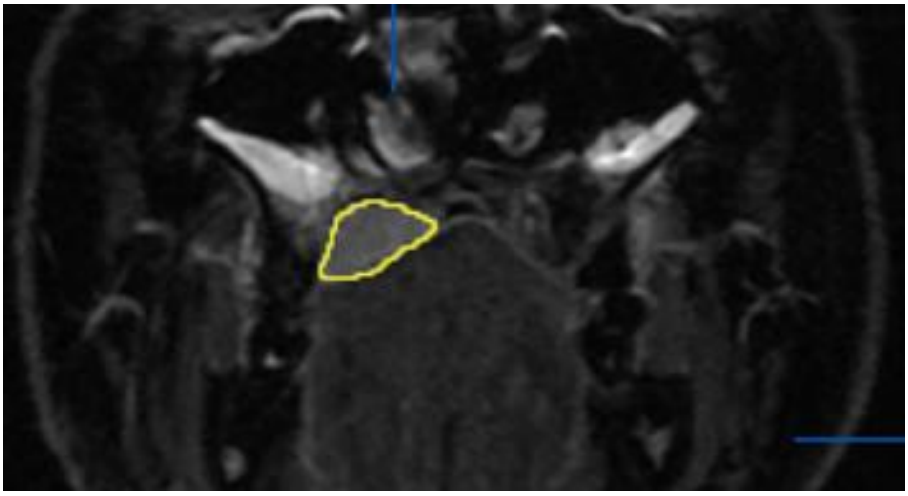


***Figure 67: Tumour volume measurement of a maxillary SCC on coronal MRI.***

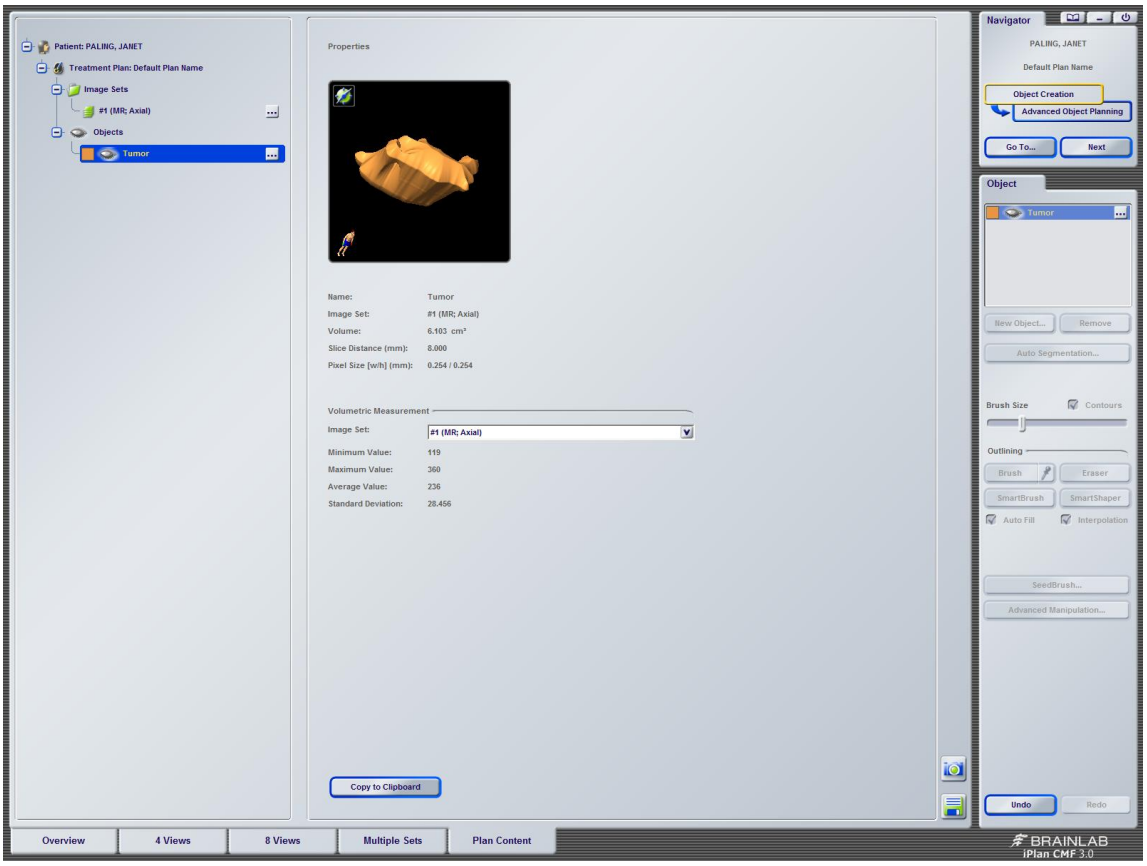



*Figure 68: Screenshot of "Plan Content" view of BrainLab software, demonstrating 3D reconstruction of tumour, and the tumour volume calculations.*

A mean result was calculated for each sequence per patient, and the greatest Tv utilised for subsequent analysis. Where tumour delineation was not clear, review with a head & neck radiologist (SJG) was completed to aid interpretation. A volume of 0cm$^3$ was assigned in cases where the tumour could not be detected on MRI.

To explore intraobserver variability for Tv, measurements were completed on ten occasions for one dataset, with 24 hours awaited between repeated attempts.

In view of the retrospective nature of the study some patients underwent MRI examination at the referring centre resulting in some variability in the MRI protocols used. In the majority of cases, axial T2 and/or coronal T2 imaging were available *(Table 39).*

| MRI Sequence | Available (n) | Used for Tumour Volume (n) |
|---|---|---|
| **Axial T2** | 34 | 26 |
| **Coronal T2** | 34 | 28 |
| **Axial T1 post-contrast** | 9 | 1 |
| **Coronal T1 post-contrast** | 13 | 3 |
| **Axial STIR** | 1 | 0 |
| **Coronal STIR** | 4 | 0 |
| **"Black Bone"** | 6 | 0 |

***Table 39: Available imaging sequences and those used for tumour volume measurements. Image sets were not used if the tumour could not be seen clearly, for example because of artefact.***

### *Clinical Outcome Measures*

Patient medical records were reviewed to identify age at diagnosis, sex, clinical site of tumour, surgical procedure completed (including neck dissection and reconstruction methods), adjuvant therapy, evidence of local or regional recurrence, date of last review, date of death (if applicable) and the histopathology and imaging findings of the primary tumour and any subsequent head and neck malignancy *(Table 40).* Tumour resection was classified according to the Brown classification.[145] The ACE-27 co-morbidity score was used to quantify past medical history *(Appendix F).* A data collection sheet was created to permit ease of data collection from review of patient medical records. This included review of the hospital patient notes, electronic patient systems including CaseNotes and PACS, and the hospital PAS system to identify date of last hospital appointment. In addition, clinic letters were reviewed on the local departmental server outlining all recent hospital clinic appointments. Computerised records were not available prior to 2005.

Data was entered onto a Microsoft Excel spreadsheet for cross-referencing prior to transfer to a Microsoft Access database to utilise enhanced data searching functionality and remove patient identifiers.

| | | |
|---|---|---|
| **Patient Identifiers:** | Hospital Number | NHS Number |
| | Sex | Date of Birth |
| **Clinical Information:** | Co-morbidity | ASA grade at surgery |
| | ACE-27 co-morbidity score | Alcohol consumption |
| | Smoking history | |
| **Tumour Details:** | Site of primary tumour | Side of tumour |
| | Date of referral | Clinical TNM staging |
| | Biopsy date | |
| **Imaging:** | Staging MRI date | Staging CT date |
| | Radiologist report of MRI | Radiologist report of CT |
| **Surgery** | Date of surgery | Surgical resection |
| | Neck dissection | Brown classification for maxillary tumours |
| **Pathology:** | TNM stage | Maximum depth of invasion |
| | Tumour grade | Tumour infiltration pattern |
| | Presence of perineural, perivascular and bony invasion | Number and levels of nodal involvement |
| | Number and level of lymph nodes with extracapsular spread | |
| **Follow up:** | Adjuvant radiotherapy dates | Adjuvant chemotherapy dates |
| | Date and location of local recurrence | Date of last hospital follow-up appointment |
| | Date and site of nodal recurrence | Date and report of last follow-up CT and/or MRI |
| | Date and cause of death | |

*Table 40: Data collection parameters.*

Patients were followed up following surgery on a monthly basis for the first year, every 2 months for the second year, every 3 months for the third year, and every 6 months subsequently until they reached 5 years and were discharged (if appropriate). A post-operative baseline MRI was completed at 6 or 12 months post-surgery, and typically on an annual basis thereafter. Overall, all cause survival (ACS) and disease-free survival (DFS) were calculated from the date of surgical resection using the actuarial method of Kaplan-Meier. Disease-free survival was calculated to the date of first clinical, radiological or pathological evidence of disease recurrence, whichever came first.

Statistical analysis was completed using Cox Regression Analysis, Kaplan-Meier plots, and Fisher's Exact test on SPSS.

### 6.1.2 Results

Of the 39 patients studied, 20 were male and 19 female, with a mean age of 70±11 years (48 – 86 years). ACE-27 co-morbidity scoring distribution is shown in *Table 41*.

| ACE-27 Grade | Frequency |
|---|---|
| **0** | 10 |
| **1** | 18 |
| **2** | 11 |

*Table 41: ACE-27 scoring distribution.*

The Brown classification for surgical resection and the reconstructive methods used are shown in *Table 42*. Elective neck dissection was performed in 24 cases, of which 3 were bilateral; 9 of the 24 patients had positive nodal disease on histology. Mean time of follow-up was 36±31 months for all patients and 47±36months for those patients who are still alive. In total, 12 patients died as a direct result of their malignancy, at a mean of 18±11 months following primary surgery.

| Brown classification[145] | Frequency |
|---|---|
| **1a** | 6 |
| **1b** | 1 |
| **2a** | 21 |
| **2b** | 5 |
| **3a** | 2 |
| **3b** | 1 |
| **4a** | 1 |
| **4b** | 1 |
| **4c** | 1 |
| **Method of reconstruction** | |
| **Obturator only** | 32 |
| **Local flap** | 1 |
| **Obturator ± free flap** | 6 |

*Table 42: Tumour resection and reconstruction method.*

Of the 9 patients with nodal disease at the time of primary surgery, 5 subsequently experienced nodal (n=4 at 3, 6, 7, and 8 months post-surgery) or local recurrence (n=1 at 10 months post-surgery). In the 13 patients who experienced nodal involvement, either at the time of primary surgery (n=9; with subsequent recurrence in n=5) or as post-operative recurrence (n=4), all cases of nodal recurrence occurred within 1 year of surgery.

### *Tumour Volume Analysis*

The Tv results obtained for assessment of intra-observer variability are shown in *Table 43*. This provided a co-efficient of variability of 3.4%.

In 23 cases more than one MRI sequence was suitable for Tv measurement, and the largest volume obtained was used for subsequent analysis. The mean discrepancy between measurements on differing MRI sequences was 2.13±3.01cm$^3$. In three cases, the tumour could not be identified on imaging, and a volume of 0cm$^3$ assigned.

The mean Tv was 12.79±24.31cm$^3$ (0 – 113cm$^3$), with a distribution according to the TNM classification shown in *Table 44.*

| Attempt | Tv Measurement |
|---|---|
| 1 | 4.596 |
| 2 | 4.384 |
| 3 | 4.439 |
| 4 | 4.598 |
| 5 | 4.443 |
| 6 | 4.147 |
| 7 | 4.648 |
| 8 | 4.345 |
| 9 | 4.460 |
| 10 | 4.311 |
| Mean±SD | 4.44±0.152 |

*Table 43: Tumour volume measurements for review of intra-observer variability.*

| T stage | Number of patients | Tumour Volume | |
|---|---|---|---|
| T1 | 7 | 1.49 ± 3.31 | [0 – 8.97] |
| T2 | 2 | 2.55 ± 3.61 | [0 - 5.11] |
| T3 | 5 | 11.86 ± 11.96 | [1.56 – 29.11] |
| T4 | 25 | 16.95 ± 29.06 | [1.15 – 113.03] |

*Table 44: Distribution of tumour volume according to T stage as per the AJCC TNM classification.*

Independent samples t test showed a significant relationship between increasing overall ACS and decreasing tumour volume (1 year: p=0.003; 5-year p=0.031). A similar finding was seen with DFS at 1 year, with increasing Tv resulting in decreased DFS (p=0.05), however, this was not significant at 5 years (p=0.104).

Timing of surgery meant that of the 39 patients studied, 2 had not yet reached 1 year of follow-up. Using the results of the remaining 37 patients for analysis, with a cut-off of 4cm$^3$ Fishers exact test revealed that those with tumours <4cm$^3$ were more likely to reach 1 year post-op (p=0.046). At 2

years (n=32 with n=21 alive), 4cm$^3$ was not significant (p=0.147), nor at 5 years post-surgery (n=27 with n=8 alive) (p=0.087).

Log rank analysis identified a Tv cut-off of 5cm$^3$ to be valuable in predicting ACS approaching significance (p=0.051) *(Figure 69).* The development of local recurrence was predicted with a Tv cut-off of 20cm$^3$ (log rank; p=0.036).

Tumour resection margins were reported as clear in 12, close in 14 and involved in 13. The effect of histological margin on DFS is shown in *Figure 69* (log rank, p=0.014).

No significant correlation was seen for nodal involvement at surgery or subsequent nodal recurrence *(Table 45).* For those patients experiencing nodal disease at or within a year of surgery mean Tv was 15.33±27.80cm$^3$ compared to 11.51±22.86cm$^3$ in those without nodal involvement.

| Tumour volume cut-off | p |
|---|---|
| **≥2cm$^3$** | 0.191 |
| **≥3cm$^3$** | 0.286 |
| **≥4cm$^3$** | 0.548 |
| **≥5cm$^3$** | 0.283 |
| **≥6cm$^3$** | 0.639 |
| **≥7cm$^3$** | 0.648 |
| **≥8cm$^3$** | 0.648 |
| **≥9cm$^3$** | 0.458 |
| **≥10cm$^3$** | 0.458 |
| **≥20cm$^3$** | 0.429 |

***Table 45: Fisher's exact test for nodal involvement at or within 1 year of surgery.***

There was no statistical significance between ACS and ACE-27 score (Chi-square test 1 year p=0.756; 2 year p=0.891).

Tv was stratified into 4 groups to correlate the results with the current TNM staging system *(Table 46).* The 1$^{st}$ and 3$^{rd}$ quartiles and the median were defined as the cut points for stratification purposes. Using this stratification, nodal involvement, neural invasion and Tv were significant for DFS and ACS prediction on Cox regression analysis *(Table 46).* Sex, ACE-27 co-morbidity grade, histological tumour differentiation, pTNM, intravascular invasion were not significant. The re-classification according to Tv stratification resulted in upstaging in four cases, and down-staging in 19 cases. The majority of cases which were downstaged had been pathologically staged as pT4 tumours *(Figure 69, Table 47).*

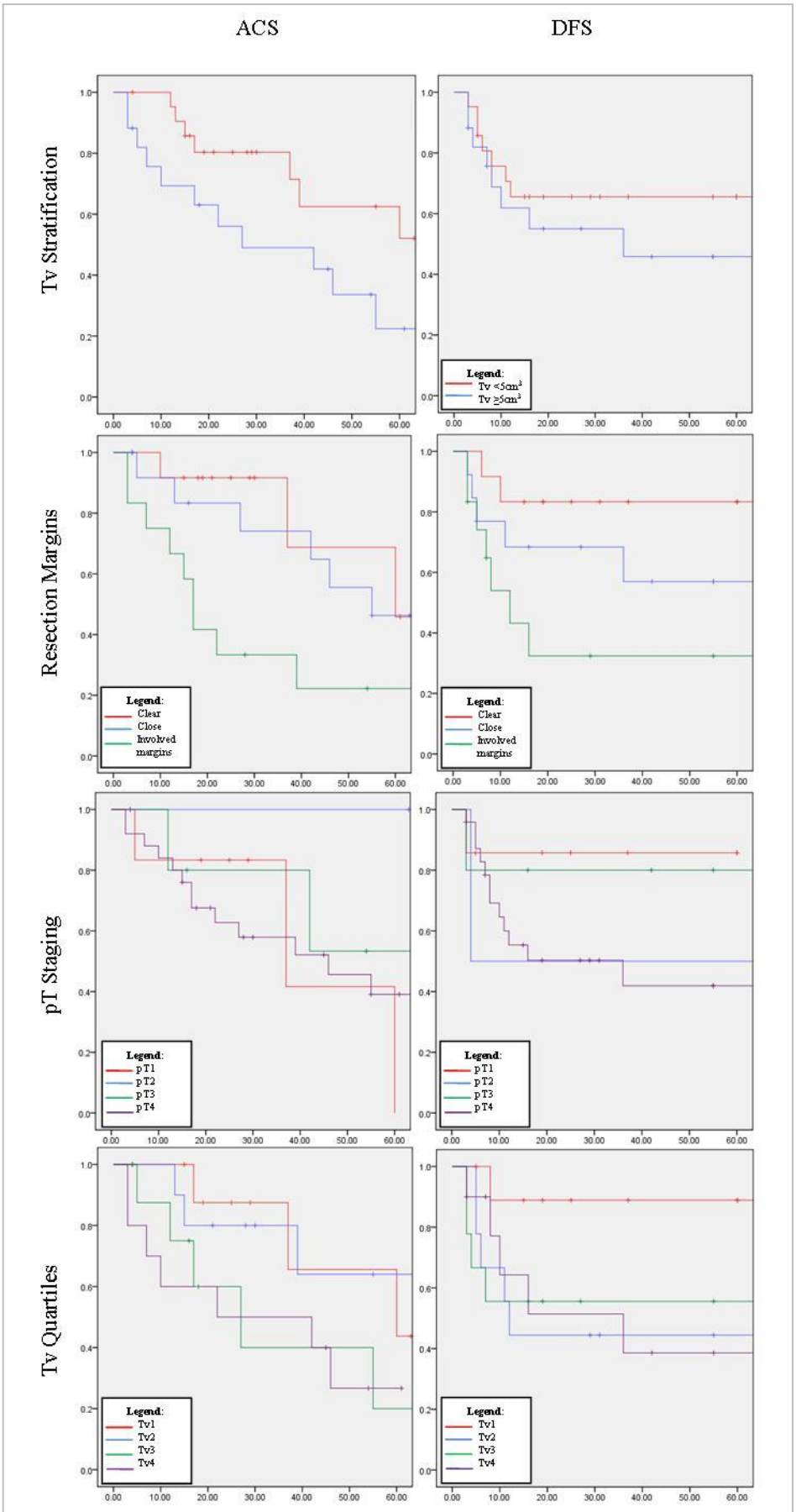



*Figure 69: Kaplan Meier plots of ACS and DFS against time (in months) for a Tv cut-off of 5cm$^3$, tumour resection margins, pT staging, and Tv stratification as quartiles.*

| Covariate | T stage | Tumour volume | Frequency | ACS p | DFS p |
|---|---|---|---|---|---|
| **Tv1** | T1 | <1.56cm$^3$ | 10 | 0.094 | 0.023* |
| **Tv2** | T2 | ≥1.56 – 4.20cm$^3$ | 10 | 0.017 * | 0.866 |
| **Tv3** | T3 | ≥4.20 – 12.32cm$^3$ | 9 | 0.051 | 0.047* |
| **Tv4** | T4 | ≥12.32cm$^3$ | 10 | 0.071 | 0.033* |
| **Nodal disease at surgery** | | | | 0.04 * | 0.001* |
| **Neural invasion** | | | | 0.019* | 0.024* |
| **Bone invasion** | | | | - | 0.065 |

*Table 46: Tumour volume cut-off to correlate with TNM staging system & significance levels in Cox Regression analysis.*

| Original Staging | Adjustment | New Stage | Frequency |
|---|---|---|---|
| **pT1** | Unchanged | | 6 |
| | Upstaged | T2 | 0 |
| | | T3 | 1 |
| **pT2** | Unchanged | | 0 |
| | Down-staged | T1 | 1 |
| | Up-Staged | T3 | 1 |
| **pT3** | Unchanged | | 2 |
| | Down-Staged | T1 | 1 |
| | | T2 | 0 |
| | Up-Staged | T4 | 2 |
| **pT4** | Unchanged | | 8 |
| | Down-staged | T1 | 2 |
| | | T2 | 10 |
| | | T3 | 5 |

*Table 47: Effect of Tv on pT staging. The majority of pT4 tumours were downstaged according to Tv.*

### 6.1.3 Discussion

In view of the small number of patients with maxillary complex tumours it was necessary to combine alveolus and maxillary sinus tumours for the purposes of this study despite these regions falling under paranasal sinuses and oral cavity tumours in the AJCC TNM staging classification. However, this has been common practice in many of the publications on tumours affecting this region.

It has been demonstrated that even with this relatively small cohort, Tv correlated significantly with outcome in terms of ACS and DFS. Tumour cut-points of 5cm$^3$ and 20cm$^3$ demonstrated significant correlation for ACS, and local recurrence respectively.

Further analysis in a larger cohort (and with single sub-site) is required to further enhance accuracy in the selection of Tv cut-offs for survival analysis. This may also yield a significant correlation between Tv and nodal status.

However, MRI measured Tv assessment appears to be a reliable predictor of survival following surgical resection of maxillary complex SCC. The next phase was to determine if Tv was also useful in mandibular tumours.

## 6.2 Tumour Volume Analysis in Mandibular SCC

Having determined that MRI based Tv measurements provide useful survival information in maxillary complex tumours, the next step was to determine if this was also the case with mandibular tumours.

### 6.2.1 Materials and Methods

The methods utilised for maxillary tumours was followed to obtain details of all patients presenting with tumours of the retromolar trigone, mandible, or floor of mouth (with bone involvement), between February 2001 and August 2011 to the OUH. The inclusion criteria were: (1) a histological diagnosis of SCC; (2) primary surgical management of the tumour with or without post-operative adjuvant chemo-radiation; (3) negative past history for head and neck malignancy or radiation therapy to the head and neck; and (4) availability of pre-treatment MRI of diagnostic quality. In total, 62 patients met the inclusion criteria.

#### *Tumour Volume (Tv) Measurement*

Tv measurements were completed following the same methodology as for maxillary complex tumours *(Figure 70)*. All MRI sequences and CT imaging were reviewed, with axial T2 and/or coronal T2 imaging used for Tv measurement in most cases *(Table 48)*.

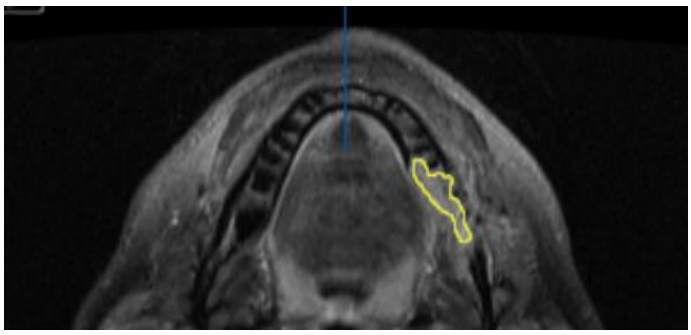


*Figure 70: Tumour volume measurement of a mandibular SCC.*

| Sequence | Available (n) | Used for tumour volume (n) |
|---|---|---|
| **Axial T2** | 49 | 42 |
| **Coronal T2** | 46 | 40 |
| **Axial T1 with contrast** | 15 | 3 |
| **Coronal T1 with contrast** | 16 | 1 |
| **Axial STIR** | 8 | 6 |
| **Coronal STIR** | 9 | 5 |
| **Axial "Black Bone"[201]** | 21 | 8 |

*Table 48: Available MRI sequences and those suitable for tumour volume measurements.*

### *Clinical Outcome Measures*

Retrospective medical note review was completed in the same manner as for maxillary complex tumours, and the data entered into the Microsoft Access database. Overall, ACS and DFS were calculated from the date of surgical resection using the actuarial method of Kaplan-Meier. DFS was calculated to the date of first clinical, radiological or pathological evidence of recurrent disease, whichever came first.

Statistical analysis was completed using Kaplan-Meier plots, Cox Regression analysis and Fisher's Exact test on SPSS.

## 6.2.2 Results

Of the 62 patients meeting the inclusion criteria, 32 were male and 30 female. The mean age was 67±14 years [38 – 89 years]. ACE-27 grading showed that the majority of patients had at least mild co-morbidity (Grade 0 n=20; Grade 1 n=26; Grade 2 n=16). In the majority of cases the primary tumour site was the mandible (n=39); with floor of mouth (with bone involvement) (n=8) and retromolar (n=15) being less frequently encountered. Neck dissection was performed in 58 cases (Right n=19; Left n=28; Bilateral n=11). Of the 62 patients studied, 58 had completed 1 year, 54 had completed 2 years, and 33 had completed 5 years of post-operative follow-up.

Pre-operative clinical TNM staging was available in 61 of the 62 cases. Following tumour resection and pathological analysis, the TNM staging remained unchanged in 39 cases. In 6 cases pTNM was downstaged compared to cTNM, and upstaged in 16 cases. In the majority of cases, upstaging was to pT4 because of bony invasion, with 46 of the 62 tumours being staged as pT4.

Two patients developed second primary tumours at 24 and 62 months post-operatively. In view of the close proximity to the original tumour site these were included as cases of recurrence for the purpose of statistical analysis.

### *Tumour Volume Analysis*

In 41 cases more than one MRI sequence was available. The maximum average discrepancy between Tv measurements on differing sequences for the same patient was 1.84±2.39cm$^3$.

The mean overall Tv measurement was 5.73±7.30cm$^3$ *(Table 49).* On univariate analysis, Tv was significant at predicting ACS at 5-years (p=0.005, independent samples t test), and DFS at 5 years (p=0.019, independent samples t-test). However significance was not reached for 1 or 2 years post-surgery.

The results of univariate analysis on DFS are shown in *Table 50*. Kaplan Meier plots and log rank were significant for a range of Tv stratifications in the prediction of outcome; a 7cm$^3$ cut-off was significant for ACS, DFS, local and nodal recurrence *(Figure 71).*

| T stage | Number of patients | Tumour Volume | |
|---|---|---|---|
| **T1** | 2 | 1.77±2.04 | [0.33-3.22] |
| **T2** | 11 | 1.70±1.78 | [0.00-5.38] |
| **T3** | 3 | 8.66±2.34 | [6.46-11.12] |
| **T4** | 46 | 6.67±8.07 | [0.75-42.30] |

***Table 49: Correlation of pT stage with tumour volume.***

| Factor | Significance |
|---|---|
| **Sex** | p=0.569 |
| **Clinical cT stage** | p=0.720 |
| **Clinical cN stage** | p=0.405 |
| **Pathological pT stage** | p=0.369 |
| **Pathological pN stage** | p=0.003 * |
| **Nodes present at surgery** | p=0.002 * |
| **Pathological tumour differentiation** | p=0.004 * |
| **Pathological invasive front** | p=0.899 |
| **Pathological tumour margin** | p=0.325 |
| **Peri-neural invasion** | p=0.933 |
| **Per-vascular invasion** | p=0.035 * |
| **Bone invasion** | p=0.073 |
| **ASA Grade** | p=0.033 * |
| **ACE-27 Score** | p=0.050 * |

***Table 50: Univariate analysis of factor effect on DFS (* signifies significance at p<0.05).***

Using the 1$^{st}$ and 3$^{rd}$ quartiles, the Tv results were stratified into low, medium and high risk groups, shown as a Kaplan-Meier plot for DFS in *Figure 72*. Cox regression analysis demonstrated significance for a model containing the stratified Tv groups and histological differentiation, for both DFS and ACS *(Table 51).*

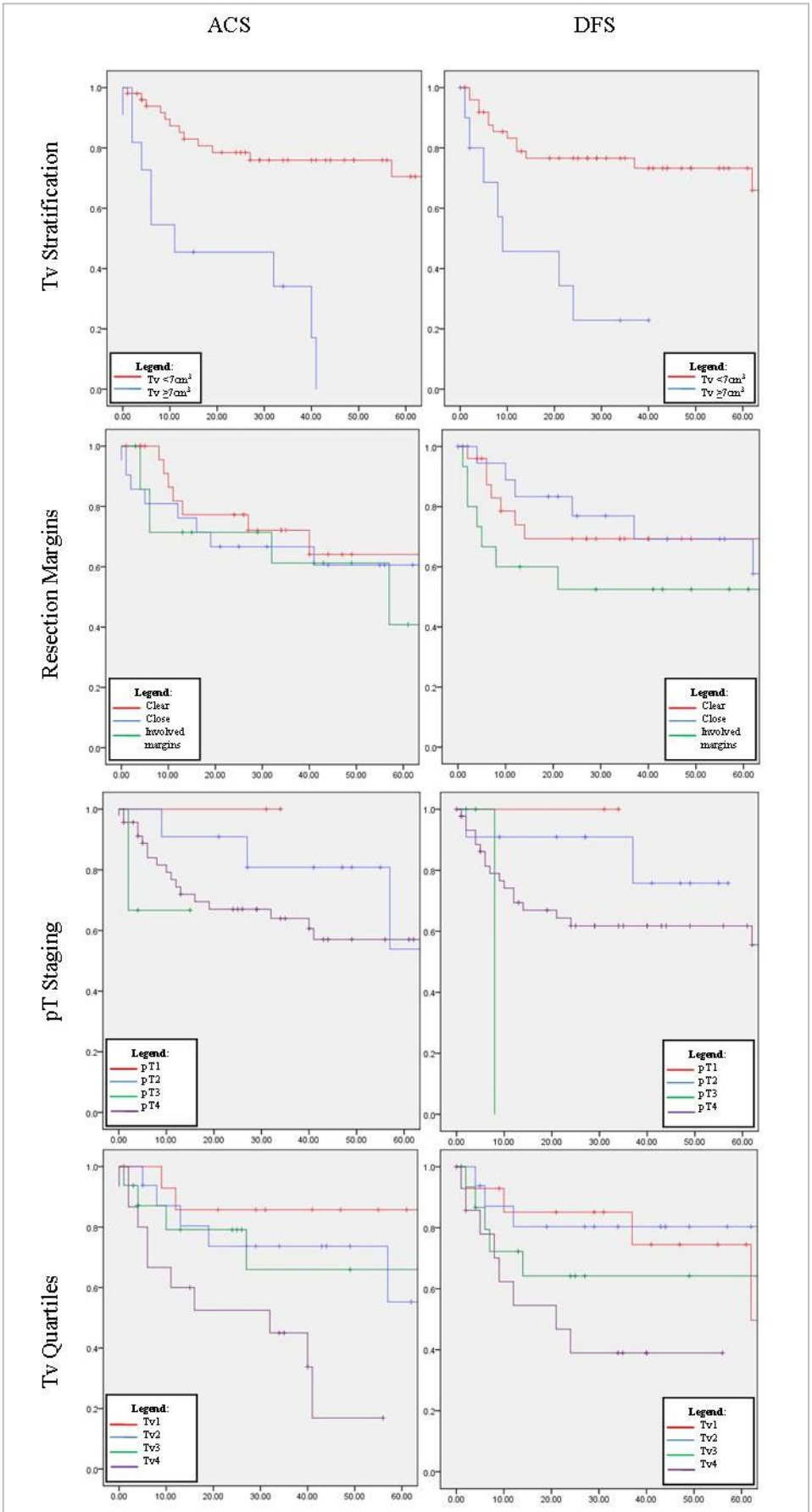



*Figure 71: Kaplan Meier plots of ACS and DFS against time (in months) for a Tv cut-off of 5cm$^3$, tumour resection margins, pT staging, and Tv stratification as quartiles.*

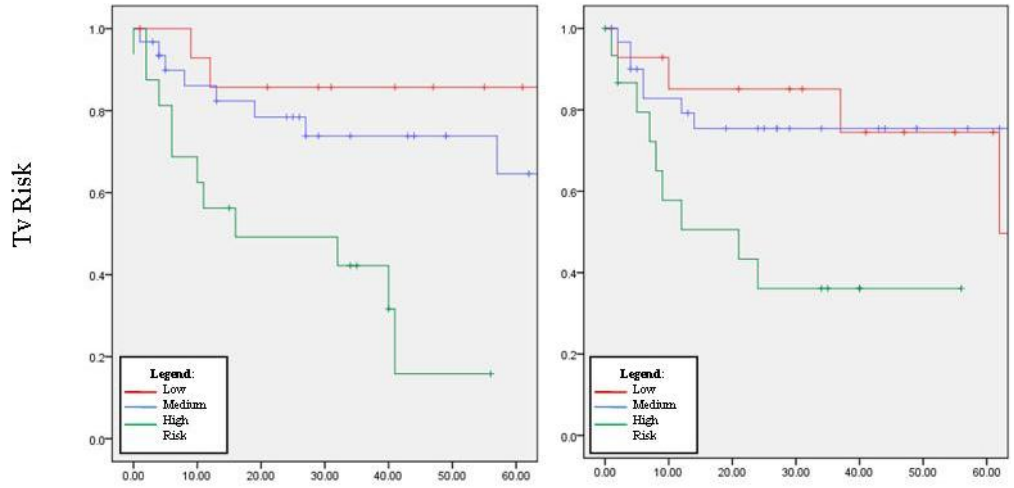



*Figure 72: Kaplan Meier plots for ACS (left) and DFS (right) with time (months) and stratification of tumour volume into low, medium and high risk groups.*

| | Hazard Ratio | 95% confidence interval | p |
|---|---|---|---|
| **Disease Free Survival** | | | |
| **Tv <1.53cm$^3$** | 0.175 | 0.044 – 0.701 | 0.014 * |
| **Tv ≥1.53 – 6.50cm$^3$** | 0.264 | 0.095 – 0.736 | 0.011 * |
| **Tv ≥6.50cm$^3$ (Reference group)** | | | 0.009 * |
| ***Histological Differentiation:*** | | | |
| **Well** | 0.057 | 0.008-0.409 | 0.004 * |
| **Moderately** | 0.064 | 0.010-0.416 | 0.004 * |
| **Poorly (Reference group)** | | | 0.012 * |
| **All Cause Survival** | | | |
| **Tv <1.53 cm$^3$** | 0.135 | 0.035-0.512 | 0.003 * |
| **Tv ≥1.53 – 6.50 cm$^3$** | 0.278 | 0.105-0.734 | 0.010 * |
| **Tv ≥6.50 cm$^3$ (Reference group)** | | | 0.004 * |
| ***Histological Differentiation:*** | | | |
| **Well** | 0.157 | 0.027-0.907 | 0.038 * |
| **Moderately** | 0.195 | 0.039-0.972 | 0.046 * |
| **Poorly (Reference group)** | | | 0.104 |

*Table 51: Cox regression analysis of DFS and ACS using Tv stratification into low, medium and high risk groups based upon the 1$^{st}$ and 3$^{rd}$ Tv quartiles.*

To permit correlation with the current TNM staging system, Tv was re-stratified using the median in addition to the 1$^{st}$ and 3$^{rd}$ quartiles *(Table 52, Figure 74)*. This resulted in down-staging of tumour stage in 40 of the 62 cases, the majority of which has been classified as pT4 tumours. Multivariate Cox regression analysis performed in a step wise fashion was significant (p=0.021) for a model using Tv stratification, and histological tumour differentiation (well, moderately or poorly differentiated) for DFS. For the current TNM system pT was not significant for DFS.

| Co-variate | TNM T-Stage | Frequency | Hazard ratio | 95% confidence | p |
|---|---|---|---|---|---|
| **Tv <1.53cm$^3$** | T1 | 35 | 0.190 | 0.047-0.774 | 0.020 * |
| **Tv ≥1.53-3.59cm$^3$** | T2 | 15 | 0.211 | 0.055-0.812 | 0.024 * |
| **Tv ≥3.59-6.50cm$^3$** | T3 | 6 | 0.479 | 0.152-1.510 | 0.209 |
| **Tv ≥6.50cm$^3$ (Reference group)** | T4 | 6 | | | 0.040 * |
| ***Histological differentiation:*** | | | | | |
| - **Well** | | | 0.054 | 0.007-0.393 | 0.004 * |
| - **Moderately** | | | 0.066 | 0.010-0.424 | 0.004 * |
| - **Poorly (Reference group)** | | | | | 0.012 * |

***Table 52: Stratification of tumour volume measurements for correlation with current TNM T staging. Co-variates included in Cox regression analysis for DFS (* significant at p<0.05).***

### 6.2.3 Discussion

In this study of 62 patients with SCC of the mandible, floor of mouth and/or retromolar trigone, Tv was an accurate predictor of outcome in terms of DFS, ACS, nodal and local recurrence. Utilising the results from univariate analysis it was possible to stratify the Tv measurements into four groups correlating to the current T stage of the TNM classification. This stratification yielded significant results in Cox Regression analysis for DFS for both T1 and T4 tumours. In view of the small number of patients within the T2 and T3 groups, Tv for these groups was not significant. However, Tv was a more useful predictor of outcome than cT or pT, which failed to yield a significant result.

In view of the relative infrequency with which tumours of these regions are encountered it was necessary to group all three subsites, which are most frequently associated with mandibular invasion. Kaplan Meier and univariate analysis demonstrated that outcome, in terms of DFS, was similar for the subsites. However, it is postulated that retromolar trigone tumours confer a poorer prognosis in view of the relatively constrictive triangular mucosal area in which cancers can readily involve other anatomic sites at this location.[202] As such, further work is required in the form of a multi-centre study to obtain sufficient numbers of tumours involving each of the oral cavity subsites. This will enhance the predictive capabilities of the Tv cut-points permitting incorporation into the TNM classification, since it is unlikely that one Tv cut-point will be a significant predictor for all subsites.

It has been demonstrated that routine MRI sequences confer a significant advantage over CT in tumours affecting the craniofacial skeleton, providing improved prediction of patient outcome than the current TNM system. The next phase of investigation was to determine if “Black Bone” could be utilised in Tv assessment.

## 6.3 Potential of "Black Bone" MRI in Tumour Assessment

This section of the thesis explores the potential of "Black Bone" MRI in tumour assessment, particularly with regard to Tv measurement, expanding on the results obtained with routine MRI sequences.

### 6.3.1 Maxillary Complex Tumours

Of the 39 patients with maxillary complex tumours, the "Black Bone" MRI sequence was available in six cases. However, in three cases there was significant movement artefact which precluded clear visualisation of the tumour. In the remaining 3 cases whilst the tumour could be identified, being particularly well defined in areas of bony loss, the true extension into the soft tissues could not be clearly delineated. This made Tv measurements unreliable. The mean Tv measurement for the patients who had undergone "Black Bone" imaging was 2.62±1.47cm$^3$, however, Tv measurements could not be reliably made on any of the "Black Bone" sequences. Examples of the tumour extent seen on the "Black Bone" sequence are shown in *Figure 73.*

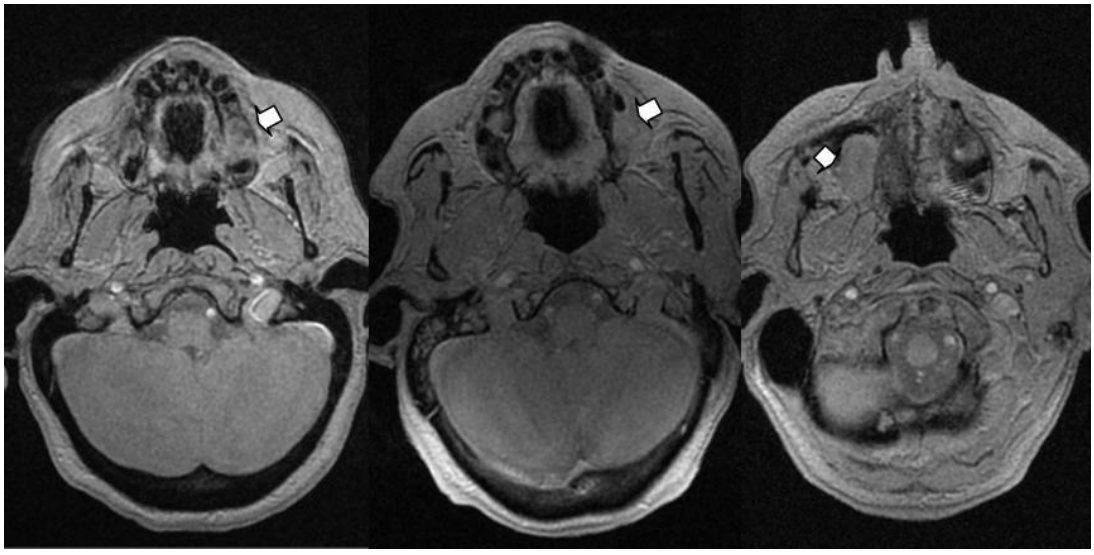


***Figure 73: Appearance of maxillary complex tumours on the "Black Bone" sequence. Breech of the cortical bone by the tumour is possible to visualise on the sequence, however due to the minimal soft tissue contrast, the true extent of soft tissue involvement cannot be delineated.***

### 6.3.2 Mandibular Region Tumours

Of the 62 patients included in the review of mandibular region tumours, 14 had "Black Bone" sequences available. In eight cases, Tv assessment was attempted; the remaining six datasets being degraded by movement or dental amalgam artefact (n=2) or the tumour extent not clearly delineated (n=4).

The Tv measurements on axial T2 imaging in 5 cases, and on coronal T2 in one case, were higher than on "Black Bone." In the remaining 2 cases, "Black Bone" offered the highest Tv measurement, and was utilised for subsequent analysis. The discrepancy in both of these cases from coronal T2 imaging was small (mean difference = 0.103cm$^3$). The overall mean difference between "Black Bone" Tv measurements and the mean result across all other available MRI measured sequences for the 8 patients was 1.19cm$^3$. Examples of the tumour extent seen in 4 of the cases are shown in *Figure 74.*

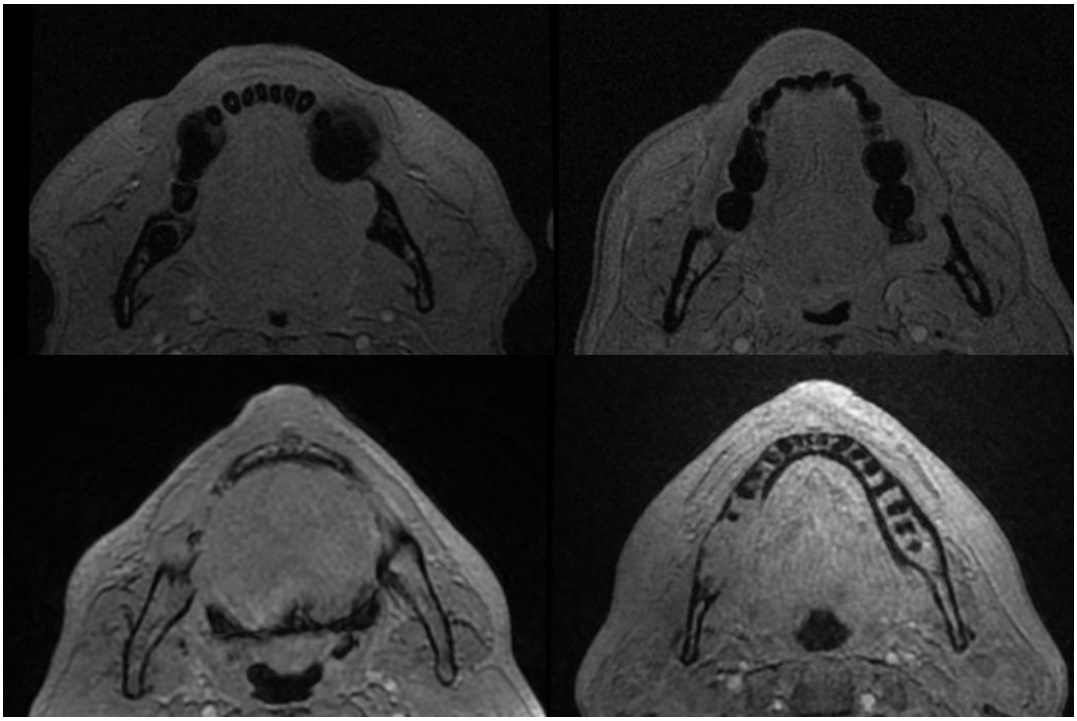


***Figure 74: Appearance of mandibular region tumours on the "Black Bone" sequence. Whilst the bony erosion and replacement of the mandible with tumour can be visualised, the soft tissue extent is not clear.***

### 6.3.3 Discussion

It is apparent, that whilst the "Black Bone" sequence is useful in determining bony erosion or replacement of bone by tumour, the true extent of the tumour cannot always be visualised if it extends into the soft tissues. In those cases where Tv measurements were possible, the results were comparable to those obtained from more routinely used sequences. In a number of cases whilst the "Black Bone" sequence had been completed, the images were not of diagnostic quality due to movement artefact. Often the "Black Bone" sequence is completed as the final sequence and since it is not deemed at present to be an "essential" sequence, it is often not repeated if subject to significant artefact. Compared to other MRI sequences it does not appear to be more susceptible to movement or dental amalgam artefact. The sequence offers useful information, and may negate the need for CT examination when investigating for tumour ingress into bone; however, it is of less value in tumour volume analysis due to the difficulties when tumour extends into the soft tissues.

Having explored the potential of "Black Bone" in Tv assessment, investigation turned to the potential of the sequence in further pathological conditions affecting the craniofacial skeleton in this adult patient group.

## 6.4 "Black Bone" MRI & Craniofacial Pathology

Having identified the limitation of the "Black Bone" sequence in the assessment of tumour volume, the next stage was to determine the potential of the sequence in radiological diagnosis of pathological conditions affecting the head and neck. This aspect of the thesis is divided into two aspects:

1. Fully anonymised review of "Black Bone" datasets
2. Review of cases where "Black Bone" MRI has been used in place of CT

### 6.4.1 "Black Bone" MRI in the Diagnosis of Craniofacial Pathology

In an attempt to further explore the potential of "Black Bone" as a diagnostic tool in craniofacial pathology a blinded review of imaging was required. However, in designing this aspect of the study there were a number of inherent limitations. These included the inability to compare the "Black Bone" sequence to other routine sequences without bias, in view of the distinct bone-soft-tissue appearance on "Black Bone." To this end, it was decided to obtain independent review of "Black Bone" datasets in isolation. Whilst not in keeping with standard radiological reporting practice devoid of clinical information, this provided the only method to independently assess the limits of "Black Bone" whilst minimising any potential bias and accepting that in combination with a clinical history the results would be enhanced.

#### 6.4.1.1 Materials and Methods

A database of patients with available "Black Bone" imaging was collated in Microsoft Excel to include clinical indication for imaging, and radiological diagnosis. Patients were identified from a departmental database of "Black Bone" and from the hospital PACS system. As PACS has no inherent searching facility for "Black Bone," sequential date review for "MRI," with review of the list of sequences performed for each patient was interrogated to identify those patients in whom the "Black Bone" sequence had been performed. PACs was introduced in 2006, and review was therefore limited to the 5 year period, 2006-2011. The images were reviewed to include only those that had been acquired in the axial plane. In total 46 axial "Black Bone" datasets were available, and the corresponding radiological reports reviewed. A further four "Black Bone" datasets from adult volunteers were included to act as controls. The 50 "Black Bone" datasets were imported into

Clear Canvas, fully anonymised and numbered randomly 1 to 50, before exporting to eFilm and saving. A scoring sheet was designed on which reviewers were asked to record their findings *(Appendix G).* The key questions were:

1. Is there any pathology present?
2. What side is the pathology?
3. What is the anatomical site of the pathology?
4. Is it a benign or malignant process
5. Is there any bony erosion?
6. What is the leading diagnosis?

Two reviewers (a head & neck radiologist and a head & neck surgeon) agreed to review the anonymised images. In addition, after waiting three month period to avoid potential bias, I acted as a third reviewer. The images were subsequently reviewed with the radiological reports and compared to the reviewers responses.

#### 6.4.1.2 Results

The tabulated results are displayed in *Appendix G*. Of the 50 datasets reviewed, 4 were from healthy volunteers in whom no pathological conditions had been identified at the time of imaging. All 3 of the assessors reported that the imaging did not contain any pathology, although in two cases it was thought that there may be an anatomical variant present.

Of the 13 patients with benign pathology, all reviewers identified that there was pathology present in all but one case for one reviewer. This was a child with a vascular malformation in the cheek tissues *(Figure 75).* In all but one case by one reviewer, the correct anatomical site for pathology was identified. In this case, there was an incidental finding of a frontal sinus effusion which led to this being attributed as the main diagnosis in this case. The process was correctly identified as being benign in 56% of cases; however, difficulty arose in cases of osteoradionecrosis, giant cell granuloma, pleomorphic adenoma, and langerhans cell histiocytosis *(Table 53).*

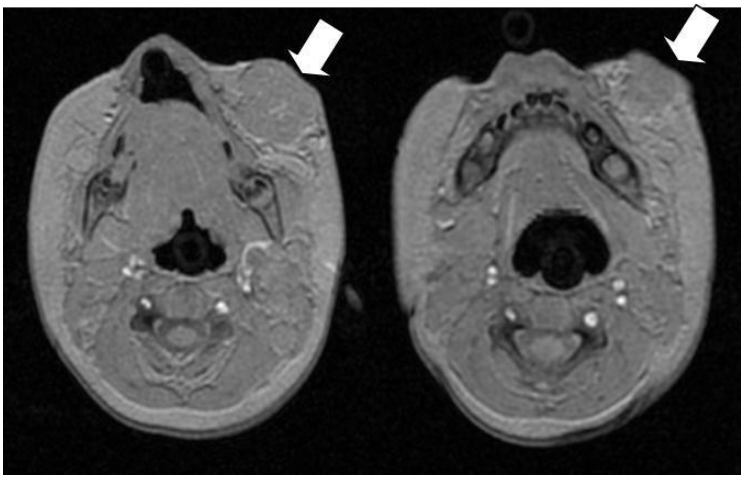


*Figure 75: Vascular malformation in cheek tissues in 1 year old child.*

| Assessors: | Frequency | | | Kappa Score | | |
|---|---|---|---|---|---|---|
| | 1 | 2 | 3 | 1 v 2 | 1 v 3 | 2 v 3 |
| **Correct identification of pathology being/not present** | 44/50 | 41/50 | 38/50 | 0.50 | 0.46 | 0.62 |
| **Correct side of pathology identified** | 28/37 | 34/37 | 30/34 | 0.71 | 0.85 | 0.78 |
| **Correct site of pathology identified** | 28/37 | 31/37 | 25/34 | 0.71 | 0.84 | 0.66 |
| **Correct identification of benign or malignant process** | 25/37 | 26/37 | 20/32 | 0.44 | 0.45 | -0.09 |
| **Correct identification of bony erosion** | 22/36 | 27/37 | 19/31 | 0.31 | 0.54 | -0.20 |

*Table 53: Frequency and inter-rater agreement for pathological diagnosis on "Black Bone" MRI.*

In 32 cases where the pathological process had been confirmed as malignant *(Figure 76)*, 14 datasets where thought to contain no pathology by at least one reviewer. These most frequently represented lesions occurring in the floor of mouth, maxilla, or around mandibular teeth. Overall, 62% of the malignant cases were correctly identified as such.

Analysing the data as a whole, the correct identification of a pathological process being present was made in 82% of cases. Overall inter-rater agreement was good with a Kappa score of 0.60. The correct side for the pathology was identified in 85%, and correct site in 78%. Greater concordance was seen between raters for selection of laterality. Identification of bony erosion was correctly documented in 65% of cases.

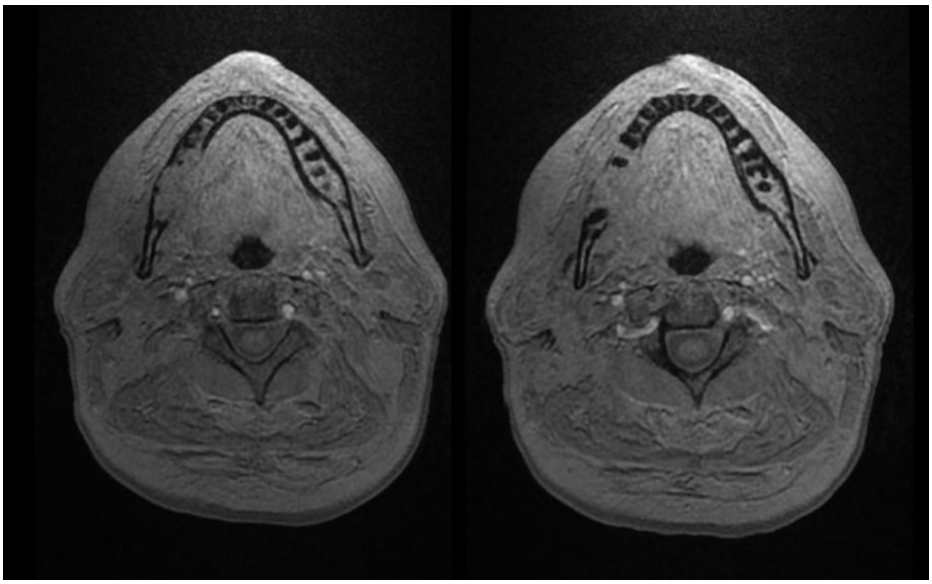


*Figure 76: Patient 35 in whom all reviewers correctly identified all aspects of the radiological diagnosis of a right mandibular SCC.*

#### 6.4.1.3 Discussion

With consideration of the lack of clinical information provided, and limitation of radiological review to "Black Bone" only, a reasonable result was obtained. The sequence appeared to demonstrate the pathological process in the majority of cases, and there was overall good agreement between raters. Assessors correctly identified those cases which had been obtained in healthy volunteers, noting that whilst there were potential anatomical variants, no pathology was present. Difficulty arose in distinguishing benign from malignant processes, particularly in cases of giant cell granuloma, and osteoradionecrosis, where clinical history and additional imaging are required in combination for an accurate diagnosis. The "Black Bone" sequence was particularly useful where the pathology involved the craniofacial skeleton. In these cases the abnormality could be clearly identified. However, with the minimal soft tissue contrast, pathology arising within the soft tissues was difficult to accurately detect.

Having explored the potential of "Black Bone" as a diagnostic tool the next stage was to review those cases where "Black Bone" has been successful in replacing CT.

## 6.5 "Black Bone" MRI Instead of CT Imaging

The "Black Bone" sequence has been utilised in routine clinical practice at OMRI and the CH for the past eight years. In view of the specialist interest of the radiologists using this technique "Black Bone" has largely been confined to the head and neck. The objectives of this aspect of the thesis were therefore to review the "Black Bone" sequences performed for head and neck pathology with regard to cases where the "Black Bone" sequence replaced ionising imaging with CT.

### 6.5.1 Materials & Methods

Utilising the database of "Black Bone" imaging previously collated the datasets and radiological reports were reviewed to identify those cases where "Black Bone" or conventional MRI sequences had been used in place of CT. The medical records for these patients were reviewed, and also for those cases where it was considered that the pathological condition requiring imaging would ordinarily be investigated with CT. MRI examination had been completed on either a 1.5T or 3T magnet at the CH or OMRI.

Whilst likely to under report the number of patient exposures, all imaging performed on the head and neck region for each patient documented on the PACs system was recorded.

### 6.5.2 Results

In total, the "Black Bone" sequence had been obtained in 69 patients as part of routine MRI of the head and neck. Of these, 33% (n=23) avoided CT examination. In these patients MRI was performed for a range of head and neck conditions including benign mandibular lesions (n=6), benign maxillary lesions (n=4), orbital fractures (n=3), facial pain (n=4), and surveillance of malignant head and neck tumours (n=6). In four cases, an MRI was performed in place of a requested CT scan. These cases are presented in Section 6.5.3 *(Table 54).* A further four cases where "Black Bone" demonstrated potential as an alternative to CT are included.

For the remaining 67% (n=46) of patients, the "Black Bone" sequence was performed in combination with CT imaging *(Table 55).* The majority of these cases had multimodal imaging performed for tumour staging or clinical suspicion of tumour recurrence. In one case, CT was

performed in addition to MRI and the "Black Bone" sequence, to further delineate the bone in a complex case of probable fibrous dysplasia.

In total 169 radiographs and 88 CT scans of the head and neck were identified on PACS for the 69 patients with "Black Bone" imaging of the head and neck. This represents an average of 1.6 plain films (n=36) and 0.8 CT scans (n=18) for patients with benign conditions, and 2.9 (n=133), and 1.5 (n=70) respectively for those with a history of head and neck malignancy.

| Patient | Age | Sex | Diagnosis | "Black Bone" sequence |
|---|---|---|---|---|
| 1 | 31 | Female | Zygomatic asymmetry | In place of requested CT |
| 2 | 38 | Male | Orbital fracture | In place of requested CT |
| 3 | 62 | Male | Mandibular keratocyst | In place of requested CT |
| 4 | 46 | Female | Maxillary giant cell granuloma | Follow up in place of CT |
| 5 | 58 | Male | Periodontal inflammation | Requested |
| 6 | 56 | Female | Mandibular keratocyst | Follow up in place of CT |
| 7 | 26 | Female | Maxillary odontogenic cyst | As part of requested MRI examination |
| 8 | 23 | Male | Zygomatic fracture | In addition to routine MRI examination |

*Table 54: Summary of presented patients undergoing "Black Bone" MRI.*

| | "Black Bone" MRI | "Black Bone" MRI + CT | Total |
|---|---|---|---|
| **Benign mandibular lesions** | 6 | 3 | **9** |
| **Benign maxillary lesions** | 4 | 4 | **8** |
| **Orbital fractures** | 3 | 0 | **3** |
| **Facial pain** | 4 | 0 | **4** |
| **Malignancy &/or surveillance** | 6 | 39 | **45** |
| **Total** | **23** | **46** | **69** |

*Table 55: "Black Bone" MRI ±CT in patients with varying pathologies of the head & neck.*

### 6.5.3 Report of Cases

***Patient 1:***

A 31 year old female was referred for CT imaging to investigate increased prominence of the right zygoma. Asymmetry of the facial features had been noted by friends of the patient two months prior to presentation, with no further progression during this period. Of note was an injury to this side of her face in childhood, which required no intervention. Radiography performed by the referring physician was normal. MRI was performed in place of the requested CT for radiation protection. Imaging demonstrated the zygomatic bodies to be within normal limits, with an acute angle between the anterior and lateral walls. The "Black Bone" sequence was useful in demonstrating a normal cortical pattern of the zygomatic bodies, with normal marrow signal from

the medulla *(Figure 77).* There was no evidence of a mass in the surrounding tissues. However, mucosal thickening in the left maxillary antrum was noted and the medial half of the anterior wall immediately below the orbital rim bulged into the cheek. The patient has been reassured that there is no significant pathology.

***Patient 2***

A 38 year old male was referred from the Emergency Department following a rugby injury. He complained of a "popping" sensation in the left globe when blowing his nose. On clinical examination there was a small palpable step in the left infraorbital rim, with no associated paraesthesia or eye symptoms. Facial radiographs performed by the referring team revealed an un-displaced fracture of the left zygoma. With no significant symptoms, the patient opted for non-surgical management, and was discharged. He re-presented 4 weeks later with diplopia on upward gaze. On clinical examination at this time he had mild enophthalmos and hypoglobus of the left orbit. CT imaging of the left orbit was requested but substituted by MRI for radiation protection. MRI demonstrated inferior displacement of almost all of the orbital floor on the left, with a mild degree of enophthalmos. A fracture was noted to extend into the inferior part of the medial wall but with no true medial wall blow-out into the ethmoid sinuses. The underlying antrum was almost completely occupied by extensive mucosal swelling with proteinaceous effusion in the remaining cavity. The "Black Bone" sequence demonstrated that the lateral antral wall was in a normal position and the zygoma appeared to be intact *(Figure 78).* He subsequently underwent open reduction and fixation of orbital fracture with autologous bone grafting.

***Patient 3:***

A 62 year old male presented with presumed recurrence of a left mandibular keratocyst, previously excised 16 years earlier. An orthopantogram (OPG) showed radiolucency of the left sigmoid notch and condyle. MRI was performed in place of the requested CT examination. The imaging confirmed a bilobed expansile lesion in the mandible on the left. Overall the lesion measured approximately 2cm x 2cm x 1cm and extended anteroinferiorly from the mandibular neck into the proximal ramus. The "Black Bone" sequence demonstrated thinning and loss of the cortex on the medial aspect of the lower margin of the lesion and again at its maximum

convexity on the medial aspect of the mandible *(Figure 79).* There was also a small area of cortical loss on the lateral aspect of the mandibular neck. However, there was no detectable extension into the soft tissues. He underwent further excision of this lesion, with histological examination confirming recurrence of the odontogenic keratocyst.

***Patient 4:***

A 46 year old female presented with buccal swelling and loosening of the upper right second premolar and first molar teeth. On OPG there was an area of radiolucency of the maxilla noted and she underwent exploration of the region, with excision of a mass. Histologically this was confirmed as a giant cell granuloma. Post-operatively she had recurrence of the mass, and was managed with calcitonin therapy, to which she had a good response. Follow up with sequential scanning has been necessary, with preference for MRI for radiation protection. "Black Bone" sequences were of sufficient quality to negate the need for CT *(Figure 80).* MRI demonstrated minimal expansion of the right antrum, which appeared to be completely occupied by the granuloma. There was expansion of the root of the right superior alveolus without displacement of the cortex or the teeth. She remains under clinical review.

***Patient 5:***

A 58 year old male presented with an intermittently painful lump in the region of the right upper second premolar tooth. This had been present for four months during which time it had gradually increased in size. On examination an 8mm bony hard lump was noted over the apex of right upper premolar. OPG showed restoration of the second premolar, but no other pathology. A "Black Bone" MRI was specifically requested to investigate this region *(Figure 81).* Imaging demonstrated no evidence of bony expansion of the right superior alveolus. There was altered signal around the roots of both right upper fifth and sixth teeth in keeping with periodontal inflammation, and a small effusion in the base of the right maxillary antrum was present. In addition, a well defined signal change was noted around the root of the right lower third tooth, in keeping with apical abscess. Under local anaesthesia the region was explored, and pus found above the disto buccal root of upper first molar tooth, which was curetted out. He was subsequently referred back to his primary care dentist for root canal therapy.

***Patient 6:***

A 56 year old female presented with recurrence of a left retromolar keratocyst. This had previously been enucleated 6 years prior to presentation. She underwent repeat enucleation and histology confirmed an odontogenic keratocyst. Recurrent imaging at 1 year demonstrated good bony infill with no evidence of cyst recurrence. The "Black Bone" sequence demonstrated normal cortical morphology, with evidence of trabecular sclerosis in keeping with healing *(Figure 82).* She remains under review.

***Patient 7:***

A 26 year old female presented with a three week history of a slowly enlarging non-painful lesion affecting the left upper jaw. Routine OPG demonstrated a radiolucency in the region of the second premolar/ first molar. MRI was requested, which demonstrated a high T2 signal lesion arising between the roots of the left upper sixth tooth. "Black bone" imaging demonstrated the lesion extended superiorly into the alveolus and breached the lateral cortex, with a dumbbell extension into the subcutaneous tissues of the cheek *(Figure 83).* The findings suggested a slow growing lesion such as a keratocyst or ameloblastoma. A fine needle aspiration of the region confirmed a diagnosis of a benign odontogenic cyst, and the remnants excised following root canal treatment of the adjacent teeth.

***Patient 8:***

A 23 year old male presented following an alleged assault, having fallen to the ground hitting his face. On examination he had mild left infraorbital anaesthesia and slight flattening of the left malar region. Radiographs showed a minimally displaced left zygomatic fracture. He failed to attend follow up, but returned 3 weeks later complaining of worsening diplopia. However, he had a longstanding squint for which he was not currently using his prescription glasses. A Hess chart used to assess diplopia (by demonstrating the position of the non-fixing eye in all positions of gaze when the other eye was fixing), showed no change. Routine MRI was requested. Coronal images demonstrated that the left orbital floor was normal. There was no evidence of surrounding fracture on the "Black Bone" images *(Figure 84).* He was reassured, and discharged from further follow-up.

All of these presented patients avoided CT examination by utilising the "Black Bone" sequence.

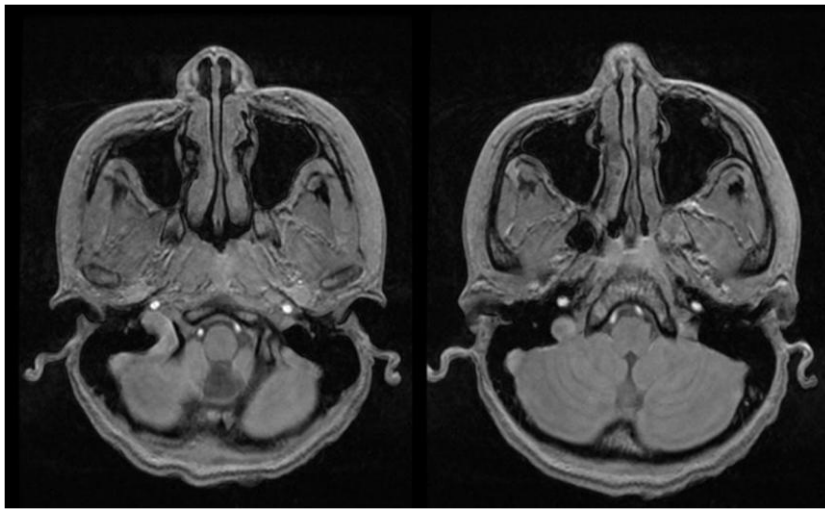


*Figure 77: Axial "Black Bone" imaging of Patient 1 demonstrating normal zygomatic bodies.*

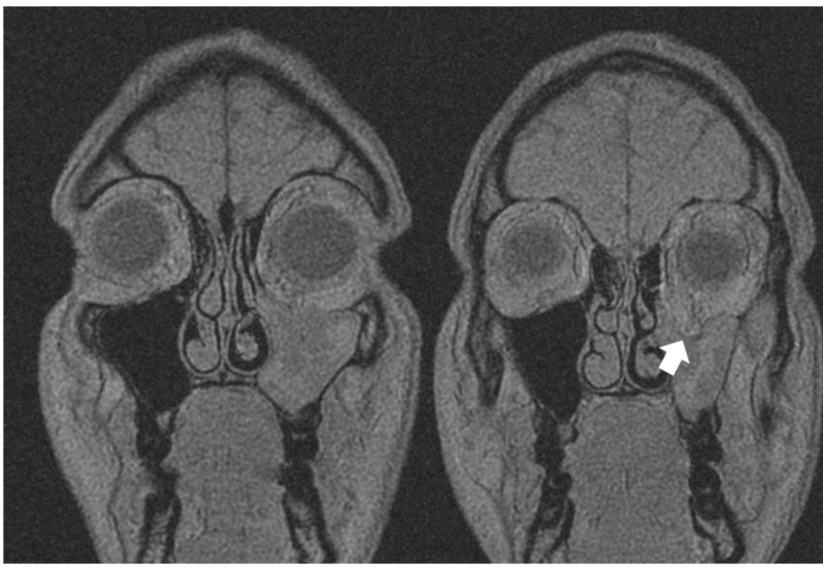


*Figure 78: Coronal "Black Bone" images of Patient 2 demonstrating inferior displacement of the left orbital floor, and fluid within the left maxillary sinus.*

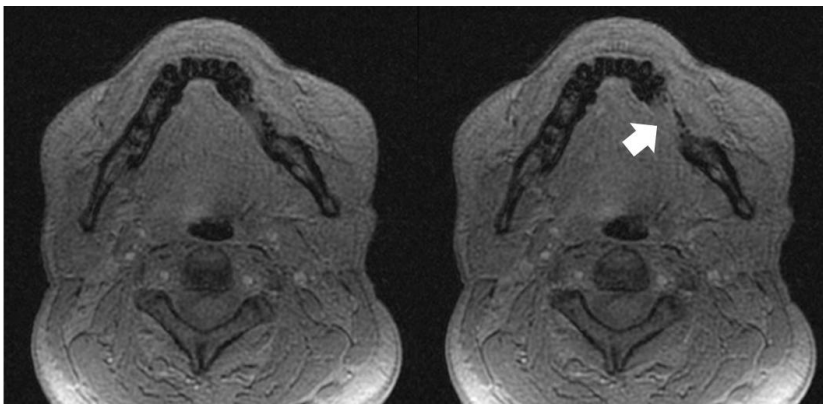


*Figure 79: Axial "Black Bone" images of Patient 3, demonstrating thinning and loss of the cortex on the medial aspect of the lower margin of the left mandibular keratocyst.*

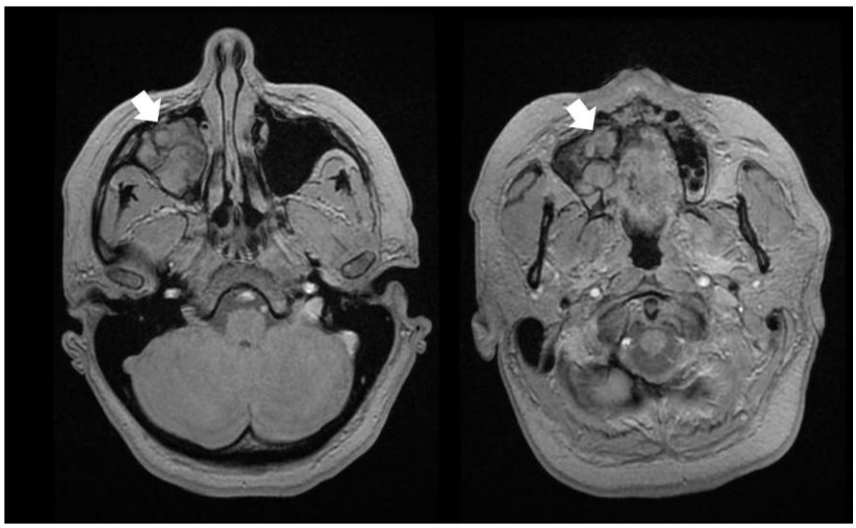


*Figure 80: Axial "Black Bone" images of Patient 4, demonstrating granuloma within the right maxillary sinus.*

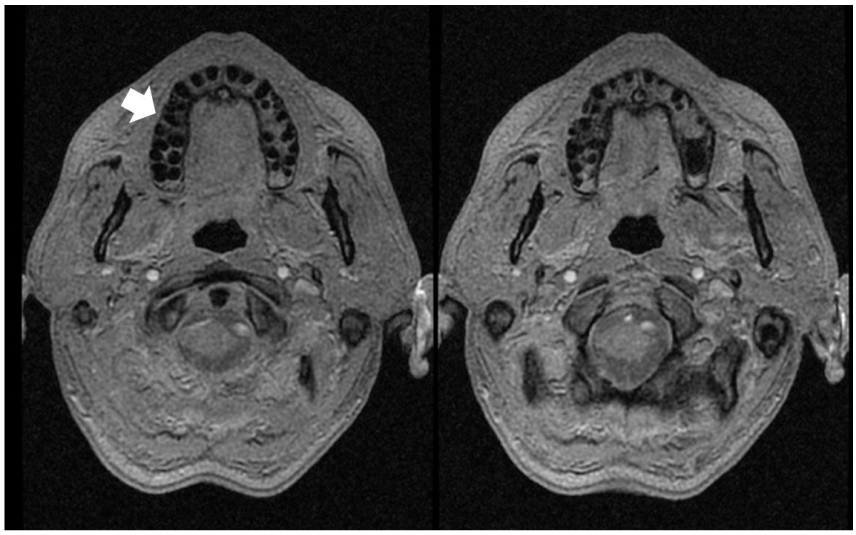


*Figure 81: Axial "Black Bone" images of Patient 5, demonstrating no evidence of bony expansion of the right superior alveolus.*

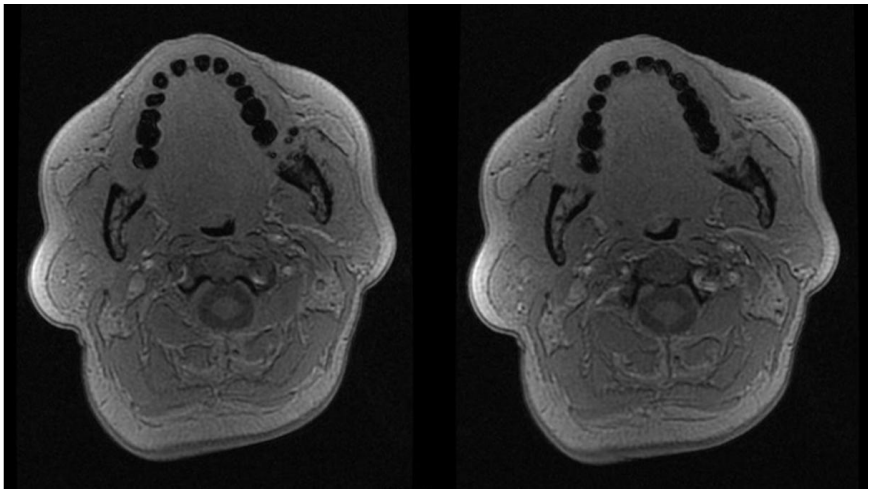


*Figure 82: Axial "Black Bone" images of Patient 6, demonstrating normal cortical morphology, with evidence of trabecular sclerosis at site of previous left retromolar keratocyst.*

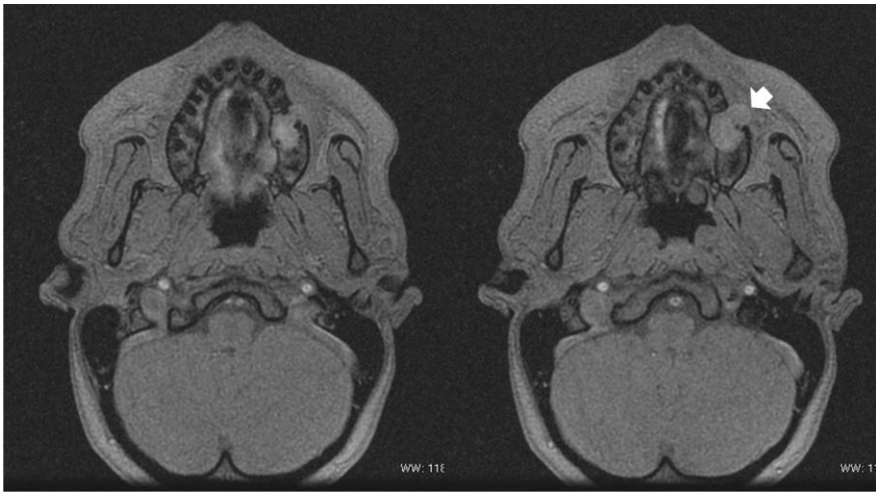


*Figure 83: Axial "Black Bone" images of Patient 7, demonstrating a lesion within the left maxillary alveolus which breaches the lateral cortex with extension into the subcutaneous tissues of the cheek.*

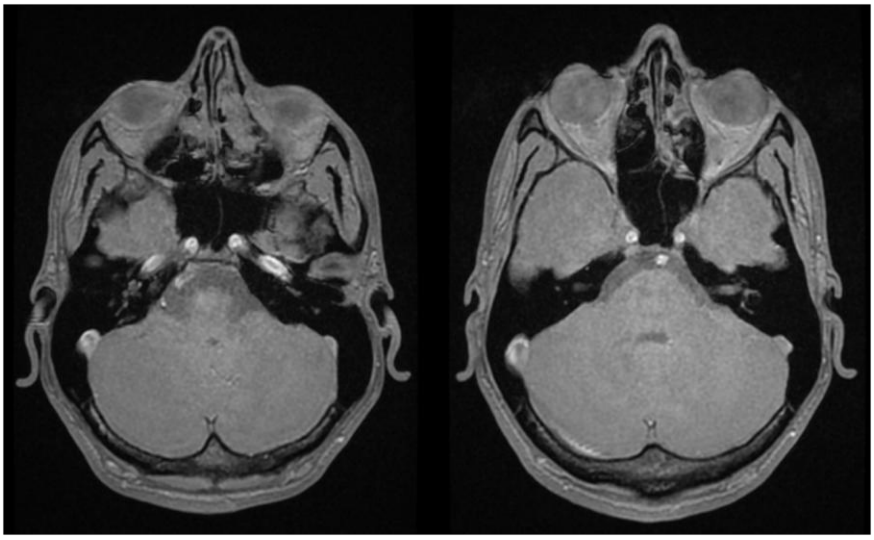


*Figure 84: Axial "Black Bone" images of Patient 8, with normal appearances of the orbital bones.*

### 6.5.4 Discussion

The potential benefits of "Black Bone" MRI when imaging the craniofacial region have been demonstrated. The key limitation of the technique is in areas where black bone abuts black air, such as the sinuses, which makes separation of the two particularly challenging. However, the sequence has been successfully utilised to both exclude and identify fractures of the facial skeleton, and for both benign and malignant infiltrating tumours. As with other MRI sequences, "Black Bone" is susceptible to artefact and degradation of image quality in the region of dental amalgam, and implanted materials.

Review of the 69 patients in this study, demonstrates that the average patient with malignancy undergoes 2-9 plain films and 1.5 CT examinations. This value is likely to severely under report the actual number of imaging procedures each patient undergoes, since further examinations are performed in primary care, and at alternative units both prior to referral and for local follow-up. Whilst the effective dose from CT scans of the head and neck are considerably lower than those for imaging the chest or abdomen, the head and neck region, as shown in this study, are more frequently imaged and the collective dose for cranial imaging therefore higher.

## Chapter Conclusion

It has been demonstrated that MRI, both routinely used sequences and "Black Bone," confers significant advantage to CT in adults when imaging the craniofacial skeleton. Tumour volume measurements provide improved prediction of clinical outcome in adults with malignancy involving the maxillary complex and mandible. "Black Bone" has been demonstrated to be a viable method of avoiding CT in a range of pathological conditions affecting the head and neck. For "Black Bone" to be widely considered in place of CT the ability to produce 3D rendered images and anatomical models of the craniofacial skeleton are required, and provides the focus of the next chapter.

# 7. 3D MRI & Anatomical Models

## 7.0. 3D Reconstruction & Anatomical Models

For “Black Bone” MRI to be of benefit to the craniofacial/maxillofacial communities, the ability to obtain 3D data sets and anatomical models of the craniofacial skeleton are required to aid with diagnosis and surgical planning. Three-dimensional reconstruction of bone using CT data has become standard practice in these specialities, made possible by the distinct Hounsfield number of bone compared to soft tissue and air. However, with MRI the pixel values of bone are also found in the soft tissues and air. With the “Black Bone” sequence, the impact of these overlapping pixels within the soft tissues is minimised, however the greatest challenge arises in areas where air and bone are in close proximity.

This section of the thesis explores a number of techniques and software to explore the potential of 3D reconstruction of “Black Bone” MRI datasets.

“Black Bone” datasets obtained from each aspect of the thesis were utilised in this section, including work with phantoms, animal models, adult volunteers, children with craniosynostosis, adolescents with facial disproportion and adults with a range of head and neck pathologies. Whilst each section is subdivided into patient groups of interest, research was conducted simultaneously for all datasets, with experimentation of techniques in one patient group resulting in advancements in another.

Experimentation and development of 3D rendering techniques using various commercially available software packages is included, with subsequent review of the accuracy of the 3D results and utilisation in the production of anatomical models.

## 7.1 3D Rendering Techniques

This section of the thesis explores the potential of a range of commercially available 3D rendering techniques to obtain 3D reconstructed images of the craniofacial skeleton from "Black Bone" datasets. All available "Black Bone" datasets were utilised for exploration including the phantom skull and cube datasets; four "Black Bone" datasets were available in children with normal cranial sutures *(Table 56)*, and 13 in children with craniosynostosis *(Table 57)*. To recap, the phantom skull consisted of an adult skull housed in a Perspex shell filled with copper sulphate solution, and the cube phantom was a Perspex cube contained within a pot filled with gelatine *(Figure 85)*.

| Patient | Age | Sex | Diagnosis |
|---|---|---|---|
| 1 | 3 years | Female | Langerhans Histiocytosis |
| 2 | 5 years | Male | Posterior fossa anaplastic ependymoma |
| 3 | 9 months | Female | Haemangioma of cheek |
| 4 | 13 months | Male | Metastatic Neuroblastoma |

*Table 56: Children with normal cranial sutures undergoing "Black Bone" MRI.*

| Patient | Age | Syndromic? | Diagnosis | Imaging location |
|---|---|---|---|---|
| **1** | 5mths | No | Sagittal synostosis | WW |
| **2** | 12mths | No | Sagittal synostosis | WW |
| **3** | 22mths | No | Sagittal synostosis | WW |
| **4** | 5mths | No | Sagittal synostosis | WW |
| **5** | 10mths | No | Right unicoronal synostosis | WW |
| **6** | 19mths | Yes - Crouzons | Sagittal & lambdoid synostosis | WW |
| **7** | 9mths | No | Right unicoronal synostosis | WW |
| **8** | 17mths | No | Metopic synostosis | WW |
| **9** | 8mths | ?Yes | Sagittal synostosis | WW |
| **10** | 9yrs | No | Sagittal synostosis | OMRI |
| **11** | 12yrs | No | Sagittal synostosis | OMRI |
| **12** | 12yrs | No | Sagittal synostosis | OMRI |
| **13** | 2mths | Yes - Aperts | Bilateral coronal synostosis | CH |

*Table 57: Children with craniosynostosis.*



*Figure 85: Phantoms used for CT and MRI imaging; skull phantom encased in Perspex shell filled with copper sulphate solution (top) and Perspex cube encased within gelatine (bottom).*

### 7.1.1. Advantage Windows Workstation

The first phase of the investigation of 3D reconstruction with "Black Bone" MRI was with an AWW. The AWW is a multi-modality workstation with image processing and analysis functions incorporating one-click applications and protocols including automatic segmentation tools for volume rendering of CT datasets.

#### 7.1.1.1 Phantom and Animal Models

The phantom skull dataset was imported into the AWW, and the threshold adjusted. Since air and bone on the "Black Bone" datasets have overlapping pixel values it was necessary to sacrifice a small amount of bone quality to minimise the surrounding air to permit visualisation of the skull and enable manual segmentation. The manual segmentation tool allows free-form selection of a region to remove or keep. This process could be completed on any of the orthogonal views or directly on the 3D rendered image. When performed on the orthogonal views it was important to adjust the cut depth to avoid interpolation to the entire dataset. The results achieved for the phantom skull are shown in *Figure 86.*

To determine the impact of soft tissues on the segmentation process, the piglet "Black Bone" dataset was used. Following the same workflow developed for the phantom skull, a threshold was selected for the piglet dataset and subsequently manually segmented. It was difficult to accurately determine the limits of the bone on the superior surface of the piglet, thus making accurate manual segmentation impossible. In the regions where the bone was segmented it was possible to visualise the posterior skull sutures and the mandibular symphysis *(Figure 86).*

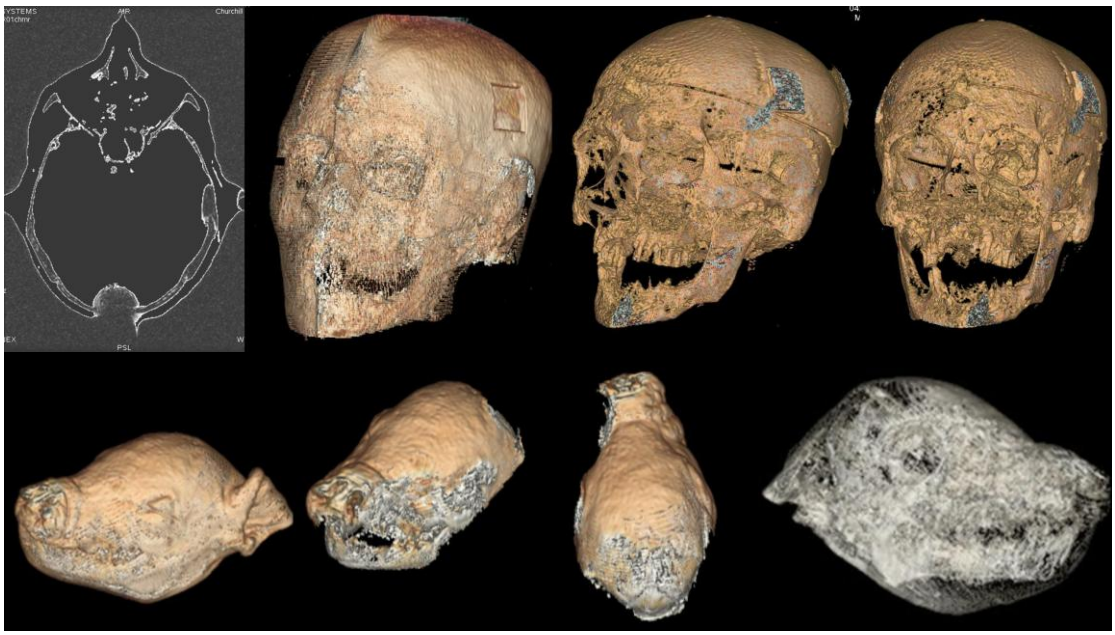


***Figure 86: Initial attempt at 3D rendering using AWW of the phantom skull dataset (top row), showing the thresholding process and manual segmentation. Note the loss of bone density as a result of compromise with the thresholding levels. Results obtained for the piglet "Black Bone" dataset (bottom row). The superior soft tissues could not be accurately removed.***

### 7.1.1.2 Adult Volunteer and Children Datasets

With one of the adult volunteer "Black Bone" datasets experimentation was undertaken with the volume rendering tools on the AWW. As with the phantom and piglet datasets it was necessary to compromise on the quality of the craniofacial skeleton to permit visualisation of the ROI for manual segmentation. The resultant 3D rendered images were of reasonable quality in terms of identification of the features of the craniofacial skeleton; however, they lacked the clarity and smoothness achievable with CT datasets *(Figure 87).*

The results obtained with one of the "Black Bone" datasets from a child with normal cranial sutures (Patient 1) are shown in *Figure 87*. Selection of a suitable threshold level for this dataset was more challenging, and attempts to manually segment the bone were particularly time consuming.

It was apparent that the segmentation tools available on the AWW were of limited value in rendering the "Black Bone" datasets and attention was turned to other software packages.

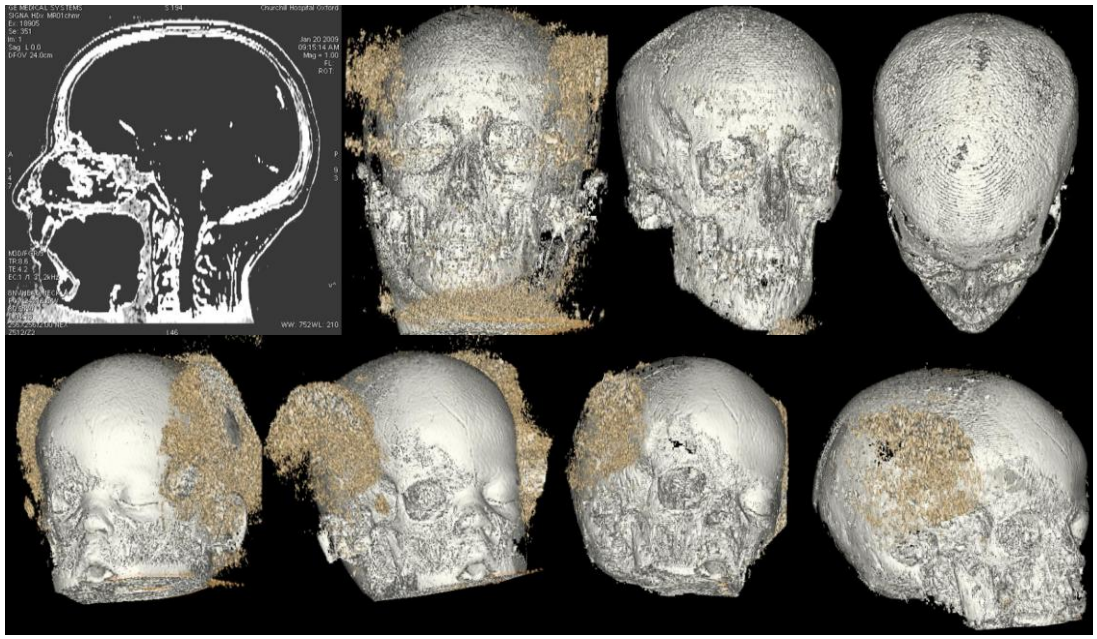


***Figure 87: Volume rendering of adult volunteer (top row) and child (bottom row) "Black Bone" datasets, demonstrating the difficulty in correct threshold selection and the process of manual segmentation.***

### 7.1.2 BrainLab

BrainLab was obtained on trial, supplied with the craniomaxillofacial (CMF) add-on package. In clinical practice the CMF applications are mainly utilised for pre-operative planning with the ability to perform virtual surgery simulation by segmentation and movement of aspects of the craniofacial skeleton independent of one another *(Figure 88).* The techniques utilised by BrainLab include atlas-based automatic segmentation of CT datasets. However, independent 3D rendering techniques for non-CT data are somewhat limited to threshold based and "magic tool" segmentation *(Figure 88).*

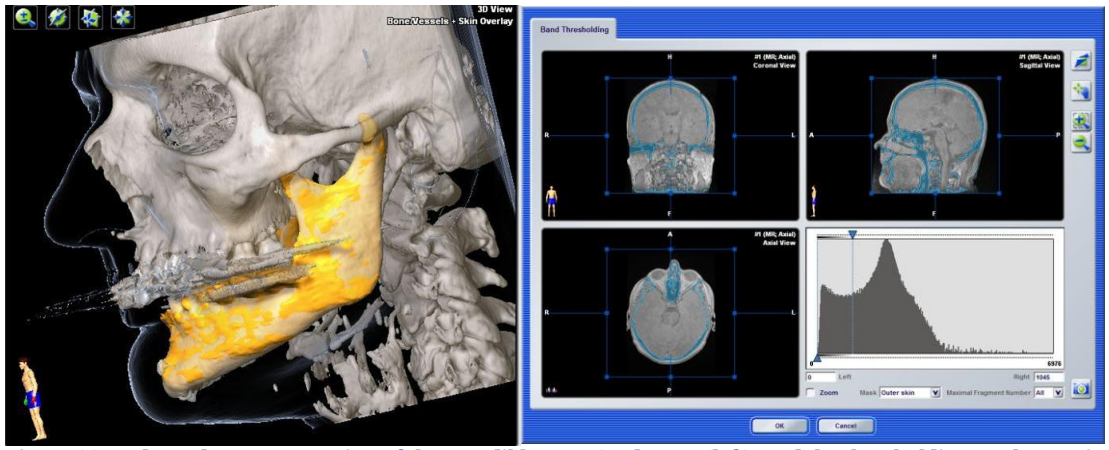



*Figure 88: Independent segmentation of the mandible on a CT dataset (left), and the thresholding workspace in BrainLab with a "Black Bone" dataset (right).*

"Black Bone" datasets obtained from adult volunteers were imported into BrainLab for exploration of the segmentation techniques. Utilising the soft tissue – bone contrast, the "Black Bone" dataset was segmented using the thresholding functions. There were two key limitations to this technique; firstly, the surrounding air was of the same pixel value as the bone and therefore also needed to be removed, and secondly, there were some areas of overlap of the pixel values between the bone and soft tissues resulting in small additional areas on the 3D image which did not truly represent bone. One method utilised to remove the surrounding air was to create a region of interest around the outer soft tissue envelope of the head, to which the thresholding process was restricted *(Figure 88).* However, again any small error in the creation of the ROI resulted in the residual air appearing as bone on the 3D image.

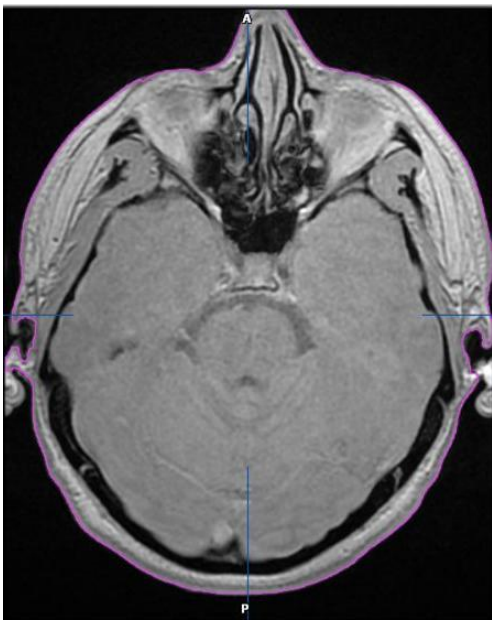


*Figure 89: Axial "Black Bone" MRI demonstrating ROI set at the limit of the soft tissue envelope.*

An alternative technique to segment the bone was to utilise the "magic brush" tool. This was successful in identifying the boundary between brain-bone and soft-tissue-bone, to permit segmentation of the intervening bone *(Figure 90).* Whilst useful for the skull cap, difficulties arose in the region of the middle ear where there was no boundary between air and bone.

Using a combination of these techniques it was possible to segment the entire craniofacial skeleton on the adult volunteer datasets *(Figure 91).* Interestingly the software had some in-built constraints in the application of colour to the segmented objects; since bone segmentation could not be performed automatically on the "Black Bone" datasets, it was not possible to assign a more traditional bone colouration to the resultant image. The software does not have any inherent ability to create or export a movie of the 3D rendered dataset, a function that has been demonstrated to be

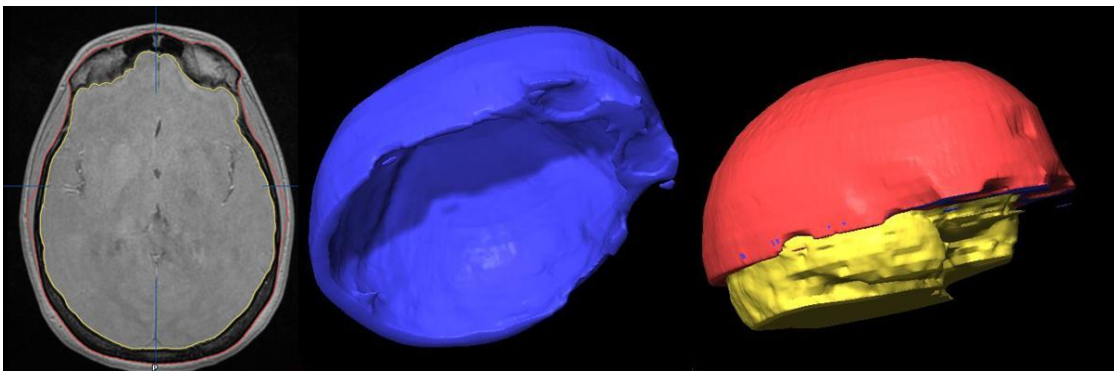


*Figure 90: Segmentation of the skull cap using the magic brush tool to independently identify the soft-tissue-bone and brain-bone boundaries (left), to obtain a 3D image of the skull cap (centre) and as a composite image including the underlying brain (right).*

particularly valuable for pre-surgical planning. With no functionality to perform fine manipulation directly on the 3D rendered image, the segmentation had to be confirmed on each axial image slice which was both challenging and time consuming to obtain an accurate result. The results of the first dataset in *Figure 91* demonstrate difficulties around the superior aspect of the piriform aperture. This highlights how a small error in the segmentation process in a very small number of axial slices can have a significant impact upon the resultant 3D image. It was concluded that whilst the images obtained were of reasonable quality, the labour intensive processes necessary to achieve them and the limited export capabilities of the software, BrainLab did not provide a suitable methodology for transfer to the clinical environment.

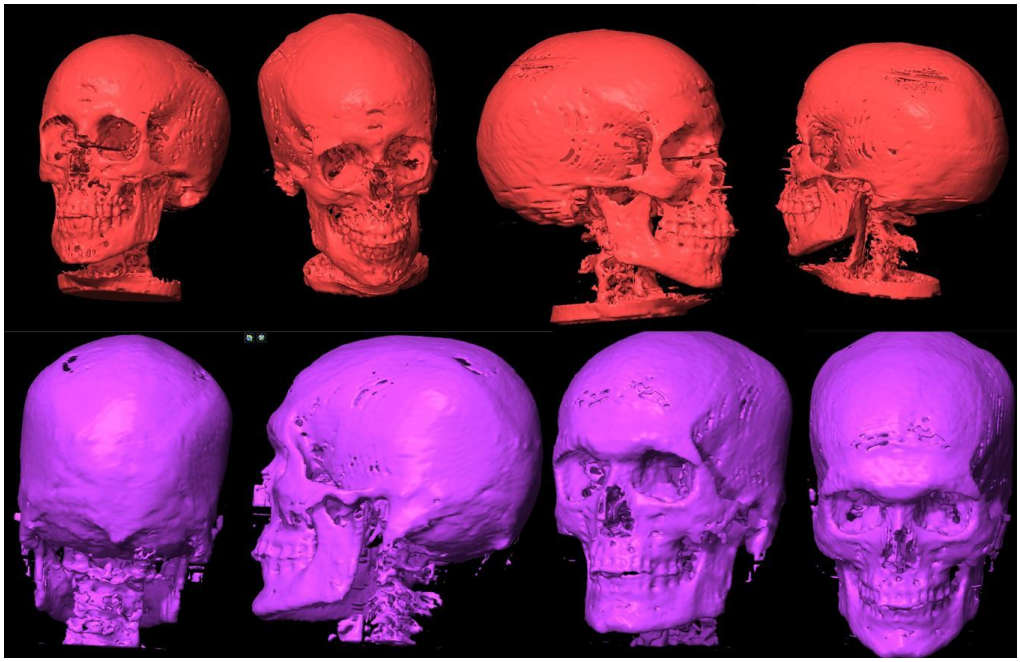


***Figure 91: 3D rendered images of adult volunteer "Black Bone" datasets using BrainLab.***

### 7.1.3 InVesalius

InVesalius is an open source imaging package developed at the Technology of Information Renato Archer Centre, of the Ministry of Science and Technology in Campinas, Brazil. Currently the user guide is only available in Portuguese, making experimentation somewhat of a trial and error process. DICOM data can be viewed in orthogonal planes with regions of interest being selected by thresholding to create the 3D surface.

#### *7.1.3.1 Phantom Datasets*

Initial exploration with InVesalius was undertaken with the skull phantom. The ROI was selected using thresholding, and the 3D surface calculated. By using the option to "select largest part" the transparency of the resultant 3D surface could be adjusted to visualise the underlying skull *(Figure 92)*. Within the advanced editing tool bar there was the ability to edit the mask using an erase tool. This however was time consuming as each individual slice needed to be edited individually. There was no method to undo any incorrect editing, which made any minor inaccuracy potentially disastrous. Overall, the results obtained with the phantom skull dataset were particularly poor. With no method to edit the 3D rendered image dataset, the potential of InVesalius with "Black Bone" datasets was deemed to be very limited, and attention was turned to other available software packages.

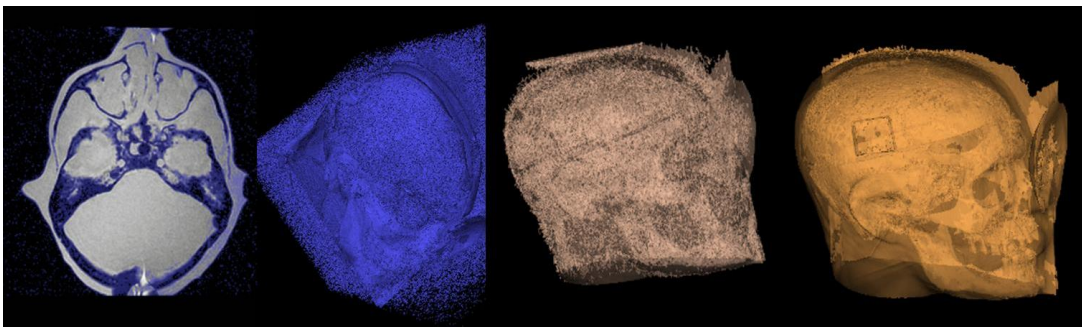


*Figure 92: Workflow in InVesalius. Segmentation of the bone was particularly challenging, and a 3D image of purely the craniofacial skeleton could not be achieved.*

### 7.1.4 MITK-3M3

MITK 3M3 is an open source software developed by the German Cancer Research Centre and Mint Medical. It enables 2D and 3D visualisation, co-registration, volumetric analysis and also has export functions.

#### *7.1.4.1 Phantom Datasets*

Initial investigation was undertaken with the phantom skull dataset. However, with difficulties in segmenting the skull, the workflow was reviewed with a CT dataset and subsequently the phantom cube "Black Bone" dataset since this provided images with no communication between the cube and surrounding air *(Figure 93).*

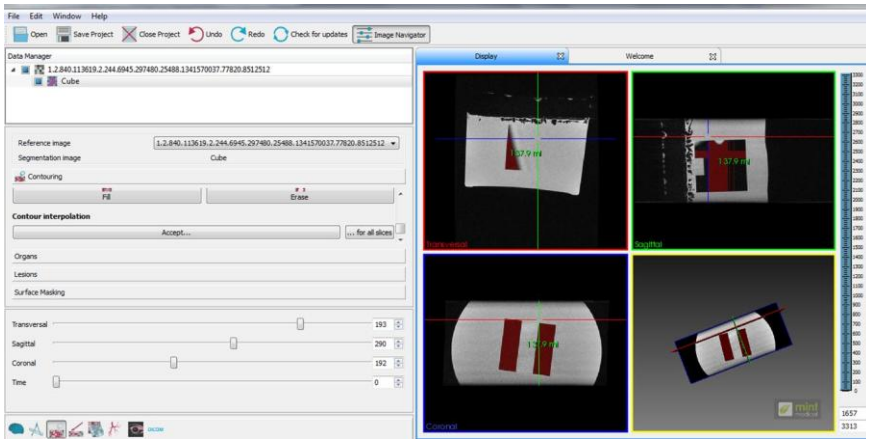



***Figure 93: Screen layout in MITK-3M3, using region growing tool with phantom cube "Black Bone" dataset.***

The thresholding function which was useful in segmenting the CT dataset was not useful for the "Black Bone" dataset; this was limited to one threshold value (rather than a range with upper and lower limits), making it impossible to distinguish the cube from the surrounding gelatine.

Use of the region growing tool was time consuming, since the ROI had to be defined on each image slice, often in all orthogonal planes. The interpolation function appeared to be of limited benefit. Once this process had been completed it was possible to produce a polygon model (3D image). However, any minor inaccuracy with the region growing process resulted in a corresponding error on the 3D image *(Figure 94).*

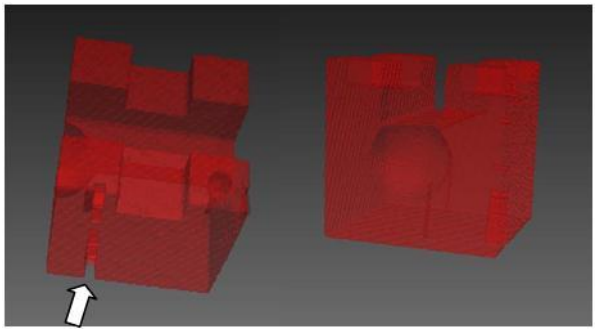


*Figure 94: Polygon model of the phantom cube. Note the inaccuracy on the front left pillar on the first image.*

On investigating the volume rendering functions, whilst these worked well with CT data, the inability to remove the surrounding air made this of limited benefit with "Black Bone" datasets *(Figure 95).*

With the skull phantom "Black Bone" dataset the threshold in which the entire phantom was included was selected and the region growing tool used to remove the surrounding copper sulphate filled shell to segment the bone. However, as shown in *Figure 96,* this was not accurate in view of the overlap in pixel values, with removal of bone on many of the slices.

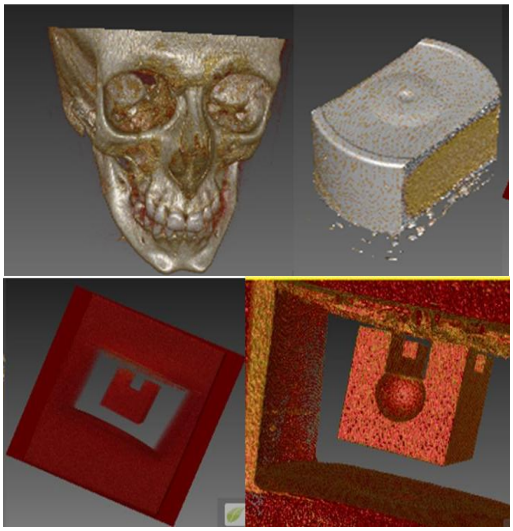


*Figure 95: Volume rendering with CT dataset (top left), and "Black Bone" phantom cube dataset. Note the inability to remove the surrounding gelatine on the first image having successfully removed air (and possibly also the cube itself). In the final two images the outside air could not be removed.*

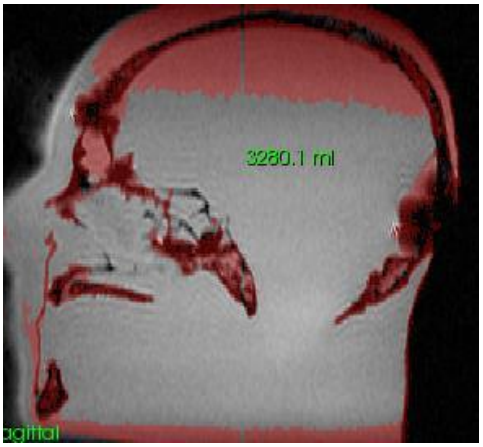



*Figure 96: Attempting to use the region growing tool to remove the surrounding copper sulphate filled shell on the phantom skull.*

### 7.1.4.2 Adult Volunteer Datasets

Using the adult volunteer datasets problems were again encountered with MITK 3M3. It was not possible to either threshold or segment the skull with the region growing tool with any accuracy. Multiple selections were required on each imaging slice with the region growing tool which made it an unfeasible method of segmenting the "Black Bone" datasets. With the volume rendering function, a reasonable 3D image of the skull was obtained but there was no facility to remove the surrounding soft tissues. Shown in *Figure 97*, is a volume rendered image, and mapped onto this, in red, is the polygon model that was produced from an attempt to segment the skull – this small area took over 30 minutes to create. MITK 3M3 was therefore also deemed unsuitable for the "Black Bone" datasets.



***Figure 97: Volume rendered image of adult "Black Bone" dataset (gold) with polygon overlay of model produced via region growing segmentation.***

### 7.1.5 Mimics

Mimics is a generic 3D visualisation tool with the ability to create and manipulate multiple image masks. Many of the techniques used by BrainLab are also used here. Additional functions include the ability to edit the image in 3D, edit the mask in the axial plane with interpolation between slices (multiple slice edit) and smooth the resultant image.

#### *7.1.5.1 Phantom and Animal Models*

Initial investigation with Mimics was undertaken with the skull phantom. Using the thresholding function, the optimal range for the craniofacial bone was selected. This resulted in the surrounding air also being included in the mask. The mask was cropped to remove as much of this air as possible, and was then edited using the "multiple slice edit" function and "edit mask in 3D" *(Figure 98)*. The resultant 3D results are shown in *Figure 99.*

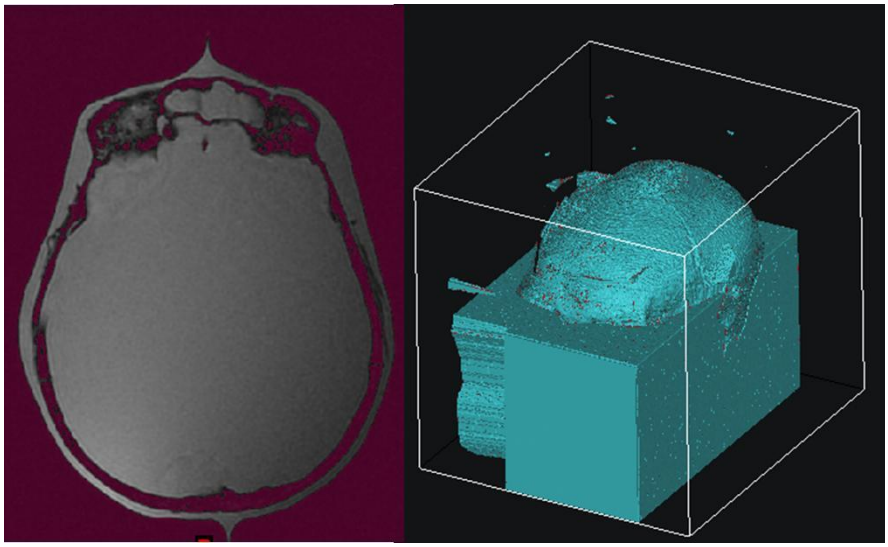


*Figure 98: Threshold selection and mask editing in 3D in Mimics.*

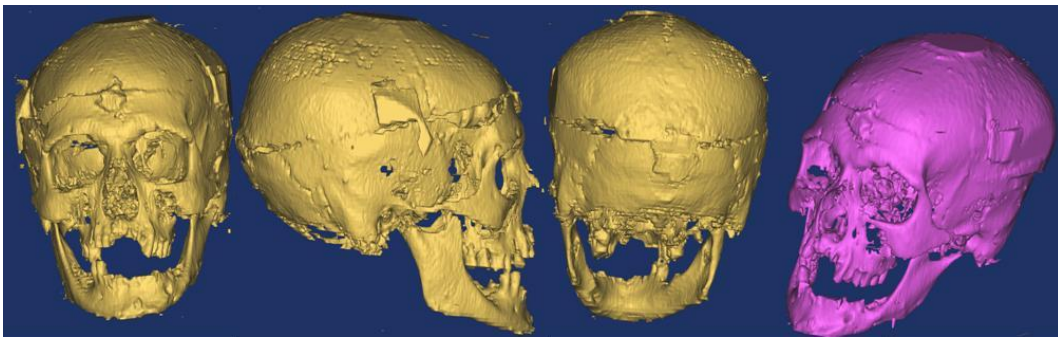


*Figure 99: 3D rendered images of the phantom in Mimics, and following application of a smoothing factor (far right pink image).*

Applying these techniques to the piglet dataset was more technically challenging as the bone was particularly thin. The final result after applying a smoothing factor is shown in *Figure 100*. The mandibular symphysis can be clearly seen, however, the cranial sutures could not be determined in view of the resultant bone loss secondary to the thresholding selection.

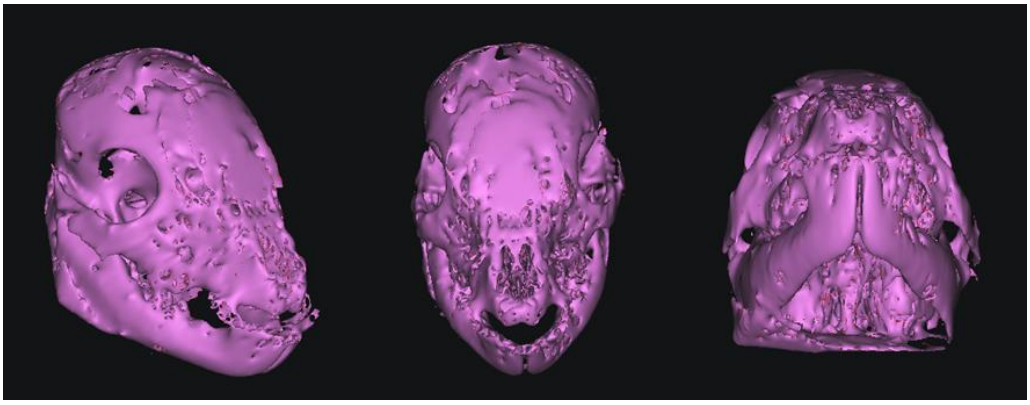


*Figure 100: 3D rendered "Black Bone" MRI dataset of piglet using Mimics.*

### *7.1.5.2 Adult Dataset*

The "Black Bone" datasets obtained from adult volunteers and adult patients undergoing imaging for a range of pathologies were individually imported into Mimics, and the 3D rendering techniques further explored. Working with the technical support team at Mimics, further options were developed to segment the craniofacial skeleton. Firstly a threshold was set which included all of the surrounding air, the mask was cropped to include only the cranium or mandible excluding any regions where there was communication between air and bone (middle ear and mouth). Using the region growing tool a second mask was created by clicking on a region of bone. It was necessary to do this on each image slice to avoid inadvertently including the surrounding air *(Figure 101).* Reasonable results were thus achieved for the cranium, brain and mandible *(Figure 102, Movie Clip 1 & 2).* However, this workflow was not suitable for any region where air and bone came into close contact, and therefore could not be utilised to segment the entire craniofacial skeleton. This would be of limited use in children, where the soft tissues are particularly thin over the cranium thus increasing the likelihood of apparent fine communication between air and bone on the image, possibly as a result of blood vessels on the bone surface.

Experimentation with the "Boolean operations" which permit the subtraction or addition of masks proved of limited benefit since the resultant mask always resulted in a small rim around the soft tissue of the skull which had to be manually segmented.

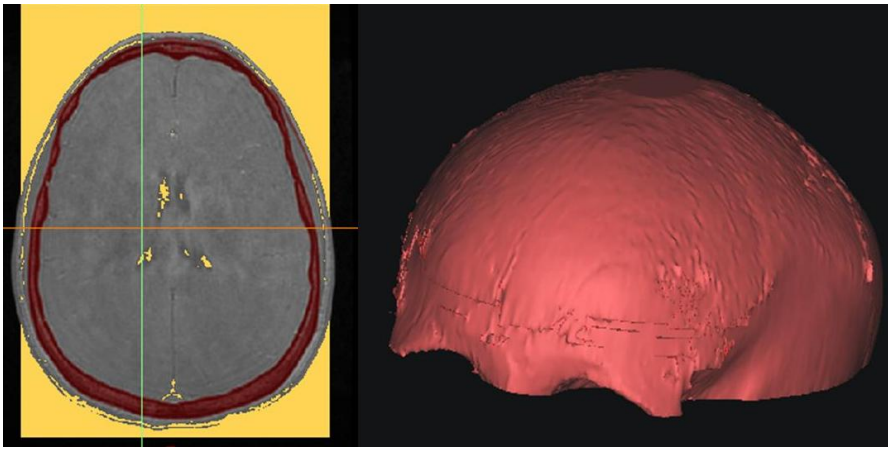


*Figure 101: Region growing tool to create second mask (red) from first (yellow) and resultant 3D image.*

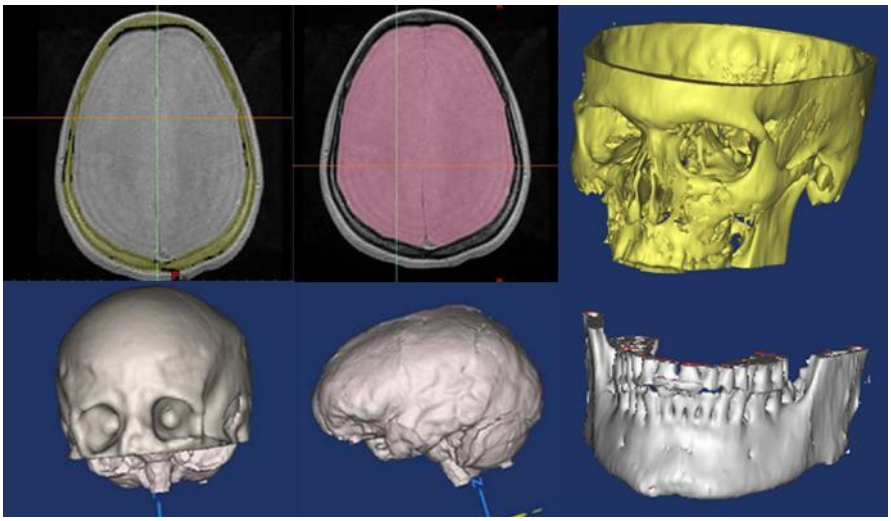


*Figure 102: Segmentation of the skull (left) and brain (centre) using region growing tool; and with multiple-slice and 3D edit (right).*

### *7.1.5.3 "Black Bone" Datasets from Children*

Utilising the techniques thus far developed in Mimics, further exploration was undertaken with three of the "Black Bone" datasets obtained from children with normal cranial sutures. The resultant 3D images are shown in *Figure 103*. What was apparent was that correct threshold selection was essential to permit distinction between the cranial bone and cranial sutures.

The use of thresholding to segment the cranial bone resulted in a number of inaccuracies and inconsistency across the datasets. Whilst the cranial sutures could be visualised in two of the children, no sutures were visible on the 3D rendered image for Patient 2. In addition, the sagittal suture was partially obscured in Patient 1. This could potentially result in an inaccurate diagnosis in cases of suspected craniosynostosis. Attempts were made to utilise the "3D live wire" tool to segment the bone as an alternative to thresholding. This is used successfully in the long bones to identify the soft-tissue-bone boundary, however, this was not useful for the craniofacial skeleton *(Figure 104).* The 3D volume rendering function was successful in identifying the underlying bone and cranial sutures through semi-transparent soft tissues *(Figure 104).* Whilst this may be of potential benefit in the distinction between normal and prematurely fused cranial sutures the inability to fully segment the bone would not enable the creation of anatomical models.

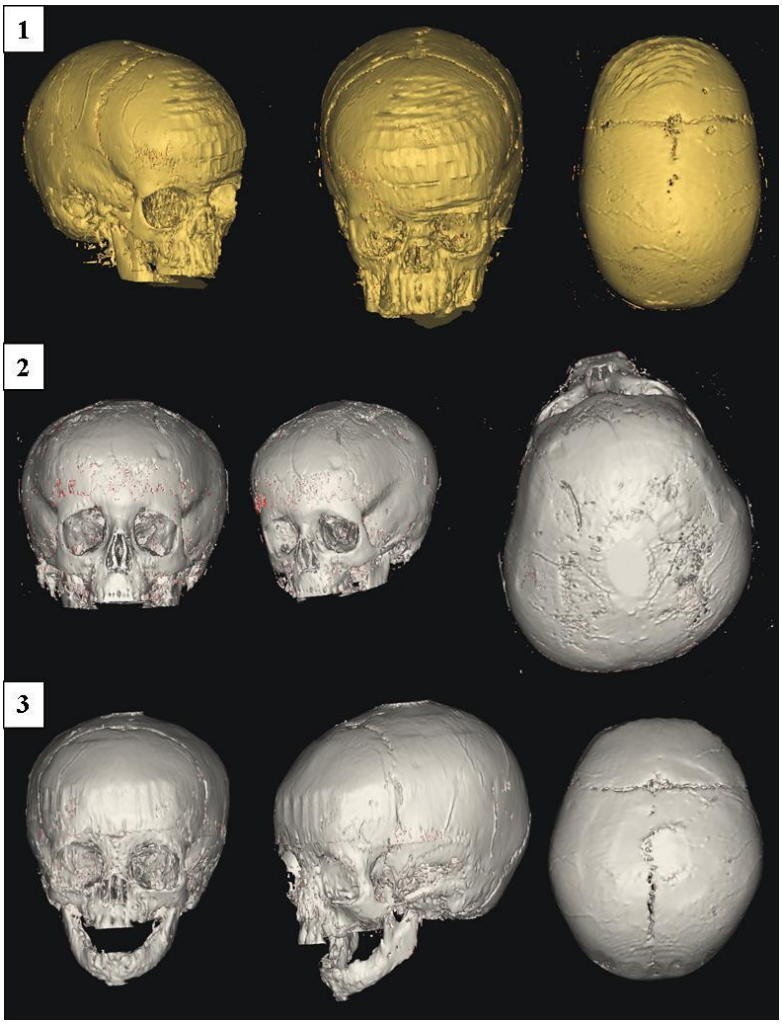



***Figure 103: 3D reconstructed images of children with normal cranial sutures using Mimics. Note that the sagittal suture is partially obscured in Patient 1.***

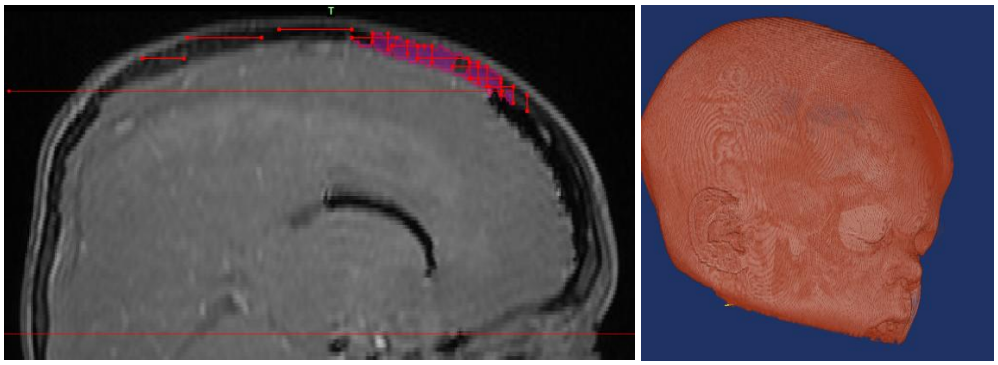


*Figure 104: Using the 3D live wire tool (left) and volume rendering functions in Mimics.*

### *7.1.5.4 Mimics and Craniosynostosis*

The results for the 13 children with craniosynostosis in Mimics are shown in *Figure 105 (Movie Clip 3 & 4)*. With these "Black Bone" datasets similar problems were encountered in attempting to segment the craniofacial skeleton. The application of a threshold was the starting point in Mimics, and whilst this could be later adjusted, it was often not until the 3D image was created that it became apparent that the wrong threshold had been set. At this stage, the mask had been edited to remove surrounding air, and any adjustment of the threshold resulted in the image being reset. The distinction between the normal and prematurely fused could therefore not always be accurately distinguished. For this reason, Mimics would seem unsuitable for reliable segmentation of these datasets in clinical practice.

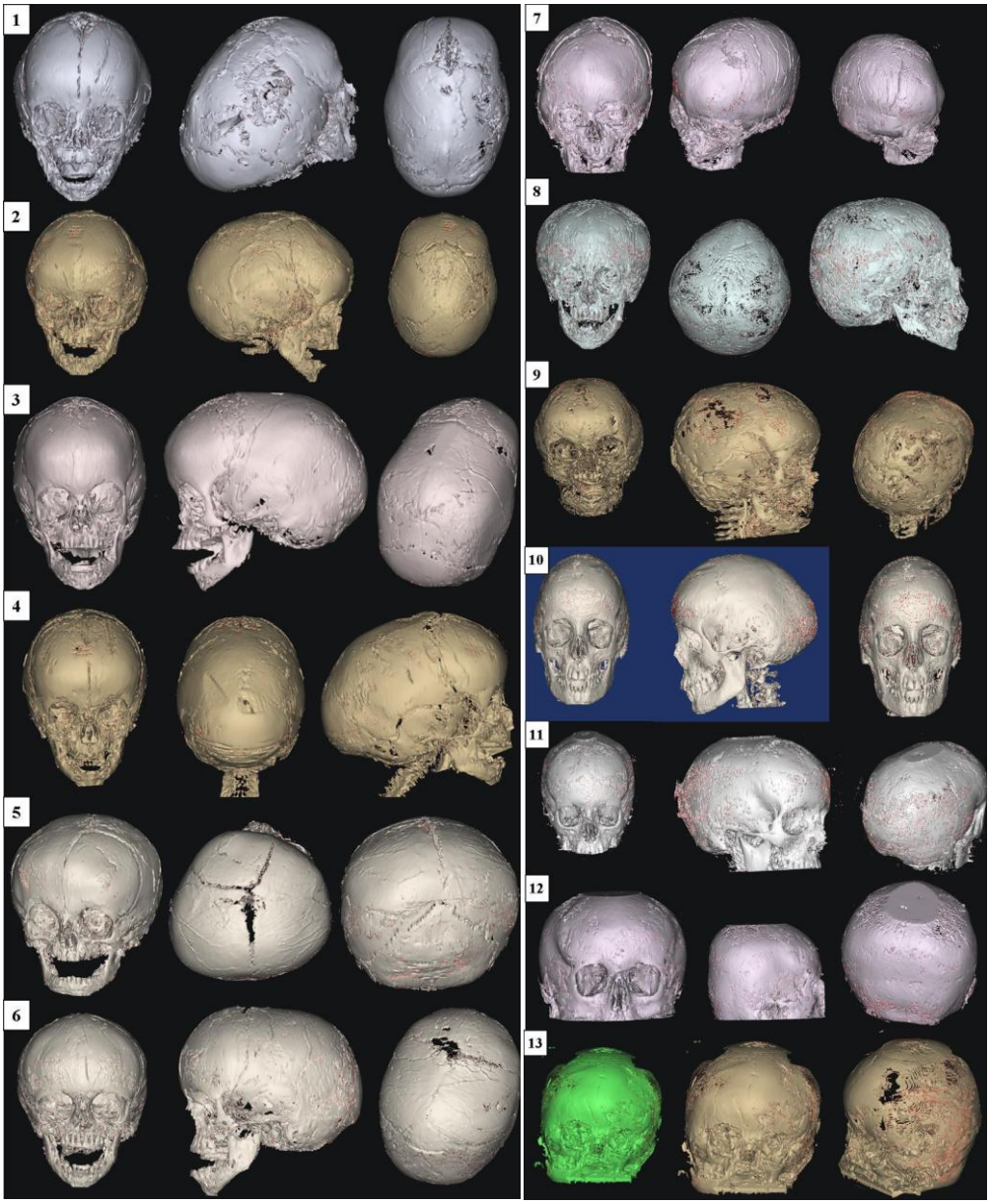



*Figure 105: 3D rendered images of "Black Bone" datasets in children with craniosynostosis using Mimics.*

### 7.1.6 Osirix

Osirix is an open source application developed for use solely on Apple Mac. Both volume and surface rendering options are available.

#### *7.1.6.1 Phantom*

The phantom skull "Black Bone" dataset was imported into Osirix. Using the surface rendering option, the skull could be identified by adjusting the transparency *(Figure 106).* Difficulties were encountered when attempting to segment the skull as a result of communication between bone and air on the "Black Bone" dataset. Attempts to achieve this were subsequently explored on the adult volunteer datasets.

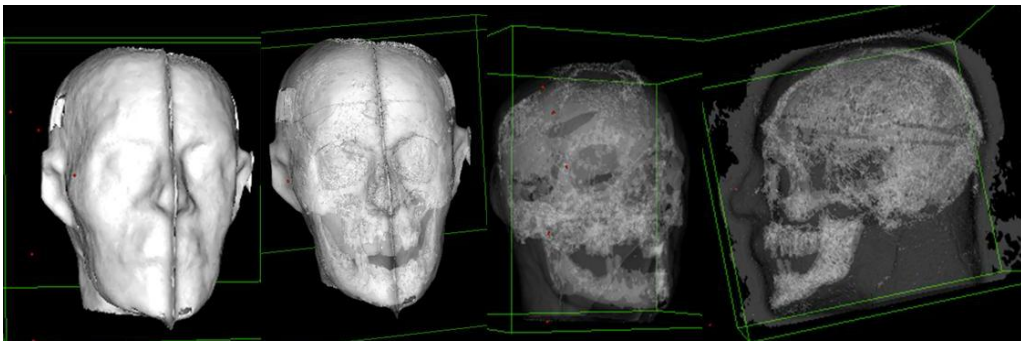


***Figure 106: Surface rendering of phantom using Osirix, with adjustment of the transparency to visualise the underlying skull.***

#### *7.1.6.2 Adult Datasets*

A ROI was created around the soft tissue edge using the closed polygon ROI editor. The pixels outside of the ROI were set to an arbitrary value that would no longer coincide with those within bone e.g. 5000, and the ROI outline then deleted. Using the threshold tool, either with threshold levels, neighbourhood or confidence interval selection, the optimal value was selected by visualisation for the bone. This became the new ROI. The pixels outside of this ROI were then set to zero, and those inside to 1000. The surface rendering menu was accessed and the pixel value set to 1000 for rendering. The dataset was also subsequently imported into the volume rendering functionality. This could only be utilised once the soft tissues had been removed as above. The results achieved with surface and volume rendering are shown in *Figure 107 (Movie Clip 5).* The advantage of using the surface rendering option was the ability to create an STL file compatible

with methods to create anatomical models, however, the results of volume rendered images were more visually appealing as a result of the application of smoothing and colouration.

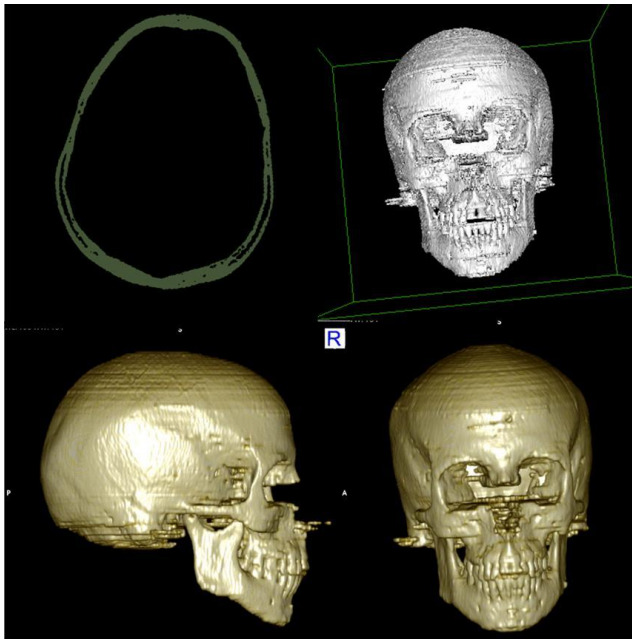



*Figure 107: Final ROI of cranial bone, surface (top right) and volume rendering (bottom) results.*

### *7.1.6.3 Datasets from Children*

Using the workflow developed with the adult volunteer datasets, "Black Bone" datasets from children with normal cranial sutures were imported and both surface and volume rendered in Osirix *(Figure 108).* To enhance visualisation of the cranial sutures and minimise the time to produce the 3D rendered images, the ROI was reduced to include only the skull cap *(Movie Clip 6)*. As can be seen in *Figure 24*, the patent cranial sutures could be visualised on the 3D rendered images. The facial skeleton was more difficult to segment, resulting in some discrepancies seen in *Figure 108.*

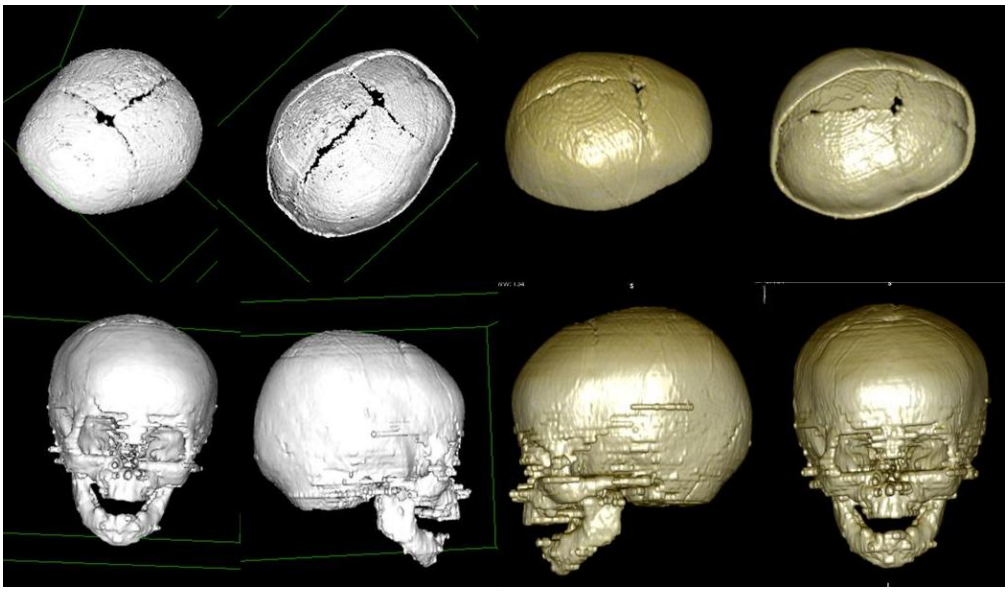


*Figure 108: 3D surface (left 2 images) and volume (right 2 images) rendered images from child with normal cranial sutures (Patient 3).*

#### *7.1.6.4 Children with Craniosynostosis*

Finally, Osirix was used to render datasets from children with craniosynostosis to determine if the appearance of the cranial sutures were consistent and if Osirix could be used to distinguish the normal from the prematurely fused cranial suture. Using the workflow previously developed the techniques were applied to each of the "Black Bone" datasets. As previously noted, the facial skeleton was particularly challenging to segment in Osirix. In the majority of cases, the patent cranial sutures could be identified *(Figure 109, Movie Clip 7 & 8).* The main limitation of Osirix was that creating 3D rendered images was time consuming as a result of the requirement to manually create a ROI around the soft tissue border on each image slice – on average a "Black Bone" dataset contained 156 axial image slices. Whilst Osirix had a function to propagate the ROI throughout the dataset and to exclude those image slices at the top and bottom of the stack outside of the skull, the ROI outline remained rigid, rather than being interpolated between slices. The result was that the ROI outline needed to be manually adjusted on a large number of slices, thus failing to offer any time saving.




*Figure 109: 3D surface (left 2 images) and volume (right 2 images) rendered images of children with craniosynostosis using Osirix (Patients 3, 5 & 10).*

### *7.1.6.5 Comparison between Mimics and Osirix*

The option to import STL files to Mimics permitted the opportunity to directly compare the STL files (surface renderings) produced in both Osirix and Mimics.

Using the "Black Bone" dataset for one of the children with craniosynostosis, 3D rendered images of the craniofacial skeleton were produced in both Osirix and Mimics, and saved as an STL file. Both files were imported and opened in Mimics and the images visually compared side-by-side. As shown in *Figure 110*, there was negligible difference between the two 3D images.

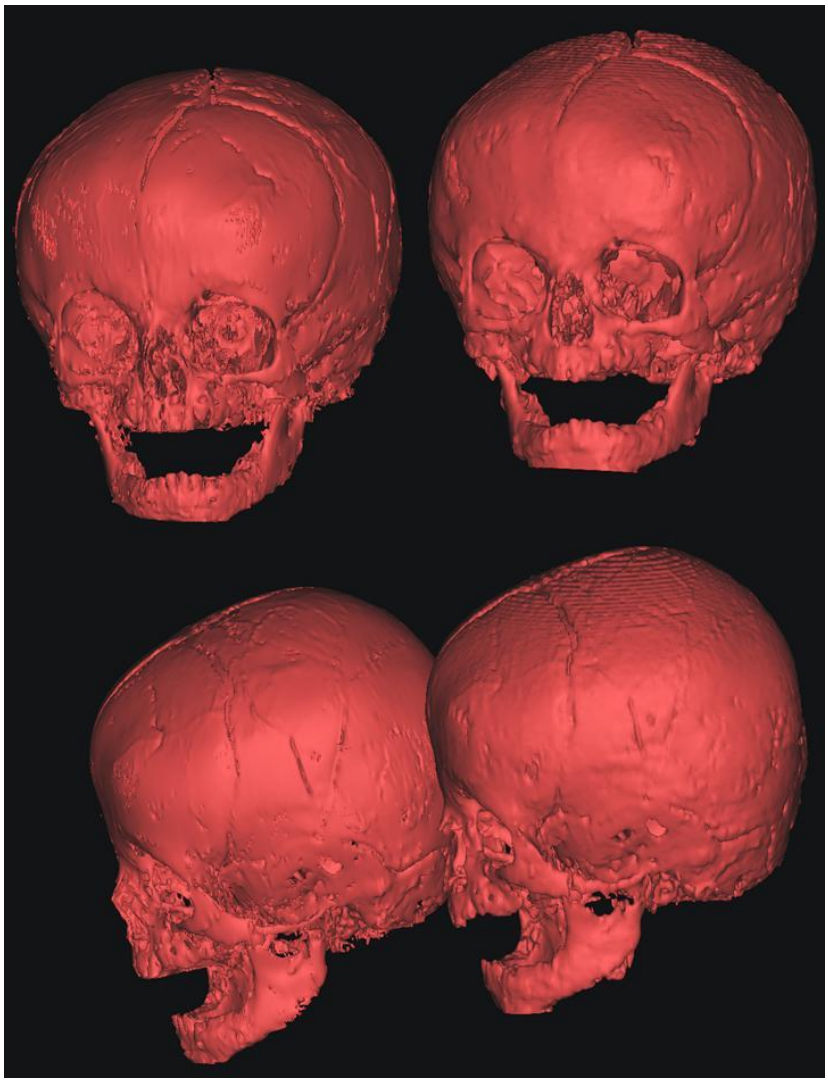


*Figure 110: Comparison between STL files created in Mimics (left) and Osirix (right).*

The software packages explored up to this point were reliant upon thresholding to segment the "Black Bone" datasets, made possible by the minimal overlap in pixel values for the soft tissue and bone. However, the inability to immediately eliminate the surrounding air resulted in time consuming processes to achieve the final result. Alternative methods of segmentation were therefore sought.

### 7.1.7 Fovia

Fovia High Definition Volume Rendering (HDVR) software was obtained on a research licence. The software is designed as an add-on for integration with manufacturers' imaging packages including Osirix, however, it can also be used independently on a personal computer (PC), which was the method utilised for this work. The software incorporates volume rendering, tools for 3D measurement, and instant free-hand-cut segmentation. Volume rendering is completed using transfer functions (TF) which maps data values to optical properties – i.e. it assigns a colour and opacity to each pixel contained in the dataset. Up to eight different TFs could be applied to one dataset. Navigation panels permitted visualisation of all functionalities in one place, simplifying the workflow. Shown in *Figure 111* is an example of the Fovia workspace. The software can handle large datasets without compromising on quality or performance and without the need for specialised hardware.

One of the benefits of the research licence was the ability to collaborate with software developers to further enhance the features of the software. Throughout the course of research period, multiple versions of the software were trialled, with each build bringing slight differences in the workflow.

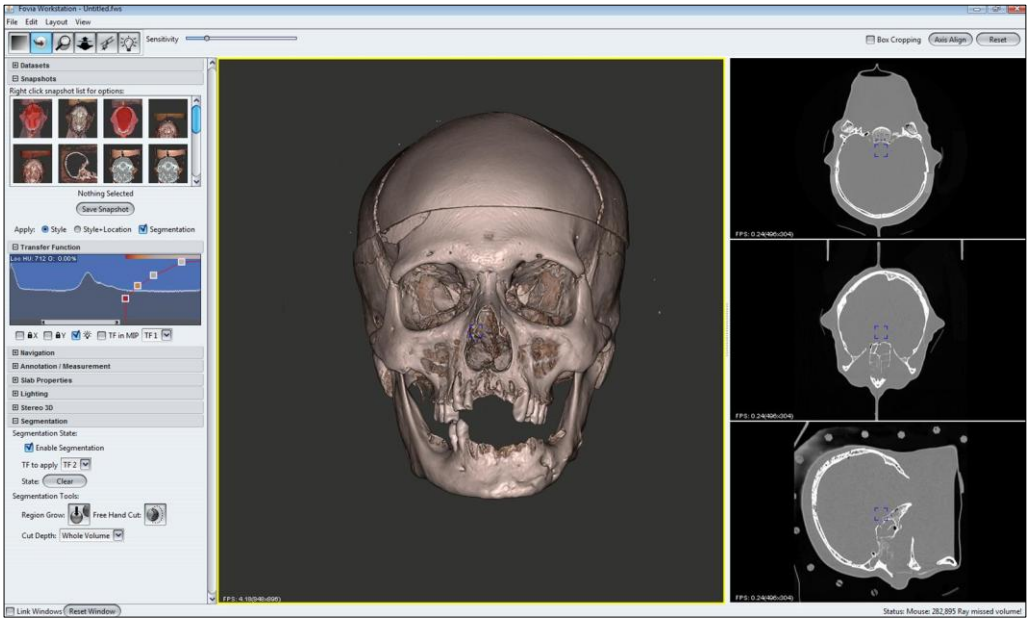



***Figure 111: Fovia workspace containing the 3D CT dataset for the skull phantom. The navigation panels on the left include the integrated "snapshots" which are preset TFs, which can be manually adjusted in the TF pane; the segmentation option are seen at the bottom of this panel. On the right orthogonal views of the dataset are included.***

#### 7.1.7.1 Phantoms and Animal Models

Utilising the dataset from the skull phantom, the initial TF was adjusted to permit visualisation of the skull through the soft tissues *(Figure 112).* Segmentation was enabled, and set to TF2 with a cut depth selection of "surface." This was applied to one side of the phantom, before rotating and applying to the other side, ensuring minimal overlap *(Figure 113).* TF2 was then deleted, thus removing the soft tissues. Any remaining areas that were not bone were removed using the cut depth of "whole volume" again with TF2. TF1 was re-adjusted to enhance the bone appearance. The workflow is shown in *Figure 113.*

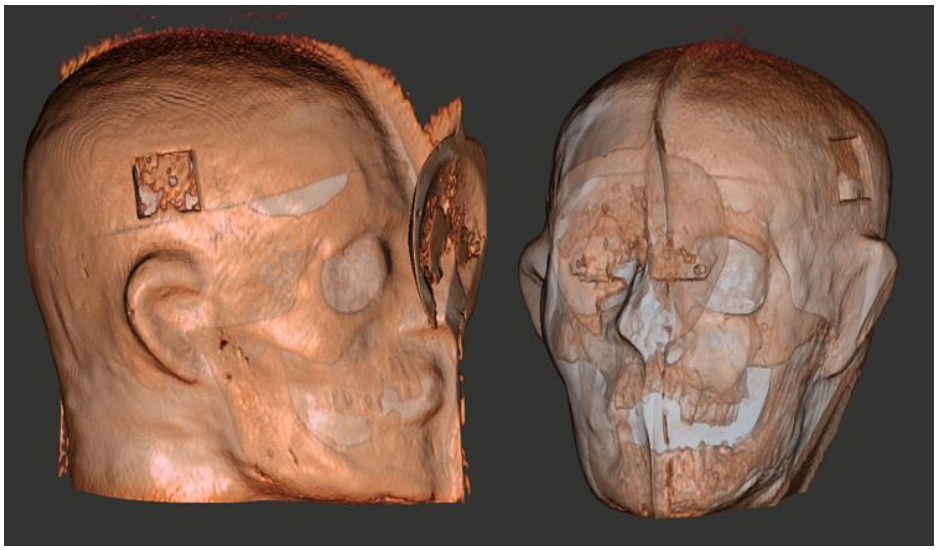


***Figure 112: TF adjusted to visualise the skull phantom through the Perspex shell and copper sulphate solutions simulating the soft tissues.***

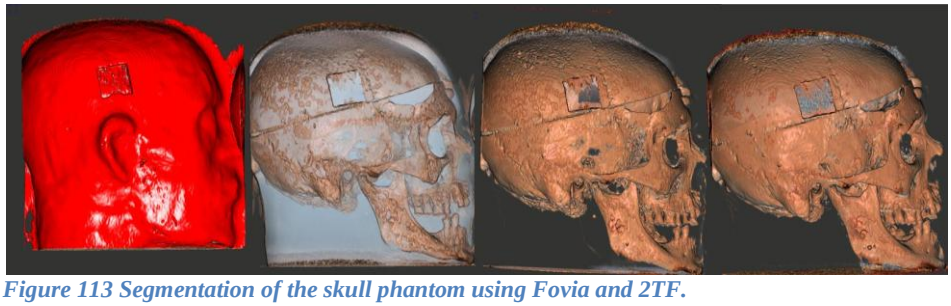


***Figure 113 Segmentation of the skull phantom using Fovia and 2TF.***

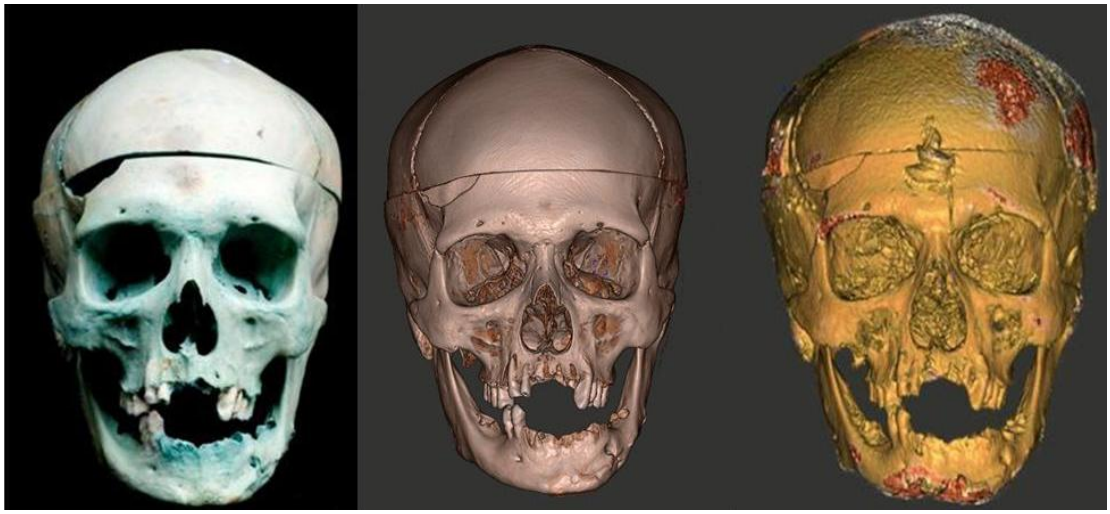


*Figure 114: Skull phantom (left), 3D rendered CT data using Fovia (centre) & 3D rendered "Black Bone" data using Fovia (right).*

Comparison of the "Black Bone" 3D results, those obtained from CT and the actual phantom are shown in *Figure 114*. The TF was adjusted to remove any colouration to permit direct comparison between the "Black Bone" and CT results *(Figure 115)*. The main areas of discrepancy were the inherent problems associated with acquiring the MRI of the phantom – firstly, there was some difficulty with leakage of copper sulphate from the Perspex shell which resulted in loss of some areas of image quality where air came into contact with the phantom; secondly, the area in the frontal region of the phantom had some metallic residue from a clip used to hold the skull cap in place. This resulted in an area of signal void, and the resultant discrepancy seen on the 3D images compared to CT.

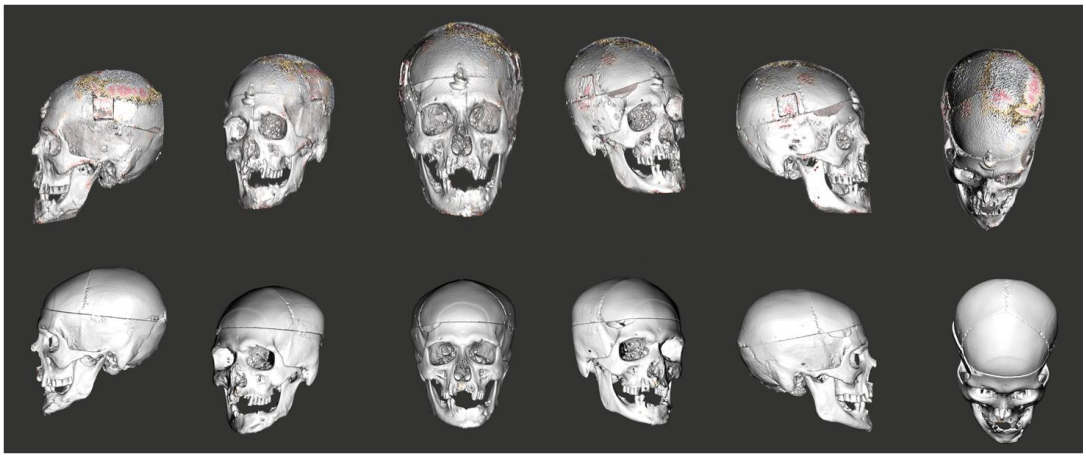


*Figure 115: 3D rendered images of phantom using "Black Bone" (top row) and CT (bottom row).*

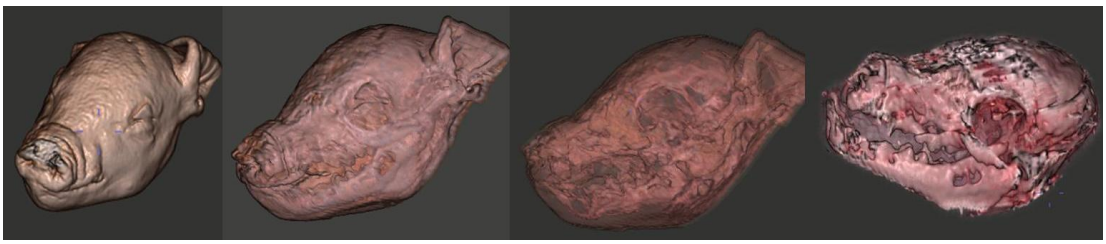


*Figure 116: 3D rendering process with "Black Bone" piglet dataset.*

Obtaining 3D rendered images from the "Black Bone" datasets from the piglet proved to be more technically challenging than for the phantom *(Figure 116).* The soft tissues were difficult to segment off of the bone, particularly in areas of dense cartilaginous tissue such as the snout. A suitable TF to permit clear visualisation of the entire skull could not be found. However, these difficult circumstances permitted the opportunity to further develop techniques to assist in such cases, such as gradual manual segmentation of the soft tissues using the "whole volume" tool. The time spent on this work with the animal datasets was limited so as to maximise efforts on patient datasets.

### *7.1.7.2 Adult Volunteers*

Having developed methods to segment the skull on a phantom, the techniques were applied to "Black Bone" datasets obtained from adult volunteers. The TF used for the phantom provided a reasonable starting point. Following the same principles, a TF was set where the soft tissues became almost transparent *(Figure 117),* before using the "one layer" segmentation tool to obtain 3D reconstruction of the craniofacial skeleton.

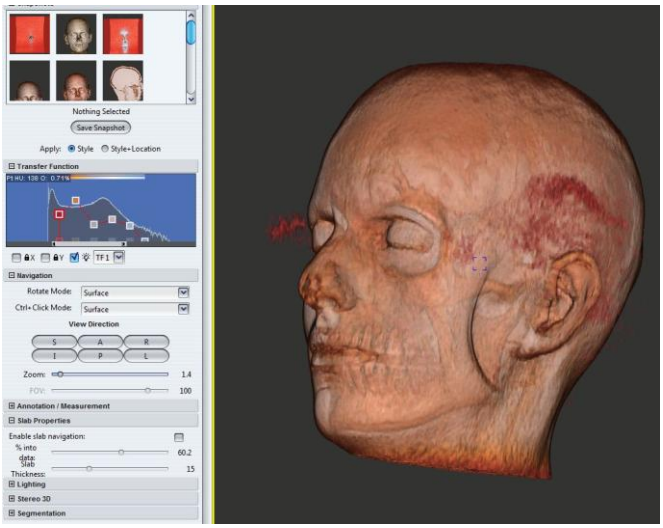



*Figure 117: Fovia window showing TF and resultant 3D image.*

Following removal of the soft tissue, the TF required further fine adjustment and any remaining areas of dense soft tissue required manual segmentation using the "whole volume" tool. These areas included those which were cartilaginous, such as the nose and ears, and also areas such as the eyes, where the soft tissue was at a deeper extent than the bone. It was also noted that the "heart-fly" preset available in Fovia provided a very good starting TF, and provided the most optimal bone appearance. The workflow for the adult datasets is shown in *Figure 118*, along with some resultant images. A movie clip to permit 360° review of these final images is included on the accompanying CD *(Movie Clip 9).* The "Black Bone" datasets used in this section represent the optimal achievable results – the volunteers were compliant with no movement or metal artefact. The next step was to test this in clinical setting.

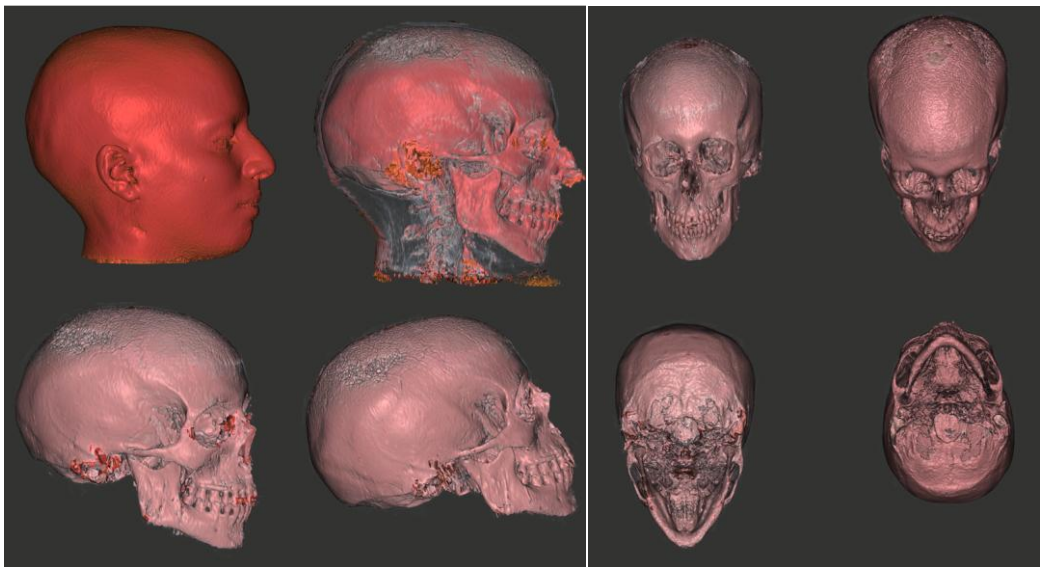


***Figure 118: Fovia workflow demonstrating TF selection, "one layer" segmentation, manual segmentation and TF adjustment and the final 3D images.***

### *7.1.7.3 Adult Patients*

To test the methods developed using ideal "Black Bone" images from volunteers in the clinical setting the "Black Bone" datasets from patients with a range of pathologies affecting the head and neck were utilised. In some cases comparable CT imaging was available to assess the accuracy of the resultant 3D "Black Bone" images. The methods previously developed were utilised for all of the datasets. Examples are shown in *Figure 119*. Whilst in some cases the final results were not fully cleaned up in terms of regions outside of the bone the results do demonstrate the potential of the techniques in each case. Having developed sufficient experience with the workflow, images

such as these were achieved in less than 10 minutes per dataset. The mandibular pathology can clearly be seen in Patients 3 and 4, with the dental roots also being visible in Patient 4. Dental amalgam has resulted in the dense appearance around the right mandibular molar teeth in Patient 1. The 3D results were consistent across all of the datasets tested. Having achieved reasonable results with adult datasets, the next step was to determine if this was also possible with "Black Bone" in children in whom the craniofacial bone is noticeably thinner.

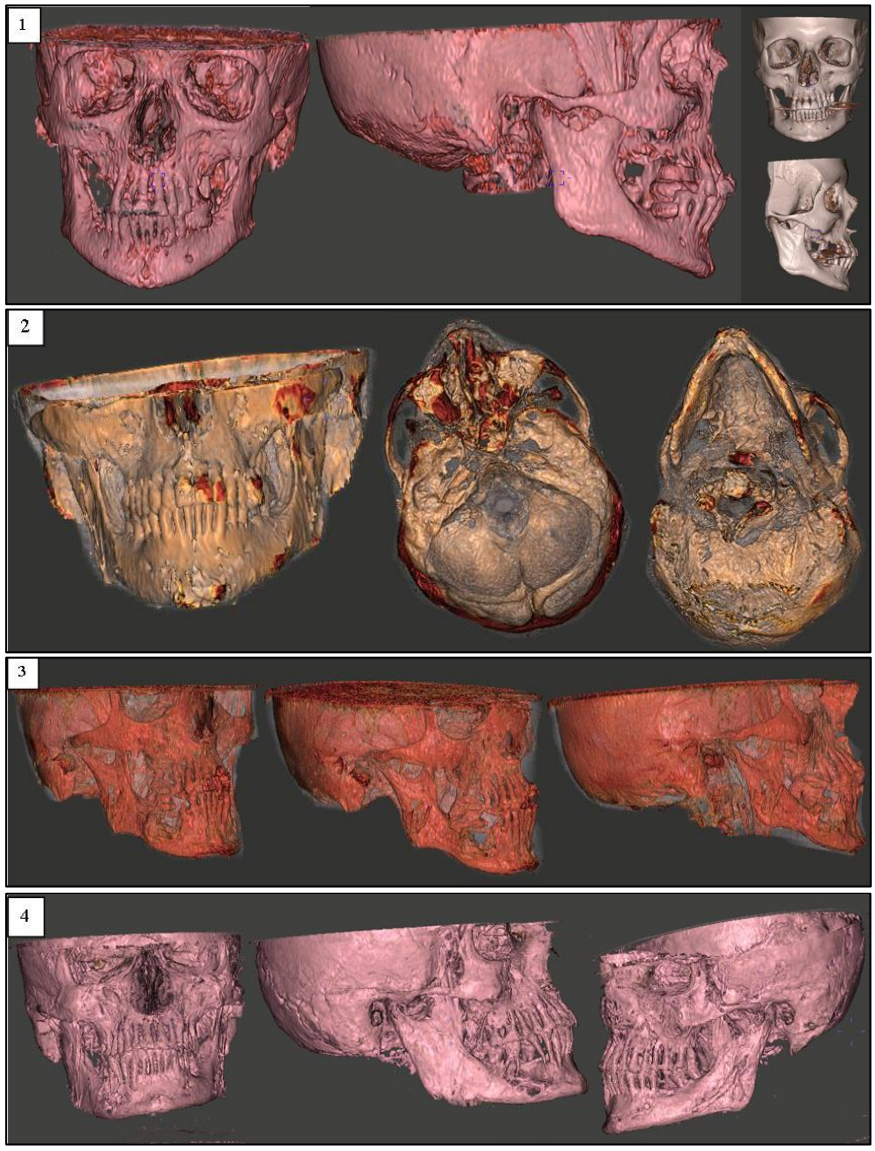



***Figure 119: 3D rendered "Black Bone" images from (1) 58 year old female with retromolar trigone SCC, with comparable CT images (right of panel); (2) 64 year old male with right maxillary alveolus SCC; (3) 69 year old male with giant cell granuloma of the right mandible; (4) 24 year old male with odontogenic myxoma of the right mandible.***

#### *7.1.7.4 Children with Normal Cranial Sutures*

Utilising the "Black Bone" datasets obtained from the 4 children with normal cranial sutures, initial investigation with Fovia was with the inherent TF presets. Using the "x-ray bone" TF preset, the clear potential of Fovia in visualisation of the cranial sutures on "Black Bone" was realised *(Figure 120).*

With slight modification of the steps utilised with the adult volunteer datasets, the results for all four children with Fovia are shown in *Figure 121 and 122*. The main difficulty in children was that the soft tissues could not always be reliably removed with the "surface" or "one layer" segmentation tool. This necessitated manual segmentation, which could be time consuming.

The 3D rendered results obtained from these datasets demonstrated good potential. It was apparent that the optimal TF for the cranial bone was different to that for the facial skeleton, and to obtain 3D rendered images of the entire skull a compromise was frequently necessary. However, the cranial sutures could be identified, and whilst there was some reliance upon manual segmentation techniques in some instances, the results appeared reliable. The results obtained in Patient 4 were degraded by the imaging artefact seen on the axial images, and this is one of the limitations of the techniques used.

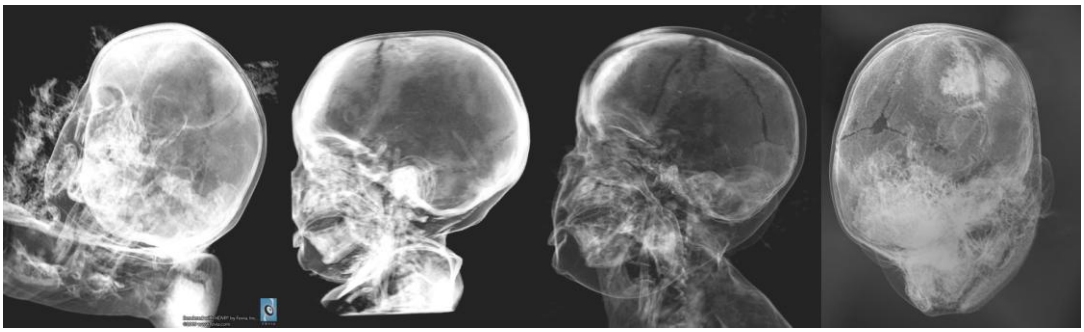


***Figure 120: Initial attempts at rendering of "Black Bone" MR images in a 3 year old child demonstrating patent cranial sutures using Fovia.***

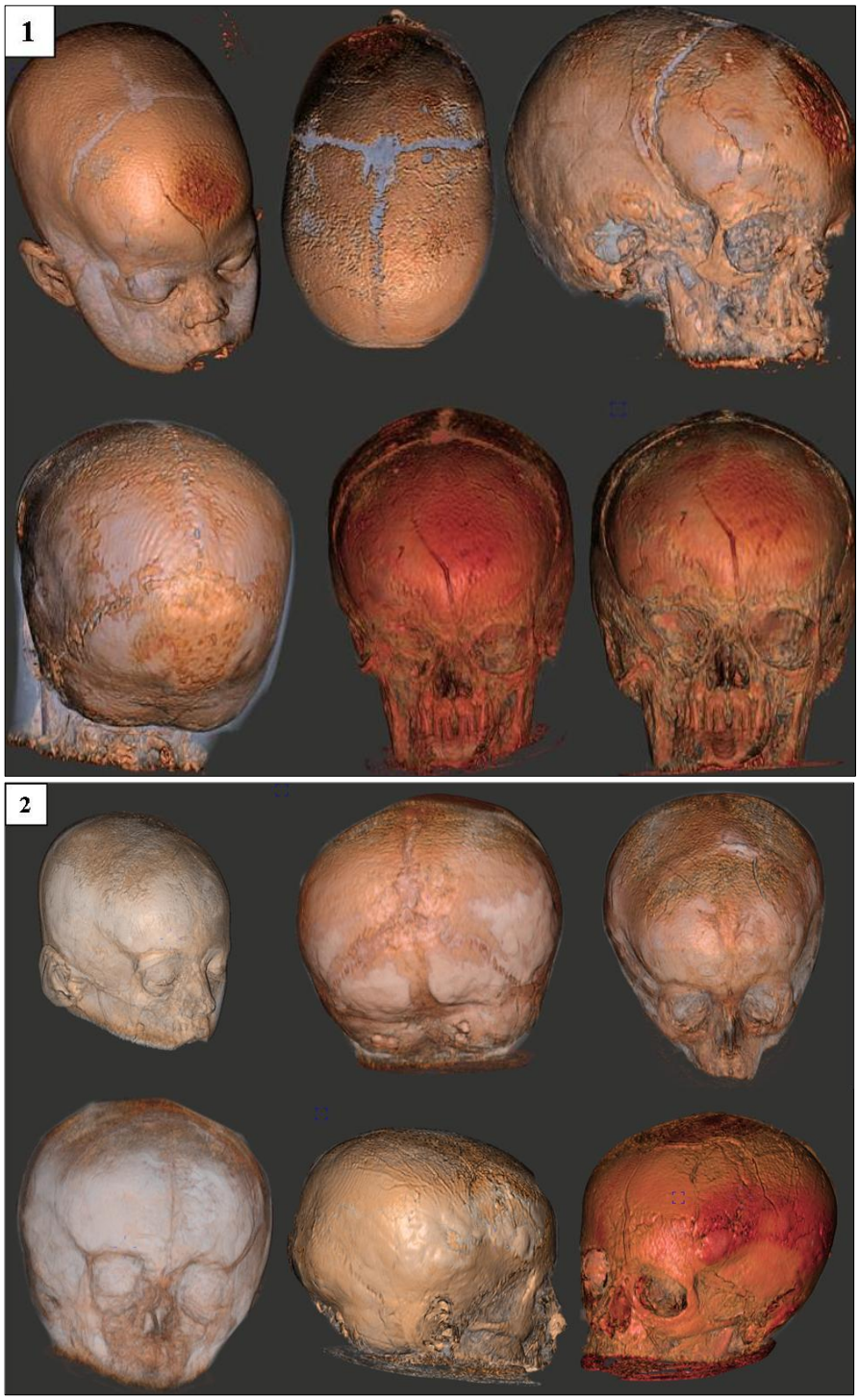



*Figure 121: 3D rendered Fovia images for Patients 1 and 2.*

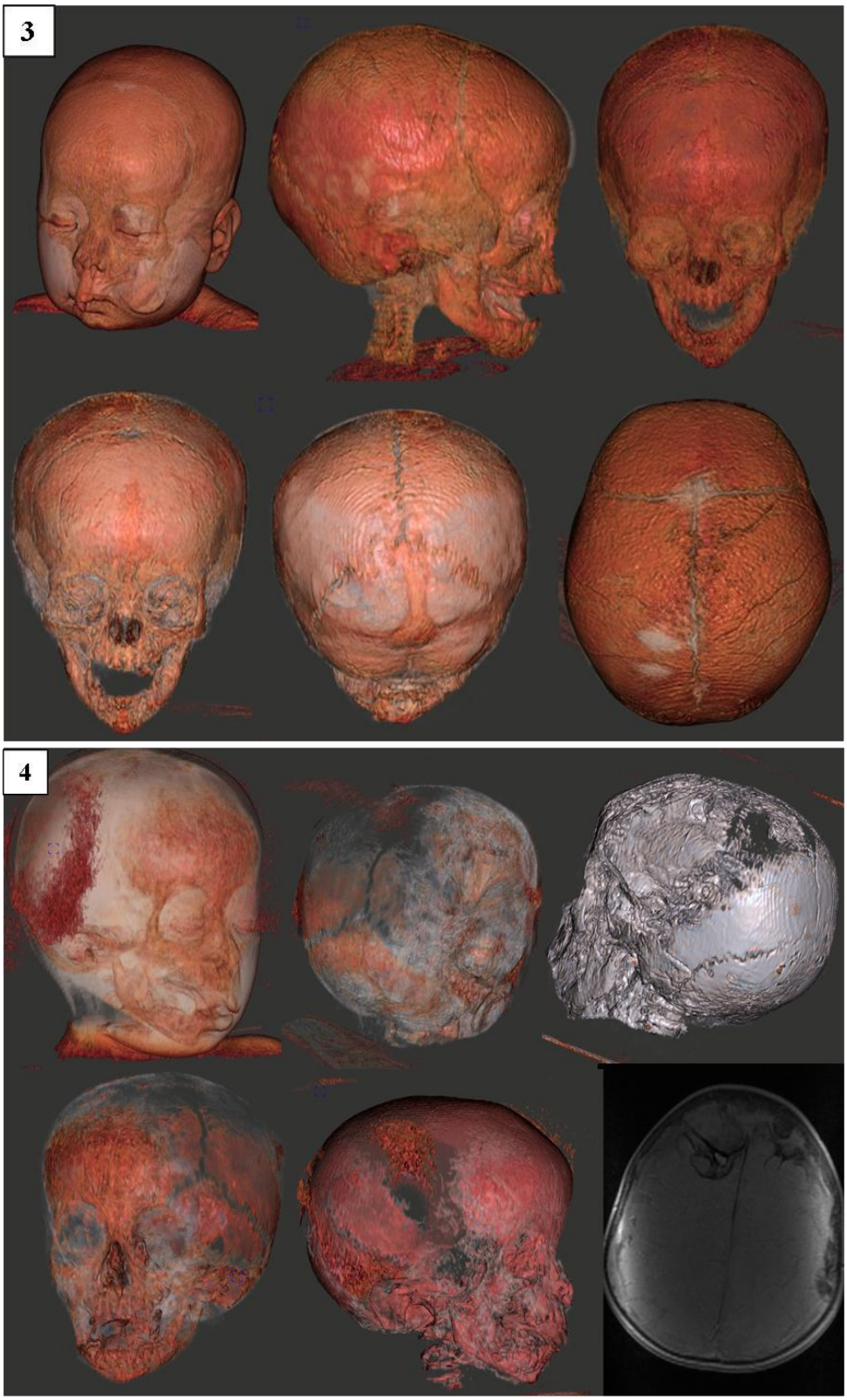



*Figure 122: 3D rendered images from children with normal sutures using Fovia. Above Patient 3, below Patient 4. Note the artefact seen in Patient 4 impacting upon the 3D results.*

### 7.1.7.5 Children with Craniosynostosis

Building upon the techniques developed in children with normal cranial sutures, the "Black Bone" datasets obtained from infants and children with craniosynostosis were rendered in Fovia *(Figures 123-29).* The comparable 3D-CT images are shown at the bottom of each panel for all of the children.

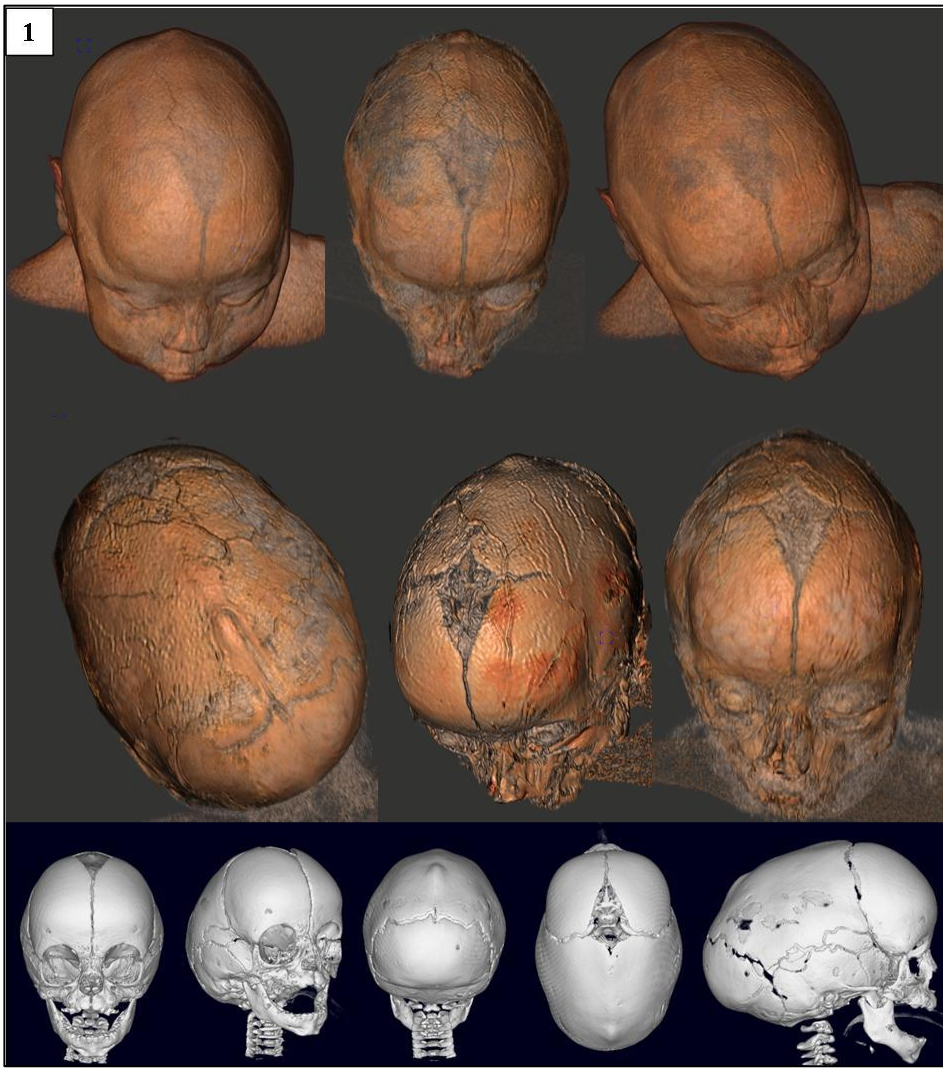



*Figure 123: Fovia Results and comparable CT images for Patient 1.*

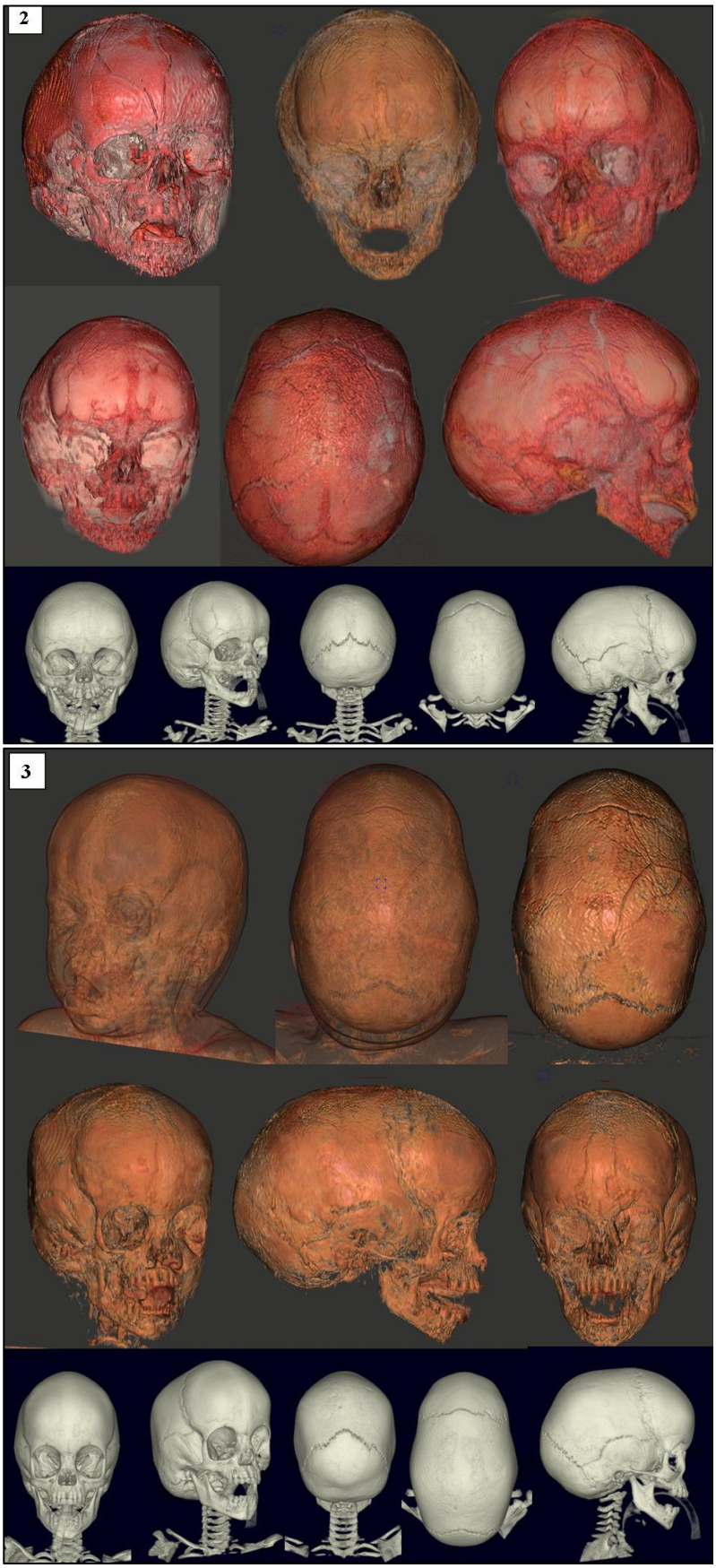



*Figure 124: Fovia results & comparable CT images for Patients' 2 & 3.*

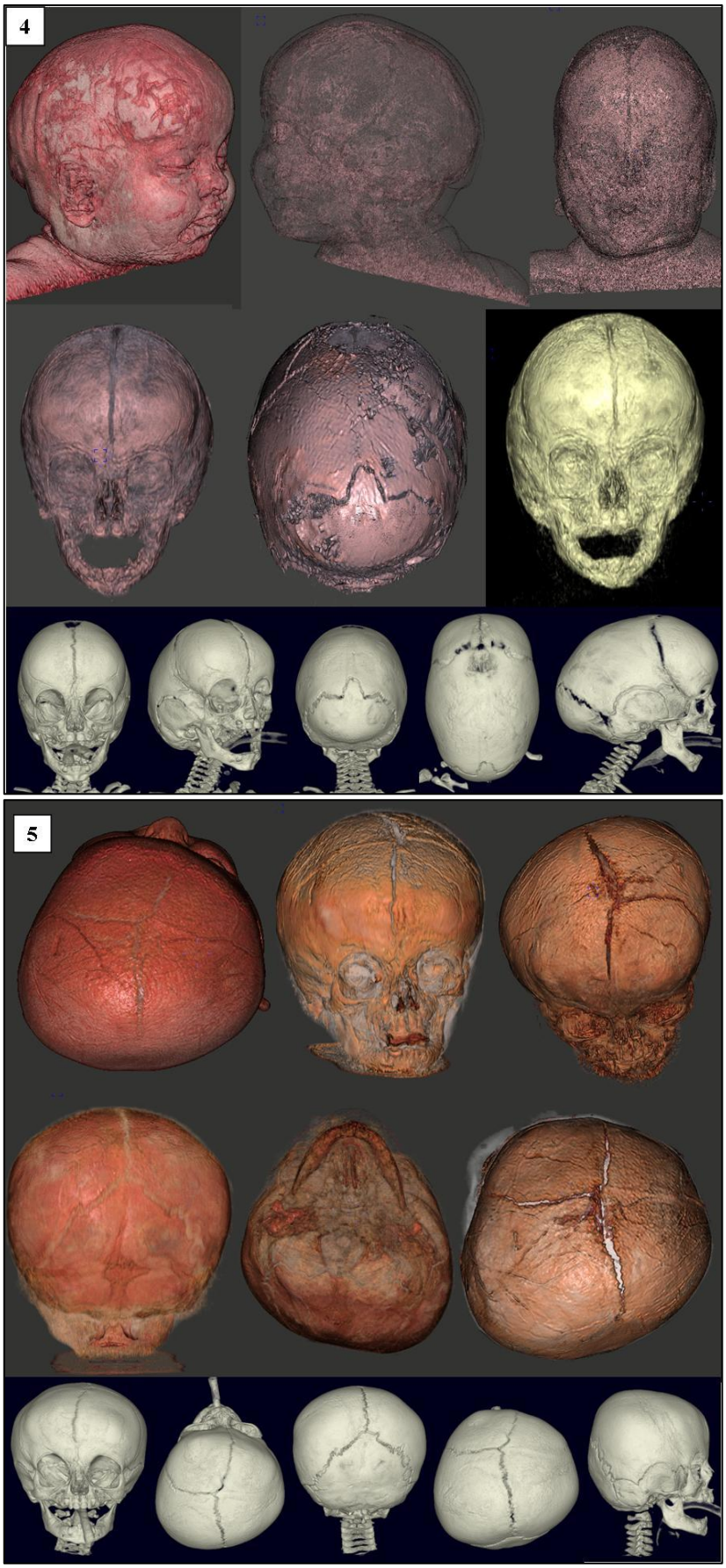



*Figure 125: Fovia results and comparable CT images for Patients' 4 & 5.*

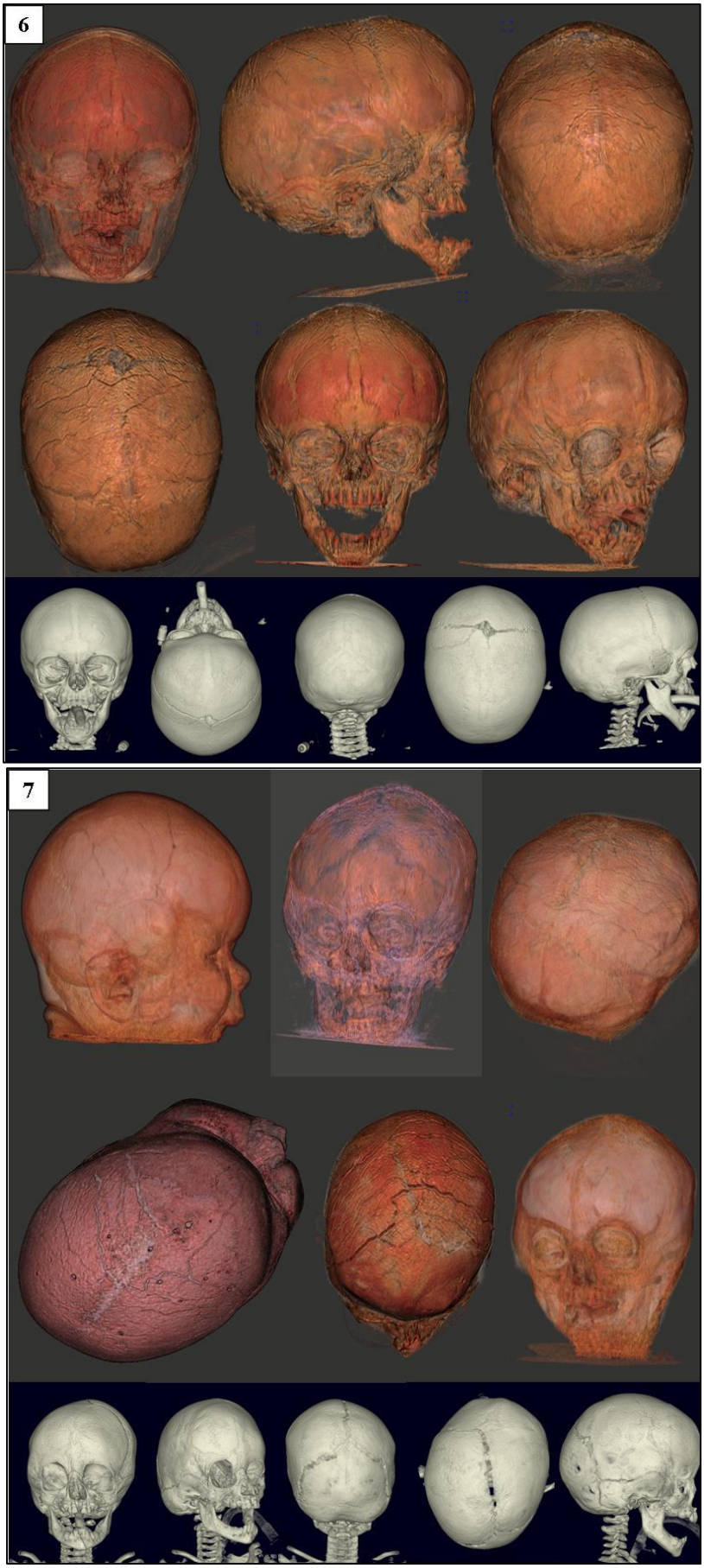



*Figure 126: Fovia results and comparable CT images for Patients' 6 & 7.*

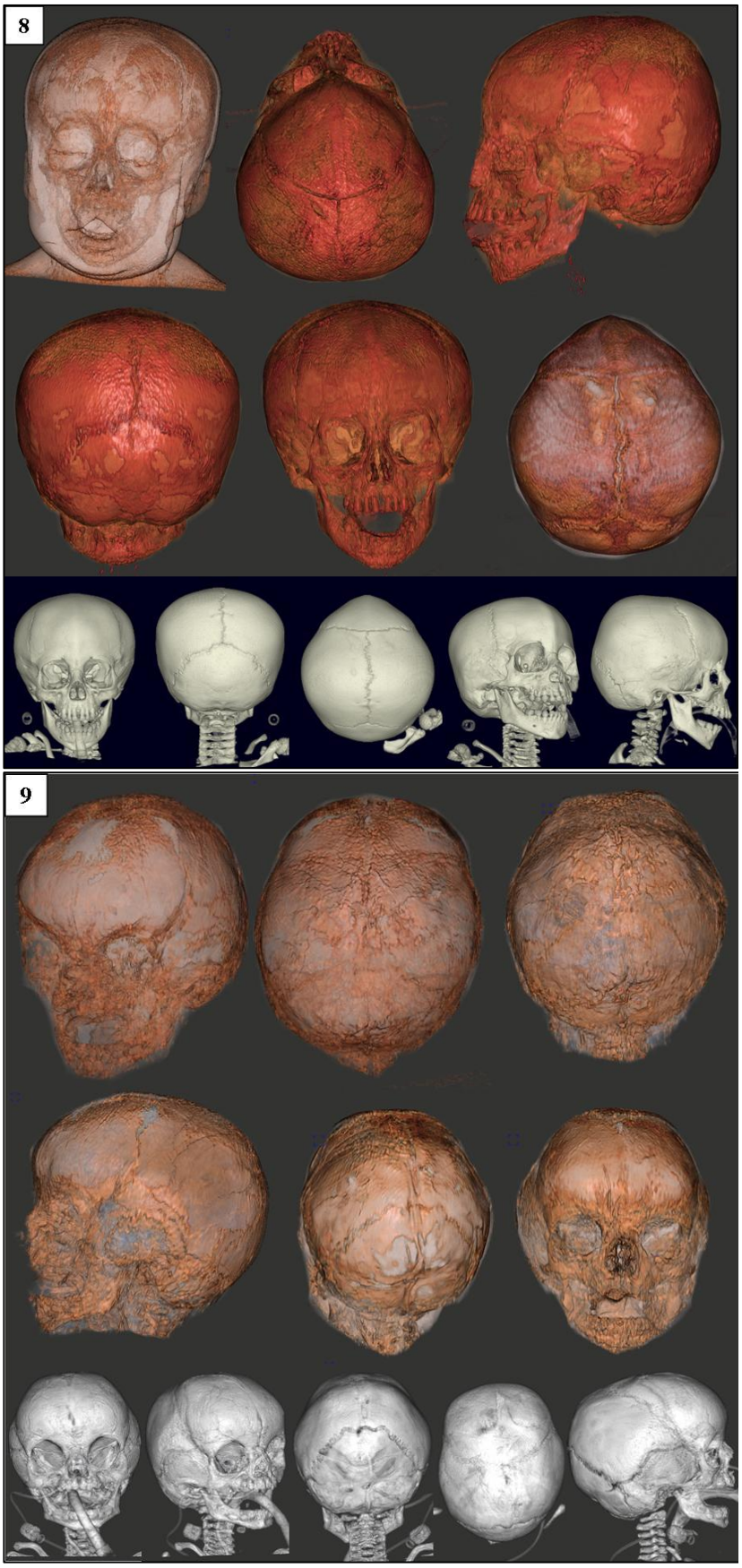



*Figure 127: Fovia results and comparable CT images for Patients' 8 & 9.*

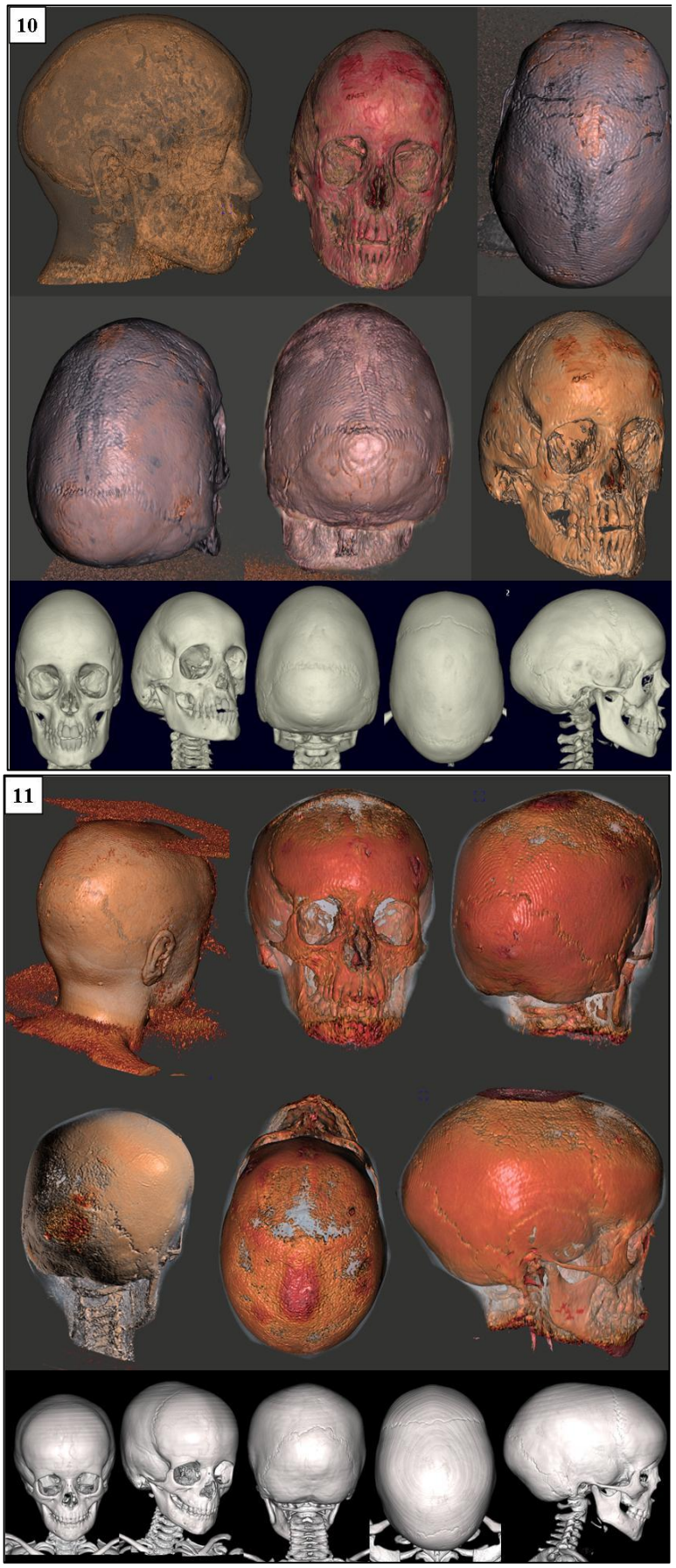



*Figure 128: Fovia results and comparable CT images for Patients' 10 & 11.*

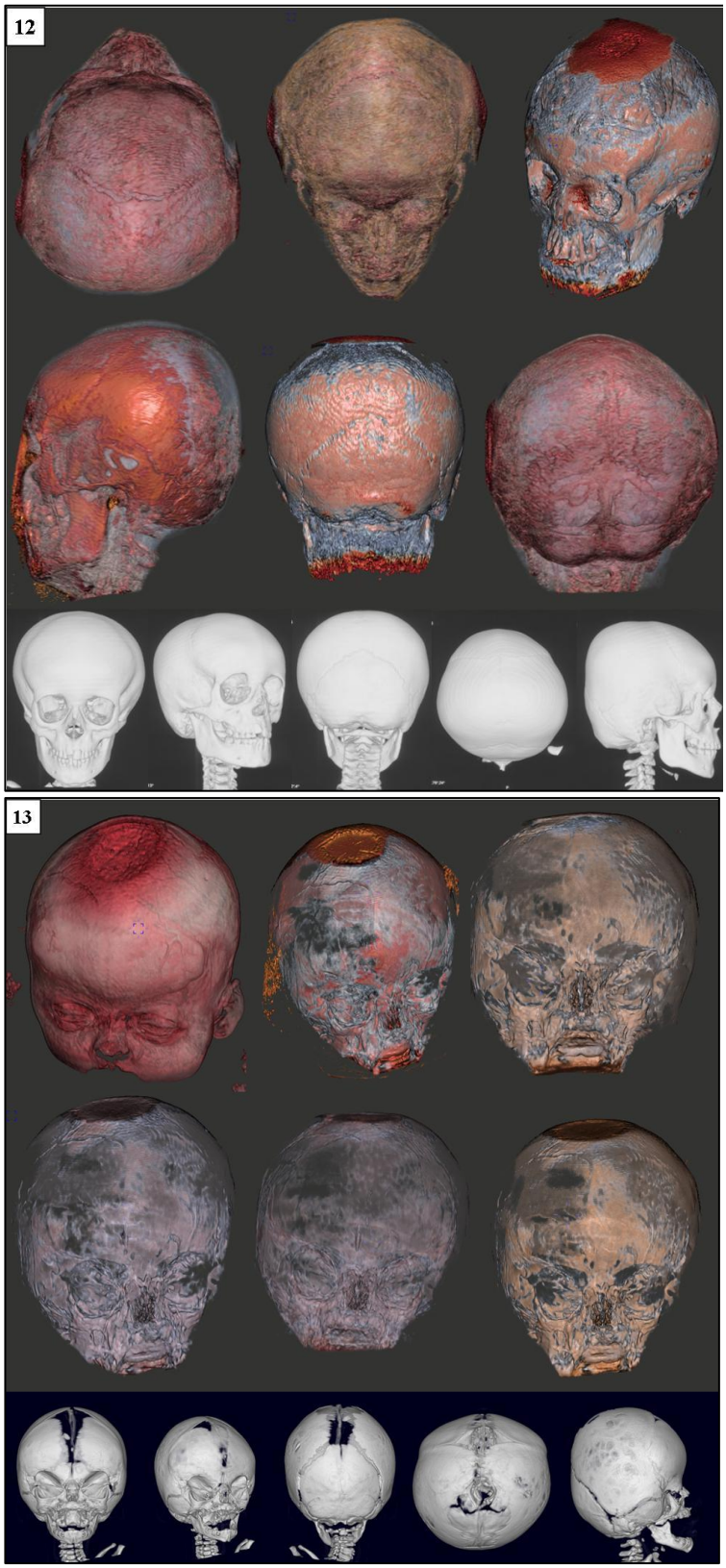



*Figure 129: Fovia results and comparable CT images for Patients' 12 & 13. Note the particularly thin cranial bone seen on CT for Patient 13.*

The first step was to obtain images of the bone and cranial sutures visible through the soft tissues. This could be achieved relatively simply by adjustment of the TF. Unfortunately the semi-automated processes developed for removing the soft tissues in the adult patient datasets did not work for the craniosynostosis datasets. This was most likely the result of the particularly thin bone in the infants. The soft tissues could be manually removed, but this was time consuming, and particularly challenging for the facial skeleton. Since the cranial sutures could be clearly visualised through the soft tissues, and the diagnosis of craniosynostosis could be made, it was questioned if it was necessary to fully segment the underlying bone. Certainly from a diagnostic perspective this would seem unnecessary, however, as will be explored in Section 7.5 full segmentation of the skull is required to produce anatomical models.

By adjusting the TF, the bone density appearance could be improved, but this invariably resulted in the visualisation of vessels on the skull surface. Whilst unlikely to be mistaken for cranial sutures, this was a possibility, and attempts to remove these were made. This was with variable success, since the segmentation tools were not sensitive enough to accurately remove such a small area. As previously noted, the optimal TF for the cranium and facial skeleton were frequently different, requiring compromise to obtain 3D images of the entire skull. This was particularly seen in Patient 13, where the bone was particularly thin.

The results obtained across the 13 children with craniosynostosis were somewhat variable. The reason for this was largely due to the problems associated with obtaining accurate imaging parameters in the WW with resultant image artefact. In cases where the parameters were not ideal, which resulted in increased soft tissue contrast, the 3D results were notably sub-optimal. For the three children imaged in OMRI, where the imaging parameters had been previously fully optimised, the bone appeared to be more defined. However, these children were also older than those scanned in the WW, and this is likely to have contributed to this finding. For the infant scanned at the CH, the Fovia results were particularly poor. This was the result of a combination of movement artefact, the very young age and syndromic diagnosis of Apert syndrome associated with particularly thin bone. This appears to be one of the limitations of “Black Bone” in this patient group.

In addition to the problems associated with fine-tuning of the "Black Bone" sequence in the WW the datasets also suffered from chemical shift artefact. This resulted in an area which had an appearance similar to bone, and had to be manually removed. One attempt to minimise the impact of the artefact was to switch the phase and frequency directions in an attempt to transpose the artefact into an area where segmentation would be simpler. However, this proved to be of limited assistance, as this failed to shift the artefact a sufficient distance away from the cranial bone.

The TF required fine manipulation for each dataset; in clinical practice having one pre-set which would be suitable for all patients, similar to the process for 3D-CT, whilst ideal does not appear to be possible for "Black Bone." However, one of the benefits of the more recent Fovia builds was the ability to save and import pre-set TF's. Once optimised for one dataset this could be imported for other patients, and provided a good starting point. Whilst minor adjustments were necessary the time required to render the image was greatly reduced. Experience with the software was required; in the early stages of working with Fovia each 3D dataset required 30-60 minutes to obtain an acceptable volume rendering result. This was reduced to less than 10 minutes once sufficient experience with Fovia had been gained.

#### *7.1.7.6 Alternative MRI Sequences*

The Fovia techniques developed were finally applied to all other MRI sequences that were available, including UTE, FIESTA, FLAIR, T1, and T2 sequences that had been completed as part of the clinical examination for the patients studied or as part of the research exploration. This was to determine if any of these routine sequences were able to yield results comparable to those from "Black Bone" MRI. Shown in *Figure 130* are the results obtained with T1, T2 and FIESTA sequences. It was not possible to obtain a good quality 3D rendered image of the craniofacial skeleton on any of these sequences due to the increased soft tissue signal. As can be seen in the image created from the FIESTA dataset, the facial musculature appears dense, and was difficult to segment off of the underlying bone. Experimentation with all available sequences did not yield any which provided reasonable segmentation of the craniofacial skeleton. "Black Bone" MRI therefore appears to offer a unique functionality in lending itself to 3D reconstruction.

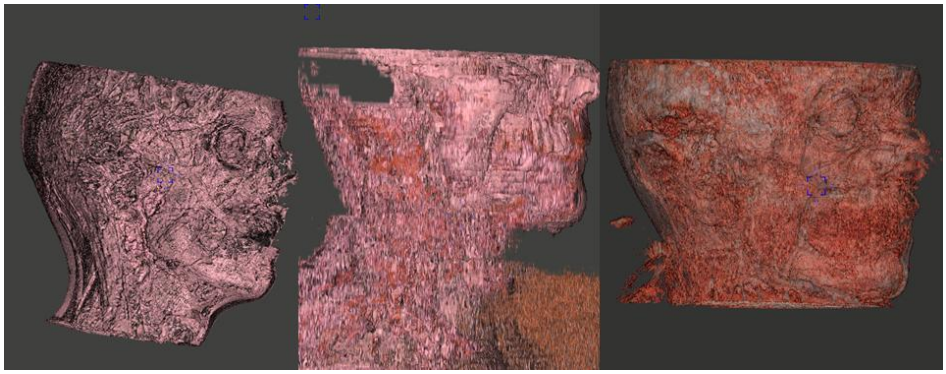


*Figure 130: Fovia results with T1 (left), T2 (centre) and FIESTA (right) sequences.*

The results obtained using Fovia with "Black Bone" datasets almost approach the quality of that expected from CT. It has been possible to develop semi-automated techniques, with the production of reasonable results within 10 minutes using a simplified workflow. Whilst Fovia permits the ability to import previously optimised TFs these frequently require fine manipulation, resulting in some variability in the final result. Since the results are user dependent, in the current format they would not be suitable for use in the general clinical environment without training. The results obtained from datasets acquired from adults and children imaged in OMRI/CH yielded the most optimal results. Difficulties arose as a result of the chemical shift artefact seen with datasets acquired in the WW, in cases where the imaging parameters were suboptimal, along with the technical challenges of segmentation in children who have thin craniofacial bone. However, the distinction between normal cranial sutures and craniosynostosis could be made in almost all cases reviewed.

### 7.1.8 3D Doctor

3D doctor is a commercially available software for 3D modelling, image processing and measurements. It supports both greyscale and colour images stored in a range of formats, to create 3D surface models and volume rendering. An academic license of 3D Doctor was purchased from Able Software Corp for this aspect of work.

#### *7.1.8.1 Phantom Datasets*

Initial work with 3D doctor was with the cube phantom "Black Bone" dataset, which provided the opportunity to explore the functions available within the software. The segmentation process could be performed manually or automatically with an interactive component. With the cube phantom, the simplest method to segment the cube was to utilise the thresholding function to create a boundary assigned to all slices within the dataset. A 3D rendered image was subsequently created from the boundary lines. The result from "Black Bone" was compared to that achieved with a CT dataset *(Figure 131);* no obvious discrepancies between the two 3D images could be identified.

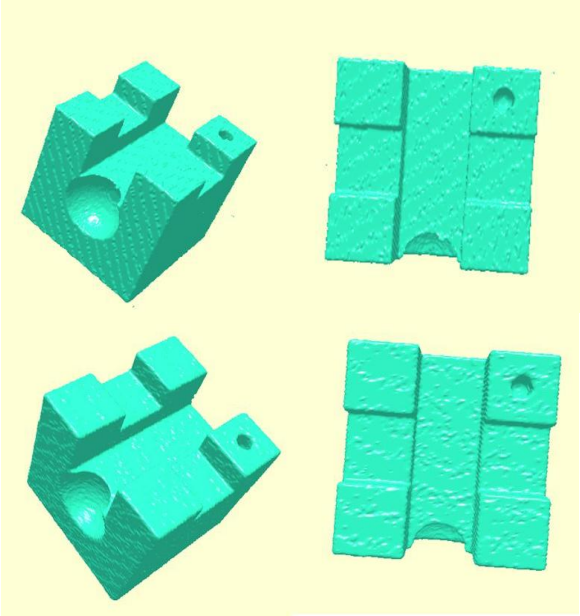


***Figure 131: 3D rendered images of the phantom cube with 3D doctor. No significant differences were noted between the "Black Bone" dataset (top) and the CT dataset (bottom).***

### 7.1.8.2 Adult Volunteer Datasets

The main difficulty associated with 3D doctor was the correct selection of the method to perform segmentation of the dataset; where too many boundaries were created, these needed to be manually removed which could be time consuming. Failure to identify and remove all of these additional boundaries resulted in their inclusion in the final 3D image *(Figure 132).* One of the main benefits however of 3D doctor was the ability to edit the boundary lines. This was of particular value in the regions where air and bone met, such as the ear canal and mouth. By closing these boundaries, which again could be time consuming, often achieved a good 3D result *(Figure 133, Movie Clip 14).*

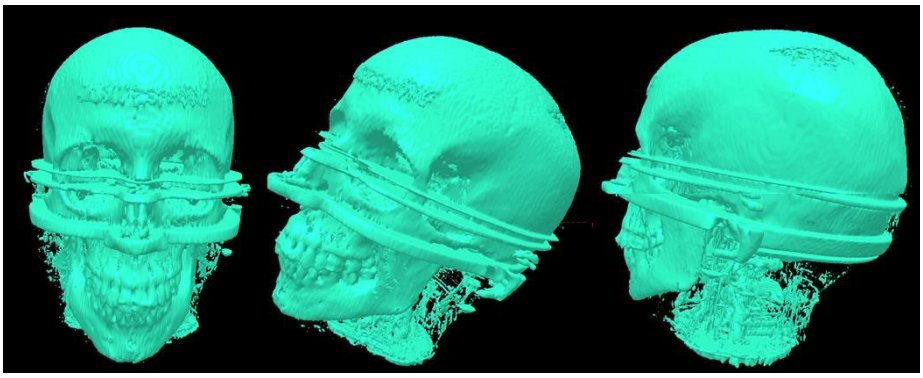


***Figure 132: Initial attempt at rendering adult "Black Bone" dataset, with failure to remove all of the soft tissue boundary lines.***

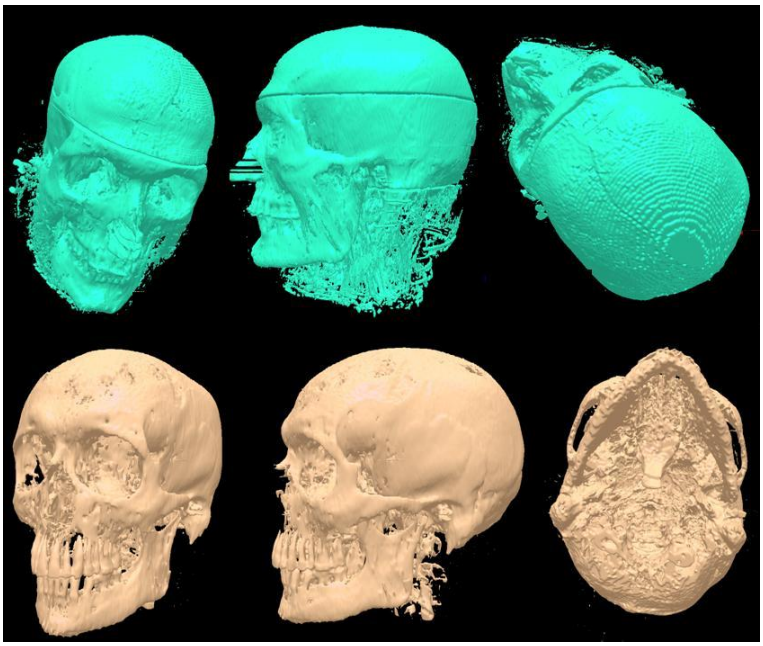


***Figure 133: 3D rendering of adult volunteer "Black Bone" datasets with 3D-Doctor.***

In an attempt to decrease the time required to render images with 3D doctor attempts to artificially close the communication between air within the ear canal and outside of the body was conducted. With an adult volunteer (KE), cotton wool soaked in olive oil was placed into the ears prior to obtaining "Black Bone" imaging *(Figure 134)*. This method was successful in providing an artificial barrier, aiding boundary identification, and could be utilised in the patient population without concern.

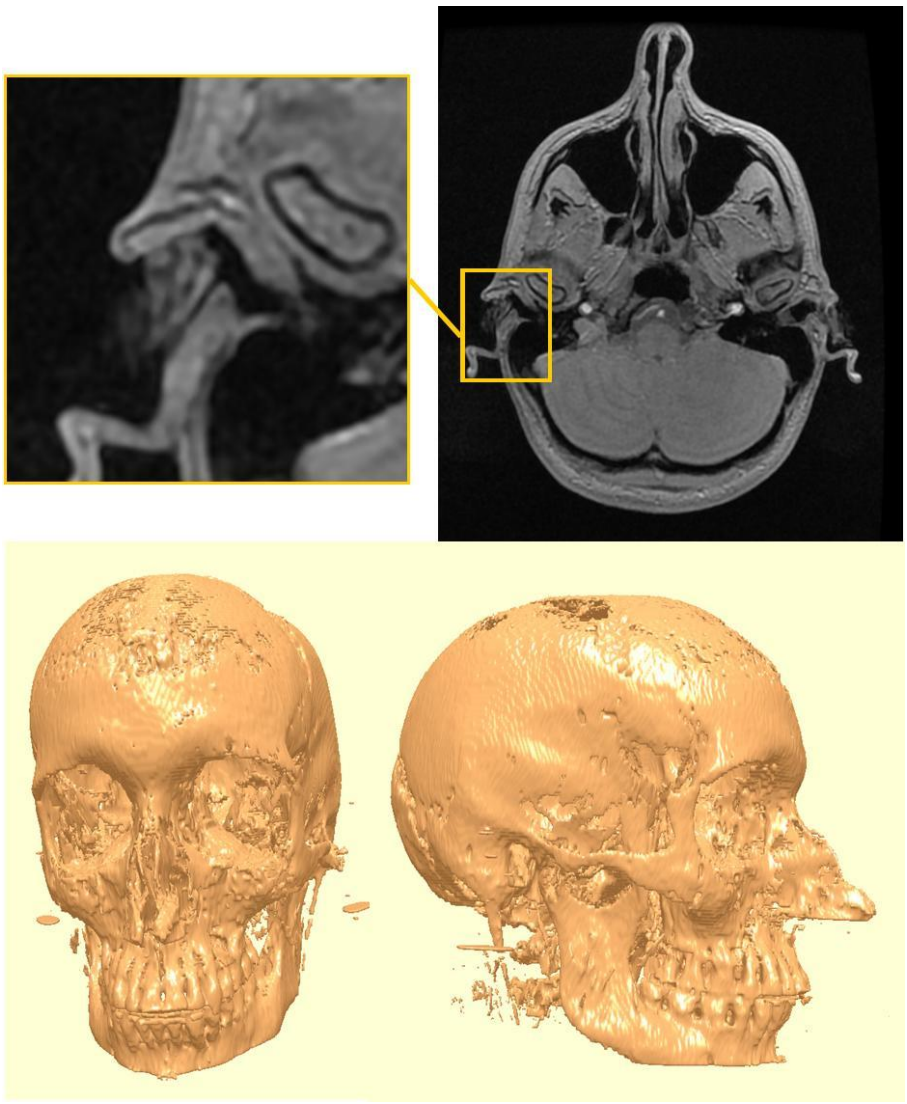


***Figure 134: Axial "Black Bone" images demonstrating artificial boundary provided by olive oil soaked cotton wool (top), and resultant 3D images.***

### 7.1.8.3 Children with Craniosynostosis

Using the automatic segmentation function, the "Black Bone" dataset of one of the infants with craniosynostosis was segmented. As shown in *Figure 135*, multiple boundaries were detected, and those not associated with bone were deleted. This was a simple process for those colours where there was no overlap, since the whole boundary set associated with this particular colour could be deleted. In cases where some of the boundary included bone, this required a more labour intensive process.

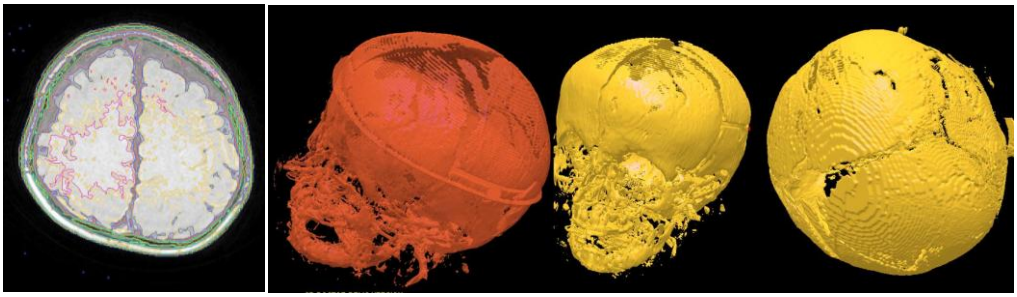


***Figure 135: Automatic detection of boundaries on axial "Black Bone" image (left), and 3D results after editing boundaries.***

Whilst 3D doctor was able to identify the boundaries on the "Black Bone" datasets, by locating so many potential boundaries it resulted in a large amount of subsequent editing to achieve the final result. Simple thresholding techniques provide a useful starting point with the datasets, but were of less benefit in children where the bone was less dense.

Attention was therefore turned to methods to automatically segment the datasets to create a useful adjunct for clinical practice.

### 7.1.9 Image J

Image J is an open source software written in Java and therefore available on all operating systems. It provides the freedom to edit the way that the program operates, with many available add-ons written by other users free to download. Multiple images can be viewed on screen as an image stack and Image J has the ability to import all types of image formats including TIFF, JPEG and DICOM. The software was downloaded from the Image J website and used on a windows platform.

#### *7.1.9.1 Phantom Datasets*

Initial investigation with Image J was completed with the phantom cube dataset. The dataset was imported as a virtual stack, and duplicated to permit manipulation within Image J. In an attempt to distinguish the cube from the outside air, the tool to subtract the background was used. Whilst this resulted in a white background thus succeeding in distinguishing itself from the cube, an outline around the object remained which would also require subsequent removal *(Figure 136).* Attempts to remove this via an automated process were unsuccessful.

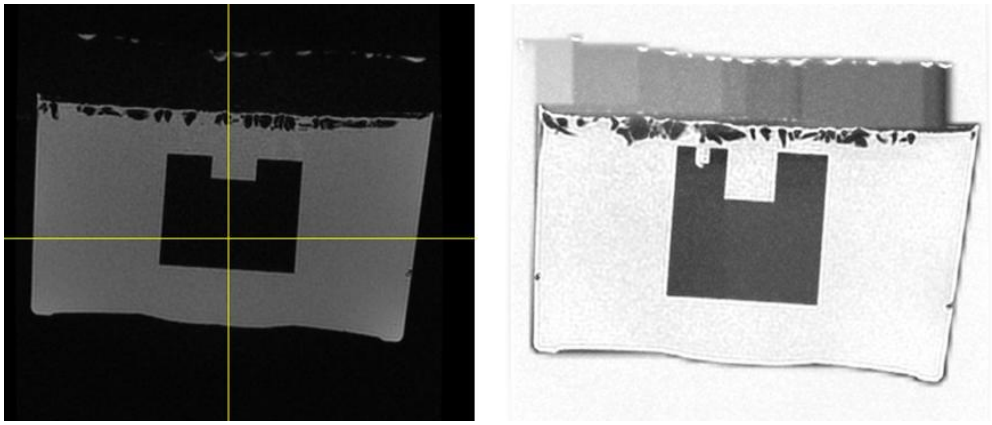


*Figure 136: Subtracting the background of the phantom cube dataset in Image J.*

An alternative method to remove the air was to use the flood tool to assign a different colour; however, this had to be completed on each individual image slice, and any remaining areas had to be removed with the paint tool *(Figure 137).*

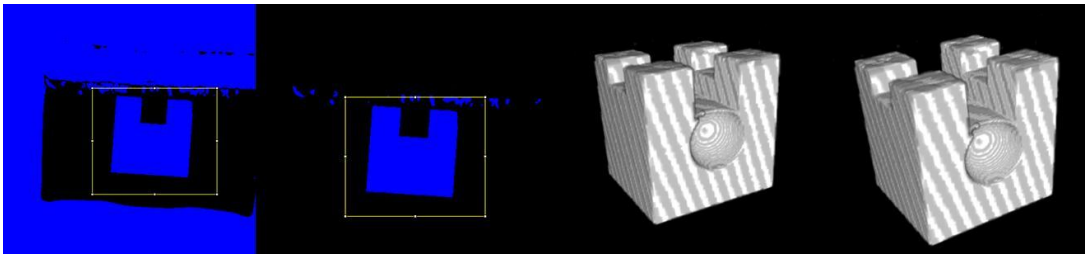


*Figure 137: Utilising the flood fill and paint tools in Image J (shown in blue) to remove the air. This enabled the creation of 3D reconstructed images of the cube phantom.*

Only once this process had been completed could the edge detection function be utilised *(Figure 138).* Whilst this provided a clear outline of the cube, the failure to successfully identify the edges of the object prior to segmentation made this of limited benefit for the "Black Bone" datasets.

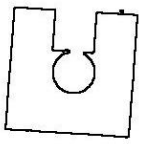


*Figure 138: Edge detection function after segmentation in Image J.*

Another successful method to segment the phantom cube dataset was to create a freehand ROI around the cube which was applied to the entire dataset, and the region outside of the boundary was cleared. This could then be converted to binary format, and inverted to enable production of a 3D image *(Figure 139).*

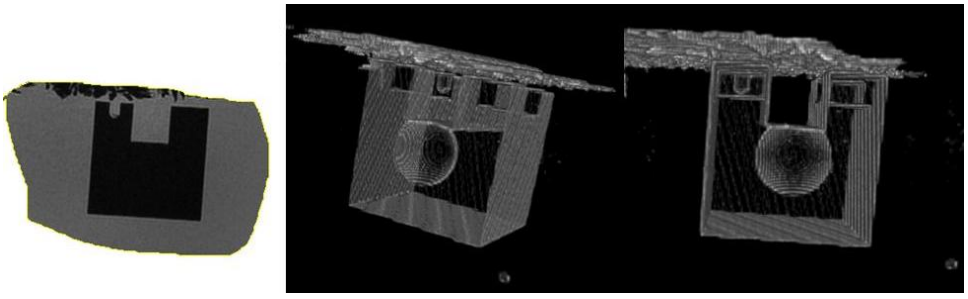


*Figure 139: Applying a freehand ROI to permit removal of everything outside of the ROI, to enable creation of a 3D reconstructed image.*

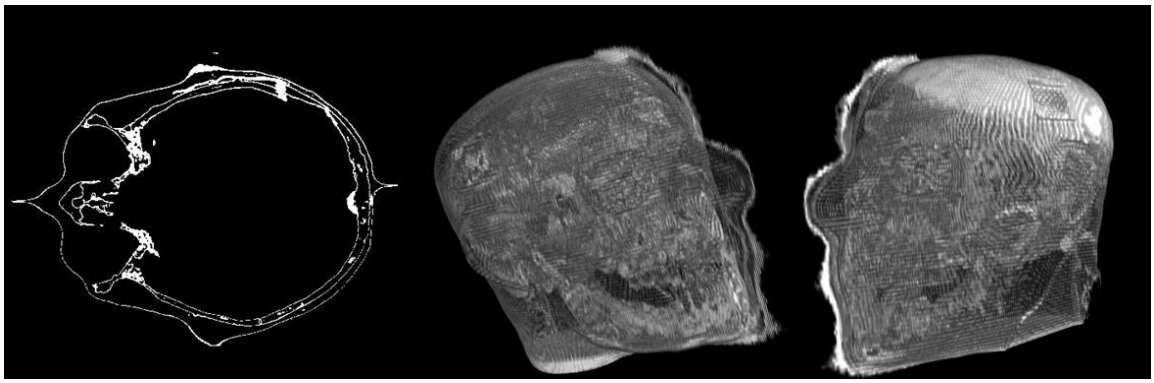


*Figure 140: Attempt to 3D render the phantom skull "Black Bone" dataset with Image J.*

With the "Black Bone" phantom skull dataset, a method to automatically remove the outer shell could not be found *(Figure 140).*

### *7.1.9.2 Adult Volunteer Datasets*

Similar problems were encountered with the adult "Black Bone" datasets, and despite multiple permutations of functions and sequence, a method to remove the outer soft tissue envelope could not be achieved *(Figure 141).*

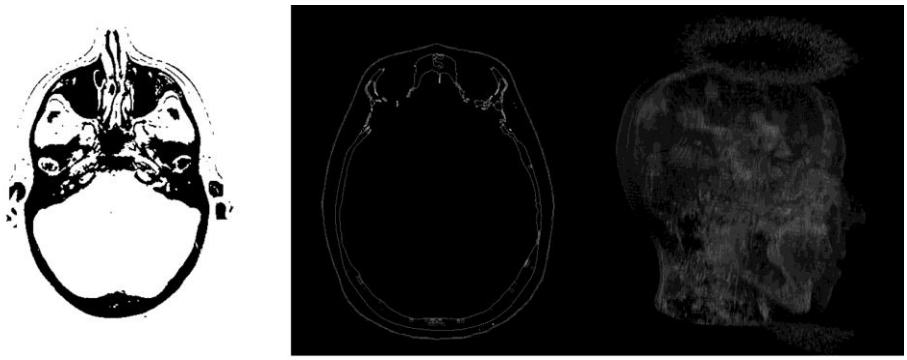


*Figure 141: Attempts to segment and render adult "Black Bone" dataset in Image J.*

For ImageJ to be of value in clinical practice with the "Black Bone" datasets, an add-on software code would be required to identify and remove the soft tissue envelope. This could not be achieved in the period of this research but provides further scope for development.

### 7.1.10 Mirada

Through collaboration with Mirada Medical Ltd a research license was granted for their proprietary imaging software. Whilst this does not currently include a 3D viewer, experimentation was undertaken to determine if this could provide a method for automatic edge detection suitable for the "Black Bone" datasets.

#### *7.1.10.1 Phantom Datasets*

With the phantom cube dataset, the ability to identify the "Black Bone" boundaries was achieved by placing a seed point in the centre of the cube and adjusting the threshold. With no communication between the cube and the outside air, all boundaries for the cube were rapidly identified, as seen in the orthogonal views in *Figure 142.*

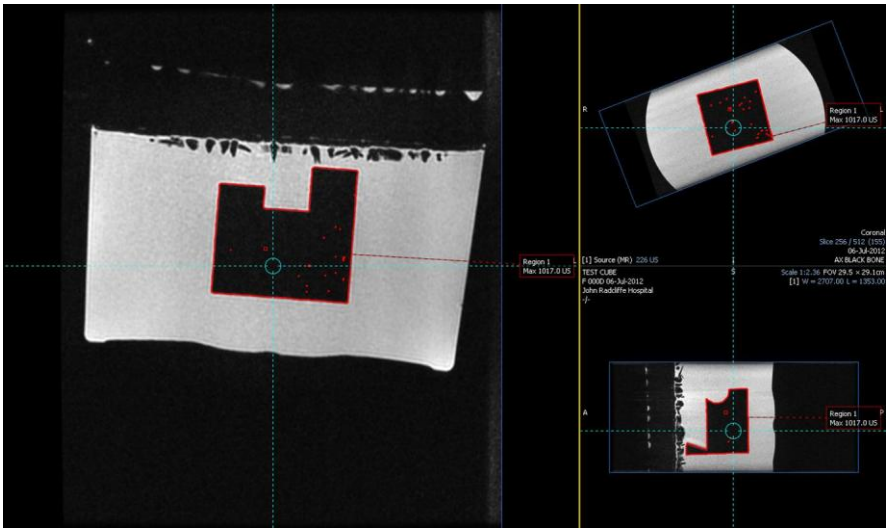


*Figure 142: Identifying the cube boundaries (red) in Mirada software.*

#### *7.1.10.2 Adult Volunteer Datasets*

With the adult "Black Bone" datasets, the bone boundaries were rapidly identified using an absolute threshold edge detection tool. With gradual drawing of the ROI around one of the image slices, all boundaries where there was a distinct change in threshold were identified. The result was visualised in the orthogonal views, and the boundaries automatically applied to the entire image stack. Whilst a boundary was produced of the outer soft tissues which required manual removal, this was achieved rapidly using the eraser tool. This was also automatically interpolated between

slices, and could be applied to any of the orthogonal views. The bone boundaries were therefore identified and unwanted boundaries removed more rapidly than with any of the other software investigated *(Figure 143).*

With the addition of a 3D viewer and associated functionalities required for optimal visualisation and the creation of anatomical models, this software could potentially be very useful in clinical practice with "Black Bone" datasets.

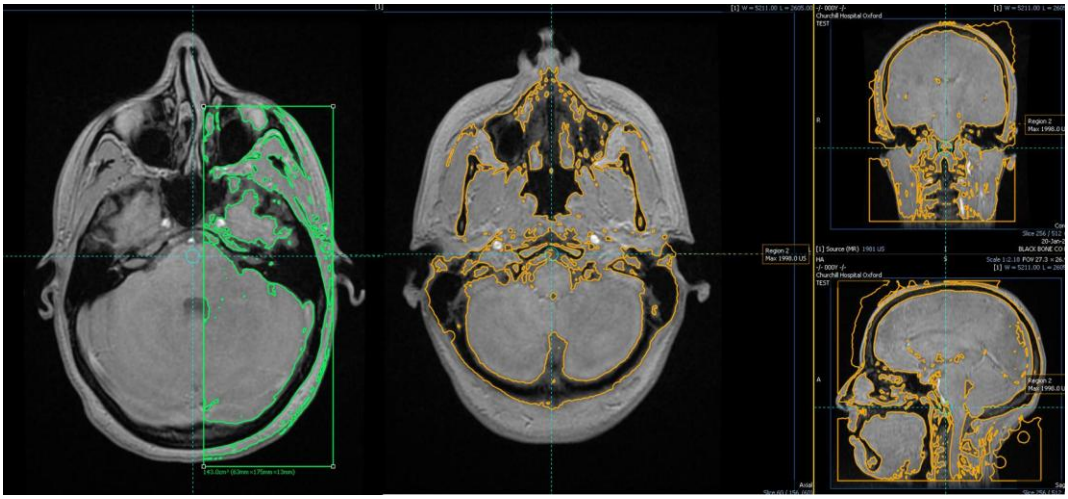


***Figure 143: Edge detection with adult "Black Bone" dataset, and removal of outer soft tissue boundary.***

### 7.1.11 ZIBAmira

Following presentation of the results thus far achieved with "Black Bone" datasets at an International Conference, collaboration was commenced with the Konrad-Zuse-Zentrum Institute Medical Imaging group in Berlin. The group were particularly interested in the "Black Bone" sequence as a method to obtain further datasets required to develop their atlas based segmentation tools, without exposing volunteers to ionising radiation.

ZIBAmira is the software developed by group, which is now commercially available. ZIBAmira is a 3D data visualisation, analysis and modelling system with the ability to visualise scientific data sets from various application areas.

Two adult volunteer "Black Bone" dataset were provided to the team, and their attempts at segmentation of the mandible using an atlas based method with subsequent fine adjustment, are shown in *Figure 144*.

A research license for ZIBAmira was very recently obtained, and initial investigation with "Black Bone" datasets completed. Shown in *Figure 144* is the typical screen layout for the software, which requires sequential addition of modules to segment, produce and visualise the 3D images. Initial experimentation with the software was completed with the phantom cube datasets. The ability to crop the dataset to include only the cube and surrounding gelatine, thus removing the outside air, meant that the cube could be segmented simply using the threshold tool *(Figure 145).*

Further collaboration is likely to result in atlas based segmentation techniques for "Black Bone" datasets of the entire craniofacial skeleton, thus making incorporation into routine clinical practice feasible in the near future.

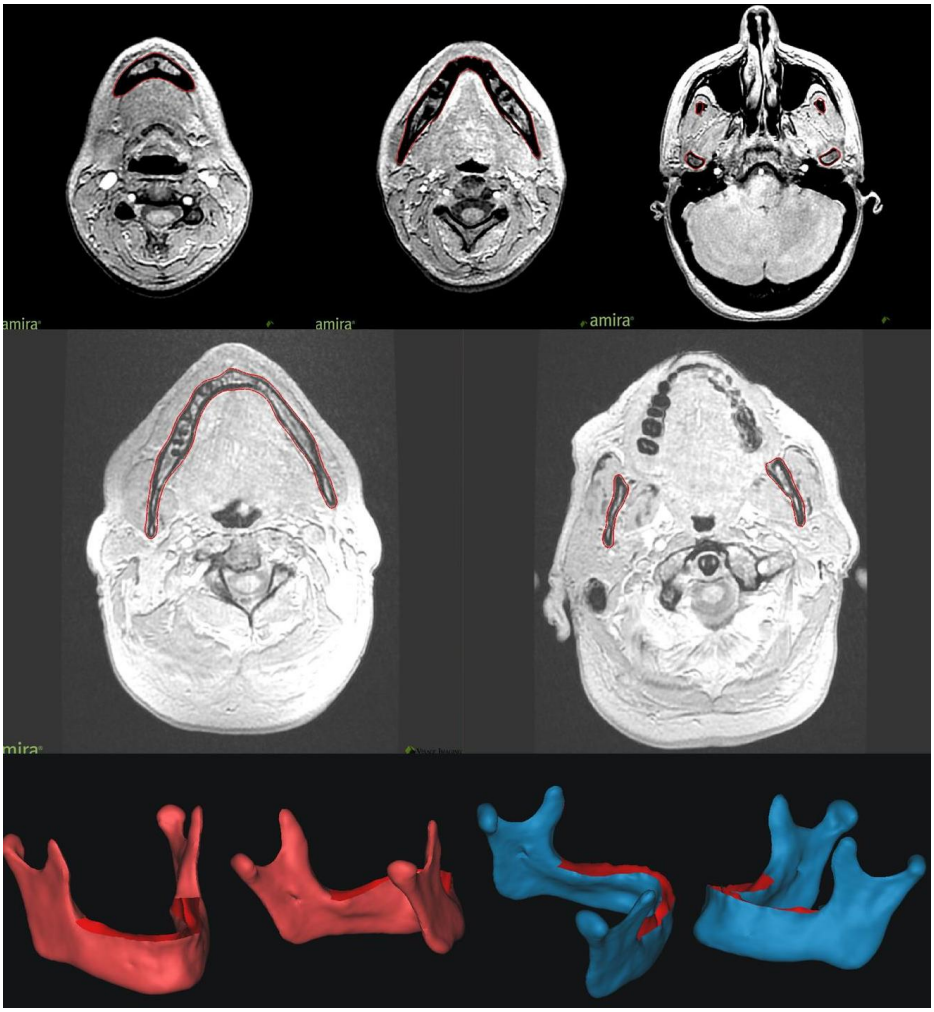


*Figure 144: Initial results obtained by ZIBAmira research team using adult volunteer "Black Bone" datasets. Segmentation for two datasets are shown (top and middle rows) with reasonable accuracy for the mandible; resultant 3D images (bottom row).*

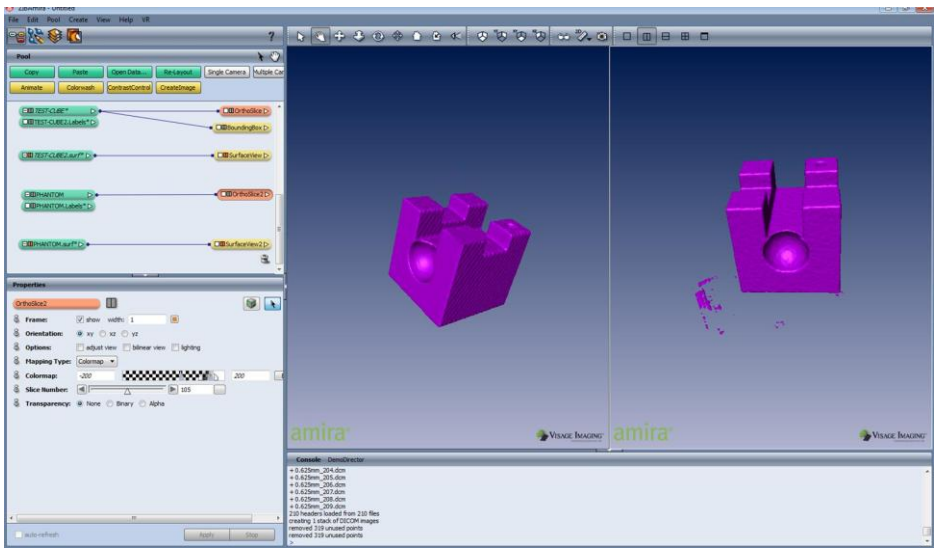


*Figure 145: Screen layout for ZIBAmira; the 3D images of the phantom cube from "Black Bone" (left), and CT (right) are shown.*

### 7.1.12 Matlab

Collaboration with Professor Zhang and Dr Crooks in the department of mathematics at the University of Swansea was established following discussion with the mathematics department at the University of Oxford.

The question posed to the mathematics team was "is there a mathematical method to define and quantify the bony edge on CT and "Black Bone" datasets?" This would therefore permit the opportunity to further validate the "Black Bone" sequence and to incorporate any edge detection techniques into imaging software.

Comparable "Black Bone" and CT datasets were supplied to the mathematics department. Shown in *Figure 146* are the preliminary results obtained by the team to identify the boundaries using Matlab. Matlab is a programming software for algorithm development, data visualisation and numerical computation. As shown in the images in *Figure 146* the boundaries on both the CT and "Black Bone" datasets were accurately identified. The inclusion of the outer soft tissue boundary, (as with the other software investigated), would result in this being in any subsequent 3D reconstruction, and would therefore necessitate an automated means of removal for Matlab to be of clinical benefit for the "Black Bone" datasets. Automated deduction of the outer boundary may be achievable with Matlab, however, this has unfortunately not yet been investigated and provides scope for further investigation.

### 7.1.13 Discussion

It has been demonstrated that 3D rendered images of the craniofacial skeleton are achievable with "Black Bone" datasets, with results approaching those obtainable with CT. The most useful software in terms of consistency of results was Fovia. Whilst the 3D reconstructed images correlated with the CT findings in the majority of cases, before these techniques could be introduced into routine clinical practice it was necessary to confirm the accuracy of the 3D rendered images. This is explored in the next section.

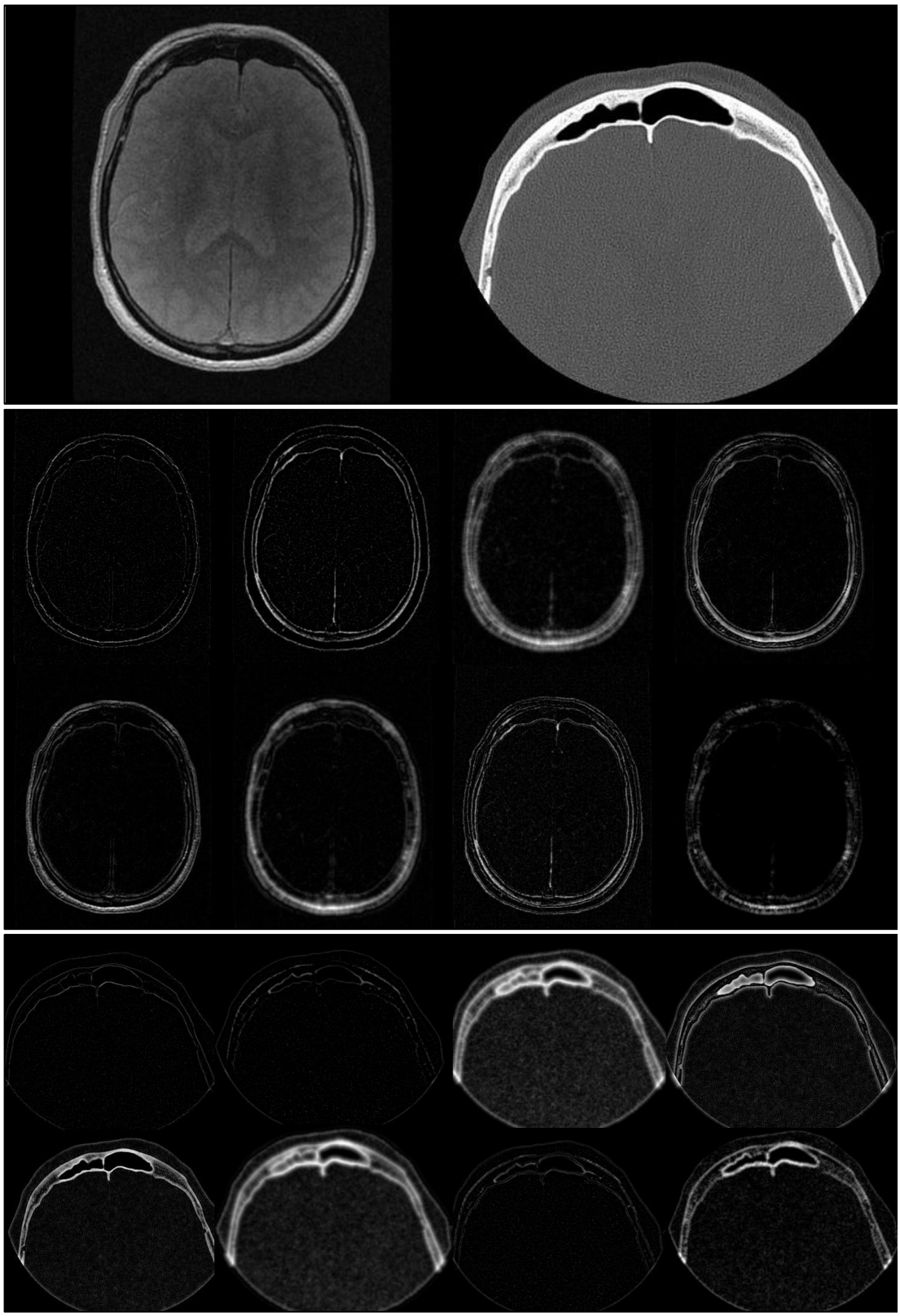


*Figure 146: Axial "Black Bone" and CT image on which investigation was conducted (Top), "Black Bone" (middle panel) and CT (bottom panel) results. Results are displayed from left to right in the following order for both datasets: Top Row - Bright corner map; Dark corner map; Edge map; Valley map; Bottom row – Ridge map; Oscillation map; Level 1 corner map; Level 3 corner map.*

## 7.2 3D Accuracy of "Black Bone" MRI

The accuracy of the resultant "Black Bone" 3D images were explored using onscreen measurements, volume analysis and mathematical modelling.

### 7.2.1 Direct Measurements

The phantom cube datasets were deemed the most suitable for completion of this aspect of the investigation; it provided the opportunity to compare "Black Bone" and CT with measurements completed directly on the cube. The imaging datasets utilised are shown in *Table 58.*

| | Slice Thickness (mm) | Overlap (mm) | Voxel Size (mm) |
|---|---|---|---|
| **CT** | | | |
| Low dose Face Protocol: | | | |
| • *Soft Tissue Algorithm* | 0.625 | - | 0.29x0.29x0.625 |
| | 1.25 | - | 0.29x0.29x1.25 |
| | 2.5 | - | 0.29x0.29x2.50 |
| • *Bone Algorithm* | 0.625 | - | 0.29x0.29x0.625 |
| | 1.25 | - | 0.29x0.29x1.25 |
| | 2.5 | - | 0.29x0.29x2.5 |
| Standard Helical Head Protocol: | | | |
| • *Soft Tissue Algorithm* | 0.625 | - | 0.3x0.3x0.625 |
| | 1.25 | - | 0.3x0.3x1.25 |
| | 2.5 | - | 0.3x0.3x2.50 |
| • *Bone Algorithm* | 0.625 | - | 0.3x0.3x0.625 |
| | 1.25 | - | 0.3x0.3x1.25 |
| | 2.5 | - | 0.3x0.3x2.50 |
| **"Black Bone" MRI** | | | |
| 1.5 T Magnet | 0.8 | 0.4 | 0.47x0.47x0.40 |
| | 1.2 | 0.6 | 0.47x0.47x0.60 |
| | 2.0 | 1.0 | 0.47x0.47x1.00 |
| | 2.4 | 1.2 | 0.47x0.47x1.20 |
| 3.0 T Magnet | 0.8 | 0.4 | 0.50x0.50x0.40 |
| | 1.2 | 0.6 | 0.50x0.50x0.60 |
| | 2.0 | 1.0 | 0.50x0.50x1.00 |
| | 2.4 | 1.2 | 0.50x0.50x1.20 |

***Table 58: Slice thickness of CT and "Black Bone" MRI phantom cube datasets for determination of accuracy.***

Eleven individual measurements *(Figure 147)* were made on each 3D rendered dataset, on 10 occasions. These were compared to measurements completed directly on the cube phantom using vernier callipers, again on 10 occasions *(Appendix H).*

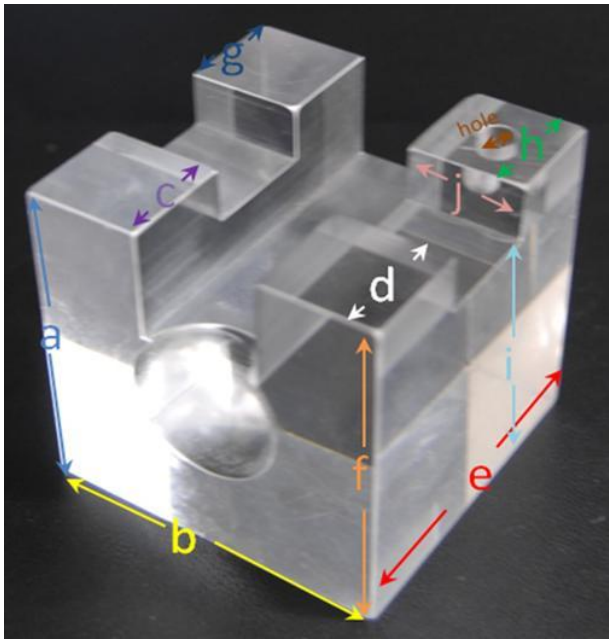



*Figure 147: Measurements on cube phantom.*

### 7.2.1.1 Fovia

In Fovia, each dataset was sequentially imported and a TF selected which provided the most visually accurate result for the cube. For the "Black Bone" datasets this required the surrounding pot to be removed by utilising the "whole volume" segmentation tool. Once a TF had been selected for the first dataset, this was imported and utilised for all datasets from the same imaging modality. The 3D rendered image was enlarged onscreen to optimise visualisation of the ROI *(Figure 148)*. Using the onscreen measuring device, measurements were recorded for each of the 11 dimensions shown in *Figure 147*. This was repeated on 10 occasions for each dataset.

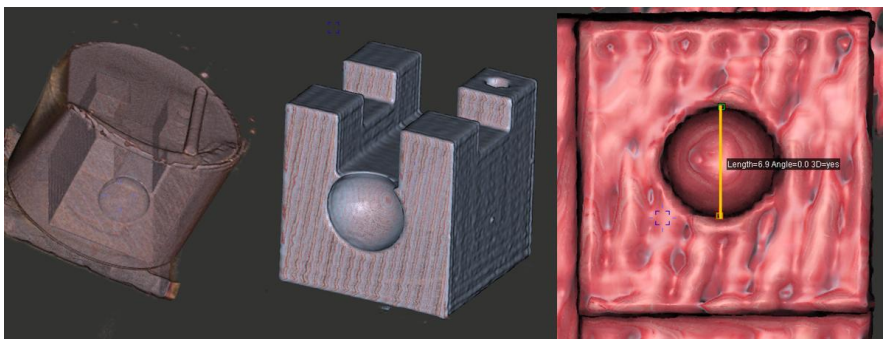


*Figure 148: Volume rendering of "Black Bone" phantom cube dataset, removing the surrounding pot and measuring one of the dimensions (the hole on the superior aspect).*

The measurements obtained for Fovia are included in *Appendix H.* Statistical analysis was performed to compare measurements across imaging modalities and with measurements made directly on the phantom *(Appendix H).* Whilst an independent t-test identified a significant difference between results from direct measurements and those performed on Fovia, the discrepancy in the majority of cases was less than 1mm. A mean difference was calculated for each of the measurements across the 10 repeated attempts. These results were combined to obtain an overall mean for each imaging dataset *(Table 59).* The overall difference for all "Black Bone" and CT datasets are also shown in *Table 59*. For the "Black Bone" datasets, the 1.5T 0.8mm dataset had the smallest mean difference from the measurements obtained directly from the phantom. For the CT datasets, the CT Helical Bone 0.625mm demonstrated the smallest mean discrepancy from the direct phantom measurements. The accuracy of the 3D image was limited by the voxel size of the dataset.

| | Mean | SD |
|---|---|---|
| **Direct v BB 1.5T 0.8mm** | 0.12 | 0.10 |
| **Direct v BB 1.5T 1.2mm** | 0.25 | 023 |
| **Direct v BB 1.5T 2.0mm** | 0.39 | 0.35 |
| **Direct v BB 1.5T 2.4mm** | 0.33 | 0.48 |
| **Direct v BB 3.0T 0.8mm** | 1.13 | 0.31 |
| **Direct v BB 3.0T 1.2mm** | 1.48 | 0.23 |
| **Direct v BB 3.0T 2.0mm** | 0.80 | 0.29 |
| **Direct v BB 3.0T 2.4mm** | 1.17 | 0.38 |
| **Direct v CT Face ST 0.625mm** | 0.56 | 0.29 |
| **Direct v CT Face ST 1.25mm** | 0.42 | 0.18 |
| **Direct v CT Face ST 2.5mm** | 0.62 | 0.45 |
| **Direct v CT Face Bone 0.625mm** | 0.24 | 0.13 |
| **Direct v CT Face Bone 1.25mm** | 0.42 | 0.33 |
| **Direct v CT Face Bone 2.5mm** | 0.36 | 0.25 |
| **Direct v CT Helical ST 0.625mm** | 0.23 | 0.15 |
| **Direct v CT Helical ST 1.25mm** | 0.37 | 0.20 |
| **Direct v CT Helical ST 2.5mm** | 0.48 | 0.31 |
| **Direct v CT Helical Bone 0.625mm** | 0.18 | 0.13 |
| **Direct v CT Helical Bone 1.25mm** | 0.24 | 0.17 |
| **Direct v CT Helical Bone 2.5mm** | 0.29 | 0.20 |
| **Overall Direct v BB** | 0.71 | 0.56 |
| **Overall Direct v CT** | 0.37 | 0.27 |

***Table 59: Overall mean difference in measurements between direct phantom measurement and imaging dataset.***

Independent samples t-test was completed to compare measurements obtained from the "Black Bone" 1.5T 0.8mm and CT Helical Brain Bone Algorithm 0.625mm datasets *(Appendix H).* These datasets were selected for comparison as they represented the parameters most likely to be selected when imaging the craniofacial skeleton, albeit with a smaller slice thickness in view of the small

size of the phantom cube. No statistical difference was found for four of the eleven sets of measurements. The overall mean difference in measurements was 0.18±0.13mm.

#### 7.2.1.2 Mimics

The 20 datasets were individually imported into Mimics. A threshold was selected, and the ROI cropped to segment the phantom cube. The 3D rendered image was enlarged onscreen to obtain the most optimal visualisation of the cube *(Figure 149).* Using the onscreen measuring device, measurements were recorded for each of the 11 dimensions. This was repeated on 10 occasions for each dataset. The individual measurements obtained are included in the *Appendix H*. Statistical analysis was completed with independent t-test between direct phantom measurements and those completed on Mimics *(Appendix H).*

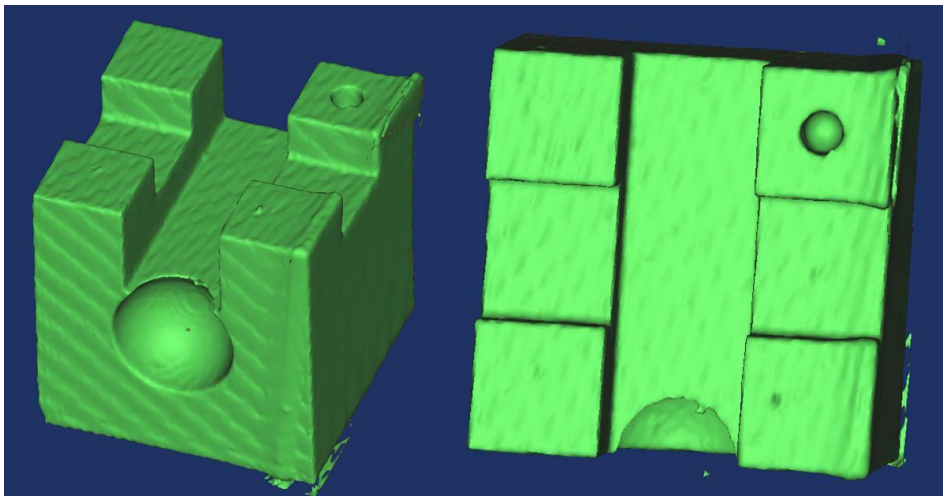


*Figure 149: Phantom cube 3D rendered with Mimics.*

| | Mean | SD |
|---|---|---|
| **Direct v BB 1.5T 0.8mm** | 0.23 | 0.20 |
| **Direct v BB 1.5T 1.2mm** | 0.15 | 0.11 |
| **Direct v BB 1.5T 2.0mm** | 0.25 | 0.34 |
| **Direct v BB 1.5T 2.4mm** | 0.42 | 0.21 |
| **Direct v BB 3.0T 0.8mm** | 0.58 | 0.27 |
| **Direct v BB 3.0T 1.2mm** | 0.17 | 0.12 |
| **Direct v BB 3.0T 2.0mm** | 0.18 | 0.09 |
| **Direct v BB 3.0T 2.4mm** | 0.24 | 0.14 |
| **Direct v CT Face Bone 0.625mm** | 0.25 | 0.25 |
| **Direct v CT Face Bone 1.25mm** | 0.24 | 0.27 |
| **Direct v CT Face Bone 2.5mm** | 0.26 | 0.22 |
| **Direct v CT Face ST 0.625mm** | 0.60 | 0.67 |
| **Direct v CT Face ST 1.25mm** | 0.41 | 0.16 |
| **Direct v CT Face ST 2.5mm** | 0.17 | 0.16 |
| **Direct v CT Helical Bone 0.625mm** | 0.27 | 0.14 |
| **Direct v CT Helical Bone 1.25mm** | 0.14 | 0.07 |
| **Direct v CT Helical Bone 2.5mm** | 0.23 | 0.14 |
| **Direct v CT Helical ST 0.625mm** | 0.18 | 0.11 |
| **Direct v CT Helical ST 1.25mm** | 0.10 | 0.08 |
| **Direct v CT Helical ST 2.5mm** | 0.22 | 0.16 |
| **Overall Direct v BB** | 0.28 | 0.24 |
| **Overall Direct v CT** | 0.26 | 0.28 |

***Table 60: Overall mean difference in measurements between direct phantom measurement and imaging dataset.***

A mean difference was calculated for each of the measurements across the 10 repeated attempts. These results were combined to obtain an overall mean for each imaging dataset *(Table 60).* The overall difference for all "Black Bone" and CT datasets are also shown in *Table 60.* Independent samples t-test was completed to compare measurements obtained from the "Black Bone" 1.5T 0.8mm and CT Helical Brain Bone Algorithm 0.625mm datasets *(Appendix H).* No statistical difference was found for six of the eleven sets of measurements. The overall mean difference in measurements was 0.21±0.20mm.

#### 7.2.1.3 Osirix

The same CT and "Black Bone" datasets were imported into Osirix for the final software measurement comparisons. Images were segmented by thresholding with removal of the outer container using the 3D segmentation tool. The 3D images were magnified on screen, and measurements completed 10 times using the integral measuring device *(Figure 150, Appendix H).*

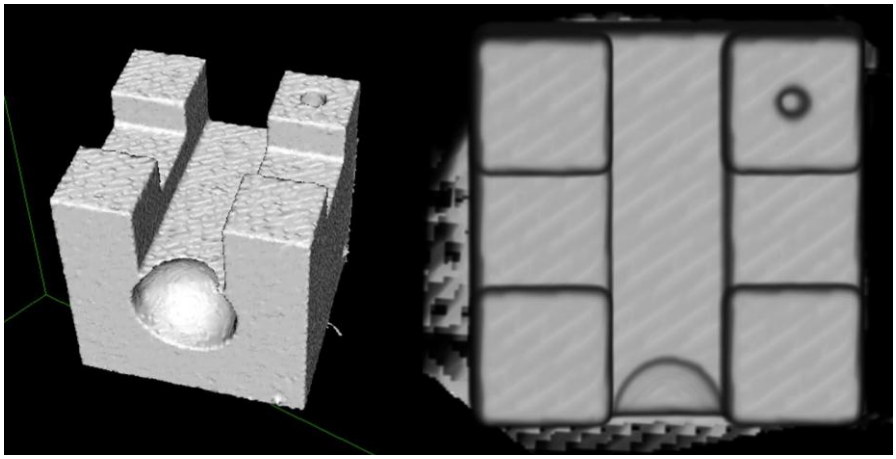


*Figure 150: Phantom cube 3D rendered with Osirix.*

| | Mean | SD |
|---|---|---|
| **Direct v BB 1.5T 0.8mm** | 0.30 | 0.43 |
| **Direct v BB 1.5T 1.2mm** | 0.17 | 0.18 |
| **Direct v BB 1.5T 2.0mm** | 0.38 | 0.72 |
| **Direct v BB 1.5T 2.4mm** | 0.51 | 0.29 |
| **Direct v BB 3.0T 0.8mm** | 0.17 | 0.08 |
| **Direct v BB 3.0T 1.2mm** | 0.51 | 0.62 |
| **Direct v BB 3.0T 2.0mm** | 0.60 | 1.54 |
| **Direct v BB 3.0T 2.4mm** | 0.24 | 0.13 |
| **Direct v CT Face Bone 0.625mm** | 0.53 | 1.37 |
| **Direct v CT Face Bone 1.25mm** | 0.14 | 0.16 |
| **Direct v CT Face Bone 2.5mm** | 0.17 | 0.28 |
| **Direct v CT Face ST 0.625mm** | 0.19 | 0.14 |
| **Direct v CT Face ST 1.25mm** | 0.36 | 0.31 |
| **Direct v CT Face ST 2.5mm** | 0.32 | 0.21 |
| **Direct v Helical Bone 0.625mm** | 0.20 | 0.11 |
| **Direct v Helical Bone 1.25mm** | 0.07 | 0.13 |
| **Direct v Helical Bone 2.5mm** | 0.19 | 0.28 |
| **Direct v Helical ST 0.625mm** | 0.20 | 0.17 |
| **Direct v Helical ST 1.25mm** | 0.24 | 0.18 |
| **Direct v Helical ST 2.5mm** | 0.31 | 0.38 |
| **Overall Direct v BB** | 0.36 | 0.66 |
| **Overall Direct v CT** | 0.24 | 0.45 |

*Table 61: Overall mean difference in measurements between direct phantom measurement and imaging dataset.*

A mean difference was calculated for each of the measurements across the 10 repeated attempts. These results were combined to obtain an overall mean for each imaging dataset *(Table 61)*. The overall difference for all "Black Bone" and CT datasets are also shown in *Table 61*. Independent samples t-test was completed to compare measurements obtained from the "Black Bone" 1.5T 0.8mm and CT Helical Brain Bone Algorithm 0.625mm datasets *(Appendix H)*. No statistical difference was found for three of the eleven sets of measurements. The overall mean difference in measurements was 0.3±0.33mm.

#### 7.2.1.4 Discussion

The discrepancy between measurements obtained between "Black Bone," CT and direct phantom measurements, overall were small. The mean difference between "Black Bone" and direct phantom measurements ranged between 0.12-1.17mm, and between CT and direct phantom measurements of 0.07-0.71mm. The mean discrepancy between the "Black Bone" 1.5T 0.8mm and CT Helical Brain Bone Algorithm 0.625mm datasets ranged between 0.18-0.3mm. It must be noted that the voxel size of the "Black Bone" datasets were larger than those of CT. However, "Black Bone" produced 3D images of comparable accuracy to those from CT.

### 7.2.2 Volume Measurements

An alternative method to directly compare the 3D rendered "Black Bone" and CT datasets in terms of accuracy was to calculate the volume of the 3D structure achieved for each modality.

#### 7.2.2.1 Direct Volume Measurements of Cube Phantom

To obtain the volume measurement of the cube phantom and thus permit comparison to the volume calculations obtained on imaging, Archimedes' principle was utilised. This law of physics states that the upward buoyant force exerted on an object immersed in fluid is equal to the weight of the fluid it actually displaces. Using a measuring jug filled with water, the fluid level was marked. The phantom cube was then placed into the jug, and allowed to freely sink to the bottom. The jug was gently tapped to remove any large water bubbles in the water, and the fluid level again marked. Using a syringe, water was removed from the jug down to the starting level, and the volume of water removed in (millilitres) recorded. Since 1ml of water is equivalent to $1cm^3$, the volume of water displaced provided the volume of the phantom cube. The process was completed on six occasions, each time commencing with a completely dry phantom *(Table 62).* Whilst attempts were made to minimise any potential error associated with measurement, a $5cm^3$ difference between the smallest and largest volume calculations was observed.

| Measurement Attempt | Volume of Phantom ($cm^3$) |
|---|---|
| 1 | 175 |
| 2 | 177 |
| 3 | 179 |
| 4 | 178 |
| 5 | 177 |
| 6 | 180 |
| Mean | 177.7 |
| SD | 1.8 |

*Table 62: Measurement of phantom cube volume from the amount of displaced water.*

#### 7.2.2.2 Osirix

To compare the accuracy of the "Black Bone" dataset to CT, volume measurements were completed in Osirix. In an attempt to minimise any potential bias in the identification of the edges of the cube, a threshold confidence level was set for both imaging datasets; however, in view of the differing methods of imaging the levels could not be standardised across both datasets. The result was visually inspected to confirm an accurate segmentation process. For the CT dataset the plinth on which the cube was set needed to be manually removed using the 3D rendering function. The volume of the ROI was calculated within Osirix on 5 occasions for both the "Black Bone"1.5T 0.8mm and CT 0.625 ST dataset *(Table 63).*

| | "Black Bone" MRI | CT |
|---|---|---|
| 1 | 173.3964 | 173.8411 |
| 2 | 174.1862 | 174.0714 |
| 3 | 174.8134 | 174.0714 |
| 4 | 174.3946 | 174.0866 |
| 5 | 174.9501 | 175.8914 |
| Mean | 174.3481 | 174.3924 |
| SD | 0.6150 | 0.8441 |
| Median | 174.3946 | 174.0714 |

*Table 63: Volume measurements of phantom cube using Osirix with "Black Bone" and CT datasets.*

Independent samples t test identified no significant difference between volume measurements on the "Black Bone" and CT datasets (p=0.927). However, a significant difference was noted between measurements obtained using Osirix for both the "Black Bone" and CT datasets when compared to the volume measurements obtained using the Archimedes principal with the phantom cube. This was most likely due to the inaccuracy associated with attempts to directly calculate the volume of the phantom cube.

#### 7.2.2.3 Mirada

Datasets were imported into Mirada software, and a seed point placed in the centre of the cube with adjustment of the threshold to achieve an accurate outline of the cube boundaries in all planes. The volume of the ROI was automatically calculated by the software. Measurements were completed on five occasions for the "Black Bone" 1.5T 0.8mm dataset, and compared to the CT datasets acquired using the standard helical head protocol and low dose face protocol:

1. CT Face protocol with bone algorithm 0.625mm
2. CT Face protocol with soft tissue algorithm 0.625mm
3. CT Helical head with bone algorithm 0.625mm
4. CT Helical head with soft tissue algorithm 0.625mm

The results obtained for these volume measurements are displayed in *Table 64.*

| | "Black Bone" | CT 1 | CT 2 | CT 3 | CT 4 |
|---|---|---|---|---|---|
| **1** | 176.3 | 169.0 | 175.1 | 179.1 | 176.3 |
| **2** | 177.4 | 173.5 | 181.9 | 179.1 | 176.3 |
| **3** | 175.3 | 173.6 | 174.5 | 179.8 | 177.3 |
| **4** | 177.9 | 178.0 | 174.8 | 179.1 | 177.6 |
| **5** | 176.8 | 175.5 | 175.1 | 182.7 | 177.8 |
| **Mean** | 176.7 | 173.9 | 176.3 | 180.0 | 177.1 |
| **SD** | 1.0 | 3.3 | 3.2 | 1.6 | 0.7 |
| **Median** | 176.8 | 173.6 | 175.1 | 179.1 | 177.3 |

*Table 64: Volume calculations of the phantom cube obtained on "Black Bone" and CT.*

An independent samples t-test was performed to compare the volume measurements obtained from the "Black Bone" and CT datasets *(Table 65).* There was no significant difference between "Black Bone" measurements and three of the four CT datasets. There was no significant difference between the direct cube volume measurements and those obtained from the "Black Bone," CT2 and CT4 datasets using Mirada software.

| | Significance |
|---|---|
| **"Black Bone" v CT 1** | 0.105 |
| **"Black Bone" v CT 2** | 0.764 |
| **"Black Bone" v CT 3** | 0.005 |
| **"Black Bone" v CT 4** | 0.578 |
| **Direct v "Black Bone"** | 0.324 |
| **Direct v CT1** | 0.039 |
| **Direct v CT2** | 0.379 |
| **Direct v CT3** | 0.049 |
| **Direct v CT4** | 0.489 |

*Table 65: Independent samples t-test for comparison between volume measurements obtained from "Black Bone" and CT, and between those directly obtained on the phantom.*

The main limitation of utilising volume measurements as a method to compare accuracy between "Black Bone" and CT datasets was the reliance upon accurate segmentation of the dataset. For both Osirix and Mirada software segmentation was completed using thresholding, which was particularly challenging in some of the CT datasets as a result of the close Hounsfield numbers of the cube and surrounding gelatine.

### 7.2.3 Mathematical Modelling

In an attempt to obtain a more accurate method of comparison between "Black Bone" and CT datasets, a mathematical method of comparison was sort. Collaboration had been established with the mathematics department at the University of Swansea, and on initial discussion the comparison between the two datasets was deemed a simple mathematical process. However, the team encountered some difficulties with the pre-processing steps required to align the two datasets; this was particularly challenging for the "Black Bone" dataset. Comparisons were made between the CT Face Protocol with Soft Tissue Reconstruction Algorithm and Slice Thickness 2.5mm, and the CT Helical Head Protocol with Soft Tissue Reconstruction Algorithm and Slice Thickness 2.5mm. The full report is included in the *Appendix H.* The process used to compare the two datasets was threshold based segmentation, with subsequent realignment of the edge points using the segmentations. Measurements were completed mathematically between the two datasets; firstly taking the maximum of the distance of each point on one volume to the nearest point on the other volume, and secondly the average distance for all points on one volume and the nearest point on the other volume. Since these measurements depend upon which dataset is the reference volume, the measurements were completed for each dataset as the reference object and the maximum result obtained. Overall, a maximum error of 1mm and an average error of 0.25mm were obtained for these CT datasets.

### 7.2.4 ZIBAmira

One of the functions available within ZIBAmira is the ability to compare two segmented objects. This provided a further method to explore the accuracy of the "Black Bone" phantom cube dataset.

The CT helical head with soft tissue algorithm and slice thickness of 0.625mm was used for comparison with the "Black Bone" phantom cube dataset. Both datasets were imported into

ZIBAmira, and segmented using a combination of thresholding and the "blow" tool. The resultant 3D rendered images were viewed, and manually re-aligned to correspond with each other three-dimensionally in space. The final alignment was performed using the "align surfaces" function. To calculate the mean difference in measurements between the two datasets the "SurfaceDistance" function with "two way" comparison was used *(Figure 151)*. This yielded a mean discrepancy result of 0.138±0.103 mm, with a maximum difference of 1.15mm, and median 0.121 mm. These results were displayed graphically on the cube to determine the areas of greatest discrepancy. As shown in *Figure 152*, the greatest discrepancy (shown in red) was around the superior aspect of the circular cut out on the front face of the cube.

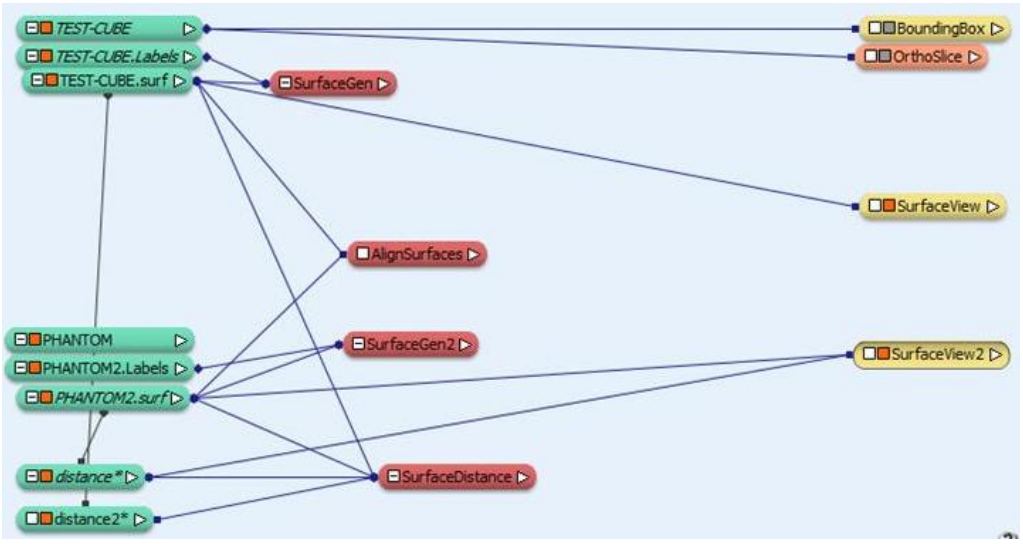



***Figure 151: ZIBAmira workflow to compare "Black Bone" and CT phantom cube datasets and obtain subsequent visual display.***

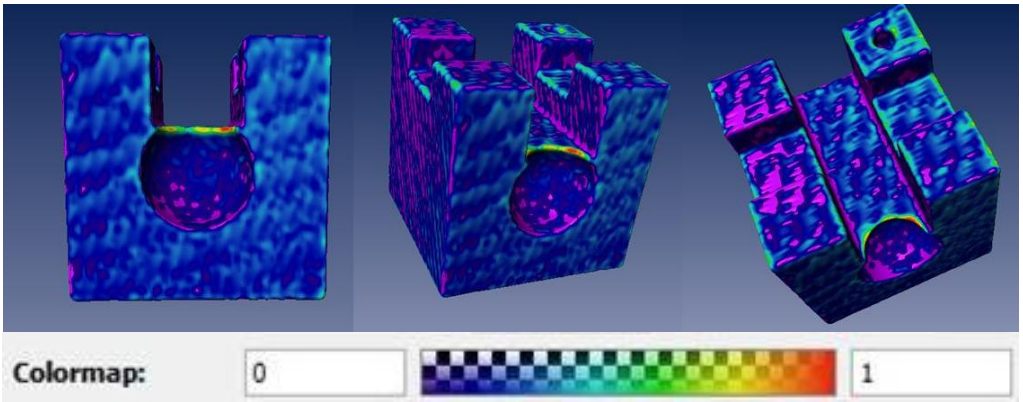



***Figure 152: Graphical display of difference between 3D rendered "Black Bone" and CT phantom cube datasets. The colour map demonstrates gradated differences between 0mm (purple) and 1mm (red).***

### 7.2.5 Discussion

It has been demonstrated via volume measurement, mathematical modelling, and image fusion, that 3D datasets from “Black Bone” and CT are comparable, with discrepancies in most cases being less than 1mm for the phantom cube datasets. However, it must be noted that “Black Bone” imaging of the cube phantom was based upon the void created within the surrounding gelatine, and thus any air-containing space between the cube and gelatine results in inaccuracy of volume measurements.

The phantom cube was selected for investigation of the accuracy of 3D rendering of “Black Bone” in view of the ease with which segmentation could be performed and the ability to align the datasets. Whilst comparison between “Black Bone” and CT datasets of the craniofacial skeleton would be the ideal measure of accuracy, particularly in ZIBAmira with display of a colour map, multiple difficulties arose when attempting to align the two complex shapes in the software and comparison was not feasible.

A further potential confounding aspect to accuracy of 3D “Black Bone” images was the application of a “smoothing factor” and this is explored in the next section.

## 7.3 Smoothing Effects

The majority of software packages incorporate the ability to smooth the resultant 3D image, thus improving its appearance. However, incorrect selection of the smoothing factor results in inaccuracies in terms of dimension and with potential loss of detail.

The impact of the smoothing factor and iterations was explored on the "Black Bone" phantom cube dataset with Mimics. The dataset was segmented using a combination of thresholding and magic tool edge detection. A smoothing factor with varying number of iterations was then applied to the 3D image *(Table 66)*; the same 3D image was used as the starting point for all smoothing applications. The resultant effects were assessed in two ways; firstly by visualisation of the effect on the cube, and secondly by measurement. Measurements were completed by magnification of the cube onscreen utilising the integral measuring device on 10 occasions for the 11 measurements shown in *Figure 147*. These were compared to measurements obtained before application of any smoothing factor.

| | | Iterations | | | | | | |
|---|---|---|---|---|---|---|---|---|
| | | 2 | 5 | 25 | 50 | 100 | 250 | 500 |
| Smoothing | 0.0001 | ✓ | ✓ | ✓ | ✓ | ✓ | ✓ | ✓ |
| | 0.001 | | | | | | | |
| | 0.01 | ✓ | ✓ | ✓ | ✓ | ✓ | ✓ | ✓ |
| | 0.1 | | | | | | | |
| | 0.2 | ✓ | ✓ | | | | | |
| | 0.5 | | | | | | | |
| | 0.8 | | | | | | | |
| | 1 | ✓ | | | | | | |

*Table 66: Smoothing factor and number of iterations applied to the phantom cube 3D dataset.*

The effects on the 3D cube are shown in *Figure 153*. With a smaller smoothing factor a larger number of iterations could be performed before there was any noticeable distortion on the resultant image. For the typical amount of smoothing required for the datasets, the resultant adverse effects were minimal.

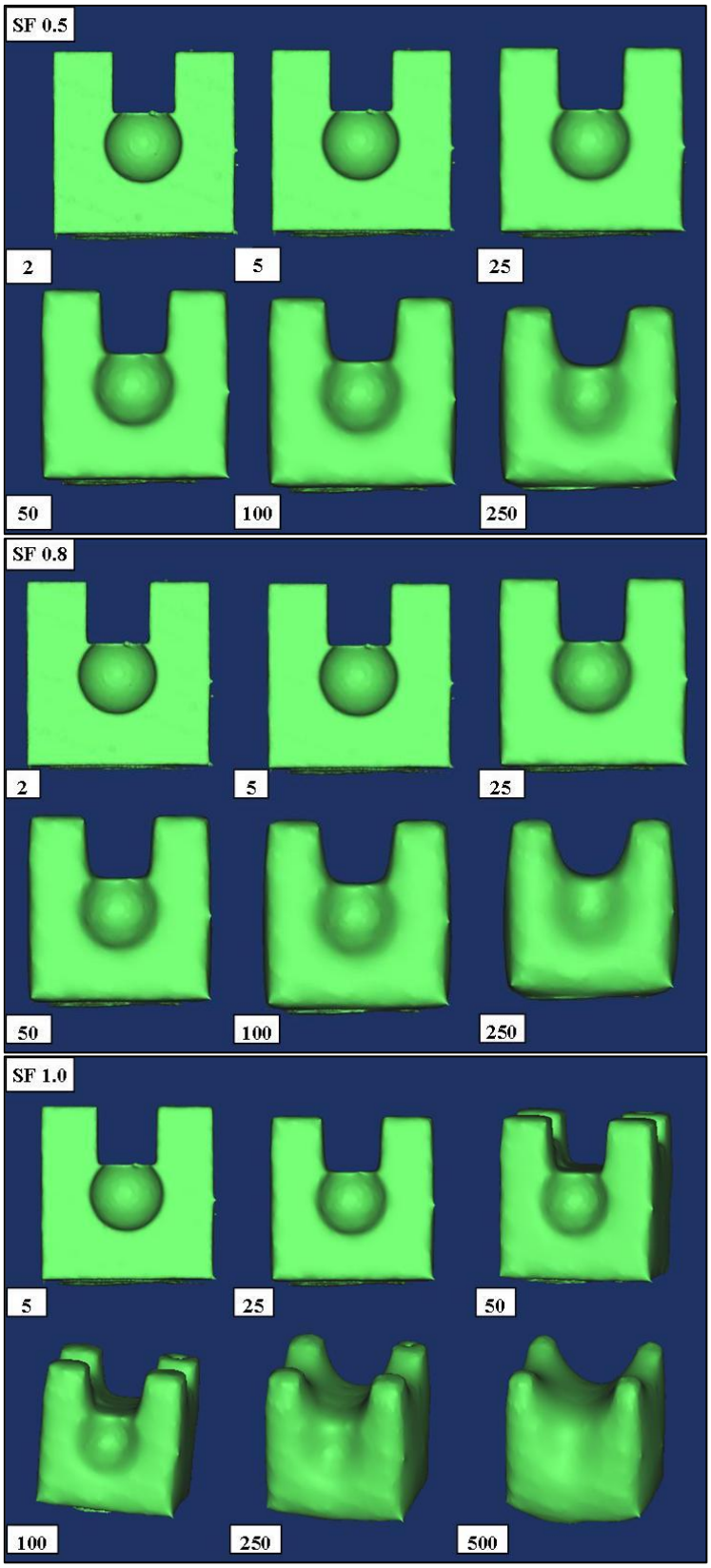



*Figure 153: Effect of varying the smoothing factor (SF) and number of iterations (2, 5, 25, 20, 100, 250 & 500).*

The measurements obtained for each combination of smoothing factor and iterations investigated are included in the *Appendix H.*

A mean difference was calculated for each of the measurements across the 10 repeated attempts. These results were combined to obtain an overall mean for each imaging dataset *(Table 67).*

| | Mean | SD |
|---|---|---|
| **None v Smooth 0.0001, Iterations 2** | 0.37 | 0.62 |
| **None v Smooth 0.0001, Iterations 5** | 0.23 | 0.55 |
| **None v Smooth 0.0001, Iterations 25** | 0.24 | 0.57 |
| **None v Smooth 0.0001, Iterations 50** | 0.26 | 0.59 |
| **None v Smooth 0.0001, Iterations 100** | 0.26 | 0.60 |
| **None v Smooth 0.0001, Iterations 250** | 0.26 | 0.61 |
| **None v Smooth 0.0001, Iterations 500** | 0.35 | 0.63 |
| **None v Smooth 0.01, Iterations 2** | 0.37 | 0.63 |
| **None v Smooth 0.01, Iterations 5** | 0.25 | 0.58 |
| **None v Smooth 0.01, Iterations 25** | 0.28 | 0.59 |
| **None v Smooth 0.01, Iterations 50** | 0.26 | 0.63 |
| **None v Smooth 0.01, Iterations 100** | 0.23 | 0.60 |
| **None v Smooth 0.01, Iterations 250** | 0.26 | 0.63 |
| **None v Smooth 0.01, Iterations 500** | 0.33 | 0.67 |
| **None v Smooth 0.2, Iterations 2** | 0.23 | 0.62 |
| **None v Smooth 0.2, Iterations 5** | 0.23 | 0.60 |
| **None v Smooth 1, Iterations 2** | 0.29 | 0.60 |

***Table 67: Mean discrepancy between measurements obtained with various smoothing factors and those prior to application of smoothing.***

With an overall mean discrepancy of between 0.23 – 0.37mm with various combinations of smoothing factor and iterations, the resultant effect on accuracy associated with this function must be born in mind.

### 7.3.1 Discussion

This section of the thesis has demonstrated that the level of smoothing utilised to enhance the visual appearance of 3D reconstructed images has a negligible effect on the resultant accuracy. Utilisation of such function is particularly valuable in improving the bony appearance on 3D rendered "Black Bone" images.

Having determined the potential of "Black Bone" in 3D reconstruction and its associated accuracy, the next section explores the potential to further enhance 3D "Black Bone" images of the orbit, in view of the particular concern for radiation protection in this region.

## 7.4 Imaging the Orbits

One of the anatomical regions which would benefit greatly from the use of "Black Bone" as an alternative to CT are the orbits in view of the threshold dose limit associated with development of cataracts. To explore if this region could be accurately imaged with "Black Bone," imaging was obtained on an adult volunteer (KE) at OMRI on a 3T magnet. The FOV was reduced to permit the smallest possible voxel size (0.43 x 0.43 x 0.4 mm). The resultant images were rendered using Mimics, Osirix and Fovia *(Figure 154).*

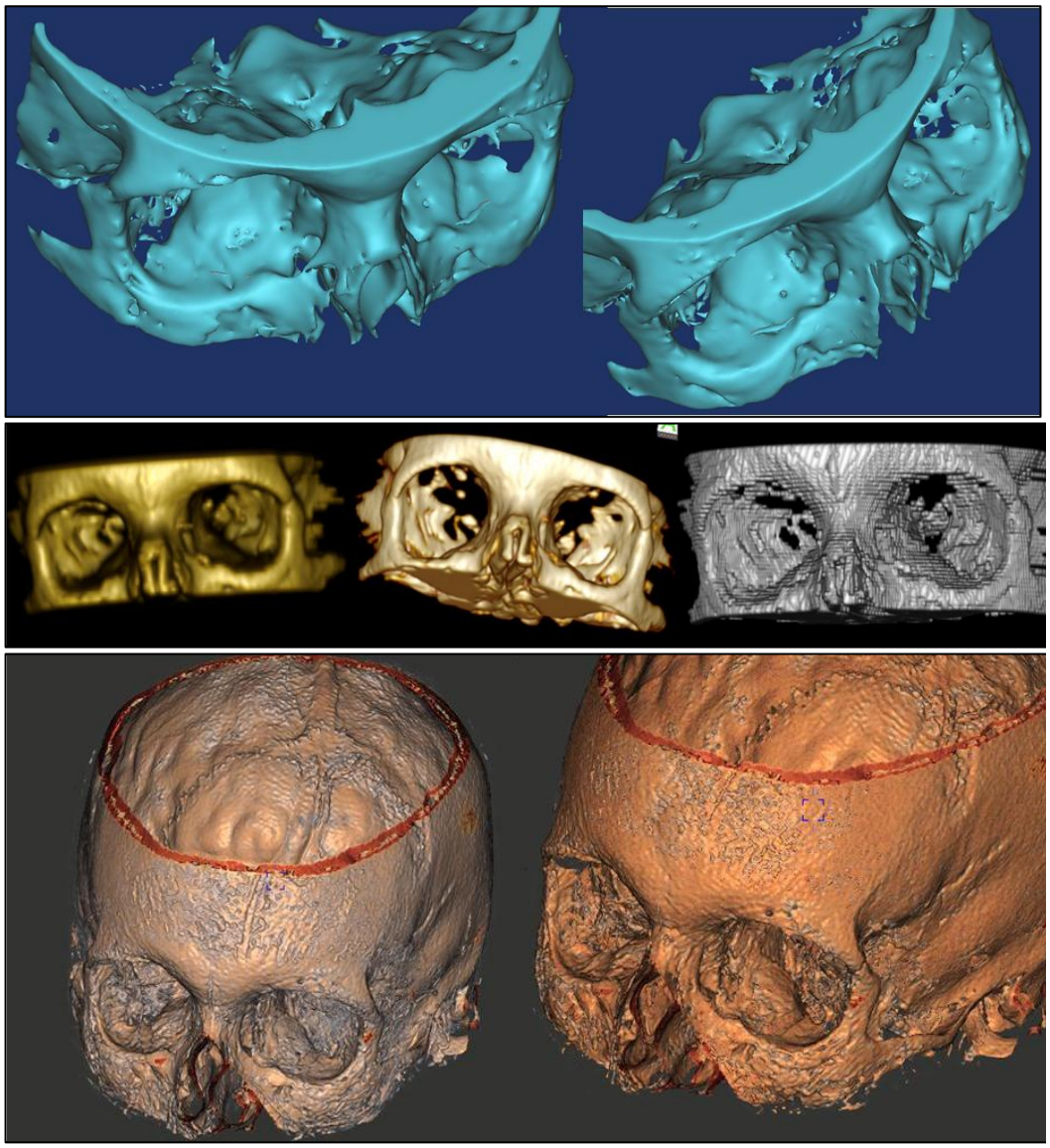


*Figure 154: 3D rendering of the orbits using Mimics (top), Osirix (middle) and Fovia (bottom).*

The main difficulties associated with segmenting bone around the orbits can be seen in *Figure 155.* The bone in this region is particularly thin. It was not possible to accurately distinguish the orbital floor from the maxillary sinus. Whilst it was possible to utilise the air in the maxillary sinus as a pseudo orbital floor resulting in a clear image in normal patients, this was a potential source of inaccuracy in cases of orbital floor fracture, one of the most common reasons for imaging this region. A "Black Bone" dataset from a patient with an orbital floor fracture was imported into Mimics, and segmented by selecting an appropriate threshold. As shown in *Figure 156*, the maxillary antrum was full of extensive mucosal swelling and proteinaceous effusion. The result on the 3D rendered image was loss of the orbital floor, and loss of bone density around the maxillary sinus. It was not possible to clearly define the extent of the fracture in this case on the 3D rendered image. As previously discovered, segmentation based purely on thresholding techniques results in somewhat variable results, and an alternative method of edge detection may yield improved results for the orbit, particularly in cases of fracture.



***Figure 155: Coronal, axial and sagittal "Black Bone" image of a normal orbit. Note the thin bone, and similar pixel value of the eye muscles.***

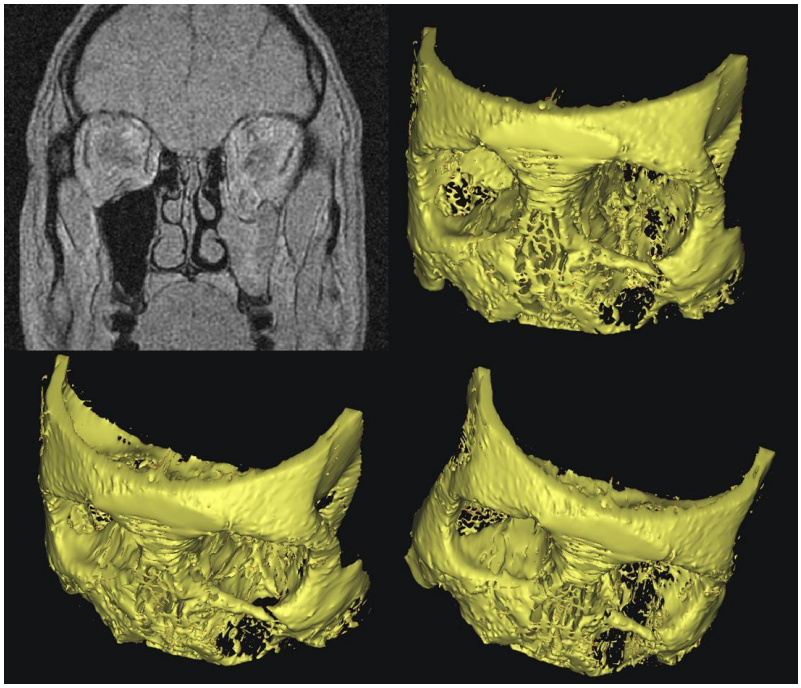


*Figure 156: Coronal "Black Bone" image, and 3D reconstructions in patient with orbital floor fracture.*

### 7.4.1 Discussion

3D reconstructed images of the orbit were achievable with "Black Bone," enhanced with the acquisition of datasets with a small voxel size. Difficulty arose in the orbital floor as a result of the inability to distinguish the bone from air within the maxillary sinus. This may result in 3D reconstructed "Black Bone" images being less reliable in patients with orbital floor fractures. However, only one dataset was available to explore this potential, and provides further scope for this work.

In the cranio-maxillofacial specialities, the production of anatomical models is of great benefit in surgical planning. Having established the potential for 3D reconstruction of "Black Bone" datasets, attention was turned to the utilisation of these reconstructed images for the production of anatomical models.

## 7.5 Anatomical Models

To enhance surgical planning the ability to create 3D anatomical models from “Black Bone” MRI images is required. This section of the thesis builds upon work in previous sections and explores the potential and accuracy of “Black Bone” in the modelling process.

A Z-Printer 650 rapid prototyping machine was available in the department for this aspect of the work *(Figure 157).* The z-printer uses an additive layer process, adding binder to a powder layer by layer to gradually build the model. The excess powder is removed by dusting it off with a brush, and with the aid of a fine high-powered jet of air. The resultant model is weak and requires finishing in one of two ways; the first, and cheapest method, is to spray the model with Epson salts and to allow the model to dry. This is repeated a number of times. This is suitable for models that are only required for a short period as they remain fragile. The second method is to cover the model with a cyanoacrylate solution. The cyanoacrylate is poured over the model, and the excess removed with rapid dabbing of the model with paper towels. Using this method the model cures quickly, and the resultant model is strong and durable.



***Figure 157: Z-printer 650.***

### 7.5.1 Accuracy of the Model Process with CT data

Prior to developing methods to create anatomical models from "Black Bone" datasets it was necessary to explore the accuracy of models created from CT data with the Z-printer, to permit comparison.

#### 7.5.1.1 Materials and Methods

The geometric Perspex cube acted as the phantom in this case *(Figure 158).* The cube was scanned using CT, and the DICOM files saved from efilm. These were imported into Mimics and the Hounsfield number adjusted to obtain an optimal 3D rendered image. An STL file was created, and imported into ZPrint 7.6 software to communicate with the zprinter. The data was subsequently converted to an STL file, and transferred to the zprinter to produce the model. The model was sprayed with Epson salts and allowed to dry. The distances which could be optimally measured using vernier callipers were selected on the cube *(Figure 158),* and each distance measured 10 times on the Perspex cube and the model. Data were entered into Microsoft Excel, and analysis performed using SPSS.

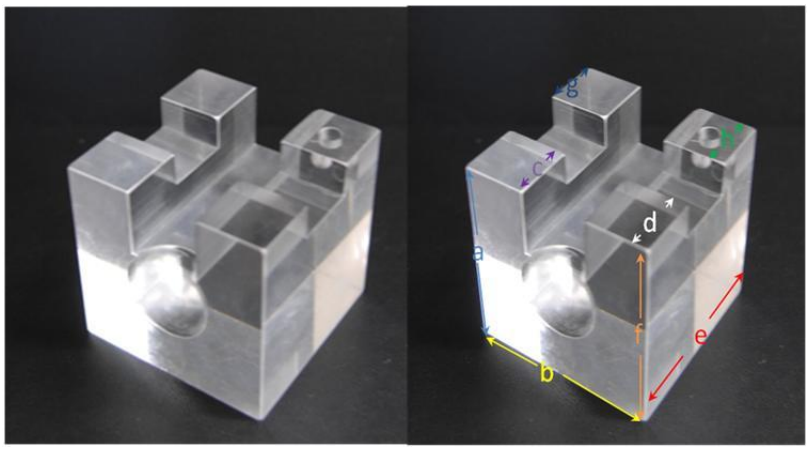



***Figure 158: The cue phantom, and the measurements used to determine accuracy of the resultant model.***

#### 7.5.1.2 Results

The model created from the CT dataset is shown in *Figure 159,* and the corresponding measurements obtained directly from the cube phantom and the model are shown in *Table 68.*

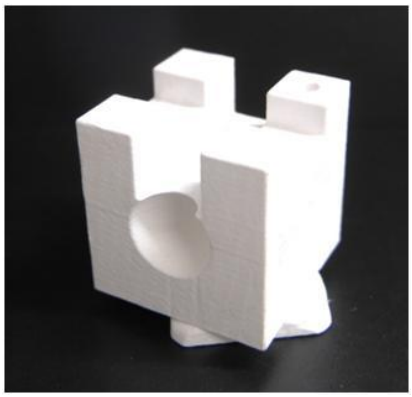


*Figure 159: Model of cube phantom created from CT dataset on z-corp printer.*

| | Measurement | | | | | | | |
|---|---|---|---|---|---|---|---|---|
| | a | b | c | d | e | f | g | h |
| | **Phantom** | | | | | | | |
| **1** | 60.09 | 60.10 | 20.11 | 20.16 | 60.09 | 60.08 | 19.86 | 19.86 |
| **2** | 60.09 | 60.10 | 20.12 | 20.06 | 60.09 | 60.07 | 19.88 | 19.89 |
| **3** | 60.09 | 60.09 | 20.05 | 20.13 | 60.09 | 60.08 | 19.86 | 19.93 |
| **4** | 60.06 | 60.09 | 20.09 | 20.12 | 60.13 | 60.07 | 19.9 | 19.94 |
| **5** | 60.06 | 60.08 | 20.06 | 20.04 | 60.15 | 60.19 | 19.86 | 19.90 |
| **6** | 60.07 | 60.10 | 20.05 | 20.11 | 60.09 | 60.15 | 19.86 | 19.95 |
| **7** | 60.05 | 60.10 | 20.05 | 20.08 | 60.09 | 60.15 | 19.88 | 19.93 |
| **8** | 60.09 | 60.11 | 20.05 | 20.10 | 60.09 | 60.13 | 19.85 | 19.89 |
| **9** | 60.20 | 60.10 | 20.08 | 20.06 | 60.10 | 60.11 | 19.86 | 19.89 |
| **10** | 60.08 | 60.11 | 20.06 | 20.07 | 60.09 | 60.11 | 19.85 | 19.88 |
| **Mean** | 60.09 | 60.10 | 20.07 | 20.09 | 60.10 | 60.11 | 19.87 | 19.91 |
| **SD** | 0.04 | 0.01 | 0.03 | 0.04 | 0.02 | 0.04 | 0.02 | 0.03 |
| | **Model** | | | | | | | |
| **1** | 60.44 | 59.87 | 19.9 | 19.74 | 59.76 | 60.40 | 19.78 | 19.62 |
| **2** | 60.32 | 59.87 | 19.84 | 19.99 | 59.74 | 60.27 | 19.68 | 19.63 |
| **3** | 60.28 | 60.01 | 19.68 | 19.90 | 59.71 | 60.39 | 19.72 | 19.70 |
| **4** | 60.29 | 59.86 | 19.74 | 19.71 | 59.77 | 60.43 | 19.76 | 19.68 |
| **5** | 60.42 | 59.98 | 19.71 | 19.83 | 59.71 | 60.41 | 19.75 | 19.72 |
| **6** | 60.30 | 59.86 | 19.70 | 19.70 | 59.70 | 60.40 | 19.68 | 19.78 |
| **7** | 60.29 | 59.82 | 19.68 | 19.96 | 59.83 | 60.26 | 19.74 | 19.72 |
| **8** | 60.30 | 59.89 | 19.69 | 19.93 | 59.65 | 60.41 | 19.68 | 19.70 |
| **9** | 60.26 | 60.03 | 19.83 | 19.89 | 59.70 | 60.48 | 19.75 | 19.77 |
| **10** | 60.23 | 59.95 | 19.81 | 19.99 | 59.76 | 60.45 | 19.69 | 19.76 |
| **Mean** | 60.31 | 59.91 | 19.76 | 19.86 | 59.73 | 60.39 | 19.72 | 19.71 |
| **SD** | 0.07 | 0.07 | 0.08 | 0.11 | 0.05 | 0.07 | 0.04 | 0.05 |

*Table 68: Measurements obtained on phantom and resultant model.*

An independent samples t-test identified a statistically significant difference ($p<0.05$) between measurements performed directly on the phantom and those on the model. To determine the level of discrepancy between the measurements, the difference was calculated for each measurement, and the mean difference determined *(Table 69).* The maximum mean discrepancy was 0.37mm, a level that would be deemed insignificant clinically.

| | a | b | c | d | e | f | g | h |
|---|---|---|---|---|---|---|---|---|
| **Mean** | 0.22 | 0.18 | 0.31 | 0.23 | 0.37 | 0.28 | 0.14 | 0.20 |
| **SD** | 0.09 | 0.08 | 0.06 | 0.14 | 0.05 | 0.08 | 0.04 | 0.05 |
| **Min** | 0.06 | 0.07 | 0.21 | 0.07 | 0.26 | 0.11 | 0.08 | 0.12 |
| **Max** | 0.36 | 0.28 | 0.37 | 0.42 | 0.44 | 0.37 | 0.20 | 0.26 |

*Table 69: Discrepancy between distances on phantom and CT model.*

Having determined the level of accuracy of models created with CT data using the zprinter, the next phase was to explore the potential of "Black Bone" MRI.

### 7.5.2 Anatomical Models from "Black Bone" MRI

Building on the preceding work on 3D rendering, the "Black Bone" 3D dataset was converted into a format compatible with the z-printer. During the course of the research period Fovia released a polygon export, equivalent to producing STL files directly. This has recently been tested with "Black Bone" datasets and required the outside air to be removed. However, there have been some problems with the resultant STL files and exploration of Fovia in anatomical modelling provides further scope for this work. Of the software utilised in Section 8, Mimics, Osirix and 3D doctor offer STL export functionalities and these were utilised in this section.

#### 7.5.2.1 Anatomical Models using Adult "Black Bone" datasets

The technical feasibility of producing anatomical models from "Black Bone" datasets was explored using an adult volunteer "Black Bone" dataset. The mandible was selected in view of the relative simplicity in 3D rendering this region, and its comparatively small size. The mandible was segmented in Mimics by applying a threshold and manually removing regions outside of the ROI *(Figure 163).* An STL file was created from the surface of the 3D rendered image, and imported into the ZPrint software to permit printing. The processes involved in finishing the model are shown in *Figure 164*, and the final result in *Figure 165 (Movie Clip 15).*

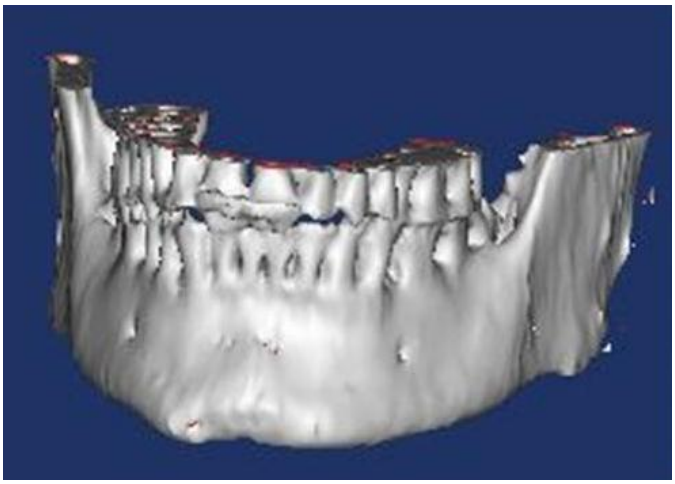


*Figure 160: 3D rendered image of mandible produced in Mimics from adult volunteer "Black Bone" dataset.*

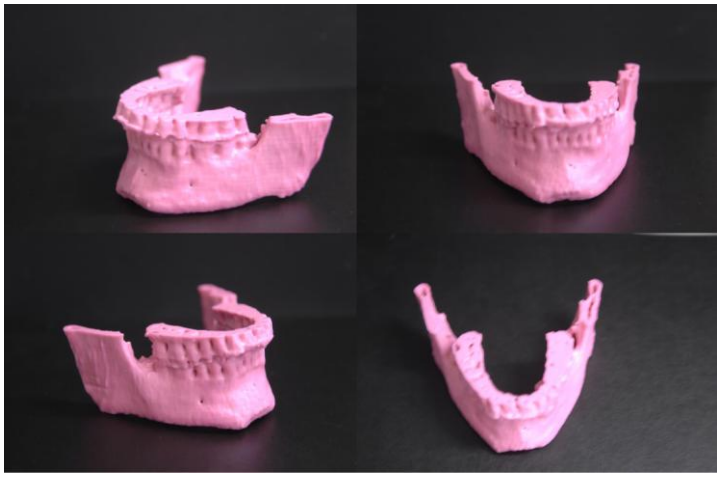


*Figure 161: Images of the finished anatomical model of the mandible from adult volunteer "Black Bone" dataset.*

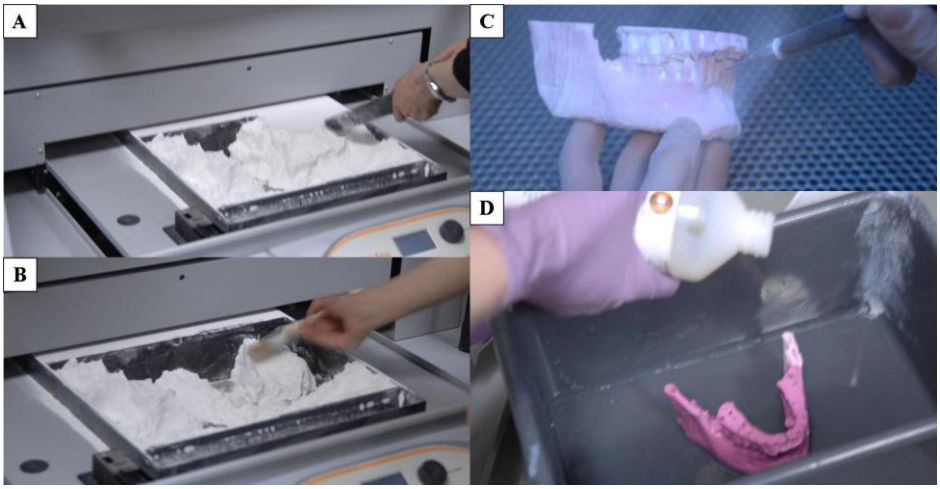



*Figure 162: Processes involved in finishing the model: (A) Removal of excess powder using vacuum; (B) removal of excess powder with brush; (C) removal of residual powder with air gun; (D) application of cyanoacrylate.*

The production of the first anatomical model from "Black Bone" data demonstrated the considerable potential of this imaging technique. This was considered to be the first ever anatomical model produced from MRI data of the craniofacial skeleton.

### 7.5.3 Accuracy of the Model Process with "Black Bone"

Having demonstrated the feasibility of utilising "Black Bone" datasets to create anatomical models, the next stage was to confirm that the resultant models were of comparable accuracy to those created from CT datasets. "Black Bone" datasets of the phantom cube were acquired with both 1.5T and 3.0T magnet. Comparable CT datasets of the cube phantom were obtained. Images were rendered using Osirix and Mimics to permit comparison between the two software's. To standardise the results, a smooth factor of 30 was used in Osirix for all of the datasets. The resultant STL files were printed with the z-printer, and after finishing, measurements were obtained of the models on ten occasions with vernier callipers. Measurements were obtained on the phantom on two occasions, with the addition of three further measurements thus resulting in 11 individual distances *(Figure 163)*. Comparisons were made between models produced with "Black Bone" and CT data, and between the models and the phantom. This was completed with independent samples t-test, and by calculating the discrepancy between the two measurement sets.

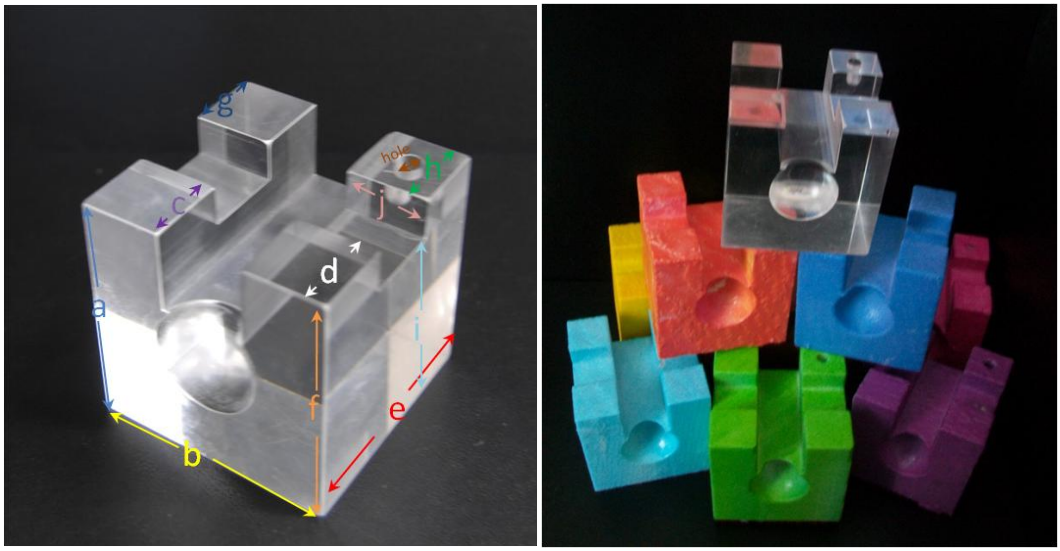



*Figure 163: The eleven measurements completed directly on phantom cube and models (left); the resultant models obtained from CT and "Black Bone."*

#### 7.5.3.1 Between Phantom and Model

The measurements obtained directly from the phantom cube are shown in *Table 70*. The measurements obtained from the resultant models for both CT and "Black Bone" datasets are included in *Appendix I.*

| | a | b | c | d | e | f | g | h | i | j | hole |
|---|---|---|---|---|---|---|---|---|---|---|---|
| **1** | 60.11 | 60.07 | 20.10 | 20.05 | 60.07 | 60.09 | 19.9 | 19.94 | 49.96 | 19.97 | 5.82 |
| **2** | 60.16 | 60.08 | 20.00 | 20.03 | 60.14 | 60.09 | 19.84 | 19.94 | 49.89 | 19.98 | 5.84 |
| **3** | 60.09 | 60.06 | 20.08 | 20.07 | 60.12 | 60.11 | 19.87 | 19.97 | 49.87 | 19.97 | 5.81 |
| **4** | 60.13 | 60.12 | 20.09 | 20.07 | 60.11 | 60.12 | 19.88 | 19.87 | 49.89 | 20.01 | 5.85 |
| **5** | 60.17 | 60.09 | 20.04 | 20.15 | 60.16 | 60.09 | 19.87 | 19.89 | 49.87 | 20.01 | 5.85 |
| **6** | 60.10 | 60.07 | 20.07 | 20.09 | 60.09 | 60.08 | 19.89 | 19.90 | 49.88 | 19.99 | 5.87 |
| **7** | 60.11 | 60.10 | 20.07 | 20.12 | 60.12 | 60.10 | 19.93 | 19.89 | 49.86 | 19.98 | 5.86 |
| **8** | 60.09 | 60.08 | 20.06 | 20.06 | 60.08 | 60.08 | 19.87 | 19.9 | 49.92 | 19.98 | 5.87 |
| **9** | 60.10 | 60.09 | 20.07 | 20.09 | 60.08 | 60.12 | 19.92 | 19.91 | 49.85 | 20.00 | 5.73 |
| **10** | 60.11 | 60.10 | 20.09 | 20.07 | 60.09 | 60.11 | 19.87 | 19.91 | 49.91 | 20.00 | 5.87 |

*Table 70: Direct measurements of phantom cube.*

##### CT

Independent samples t-test identified a significant difference between the phantom and the model produced with the CT dataset on Mimics for all distances, and for all but two distances for the Osirix produced model. The mean±SD difference between measurements on the phantom and resultant model with both Osirix and Mimics for each distance are shown in *Table 71*. Overall, the mean discrepancy between CT and the model produced using Osirix was 0.36±0.32mm, and for Mimics 0.86±0.19mm.

##### "Black Bone"

Independent samples t-test identified a significant difference between the phantom and the model produced with the 1.5T dataset on Mimics for all distances; all but 3 distances with the 1.5T dataset with Osirix; all distances with the 3T dataset with Mimics; and all but 3 distances with the 3T dataset with Osirix. The mean and SD discrepancies for each distance between model and phantom are shown in *Table 71*. Overall, the mean discrepancy between phantom and model was 0.32±0.19mm for the 1.5T dataset on Mimics, 0.17±0.11mm for the 1.5T dataset on Osirix, 0.49±0.30mm for the 3T dataset on Mimics, and 0.33±0.24mm for the 3T dataset on Osirix.

| | CT Mimics | CT Osirix | BB 1.5T Mimics | BB 1.5T Osirix | BB 3T Mimics | BB 3T Osirix |
|---|---|---|---|---|---|---|
| **a** | 0.96±0.08 | 0.85±0.04 | 0.07±0.03 | 0.10±0.05 | 0.82±0.12 | 0.30±0.09 |
| **b** | 0.73±0.07 | 0.47±0.15 | 0.13±0.07 | 0.26±0.07 | 0.14±0.02 | 0.08±0.06 |
| **c** | 0.82±0.05 | 0.17±0.08 | 0.34±0.05 | 0.24±0.15 | 0.42±0.07 | 0.41±0.04 |
| **d** | 0.76±0.04 | 0.07±0.07 | 0.24±0.08 | 0.26±0.07 | 0.59±0.05 | 0.31±0.04 |
| **e** | 0.86±0.04 | 0.03±0.02 | 0.66±0.06 | 0.17±0.07 | 0.14±0.05 | 0.73±0.15 |
| **f** | 0.94±0.09 | 0.69±0.04 | 0.07±0.05 | 0.04±0.05 | 0.89±0.10 | 0.27±0.08 |
| **g** | 0.73±0.03 | 0.13±0.08 | 0.42±0.08 | 0.11±0.11 | 0.30±0.04 | 0.55±0.04 |
| **h** | 0.71±0.03 | 0.17±0.05 | 0.30±0.07 | 0.18±0.09 | 0.34±0.08 | 0.68±0.05 |
| **i** | 1.18±0.18 | 0.91±0.15 | 0.29±0.13 | 0.1±0.07 | 0.70±0.04 | 0.11±0.08 |
| **j** | 0.65±0.03 | 0.13±0.02 | 0.46±0.02 | 0.26±0.02 | 0.16±0.03 | 0.02±0.03 |
| **hole** | 1.16±0.16 | 0.29±0.21 | 0.50±0.13 | 0.15±0.08 | 0.92±0.07 | 0.20±0.12 |

*Table 71: Mean±SD difference between Phantom and model using CT and "Black Bone" datasets on Mimics and Osirix.*

Overall, the discrepancy between the phantom and model produced both with CT and "Black Bone" datasets were within an acceptable level of accuracy (<1mm discrepancy). The models produced using the "Black Bone" datasets were more accurate than the model produced with CT data using Mimics.

#### *7.5.3.2 Between Model from CT and Model from "Black Bone"*

To compare the models created from CT and "Black Bone" datasets, the mean difference in the distances were calculated in a similar manner to those exploring the phantom and model discrepancies. The mean results are shown in *Table 72*. Overall, the mean discrepancy between Osirix rendered models using CT and the 1.5T "Black Bone" dataset was 0.39±0.34mm, and 0.46±0.24mm for the CT and 3T "Black Bone" datasets. For the models rendered with Mimics, the overall mean discrepancy was 0.55±0.27mm for the CT and 1.5T "Black Bone" datasets, and 0.38±0.20mm for the CT and 3T "Black Bone" datasets.

| | Osirix | | Mimics | |
|---|---|---|---|---|
| | CT v 1.5T BB | CT v 3T BB | CT v 1.5T BB | CT v 3T BB |
| **A** | 0.90±0.07 | 0.55±0.07 | 0.89±0.07 | 0.16±0.14 |
| **b** | 0.73±0.17 | 0.38±0.15 | 0.60±0.10 | 0.59±0.07 |
| **c** | 0.11±0.10 | 0.24±0.10 | 0.48±0.07 | 0.40±0.05 |
| **d** | 0.30±0.11 | 0.34±0.06 | 0.53±0.09 | 0.17±0.05 |
| **e** | 0.15±0.07 | 0.71±0.14 | 0.20±0.05 | 0.72±0.06 |
| **F** | 0.67±0.08 | 0.43±0.07 | 0.87±0.09 | 0.12±0.10 |
| **G** | 0.11±0.05 | 0.42±0.10 | 0.31±0.09 | 0.43±0.04 |
| **h** | 0.08±0.04 | 0.50±0.04 | 0.42±0.10 | 0.37±0.07 |
| **I** | 0.86±0.21 | 0.94±0.18 | 0.89±0.15 | 0.48±0.18 |
| **j** | 0.12±0.03 | 0.14±0.05 | 0.19±0.02 | 0.49±0.03 |
| ***hole*** | *0.25±0.23* | *0.38±0.27* | *0.65±0.27* | *0.24±0.14* |

***Table 72: Mean±SD discrepancy between models created with CT and "Black Bone" datasets using Osirix and Mimics.***

Models produced with CT data are currently the "gold standard" in terms of anatomical modelling. The models produced with "Black Bone" datasets demonstrate a comparable level of accuracy to those from CT datasets, with overall discrepancy of less than 1mm.

### 7.5.4 Application of Techniques to Children with Craniosynostosis

The final stage in this Section of the thesis, was to apply the techniques to produce an anatomical model of the craniofacial skeleton in a child with craniosynostosis. The 3D rendered dataset of a child with unicoronal synostosis produced using Mimics was utilised for this purpose. The resultant anatomical model is shown in *Figure 164*. This model had some technical difficulties in the production stage in view of the particularly thin bone of the facial skeleton.

As a result of the manufacturing process there was problems with the thin structure of the skull base. Since the model was printed on its side, there was a large amount of residual powder left inside of the structure. When lifted out of the build chamber, this excess weight resulted in breakage of the skull base region. It was therefore noted that the skull should be printed upright to permit this excess to fall naturally through the foramen magnum.



*Figure 164: Frontal and superior views of anatomical model from "Black Bone" dataset of infant with unicoronal synostosis.*

### 7.5.5 Discussion

The main limitation in creating models from "Black Bone" datasets was obtaining STL files of the 3D rendered images. This was possible with both Mimics and Osirix, but as previously discussed these software packages are reliant upon thresholding for segmentation, resulting in a time consuming process. This resulted in difficulties in model production particularly where the bone was thin, as seen with the craniofacial skeleton in the infant with craniosynostosis. However, it has been demonstrated that "Black Bone" datasets can be utilised successfully to produce anatomical models. These have comparable accuracy to models created with CT datasets, and therefore "Black Bone" demonstrates considerable promise as a non-ionising alternative in craniofacial surgical planning.

## 7.6 Future Applications

Having demonstrated the potential of "Black Bone" in 3D reconstruction of the craniofacial skeleton, the final section of this chapter explores the potential of 3D rendering of other aspects of the bony skeleton. This provides an insight into the potential benefits of the sequence in reducing ionising radiation exposure to patients in whom CT would ordinarily be the imaging modality of choice.

### 7.6.1 Cervical Fractures

The "Black Bone" sequence was obtained in two patients with suspected fractures of the cervical spine.

#### *Patient 1*

A 9 year old female presented with cervical spine pain and bony tenderness after a friend fell onto her neck. Plain radiography demonstrated a lucent line projected through the body of the peg, with associated pre-vertebral soft tissue swelling. In addition the distance between the anterior aspect of the peg and posterior aspect of the anterior arch of C1 was mildly increased (6mm). These appearances were suspicious of a transverse fracture through the mid-portion of the odontoid peg (type II), and MRI was obtained. MRI including "Black Bone" was normal, with no evidence of bony or soft tissue injury *(Figure 165).*

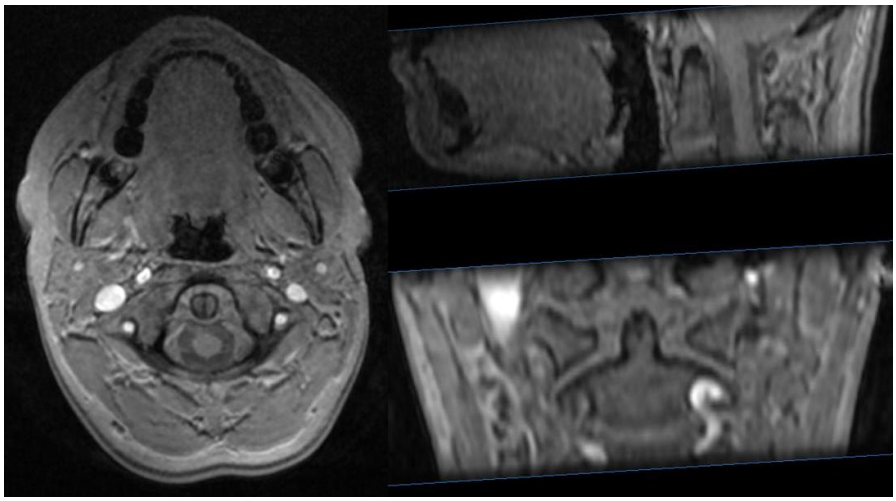


***Figure 165: Axial "Black Bone" MRI with orthogonal reconstructions of Patient 1 demonstrating normal odontoid peg.***

### *Patient 2*

A 44 year old female was transferred to OUH after being hit on the head by a horse. Initial plain radiography at the referring unit demonstrated a possible fracture at C1, and she underwent MRI on arrival. MRI including "Black Bone" demonstrated a fracture of the right anterior arch of C1 with lateral displacement *(Figure 166).* In addition, there was tearing of the right transverse ligament with a small bone fragment seen lateral to the odontoid peg on the right side. Normal alignment was maintained, with no spinal cord compression.

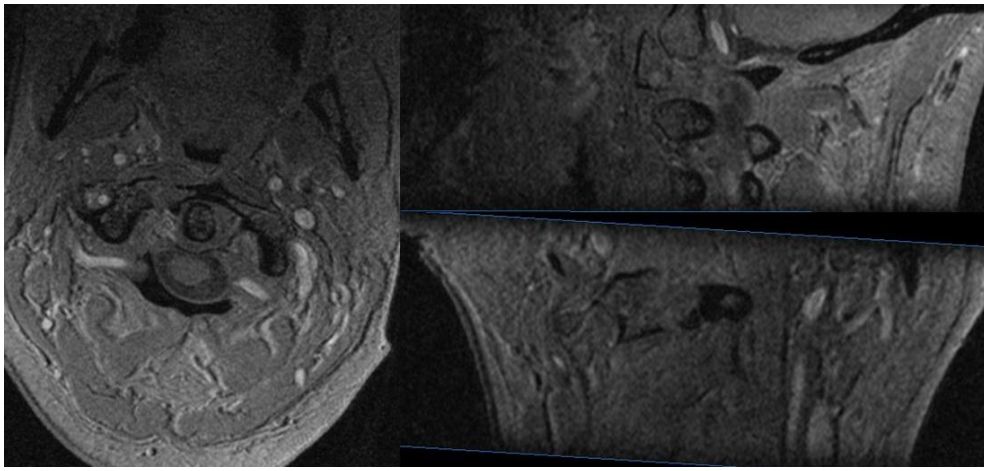


***Figure 166: Axial "Black Bone" MRI with orthogonal reconstructions of Patient 2 demonstrating fracture of the right anterior arch of C1 with lateral displacement.***

### *3D Rendering*

The datasets for both patients were imported into Fovia to obtain the 3D rendered images in *Figure 167*. Difficulties arose in creating these 3D datasets in view of the small field of view - which resulted in the inevitable poor SNR areas at the extremes of the image stack encroaching into the area of interest. The images from Patient 1 were particularly problematic, most likely a result of the decreased cortical bone density due to the young age of the patient. In both cases the cervical bones can be visualised and in Patient 2 the fracture can be seen on the final image.

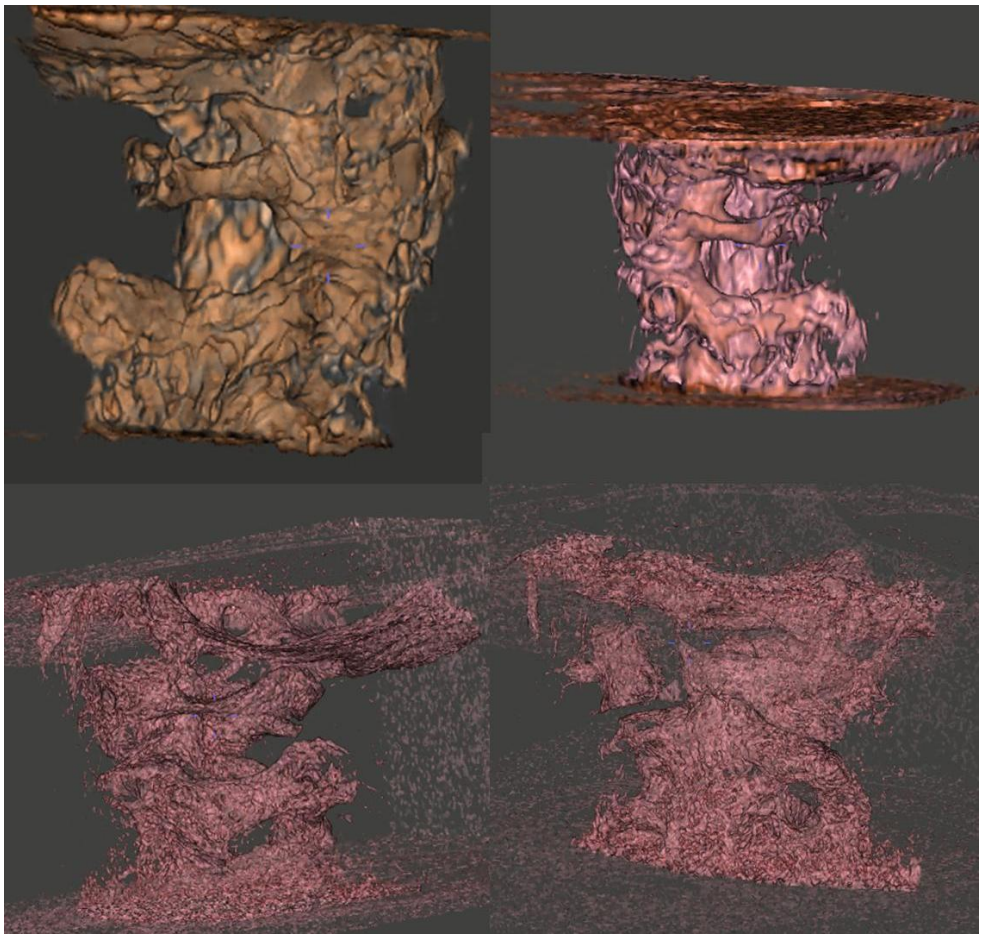


*Figure 167: 3D rendered cervical spine images of Patient 1 (top) and patient 2 (bottom). Note the fracture seen in Patient 2 on the final image.*

### 7.6.2 Imaging of the Hip

Imaging is frequently required of the hip in young patients. In view of the proximity to the reproductive organs, the hip and pelvis are regions of concern in terms of radiation protection. To explore the potential of "Black Bone" in this region, the sequence was obtained of the hip and pelvis in an adult volunteer. This was completed on a 3T magnet at the JR acquired in the coronal plane for the pelvis, and the axial plane for the hip in isolation *(Figure 168 & 169).*



*Figure 168: Axial "Black Bone" imaging of the pelvis at the level of the femoral heads.*

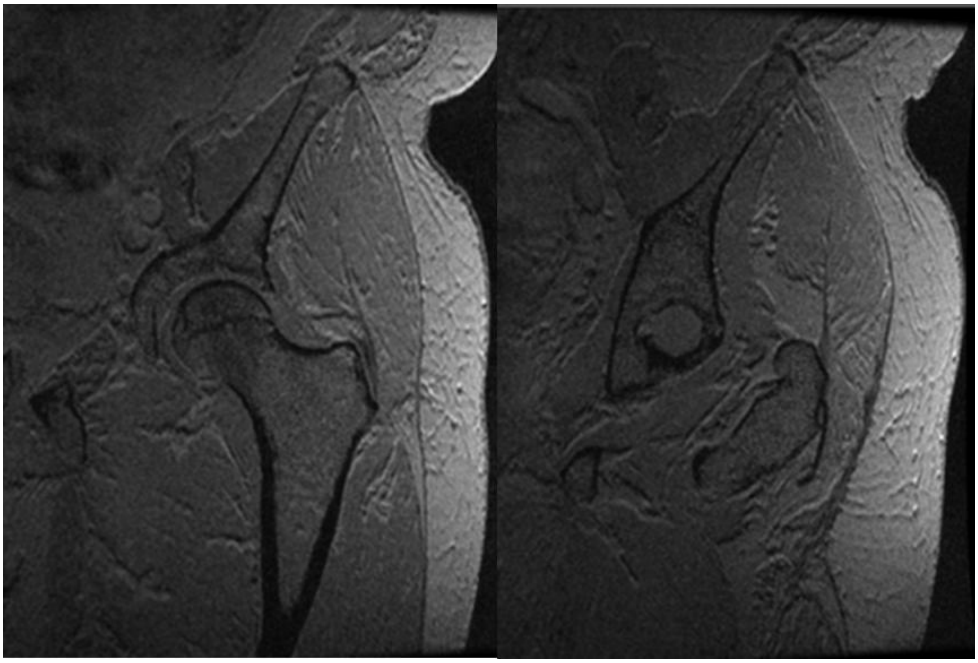


*Figure 169: Coronal "Black Bone" MRI of hip joint demonstrating the femoral head within the acetabulum.*

### 3D Rendering

The "Black Bone" datasets were imported into Fovia and Mimics to obtain the images in *Figure 170*. There was some difficulty around the greater trochanter, which resulted in the 3D reconstruction appearing "moth eaten" in this region. Further cleaning of the images would be required in clinical practice, and this would be achievable with both of the imaging software used.

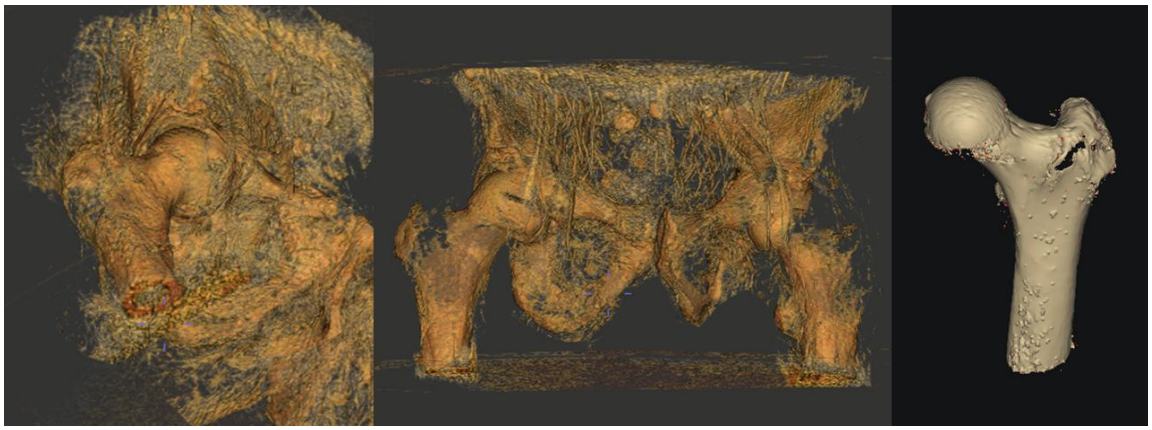


*Figure 170: 3D rendered images from axial imaging (left), and coronal imaging (centre) using Fovia, and from axial imaging using Mimics (right).*

### 7.6.3 Imaging of the Tibia & Fibula

Whilst less of a region of concern in terms of radiation protection, investigation moved to the tibia and fibula. Imaging was obtained on an adult volunteer (KE) on a 1.5T magnet in OMRI. In an attempt to improve the image resolution by maintaining a small slice thickness, imaging was completed of the proximal and distal half of the long bones separately *(Figure 171).*



*Figure 171: Axial imaging of the tibia and fibula with orthogonal reconstructions. Note the decreased SNR occurring at the distal aspect, making the talus and calcaneus more difficult to clearly visualise.*

### *3D Reconstruction*

The datasets were imported into Fovia and Mimics. Segmentation of the bones was a straight forward process in view of their uniform paths. Again there was some loss of image quality at the proximal and distal extremes. Visualisation of the cortex distinct from the medullary bone can be clearly seen on the Mimics rendered image, which has also been smoothed *(Figure 172).*

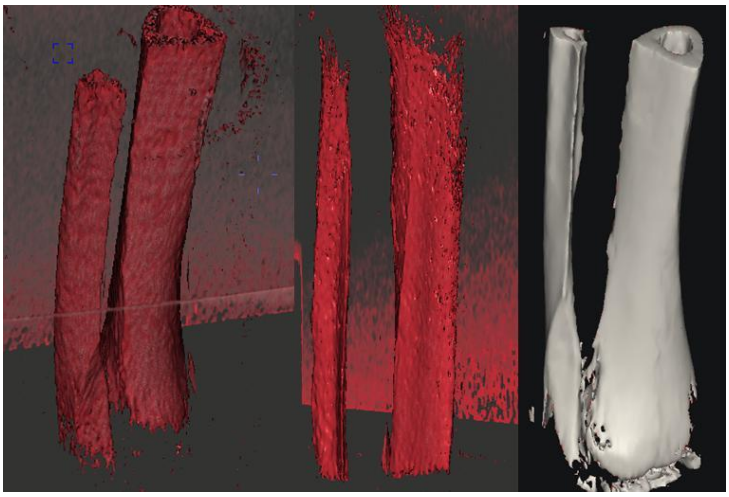


***Figure 172: 3D rendered images of tibia and fibula using Fovia (left & centre) and Mimics (right).***

## 7.6.4 Imaging of the Hand and Wrist

Imaging of the wrist is most frequently obtained in cases of suspected scaphoid fracture. MRI of this region is usually acquired with the patient lying prone in the scanner with their hand outstretched. Most patients can only tolerate this position for one or two sequences. As we have seen with the "Black Bone" sequence it offers the benefit of visualisation in any plane (albeit with a small amount of image quality loss) since it is acquired as a 3D volume. This could be of particular value when imaging this anatomical region. "Black Bone" imaging of the hand was obtained on an adult volunteer (KE) on a 1.5T magnet at OMRI *(Figure 173).*

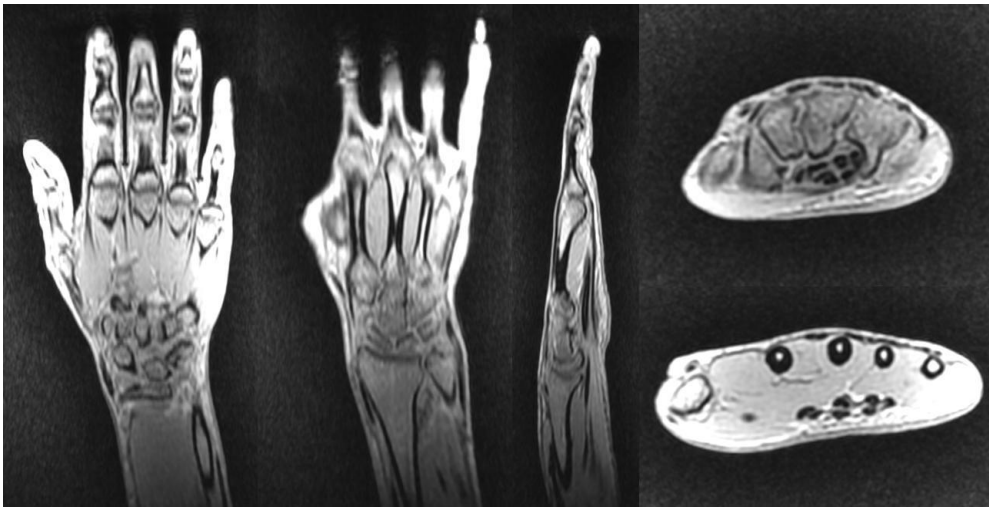


*Figure 173: Axial "Black Bone" MRI of the hand with orthogonal reconstructions. Note how the tendons are also clearly seen.*

### 3D Reconstruction

The dataset was imported into Fovia, to obtain the rendered images in *Figure 174*. With the soft tissues intact the deeper structures could be visualised. This was further enhanced with removal of the soft tissues, where the path of the flexor and extensor tendons could be seen inserting into the phalanges. There was some signal loss in the wrist region.



*Figure 174: 3D rendered images of the hand. Note how the tendon paths can be clearly seen.*

### 7.6.5 Discussion

The “Black Bone” sequence offers potential in a range of imaging applications. It has been shown to be of benefit in the visualisation of fractures, both in the orbit and cervical spine. When combined with routine MRI sequences in the cervical spine region this provides the opportunity to acquire all of the clinical information in one examination, negating the requirement for CT. Clear imaging of the bony structures in both the upper and lower limbs was obtained with “Black Bone” and in all cases 3D visualisation could be completed. In the hand, the path of the flexor and extensor tendons could be followed to their insertion in the phalanges in 3D which provides a further application of the technique, in addition to providing an opportunity for anatomical teaching. Further refinement in the 3D rendering techniques would enhance the resultant images and decrease the time necessary to produce them. When setting the FOV at the time of image acquisition, recognition that there is inevitable image degradation at both extremes, would ensure that this is centred over the area of interest with sufficient clearance.

## Chapter Conclusion

It has been demonstrated that “Black Bone” datasets can be utilised to produce 3D reconstructed images of the craniofacial skeleton with comparable accuracy and appearance to those produced with CT datasets. The utilisation of a smoothing function to enhance the resultant images has negligible effect on the accuracy and can therefore be used without concern with “Black Bone” datasets which greatly benefit from this additional function. The ability to subsequently utilise the 3D reconstructed “Black Bone” datasets for the production of anatomical models makes “Black Bone” a viable alternative to CT for the craniofacial skeleton. In addition, the exploration of 3D rendering of various aspects of bony anatomy has demonstrated that the “Black Bone” sequence offers a wide variety of potential applications outside of the craniofacial skeleton.

# 8. General Discussion & Conclusion

## 8.1 Discussion

The starting point for this research was concern related to the ionising radiation exposure in three patient groups, from infancy to advanced age, with a range of benign and malignant pathologies affecting the craniofacial skeleton. Whilst MRI offered a non-ionising method of imaging, it was not routinely used for bony imaging in this anatomical region.

The potential of routinely available MRI sequences have been explored in the three patient groups. These were of limited value in delineating the cranial sutures in infants making them unreliable in the diagnosis of craniosynostosis. Inaccuracies were also seen in cephalometric analyses in adolescents with facial disproportion on T1 and T2 weighted images. Routinely used MRI sequences were, however, of more value in the adult patient group, permitting tumour volume measurements providing an improved method of predicting outcome in patients with maxillary complex and mandibular SCC.

The "Black Bone" MRI sequence was optimised to minimise the soft tissue contrast, thus improving the boundary between the bone and soft tissues. It was not possible to confirm the optimal appearance mathematically using mean and standard deviation in terms of pixel values of the bone and soft tissues, respectively. These results suggested that a lower flip angle provided the most optimal results, yet visually there was apparent degradation of image quality when the flip angle was reduced below 5°. The main limitation of this work was the inability to calibrate the measurements between datasets.

"Black Bone" was demonstrated to be biometrically accurate, with an overall mean discrepancy between measurements on CT and "Black Bone" of 0.38mm. Comparable differences between imaging with CT and "Black Bone" and direct anatomical measurements on a phantom were found, with a mean error of 0.75%. This was consistent with the error associated with CT analysis, and demonstrated the potential of "Black Bone" as a viable alternative to CT. [106,110,185] The full potential of the sequence has been explored in the three patient groups, demonstrating considerable promise as a diagnostic and planning tool. "Black Bone" was accurate in the

diagnosis of craniosynostosis, and a range of benign and malignant pathologies affecting the head and neck.

The appearance of the cranial sutures was considerably enhanced on "Black Bone" when compared to other more routinely used MRI sequences, appearing as areas of increased signal distinct from the cranial bone and with comparable width measurements to CT.[74] In cases of craniosynostosis, the suture was clearly absent permitting accurate diagnosis. This was confirmed on blinded review, with the correct diagnosis being made in all cases by the neuroradiologist most familiar with craniofacial anomalies.

Difficulties were encountered with both Philips and Siemens MRI scanners since all prior exploration work had been conducted on GE scanners. This highlighted the need for sequence optimisation prior to widespread incorporation into clinical practice. Whilst this was beyond the scope of this work, the likely cause of these discrepancies was the inherent differences between the basic gradient echo sequence to which the "Black Bone" parameters were applied. The consequences of a non-fully optimised sequence were seen in the children with craniosynostosis, where there was some variability in results, and a chemical shift artefact.

The limitation of the "Black Bone" sequence in children with craniosynostosis appeared to be young infants with syndromic synostosis in whom the cranial bone was particularly thin; however, imaging was acquired in only one such infant which was associated with significant movement artefact. Evaluation with a larger patient cohort is required to fully explore if "Black Bone" provides a reliable alternative to CT in all children with craniosynostosis. The addition of a T2 weighted MRI of the brain in these children provided the opportunity to identify evidence of raised intracranial pressure, the findings of which have been shown to be non-specific on CT.[189,203-204]

In adolescents with facial disproportion "Black Bone" provides the potential for 3D cephalometric analysis, having demonstrated improved accuracy in landmark identification when compared to T1 and T2 weighted sequences on which the literature has focused.[164,205] The

main difficulty of establishing a new method of cephalometrics is the need for comparative normative values, which is both a costly process both in terms of time and expense of the required imaging. However, "Black Bone" offers an ethically acceptable method for recruitment since it does not subject healthy volunteers to ionising radiation. Discrepancies between "Black Bone" and lateral cephalogram measurements were in the range of 2-4mm, compounded by the inherent inaccuracies associated with the lateral cephalogram. As demonstrated with the work with the skull phantom exploring the biometric accuracy, "Black Bone" is likely to offer a more reliable method of skeletal measurements than conventional radiography.

Whilst some authors have reported smaller discrepancies between lateral cephalogram and comparator (such as CBCT), it is not clear if directional components between the two groups of measurements were removed, as was the case with this work. Failure to remove these components would inevitably result in an apparent decreased discrepancy due to the addition of negative integers.

The main limitation of "Black Bone" in cephalometric analysis is its restriction to pre-treatment planning as a result of the image degradation when fixed orthodontic appliances are in place.

In the adult patient group, "Black Bone" conferred particular advantage over more routine MRI sequences in the identification of bony erosion and tumour ingress. Even when imaging was reviewed without clinical information a reasonable level of accuracy was obtained by the assessors in terms of the distinction between benign and malignant processes. In view of the minimal soft tissue contrast, "Black Bone" was less valuable in tumour volume assessments in patients with maxillary complex and mandibular SCC, being overshadowed by the enhanced tumour appearance on T2 weighted images. Tumours in these regions were often poorly defined on CT imaging making tumour volume assessments on CT inaccurate, and demonstrating the added advantage of MRI examination. The measurement of tumour volume provided improved correlation with patient outcome in terms of disease free survival when compared to the current

TNM staging system. The main limitation to this work was the small sample size, and the need to group tumours of the hard palate, maxillary sinus and maxilla, despite tumours of the paranasal sinuses and oral cavity being classified separately in the TNM system. However, this has been consistent practice as a result of the infrequency with which tumours at these sites are encountered.[132,144] This was also the case for tumours involving the mandible with the grouping of retromolar, floor of mouth and alveolus subsites. During the 10 year period of the study there were three editions of the AJCC TMN classification ($5^{th}$ – $7^{th}$ Editions) published. For oral cavity tumours the key changes between the $5^{th}$ and $6^{th}$ editions included the subdivision of T4 tumours dependent upon anatomical boundaries, and tumours of the maxillary sinus tumours were similarly subdivided. To avoid potential bias associated with these changes, T4 tumours were analysed as one group for the purposes of this study, which may have resulted in the decreased predictive capabilities seen with the TNM system. The retrospective nature of the study resulted in findings being dependent upon accurate interpretation of the medical records and whilst this was enhanced by clinical experience in the speciality difficulties arose when determining the date of tumour recurrence due to incomplete documentation.

Tumour volume measurements were completed by only one assessor, and whilst consistency was demonstrated with a low coefficient of variation, inevitable discrepancies are likely between assessors as a result of familiarity and subjective interpretation of surrounding oedema. Inter- and intra-observer variability has been assessed in nasopharyngeal tumour volume measurements on CT demonstrating that interobserver variability was the major component of total variability.[206] An automated method of tumour segmentation would therefore provide a method of standardising the tumour volume measurements and enhance incorporation into routine practice.

One of the most useful applications of "Black Bone" for all three patient groups is the ability to create 3D rendered images of the craniofacial skeleton with subsequent creation of anatomical models. The accuracy of these techniques have been demonstrated with results comparable to CT.

Such ability to create 3D rendered images, and the accuracy of the "Black Bone" sequence, permits the opportunity to develop 3D cephalometry techniques, which will permit 3D surgical planning in patients with facial disproportion. Whilst the cephalometric landmarks that would be useful in such work were postulated, the development of these techniques was limited by the inability to complete measurements across multiple imaging slices on the software available. Mimics have recently developed a cephalometric module for their software which may provide methods of completing these measurements. This provides scope for further investigation.

The volume rendering software Fovia was of most benefit in 3D visualisation of the craniofacial skeleton with "Black Bone" datasets, being unhindered by the communication between air within the ear canal and outside of the body. This could be overcome by the use of artificial separators such as cotton wool soaked in olive oil placed in the ear, and demonstrated to be a useful method for boundary identification with 3D-doctor. However, the communication of air at the lips can be more difficult to overcome, particularly in patients with facial disproportion where lip incompetence is frequently encountered.

The need for manual segmentation of the soft tissues with Fovia would restrict its use in the clinical environment to personnel with sufficient experience with the software. The need to ultimately subtract the surrounding air prior to creation of STL files required for anatomical models also adds a layer of associated difficulty. The greatest potential therefore lies in automatic edge detection of bone on "Black Bone" datasets and further collaboration is required to permit "Black Bone" to become a truly viable alternative to CT in 3D visualisation of the craniofacial skeleton.

## 8.2 Scope for Further Work

This thesis has explored the potential of routine MRI sequences and "Black Bone" MRI as an alternative to CT when imaging the craniofacial skeleton. In doing so, a number of potential avenues for further investigation have been identified.

In children with craniosynostosis, a larger scale study is required to fully evaluate the accuracy and limitations of "Black Bone" in this patient group. This would be enhanced by collaboration with a craniofacial centre where MRI examination is routinely performed. A unit where MRI is more frequently obtained than at the OUH has been identified in the literature.[154] Work in this patient group identified the difficulties associated with importing the "Black Bone" parameters into non-GE scanners. Further exploration is warranted to further optimise the sequence, and to eliminate the chemical shift artefact.

In the adolescent group, further "Black Bone" imaging is required on a larger scale to obtain normative data, and to further develop a 3D cephalometric analysis tool. This would be enhanced by a software package capable of measurements across multiple slices and directly on a 3D reconstruction of the craniofacial skeleton. The potential of the cephalometric module in Mimics is currently being evaluated for this task.

In adults with SCC of the mandible and maxillary complex, a multi-centre trial is required to fully explore the correlation of tumour volume with patient outcome. This would provide the opportunity to acquire sufficient numbers of patients to avoid grouping tumours of different oral cavity subsites which invariably have different prognoses. A method of automated tumour segmentation is also required to eliminate inter-observer variability and enable incorporation of tumour volume measurements into widespread clinical practice. The development of a multi-centre study is currently underway to fulfil these aims and to provide sufficient statistical power to incorporate tumour volume into the TNM system.

Further potential applications of "Black Bone" have been considered including evaluation of the bone around the foramen magnum prior to surgery for chiari malformation, and the use of "Black Bone" in Positron Emission Tomography with MRI (PET-MR).

In terms of 3D reconstruction, collaboration continues with the Berlin group, and both Fovia and Mirada software developers in order to develop an automated method of segmentation of the craniofacial skeleton from "Black Bone" datasets, which will permit MRI to become a truly viable alternative to CT in clinical practice.

Outside of the craniofacial skeleton, it has been demonstrated that "Black Bone" offers potential for 3D reconstruction of a range of bony anatomy, and also provides considerable scope for further exploration.

## 8.3 Conclusion

In conclusion, it has been demonstrated that routine and "Black Bone" MRI, offer a reliable alternative to CT when examining the craniofacial skeleton, both in terms of diagnosis, 3D reconstruction and anatomical models. "Black Bone" has widespread application and used in combination with routine MRI sequences yields additional prognostic information that may ultimately eliminate ionising radiation exposure to the craniofacial region in the future.

# References


1. Hounsfield GN. Computerized transverse axial scanning (tomography): Part I. Description of system. Br J Radiol 1973;46:1016-1022.
2. Lewis MA, Edyvean S. Patient dose reduction in CT. Br J Radiol 2005;78:880-883.
3. Eley KA. Magnetic Resonance Imaging as a diagnostic tool in craniosynostosis. Oxford: University of Oxford; 2009. 100 p.
4. Dendy P, Heaton B. Physics for diagnostic radiology: IOP Publishing Ltd; 1999
5. Bushberg JT, Seibert JA, Leidholdt EM, Boone JM. The Essential Physics of Medical Imaging 2nd Edition: Lippincott Williams & Wilkins; 2002
6. Kalender WA. Computed Tomography. Munich: Publicis MCD Verlag; 2000
7. Hsieh. Computed tomography principles, design, artifacts and recent advances. Washington: SPIE; 2009
8. Romans LE. Introduction to computed tomography. PA: Williams & Wilkins; 1995
9. Allisy-Roberts P, Williams J. Farr's Physics for Medical Imaging. Philadelphia: Saunders Elservier; 2008
10. Armstrong P, Wastie ML. A concise textbook of radiology: Arnold; 2001
11. Arai Y, Tammisalo E, Iwai K, Hashimoto K, Shinoda K. Development of a compact computed tomographic apparatus for dental use. Dentomaxillofac Radiol 1999;28:245-248.
12. Mozzo P, Procacci C, Tacconi A, Tinazzi Martini P, ;, Bergamo Andreis IA. A new volumetric CT machine for dental imaging based on the cone-beam technique: preliminary results. Eur Radiol 1998;8:1558-1564.
13. De Vos W, Casselman J, Swennen GRJ. Cone-beam computed tomography (CBCT) imaging of the oral and maxillofacial region: A systematic review of the literature. Int J Oral Maxillofac Surg 2009;38(6):609-625.
14. Kau CH, Abramovitch K, Kamel SG, Bozic M. Cone beam CT of the head and neck. An anatomical atlas: Springer; 2011
15. Scarfe WC, Farman AG. What is cone-beam CT and how does it work? Dent Clin N Am 2008;52:707-730.
16. Pykett IL, Newhouse JH, Buonanno FS, Brady TJ, Goldman MR, Kistler JP, Pohost GM. Principles of Nuclear Magnetic Resonance Imaging. Radiology 1982;143:157-168.
17. Westbrook C. MRI at a glance. Oxford: Blackwell Science Ltd; 2002
18. Weishaupt D, Kochli VD, Marincek B. How does MRI work? Berlin: Springer; 2006
19. Andrews C, Simmons A, Williams S. Magnetic resonance imaging and spectroscopy. Physics Education 2001;31:80-85.
20. Henderson RG. Nuclear Magnetic resonance imaging: a review. J Royal Society Medicine 1983;76:206-212.
21. Phan CM, Matsuura M, Bauer JS, Dunn TC, Newitt D, Lochmueller EM, Eckstein F, Majumdar S, Link TM. Trabecular bone structure of the calcaneous: comparison of MR imaging at 3.0 and 1.5T with micro CT as the standard of reference. Radiology 2006;239(2):488-496.
22. Cotten A, Kermarrex E, Moraux A, Budzik J. New MRI sequences. Joint Bone Spine 2009;76:588-590.
23. Heidemann RM, Ozsarlak O, Parizel PM, Michiels J, Kiefer B, Jellus V, Muller M, Breuer F, Blaimer M, Griswold MA, Jakob PM. A brief review of parallel magnetic resonance imaging. Eur Radiol 2003;13:2323-2337.
24. Nitz WR. Fast and ultrafast non-echo-planar MR imaging techniques. Eur Radiol 2002;12:2866-2882.
25. McCollough CH, Schueler BA. Calculation of effective dose. Med Phys 2000;27(5):828-837.
26. HPA. Guidance on the safe use of dental cone beam CT (Computed Tomography) equipment. Equipment HPAWPoDCBC, editor: Health Protection Agency; 2010
27. Huda W, Vance A. Patient radiation doses from adult and paediatric CT. AJR 2007;188:540-546.
28. Brenner DJ. Effective dose: a flawed concept that could and should be replaced. British J Radiology 2008;81:521-523.
29. FDA NEWS RELEASE: FDA working to prevent radiation overdoses during CT scans. http://www.fda.gov/NewsEvents/Newsroom/PressAnnouncements/ucm233245.htm
30. UNSCEAR. Sources and effects of ionizing radiation. United Nations Scientific Committee on the effects of atomic radiation report to the general assembly United Nations, New York 2000.
31. Meinert R, Kaletsch U, Kaatsch P, Schuz J, Michaelis J. Associations between childhood cancer and ionizing radiation: results of a population-based case-control study in Germany. Cancer Epidemiology, Biomarkers & Prevention 1999;8:793-799.
32. Polhemus DW, Koch R. Leukemia and medical radiation. Pediatrics 1959;23:453-461.
33. Brenner DJ, Doll R, Goodhead DT, Hall EJ, Land CE, Little JB, Lubin JH, Preston DL, Preston RJ, Puskin JS, Ron E, Sachs RK, Samet JM, Setlow RB, Zaider M. Cancer risks attributable to low doses of ionizing radiation: Assessing what we really know. Proceedings National Academy of Sciences USA 2003;100(24):13761-13766.
34. Brenner DJ, Hall EJ. Computed Tomography - An increasing source of radiation exposure. N Engl J Med 2007;357:2277-2284.
35. Doody MM, Lonstein JE, Stovall M, Hacker DG, Luckyanov N, Land CE. Breast cancer mortality after diagnostic radiography. Spine 2000;25(16):2052-2063.

36. Feng ST, Law MWM, Huang B, Ng S, Li Z, Meng QF, Khong PL. Radiation dose and cancer risk from pediatric CT examinations on 64-slice CT: A phantom study. European Journal Radiology 2010;76:e19-e23.
37. Bartley K, Metayer C, Selvin S, Ducore J, Buffler P. Diagnostic x-rays and risk of childhood leukaemia. Int J Epidemiol 2010;October 1:1-10.
38. Hammer GP, Seidenbusch MC, Schneider K, Regulla DF, Zeeb H, Spix C, Blettner M. A cohort study of childhood cancer incidence after postnatal diagnostic x-ray exposure. Radiation Research 2009;171:504-512.
39. Mole RH. Childhood cancer after prenatal exposure to diagnostic x-ray examinations in Britain. Br J Cancer 1990;62:152-168.
40. Doll R, Wakeford R. Risk of childhood cancer from fetal irradiation. Br J Radiol 1997;70:130-139.
41. Court-Brown CM, Doll R, Bradford-Hill A. Incidence of leukaemia after exposure to diagnostic radiation in utero. BMJ 1960;Nov 26:1539-1545.
42. Mole RH. Childhood cancer after prenatal exposure to diagnostic X-ray examinations in Britain. Br J Cancer 1990;62(1):152-168.
43. Domeshek LF, Mukundan S, Yoshizumi T, Marcus JR. Increasing concern regarding Computed Tomography irradiation in craniofacial surgery. Plast Reconstr Surg 2009;123:1313-1320.
44. Hall EJ. CT scanning: risk versus benefit. J Radiological Protection 2000;20(4):347.
45. Hospital activity statistics - Imaging and Radiodiagnostics. 2010 http://www.dh.gov.uk/en/Publicationsandstatistics/Statistics/Performancedataandstatistics/HospitalActivityStatistics/DH_077487
46. Tack D, Gevenois PA. Radiation dose from adult and paediatric multidetector computed tomography: Springer; 2007
47. Shrimpton PC, Hillier MC, Lewis MA, Dunn M. Doses from Computed Tomography (CT) examinations in the UK - 2003 review. NRPB W67 National Radiological Protection Board, Chilton 2003.
48. Hall EJ, Brenner DJ. Cancer risks from diagnostic radiology. Br J Radiol 2008;81(965):362-378.
49. Chan CY, Wong YC, Chau LF, Yu SK, Lau PC. Radiation dose reduction in paediatric cranial T. Pediatr Radiol 1999;29:770-775.
50. Herzog P, Rieger CT. Risk of cancer from diagnostic x-rays. Lancet 2004;363:340-341.
51. The American Association of Physicists in Medicine. http://www.aapm.org/pubs/CTProtocols/
52. Yates SJ, Pike LC, Goldstone KE. Effect of multislice scanners on patient dose from routine CT examinations in East Anglia. Br J Radiol 2004;77:472-478.
53. Nishizawa K, Mori SI, Ohno M, Yanagawa N, Yoshida T, Akahane K, Iwai K, Wada SI. Patient dose estimation for multi-detector-row CT examinations. Radiation Protection dosimetry 2007;128(1):98-105.
54. Mettler FA, Wiest PW, Locken JA, Kelsey CA. CT scanning: patterns of use and dose. J Radiological Protection 2000;20:353-359.
55. Brenner DJ. Estimating cancer risks from pediatric CT: going from the qualitative to the quantitative. Pediatr Radiol 2002;32:228-231.
56. Huda W, Chamberlain CC, Rosenbaum AE, Garrisi W. Radiation doses to infants and adults undergoing head CT examinations. Med Phys 2001;28(3):393-399.
57. Smith A, Shah GA, Kron T. Variation of patient dose in head CT. Br J Radiol 1998;71:1296-1301.
58. Smyth MD, Narayan P, Tubbs RS, Leonard JR, Park TS, Loukas M, Grabb PA. Cumulative diagnostic radiation exposure in children with ventriculoperitoneal shunts: a review. Child's Nerv Syst 2008;24:493-497.
59. Stein SC, Hurst RW, Sonnad SS. Meta-analysis of cranial CT scans in children. Pediatr Neurosurg 2008;44:448-457.
60. Rice DP. Developmental anatomy of craniofacial sutures. In: Rice DP, editor. Craniofacial Sutures, Development, Disease and Treatment. 1st ed. Switzerland: Karger; 2008.
61. Martinez-Lage JF, Alamo L, Poza M. Raised intracranial pressure in minimal forms of craniosynostosis. Childs Nervous System 1999;15:11-16.
62. Craniosynostosis. Cincinnati Childrens Hospital.http://www.cincinnatichildrens.org/health/c/craniosynostosis/
63. Thomas GPL, Wilkie AOM, Richards PG, Wall SA. FGFR3 P250R Mutation Increases the Risk of Reoperation in Apparent 'Nonsyndromic' Coronal Craniosynostosis. J Craniofac Surg 2005;16(3):347-352.
64. Rice DP. Craniofacial Sutures Development, Disease and Treatment. Sharpe P, editor. Basel: Karger; 2008
65. Hukki J, Saarinen P, Kangasniemi M. Single suture craniosynostosis: Diagnosis and imaging. In: Rice DP, editor. Craniofacial Sutures, Development, Disease and Treatment. Volume 12: Karger; 2008.
66. Passos-Bueno MR, Sertie AL, Jehee FS, Fanganiello R, Yeh E. Genetics of craniosynostosis: Genes, syndromes, mutations and genotype-phenotype correlations. In: Rice DP, editor. Craniofacial Sutures, Development, Disease and Treatment. Volume 12. Switzerland: Karger; 2008.
67. Inagaki T, Kyutoku S, Seno T, Kawaguchi T, Yamahara T, Oshige H, Yamanouchi Y, Kawamoto K. The intracranial pressure of the patients with mild form of craniosynostosis. Childs Nervous System 2007;23(12):1455-1459.

68. Tamburrini G, Caldarelli M, Santini P, Di Rocco C. Intracranial pressure monitoring in children with single suture and complex craniosynostosis: a review. Childs Nervous System 2005;21:913-921.
69. Kotrikova B, Krempien R, Freier K, Muhling J. Diagnostic imaging in the management of craniosynostosis. Eur Radiol 2007;17:1968-1978.
70. Chatterjee JS, Mahmoud M, Karthikeyan S, Duncan C, Dover MS, Nishikawa H. Referral pattern and surgical outcome of sagittal synostosis. J Plast Reconstr Aesthet Surg 2009;62(2):211-215.
71. Esparza J, Hinojosa J, Garcia-Recuero I, Romance A, Pascual B, Martinez de Aragon A. Surgical treatment of isolated and syndromic craniosynostosis. Results and complications in 283 consecutive cases. Neurocirugia (Astur) 2008;19(6):509-529.
72. Craniosynostosis. Doernbecher Children's Hospital, Oregon Health & Science University.http://www.ohsu.edu/xd/health/services/doernbecher/programs-services/craniosynostosis.cfm
73. Tartaro A, Larici AR, Antonucci D, Merlino B, Colosimo C, Bonomo L. Optimization and diagnostic accuracy of computerized tomography with tridimensional spiral technique in the study of craniosynostosis. Radiol Med 1998;96:10-17.
74. Mitchell LA, Kitley CA, Armitage TL, Krasnokutsky MV, Rooks VJ. Normal Sagittal and Coronal Suture Widths by Using CT Imaging. AJNR American journal of neuroradiology 2011;32(10):1801-1805.
75. Soboleski D, McCloskey D, Mussari B, Sauerbrei E, Clarke M, Fletcher A. Sonography of normal cranial sutures. AJR Am J Roentgenol 1997;168(3):819-821.
76. Jeffurs D, Denny A. Diagnostic pediatric Computed Tomographic scans of the head: actual dosage versus estimated risk. Plast Reconstr Surg 2009;124:1254-1260.
77. Fearon JA, Singh DJ, Beals SP, Yu JC. The diagnosis and treatment of single-sutural synostoses: Are computed tomographic scans necessary? Plastic and Reconstructive Surgery 2007;120:1327-1331.
78. Binning M, Ragel B, Brockmeyer DL, Walker ML, Kestle JRW. Evaluation of the necessity of postoperative imaging after craniofacial surgery. J Neurosurg 2007;107:43-45.
79. Harshbarger R, Kelley P, Leake D, George T. Low dose craniofacial CT/Rapid access MRI protocol in craniosynostosis patients: decreased radiation exposure and cost savings. Plast Reconstr Surg 2010 126(4):4-5.
80. Ochoa BK, Nanda RS. Comparison of maxillary and mandibular growth. Am J Orthod Dentofacial Orthop 2004;125(2):148-159.
81. Proffit WR, White RP. Surgical orthodontic treatment. St Louis: Mosby; 1991
82. Plooij JM, Maal TJJ, Haers P, Borstlap WA, Kuijpers-Jagtman AM, Berge SJ. Digital three-dimensional image fusion processes for planning and evaluating orthodontics and orthognathic surgery. A systematic review. Int J Oral Maxillofac Surg 2010;Epub.
83. Jaw Deformities Center. Division of Plastic and Maxillofacial Surgery, Childrens Hospital, Los Angeles.http://www.hopeforkids.com/site/c.lpISKYOvFkG/b.4204965/k.6500/Jaw_Deformities_Center.htm
84. Tsang KHS, Cooke MS. Comparison of cephalometric analysis using a non-radiographic sonic digitizer (DigiGraph Workstation) with conventional radiography. Eur J Orthodont 1999;21:1-13.
85. Kumar V, Ludlow J, Cevidanes LHS, Mol A. In Vivo comparison of conventional and Cone Beam CT synthesized cephalograms. Angle Orthodontist 2008;78(5):873-879.
86. Broadbent BH. A new x-ray technique and its application to orthodontia. Angle Orthodontist 1931;1(2):45-66.
87. Waitzman AA, Posnick JC, Armstrong DC, Pron GE. Craniofacial skeletal measurements based on computed tomography: Part II. Normal values and growth trends. Cleft Palate-Craniofacial Journal 1992;29(2):118-128.
88. Gray J. Cephalometric instruments and cephalograms. Journal of the Anthropological Institute Great Britain and Ireland 1901;31:111-115.
89. Gladstone RJ. Preliminary commuication on some cephalometric data bearing upon the relation of the size and shape of the head to mental ability. J Anat Physiol 1903;37(4):333-346.
90. Schwarz R. New cephalometric method and apparatus and its application to orthodontia. Int J Orthodontia Oral Surg Rad 1925;11(11):989-1017.
91. Grybauskas S, Balciuniene I, Vetra J. Validity and reproducibility of cephalometric measurements obtained from digital photographs of analogue headfilms. Stomatologija Baltic Dental Maxillofac J 2007;9(4):114-120.
92. Geelen W, Wenzel A, Gotfredsen E, Kruger M, Hansson LG. Reproducibility of cephalometric landmarks on conventional film, hardcopy, and monitor-displayed images obtained by the storage phosphor tecnhique. European J Orthodontics 1998;20:331-340.
93. Uysal T, Baysal A, Yagci A. Evaluation of speed, repeatability, and reproducibility of digital radiography with manual versus computer-assited cephalometric analyses. European J Orthodontics 2009;31:523-528.
94. Leonardi R, Giordano D, Maiorana F, Spampinato C. Automatic cephalometric analysis. Angle Orthodontist 2008;78(1):145-151.

95. Baumrind S, Frantz RC. The reliability of head film measurements. American J Orthodontics 1971;60(2):111-127.
96. Baumrind S, Frantz RC. The reliability of head film measurements. Conventional angular and linear measures. Am J Orthodontics 1971;60(5):505-517.
97. Moyers RE, Bookstein FL. The inappropriateness of conventional cephalometrics. Am J Orthodontics 1979;75(6):599-617.
98. Palomo JM, Yang C-Y, Hans MG. Clinical application of three-dimensional craniofacial imaging in orthodontics. J Med Sci 2005;25(6):269-278.
99. Papadopoulos MA, Jannowitz C, Boettcher P, Henke J, Stolla R, Zeilhofer H, Kovacs L, Erhardt W, Biemer E, Papadopulos NA. Three-dimensional fetal cephalometry: An evaluation of the reliability of cephalometric measurements based on three-dimensional CT reconstructions and on dry skulls of sheep fetuses. J Cranio-Maxillofac Surg 2005;33:229-237.
100. Kragskov J, Bosch C, Gyldensted C, Sindet-Pedersen S. Comparison of the reliability of craniofacial anatomic landmarks based on cephalometric radiographs and three-dimensional CT scans. Cleft Palate-Craniofacial Journal 1997;34(2):111-116.
101. Huja SS, Grubaugh EL, Rummel AM, Fields HW, Beck FM. Comparison of hand-traced and computer-based cephalometric superimpositions. Angle Orthodontist 2009;79(3):428-435.
102. Power G, Breckon J, Sherriff M, McDonald F. Dolphin imaging software: An analysis of the accuracy of cephalometric digitization and orthognathic prediction. Int J Oral Maxillofac Surg 2005;34:619-626.
103. Sayinsu K, Isik F, Trakyali G, Arun T. An evaluation of the errors in cephalometric measurements on scanned cephalometric images and conventional tracings. European J Orthodontics 2007;29:105-108.
104. El H, Palomo JM. Measuring the airway in 3 dimensions: A reliability and accuracy study. Am J Orthod Dentofacial Orthop 2010;137:850-852.
105. Lopes PML, Moreira CR, Perrella A, Antunes JL, Cavalcanti MGP. 3-D volume rendering maxillofacial analysis of angular measurements by multislice CT. Oral Surg Oral Med Oral Path Oral Radiol Endod 2008;105:224-230.
106. Waitzman AA, Posnick JC, Armstrong DC, Pron GE. Craniofacial skeletal measurements based on Computed Tomography: Part I. Accuracy and Reproducibility. Cleft Palate-Craniofacial Journal 1992;29(2):112-117.
107. Cavalcanti MGP, Haller JW, Vannier MW. Three-dimensional computed tomography landmark measurement in craniofacial surgical planning: Experimental validation in vitro. J Oral Maxillofac Surg 1999;57:690-694.
108. Citardi MJ, Herrmann B, Hollenbeak CS, Stack BC, Cooper M, Bucholz RD. Comparison of scientific calipers and computer-enabled CT review for the measurement of skull base and craniomaxillofacial dimensions. Skull Base: An interdisciplinary approach 2001;11(1):5-11.
109. Periago DR, Scarfe WC, Moshiri M, Scheetz JP, Silveira AM, Farman AG. Linear accuracy and reliability of cone beam CT derived 3-dimensional images constructed using an orthodontic volumetric rendering program. Angle Orthodontist 2008;78(3):387-395.
110. Cavalcanti MGP, Rocha SS, Vannier MW. Craniofacial measurements based on 3D -CT volume rendering: implications for clinical applications. Dentomaxillofac Radiol 2004;33:170-176.
111. Kitaura H, Yonetsu K, Kitamori H, Kobayashi K, Natkamura T. Standardization of 3D CT measurements for length and angles by matrix transformation in the 3D coordinate system. Cleft Palate-Craniofacial Journal 2000;37(4):349-356.
112. deOliveira AE, Cevidanes LHS, Phillips C, Motta A, Burke B, Tyndall D. Observer reliability of three-dimensional cephalometric landmark identification on cone-beam computerized tomography. Oral Surg Oral Med Oral Path Oral Radiol Endod 2009;107(2).
113. Prawat JS, Nieberg L, Cisneros GJ, Acs G. A comparison between radiographic and sonically produced cephalometric values. Angle Orthodontist 1995;65:271-276.
114. Oral Cancer Screening. National Cancer Institute.http://www.cancer.gov/cancertopics/pdq/screening/oral/Patient/page2/Print
115. Do L, Syed N, Puthawala A, Azawi S, Williams R, Vora N. Prognostic significance of bone or cartilage invasion of locally advanced head and neck cancers. Am J Clin Oncol 2010;33(6):591-594.
116. Van Cann EM, Rijpkema M, Heerschap A, van der Bilt A, Koole R, Stoelinga PJW. Quantitative dynamic contrast-enhanced MRI for the assessment of mandibular invasion by squamous cell carcinoma. Oral Oncol 2008;44:1147-1154.
117. Chen C, Ashjian P, Disa J, Cordeiro P, Pusic A, Mehrara B. Is the use of intraoperative heparin safe? 2008;121.
118. Joseph AW, D'Souza G. Epidemiology of human papillomavirus-related head and neck cancer. Otolaryngol Clin North Am 2012;45(4):739-764.
119. Lee LA, Huang CG, Liao CT, Lee LY, Hsueh C, Chen TC, Lin CY, Fan KH, Wang HM, Huang SF, Chen IH, Kang CJ, Ng SH, Yang SL, Tsao KC, Chang YL, Yen TC. Human papillomavirus-16 infection in advanced oral cavity cancer patients is related to an increased risk of distant metastases and poor survival. PLoS One 2012;7(7):e40767.

120. Stavrianos S, Camilleri I, McLean N, Piggot T, Kelly C, Soames J. Malignant tumours of the maxillary complex: an 18-year review. British journal of plastic surgery 1998;51(8):584-588.
121. Poeschl PW, Russmueller G, Seemann R, Klug C, Poeschl E, Sulzbacher I, Ewers R. Staging and Grading as Prognostic Factors in Maxillary Squamous Cell Carcinoma. Journal of Oral and Maxillofacial Surgery 2011.
122. Brown JS, Lewis-Jones H. Evidence for imaging the mandible in the management of oral squamous cell carcinoma: a review. Br J Oral & Maxilofac Surg 2001;39:411-418.
123. Rajesh A, Khan A, Kendall C, Hayter J, Cherryman G. Can magnetic resonance imaging replace single photon computed tomography and computed tomography in detecting bony invasion in patients with oral squamous cell carcinoma? British Journal of Oral and Maxillofacial Surgery 2008;46(1):11-14.
124. Ariyoshi Y, Shimahara M. Magnetic resonance imaging of maxillary cancer—possibility of detecting bone destruction. Oral oncology 2000;36(6):499-507.
125. Le QT, Fu KK, Kaplan M, Terris DJ, Fee WE, Goffinet DR. Treatment of maxillary sinus carcinoma. Cancer 1999;86(9):1700-1711.
126. Been MJ, Watkins J, Manz RM, Gentry LR, Leverson GE, Harari PM, Hartig GK. Tumor volume as a prognostic factor in oropharyngeal squamous cell carcinoma treated with primary radiotherapy. Laryngoscope 2008;118(8):1377-1382.
127. Gomez D, Faucher A, Picot V, Siberchicot F, Renaud-Salis JL, Bussières E, Pinsolle J. Outcome of squamous cell carcinoma of the gingiva: a follow-up study of 83 cases. Journal of Cranio-Maxillofacial Surgery 2000;28(6):331-335.
128. Bhattacharyya N. Factors affecting survival in maxillary sinus cancer. Journal of Oral and Maxillofacial Surgery 2003;61(9):1016-1021.
129. Hayashi T, Nonaka S, Bandoh N, Kobayashi Y, Imada M, Harabuchi Y. Treatment outcome of maxillary sinus squamous cell carcinoma. Cancer 2001;92(6):1495-1503.
130. Ebrahimi A, Murali R, Gao K, Elliott MS, Clark JR. The prognostic and staging implications of bone invasion in oral squamous cell carcinoma. Cancer 2011;117(19):4460-4467.
131. Waldron JN, O'Sullivan B, Gullane P, Witterick IJ, Liu FF, Payne D, Warde P, Cummings B. Carcinoma of the maxillary antrum: a retrospective analysis of 110 cases. Radiotherapy and Oncology 2000;57(2):167-173.
132. Binahmed A, Nason RW, Hussain A, Abdoh AA, Sándor GKB. Treatment outcomes in squamous cell carcinoma of the maxillary alveolus and palate: a population-based study. Oral Surgery, Oral Medicine, Oral Pathology, Oral Radiology, and Endodontology 2008;105(6):750-754.
133. Lin HW, Bhattacharyya N. Survival impact of nodal disease in hard palate and maxillary alveolus cancer. Laryngoscope 2009;119(2):312-315.
134. Lenz M, Skalej M, Ozdoba C, Bongers H. [Magnetic resonance tomography of the oral cavity, the oropharynx and the mouth floor: comparison with computed tomography]. RoFo : Fortschritte auf dem Gebiete der Rontgenstrahlen und der Nuklearmedizin 1989;150(4):425-433.
135. Boland PW, Watt-Smith SR, Pataridis K, Alvey C, Golding SJ. Evaluating lingual carcinoma for surgical management: what does volumetric measurement with MRI offer? The British journal of radiology 2010;83(995):927-933.
136. Hibbert J, Marks NJ, Winter PJ, Shaheen OH. Prognostic factors in oral squamous carcinoma and their relation to clinical staging. Clinical otolaryngology and allied sciences 1983;8(3):197-203.
137. Beahrs OH, American Joint Committee on Cancer., American Cancer Society. Manual for staging of cancer. Philadelphia: Lippincott; 1988
138. Mucke T, Holzle F, Wagenpfeil S, Wolff KD, Kesting M. The role of tumor invasion into the mandible of oral squamous cell carcinoma. J Cancer Res Clin Oncol 2011;137(1):165-171.
139. Yokoo S, Umeda M, Komatsubara H, Shibuya Y, Komori T. Evaluation of T-classifications of upper gingival and hard palate carcinomas—a proposition for new criterion of T4. Oral oncology 2002;38(4):378-382.
140. Sasaki T, Imai Y, Fujibayashi T. New proposal for T classification of gingival carcinomas arising in the maxilla. International journal of oral and maxillofacial surgery 2004;33(4):349-352.
141. Le QT, Fu KK, Kaplan MJ, Terris DJ, Fee WE, Goffinet DR. Lymph node metastasis in maxillary sinus carcinoma. International Journal of Radiation Oncology* Biology* Physics 2000;46(3):541-549.
142. Simental Jr AA, Johnson JT, Myers EN. Cervical metastasis from squamous cell carcinoma of the maxillary alveolus and hard palate. Laryngoscope 2006;116(9):1682-1684.
143. Montes DM, Carlson ER, Fernandes R, Ghali G, Lubek J, Ord R, Bell B, Dierks E, Schmidt BL. Oral maxillary squamous carcinoma: An indication for neck dissection in the clinically negative neck. Head Neck 2010.
144. Beltramini GA, Massarelli O, Demarchi M, Copelli C, Cassoni A, Valentini V, Tullio A, Giannì AB, Sesenna E, Baj A. Is neck dissection needed in squamous-cell carcinoma of the maxillary gingiva, alveolus, and hard palate? A multicentre Italian study of 65 cases and literature review. Oral oncology 2011.
145. Brown J, Rogers S, McNally D. A modified classification for the maxillectomy defect. Head Neck 2000;22:17-26.
146. Jimi E, Furuta H, Matsuo K, Tominaga K, Takahashi T, Nakanishi O. The cellular and molecular mechanisms of bone invasion by oral squamous cell carcinoma. Oral Dis 2011;17(5):462-468.

147. Brown JS, Griffith JF, Phelps PD, Browne RM. A comparison of different imaging modalities and direct inspection after periosteal stripping in predicting the invasion of the mandible by oral squamous cell carcinoma. Br J Oral & Maxilofac Surg 1994;32:347-359.
148. Slootweg PJ. Complex head and neck specimens and neck dissections. How to handle them. J Clin Pathol 2005;58(3):243-248.
149. Reuben AD, Watt-Smith SR, Dobson D, Golding SJ. A comparative study of evaluation of radiographs, CT and 3D reformatted CT in facial trauma: what is the role of 3D? Br J Radiol 2005;78(927):198-201.
150. Bibb R. Pre-operative management - Modelling and rapid prototyping. Imaging and planning in surgery: A guide to research. Switzerland: AO Publishing; 2008.
151. Erickson DM, Chance D, Schmitt S, Mathis J. An opinion survey of reported benefits from the use of stereolithographic models. J Oral Maxillofac Surg 1999;57(9):1040-1043.
152. Fruhwald J, Schicho KA, Figl M, Benesch T, Watzinger F, Kainberger F. Accuracy of craniofacial measurements: Computed Tomography and three-dimensional computed tomography with stereolithographic models. J Craniofac Surg 2008;19(1):22-26.
153. Hayward R, Harkness W, Kendall B, Jones B. Magnetic Resonance Imaging in the assessment of craniosynostosis. Scand J Plast Reconstr Hand Surg 1992;26:287-292.
154. Engel M, Hoffmann J, Muhling J, Castrillon-Oberndorfer G, Seeberger R, Freudlsperger C. Magnetic resonance imaging in isolated sagittal synostosis. J Craniofac Surg 2012;23(4):e366-369.
155. Fjortoft MI, Sevely A, Boetto S, Kessler S, Sarramon MF, Rolland M. Prenatal diagnosis of craniosynostosis: value of MR imaging. Neuroradiology 2007;49(6):515-521.
156. Cotton F, Rozzi F, Vallee B, Pachai C, Hermier M, Guihard-Costa A, Froment J. Cranial sutures and craniometric points detected on MRI. Surg Radiol Anat 2005;27(1):64-70.
157. Cotton F, Rozzi FR, Vallee B, Pachai C, Hermier M, Guihard-Costa AM, Froment JC. Cranial sutures and craniometric points detected on MRI. Surg Radiol Anat 2005;27(1):64-70.
158. Serafini G, Ongaro L, Mori A, Rossi C, Cavalloro F, Tagliaferri C, Mencherini S, Braschi A. Anesthesia for MRI in the pediatric patient. Minerva Anestesiol 2005;71(6):361-366.
159. Malviya S, Voepel-Lewis T, Eldevik OP, Rockwell DT, Wong JH, Tait AR. Sedation and general anaesthesia in children undergoing MRI and CT: adverse events and outcomes. Br J Anaesth 2000;84(6):743-748.
160. Haynes SR, Lawler PG. An assessment of the consistency of ASA physical status classification allocation. Anaesthesia 1995;50(3):195-199.
161. Bharadwaj R, Ravikumar A, Krishnaswamy NR. Evaluation of craniofacial morphology in patients with obstructive sleep apnea using lateral cephalometry and dynamic MRI. Indian J Dent Res 2011;22(6):739-748.
162. Pirila-Parkkinen K, Lopponen H, Nieminen P, Tolonen U, Paakko E, Pirttiniemi P. Validity of upper airway assessment in children: a clinical, cephalometric, and MRI study. Angle Orthod 2011;81(3):433-439.
163. Lee RW, Sutherland K, Chan AS, Zeng B, Grunstein RR, Darendeliler MA, Schwab RJ, Cistulli PA. Relationship between surface facial dimensions and upper airway structures in obstructive sleep apnea. Sleep 2010;33(9):1249-1254.
164. Cevidanes LHS, Busby B, Cheek C, Proffit WR, Gerig G, Franco AA, Vigorito JW. Precision of 3D craniofacial landmark data using magnetic resonance scans (Abstract). International Association for Dental Research, Conference Abstracts 2002:3128.
165. Christianson R, Lufkin RB, Abemayor E, Hanafee W. MRI of the mandible. Surg Radiol Anat 1989;11:163-169.
166. Bolzoni A, Cappiello J, Piazza C, Peretti G, Maroldi R, Farina D, Nicolai P. Diagnostic accuracy of magnetic resonance imaging in the assessment of mandibular involvement in oral-oropharyngeal squamous cell carcinoma. Arch Otolaryngol Head Neck Surg 2004;130:837.
167. Eley KA, Boland PW, Potter M, Watt-Smith SR, Golding SJ. Pre-treatment tumour volume, as measured on MRI, reliably predicts survival in maxillary squamous cell carcinoma following surgical resection. Under Review.
168. Baghi M, Mack MG, Hambek M, Bisdas S, Muerthel R, Wagenblast J, Gstoettner W, Vogl T, Knecht R. Usefulness of MRI volumetric evaluation in patients with squamous cell cancer of the head and neck treated with neoadjuvant chemotherapy. Head Neck 2007;29(2):104-108.
169. Partridge SC, Gibbs JE, Lu Y, Esserman LJ, Tripathy D, Wolverton DS, Rugo HS, Hwang ES, Ewing CA, Hylton NM. MRI measurements of breast tumor volume predict response to neoadjuvant chemotherapy and recurrence-free survival. American Journal of Roentgenology 2005;184(6):1774-1781.
170. Wang TC, Hua CH, Lin CC, Tsou YA, Tseng HC, Tsai MH. Risk factors affect the survival outcome of hard palatal and maxillary alveolus squamous cell carcinoma: 10-year review in a tertiary referral center. Oral Surgery, Oral Medicine, Oral Pathology, Oral Radiology, and Endodontology 2010;110(1):11-17.
171. Studer G, Lütolf U, El-Bassiouni M, Rousson V, Glanzmann C. Volumetric staging (VS) is superior to TNM and AJCC staging in predicting outcome of head and neck cancer treated with IMRT. Acta Oncologica 2007;46(3):386-394.
172. Gibbs P, Buckley D, Blackband S, Horsman A. Tumour volume determination from MR images by morphological segmentation. Physics in Medicine and Biology 1996;41:2437.

173. Munajat I, Zulmi W, Norazman M, Wan Faisham W. Tumour volume and lung metastasis in patients with osteosarcoma. J Orthop Surg 2008;16:182-185.
174. Kimura Y, Sumi M, Ichikawa Y, Kawai Y, Nakamura T. Volumetric MR imaging of oral, maxillary sinus, oropharyngeal, and hypopharyngeal cancers: correlation between tumor volume and lymph node metastasis. American journal of neuroradiology 2005;26(9):2384-2389.
175. Gordon AR, Loevner LA, Shukla-Dave A, Redfern RO, Sonners AI, Kilger AM, Elliott MA, Machtay M, Weber RS, Glickson JD. Intraobserver variability in the MR determination of tumor volume in squamous cell carcinoma of the pharynx. American journal of neuroradiology 2004;25(6):1092-1098.
176. Robson MD, Gatehouse PD, So PW, Bell JD, Bydder GM. Contrast enhancement of short T2 tissues using ultrashort TE (UTE) pulse sequences. Clinical Radiology 2004;59:720-726.
177. Robson MD, Bydder GM. Clinical ultrashort echo time imaging of bone and other connective tissues. NMR Biomed 2006;19:765-780.
178. Robson MD, Benjamin M, Gishen P, Bydder GM. Magnetic resonance imaging of the Achilles tendon using ultrashort TE (UTE) pulse sequences. Clinical Radiology 2004;59:727-735.
179. Waldman A, Rees JH, Brock CS, Robson MD, Gatehouse PD, Bydder GM. MRI of the brain with ultra-short echo-time pulse sequences. Neuroradiology 2003;45:887-892.
180. Dogdas B, Shattuck DW, Leahy RM. Segmentation of skull and scalp in 3-D human MRI using mathematical morphology. Hum Brain Mapp 2005;26(4):273-285.
181. Daliri M, Abrishami Moghaddam H, Ghadimi S, Momeni M, Harirchi F, Giti M. Skull segmentation in 3D neonatal MRI using hybrid Hopfield Neural Network. Conf Proc IEEE Eng Med Biol Soc 2010;2010:4060-4063.
182. Wang D, Shi L, Chu WC, Cheng JC, Heng PA. Segmentation of human skull in MRI using statistical shape information from CT data. J Magn Reson Imaging 2009;30(3):490-498.
183. Goto TK, Nishida S, Nakamura Y, Tokumori K, Nakamura Y, Kobayashi K, Yoshida Y, Yoshiura K. The accuracy of 3-dimensional magnetic resonance 3D vibe images of the mandible: an in vitro comparison of magnetic resonance imaging and computed tomography. Oral Surg Oral Med Oral Path Oral Radiol Endod 2006;103(4):550-559.
184. Golding SJ, Saeed R, Alvey C, Evangelou I, McIntyre A, Watt-Smith S. Imaging Cortical Bone by MRI: a new approach to image-guided planning for reconstructive surgery of the face. European Congress of Radiology, ECR, Abstract. European Radiology Supplements 2005;15(1):1-688.
185. Connor SEJ, Arscott T, Berry J, Greene L, Gorman RO. Precision and accuracy of low-dose CT protocols in the evaluation of skull landmarks. Dentomaxillofac Radiol 2007;36(5):270-276.
186. Online Kappa calculator. 2011 http://justus.randolph.name/kappa
187. Soboleski D, Mussari B, McCloskey D, Sauerbrei E, Espinosa F, Fletcher A. High-resolution sonography of the abnormal cranial suture. Pediatr Radiol 1998;28(2):79-82.
188. Siegel MI, Mooney MP. Appropriate animal models for craniofacial biology. Cleft Palate J 1990;27(1):18-25.
189. Geeraerts T, Newcombe VF, Coles JP, Abate MG, Perkes IE, Hutchinson PJ, Outtrim JG, Chatfield DA, Menon DK. Use of T2-weighted magnetic resonance imaging of the optic nerve sheath to detect raised intracranial pressure. Crit Care 2008;12(5):R114.
190. Premkumar S. Orthodontics Prep Manual for Undergraduates: Elsevier; 2008
191. Larrabee WF, Makielski KH, Henderson JL. Surgical anatomy of the face. Philadelphia, PA: Lippincott Williams & Wilkins; 2004
192. Scheideman GB, Bell WH, Legan HL, Finn RA, Reisch JS. Cephalometric analysis of dentofacial normals. Am J Orthod 1980;78(4):404-420.
193. Burstone CJ, James RB, Legan H, Murphy GA, Norton LA. Cephalometrics for orthognathic surgery. J Oral Surg 1978;36(4):269-277.
194. Legan HL, Burstone CJ. Soft tissue cephalometric analysis for orthognathic surgery. J Oral Surg 1980;38(10):744-751.
195. Frongia G, Piancino MG, Bracco P. Cone-Beam Computed Tomography: Accuracy of Three-dimensional Cephalometry Analysis and Influence of Patient Scanning Position. J Craniofac Surg 2012;23(4):1038-1043.
196. Zamora N, Llamas JM, Cibrian R, Gandia JL, Paredes V. A study on the reproducibility of cephalometric landmarks when undertaking a three-dimensional (3D) cephalometric analysis. Med Oral Patol Oral Cir Bucal 2012;17(4):e678-688.
197. Oz U, Orhan K, Abe N. Comparison of linear and angular measurements using two-dimensional conventional methods and three-dimensional cone beam CT images reconstructed from a volumetric rendering program in vivo. Dentomaxillofac Radiol 2011;40(8):492-500.
198. Bholsithi W, Tharanon W, Chintakanon K, Komolpis R, Sinthanayothin C. 3D vs. 2D cephalometric analysis comparisons with repeated measurements from 20 Thai males and 20 Thai females. Biomed Imaging Interv J 2009;5(4):e21.
199. van Vlijmen OJ, Maal T, Berge SJ, Bronkhorst EM, Katsaros C, Kuijpers-Jagtman AM. A comparison between 2D and 3D cephalometry on CBCT scans of human skulls. Int J Oral Maxillofac Surg 2010;39(2):156-160.

200. http://www.brainlab.com. 2011
201. Eley KA, McIntyre A, Watt-Smith SR, Golding SJ. "Black Bone" MRI: A partial flip angle technique for radiation reduction in craniofacial imaging. British J Radiology 2012;85(1011):272-278.
202. Hao SP, Tsang NM, Chang KP, Chen CK, Huang SS. Treatment of squamous cell carcinoma of the retromolar trigone. Laryngoscope 2006;116(6):916-920.
203. Wiegand C, Richards P. Measurement of intracranial pressure in children: a critical review of current methods. Developmental Medicine Child Neurology 2007;49:935-941.
204. Raboel PH, Bartek J, Jr., Andresen M, Bellander BM, Romner B. Intracranial Pressure Monitoring: Invasive versus Non-Invasive Methods-A Review. Crit Care Res Pract 2012;2012:950393.
205. Tai K, Park JH, Hayashi K, Yanagi Y, Asaumi JI, Iida S, Shin JW. Preliminary study evaluating the accuracy of MRI images on CBCT images in the field of orthodontics. J Clin Pediatr Dent 2011;36(2):211-218.
206. Chang CC, Chen MK, Wu HK, Liu MT. Nasopharyngeal carcinoma volume measurements determined with computed tomography: study of intraobserver and interobserver variability. J Otolaryngol 2002;31(6):361-365.
207. Sobin LH, Gospodarowicz MK, Wittekind C, International Union against Cancer. TNM classification of malignant tumours. Chichester, West Sussex, UK ; Hoboken, NJ: Wiley-Blackwell; 2010

# Appendices

# Appendices


Appendix A: Optimal "Black Bone" flip angle ..... 296
A.1. Optimal "Black Bone" flip angle results - Osirix ..... 297
A.2. Optimal "Black Bone" flip angle results - Advantage windows ..... 297
A.3. Optimal "Black Bone" flip angle results - Adobe Photoshop ..... 298
A.4. Optimal "Black Bone" Parameters ..... 298
Appendix B: Biometric Accuracy of "Black Bone" MRI ..... 299
B.1. Biometric Accuracy Results of Phantom Skull ..... 300
Appendix C: Cranial Sutures on MRI ..... 302
C.1. Cranial sutures on MRI Reviewers' sheet ..... 303
Appendix D: "Black Bone" MRI in craniosynostosis ..... 305
D.1. "Black Bone" MRI in craniosynostosis Ethics ..... 306
D.1 Parental Information Sheet for CT & MRI ..... 306
D.2 Parental Consent Form for CT & MRI ..... 309
D.3 Patient/Parent Information Sheet for MRI only ..... 310
D.4 Reviewers' sheet for "Black Bone" MRI & craniosynostosis ..... 313
D.5 Assessor results for review of "Black Bone" in craniosynostosis ..... 314
D.6 Cranial Suture widths on "Black Bone" ..... 314
Appendix E: Cephalometrics ..... 315
E.1. Cephalometric accuracy of "Black Bone" MRI ..... 316
E.1.1. Patient Information Sheet for MRI ..... 316
E.1.2. Patient Consent form for MRI ..... 319
E.1.3. Consent form for patients under 16 years of age ..... 320
E.2. AWW Cephalometric Results ..... 321
E.2.1. Volunteer 1: Lateral Cephalogram ..... 321
E.2.1. Volunteer 2: Lateral Cephalogram ..... 322
E.2.2. Volunteer 3: Lateral Cephalogram ..... 323
E.2.3. Volunteer 1: "Black Bone" ..... 324
E.2.4. Volunteer 2: "Black Bone" ..... 325
E.2.5. Volunteer 3: "Black Bone" ..... 326
E.2.6. Volunteer 1: MRI T1 ..... 327
E.2.7. Volunteer 2: MRI T1 ..... 328
E.2.8. Volunteer 3: MRI T1 ..... 328
E.2.9. Patient 1: Lateral Cephalogram ..... 329
E.2.10. Patient 2: Lateral Cephalogram ..... 330
E.2.11. Patient 3: Lateral Cephalogram ..... 331
E.2.12. Patient 4: Lateral Cephalogram ..... 331
E.2.13. Patient 5: Lateral Cephalogram ..... 331
E.2.14. Patient 1: "Black Bone" ..... 332
E.2.15. Patient 2: "Black Bone" ..... 333
E.2.16. Patient 3: "Black Bone" ..... 334
E.2.17. Patient 4: "Black Bone" ..... 334
E.2.18. Patient 5: "Black Bone" ..... 335
E.2.19. Patient 3: MRI T1 ..... 335
E.2.20. Patient 4: MRI T1 ..... 335
E.2.21. Patient 5: MRI T1 ..... 335
E.2.22. Patient 3: MRI T2 ..... 336
E.2.23. Patient 4: MRI T2 ..... 336
E.2.24. Patient 5: MRI T2 ..... 336
E.3. Repeatability of Dolphin Measurements ..... 337
E.4. Co-ordinates of repeated digitisations of "Black Bone" using Dolphin with 1st digitisation as reference ..... 337

Appendix F: Tumour Volume ..... 338
F.1 Staging of head & neck malignancy ..... 339
Lip & Oral Cavity ..... 339
Nasal Cavity and Paranasal Sinuses ..... 340
F.2 ACE-27 Co-morbidity Scoring ..... 341
F.3 Maxillary Tumour Volume: Patient Data Summary ..... 343
F.4 Maxillary Tumour Volume MRI Parameters ..... 345
F.5 Mandible Tumour Volume: Patient Data Summary ..... 346
F.6 Mandible Tumour Volume MRI Parameters: ..... 348
Appendix G: “Black Bone” MRI & Pathology ..... 349
G.1 Reviewers’ scoring sheet ..... 350
G.2 “Black Bone” Pathology Reviewers’ Responses ..... 351
Appendix H: 3D “Black Bone” ..... 352
H.1 Direct Phantom Cube Direct Measurements ..... 353
H.2 Phantom Cube Measurements on Software ..... 353
H.2.1 Statistical Analysis Phantom Cube Measurements on Software ..... 363
H.2.1.1. Fovia ..... 363
H.2.1.2. Mimics ..... 377
H.2.1.3. Osirix ..... 391
H.3 Mathematical Modelling ..... 406
H.4 Smoothing effects of Mimics on Phantom cube measurements ..... 415
H.4.1. Smoothing Effects ..... 418
Appendix I: “Black Bone” & Anatomical Models ..... 430
I.1. Model Cube measurements ..... 431

# Appendix A: Optimal “Black Bone” flip angle

## A.1. Optimal "Black Bone" flip angle results - Osirix

| Flip Angle | Location | Region | Area | Mean | SD | Variance | Min | Max |
|---|---|---|---|---|---|---|---|---|
| 1 | 84.23 | Bone vertex | 7.473 | 57.802 | 15.374 | 236.3599 | 24 | 127 |
| 3 | | | | 85.23 | 35.993 | 1295.496 | 30 | 297 |
| 5 | | | | 106.473 | 58.867 | 3465.324 | 24 | 451 |
| 7 | | | | 130.984 | 74.09 | 5489.328 | 34 | 570 |
| 10 | | | | 160.147 | 104.069 | 10830.36 | 29 | 709 |
| 15 | | | | 167.206 | 111.462 | 12423.78 | 27 | 808 |
| 20 | | | | 170.694 | 118.338 | 14003.88 | 32 | 832 |
| 45 | | | | 216.634 | 133.001 | 17689.27 | 40 | 1037 |
| 60 | | | | 239.641 | 139.512 | 19463.6 | 42 | 1087 |
| 1 | 67.73 | ST Brain | 34.366 | 227.794 | 25.944 | 673.0911 | 146 | 344 |
| 3 | | | | 495.396 | 32.348 | 1046.393 | 344 | 622 |
| 5 | | | | 677.705 | 35.542 | 1263.234 | 422 | 875 |
| 7 | | | | 792.265 | 40.596 | 1648.035 | 550 | 984 |
| 10 | | | | 948.703 | 52.6 | 2766.76 | 564 | 1187 |
| 15 | | | | 1026.325 | 99.52 | 9904.23 | 380 | 1637 |
| 20 | | | | 1014.183 | 149.976 | 22492.8 | 245 | 2018 |
| 45 | | | | 761.339 | 342.18 | 117087.2 | 18 | 3036 |
| 60 | | | | 677.549 | 391.361 | 153163.4 | 97 | 3255 |
| 1 | -86.77 | ST Tongue | 7.319 | 204.293 | 22.201 | 492.8844 | 137 | 309 |
| 3 | | | | 489.518 | 32.919 | 1083.661 | 365 | 686 |
| 5 | | | | 662.605 | 37.496 | 1405.95 | 513 | 838 |
| 7 | | | | 751.215 | 42.634 | 1817.658 | 583 | 922 |
| 10 | | | | 833.37 | 65.783 | 4327.403 | 465 | 1119 |
| 15 | | | | 867.049 | 88.13 | 7766.897 | 428 | 1220 |
| 20 | | | | 848.81 | 111.408 | 12411.74 | 383 | 1283 |
| 45 | | | | 700.636 | 183.282 | 33592.29 | 220 | 1698 |
| 60 | | | | 614.453 | 207.501 | 43056.67 | 130 | 1782 |
| 1 | -86.77 | Mandible | 0.715 | 76.562 | 31.823 | 1012.703 | 26 | 212 |
| 3 | | | | 146.614 | 127.842 | 16343.58 | 34 | 554 |
| 5 | | | | 183.25 | 164.036 | 26907.81 | 31 | 801 |
| 7 | | | | 261.551 | 243.493 | 59288.84 | 35 | 999 |
| 10 | | | | 233.852 | 231.303 | 53501.08 | 41 | 1094 |
| 15 | | | | 292.526 | 329.025 | 108257.5 | 33 | 1462 |
| 20 | | | | 323.256 | 386.8 | 149614.2 | 51 | 1811 |
| 45 | | | | 406.778 | 514.514 | 264724.7 | 41 | 2409 |
| 60 | | | | 458.426 | 628.996 | 395636 | 46 | 2647 |
| 1 | 30.23 | Brain | 93.911 | 243.238 | 36.168 | 1308.124 | 144 | 400 |
| 3 | | | | 533.118 | 39.614 | 1569.269 | 385 | 709 |
| 5 | | | | 717.987 | 54.153 | 2932.547 | 432 | 946 |
| 1 | 21.23 | Brain | 15.907 | 246.138 | 38.231 | 1461.609 | 132 | 364 |
| 3 | | | | 530.676 | 35.932 | 1291.109 | 389 | 680 |
| 5 | | | | 701.405 | 56.262 | 3165.413 | 489 | 901 |

## A.2. Optimal "Black Bone" flip angle results - Advantage windows

| Flip Angle | Image Location | Region | Area | Mean | SD | Min | Max |
|---|---|---|---|---|---|---|---|
| 1 | 69.2 | Brain | 987 | 229.06 | 24.81 | 148 | 321 |
| 3 | | | | 497.21 | 29.6 | 367 | 608 |
| 5 | | | | 676.84 | 32.32 | 503 | 818 |
| 7 | | | | 792.05 | 33.61 | 635 | 916 |
| 10 | | | | 938.71 | 44.07 | 706 | 1157 |
| 15 | | | | 1007.41 | 69.69 | 610 | 1616 |
| 20 | | | | 998.92 | 92.68 | 638 | 2019 |
| 45 | | | | 713.36 | 210.42 | 407 | 3057 |
| 60 | | | | 629.7 | 245.45 | 274 | 3313 |
| 1 | 84.2 | Bone Vertex | 450 | 59.55 | 16.56 | 27 | 127 |
| 3 | | | | 84.55 | 26.04 | 32 | 177 |
| 5 | | | | 94.11 | 33.77 | 31 | 233 |
| 7 | | | | 122.74 | 46.43 | 33 | 439 |
| 10 | | | | 122.67 | 45.92 | 29 | 381 |
| 15 | | | | 130.39 | 54.35 | 27 | 479 |
| 20 | | | | 137.58 | 65.78 | 32 | 577 |
| 45 | | | | 185.89 | 77.19 | 40 | 535 |
| 60 | | | | 201.42 | 78.47 | 55 | 603 |
| 1 | 88.3 | Mandible/ tongue | 987 | 184.18 | 46.32 | 24 | 285 |
| 3 | | | | 440.06 | 117.9 | 37 | 588 |
| 5 | | | | 607.92 | 159.94 | 42 | 820 |
| 7 | | | | 698.14 | 175.82 | 33 | 439 |
| 10 | | | | 759.52 | 203.61 | 19 | 1073 |
| 15 | | | | 804.48 | 220.12 | 32 | 1266 |
| 20 | | | | 782.81 | 237.86 | 34 | 1506 |
| 45 | | | | 666.73 | 268.0 | 39 | 2285 |
| 60 | | | | 585.53 | 292.49 | 44 | 2408 |

## A.3. Optimal "Black Bone" flip angle results - Adobe Photoshop

| Flip Angle | Image | Mean | SD | Median | Pixels |
|---|---|---|---|---|---|
| **1** | 28 – Tongue ST | 153.47 | 15.17 | 153 | 3264 |
| **3** | | 148.87 | 8.51 | 149 | 3465 |
| **5** | | 123.8 | 6.30 | 123 | 3328 |
| **7** | | 116.84 | 5.86 | 117 | 3575 |
| **10** | | 97.18 | 5.42 | 97 | 3770 |
| **15** | | 90.83 | 6.64 | 91 | 3752 |
| **20** | | 90.47 | 7.81 | 90 | 3717 |
| **45** | | 47.0 | 8.52 | 46 | 3190 |
| **60** | | 39.33 | 10.34 | 37 | 2728 |
| **1** | 138 – Vertex Bone | 53.84 | 13.72 | 52 | 2660 |
| **3** | | 32.47 | 10.36 | 31 | 2624 |
| **5** | | 24.32 | 9.01 | 23 | 2332 |
| **7** | | 25.32 | 9.88 | 24 | 2310 |
| **10** | | 25.25 | 9.94 | 23 | 2106 |
| **15** | | 23.18 | 9.01 | 22 | 1683 |
| **20** | | 21.63 | 10.21 | 19 | 2242 |
| **45** | | 24.04 | 9.98 | 22 | 2214 |
| **60** | | 23.76 | 9.05 | 22 | 2173 |
| **1** | 128 – Brain ST | 174.49 | 19.76 | 174 | 14378 |
| **3** | | 162.08 | 10.27 | 162 | 11692 |
| **5** | | 168.03 | 9.16 | 168 | 14790 |
| **7** | | 174.16 | 8.97 | 175 | 13706 |
| **10** | | 176.62 | 10.57 | 176 | 12166 |
| **15** | | 152.90 | 14.42 | 151 | 12264 |
| **20** | | 127.84 | 18.62 | 124 | 13706 |
| **45** | | 63.82 | 28.55 | 55 | 14151 |
| **60** | | 52.48 | 31.03 | 43 | 13300 |

## A.4. Optimal "Black Bone" Parameters

Scanning parameters for GE and Philips MRI scanners:

| | GE | Philips |
|---|---|---|
| **Scanning sequence** | GR | GR |
| **Sequence variant** | OSP | SS\SK |
| **MR acquisition type** | 3D | 3D |
| **Slice thickness** | 2.4 | 2.4 |
| **TR** | 8.32 | 8.19 |
| **TE** | 4.2 | 4.01 |
| **Number of averages** | 2 | 4 |
| **Imaging frequency** | 63.865 | 63.890 |
| **Echo number** | 1 | 1 |
| **Spacing between slices** | 1.2 | 1.2 |
| **Echo train length** | 1 | 1 |
| **Pixel bandwidth** | 122.07 | 180 |
| **Phase encoding direction** | Row | Row |
| **Flip angle** | 5 | 5 |
| **Rows** | 512 | 512 |
| **Columns** | 512 | 512 |
| **Photometric interpretation** | Monochrome2 | Monochrome2 |

# Appendix B: Biometric Accuracy of “Black Bone” MRI

## B.1. Biometric Accuracy Results of Phantom Skull

1. Maximum cranial-caudal aperture of the right orbit
2. Maximum cranial-caudal aperture of the left orbit
3. Maximum height of the mandible from chin point in the midline
4. Maximum coronal dimension of the skull at the disarticulation point
5. Maximum coronal dimension of the skull cap at the disarticulation point
6. Distance between the lateral most aspect of the paired infraorbital foramen
7. Maximum cranial-caudal aperture of the piriform aperture
8. Maximum coronal aperture of the piriform aperture
9. Distance between the lateral most aspect of the paired mental foramen
10. Distance between the lateral most aspect of the paired mandibular condyles
11. Maximum dimension of the posterior hard palate between the most posterior identifiable molar teeth
12. Maximum distance between the lateral surfaces of the paired posterior upper molar teeth

| | A | B | C | D | E | F | G | H | I. | J | K | L |
|---|---|---|---|---|---|---|---|---|---|---|---|---|
| | **Direct Measurements** | | | | | | | | | | | |
| 1 | 32.61 | 33.00 | 27.67 | 139.52 | 139.96 | 55.91 | 32.34 | 21.11 | 44.3 | 110.25 | 57.89 | 40.46 |
| 2 | 32.42 | 33.04 | 27.45 | 139.41 | 140.5 | 55.78 | 32.34 | 21.18 | 44.25 | 110.04 | 58.56 | 40.75 |
| 3 | 32.78 | 32.85 | 27.53 | 139.81 | 140.8 | 55.85 | 32.28 | 21.00 | 44.85 | 110.05 | 58.25 | 40.46 |
| 4 | 32.49 | 32.74 | 27.67 | 139.87 | 140.92 | 55.81 | 32.54 | 21.82 | 44.71 | 110.18 | 58.21 | 40.63 |
| 5 | 32.41 | 32.93 | 27.51 | 139.3 | 140.37 | 55.75 | 32.23 | 21.33 | 44.36 | 109.49 | 58.04 | 40.81 |
| 6 | 32.74 | 33.01 | 27.65 | 139.74 | 140.77 | 55.82 | 32.38 | 21.27 | 44.70 | 109.72 | 57.79 | 40.76 |
| 7 | 32.77 | 32.82 | 27.63 | 139.5 | 140.48 | 55.77 | 32.39 | 21.4 | 44.42 | 109.78 | 58.03 | 40.59 |
| 8 | 32.93 | 32.92 | 27.56 | 139.51 | 140.81 | 55.72 | 32.24 | 21.5 | 44.20 | 109.4 | 58.25 | 40.74 |
| 9 | 32.72 | 32.78 | 28.06 | 139.11 | 140.96 | 55.84 | 32.39 | 21.72 | 44.54 | 109.98 | 57.83 | 40.36 |
| 10 | 32.93 | 32.66 | 27.91 | 139.43 | 140.96 | 55.84 | 32.29 | 21.93 | 44.87 | 110.02 | 58.19 | 40.54 |
| 11 | 32.96 | 32.98 | 28.03 | 139.42 | 140.82 | 55.73 | 32.22 | 21.61 | 44.49 | 109.86 | 58.28 | 40.61 |
| 12 | 32.73 | 33.06 | 27.48 | 140.22 | 140.9 | 55.75 | 32.24 | 21.59 | 44.34 | 110.03 | 58.33 | 40.43 |
| 13 | 32.74 | 32.77 | 27.43 | 139.42 | 140.91 | 55.77 | 32.3 | 21.53 | 44.77 | 109.44 | 58.41 | 40.44 |
| 14 | 32.75 | 32.88 | 27.44 | 140.06 | 140.83 | 55.81 | 32.1 | 21.44 | 44.33 | 109.76 | 58.28 | 40.56 |
| 15 | 32.68 | 32.95 | 27.96 | 139.23 | 140.8 | 55.81 | 32.19 | 21.81 | 44.04 | 110.48 | 57.60 | 40.41 |
| 16 | 32.91 | 32.58 | 27.55 | 139.22 | 140.84 | 55.84 | 32.31 | 21.14 | 44.11 | 110.5 | 57.79 | 40.41 |
| 17 | 32.97 | 32.83 | 28.12 | 139.52 | 140.56 | 55.82 | 32.18 | 21.71 | 44.37 | 110.76 | 58.06 | 40.39 |
| 18 | 32.85 | 33.02 | 27.32 | 139.28 | 140.97 | 55.84 | 32.26 | 21.77 | 44.35 | 110.58 | 58.00 | 40.58 |
| 19 | 32.98 | 32.97 | 27.52 | 139.27 | 140.88 | 55.83 | 32.30 | 21.38 | 44.86 | 110.48 | 58.10 | 40.61 |
| 20 | 32.99 | 32.98 | 27.50 | 139.2 | 140.38 | 55.82 | 32.25 | 21.61 | 44.52 | 110.49 | 57.57 | 40.62 |
| 21 | 32.91 | 32.69 | 27.55 | 139.54 | 140.85 | 55.88 | 32.49 | 21.44 | 44.25 | 110.43 | 58.47 | 40.34 |
| 22 | 32.96 | 32.91 | 27.98 | 139.11 | 140.96 | 55.84 | 32.53 | 21.37 | 44.62 | 109.41 | 58.26 | 40.50 |
| 23 | 32.80 | 33.06 | 27.37 | 139.18 | 140.68 | 55.80 | 32.45 | 21.14 | 44.80 | 109.60 | 57.67 | 40.42 |
| 24 | 32.99 | 33.03 | 27.79 | 139.41 | 140.85 | 55.83 | 32.39 | 21.62 | 44.41 | 109.57 | 58.30 | 40.54 |
| 25 | 32.92 | 32.94 | 27.53 | 139.18 | 140.76 | 55.84 | 32.15 | 21.5 | 44.88 | 109.54 | 58.35 | 40.57 |
| 26 | 32.38 | 33.08 | 27.37 | 139.39 | 140.53 | 55.85 | 32.28 | 21.37 | 44.72 | 110.23 | 58.85 | 40.46 |
| 27 | 32.97 | 32.89 | 27.48 | 139.44 | 140.45 | 55.92 | 32.56 | 21.51 | 44.35 | 110.49 | 58.67 | 40.48 |
| 28 | 32.85 | 32.96 | 28.04 | 139.94 | 140.44 | 55.81 | 32.14 | 21.26 | 44.04 | 110.78 | 58.34 | 40.97 |
| 29 | 32.77 | 32.67 | 27.48 | 139.62 | 140.16 | 55.80 | 32.56 | 21.40 | 44.27 | 110.63 | 58.55 | 40.47 |
| 30 | 32.9 | 32.98 | 27.64 | 139.37 | 139.86 | 55.85 | 32.38 | 21.98 | 44.67 | 110.71 | 58.52 | 40.56 |
| 31 | 32.08 | 32.82 | 27.93 | 139.76 | 140.19 | 55.83 | 32.43 | 21.54 | 44.15 | 109.43 | 58.03 | 40.36 |
| 32 | 32.87 | 32.7 | 27.61 | 139.53 | 140.78 | 55.76 | 32.48 | 21.92 | 44.28 | 109.53 | 58.42 | 40.48 |
| 33 | 32.3 | 32.87 | 28.17 | 139.66 | 140.51 | 55.65 | 32.34 | 21.45 | 44.77 | 110.33 | 57.46 | 40.35 |
| 34 | 32.96 | 32.97 | 27.82 | 139.62 | 140.28 | 55.77 | 32.3 | 21.39 | 44.75 | 110.61 | 57.55 | 40.56 |
| 35 | 32.21 | 33.01 | 28.16 | 139.31 | 140.54 | 55.74 | 32.45 | 21.72 | 44.25 | 110.76 | 57.48 | 40.65 |
| 36 | 32.82 | 32.91 | 28.15 | 139.19 | 140.53 | 55.84 | 32.65 | 21.65 | 44.26 | 109.68 | 57.41 | 40.57 |
| 37 | 32.43 | 32.68 | 27.7 | 139.46 | 140.56 | 55.81 | 32.8 | 21.96 | 44.05 | 110.59 | 57.38 | 40.26 |
| 38 | 32.98 | 32.89 | 27.57 | 139.58 | 140.49 | 55.83 | 32.1 | 21.68 | 44.17 | 110.52 | 58.48 | 40.25 |
| 39 | 32.74 | 32.98 | 27.91 | 139.39 | 140.83 | 55.8 | 32.42 | 21.85 | 44.87 | 110.63 | 58.54 | 40.75 |
| 40 | 32.55 | 32.94 | 27.44 | 139.50 | 140.3 | 55.84 | 32.29 | 21.98 | 44.69 | 110.42 | 58.38 | 40.79 |
| | **"Black Bone" MRI Measurements** | | | | | | | | | | | |
| 1 | 33.2 | 32.8 | 28.7 | 139.8 | 140.1 | 55.9 | 32.2 | 22.1 | 43.3 | 109.6 | 58.2 | 40.4 |
| 2 | 32.3 | 32.8 | 28.0 | 139.8 | 140.6 | 56.0 | 32.4 | 22.0 | 43.3 | 109.6 | 58.4 | 40.2 |
| 3 | 33.0 | 33.0 | 27.9 | 139.5 | 140.8 | 56.4 | 32.1 | 22.5 | 43.4 | 110.0 | 58.3 | 40.7 |
| 4 | 32.6 | 33.2 | 27.7 | 139.7 | 140.3 | 56.1 | 32.6 | 22.5 | 43.8 | 110.7 | 58.3 | 40.6 |
| 5 | 33.3 | 32.8 | 28.3 | 140.1 | 140.3 | 56.3 | 32.9 | 22.4 | 44.0 | 109.5 | 58.1 | 40.6 |
| 6 | 33.2 | 33.0 | 27.9 | 139.6 | 140.0 | 56.1 | 32.3 | 22.5 | 43.9 | 110.0 | 57.8 | 40.1 |
| 7 | 32.9 | 32.6 | 27.7 | 139.8 | 140.3 | 55.9 | 32.5 | 22.7 | 43.8 | 110.4 | 57.6 | 40.7 |
| 8 | 32.2 | 32.8 | 27.5 | 139.6 | 140.7 | 55.9 | 32.2 | 22.1 | 44.0 | 110.9 | 57.8 | 40.9 |
| 9 | 32.8 | 33.0 | 27.8 | 139.8 | 139.8 | 56.3 | 32.0 | 22.3 | 43.5 | 111.1 | 58.0 | 41.1 |
| 10 | 33.2 | 33.0 | 27.5 | 140.0 | 140.1 | 56.1 | 32.2 | 22.5 | 43.5 | 110.7 | 58.0 | 41.3 |
| 11 | 33.1 | 32.8 | 27.4 | 139.8 | 139.8 | 56.8 | 32.5 | 21.9 | 43.7 | 110.0 | 58.1 | 40.9 |
| 12 | 32.9 | 33.2 | 28.1 | 139.8 | 140.3 | 55.9 | 32.5 | 22.0 | 43.4 | 110.9 | 58.0 | 41.1 |
| 13 | 33.3 | 32.8 | 27.9 | 140.3 | 140.0 | 56.4 | 32.4 | 22.7 | 43.8 | 111.1 | 58.1 | 41.2 |
| 14 | 33.0 | 32.8 | 28.0 | 140.0 | 140.1 | 56.2 | 32.4 | 22.4 | 43.7 | 110.9 | 57.8 | 40.8 |
| 15 | 32.9 | 33.0 | 27.8 | 139.8 | 140.5 | 56.1 | 32.4 | 22.5 | 43.8 | 110.7 | 58.1 | 40.9 |
| 16 | 32.7 | 33.0 | 28.1 | 139.8 | 140.3 | 56.5 | 32.4 | 22.1 | 43.7 | 110.9 | 57.6 | 40.9 |
| 17 | 32.9 | 32.4 | 28.8 | 139.8 | 139.8 | 56.2 | 32.6 | 21.9 | 43.5 | 111.2 | 57.5 | 40.6 |
| 18 | 33.4 | 32.8 | 28.0 | 140.1 | 140.3 | 56.5 | 32.2 | 22.0 | 43.5 | 111.2 | 58.1 | 40.7 |
| 19 | 33.2 | 32.6 | 28.1 | 140.5 | 140.8 | 56.1 | 32.1 | 22.2 | 43.7 | 110.2 | 58.0 | 40.7 |
| 20 | 32.7 | 32.4 | 28.2 | 140.3 | 140.5 | 56.5 | 32.8 | 22.1 | 43.4 | 110.5 | 58.0 | 40.1 |

| | A | B | C | D | E | F | G | H | I. | J | K | L |
|---|---|---|---|---|---|---|---|---|---|---|---|---|
| **21** | 32.6 | 33.0 | 28.1 | 139.8 | 140.6 | 55.6 | 32.2 | 22.2 | 43.7 | 110.9 | 58.1 | 40.6 |
| **22** | 33.0 | 33.2 | 27.3 | 140.1 | 140.0 | 56.2 | 32.6 | 22.2 | 43.6 | 110.2 | 58.1 | 40.7 |
| **23** | 33.0 | 33.0 | 27.7 | 140.1 | 140.3 | 55.9 | 32.4 | 22.1 | 43.7 | 111.1 | 58.1 | 40.8 |
| **24** | 33.0 | 32.8 | 28.1 | 139.9 | 140.7 | 56.6 | 32.6 | 22.2 | 43.3 | 109.7 | 57.8 | 40.7 |
| **25** | 33.4 | 33.0 | 28.3 | 139.9 | 140.5 | 56.1 | 32.7 | 22.1 | 43.3 | 110.5 | 58.1 | 40.2 |
| **26** | 33.3 | 32.8 | 28.2 | 140.1 | 140.3 | 56.1 | 32.5 | 22.1 | 43.5 | 110.2 | 57.6 | 40.8 |
| **27** | 33.0 | 32.8 | 28.3 | 139.9 | 140.3 | 56.5 | 32.9 | 22.3 | 43.6 | 110.7 | 57.3 | 41.2 |
| **28** | 33.0 | 32.8 | 28.2 | 140.3 | 140.2 | 56.6 | 32.7 | 21.8 | 43.6 | 110.5 | 57.6 | 41.4 |
| **29** | 32.8 | 32.8 | 28.1 | 140.3 | 140.3 | 56.1 | 32.2 | 22.2 | 43.5 | 110.4 | 58.4 | 40.6 |
| **30** | 33.0 | 33.2 | 27.9 | 139.8 | 140.3 | 56.3 | 32.2 | 22.2 | 43.4 | 110.7 | 58.6 | 40.7 |
| **31** | 33.0 | 32.8 | 28.1 | 140.1 | 140.3 | 55.9 | 32.4 | 22.2 | 43.4 | 109.5 | 58.3 | 40.7 |
| **32** | 33.2 | 33.0 | 28.0 | 140.1 | 140.3 | 56.2 | 32.5 | 22.9 | 43.9 | 109.2 | 58.3 | 40.1 |
| **33** | 33.2 | 32.8 | 28.4 | 139.8 | 140.1 | 55.8 | 32.0 | 22.3 | 43.8 | 110.9 | 58.3 | 40.7 |
| **34** | 33.2 | 33.0 | 27.8 | 139.9 | 140.1 | 56.6 | 32.1 | 22.1 | 44.0 | 109.7 | 58.6 | 40.4 |
| **35** | 33.3 | 32.8 | 27.8 | 140.1 | 140.4 | 56.2 | 32.1 | 22.2 | 43.6 | 109.7 | 58.3 | 40.6 |
| **36** | 32.7 | 32.8 | 27.3 | 140.1 | 139.9 | 55.9 | 32.5 | 22.2 | 43.7 | 110.2 | 58.1 | 40.4 |
| **37** | 33.2 | 33.0 | 28.1 | 139.8 | 140.0 | 56.0 | 32.5 | 22.1 | 43.5 | 110.2 | 58.1 | 40.4 |
| **38** | 32.6 | 32.6 | 27.8 | 140.0 | 140.6 | 56.2 | 32.5 | 22.1 | 43.5 | 110.2 | 58.6 | 40.9 |
| **39** | 32.6 | 32.6 | 28.6 | 140.0 | 140.3 | 56.4 | 32.5 | 22.3 | 43.6 | 110.9 | 58.6 | 40.5 |
| **40** | 33.0 | 33.0 | 28.0 | 140.1 | 140.1 | 56.2 | 31.9 | 22.6 | 43.7 | 110.4 | 58.1 | 40.9 |
| | **CT Measurements** | | | | | | | | | | | |
| **1** | 32.2 | 33.0 | 27.9 | 139.0 | 140.3 | 56.5 | 32.2 | 21.6 | 45.1 | 110.5 | 58.6 | 40.6 |
| **2** | 32.0 | 32.7 | 27.8 | 139.3 | 140.4 | 57.4 | 33.1 | 21.5 | 45.3 | 110.5 | 59.3 | 40.8 |
| **3** | 32.7 | 32.7 | 28.0 | 139.9 | 140.2 | 56.5 | 32.7 | 21.7 | 45.8 | 110.3 | 58.9 | 40.8 |
| **4** | 32.1 | 33.1 | 28.5 | 139.7 | 140.2 | 56.3 | 33.0 | 22.1 | 44.4 | 110.8 | 58.9 | 40.5 |
| **5** | 32.7 | 32.9 | 28.5 | 139.8 | 140.1 | 56.7 | 33.2 | 22.1 | 44.8 | 110.8 | 59.0 | 40.5 |
| **6** | 33.4 | 32.4 | 27.8 | 139.9 | 140.3 | 56.9 | 33.2 | 21.6 | 44.5 | 110.8 | 58.4 | 40.6 |
| **7** | 33.3 | 32.8 | 28.0 | 140.4 | 140.5 | 55.9 | 32.5 | 21.8 | 44.7 | 110.8 | 57.8 | 40.8 |
| **8** | 32.5 | 33.5 | 28.3 | 139.8 | 139.6 | 57.2 | 33.0 | 22.0 | 44.4 | 110.8 | 58.0 | 40.8 |
| **9** | 33.0 | 32.8 | 28.1 | 140.4 | 140.0 | 56.7 | 32.6 | 21.4 | 44.6 | 110.8 | 57.8 | 40.9 |
| **10** | 32.5 | 33.2 | 28.7 | 140.4 | 140.2 | 56.1 | 33.0 | 21.8 | 45.0 | 111.1 | 57.6 | 40.8 |
| **11** | 32.2 | 33.1 | 28.1 | 140.1 | 140.3 | 56.7 | 33.1 | 21.7 | 44.8 | 110.9 | 57.8 | 40.6 |
| **12** | 32.4 | 32.7 | 28.0 | 140.1 | 140.2 | 57.1 | 33.1 | 21.8 | 44.3 | 110.8 | 58 | 40.6 |
| **13** | 32.6 | 32.3 | 27.2 | 139.7 | 140.1 | 56.9 | 32.8 | 21.9 | 44.7 | 110.8 | 57.8 | 40.8 |
| **14** | 32.3 | 33.1 | 27.6 | 139.7 | 140.0 | 57.3 | 32.6 | 22.1 | 44.2 | 111.2 | 57.7 | 40.6 |
| **15** | 32.8 | 33.3 | 27.6 | 139.8 | 140.3 | 56.7 | 32.7 | 21.8 | 44.2 | 111.1 | 57.9 | 40.5 |
| **16** | 32.5 | 32.6 | 27.8 | 140.2 | 140.4 | 56.3 | 32.9 | 21.9 | 44.6 | 110.9 | 57.8 | 40.8 |
| **17** | 32.1 | 32.6 | 27.8 | 140.3 | 140.2 | 57.6 | 33.2 | 21.1 | 44.5 | 110.8 | 58.1 | 40.3 |
| **18** | 32.3 | 33.3 | 27.9 | 140 | 140.4 | 56.9 | 33.1 | 22.0 | 44.7 | 111.4 | 58.1 | 40.8 |
| **19** | 32.4 | 32.4 | 27.8 | 140.1 | 140 | 57.0 | 33.4 | 21.6 | 44.9 | 111.2 | 58.2 | 40.6 |
| **20** | 33.0 | 32.4 | 28.3 | 139.8 | 140.1 | 57.3 | 33.1 | 21.4 | 44.6 | 110.9 | 58.1 | 40.5 |
| **21** | 32.6 | 32.7 | 28.3 | 140.1 | 140.3 | 56.7 | 32.8 | 21.9 | 44.7 | 110.9 | 57.9 | 40.9 |
| **22** | 32.0 | 32.8 | 28.3 | 140.1 | 140.2 | 56.7 | 33.1 | 22.2 | 44.6 | 110.9 | 58.2 | 40.3 |
| **23** | 32.8 | 33.3 | 28.3 | 140.1 | 139.9 | 57.1 | 32.5 | 21.9 | 44.5 | 111.2 | 57.9 | 40.6 |
| **24** | 32.0 | 33.0 | 27.4 | 140.7 | 139.9 | 56.9 | 32.8 | 21.8 | 45.0 | 111.2 | 57.7 | 40.6 |
| **25** | 32.8 | 32.7 | 27.4 | 140.3 | 140.0 | 57.1 | 33.5 | 21.6 | 44.4 | 111.1 | 57.8 | 40.2 |
| **26** | 32.0 | 32.3 | 28.3 | 140.4 | 140.0 | 56.9 | 32.9 | 22.0 | 44.8 | 111.1 | 58.2 | 40.5 |
| **27** | 32.1 | 32.5 | 27.7 | 140.5 | 140.4 | 56.9 | 33.2 | 21.7 | 44.8 | 110.9 | 58.4 | 40.6 |
| **28** | 32.6 | 32.6 | 27.6 | 140.1 | 140.1 | 56.7 | 32.9 | 21.7 | 44.9 | 110.8 | 58.9 | 40.3 |
| **29** | 32.5 | 32.8 | 27.9 | 140.3 | 139.8 | 56.7 | 33.1 | 21.3 | 45.0 | 110.9 | 58.3 | 40.3 |
| **30** | 32.1 | 33.1 | 28.3 | 140.9 | 139.6 | 56.9 | 33.0 | 21.7 | 45.0 | 111.1 | 58.5 | 40.6 |
| **31** | 32.7 | 32.7 | 28.1 | 140.2 | 140.0 | 56.7 | 33.2 | 21.7 | 44.7 | 111.1 | 59.5 | 40.4 |
| **32** | 32.9 | 32.6 | 27.9 | 140.1 | 139.4 | 56.9 | 33.1 | 22.0 | 45.2 | 111.4 | 58.5 | 40.5 |
| **33** | 32.2 | 32.9 | 28.1 | 140.2 | 139.7 | 57.1 | 33.0 | 21.5 | 45.0 | 110.8 | 58.6 | 40.3 |
| **34** | 32.5 | 32.3 | 27.6 | 140.1 | 139.9 | 56.5 | 33.3 | 21.7 | 45.1 | 110.7 | 58.5 | 40.5 |
| **35** | 32.0 | 32.2 | 27.4 | 139.9 | 139.9 | 56.7 | 32.7 | 21.8 | 45.1 | 110.7 | 57.7 | 40.1 |
| **36** | 32.8 | 33.3 | 27.6 | 139.7 | 139.6 | 56.9 | 32.8 | 21.6 | 44.8 | 111.2 | 57.9 | 40.2 |
| **37** | 32.1 | 32.9 | 27.7 | 139.8 | 139.9 | 57.1 | 33.1 | 21.8 | 45.0 | 111.1 | 58.2 | 40.5 |
| **38** | 32.5 | 33.0 | 27.8 | 139.7 | 140.2 | 56.9 | 32.9 | 21.6 | 44.8 | 111.1 | 58.3 | 40.6 |
| **39** | 32.6 | 32.8 | 28.1 | 140.0 | 140.2 | 56.7 | 33.2 | 21.4 | 44.7 | 111 | 58.4 | 40.9 |
| **40** | 32.9 | 32.7 | 27.6 | 140.1 | 140.4 | 57.0 | 32.9 | 22.1 | 45.0 | 110.9 | 58.2 | 40.5 |

# Appendix C: Cranial Sutures on MRI

## C.1. Cranial sutures on MRI Reviewers' sheet

**Cranial Sutures on MRI**

Thank you for taking part in this study to identify which MR sequence is optimal at identifying cranial sutures.

The MR images have been anonymised, arranged in a random order and numbered 1 to 100. The numbering system permits identification at the end of review – so please ensure your responses correlate with the patient number on the image!

Axial, sagittal and coronal imaging, with varying sequences are included. All images are from children under one year of age.

Please use the attached marking sheets to circle the coronal, sagittal and lambdoid sutures, as follows:

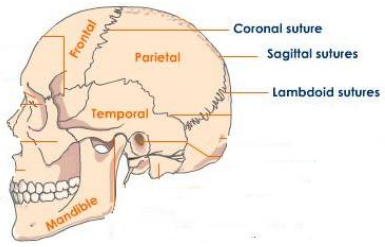
0 = suture cannot be identified

1 = suture is partially identifiable

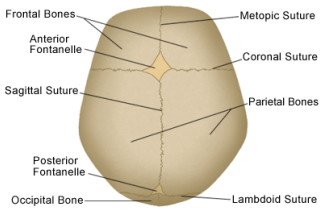
2 = suture fully identifiable & confident of its presence

You do not need to try and differentiate between the open and fused suture.

Please note in the comments section any problems/comments related to the imaging





**Identification of Cranial Sutures on MRI**

Please Circle

**0** = Unable to visualise suture;

**1** = Suture partially visible;

**2** = Suture fully identifiable/ confident regarding presence

| Patient | Coronal | | | Sagittal | | | Lambdoids | | | Comments |
|---|---|---|---|---|---|---|---|---|---|---|
| 1 | 0 | 1 | 2 | 0 | 1 | 2 | 0 | 1 | 2 | |
| 2 | 0 | 1 | 2 | 0 | 1 | 2 | 0 | 1 | 2 | |
| 3 | 0 | 1 | 2 | 0 | 1 | 2 | 0 | 1 | 2 | |
| 4 | 0 | 1 | 2 | 0 | 1 | 2 | 0 | 1 | 2 | |
| 5 | 0 | 1 | 2 | 0 | 1 | 2 | 0 | 1 | 2 | |
| 6 | 0 | 1 | 2 | 0 | 1 | 2 | 0 | 1 | 2 | |
| 7 | 0 | 1 | 2 | 0 | 1 | 2 | 0 | 1 | 2 | |
| 8 | 0 | 1 | 2 | 0 | 1 | 2 | 0 | 1 | 2 | |
| 9 | 0 | 1 | 2 | 0 | 1 | 2 | 0 | 1 | 2 | |
| 10 | 0 | 1 | 2 | 0 | 1 | 2 | 0 | 1 | 2 | |
| 11 | 0 | 1 | 2 | 0 | 1 | 2 | 0 | 1 | 2 | |
| 12 | 0 | 1 | 2 | 0 | 1 | 2 | 0 | 1 | 2 | |
| 13 | 0 | 1 | 2 | 0 | 1 | 2 | 0 | 1 | 2 | |
| 14 | 0 | 1 | 2 | 0 | 1 | 2 | 0 | 1 | 2 | |
| 15 | 0 | 1 | 2 | 0 | 1 | 2 | 0 | 1 | 2 | |
| 16 | 0 | 1 | 2 | 0 | 1 | 2 | 0 | 1 | 2 | |
| 17 | 0 | 1 | 2 | 0 | 1 | 2 | 0 | 1 | 2 | |
| 18 | 0 | 1 | 2 | 0 | 1 | 2 | 0 | 1 | 2 | |
| 19 | 0 | 1 | 2 | 0 | 1 | 2 | 0 | 1 | 2 | |
| 20 | 0 | 1 | 2 | 0 | 1 | 2 | 0 | 1 | 2 | |
| 21 | 0 | 1 | 2 | 0 | 1 | 2 | 0 | 1 | 2 | |
| 22 | 0 | 1 | 2 | 0 | 1 | 2 | 0 | 1 | 2 | |
| 23 | 0 | 1 | 2 | 0 | 1 | 2 | 0 | 1 | 2 | |
| 24 | 0 | 1 | 2 | 0 | 1 | 2 | 0 | 1 | 2 | |
| 25 | 0 | 1 | 2 | 0 | 1 | 2 | 0 | 1 | 2 | |
| 26 | 0 | 1 | 2 | 0 | 1 | 2 | 0 | 1 | 2 | |
| 27 | 0 | 1 | 2 | 0 | 1 | 2 | 0 | 1 | 2 | |
| 92 | 0 | 1 | 2 | 0 | 1 | 2 | 0 | 1 | 2 | |
| 93 | 0 | 1 | 2 | 0 | 1 | 2 | 0 | 1 | 2 | |
| 94 | 0 | 1 | 2 | 0 | 1 | 2 | 0 | 1 | 2 | |
| 95 | 0 | 1 | 2 | 0 | 1 | 2 | 0 | 1 | 2 | |
| 96 | 0 | 1 | 2 | 0 | 1 | 2 | 0 | 1 | 2 | |
| 97 | 0 | 1 | 2 | 0 | 1 | 2 | 0 | 1 | 2 | |
| 98 | 0 | 1 | 2 | 0 | 1 | 2 | 0 | 1 | 2 | |
| 99 | 0 | 1 | 2 | 0 | 1 | 2 | 0 | 1 | 2 | |
| 100 | 0 | 1 | 2 | 0 | 1 | 2 | 0 | 1 | 2 | |

# Appendix D: “Black Bone” MRI in craniosynostosis

# D.1. "Black Bone" MRI in craniosynostosis Ethics

## D.1 Parental Information Sheet for CT & MRI

### PARENT INFORMATION SHEET

### Magnetic Resonance Imaging as a Diagnostic Tool in Craniosynostosis

**REC Ref: 09/H0606/2**

**A study to determine if MRI scans can be used to accurately diagnose and follow-up children with craniosynostosis.**

**PART ONE – INVITATION TO JOIN THE STUDY**

We would like to invite your child to take part in this research study. Before you decide whether to participate it is important for you to understand why the research is being done and what it would involve. You should understand enough about its risks and benefits to be able to make an informed decision. This process is known as informed consent. Please take time to read the following information carefully and discuss it with your family if you wish. Ask if there is anything that is not clear or if you would like more information. Take time to decide whether or not you wish to take part, and thank you for reading this sheet.

**What is the purpose of the study?**

Currently, children who are suspected of having craniosynostosis (the early fusion of parts of the skull) require a CT scan to confirm this. CT stands for computerized tomography. This scan takes pictures of the body and uses a computer to put them together. A CT scanner uses X-rays and is a painless procedure in which the scanner takes a series of X-rays of the body at slightly difference angles to provide very detailed pictures of the inside of the body. The CT scanner is a large machine and looks like a giant doughnut, and the pictures are taken while lying inside it. A lot of people are put to sleep (anaesthetised) whilst having a scan, as the machine needs patients to be very still.

There is however another form of scanning (imaging) called MRI. MRI stands for magnetic resonance imaging. This scanner looks similar to the CT scanner and is located in the same place in the hospital. An MRI scanner instead of using X-rays uses magnets and radio waves to create pictures of the body. Traditionally, MRI scanners are used to examine tissues and organs in the body.

We want to test whether MRI scanners could give doctors just as good pictures of the skull as CT scanners. The reason why we want to test this is if MRI scans could produce just as good pictures as CT scans then patients would not need to be exposed to x-rays, as x-rays do expose the body to small amounts of radiation – if we could eliminate this, this would be beneficial for all patients, but especially so for those people that need to have regular CT scans throughout their lifetime.

**Why have I been chosen?**

The doctors that you have seen today need further scans (images) of your child and have requested a CT scan. These scans will occur for all patients in and outside of this study. However for those that agree to take part in this study, an extra scan will be taken - an MRI.

**Do I have to take part?**

Children in whom a diagnosis of craniosynostosis is suspected are being invited to participate in the study, because the condition is limited to this age group. However it is up to you to decide whether or not your child should take part. If you do decide to allow your child to take part you will be given this information sheet to

keep and be asked to sign a consent form, and you would be free to withdraw at any time and without giving a reason. A decision to withdraw at any time, or a decision not to take part, would not affect the standard of care they receive.

**What will happen to me if I take part?**

For parents of patients who agree for their child to enter the study, their care will not change. All patients will still receive a CT scan. For those that agree to take part in this study, there would be another scan – an MRI. After the CT scan has been performed, and whilst still asleep with anaesthetic, your child would be transferred to the MRI scanner in the next room. The MRI scan would take approximately 20 minutes to complete. After the scans your child would be woken up and looked after in the usual manner. The care before and after the MRI scan will be identical to that of those children not participating in the study.

If, after reading Part One, the study sounds like something you might agree to your child taking part in, you may find it helpful to read the further information in Part Two before you make your decision.

**PART TWO – ADDITIONAL INFORMATION ABOUT THE BLACK BONE STUDY**

**Who is organising and funding the research?**

Members of the radiology, and craniofacial departments within the Oxford Radcliffe Hospital NHS Trust are organising this research. The AO Foundation and New Life Foundation are funding this research.

**Who has approved the study?**

Any research conducted on patients has to be first approved by a NHS Research Ethics Committee (REC). RECs look after the rights, well being and dignity of patients. This study has been reviewed by NRES Committee South Central – Oxford C and given a favourable opinion and the reference 09/H0606/2

**Is there a contact point where I can seek independent advice about participating in this study?**

Yes, general information regarding research can be obtained from the Trust's Patient Advice and Liaison Service (PALS). Further information can be obtained via the Oxford Craniofacial Unit Website (http://www.oxford-craniofacial.org) where there are contact details for independent Craniofacial organisations.

**Are there any risks?**

There are no known risks to having a MRI, however in order to have the MRI, the anaesthetic given to your child would take a little longer than normal due to this extra scan (about 20 minutes longer), but this should not affect your child in any way.

**What if something goes wrong?**

This study is investigating a very established scanning (imaging) method – however it is being used to look at bone (the Skull) where it has traditionally been used to look at soft tissues and organs. MRI scans are used all over the world and have been shown to be safe. However, NHS bodies are legally liable for the negligent acts and omissions of their employees. If your child is harmed whilst taking part in a clinical trial as a result of negligence on the part of a member of the study team this liability cover would apply.

Non-negligent harm is not covered by the NHS indemnity scheme. The Oxford Radcliffe NHS Trust, therefore, cannot agree in advance to pay compensation in these circumstances. In exceptional circumstances an ex-gratia payment may be offered.

**What are the possible benefits of taking part?**

It is hoped in the longer term that this study will contribute to improved standards of care for patients with craniosynostosis, based on the information we record on patients in this study. There are no immediate benefits to participating in the study. Should the study be successful, MRI may replace CT as a method of imaging children in the future.

**Would my taking part in this study be kept confidential?**

All information which would be collected about participants during the course of the study would be kept strictly confidential and would include information such as the scans taken. As the MRI scan may be of potential benefit in the care of your child, the imaging will remain on their medical records so that they can be looked at a future date. As the scans will include the brain, these will be looked at by consultant radiologists.

**What happens if I have any questions, or concerns about the study?**

If you have any questions concerning the study, please ask the person presenting this form to you, or contact Miss Eley on 01865 743103, or by writing to Nuffield Department of Surgical Sciences, Level 6 Academic Block, John Radcliffe Hospital, Headley Way, Oxford OX3 9DU.

**What if I wish to complain?**

If you have any comments, concerns or complaints about any aspect of the way you have been approached or treated during the course of this study, you should contact the Patient Advice Liaison Service (PALS) at John Radcliffe Hospital, who will be able to guide you through the hospital complaints process.

**Where can I find the results of the study?**

The results are estimated to be published in late 2012. If you would like a copy, please contact Miss Eley, Nuffield Department of Surgical Sciences, Level 6, John Radcliffe Hospital, Headley Way, Headington, Oxford, OX3 9DU.

## D.2 Parental Consent Form for CT & MRI

# PARENTAL CONSENT FORM FOR CT & MRI

## MRI as a diagnostic tool in craniosynostosis

**REC Ref No: 09/H0606/2**

**Title of project: A study to determine if MRI scans can be used to accurately diagnose and follow-up children with craniosynostosis.**

**Please initial boxes**

| | | |
|---|---|---|
| 1 | I confirm that I have read and understood the information sheet dated September 2011, Version 04 for the above study and have had the opportunity to ask questions …….……..... | ☐ |
| 2 | I confirm that I have had sufficient time to consider whether or not to include my child in this study…….... | ☐ |
| 3 | I understand that my child's participation is voluntary & that I am free to withdraw them at any time, without giving any reason & without my child's medical care or legal rights being affected…….... | ☐ |
| 4 | I understand that sections of any of my child's medical notes may be looked at by responsible individuals involved with the study. I give permission for these individuals to have access to these records …….... | ☐ |
| 5 | I give permission that anonymised data may be made available to other groups for the purposes of improving clinical diagnosis and treatment..... | ☐ |
| 6 | I agree for my child to take part in the above study …….... | ☐ |

| Name of child | Name of child's parent or guardian | Date | Signature |
|---|---|---|---|
| | | | |

| Name of person taking consent | Date | Signature |
|---|---|---|
| | | |

MRI as a diagnostic tool in craniosynostosis Study number ___ ___

Original: To be retained by the Chief Investigator

Copies: 1 for patient, 1 to be kept with hospital notes

## D.3 Patient/Parent Information Sheet for MRI only

# PATIENT/ PARENT INFORMATION SHEET

## Magnetic Resonance Imaging as a Diagnostic Tool in Craniosynostosis

**REC Ref: 09/H0606/2**

**A study to determine if MRI scans can be used to accurately diagnose and follow-up children with craniosynostosis.**

### PART ONE – INVITATION TO JOIN THE STUDY

We would like to invite you/your child to take part in this research study. Before you decide whether to participate it is important for you to understand why the research is being done and what it would involve. You should understand enough about its risks and benefits to be able to make an informed decision. This process is known as informed consent. Please take time to read the following information carefully and discuss it with your family if you wish. Ask if there is anything that is not clear or if you would like more information. Take time to decide whether or not you wish to take part, and thank you for reading this sheet.

**What is the purpose of the study?**

Currently, children who are suspected of having craniosynostosis (the early fusion of parts of the skull) require a CT scan to confirm this. CT stands for computerized tomography. This scan takes pictures of the body and uses a computer to put them together. A CT scanner uses X-rays and is a painless procedure in which the scanner takes a series of X-rays of the body at slightly difference angles to provide very detailed pictures of the inside of the body. The CT scanner is a large machine and looks like a giant doughnut, and the pictures are taken while lying inside it. There is however another form of scanning (imaging) called MRI. MRI stands for magnetic resonance imaging. This scanner looks similar to the CT scanner and is located in the same place in the hospital. An MRI scanner instead of using X-rays uses magnets and radio waves to create pictures of the body. Traditionally, MRI scanners are used to examine tissues and organs in the body.

We want to test whether MRI scanners could give doctors just as good pictures of the skull as CT scanners. The reason why we want to test this is if MRI scans could produce just as good pictures as CT scans then patients would not need to be exposed to x-rays, as x-rays do expose the body to small amounts of radiation – if we could eliminate this, this would be beneficial for all patients, but especially so for those people that need to have regular CT scans throughout their lifetime.

**Why have I been chosen?**

The doctors looking after you/your child have identified the early fusion of skull sutures, and believe that you/your child would be suitable to participate in the study.

**Do I have to take part?**

Children/adults with a diagnosis of craniosynostosis who have not had surgery are being invited to participate in the study. However it is up to you to decide whether or not you/your child should take part. If you do decide to allow your child to take part you will be given this information sheet to keep and be asked to sign a consent form, and you would be free to withdraw at any time and without giving a reason. A decision to withdraw at any time, or a decision not to take part, would not affect the standard of care you/they receive.

**What will happen to me if I take part?**

For parents of patients who agree for their child to enter the study, their care will not change. For those that agree to take part in this study, they will receive an MRI.

If, after reading Part One, the study sounds like something you might agree to your child taking part in, you may find it helpful to read the further information in Part Two before you make your decision.

## PART TWO – ADDITIONAL INFORMATION ABOUT THE BLACK BONE STUDY

**Who is organising and funding the research?**

Members of the radiology and craniofacial departments within the Oxford Radcliffe Hospital NHS Trust are organising this research. The AO Foundation and New Life Foundation are funding this research.

**Who has approved the study?**

Any research conducted on patients has to be first approved by a NHS Research Ethics Committee (REC). RECs look after the rights, well being and dignity of patients. This study has been reviewed by NRES Committee South Central – Oxford C and given a favourable opinion and the reference 09/H0606/2

**Is there a contact point where I can seek independent advice about participating in this study?**

Yes, general information regarding research can be obtained from the Trust's Patient Advice and Liaison Service (PALS). Further information can be obtained via the Oxford Craniofacial Unit Website (http://www.oxford-craniofacial.org) where there are contact details for independent Craniofacial organisations.

**Are there any risks?**

There are no known risks to having a MRI. Some people find the scans a little claustrophobic or noisy, but you/your child will be given ear protection.

**What if something goes wrong?**

This study is investigating a very established scanning (imaging) method – however it is being used to look at bone (the Skull) where it has traditionally been used to look at soft tissues and organs. MRI scans are used all over the world and have been shown to be safe. However, NHS bodies are legally liable for the negligent acts and omissions of their employees. If your child is harmed whilst taking part in a clinical trial as a result of negligence on the part of a member of the study team this liability cover would apply.

Non-negligent harm is not covered by the NHS indemnity scheme. The Oxford Radcliffe NHS Trust, therefore, cannot agree in advance to pay compensation in these circumstances. In exceptional circumstances an ex-gratia payment may be offered.

**What are the possible benefits of taking part?**

It is hoped in the longer term that this study will contribute to improved standards of care for patients with craniosynostosis, based on the information we record on patients in this study. There are no immediate benefits to participating in the study. Should the study be successful, MRI may replace CT as a method of imaging children in the future.

**Would my taking part in this study be kept confidential?**

All information which would be collected about participants during the course of the study would be kept strictly confidential and would include information such as the scans taken. As the MRI scan may be of potential benefit in the care of you/your child, the imaging will remain on their medical records so that they can be looked at at a future date. As the scans will include the brain, these will be looked at by consultant radiologists.

**What happens if I have any questions, or concerns about the study?**

If you have any questions concerning the study, please ask the person presenting this form to you, or contact Eley on 01865 743103, or in writing to Nuffield Department of Surgical Sciences, Level 6, John Radcliffe Hospital, Headley Way, Headington, Oxford, OX3 9DU

**What if I wish to complain?**

If you have any comments, concerns or complaints about any aspect of the way you have been approached or treated during the course of this study, you should contact the Patient Advice Liaison Service (PALS) at John Radcliffe Hospital, who will be able to guide you through the hospital complaints process.

**Where can I find the results of the study?**

The results are estimated to be published in late 2012. If you would like a copy, please contact Miss Eley, Nuffield Department of Surgical Sciences, Level 6, John Radcliffe Hospital, Headley Way, Headington, Oxford, OX3 9DU.

## D.4 Reviewers' sheet for "Black Bone" MRI & craniosynostosis

**Accuracy of diagnosis of craniosynostosis on Black Bone MRI**

The purpose of this study is to determine if prematurely fused sutures (craniosynostosis) can be distinguished from normal sutures.

Please review each of the anonymised Black Bone MRI data-sets, and assess the cranial sutures independently by circling a score as per the key below.

If you believe the reason that you are unable to visualise the suture is a result of craniosynostosis, please tick the appropriate box.

Please Circle: **0** = Unable to visualise suture;
**1** = Suture partially visible;
**2** = Suture fully identifiable/ confident regarding presence

| Patient | Identification of Cranial Sutures (circle) | | | | | | | | | | | | | | | | | | Evidence of Synostosis? (tick if yes) | | | | | | Comments |
|---|---|---|---|---|---|---|---|---|---|---|---|---|---|---|---|---|---|---|---|---|---|---|---|---|---|
| | Metopic | | | Coronal | | | | | | Sagittal | | | Lambdoids | | | | | | Metopic | Coronal | | Sagittal | Lambdoid | | |
| | | | | Right | | | Left | | | | | | Right | | | Left | | | | Right | Left | | Right | Left | |
| 1 | 0 | 1 | 2 | 0 | 1 | 2 | 0 | 1 | 2 | 0 | 1 | 2 | 0 | 1 | 2 | 0 | 1 | 2 | | | | | | | |
| 2 | 0 | 1 | 2 | 0 | 1 | 2 | 0 | 1 | 2 | 0 | 1 | 2 | 0 | 1 | 2 | 0 | 1 | 2 | | | | | | | |
| 3 | 0 | 1 | 2 | 0 | 1 | 2 | 0 | 1 | 2 | 0 | 1 | 2 | 0 | 1 | 2 | 0 | 1 | 2 | | | | | | | |
| 4 | 0 | 1 | 2 | 0 | 1 | 2 | 0 | 1 | 2 | 0 | 1 | 2 | 0 | 1 | 2 | 0 | 1 | 2 | | | | | | | |
| 5 | 0 | 1 | 2 | 0 | 1 | 2 | 0 | 1 | 2 | 0 | 1 | 2 | 0 | 1 | 2 | 0 | 1 | 2 | | | | | | | |
| 6 | 0 | 1 | 2 | 0 | 1 | 2 | 0 | 1 | 2 | 0 | 1 | 2 | 0 | 1 | 2 | 0 | 1 | 2 | | | | | | | |
| 7 | 0 | 1 | 2 | 0 | 1 | 2 | 0 | 1 | 2 | 0 | 1 | 2 | 0 | 1 | 2 | 0 | 1 | 2 | | | | | | | |
| 8 | 0 | 1 | 2 | 0 | 1 | 2 | 0 | 1 | 2 | 0 | 1 | 2 | 0 | 1 | 2 | 0 | 1 | 2 | | | | | | | |
| 9 | 0 | 1 | 2 | 0 | 1 | 2 | 0 | 1 | 2 | 0 | 1 | 2 | 0 | 1 | 2 | 0 | 1 | 2 | | | | | | | |
| 10 | 0 | 1 | 2 | 0 | 1 | 2 | 0 | 1 | 2 | 0 | 1 | 2 | 0 | 1 | 2 | 0 | 1 | 2 | | | | | | | |
| 11 | 0 | 1 | 2 | 0 | 1 | 2 | 0 | 1 | 2 | 0 | 1 | 2 | 0 | 1 | 2 | 0 | 1 | 2 | | | | | | | |
| 12 | 0 | 1 | 2 | 0 | 1 | 2 | 0 | 1 | 2 | 0 | 1 | 2 | 0 | 1 | 2 | 0 | 1 | 2 | | | | | | | |

## D.5 Assessor results for review of "Black Bone" in craniosynostosis

| | Metopic | | | Right Coronal | | | Left Coronal | | | Sagittal | | | Right Lambdoid | | | Left Lambdoid | | |
|---|---|---|---|---|---|---|---|---|---|---|---|---|---|---|---|---|---|---|
| | 1 | 2 | 3 | 1 | 2 | 3 | 1 | 2 | 3 | 1 | 2 | 3 | 1 | 2 | 3 | 1 | 2 | 3 |
| **1** | 2 | 0 | 0 | 2 | 1 | 2 | 2 | 1 | 2 | 0 | 0 | 0 | 2 | 1 | 2 | 2 | 1 | 2 |
| **2** | 1 | 0 | 0 | 2 | 0 | 2 | 2 | 0 | 2 | 0 | 0 | 0 | 2 | 2 | 2 | 2 | 2 | 2 |
| **3** | 0 | 0 | 0 | 1 | 0 | 0 | 1 | 0 | 2 | 1 | 1 | 2 | 1 | 0 | 2 | 1 | 0 | 2 |
| **4** | 2 | 0 | 0 | 2 | 2 | 2 | 2 | 2 | 2 | 2 | 2 | 2 | 1 | 2 | 2 | 1 | 2 | 2 |
| **5** | 0 | 1 | 0 | 2 | 2 | 2 | 2 | 2 | 2 | 2 | 2 | 2 | 2 | 2 | 2 | 2 | 2 | 2 |
| **6** | 2 | 1 | 0 | 2 | 1 | 2 | 2 | 1 | 2 | 0 | 0 | 0 | 2 | 1 | 2 | 2 | 1 | 2 |
| **7** | 1 | 1 | 0 | 2 | 2 | 2 | 2 | 2 | 2 | 2 | 2 | 2 | 1 | 2 | 2 | 1 | 2 | 2 |
| **8** | 2 | 1 | 2 | 0 | 0 | 0 | 2 | 0 | 2 | 2 | 2 | 2 | 2 | 2 | 2 | 2 | 2 | 2 |
| **9** | 0 | 0 | 0 | 2 | 1 | 2 | 2 | 1 | 2 | 0 | 0 | 0 | 2 | 1 | 2 | 2 | 1 | 2 |
| **10** | 0 | 0 | 0 | 2 | 1 | 2 | 2 | 1 | 2 | 0 | 0 | 0 | 2 | 2 | 2 | 2 | 2 | 2 |
| **11** | 2 | 0 | 2 | 2 | 1 | 2 | 2 | 1 | 2 | 0 | 0 | 0 | 2 | 1 | 2 | 2 | 1 | 2 |
| **12** | 0 | 0 | 0 | 2 | 2 | 2 | 2 | 2 | 2 | 2 | 1 | 2 | 2 | 2 | 2 | 2 | 2 | 2 |

## D.6 Cranial Suture widths on "Black Bone"

Cranial suture width measurements (mm) on "Black Bone" in two children with normal cranial sutures.

| Sagittal | | | | Coronal | | | |
|---|---|---|---|---|---|---|---|
| Patient 1 | | Patient 3 | | Patient 1 | | Patient 3 | |
| Anterior | Posterior | Anterior | Posterior | Right | Left | Right | Left |
| 0.9 | 0.8 | 1.2 | 1 | 0.7 | 0.7 | 1 | 1 |
| 0.7 | 0.8 | 1 | 1.2 | 1 | 0.9 | 1.2 | 1.2 |
| 0.8 | 1 | 1.2 | 1 | 0.8 | 0.6 | 0.7 | 1 |
| 1 | 0.9 | 1.2 | 0.8 | 0.6 | 0.7 | 1 | 1.3 |
| 1.1 | 1 | 1 | 1 | 0.8 | 0.7 | 1 | 1.2 |
| 1 | 0.9 | 1.2 | 0.8 | 0.7 | 0.7 | 0.8 | 0.8 |
| 0.9 | 0.9 | 1.1 | 1 | 1 | 1 | 1.3 | 1 |
| 1 | 1.2 | 1 | 0.8 | 1 | 1.1 | 1.2 | 1.3 |
| | 1.1 | 1.2 | 1.1 | 1.1 | 0.8 | 1 | 1.3 |
| | 0.8 | 1.2 | 1 | 1.2 | 0.9 | 0.9 | 1.3 |
| | 0.7 | 0.9 | 0.8 | 1.1 | 1.1 | 0.8 | 1.1 |
| | 1 | 0.8 | 1 | 0.8 | 1.1 | 0.8 | 1.1 |
| | | 1.3 | 1.2 | 1.2 | 0.9 | | |
| | | 1 | 1.2 | 1.2 | 1.1 | | |
| | | | 1.3 | 1.3 | 0.8 | | |
| | | | 1.6 | 1.3 | 1 | | |
| | | | 1.3 | | | | |
| | | | 1.3 | | | | |
| | | | 0.9 | | | | |
| | | | 0.8 | | | | |
| | | | 1 | | | | |
| | | | 1.2 | | | | |
| | | | 0.8 | | | | |
| | | | 0.8 | | | | |
| | | | 1 | | | | |
| | | | 1 | | | | |
| | | | 1.1 | | | | |
| | | | 1.1 | | | | |
| | | | 1.1 | | | | |
| | | | 1.3 | | | | |
| | | | 1.2 | | | | |
| | | | 1 | | | | |

# Appendix E: Cephalometrics

## E.1. Cephalometric accuracy of "Black Bone" MRI

### E.1.1. Patient Information Sheet for MRI

# PATIENT INFORMATION SHEET

## The cephalometric accuracy of Magnetic Resonance Imaging

**REC Ref: 09/H0505/120**

**A study to determine if MRI scans can be used to obtain cephalometrically accurate measurements.**

**PART ONE – INVITATION TO JOIN THE STUDY**

We would like to invite you to take part in this research study. Before you decide whether to participate it is important for you to understand why the research is being done and what it would involve. You should understand enough about its risks and benefits to be able to make an informed decision. This process is known as informed consent. Please take time to read the following information carefully and discuss it with your family if you wish. Ask if there is anything that is not clear or if you would like more information. Take time to decide whether or not you wish to take part, and thank you for reading this sheet.

**What is the purpose of the study?**

There is a form of scanning (imaging) called MRI, which can produce high quality images of your head. MRI stands for magnetic resonance imaging. An MRI scanner instead of using X-rays uses magnets and radio waves to create pictures of the body. As MRI does not use x-rays there is no associated radiation risk. Traditionally, MRI scanners are used to examine tissues and organs in the body.

We want to test whether MRI scans can provide accurate measurements of the skull and facial skeleton. If MRI scans could produce accurate measurements then patients would not need to be exposed to x-rays, which would be beneficial for all patients, but especially so for those people that need regular imaging throughout their lifetime.

**Why have I been chosen?**

The doctors that you have seen today need plain x-rays of the facial skeleton as part of orthodontic assessment, or oral surgery. These x-rays are essential whether included in the study or not. However for those that agree to take part in this study, an extra scan (image) will be taken - an MRI.

**Do I have to take part?**

Patients in whom cephalometric x-rays are being requested are being invited to participate, since the x-rays can be compared to the measurements obtained from MRI. However it is up to you to decide whether or not you should take part. If you do decide to participate you will be given this information sheet to keep and be asked to sign a consent form, and you would be free to withdraw at any time and without giving a reason. A decision to withdraw at any time, or a decision not to take part, would not affect the standard of care you receive.

**What will happen to me if I take part?**

For patients who agree to enter the study, their care will not change. All patients will still receive plain x-rays. For those that agree to take part in this study, there would be an additional MRI scan. The MRI scan would take approximately 20 minutes to complete, and would take place at the John Radcliffe or Churchill Hospital site.

If, after reading Part One, the study sounds like something you might agree to taking part in, you may find it helpful to read the further information in Part Two before you make your decision.

**PART TWO – ADDITIONAL INFORMATION ABOUT THE BLACK BONE STUDY**

**Who is organising and funding the research?**

Members of the radiology, and craniofacial departments within the Oxford Radcliffe Hospital NHS Trust are organising this research. AO Foundation is funding this research, and it is being sponsored by the Oxford Radcliffe Hospitals NHS Trust.

**Who has approved the study?**

Any research conducted on patients has to be first approved by a NHS Research Ethics Committee (REC). RECs look after the rights, well being and dignity of patients. This study has been reviewed by a REC and given a favourable opinion and the reference 09/H0505/120

**Is there a contact point where I can seek independent advice about participating in this study?**

Yes, general information regarding research can be obtained from the Trust's Patient Advice and Liaison Service (PALS). Further information regarding MRI scans can be obtained via the NHS website (www.nhs.uk).

**Are there any risks?**

There are no known risks to having a MRI. Occasionally, people find the scan a little noisy, or claustrophobic. You will be given ear plugs to help with the noise, and if you cannot tolerate the scan for whatever reason, the scan will be stopped.

**What if something goes wrong?**

This study is investigating a very established scanning (imaging) method – however it is being used to look at bone (the Skull) where it has traditionally been used to look at soft tissues and organs. MRI scans are used all over the world and have been shown to be safe. However, NHS bodies are legally liable for the negligent acts and omissions of their employees. If you are harmed whilst taking part in a clinical trial as a result of negligence on the part of a member of the study team this liability cover would apply.

Non-negligent harm is not covered by the NHS indemnity scheme. The Oxford Radcliffe NHS Trust, therefore, cannot agree in advance to pay compensation in these circumstances. In exceptional circumstances an ex-gratia payment may be offered.

**What are the possible benefits of taking part?**

It is hoped in the longer term that this study will contribute to improved standards of care for patients with abnormalities of the skull and facial skeleton, based on the information we record on patients in this study. There are no immediate benefits to participating in the study.

**Would my taking part in this study be kept confidential?**

All information which would be collected about participants during the course of the study would be kept strictly confidential and would include information such as the scans taken. All data collected would be "anonymised"- that is, any information that leaves the hospital would have all names and address removed. Individuals could not be recognised from it. Anonymised data may be made available to other groups for the purposes of improving clinical diagnosis and treatment.

**What happens if I have any questions, or concerns about the study?**

If you have any questions concerning the study, please ask the person presenting this form to you, or contact Miss Eley, on 01865 743103, or by writing to Mr Watt-Smith or in writing to Nuffield Department of Surgical Sciences, Level 6 Academic Block, John Radcliffe Hospital, Headley Way, Oxford OX3 9DU.

**What if I wish to complain?**

If you have any comments, concerns or complaints about any aspect of the way you have been approached or treated during the course of this study, you should contact the Patient Advice Liaison Service (PALS) at John Radcliffe Hospital, who will be able to guide you through the hospital complaints process.

**Where can I find the results of the study?**

The results are estimated to be published in 2010. If you would like a copy, please contact Miss Eley, Nuffield Department of Surgical Sciences, Level 6 Academic Block, John Radcliffe Hospital, Headley Way, Headington, Oxford, OX3 9DU.

### E.1.2. Patient Consent form for MRI

# PATIENT CONSENT FORM

## Cephalometric accuracy of MRI

**REC Ref No: 09/H0505/120**

**Title of project: A study to determine if MRI scans can be used to obtain accurate cephalometric measurements**

**Please initial boxes**

| | | |
|---|---|---|
| 1. | I confirm that I have read and understood the information sheet dated November 2009, Version 02 for the above study and have had the opportunity to ask questions ……..……..... | ☐ |
| 2 | I confirm that I have had sufficient time to consider whether or not to participate in this study…….... | ☐ |
| 3 | I understand that my participation is voluntary & that I am free to withdraw at any time, without giving any reason & without my medical care or legal rights being affected..... | ☐ |
| 4 | I understand that relevant sections of my medical notes and data collected during the study may be looked at by individuals from regulatory authorities or from the NHS Trust, where it is relevant to my taking part in this research. I give my permission for these individuals to have access to my records……..... | ☐ |
| 5 | I understand that my scan will be reviewed by a consultant radiologist, and if any unexpected abnormalities are detected, I agree for my hospital doctors and GP to be informed so that I have the opportunity to discuss further imaging options…… | ☐ |
| 6 | I give permission that anonymised data may be made available to other groups for the purposes of improving clinical diagnosis and treatment…… | ☐ |
| 7 | I agree to take part in the above study ……..… | ☐ |

| | | |
|---|---|---|
| _____ | _____ | _____ |
| Name of patient | Date | Patient Signature |
| _____ | _____ | _____ |
| Name of person taking consent | Date | Signature |

Please check this box if you would like to receive a copy of the results of this study once available ☐

Cephalometric accuracy of MRI Study number ___ ___

Original: To be retained by the Chief Investigator; Copies: 1 for patient, 1 to be kept with hospital notes

### E.1.3. Consent form for patients under 16 years of age

## CONSENT FORM FOR PARTICIPANTS UNDER 16 YEARS OF AGE

## Cephalometric accuracy of MRI

**REC Ref No: 09/H0505/120**

**Title of project: A study to determine if MRI scans can be used to obtain accurate cephalometric measurements**

**Please initial boxes**

| | | |
|---|---|---|
| E.1. | I confirm that I have read and understood the information sheet dated October 2010, Version 02 for the above study and have had the opportunity to ask questions ……..…… | ☐ |
| 2 | I confirm that I have had sufficient time to consider whether or not to include my child in this study……. | ☐ |
| 3 | I understand that my child's participation is voluntary & that I am free to withdraw them at any time, without giving any reason & without my child's medical care or legal rights being affected…… | ☐ |
| 4 | I understand that relevant sections of my child's medical notes and data collected during the study may be looked at by individuals from regulatory authorities or from the NHS Trust, where it is relevant to my taking part in this research. I give my permission for these individuals to have access to my child's records…..... | ☐ |
| 5 | I understand that my child's scan will be reviewed by a consultant radiologist, and if any Unexpected abnormalities are detected, I agree for my child's hospital doctors and GP to be informed so that we have the opportunity to discuss further imaging options…… | ☐ |
| 6 | I give permission that anonymised data may be made available to other groups for the purposes of improving clinical diagnosis and treatment…… | ☐ |
| 7 | I agree to my child taking part in the above study …… | ☐ |
| 8 | I have had the opportunity to ask any questions …… | ☐ |

| Name of child | Date | Name of Parent or Guardian | Relationship to child | Parent or guardian Signature |
|---|---|---|---|---|
| | | | | |

| Name of person taking consent | Date | Signature |
|---|---|---|
| | | |

**PATIENT CONSENT**

I have read and understood the patient information sheet, and I agree to participate in the study
I have had the opportunity to ask any questions

| Name of patient | Date | Signature |
|---|---|---|
| | | |

| Name of person taking consent | Date | Signature |
|---|---|---|
| | | |

Please check this box if you would like to receive a copy of the results of this study once available ☐

Cephalometric accuracy of MRI Study number ___ ___
Original: To be retained by the Chief Investigator; Copies: 1 for patient, 1 to be kept with hospital notes

## E.2. AWW Cephalometric Results

### E.2.1. Volunteer 1: Lateral Cephalogram

| | SNA Angle | SNB Angle | ANB Angle | Interincisal Angle | 1-NA angle | 1-NA | 1-NB Angle | 1-NB | S-N | PNS-ANS | S-ANS | Me-ANS | N-Pog | S-Gn | N-A | N-B |
|---|---|---|---|---|---|---|---|---|---|---|---|---|---|---|---|---|
| 1 | 83 | 79 | 5 | 127 | 23 | 3.4 | 25 | 5.7 | 68.2 | 54.4 | 86.3 | 63 | 99 | 112.6 | 51.6 | 87.3 |
| 1 | 83 | 78 | 5 | 127 | 23 | 3.7 | 25 | 5.7 | 68.7 | 54.2 | 86.3 | 63.2 | 99.2 | 112.2 | 51.4 | 87.3 |
| 1 | 83 | 78 | 4 | 127 | 23 | 3.2 | 25 | 6.1 | 68.1 | 54.5 | 86.1 | 62.8 | 99.5 | 112.2 | 51.6 | 87.7 |
| 1 | 83 | 78 | 5 | 127 | 23 | 3.9 | 25 | 5.5 | 68.1 | 54.2 | 86.4 | 63 | 99.4 | 112.2 | 51.2 | 87.5 |
| 1 | 83 | 78 | 4 | 127 | 23 | 3.9 | 25 | 5.7 | 68.5 | 54.5 | 86.3 | 63 | 99.6 | 112.6 | 51.6 | 87.5 |
| 1 | 83 | 78 | 4 | 127 | 23 | 3.9 | 25 | 5.7 | 68.6 | 54.2 | 86.5 | 62.8 | 99.5 | 112.4 | 51.4 | 87.5 |
| 1 | 83 | 78 | 4 | 127 | 23 | 3.9 | 25 | 5.4 | 68.7 | 54.2 | 86.5 | 62.8 | 99.2 | 112.1 | 51.4 | 87.5 |
| 1 | 83 | 79 | 5 | 127 | 23 | 3.4 | 25 | 5.7 | 68.5 | 54 | 86.1 | 63.1 | 99.2 | 112.9 | 51.4 | 87.6 |
| 1 | 83 | 78 | 4 | 127 | 23 | 3.4 | 25 | 5.7 | 68.3 | 54.5 | 86 | 62.8 | 99.2 | 113 | 51.4 | 87.6 |
| 1 | 83 | 78 | 5 | 127 | 23 | 3.2 | 25 | 5.4 | 68.4 | 54.4 | 86 | 62.9 | 99.6 | 112.5 | 51.4 | 87.5 |
| 2 | 83 | 79 | 4 | 114 | 31 | 3.9 | 32 | 5.7 | 67.6 | 51.1 | 83.1 | 63.2 | 99.8 | 112.7 | 50.6 | 88.2 |
| 2 | 83 | 79 | 4 | 114 | 31 | 3.9 | 32 | 5.4 | 68 | 51 | 83 | 62.7 | 99.6 | 112.8 | 50.6 | 88.5 |
| 2 | 83 | 79 | 4 | 114 | 31 | 3.9 | 32 | 5.5 | 67.6 | 51.4 | 83.2 | 62.7 | 99.6 | 112.3 | 50.6 | 88 |
| 2 | 83 | 79 | 4 | 114 | 31 | 4.3 | 32 | 5.5 | 67.6 | 51.4 | 83.1 | 63 | 99.8 | 112.6 | 50.6 | 88.8 |
| 2 | 83 | 79 | 4 | 114 | 31 | 4 | 32 | 5.3 | 67.8 | 51.1 | 82.9 | 62.8 | 99.6 | 112.6 | 50.8 | 88.2 |
| 2 | 83 | 79 | 4 | 114 | 31 | 4 | 32 | 5.5 | 67.6 | 51 | 83.2 | 62.9 | 99.5 | 112.5 | 50.8 | 88.3 |
| 2 | 83 | 79 | 4 | 114 | 31 | 3.7 | 32 | 5.3 | 68.3 | 51.1 | 83.5 | 62.7 | 99.6 | 112.8 | 51.2 | 88.3 |
| 2 | 83 | 79 | 4 | 114 | 31 | 4.1 | 32 | 5.3 | 67.8 | 51.1 | 83 | 63.2 | 99.4 | 112.5 | 50.6 | 88.3 |
| 2 | 83 | 79 | 4 | 114 | 31 | 3.9 | 32 | 5.4 | 67.8 | 51 | 83.2 | 62.7 | 99.6 | 112.4 | 50.4 | 88.6 |
| 2 | 83 | 79 | 4 | 114 | 31 | 3.9 | 32 | 5.1 | 67.9 | 51.1 | 82.6 | 63.2 | 99.6 | 112.3 | 50.6 | 88 |
| 3 | 83 | 79 | 4 | 108 | 29 | 3.2 | 39 | 5.5 | 68.2 | 52.2 | 84 | 62.6 | 100.7 | 112.8 | 50.6 | 88.5 |
| 3 | 83 | 79 | 4 | 108 | 29 | 3.7 | 39 | 5.5 | 68.2 | 52.2 | 83.9 | 62.9 | 100.6 | 112.8 | 50.8 | 88.9 |
| 3 | 83 | 79 | 4 | 108 | 29 | 3.8 | 39 | 5.3 | 68.1 | 52.2 | 83.9 | 63.2 | 100.7 | 112.7 | 51.1 | 89.1 |
| 3 | 83 | 79 | 4 | 108 | 29 | 3.7 | 39 | 4.9 | 68.1 | 51.8 | 84 | 62.7 | 100.4 | 112.6 | 50.4 | 88.9 |
| 3 | 83 | 79 | 4 | 108 | 29 | 3.4 | 39 | 5.3 | 68.1 | 51.8 | 93.9 | 62.6 | 100.9 | 112.6 | 50.8 | 88.9 |
| 3 | 83 | 79 | 4 | 108 | 29 | 3.2 | 39 | 5.3 | 68.1 | 52.2 | 84.2 | 62.8 | 100.6 | 112.5 | 50.8 | 88.9 |
| 3 | 83 | 79 | 4 | 108 | 29 | 3.4 | 39 | 5.4 | 68.2 | 52 | 83.9 | 62.9 | 100.9 | 112.8 | 50.8 | 89.1 |
| 3 | 83 | 79 | 4 | 108 | 29 | 3.7 | 39 | 5.4 | 68.2 | 52.2 | 83.7 | 63.3 | 100.9 | 112.8 | 51 | 88.9 |
| 3 | 83 | 79 | 4 | 108 | 29 | 3.7 | 39 | 5.3 | 68.1 | 52.2 | 83.7 | 62.7 | 100.9 | 112.5 | 51.1 | 89.4 |
| 3 | 83 | 79 | 4 | 108 | 29 | 3.7 | 39 | 5.5 | 68.1 | 52.4 | 83.8 | 62.9 | 100.5 | 112.8 | 50.8 | 88.9 |
| 4 | 84 | 79 | 5 | 107 | 35 | 3.5 | 34 | 5.9 | 67.6 | 53.2 | 84.7 | 63 | 99.4 | 112.5 | 50.6 | 88.5 |
| 4 | 84 | 79 | 5 | 107 | 35 | 3.9 | 34 | 5.9 | 67.8 | 53 | 85 | 62.7 | 99.2 | 112.6 | 50.2 | 88.5 |
| 4 | 84 | 79 | 5 | 107 | 35 | 3.4 | 34 | 5.9 | 67.9 | 53 | 84.9 | 62.6 | 98.9 | 112.6 | 50.4 | 88.3 |
| 4 | 84 | 79 | 5 | 107 | 35 | 3.9 | 34 | 5.7 | 67.9 | 53.6 | 84.6 | 62.7 | 99 | 112.3 | 50.4 | 88.3 |
| 4 | 84 | 79 | 5 | 107 | 35 | 3.5 | 34 | 5.7 | 67.6 | 53.2 | 85 | 62.6 | 99.4 | 112.5 | 50.4 | 88.7 |
| 4 | 84 | 79 | 5 | 107 | 35 | 3.9 | 34 | 5.9 | 68.1 | 53 | 84.8 | 62.8 | 99 | 112.5 | 50.3 | 88.5 |
| 4 | 84 | 79 | 5 | 107 | 35 | 3.9 | 34 | 5.7 | 67.8 | 53.2 | 84.9 | 62.9 | 99.2 | 112.5 | 50.4 | 88.5 |
| 4 | 84 | 79 | 5 | 107 | 35 | 3.5 | 34 | 5.9 | 67.8 | 53.2 | 84.7 | 62.6 | 99.2 | 112.5 | 50.2 | 88.6 |
| 4 | 84 | 79 | 5 | 107 | 35 | 3.7 | 34 | 5.7 | 67.8 | 53.4 | 84.6 | 62.6 | 99.2 | 112.8 | 50.2 | 88.3 |
| 4 | 84 | 79 | 5 | 107 | 35 | 3.9 | 34 | 5.9 | 67.8 | 52.8 | 84.9 | 62.6 | 99.2 | 112.8 | 50.4 | 88.6 |
| 5 | 83 | 79 | 4 | 114 | 30 | 3.2 | 31 | 5.5 | 68.1 | 53.4 | 85.2 | 63.3 | 99.4 | 112.5 | 50.6 | 88.5 |
| 5 | 83 | 79 | 4 | 114 | 30 | 3.5 | 31 | 5.4 | 68 | 53.6 | 84.6 | 63.1 | 99.4 | 112.5 | 50.4 | 88.5 |
| 5 | 83 | 79 | 4 | 114 | 30 | 3.9 | 31 | 6.1 | 68.1 | 53.6 | 85 | 63.2 | 99.4 | 112.6 | 50.2 | 88.3 |
| 5 | 83 | 79 | 4 | 114 | 30 | 3.4 | 31 | 5.5 | 67.5 | 53.8 | 85.2 | 62.9 | 99.4 | 112.4 | 50.4 | 88.5 |
| 5 | 83 | 79 | 4 | 114 | 30 | 3.5 | 31 | 5.4 | 68 | 53.2 | 85.3 | 62.8 | 99.4 | 112.6 | 50.6 | 88.6 |
| 5 | 83 | 79 | 4 | 114 | 30 | 3.9 | 31 | 5.9 | 67.8 | 53.8 | 84.8 | 63.4 | 99.2 | 112.3 | 50.6 | 88.1 |
| 5 | 83 | 79 | 4 | 114 | 30 | 3.4 | 31 | 5.5 | 68.1 | 53.6 | 84.9 | 62.9 | 99.6 | 112.5 | 50.8 | 88.5 |
| 5 | 83 | 79 | 4 | 114 | 30 | 3.4 | 31 | 5.4 | 68.1 | 53.6 | 84.8 | 63.1 | 99.4 | 112.5 | 50.6 | 88.9 |
| 5 | 83 | 79 | 4 | 114 | 30 | 3.7 | 31 | 5.5 | 68 | 53.8 | 85 | 63.1 | 99.6 | 112.1 | 50.8 | 88.5 |
| 5 | 83 | 79 | 4 | 114 | 30 | 3.9 | 31 | 5.5 | 68.1 | 53.6 | 85 | 63.2 | 99.2 | 112.5 | 50.6 | 88.3 |

## E.2.1. Volunteer 2: Lateral Cephalogram

| | SNA Angle | SNB Angle | ANB Angle | Interincisal Angle | 1-NA angle | 1-NA | 1-NB Angle | 1-NB | S-N | PNS-ANS | S-PNS | S-ANS | Me-ANS | N-Pog | S-Gn | N-A | N-B |
|---|---|---|---|---|---|---|---|---|---|---|---|---|---|---|---|---|---|
| 1 | 89.0 | 91.0 | 2.0 | 138.0 | 28.0 | 6.2 | 15.0 | 0.8 | 63.5 | 49.4 | 45.2 | 80.0 | 61.9 | 98.8 | 121.9 | 44.0 | 84.2 |
| 1 | 89.0 | 91.0 | 2.0 | 138.0 | 28.0 | 6.0 | 15.0 | 1.3 | 63.5 | 49.8 | 45.1 | 79.9 | 62.0 | 98.4 | 121.7 | 44.5 | 84.6 |
| 1 | 89.0 | 91.0 | 2.0 | 138.0 | 28.0 | 6.3 | 15.0 | 1.3 | 63.5 | 49.8 | 45.4 | 79.8 | 62.1 | 98.8 | 121.4 | 44.2 | 84.4 |
| 1 | 89.0 | 91.0 | 2.0 | 138.0 | 28.0 | 5.5 | 15.0 | 1.1 | 63.3 | 49.6 | 45.7 | 80.0 | 62.0 | 98.6 | 121.6 | 44.6 | 84.4 |
| 1 | 89.0 | 91.0 | 2.0 | 138.0 | 28.0 | 5.6 | 15.0 | 1.1 | 63.3 | 49.4 | 45.5 | 80.2 | 62.0 | 98.6 | 121.9 | 44.6 | 84.6 |
| 1 | 89.0 | 91.0 | 2.0 | 138.0 | 28.0 | 6.2 | 15.0 | 0.8 | 63.0 | 49.6 | 45.2 | 79.8 | 62.0 | 99.2 | 121.7 | 44.5 | 84.4 |
| 1 | 89.0 | 91.0 | 2.0 | 138.0 | 28.0 | 5.6 | 15.0 | 1.1 | 63.3 | 49.6 | 45.5 | 80.1 | 62.0 | 98.6 | 122.1 | 44.2 | 84.6 |
| 1 | 89.0 | 91.0 | 2.0 | 138.0 | 28.0 | 5.8 | 15.0 | 1.1 | 62.9 | 49.2 | 45.3 | 80.1 | 62.1 | 98.4 | 121.7 | 44.6 | 84.2 |
| 1 | 89.0 | 91.0 | 2.0 | 138.0 | 28.0 | 6.2 | 15.0 | 0.8 | 63.7 | 49.6 | 45.7 | 79.8 | 62.0 | 99.0 | 121.4 | 44.5 | 84.4 |
| 1 | 89.0 | 91.0 | 2.0 | 138.0 | 28.0 | 6.0 | 15.0 | 1.1 | 63.3 | 49.6 | 45.2 | 79.8 | 62.1 | 98.8 | 121.6 | 44.2 | 84.2 |
| 2 | 89.0 | 91.0 | 2.0 | 138.0 | 28.0 | 6.2 | 15.0 | 0.8 | 63.5 | 49.4 | 45.2 | 80.0 | 61.9 | 98.8 | 121.9 | 44.0 | 84.2 |
| 2 | 89.0 | 91.0 | 2.0 | 138.0 | 28.0 | 6.0 | 15.0 | 1.3 | 63.5 | 49.8 | 45.1 | 79.9 | 62.0 | 98.4 | 121.7 | 44.5 | 84.6 |
| 2 | 89.0 | 91.0 | 2.0 | 138.0 | 28.0 | 6.3 | 15.0 | 1.3 | 63.5 | 49.8 | 45.4 | 79.8 | 62.1 | 98.8 | 121.4 | 44.2 | 84.4 |
| 2 | 89.0 | 91.0 | 2.0 | 138.0 | 28.0 | 5.5 | 15.0 | 1.1 | 63.3 | 49.6 | 45.7 | 80.0 | 62.0 | 98.6 | 121.6 | 44.6 | 84.4 |
| 2 | 89.0 | 91.0 | 2.0 | 138.0 | 28.0 | 5.6 | 15.0 | 1.1 | 63.3 | 49.4 | 45.5 | 80.2 | 62.0 | 98.6 | 121.9 | 44.6 | 84.6 |
| 2 | 89.0 | 91.0 | 2.0 | 138.0 | 28.0 | 6.2 | 15.0 | 0.8 | 63.0 | 49.6 | 45.2 | 79.8 | 62.0 | 99.2 | 121.7 | 44.5 | 84.4 |
| 2 | 89.0 | 91.0 | 2.0 | 138.0 | 28.0 | 5.6 | 15.0 | 1.1 | 63.3 | 49.6 | 45.5 | 80.1 | 62.0 | 98.6 | 122.1 | 44.2 | 84.6 |
| 2 | 89.0 | 91.0 | 2.0 | 138.0 | 28.0 | 5.8 | 15.0 | 1.1 | 62.9 | 49.2 | 45.3 | 80.1 | 62.1 | 98.4 | 121.7 | 44.6 | 84.2 |
| 2 | 89.0 | 91.0 | 2.0 | 138.0 | 28.0 | 6.2 | 15.0 | 0.8 | 63.7 | 49.6 | 45.7 | 79.8 | 62.0 | 99.0 | 121.4 | 44.5 | 84.4 |
| 2 | 89.0 | 91.0 | 2.0 | 138.0 | 28.0 | 6.0 | 15.0 | 1.1 | 63.3 | 49.6 | 45.2 | 79.8 | 62.1 | 98.8 | 121.6 | 44.2 | 84.2 |
| 3 | 89.0 | 91.0 | 2.0 | 135.0 | 30.0 | 6.0 | 18.0 | 0.6 | 63.5 | 50.0 | 46.1 | 80.3 | 62.5 | 99.6 | 120.7 | 44.2 | 83.7 |
| 3 | 89.0 | 91.0 | 2.0 | 135.0 | 30.0 | 5.8 | 18.0 | 0.6 | 63.3 | 50.3 | 46.3 | 80.4 | 62.8 | 99.2 | 121.1 | 44.5 | 83.2 |
| 3 | 89.0 | 91.0 | 2.0 | 135.0 | 30.0 | 6.0 | 18.0 | 0.8 | 63.1 | 50.3 | 46.2 | 80.3 | 62.7 | 99.2 | 120.8 | 44.5 | 83.4 |
| 3 | 89.0 | 91.0 | 2.0 | 135.0 | 30.0 | 5.8 | 18.0 | 0.8 | 63.5 | 50.0 | 45.7 | 80.4 | 62.4 | 99.2 | 121.1 | 44.5 | 83.7 |
| 3 | 89.0 | 91.0 | 2.0 | 135.0 | 30.0 | 6.3 | 18.0 | 0.6 | 63.5 | 49.8 | 46.0 | 80.4 | 62.2 | 99.2 | 121.3 | 44.5 | 83.4 |
| 3 | 89.0 | 91.0 | 2.0 | 135.0 | 30.0 | 6.0 | 18.0 | 0.6 | 63.1 | 49.6 | 45.8 | 80.1 | 62.5 | 99.6 | 120.6 | 44.0 | 83.8 |
| 3 | 89.0 | 91.0 | 2.0 | 135.0 | 30.0 | 5.8 | 18.0 | 0.9 | 63.3 | 50.1 | 45.9 | 80.4 | 62.1 | 99.0 | 120.8 | 44.5 | 83.7 |
| 3 | 89.0 | 91.0 | 2.0 | 135.0 | 30.0 | 6.0 | 18.0 | 0.9 | 63.3 | 50.1 | 46.3 | 80.4 | 62.5 | 99.5 | 120.9 | 44.5 | 83.6 |
| 3 | 89.0 | 91.0 | 2.0 | 135.0 | 30.0 | 6.0 | 18.0 | 1.3 | 62.9 | 49.6 | 46.3 | 80.1 | 62.5 | 99.0 | 121.2 | 44.5 | 83.8 |
| 3 | 89.0 | 91.0 | 2.0 | 135.0 | 30.0 | 5.8 | 18.0 | 0.6 | 63.1 | 50.3 | 45.5 | 80.1 | 62.4 | 98.8 | 120.9 | 44.3 | 84.0 |
| 4 | 89.0 | 91.0 | 2.0 | 135.0 | 28.0 | 6.4 | 18.0 | 0.6 | 63.5 | 47.8 | 46.6 | 79.1 | 62.4 | 97.6 | 121.4 | 44.5 | 84.0 |
| 4 | 89.0 | 91.0 | 2.0 | 135.0 | 28.0 | 6.6 | 18.0 | 0.6 | 63.3 | 47.6 | 46.1 | 79.3 | 62.1 | 97.6 | 121.0 | 44.6 | 84.2 |
| 4 | 89.0 | 91.0 | 2.0 | 135.0 | 28.0 | 6.0 | 18.0 | 0.6 | 63.3 | 47.9 | 46.6 | 79.4 | 62.0 | 97.6 | 121.1 | 44.8 | 84.3 |
| 4 | 89.0 | 91.0 | 2.0 | 135.0 | 28.0 | 6.6 | 18.0 | 1.1 | 63.5 | 47.8 | 46.5 | 79.5 | 62.1 | 97.6 | 120.8 | 44.6 | 84.5 |
| 4 | 89.0 | 91.0 | 2.0 | 135.0 | 28.0 | 6.0 | 18.0 | 0.9 | 63.3 | 47.6 | 46.1 | 79.3 | 62.1 | 97.8 | 121.1 | 44.8 | 84.3 |
| 4 | 89.0 | 91.0 | 2.0 | 135.0 | 28.0 | 6.3 | 18.0 | 1.1 | 63.3 | 47.9 | 46.8 | 79.5 | 62.1 | 97.3 | 121.0 | 44.5 | 84.0 |
| 4 | 89.0 | 91.0 | 2.0 | 135.0 | 28.0 | 5.8 | 18.0 | 0.6 | 63.7 | 47.9 | 46.5 | 79.6 | 62.0 | 97.3 | 120.6 | 44.5 | 84.5 |
| 4 | 89.0 | 91.0 | 2.0 | 135.0 | 28.0 | 6.2 | 18.0 | 0.8 | 63.3 | 47.9 | 46.4 | 79.3 | 62.3 | 97.8 | 121.0 | 44.8 | 84.0 |
| 4 | 89.0 | 91.0 | 2.0 | 135.0 | 28.0 | 6.2 | 18.0 | 0.9 | 63.3 | 48.2 | 46.4 | 79.2 | 62.3 | 97.8 | 121.3 | 44.8 | 84.6 |
| 4 | 89.0 | 91.0 | 2.0 | 135.0 | 28.0 | 5.6 | 18.0 | 0.8 | 63.5 | 47.9 | 46.4 | 79.5 | 62.0 | 97.8 | 120.8 | 44.8 | 84.6 |
| 5 | 89.0 | 90.0 | 1.0 | 136.0 | 28.0 | 5.4 | 16.0 | 0.6 | 62.8 | 48.8 | 45.0 | 79.6 | 62.4 | 99.3 | 121.3 | 46.2 | 86.0 |
| 5 | 89.0 | 90.0 | 1.0 | 136.0 | 28.0 | 5.4 | 16.0 | 0.4 | 62.8 | 49.0 | 44.8 | 79.7 | 62.0 | 99.0 | 121.3 | 46.2 | 85.7 |
| 5 | 89.0 | 90.0 | 1.0 | 136.0 | 28.0 | 5.2 | 16.0 | 0.6 | 62.8 | 48.6 | 45.4 | 79.8 | 62.1 | 99.0 | 121.0 | 46.2 | 86.0 |
| 5 | 89.0 | 90.0 | 1.0 | 136.0 | 28.0 | 4.7 | 16.0 | 0.6 | 62.8 | 48.8 | 45.6 | 79.5 | 62.1 | 99.7 | 121.3 | 46.2 | 85.7 |
| 5 | 89.0 | 90.0 | 1.0 | 136.0 | 28.0 | 5.2 | 16.0 | 1.1 | 62.8 | 48.8 | 45.3 | 79.5 | 62.0 | 99.5 | 121.0 | 46.3 | 85.7 |
| 5 | 89.0 | 90.0 | 1.0 | 136.0 | 28.0 | 5.0 | 16.0 | 0.8 | 62.9 | 48.6 | 45.4 | 79.6 | 62.4 | 99.6 | 121.3 | 46.3 | 85.5 |
| 5 | 89.0 | 90.0 | 1.0 | 136.0 | 28.0 | 5.6 | 16.0 | 0.8 | 62.8 | 48.8 | 45.4 | 79.6 | 62.0 | 99.3 | 121.1 | 46.2 | 85.9 |
| 5 | 89.0 | 90.0 | 1.0 | 136.0 | 28.0 | 5.2 | 16.0 | 0.8 | 62.8 | 48.8 | 45.6 | 79.6 | 61.5 | 99.6 | 121.0 | 45.9 | 85.4 |
| 5 | 89.0 | 90.0 | 1.0 | 136.0 | 28.0 | 5.4 | 16.0 | 1.3 | 63.1 | 49.0 | 45.4 | 80.0 | 62.1 | 99.5 | 121.0 | 45.6 | 85.7 |
| 5 | 89.0 | 90.0 | 1.0 | 136.0 | 28.0 | 5.4 | 16.0 | 0.8 | 62.9 | 49.0 | 45.4 | 79.8 | 62.1 | 99.3 | 121.1 | 46.2 | 86.0 |

## E.2.2. Volunteer 3: Lateral Cephalogram

| | SNA Angle | SNB Angle | ANB Angle | Interincisal Angle | 1-NA angle | 1-NA | 1-NB Angle | 1-NB | S-N | PNS-ANS | S-PNS | S-ANS | Me-ANS | N-Pog | S-Gn | N-A | N-B |
|---|---|---|---|---|---|---|---|---|---|---|---|---|---|---|---|---|---|
| 1 | 85.0 | 81.0 | 4.0 | 156.0 | 7.0 | 1.1 | 14.0 | 1.4 | 68.8 | 50.2 | 5.5 | 86.9 | 61.7 | 107.5 | 122.2 | 56.1 | 90.3 |
| 1 | 85.0 | 81.0 | 4.0 | 156.0 | 7.0 | 1.4 | 14.0 | 1.9 | 68.4 | 50.0 | 50.8 | 86.9 | 62.1 | 107.5 | 122.5 | 55.9 | 90.1 |
| 1 | 85.0 | 81.0 | 4.0 | 156.0 | 7.0 | 1.3 | 14.0 | 1.7 | 68.6 | 49.8 | 50.7 | 86.6 | 62.1 | 107.7 | 122.1 | 55.9 | 90.1 |
| 1 | 85.0 | 81.0 | 4.0 | 156.0 | 7.0 | 1.4 | 14.0 | 1.4 | 68.4 | 49.8 | 50.3 | 86.6 | 62.1 | 107.3 | 122.2 | 56.3 | 90.1 |
| 1 | 85.0 | 81.0 | 4.0 | 156.0 | 7.0 | 0.8 | 14.0 | 1.7 | 68.4 | 50.3 | 50.4 | 86.7 | 61.8 | 107.7 | 122.4 | 55.7 | 90.3 |
| 1 | 85.0 | 81.0 | 4.0 | 156.0 | 7.0 | 1.1 | 14.0 | 1.4 | 68.6 | 50.0 | 50.4 | 86.9 | 61.7 | 107.3 | 122.2 | 56.7 | 89.9 |
| 1 | 85.0 | 81.0 | 4.0 | 156.0 | 7.0 | 1.4 | 14.0 | 1.4 | 68.6 | 50.0 | 50.7 | 87.1 | 61.8 | 107.5 | 122.6 | 55.9 | 90.1 |
| 1 | 85.0 | 81.0 | 4.0 | 156.0 | 7.0 | 1.4 | 14.0 | 1.4 | 68.6 | 50.2 | 50.7 | 87.0 | 62.0 | 107.5 | 122.0 | 56.3 | 90.1 |
| 1 | 85.0 | 81.0 | 4.0 | 156.0 | 7.0 | 1.3 | 14.0 | 1.9 | 68.2 | 50.0 | 50.2 | 87.1 | 62.4 | 107.5 | 122.4 | 56.1 | 90.1 |
| 1 | 85.0 | 81.0 | 4.0 | 156.0 | 7.0 | 1.3 | 14.0 | 1.9 | 68.8 | 50.0 | 50.8 | 86.8 | 60.4 | 107.9 | 122.5 | 56.1 | 89.9 |
| 2 | 85.0 | 81.0 | 4.0 | 159.0 | 8.0 | 0.8 | 11.0 | 2.2 | 67.3 | 51.3 | 51.4 | 87.9 | 63.5 | 106.3 | 122.1 | 83.6 | 90.7 |
| 2 | 85.0 | 81.0 | 4.0 | 159.0 | 8.0 | 1.7 | 11.0 | 1.9 | 67.9 | 51.5 | 51.8 | 87.8 | 63.3 | 106.4 | 121.6 | 83.3 | 90.7 |
| 2 | 85.0 | 81.0 | 4.0 | 159.0 | 8.0 | 1.3 | 11.0 | 2.3 | 67.4 | 51.3 | 51.7 | 87.7 | 63.5 | 106.4 | 121.9 | 83.5 | 90.7 |
| 2 | 85.0 | 81.0 | 4.0 | 159.0 | 8.0 | 1.1 | 11.0 | 1.9 | 67.9 | 51.5 | 51.8 | 87.6 | 63.3 | 106.9 | 122.2 | 83.5 | 90.7 |
| 2 | 85.0 | 81.0 | 4.0 | 159.0 | 8.0 | 1.4 | 11.0 | 2.2 | 67.3 | 51.5 | 51.3 | 87.5 | 63.4 | 106.7 | 121.9 | 83.7 | 91.2 |
| 2 | 85.0 | 81.0 | 4.0 | 159.0 | 8.0 | 1.4 | 11.0 | 2.3 | 67.8 | 51.3 | 51.6 | 87.6 | 63.3 | 106.4 | 122.4 | 83.7 | 90.9 |
| 2 | 85.0 | 81.0 | 4.0 | 159.0 | 8.0 | 1.4 | 11.0 | 2.5 | 67.8 | 51.5 | 51.2 | 87.9 | 63.8 | 106.4 | 122.2 | 83.8 | 91.2 |
| 2 | 85.0 | 81.0 | 4.0 | 159.0 | 8.0 | 1.7 | 11.0 | 2.1 | 67.6 | 51.3 | 51.6 | 87.3 | 63.3 | 106.3 | 122.2 | 83.5 | 91.2 |
| 2 | 85.0 | 81.0 | 4.0 | 159.0 | 8.0 | 1.4 | 11.0 | 1.9 | 67.8 | 51.5 | 51.4 | 87.8 | 63.3 | 106.7 | 122.3 | 83.7 | 90.9 |
| 2 | 85.0 | 81.0 | 4.0 | 159.0 | 8.0 | 1.7 | 11.0 | 2.2 | 67.8 | 51.8 | 51.2 | 87.9 | 63.3 | 106.7 | 121.9 | 83.8 | 91.2 |
| 3 | 86.0 | 82.0 | 4.0 | 155.0 | 8.0 | 1.3 | 15.0 | 1.7 | 68.7 | 49.8 | 51.9 | 87.7 | 62.0 | 107.5 | 123.0 | 54.5 | 90.3 |
| 3 | 86.0 | 82.0 | 4.0 | 155.0 | 8.0 | 1.7 | 15.0 | 1.9 | 68.7 | 50.0 | 51.7 | 87.5 | 62.0 | 107.3 | 123.3 | 54.5 | 90.3 |
| 3 | 86.0 | 82.0 | 4.0 | 155.0 | 8.0 | 1.9 | 15.0 | 2.1 | 69.0 | 49.8 | 51.3 | 87.6 | 62.1 | 107.5 | 123.3 | 54.1 | 90.5 |
| 3 | 86.0 | 82.0 | 4.0 | 155.0 | 8.0 | 1.7 | 15.0 | 1.7 | 68.5 | 50.0 | 52.0 | 87.5 | 62.1 | 107.3 | 123.3 | 54.5 | 90.5 |
| 3 | 86.0 | 82.0 | 4.0 | 155.0 | 8.0 | 1.4 | 15.0 | 1.7 | 68.5 | 49.8 | 51.9 | 87.2 | 62.2 | 107.1 | 123.5 | 54.5 | 90.3 |
| 3 | 86.0 | 82.0 | 4.0 | 155.0 | 8.0 | 1.4 | 15.0 | 1.7 | 68.4 | 49.6 | 51.8 | 87.4 | 61.9 | 107.3 | 123.6 | 54.3 | 90.5 |
| 3 | 86.0 | 82.0 | 4.0 | 155.0 | 8.0 | 1.7 | 15.0 | 1.9 | 68.8 | 50.3 | 51.9 | 87.6 | 61.4 | 107.1 | 123.3 | 54.5 | 89.9 |
| 3 | 86.0 | 82.0 | 4.0 | 155.0 | 8.0 | 1.9 | 15.0 | 1.9 | 68.5 | 50.3 | 51.3 | 87.8 | 62.0 | 107.5 | 123.1 | 54.3 | 90.5 |
| 3 | 86.0 | 82.0 | 4.0 | 155.0 | 8.0 | 1.9 | 15.0 | 1.9 | 68.8 | 50.0 | 51.7 | 87.6 | 62.1 | 107.1 | 123.5 | 54.5 | 90.3 |
| 3 | 86.0 | 82.0 | 4.0 | 155.0 | 8.0 | 1.9 | 15.0 | 2.1 | 68.8 | 49.8 | 51.8 | 87.9 | 62.4 | 107.3 | 123.5 | 54.5 | 90.1 |
| 4 | 87.0 | 83.0 | 4.0 | 157.0 | 7.0 | 1.4 | 13.0 | 2.3 | 69.0 | 50.5 | 51.8 | 86.9 | 63.3 | 104.4 | 122.6 | 53.0 | 91.3 |
| 4 | 87.0 | 83.0 | 4.0 | 157.0 | 7.0 | 1.9 | 13.0 | 2.3 | 68.4 | 50.5 | 52.0 | 87.1 | 63.5 | 104.6 | 122.2 | 53.2 | 91.3 |
| 4 | 87.0 | 83.0 | 4.0 | 157.0 | 7.0 | 1.3 | 13.0 | 2.1 | 68.4 | 50.3 | 52.1 | 86.7 | 62.9 | 104.4 | 122.4 | 52.9 | 91.3 |
| 4 | 87.0 | 83.0 | 4.0 | 157.0 | 7.0 | 2.1 | 13.0 | 2.3 | 67.9 | 49.9 | 52.1 | 86.6 | 63.5 | 104.8 | 122.8 | 53.3 | 90.9 |
| 4 | 87.0 | 83.0 | 4.0 | 157.0 | 7.0 | 1.4 | 13.0 | 2.3 | 69.0 | 50.1 | 52.2 | 86.7 | 63.3 | 104.4 | 122.5 | 53.4 | 90.9 |
| 4 | 87.0 | 83.0 | 4.0 | 157.0 | 7.0 | 2.1 | 13.0 | 1.9 | 69.0 | 50.1 | 52.0 | 86.8 | 63.3 | 104.2 | 122.4 | 53.2 | 91.2 |
| 4 | 87.0 | 83.0 | 4.0 | 157.0 | 7.0 | 1.7 | 13.0 | 2.1 | 68.4 | 50.5 | 52.0 | 87.2 | 63.0 | 104.0 | 122.2 | 53.4 | 90.9 |
| 4 | 87.0 | 83.0 | 4.0 | 157.0 | 7.0 | 1.7 | 13.0 | 2.3 | 68.4 | 50.1 | 52.2 | 86.9 | 63.0 | 104.4 | 122.3 | 53.2 | 91.3 |
| 4 | 87.0 | 83.0 | 4.0 | 157.0 | 7.0 | 1.3 | 13.0 | 2.2 | 68.6 | 50.3 | 52.4 | 86.6 | 63.0 | 104.2 | 122.6 | 53.2 | 91.2 |
| 4 | 87.0 | 83.0 | 4.0 | 157.0 | 7.0 | 1.4 | 13.0 | 1.9 | 68.7 | 50.1 | 52.2 | 87.2 | 62.9 | 104.4 | 122.4 | 53.2 | 91.8 |
| 5 | 86.0 | 82.0 | 4.0 | 159.0 | 8.0 | 1.3 | 12.0 | 1.7 | 68.8 | 50.4 | 51.7 | 87.2 | 62.9 | 103.8 | 122.2 | 53.6 | 90.1 |
| 5 | 86.0 | 82.0 | 4.0 | 159.0 | 8.0 | 1.1 | 12.0 | 1.9 | 68.8 | 50.7 | 51.5 | 87.5 | 62.4 | 103.8 | 122.0 | 53.8 | 89.6 |
| 5 | 86.0 | 82.0 | 4.0 | 159.0 | 8.0 | 0.9 | 12.0 | 2.1 | 68.8 | 50.9 | 51.4 | 87.3 | 63.1 | 103.4 | 122.2 | 53.8 | 89.9 |
| 5 | 86.0 | 82.0 | 4.0 | 159.0 | 8.0 | 0.8 | 12.0 | 2.1 | 68.6 | 50.7 | 51.3 | 87.3 | 62.9 | 104.0 | 122.2 | 54.0 | 89.9 |
| 5 | 86.0 | 82.0 | 4.0 | 159.0 | 8.0 | 1.1 | 12.0 | 1.4 | 68.8 | 50.4 | 51.6 | 87.5 | 63.1 | 103.6 | 122.2 | 54.2 | 90.3 |
| 5 | 86.0 | 82.0 | 4.0 | 159.0 | 8.0 | 0.6 | 12.0 | 2.1 | 68.8 | 50.7 | 51.4 | 87.5 | 62.8 | 103.6 | 122.3 | 53.8 | 90.1 |
| 5 | 86.0 | 82.0 | 4.0 | 159.0 | 8.0 | 1.1 | 12.0 | 2.2 | 68.5 | 50.9 | 51.6 | 87.8 | 62.4 | 103.6 | 122.2 | 53.8 | 89.5 |
| 5 | 86.0 | 82.0 | 4.0 | 159.0 | 8.0 | 1.1 | 12.0 | 2.1 | 68.8 | 50.7 | 51.6 | 87.5 | 62.9 | 103.1 | 122.4 | 53.8 | 89.6 |
| 5 | 86.0 | 82.0 | 4.0 | 159.0 | 8.0 | 1.3 | 12.0 | 2.1 | 69.0 | 50.5 | 51.3 | 87.5 | 62.9 | 103.6 | 122.4 | 53.4 | 89.9 |
| 5 | 86.0 | 82.0 | 4.0 | 159.0 | 8.0 | 1.1 | 12.0 | 1.9 | 69.0 | 51.1 | 51.3 | 87.4 | 62.8 | 103.8 | 122.1 | 53.8 | 89.9 |

## E.2.3. Volunteer 1: "Black Bone"

| | SNA Angle | SNB Angle | ANB Angle | Interincisal Angle | 1-NA angle | 1-NA | 1-NB Angle | 1-NB | S-N | PNS-ANS | S-PNS | S-ANS | Me-ANS | N-Pog | S-Gn | N-A | N-B |
|---|---|---|---|---|---|---|---|---|---|---|---|---|---|---|---|---|---|
| **1** | 82.0 | 78.0 | 5.0 | 122.0 | 24.0 | 5.6 | 30.0 | 7.0 | 70.7 | 56.4 | 45.9 | 89.1 | 66.0 | 102.2 | 115.2 | 49.5 | 88.4 |
| **1** | 82.0 | 78.0 | 5.0 | 122.0 | 24.0 | 5.2 | 30.0 | 6.6 | 70.5 | 56.4 | 46.4 | 88.8 | 66.2 | 102.7 | 115.0 | 49.3 | 88.2 |
| **1** | 82.0 | 78.0 | 5.0 | 122.0 | 24.0 | 5.2 | 30.0 | 7.0 | 70.1 | 56.4 | 45.8 | 89.1 | 66.1 | 102.7 | 115.2 | 49.7 | 88.4 |
| **1** | 82.0 | 78.0 | 5.0 | 122.0 | 24.0 | 5.6 | 30.0 | 6.8 | 70.6 | 56.5 | 46.0 | 88.6 | 65.8 | 102.7 | 115.2 | 49.5 | 88.4 |
| **1** | 82.0 | 78.0 | 5.0 | 122.0 | 24.0 | 5.4 | 30.0 | 6.3 | 70.8 | 56.4 | 46.4 | 88.9 | 66.3 | 102.9 | 114.9 | 49.5 | 88.2 |
| **1** | 82.0 | 78.0 | 5.0 | 122.0 | 24.0 | 5.2 | 30.0 | 6.3 | 70.4 | 56.4 | 46.0 | 88.6 | 66.1 | 102.4 | 115.4 | 49.5 | 88.2 |
| **1** | 82.0 | 78.0 | 5.0 | 122.0 | 24.0 | 5.4 | 30.0 | 7.3 | 70.8 | 56.6 | 45.9 | 88.7 | 66.1 | 102.4 | 115.2 | 49.7 | 88.4 |
| **1** | 82.0 | 78.0 | 5.0 | 122.0 | 24.0 | 5.4 | 30.0 | 6.8 | 70.7 | 56.4 | 46.3 | 88.5 | 66.0 | 102.2 | 115.4 | 49.7 | 88.4 |
| **1** | 82.0 | 78.0 | 5.0 | 122.0 | 24.0 | 5.4 | 30.0 | 7.3 | 70.5 | 57.1 | 46.5 | 88.9 | 66.1 | 102.7 | 115.3 | 50.0 | 88.4 |
| **1** | 82.0 | 78.0 | 5.0 | 122.0 | 24.0 | 5.6 | 30.0 | 7.3 | 70.7 | 56.2 | 46.2 | 88.7 | 66.3 | 102.4 | 115.4 | 49.3 | 88.4 |
| **2** | 85.0 | 80.0 | 5.0 | 121.0 | 19.0 | 4.0 | 36.0 | 7.5 | 70.3 | 62.9 | 43.7 | 89.3 | 65.5 | 99.2 | 115.0 | 47.6 | 85.4 |
| **2** | 84.0 | 79.0 | 5.0 | 121.0 | 19.0 | 4.2 | 36.0 | 8.5 | 70.1 | 62.3 | 44.4 | 88.9 | 65.1 | 99.6 | 114.7 | 47.6 | 85.3 |
| **2** | 84.0 | 79.0 | 5.0 | 121.0 | 19.0 | 4.5 | 36.0 | 8.0 | 70.2 | 62.4 | 43.5 | 88.8 | 65.5 | 99.4 | 115.0 | 47.2 | 85.4 |
| **2** | 85.0 | 79.0 | 5.0 | 121.0 | 19.0 | 4.5 | 36.0 | 8.0 | 69.9 | 62.3 | 43.4 | 89.0 | 65.3 | 99.4 | 115.0 | 47.9 | 85.6 |
| **2** | 84.0 | 79.0 | 5.0 | 121.0 | 19.0 | 4.1 | 36.0 | 8.0 | 70.1 | 62.8 | 43.8 | 89.1 | 65.1 | 99.6 | 115.2 | 47.9 | 85.1 |
| **2** | 84.0 | 79.0 | 5.0 | 121.0 | 19.0 | 4.2 | 36.0 | 8.0 | 70.3 | 62.6 | 44.3 | 89.0 | 65.5 | 100.1 | 114.9 | 47.4 | 85.3 |
| **2** | 84.0 | 79.0 | 5.0 | 121.0 | 19.0 | 4.2 | 36.0 | 8.0 | 70.3 | 62.6 | 43.9 | 88.6 | 65.2 | 100.1 | 114.5 | 47.9 | 85.6 |
| **2** | 84.0 | 79.0 | 5.0 | 121.0 | 19.0 | 4.3 | 36.0 | 7.7 | 70.4 | 63.0 | 44.3 | 89.1 | 65.3 | 99.9 | 114.6 | 47.9 | 85.3 |
| **2** | 84.0 | 79.0 | 5.0 | 121.0 | 19.0 | 4.0 | 36.0 | 8.2 | 70.3 | 62.8 | 43.9 | 88.8 | 64.8 | 99.4 | 114.3 | 47.9 | 85.1 |
| **2** | 84.0 | 79.0 | 5.0 | 121.0 | 19.0 | 3.8 | 36.0 | 7.8 | 69.8 | 62.8 | 43.8 | 89.1 | 65.6 | 100.1 | 114.7 | 47.9 | 85.3 |
| **3** | 84.0 | 79.0 | 5.0 | 123.0 | 24.0 | 4.0 | 29.0 | 5.4 | 70.3 | 55.2 | 45.3 | 85.2 | 64.4 | 98.7 | 114.3 | 46.9 | 84.4 |
| **3** | 84.0 | 79.0 | 5.0 | 123.0 | 24.0 | 4.0 | 29.0 | 6.3 | 69.8 | 54.9 | 45.5 | 85.5 | 64.2 | 98.5 | 114.3 | 46.5 | 84.4 |
| **3** | 84.0 | 79.0 | 5.0 | 123.0 | 24.0 | 4.7 | 29.0 | 6.6 | 70.2 | 54.7 | 45.5 | 85.2 | 64.0 | 98.5 | 114.2 | 46.5 | 84.2 |
| **3** | 84.0 | 79.0 | 5.0 | 123.0 | 24.0 | 4.0 | 29.0 | 6.6 | 70.1 | 54.9 | 45.9 | 85.6 | 64.1 | 98.7 | 114.8 | 47.0 | 84.4 |
| **3** | 84.0 | 79.0 | 5.0 | 123.0 | 24.0 | 3.8 | 29.0 | 6.6 | 70.1 | 54.9 | 45.7 | 85.2 | 63.9 | 98.7 | 114.4 | 46.7 | 84.7 |
| **3** | 84.0 | 79.0 | 5.0 | 123.0 | 24.0 | 4.2 | 29.0 | 5.4 | 69.9 | 54.5 | 45.2 | 85.6 | 64.1 | 98.7 | 114.6 | 46.9 | 84.7 |
| **3** | 84.0 | 79.0 | 5.0 | 123.0 | 24.0 | 4.2 | 29.0 | 5.9 | 69.8 | 54.9 | 46.0 | 85.6 | 63.9 | 98.7 | 114.1 | 46.7 | 84.4 |
| **3** | 84.0 | 79.0 | 5.0 | 123.0 | 24.0 | 3.8 | 29.0 | 6.1 | 70.1 | 55.1 | 46.1 | 85.4 | 64.2 | 98.7 | 114.3 | 46.7 | 84.9 |
| **3** | 84.0 | 79.0 | 5.0 | 123.0 | 24.0 | 3.8 | 29.0 | 6.1 | 69.8 | 54.9 | 45.7 | 85.2 | 64.5 | 98.9 | 114.6 | 46.5 | 84.4 |
| **3** | 84.0 | 79.0 | 5.0 | 123.0 | 24.0 | 4.5 | 29.0 | 6.4 | 70.3 | 54.7 | 45.7 | 85.1 | 64.5 | 98.5 | 114.1 | 46.7 | 84.7 |
| **4** | 85.0 | 80.0 | 5.0 | 128.0 | 20.0 | 4.5 | 29.0 | 6.1 | 70.4 | 53.6 | 44.6 | 84.3 | 64.1 | 98.7 | 114.5 | 46.7 | 85.6 |
| **4** | 85.0 | 80.0 | 5.0 | 128.0 | 20.0 | 4.2 | 29.0 | 7.1 | 70.2 | 53.6 | 45.1 | 84.3 | 63.9 | 98.9 | 114.5 | 46.7 | 85.6 |
| **4** | 85.0 | 80.0 | 5.0 | 128.0 | 20.0 | 4.5 | 29.0 | 6.4 | 70.2 | 53.4 | 44.9 | 84.1 | 64.0 | 99.2 | 114.5 | 46.7 | 85.6 |
| **4** | 85.0 | 80.0 | 5.0 | 128.0 | 20.0 | 4.7 | 29.0 | 6.3 | 70.0 | 53.9 | 45.1 | 84.3 | 63.7 | 99.2 | 114.7 | 46.7 | 85.5 |
| **4** | 85.0 | 80.0 | 5.0 | 128.0 | 20.0 | 4.2 | 29.0 | 6.1 | 70.0 | 53.1 | 44.7 | 84.2 | 64.0 | 98.7 | 114.7 | 46.9 | 85.6 |
| **4** | 85.0 | 80.0 | 5.0 | 128.0 | 20.0 | 4.7 | 29.0 | 5.9 | 70.3 | 53.6 | 44.9 | 84.3 | 63.9 | 98.7 | 114.8 | 47.2 | 85.6 |
| **4** | 85.0 | 80.0 | 5.0 | 128.0 | 20.0 | 4.5 | 29.0 | 6.3 | 70.4 | 53.9 | 44.5 | 84.4 | 64.4 | 98.9 | 114.3 | 46.5 | 85.4 |
| **4** | 85.0 | 80.0 | 5.0 | 128.0 | 20.0 | 4.0 | 29.0 | 5.6 | 69.9 | 53.2 | 44.8 | 84.5 | 64.1 | 99.4 | 114.1 | 46.7 | 85.6 |
| **4** | 85.0 | 80.0 | 5.0 | 128.0 | 20.0 | 4.5 | 29.0 | 6.1 | 69.9 | 53.4 | 44.9 | 84.1 | 63.4 | 99.2 | 114.5 | 46.2 | 85.2 |
| **4** | 85.0 | 80.0 | 5.0 | 128.0 | 20.0 | 3.8 | 29.0 | 5.6 | 70.4 | 53.4 | 45.1 | 84.7 | 64.2 | 98.9 | 114.3 | 46.7 | 85.8 |
| **5** | 84.0 | 80.0 | 4.0 | 124.0 | 22.0 | 5.2 | 31.0 | 5.6 | 69.8 | 53.0 | 45.3 | 84.0 | 64.0 | 99.6 | 114.4 | 46.7 | 85.6 |
| **5** | 84.0 | 80.0 | 4.0 | 124.0 | 22.0 | 5.2 | 31.0 | 6.1 | 70.5 | 52.8 | 45.4 | 83.7 | 63.9 | 99.6 | 114.1 | 46.7 | 85.6 |
| **5** | 84.0 | 80.0 | 4.0 | 124.0 | 22.0 | 4.9 | 31.0 | 6.6 | 70.1 | 53.2 | 45.5 | 83.9 | 63.6 | 99.4 | 114.3 | 47.4 | 85.4 |
| **5** | 84.0 | 80.0 | 4.0 | 124.0 | 22.0 | 5.4 | 31.0 | 6.1 | 70.1 | 52.9 | 45.3 | 84.1 | 64.0 | 99.2 | 114.3 | 46.9 | 85.6 |
| **5** | 84.0 | 80.0 | 4.0 | 124.0 | 22.0 | 4.7 | 31.0 | 4.9 | 69.8 | 53.0 | 45.5 | 83.8 | 64.1 | 99.4 | 114.0 | 47.1 | 85.6 |
| **5** | 84.0 | 80.0 | 4.0 | 124.0 | 22.0 | 4.9 | 31.0 | 6.1 | 70.3 | 53.2 | 45.5 | 84.3 | 64.0 | 99.9 | 114.5 | 46.9 | 85.6 |
| **5** | 84.0 | 80.0 | 4.0 | 124.0 | 22.0 | 5.2 | 31.0 | 6.3 | 70.0 | 53.2 | 45.3 | 83.8 | 63.8 | 99.4 | 114.0 | 47.2 | 85.6 |
| **5** | 84.0 | 80.0 | 4.0 | 124.0 | 22.0 | 4.9 | 31.0 | 6.3 | 70.3 | 53.0 | 44.9 | 84.1 | 63.8 | 99.2 | 114.4 | 46.7 | 85.6 |
| **5** | 84.0 | 80.0 | 4.0 | 124.0 | 22.0 | 4.7 | 31.0 | 5.6 | 70.1 | 53.0 | 45.4 | 84.0 | 63.6 | 99.2 | 114.2 | 47.2 | 85.1 |
| **5** | 84.0 | 80.0 | 4.0 | 124.0 | 22.0 | 4.9 | 31.0 | 5.4 | 70.3 | 53.0 | 45.6 | 83.5 | 64.0 | 99.6 | 114.4 | 46.7 | 85.8 |

### E.2.4. Volunteer 2: "Black Bone"

| | SNA Angle | SNB Angle | ANB Angle | Interincisal Angle | 1-NA angle | 1-NA | 1-NB Angle | 1-NB | S-N | PNS-ANS | S-PNS | S-ANS | Me-ANS | N-Pog | S-Gn | N-A | N-B |
|---|---|---|---|---|---|---|---|---|---|---|---|---|---|---|---|---|---|
| 1 | 91.0 | 88.0 | 3.0 | 136.0 | 22.0 | 4.3 | 19.0 | 1.2 | 56.5 | 48.8 | 44.6 | 79.1 | 61.0 | 103.4 | 117.5 | 48.6 | 85.3 |
| 1 | 91.0 | 88.0 | 3.0 | 136.0 | 22.0 | 4.5 | 19.0 | 1.2 | 56.6 | 49.0 | 44.4 | 78.8 | 60.7 | 103.7 | 117.3 | 48.3 | 85.1 |
| 1 | 91.0 | 88.0 | 3.0 | 136.0 | 22.0 | 4.3 | 19.0 | 1.4 | 56.4 | 49.1 | 44.2 | 78.8 | 60.2 | 103.7 | 117.3 | 48.8 | 85.6 |
| 1 | 91.0 | 88.0 | 3.0 | 136.0 | 22.0 | 4.6 | 19.0 | 1.6 | 56.7 | 49.3 | 44.4 | 78.8 | 60.7 | 103.1 | 117.0 | 48.3 | 85.2 |
| 1 | 91.0 | 88.0 | 3.0 | 136.0 | 22.0 | 4.9 | 19.0 | 0.5 | 56.6 | 49.5 | 44.4 | 78.8 | 61.0 | 102.7 | 117.3 | 48.6 | 85.6 |
| 1 | 91.0 | 88.0 | 3.0 | 136.0 | 22.0 | 4.8 | 19.0 | 0.8 | 56.6 | 49.3 | 44.6 | 78.6 | 60.5 | 102.8 | 116.8 | 48.3 | 85.6 |
| 1 | 91.0 | 88.0 | 3.0 | 136.0 | 22.0 | 4.6 | 19.0 | 1.2 | 56.5 | 49.2 | 44.0 | 79.0 | 60.7 | 102.6 | 117.2 | 48.6 | 85.2 |
| 1 | 91.0 | 88.0 | 3.0 | 136.0 | 22.0 | 4.5 | 19.0 | 1.2 | 57.2 | 48.8 | 44.4 | 78.8 | 61.2 | 102.7 | 117.0 | 48.6 | 85.6 |
| 1 | 91.0 | 88.0 | 3.0 | 136.0 | 22.0 | 5.0 | 19.0 | 0.7 | 56.6 | 49.1 | 44.2 | 78.8 | 60.7 | 102.5 | 117.3 | 48.3 | 85.4 |
| 1 | 91.0 | 88.0 | 3.0 | 136.0 | 22.0 | 4.6 | 19.0 | 0.9 | 56.5 | 49.1 | 44.4 | 78.3 | 61.2 | 102.9 | 117.2 | 48.3 | 85.5 |
| 2 | 92.0 | 89.0 | 3.0 | 130.0 | 21.0 | 4.3 | 27.0 | 0.9 | 57.1 | 49.9 | 43.4 | 79.3 | 60.7 | 102.9 | 118.5 | 48.4 | 85.6 |
| 2 | 92.0 | 89.0 | 3.0 | 130.0 | 21.0 | 4.7 | 27.0 | 1.5 | 56.8 | 50.1 | 43.7 | 78.9 | 61.2 | 103.2 | 118.1 | 48.3 | 86.1 |
| 2 | 92.0 | 89.0 | 3.0 | 130.0 | 21.0 | 4.9 | 27.0 | 1.2 | 56.7 | 50.0 | 43.4 | 79.1 | 61.0 | 102.8 | 118.2 | 48.3 | 85.9 |
| 2 | 92.0 | 89.0 | 3.0 | 130.0 | 21.0 | 4.9 | 27.0 | 0.7 | 56.9 | 49.9 | 43.3 | 78.8 | 61.2 | 102.7 | 118.0 | 48.1 | 85.9 |
| 2 | 92.0 | 89.0 | 3.0 | 130.0 | 21.0 | 4.9 | 27.0 | 0.9 | 57.1 | 49.6 | 43.6 | 79.1 | 61.4 | 103.2 | 118.1 | 48.1 | 85.7 |
| 2 | 92.0 | 89.0 | 3.0 | 130.0 | 21.0 | 5.4 | 27.0 | 0.9 | 56.8 | 50.1 | 44.1 | 79.1 | 61.2 | 102.8 | 118.2 | 48.9 | 85.6 |
| 2 | 92.0 | 89.0 | 3.0 | 130.0 | 21.0 | 5.2 | 27.0 | 0.7 | 56.8 | 50.3 | 43.5 | 79.2 | 61.2 | 102.7 | 118.3 | 48.6 | 85.8 |
| 2 | 92.0 | 89.0 | 3.0 | 130.0 | 21.0 | 4.9 | 27.0 | 0.9 | 56.9 | 49.7 | 43.4 | 79.2 | 61.4 | 102.8 | 118.1 | 48.6 | 85.9 |
| 2 | 92.0 | 89.0 | 3.0 | 130.0 | 21.0 | 4.9 | 27.0 | 0.7 | 56.4 | 49.8 | 43.6 | 78.9 | 60.7 | 102.8 | 118.5 | 48.4 | 85.9 |
| 2 | 92.0 | 89.0 | 3.0 | 130.0 | 21.0 | 4.7 | 27.0 | 0.7 | 56.7 | 50.6 | 43.9 | 79.1 | 61.0 | 103.1 | 118.1 | 48.6 | 85.3 |
| 3 | 92.0 | 88.0 | 4.0 | 133.0 | 21.0 | 4.5 | 22.0 | 1.2 | 57.0 | 51.9 | 42.6 | 78.9 | 61.2 | 102.7 | 116.8 | 47.7 | 86.5 |
| 3 | 92.0 | 88.0 | 4.0 | 133.0 | 21.0 | 4.5 | 22.0 | 1.7 | 56.9 | 52.0 | 42.5 | 79.1 | 60.9 | 102.9 | 117.7 | 47.4 | 86.7 |
| 3 | 92.0 | 88.0 | 4.0 | 133.0 | 21.0 | 4.7 | 22.0 | 1.6 | 57.2 | 51.8 | 42.5 | 79.3 | 61.2 | 103.0 | 116.8 | 47.8 | 86.5 |
| 3 | 92.0 | 88.0 | 4.0 | 133.0 | 21.0 | 4.7 | 22.0 | 1.4 | 57.1 | 51.6 | 42.1 | 78.6 | 61.2 | 103.0 | 117.2 | 47.8 | 86.6 |
| 3 | 92.0 | 88.0 | 4.0 | 133.0 | 21.0 | 4.5 | 22.0 | 1.2 | 57.2 | 51.6 | 42.3 | 79.3 | 60.9 | 102.9 | 117.0 | 47.8 | 86.4 |
| 3 | 92.0 | 88.0 | 4.0 | 133.0 | 21.0 | 4.9 | 22.0 | 1.9 | 57.4 | 51.5 | 42.3 | 78.8 | 61.4 | 102.9 | 116.8 | 47.4 | 86.4 |
| 3 | 92.0 | 88.0 | 4.0 | 133.0 | 21.0 | 4.9 | 22.0 | 1.4 | 57.1 | 51.5 | 42.5 | 78.9 | 61.2 | 103.1 | 116.8 | 47.6 | 86.4 |
| 3 | 92.0 | 88.0 | 4.0 | 133.0 | 21.0 | 4.9 | 22.0 | 1.9 | 57.0 | 51.6 | 42.3 | 79.0 | 61.2 | 102.7 | 117.3 | 47.6 | 86.6 |
| 3 | 92.0 | 88.0 | 4.0 | 133.0 | 21.0 | 4.7 | 22.0 | 1.2 | 57.2 | 51.8 | 42.6 | 79.0 | 60.9 | 103.2 | 117.2 | 47.8 | 86.6 |
| 3 | 92.0 | 88.0 | 4.0 | 133.0 | 21.0 | 5.2 | 22.0 | 1.7 | 56.9 | 51.3 | 42.7 | 79.3 | 60.9 | 103.1 | 117.0 | 47.4 | 86.6 |
| 4 | 92.0 | 89.0 | 3.0 | 127.0 | 22.0 | 4.9 | 29.0 | 1.4 | 56.4 | 48.7 | 44.1 | 78.2 | 60.7 | 101.3 | 117.3 | 47.7 | 84.7 |
| 4 | 92.0 | 89.0 | 3.0 | 127.0 | 22.0 | 4.7 | 29.0 | 1.2 | 56.5 | 48.6 | 44.5 | 78.6 | 60.7 | 101.4 | 117.2 | 47.4 | 84.7 |
| 4 | 92.0 | 89.0 | 3.0 | 127.0 | 22.0 | 4.7 | 29.0 | 1.2 | 56.2 | 48.3 | 44.3 | 78.1 | 61.1 | 101.2 | 117.0 | 47.3 | 84.8 |
| 4 | 92.0 | 89.0 | 3.0 | 127.0 | 22.0 | 4.9 | 29.0 | 1.2 | 56.5 | 48.6 | 44.5 | 78.4 | 60.2 | 101.6 | 117.3 | 47.4 | 84.7 |
| 4 | 92.0 | 89.0 | 3.0 | 127.0 | 22.0 | 4.5 | 29.0 | 1.2 | 55.9 | 48.8 | 44.2 | 78.0 | 60.5 | 101.3 | 116.8 | 47.5 | 84.7 |
| 4 | 92.0 | 89.0 | 3.0 | 127.0 | 22.0 | 4.7 | 29.0 | 1.4 | 56.4 | 48.6 | 44.3 | 78.4 | 60.9 | 101.6 | 117.3 | 47.4 | 84.8 |
| 4 | 92.0 | 89.0 | 3.0 | 127.0 | 22.0 | 4.7 | 29.0 | 1.2 | 56.3 | 48.6 | 44.5 | 78.3 | 60.5 | 101.8 | 117.0 | 47.7 | 85.1 |
| 4 | 92.0 | 89.0 | 3.0 | 127.0 | 22.0 | 4.5 | 29.0 | 1.2 | 56.2 | 48.8 | 44.3 | 78.3 | 61.0 | 101.4 | 116.8 | 47.2 | 84.8 |
| 4 | 92.0 | 89.0 | 3.0 | 127.0 | 22.0 | 4.7 | 29.0 | 1.2 | 56.6 | 48.6 | 44.2 | 78.1 | 60.9 | 101.3 | 116.8 | 47.4 | 84.7 |
| 4 | 92.0 | 89.0 | 3.0 | 127.0 | 22.0 | 4.5 | 29.0 | 1.4 | 56.2 | 48.1 | 44.1 | 78.4 | 61.2 | 101.1 | 117.3 | 47.7 | 85.2 |
| 5 | 92.0 | 89.0 | 3.0 | 132.0 | 20.0 | 4.5 | 26.0 | 1.2 | 56.7 | 44.9 | 46.1 | 78.8 | 60.5 | 102.8 | 117.8 | 48.2 | 84.8 |
| 5 | 92.0 | 89.0 | 3.0 | 132.0 | 20.0 | 4.2 | 26.0 | 1.4 | 56.5 | 44.9 | 46.2 | 78.8 | 60.5 | 103.0 | 117.4 | 48.4 | 85.0 |
| 5 | 92.0 | 89.0 | 3.0 | 132.0 | 20.0 | 4.5 | 26.0 | 1.9 | 56.6 | 44.2 | 46.1 | 78.6 | 60.2 | 103.0 | 117.7 | 48.1 | 85.3 |
| 5 | 92.0 | 89.0 | 3.0 | 132.0 | 20.0 | 4.7 | 26.0 | 1.4 | 56.7 | 44.5 | 46.1 | 78.8 | 60.5 | 103.0 | 117.2 | 48.5 | 84.8 |
| 5 | 92.0 | 89.0 | 3.0 | 132.0 | 20.0 | 4.2 | 26.0 | 1.4 | 56.7 | 44.7 | 45.9 | 79.0 | 60.5 | 102.7 | 117.3 | 48.2 | 85.5 |
| 5 | 92.0 | 89.0 | 3.0 | 132.0 | 20.0 | 5.2 | 26.0 | 1.4 | 56.7 | 44.4 | 46.1 | 78.7 | 60.2 | 102.8 | 117.3 | 48.6 | 85.3 |
| 5 | 92.0 | 89.0 | 3.0 | 132.0 | 20.0 | 4.7 | 26.0 | 1.4 | 56.3 | 44.5 | 46.1 | 78.4 | 60.2 | 103.0 | 117.8 | 48.2 | 85.0 |
| 5 | 92.0 | 89.0 | 3.0 | 132.0 | 20.0 | 4.7 | 26.0 | 1.4 | 56.9 | 44.5 | 45.7 | 78.9 | 60.2 | 103.1 | 117.5 | 48.3 | 84.9 |
| 5 | 92.0 | 89.0 | 3.0 | 132.0 | 20.0 | 4.2 | 26.0 | 0.7 | 56.7 | 44.4 | 46.1 | 78.8 | 60.7 | 103.0 | 117.3 | 48.3 | 85.5 |
| 5 | 92.0 | 89.0 | 3.0 | 132.0 | 20.0 | 4.2 | 26.0 | 1.0 | 56.7 | 44.2 | 46.2 | 78.7 | 60.7 | 102.7 | 117.5 | 48.3 | 85.5 |

## E.2.5. Volunteer 3: "Black Bone"

| | SNA Angle | SNB Angle | ANB Angle | Interincisal Angle | 1-NA angle | 1-NA | 1-NB Angle | 1-NB | S-N | PNS-ANS | S-PNS | S-ANS | Me-ANS | N-Pog | S-Gn | N-A | N-B |
|---|---|---|---|---|---|---|---|---|---|---|---|---|---|---|---|---|---|
| 1 | 85.0 | 81.0 | 4.0 | 145.0 | 13.0 | 1.9 | 19.0 | 3.3 | 67.6 | 57.3 | 48.6 | 87.2 | 63.6 | 110.1 | 122.8 | 53.8 | 88.8 |
| 1 | 85.0 | 81.0 | 4.0 | 145.0 | 13.0 | 1.6 | 19.0 | 5.2 | 67.2 | 57.6 | 48.4 | 87.2 | 63.6 | 110.1 | 123.0 | 54.1 | 88.9 |
| 1 | 85.0 | 81.0 | 4.0 | 145.0 | 13.0 | 1.4 | 19.0 | 4.9 | 67.5 | 57.6 | 48.2 | 87.2 | 63.9 | 110.1 | 122.3 | 54.3 | 88.5 |
| 1 | 85.0 | 81.0 | 4.0 | 145.0 | 13.0 | 1.7 | 19.0 | 4.3 | 67.0 | 57.3 | 48.5 | 87.0 | 63.6 | 109.9 | 122.5 | 54.4 | 88.8 |
| 1 | 85.0 | 81.0 | 4.0 | 145.0 | 13.0 | 1.4 | 19.0 | 4.9 | 67.6 | 57.3 | 48.8 | 87.1 | 63.6 | 109.7 | 122.5 | 54.0 | 88.5 |
| 1 | 85.0 | 81.0 | 4.0 | 145.0 | 13.0 | 1.7 | 19.0 | 5.7 | 67.6 | 57.3 | 48.4 | 87.4 | 63.6 | 109.7 | 122.6 | 54.3 | 88.8 |
| 1 | 85.0 | 81.0 | 4.0 | 145.0 | 13.0 | 1.7 | 19.0 | 5.2 | 67.6 | 57.3 | 48.8 | 87.4 | 63.1 | 109.9 | 122.8 | 54.0 | 88.7 |
| 1 | 85.0 | 81.0 | 4.0 | 145.0 | 13.0 | 1.6 | 19.0 | 3.8 | 67.3 | 57.4 | 48.3 | 87.2 | 63.8 | 109.9 | 123.0 | 54.1 | 88.5 |
| 1 | 85.0 | 81.0 | 4.0 | 145.0 | 13.0 | 1.9 | 19.0 | 4.9 | 67.5 | 57.6 | 49.2 | 87.2 | 63.6 | 109.9 | 122.8 | 54.1 | 88.6 |
| 1 | 85.0 | 81.0 | 4.0 | 145.0 | 13.0 | 1.4 | 19.0 | 5.2 | 67.8 | 57.3 | 48.4 | 87.7 | 63.6 | 109.9 | 122.2 | 54.4 | 88.8 |
| 2 | 85.0 | 81.0 | 4.0 | 141.0 | 16.0 | 0.7 | 21.0 | 3.8 | 67.5 | 57.6 | 48.4 | 87.5 | 63.4 | 108.0 | 122.1 | 53.5 | 90.9 |
| 2 | 85.0 | 81.0 | 4.0 | 141.0 | 16.0 | 0.7 | 21.0 | 4.7 | 67.6 | 57.4 | 48.5 | 87.1 | 63.6 | 108.5 | 121.9 | 53.7 | 90.9 |
| 2 | 85.0 | 81.0 | 4.0 | 141.0 | 16.0 | 1.2 | 21.0 | 3.5 | 67.4 | 57.3 | 48.4 | 87.3 | 63.1 | 108.5 | 121.9 | 53.4 | 91.1 |
| 2 | 85.0 | 81.0 | 4.0 | 141.0 | 16.0 | 1.6 | 21.0 | 4.7 | 67.4 | 57.4 | 48.2 | 87.1 | 64.1 | 108.3 | 122.1 | 53.4 | 91.1 |
| 2 | 85.0 | 81.0 | 4.0 | 141.0 | 16.0 | 1.4 | 21.0 | 3.8 | 67.4 | 57.4 | 48.3 | 87.2 | 63.2 | 108.3 | 121.7 | 53.4 | 90.9 |
| 2 | 85.0 | 81.0 | 4.0 | 141.0 | 16.0 | 1.0 | 21.0 | 4.0 | 67.7 | 57.8 | 48.0 | 87.1 | 63.6 | 108.1 | 122.1 | 53.4 | 90.9 |
| 2 | 85.0 | 81.0 | 4.0 | 141.0 | 16.0 | 0.7 | 21.0 | 4.2 | 67.1 | 57.6 | 48.0 | 87.3 | 63.9 | 108.1 | 121.7 | 53.8 | 90.9 |
| 2 | 85.0 | 81.0 | 4.0 | 141.0 | 16.0 | 1.0 | 21.0 | 4.2 | 67.2 | 57.1 | 47.8 | 87.5 | 63.7 | 108.6 | 122.1 | 53.5 | 90.9 |
| 2 | 85.0 | 81.0 | 4.0 | 141.0 | 16.0 | 0.9 | 21.0 | 4.2 | 67.6 | 57.9 | 46.8 | 87.0 | 63.9 | 108.1 | 121.9 | 53.4 | 91.1 |
| 2 | 85.0 | 81.0 | 4.0 | 141.0 | 16.0 | 1.4 | 21.0 | 4.7 | 67.6 | 57.2 | 48.0 | 86.9 | 63.8 | 108.5 | 121.8 | 53.2 | 91.1 |
| 3 | 84.0 | 80.0 | 4.0 | 133.0 | 19.0 | 1.2 | 25.0 | 4.2 | 67.6 | 56.8 | 47.6 | 86.5 | 63.3 | 109.7 | 121.7 | 82.6 | 91.4 |
| 3 | 84.0 | 80.0 | 4.0 | 133.0 | 19.0 | 1.4 | 25.0 | 4.0 | 67.8 | 56.6 | 47.6 | 86.0 | 63.1 | 110.0 | 121.9 | 82.3 | 91.9 |
| 3 | 84.0 | 80.0 | 4.0 | 133.0 | 19.0 | 1.6 | 25.0 | 3.3 | 67.3 | 56.5 | 47.4 | 86.2 | 63.6 | 109.7 | 121.5 | 82.7 | 91.4 |
| 3 | 84.0 | 80.0 | 4.0 | 133.0 | 19.0 | 1.3 | 25.0 | 4.0 | 68.0 | 56.8 | 47.5 | 86.4 | 63.3 | 110.0 | 122.0 | 82.5 | 91.4 |
| 3 | 84.0 | 80.0 | 4.0 | 133.0 | 19.0 | 0.9 | 25.0 | 4.5 | 67.9 | 57.3 | 46.7 | 85.8 | 63.5 | 109.7 | 121.9 | 82.3 | 91.8 |
| 3 | 84.0 | 80.0 | 4.0 | 133.0 | 19.0 | 1.2 | 25.0 | 4.0 | 67.8 | 56.8 | 47.1 | 86.5 | 63.8 | 109.9 | 121.7 | 82.6 | 91.8 |
| 3 | 84.0 | 80.0 | 4.0 | 133.0 | 19.0 | 1.2 | 25.0 | 4.2 | 68.0 | 56.8 | 47.4 | 86.2 | 63.3 | 109.9 | 121.7 | 82.8 | 91.6 |
| 3 | 84.0 | 80.0 | 4.0 | 133.0 | 19.0 | 1.2 | 25.0 | 4.2 | 68.1 | 57.0 | 47.4 | 86.0 | 63.3 | 109.9 | 121.9 | 82.5 | 91.6 |
| 3 | 84.0 | 80.0 | 4.0 | 133.0 | 19.0 | 1.2 | 25.0 | 3.8 | 67.8 | 56.8 | 47.6 | 86.2 | 63.1 | 110.2 | 121.7 | 82.7 | 91.4 |
| 3 | 84.0 | 80.0 | 4.0 | 133.0 | 19.0 | 1.2 | 25.0 | 5.0 | 67.8 | 57.0 | 47.2 | 86.6 | 63.3 | 109.9 | 121.3 | 82.6 | 91.6 |
| 4 | 84.0 | 80.0 | 4.0 | 135.0 | 20.0 | 1.2 | 22.0 | 4.0 | 67.6 | 57.7 | 46.8 | 87.0 | 63.7 | 108.2 | 120.9 | 54.1 | 90.6 |
| 4 | 84.0 | 80.0 | 4.0 | 135.0 | 20.0 | 1.4 | 22.0 | 3.5 | 67.1 | 57.5 | 46.8 | 86.5 | 63.6 | 109.0 | 121.3 | 54.2 | 90.4 |
| 4 | 84.0 | 80.0 | 4.0 | 135.0 | 20.0 | 0.9 | 22.0 | 3.8 | 67.5 | 57.5 | 47.0 | 86.6 | 63.7 | 108.7 | 120.9 | 54.4 | 90.4 |
| 4 | 84.0 | 80.0 | 4.0 | 135.0 | 20.0 | 1.2 | 22.0 | 3.3 | 67.3 | 57.7 | 46.8 | 86.3 | 63.6 | 108.7 | 120.8 | 54.3 | 90.1 |
| 4 | 84.0 | 80.0 | 4.0 | 135.0 | 20.0 | 1.0 | 22.0 | 4.5 | 67.3 | 57.7 | 46.7 | 86.5 | 63.6 | 108.2 | 120.7 | 53.6 | 91.1 |
| 4 | 84.0 | 80.0 | 4.0 | 135.0 | 20.0 | 1.3 | 22.0 | 4.0 | 67.3 | 57.7 | 46.8 | 86.1 | 63.4 | 108.8 | 121.3 | 54.3 | 90.7 |
| 4 | 84.0 | 80.0 | 4.0 | 135.0 | 20.0 | 1.2 | 22.0 | 4.2 | 67.6 | 57.7 | 46.8 | 86.5 | 63.6 | 108.7 | 120.7 | 54.4 | 90.2 |
| 4 | 84.0 | 80.0 | 4.0 | 135.0 | 20.0 | 1.2 | 22.0 | 3.6 | 67.4 | 57.4 | 46.8 | 86.3 | 63.6 | 108.7 | 120.9 | 53.9 | 90.7 |
| 4 | 84.0 | 80.0 | 4.0 | 135.0 | 20.0 | 1.4 | 22.0 | 3.8 | 67.6 | 57.7 | 46.9 | 86.6 | 63.7 | 108.8 | 120.7 | 54.2 | 90.4 |
| 4 | 84.0 | 80.0 | 4.0 | 135.0 | 20.0 | 1.4 | 22.0 | 3.8 | 67.5 | 57.2 | 47.0 | 86.7 | 63.4 | 108.8 | 120.7 | 54.3 | 90.4 |
| 5 | 84.0 | 80.0 | 4.0 | 133.0 | 24.0 | 1.4 | 20.0 | 4.2 | 67.9 | 57.7 | 46.8 | 86.9 | 64.1 | 108.8 | 121.2 | 53.5 | 91.8 |
| 5 | 84.0 | 80.0 | 4.0 | 133.0 | 24.0 | 1.2 | 20.0 | 4.5 | 67.8 | 57.7 | 46.6 | 87.1 | 64.6 | 108.7 | 121.7 | 53.7 | 91.5 |
| 5 | 84.0 | 80.0 | 4.0 | 133.0 | 24.0 | 1.4 | 20.0 | 4.9 | 67.9 | 57.5 | 46.8 | 87.1 | 64.6 | 108.5 | 121.7 | 53.8 | 91.6 |
| 5 | 84.0 | 80.0 | 4.0 | 133.0 | 24.0 | 1.7 | 20.0 | 4.5 | 67.2 | 57.7 | 46.4 | 87.0 | 64.3 | 108.3 | 121.2 | 53.4 | 90.8 |
| 5 | 84.0 | 80.0 | 4.0 | 133.0 | 24.0 | 0.9 | 20.0 | 4.7 | 67.7 | 57.5 | 47.0 | 86.9 | 64.1 | 108.5 | 121.4 | 53.4 | 91.5 |
| 5 | 84.0 | 80.0 | 4.0 | 133.0 | 24.0 | 1.5 | 20.0 | 5.2 | 68.4 | 57.7 | 47.0 | 87.3 | 64.4 | 108.9 | 121.6 | 53.6 | 91.7 |
| 5 | 84.0 | 80.0 | 4.0 | 133.0 | 24.0 | 1.4 | 20.0 | 4.7 | 68.2 | 57.3 | 46.5 | 86.9 | 63.9 | 108.0 | 121.6 | 53.6 | 92.0 |
| 5 | 84.0 | 80.0 | 4.0 | 133.0 | 24.0 | 1.6 | 20.0 | 5.4 | 67.9 | 57.3 | 46.6 | 86.9 | 63.8 | 108.3 | 121.4 | 53.9 | 92.0 |
| 5 | 84.0 | 80.0 | 4.0 | 133.0 | 24.0 | 1.3 | 20.0 | 4.5 | 68.2 | 57.5 | 46.8 | 86.9 | 64.3 | 108.7 | 121.4 | 53.6 | 91.5 |
| 5 | 84.0 | 80.0 | 4.0 | 133.0 | 24.0 | 1.2 | 20.0 | 4.7 | 68.2 | 57.3 | 46.5 | 87.1 | 64.3 | 108.5 | 121.0 | 53.6 | 91.3 |

## E.2.6. Volunteer 1: MRI T1

| | SNA Angle | SNB Angle | ANB Angle | Interincisal Angle | 1-NA angle | 1-NA | 1-NB Angle | 1-NB | S-N | PNS-ANS | S-PNS | S-ANS | Me-ANS | N-Pog | S-Gn | N-A | N-B |
|---|---|---|---|---|---|---|---|---|---|---|---|---|---|---|---|---|---|
| 1 | 85.0 | 80.0 | 5.0 | 129.0 | 29.0 | 4.2 | 18.0 | 5.4 | 70.2 | 51.7 | 46.3 | 84.3 | 64.4 | 98.2 | 113.1 | 46.0 | 83.0 |
| 1 | 86.0 | 81.0 | 5.0 | 130.0 | 28.0 | 4.1 | 17.0 | 5.0 | 69.9 | 52.0 | 45.8 | 84.4 | 64.5 | 98.1 | 113.1 | 45.9 | 83.0 |
| 1 | 86.0 | 81.0 | 5.0 | 131.0 | 28.0 | 4.6 | 18.0 | 5.2 | 69.8 | 51.8 | 45.5 | 84.6 | 64.6 | 98.1 | 113.5 | 46.2 | 83.0 |
| 1 | 85.0 | 80.0 | 5.0 | 130.0 | 27.0 | 4.7 | 18.0 | 5.0 | 70.1 | 52.1 | 45.8 | 84.3 | 64.4 | 97.5 | 113.4 | 46.4 | 83.6 |
| 1 | 85.0 | 80.0 | 4.0 | 130.0 | 28.0 | 4.6 | 18.0 | 5.2 | 70.0 | 51.9 | 45.8 | 84.4 | 64.8 | 97.9 | 113.3 | 46.1 | 82.9 |
| 1 | 85.0 | 80.0 | 5.0 | 130.0 | 28.0 | 4.6 | 18.0 | 5.4 | 69.8 | 52.2 | 45.9 | 83.9 | 64.2 | 98.3 | 113.4 | 46.5 | 83.0 |
| 1 | 85.0 | 80.0 | 5.0 | 130.0 | 28.0 | 4.9 | 18.0 | 5.2 | 70.0 | 51.9 | 46.0 | 84.2 | 64.2 | 97.7 | 113.4 | 46.5 | 83.6 |
| 1 | 85.0 | 80.0 | 5.0 | 130.0 | 28.0 | 4.3 | 18.0 | 5.4 | 69.9 | 51.9 | 46.3 | 84.4 | 64.2 | 98.1 | 113.3 | 46.3 | 83.0 |
| 1 | 86.0 | 80.0 | 5.0 | 130.0 | 28.0 | 4.6 | 18.0 | 5.2 | 69.7 | 51.9 | 45.8 | 84.1 | 64.4 | 97.9 | 113.3 | 45.9 | 83.2 |
| 1 | 85.0 | 80.0 | 5.0 | 131.0 | 28.0 | 4.8 | 17.0 | 5.6 | 70.3 | 51.6 | 45.6 | 84.5 | 64.6 | 98.2 | 113.4 | 46.1 | 83.2 |
| 2 | 81.0 | 82.0 | 2.0 | 118.0 | 34.0 | 16.2 | 29.0 | 5.9 | 66.8 | 56.1 | 43.0 | 83.0 | 68.0 | 99.3 | 115.8 | 44.8 | 83.7 |
| 2 | 80.0 | 82.0 | 2.0 | 119.0 | 34.0 | 16.0 | 29.0 | 6.0 | 66.7 | 56.5 | 43.6 | 83.4 | 68.1 | 99.6 | 115.8 | 44.8 | 83.9 |
| 2 | 80.0 | 82.0 | 2.0 | 119.0 | 34.0 | 15.8 | 30.0 | 6.1 | 66.8 | 55.8 | 43.2 | 83.3 | 68.7 | 99.5 | 115.9 | 44.8 | 83.7 |
| 2 | 80.0 | 82.0 | 2.0 | 119.0 | 34.0 | 16.0 | 29.0 | 6.2 | 66.9 | 56.1 | 43.6 | 83.5 | 68.3 | 99.1 | 116.1 | 44.8 | 83.7 |
| 2 | 80.0 | 82.0 | 2.0 | 119.0 | 34.0 | 16.0 | 29.0 | 6.7 | 66.9 | 56.0 | 42.9 | 83.1 | 68.2 | 99.3 | 115.6 | 44.3 | 83.5 |
| 2 | 80.0 | 82.0 | 2.0 | 119.0 | 34.0 | 15.5 | 29.0 | 6.2 | 67.0 | 55.8 | 43.9 | 83.5 | 68.2 | 99.4 | 115.8 | 44.8 | 83.9 |
| 2 | 80.0 | 82.0 | 2.0 | 119.0 | 34.0 | 16.2 | 29.0 | 6.8 | 66.8 | 55.9 | 43.6 | 83.3 | 68.5 | 99.3 | 115.9 | 44.5 | 83.7 |
| 2 | 80.0 | 82.0 | 2.0 | 119.0 | 34.0 | 15.9 | 29.0 | 6.7 | 66.8 | 56.0 | 43.4 | 83.3 | 68.8 | 99.3 | 115.8 | 44.5 | 83.7 |
| 2 | 80.0 | 82.0 | 2.0 | 119.0 | 34.0 | 15.7 | 29.0 | 6.6 | 66.4 | 56.1 | 43.1 | 83.0 | 68.2 | 99.5 | 116.0 | 44.8 | 83.7 |
| 2 | 80.0 | 82.0 | 2.0 | 119.0 | 34.0 | 15.7 | 29.0 | 6.6 | 67.0 | 55.8 | 43.4 | 83.3 | 68.5 | 99.3 | 115.9 | 44.8 | 83.7 |
| 3 | 82.0 | 79.0 | 3.0 | 122.0 | 31.0 | 7.3 | 26.0 | 6.3 | 71.9 | 62.4 | 44.8 | 91.1 | 66.1 | 97.0 | 115.1 | 45.7 | 82.7 |
| 3 | 83.0 | 80.0 | 3.0 | 122.0 | 31.0 | 8.0 | 26.0 | 6.1 | 72.2 | 62.0 | 45.3 | 91.2 | 66.6 | 96.7 | 115.3 | 45.7 | 82.5 |
| 3 | 83.0 | 79.0 | 3.0 | 122.0 | 31.0 | 8.0 | 26.0 | 6.1 | 72.1 | 62.4 | 45.4 | 90.8 | 66.6 | 97.0 | 115.6 | 45.5 | 82.2 |
| 3 | 83.0 | 80.0 | 3.0 | 122.0 | 31.0 | 8.0 | 26.0 | 6.4 | 72.4 | 62.5 | 44.7 | 91.2 | 66.4 | 97.0 | 115.4 | 46.0 | 82.4 |
| 3 | 83.0 | 80.0 | 3.0 | 122.0 | 31.0 | 8.0 | 26.0 | 6.3 | 72.4 | 62.4 | 45.3 | 91.1 | 66.2 | 96.7 | 115.7 | 46.0 | 82.7 |
| 3 | 82.0 | 79.0 | 3.0 | 122.0 | 31.0 | 8.0 | 26.0 | 6.6 | 72.1 | 62.6 | 45.3 | 91.2 | 66.6 | 96.8 | 115.4 | 45.8 | 82.2 |
| 3 | 82.0 | 79.0 | 3.0 | 122.0 | 31.0 | 7.7 | 26.0 | 6.6 | 72.4 | 62.2 | 44.8 | 91.0 | 66.1 | 97.0 | 115.8 | 45.7 | 82.5 |
| 3 | 82.0 | 79.0 | 3.0 | 122.0 | 31.0 | 7.7 | 26.0 | 6.3 | 72.1 | 62.4 | 45.3 | 91.2 | 66.1 | 97.0 | 115.3 | 45.7 | 82.2 |
| 3 | 82.0 | 79.0 | 3.0 | 122.0 | 31.0 | 8.2 | 26.0 | 6.3 | 72.3 | 62.7 | 45.2 | 91.5 | 66.1 | 96.5 | 115.4 | 45.5 | 82.0 |
| 3 | 82.0 | 80.0 | 3.0 | 122.0 | 31.0 | 7.7 | 26.0 | 6.1 | 72.2 | 62.8 | 45.0 | 91.1 | 66.0 | 96.7 | 115.4 | 45.3 | 82.2 |
| 4 | 86.0 | 80.0 | 7.0 | 115.0 | 24.0 | 3.5 | 34.0 | 6.4 | 69.9 | 56.3 | 46.7 | 89.3 | 65.8 | 100.3 | 114.4 | 47.0 | 84.2 |
| 4 | 85.0 | 79.0 | 6.0 | 116.0 | 24.0 | 3.5 | 34.0 | 6.1 | 69.9 | 56.1 | 46.8 | 89.4 | 65.1 | 100.3 | 114.6 | 46.8 | 84.5 |
| 4 | 86.0 | 80.0 | 6.0 | 116.0 | 24.0 | 3.3 | 34.0 | 7.3 | 70.0 | 56.3 | 46.8 | 89.3 | 65.8 | 100.5 | 114.4 | 46.5 | 84.2 |
| 4 | 86.0 | 80.0 | 7.0 | 116.0 | 24.0 | 3.6 | 34.0 | 6.8 | 70.0 | 56.0 | 47.3 | 89.2 | 65.5 | 100.1 | 114.5 | 47.0 | 84.2 |
| 4 | 86.0 | 79.0 | 7.0 | 116.0 | 24.0 | 3.3 | 34.0 | 7.0 | 69.4 | 56.0 | 47.2 | 89.2 | 65.3 | 100.5 | 114.4 | 46.7 | 83.8 |
| 4 | 86.0 | 80.0 | 7.0 | 116.0 | 24.0 | 3.1 | 34.0 | 5.6 | 70.2 | 56.1 | 46.6 | 89.2 | 65.5 | 100.3 | 114.9 | 46.5 | 84.2 |
| 4 | 86.0 | 79.0 | 7.0 | 116.0 | 24.0 | 3.8 | 34.0 | 6.1 | 69.6 | 56.0 | 47.1 | 89.2 | 65.7 | 100.1 | 114.7 | 46.5 | 84.0 |
| 4 | 86.0 | 79.0 | 7.0 | 116.0 | 24.0 | 3.5 | 34.0 | 6.6 | 69.7 | 56.0 | 46.8 | 89.2 | 65.8 | 100.8 | 114.6 | 46.8 | 84.0 |
| 4 | 86.0 | 80.0 | 7.0 | 116.0 | 24.0 | 3.5 | 34.0 | 6.3 | 69.5 | 55.8 | 46.8 | 89.2 | 65.3 | 100.3 | 114.9 | 46.7 | 84.5 |
| 4 | 86.0 | 79.0 | 6.0 | 116.0 | 24.0 | 3.1 | 34.0 | 6.8 | 69.9 | 56.3 | 47.4 | 89.3 | 65.5 | 100.3 | 114.4 | 46.7 | 84.5 |

## E.2.7. Volunteer 2: MRI T1

| | SNA Angle | SNB Angle | ANB Angle | Interincisal Angle | 1-NA angle | 1-NA | 1-NB Angle | 1-NB | S-N | PNS-ANS | S-ANS | Me-ANS | N-Pog |
|---|---|---|---|---|---|---|---|---|---|---|---|---|---|
| 1 | 93.0 | 91.0 | 2.0 | 132.0 | 27.0 | 3.8 | 21.0 | 1.9 | 59.4 | 49.3 | 79.4 | 61.4 | 100.6 |
| 1 | 93.0 | 91.0 | 2.0 | 132.0 | 27.0 | 4.0 | 21.0 | 1.5 | 59.5 | 48.8 | 79.0 | 61.9 | 100.8 |
| 1 | 93.0 | 91.0 | 2.0 | 132.0 | 27.0 | 4.0 | 21.0 | 2.0 | 59.5 | 49.0 | 79.2 | 60.9 | 100.4 |
| 1 | 93.0 | 91.0 | 2.0 | 132.0 | 27.0 | 3.8 | 21.0 | 1.6 | 59.5 | 49.3 | 78.8 | 60.9 | 100.6 |
| 1 | 93.0 | 91.0 | 2.0 | 132.0 | 27.0 | 3.8 | 21.0 | 1.9 | 59.5 | 48.6 | 79.0 | 60.9 | 100.8 |
| 1 | 93.0 | 91.0 | 2.0 | 132.0 | 27.0 | 4.0 | 21.0 | 1.7 | 59.5 | 48.9 | 79.1 | 61.6 | 100.2 |
| 1 | 93.0 | 91.0 | 2.0 | 132.0 | 27.0 | 3.1 | 21.0 | 1.4 | 59.2 | 49.0 | 79.3 | 61.4 | 100.6 |
| 1 | 93.0 | 91.0 | 2.0 | 132.0 | 27.0 | 3.3 | 21.0 | 2.4 | 58.9 | 48.6 | 79.6 | 61.2 | 100.8 |
| 1 | 93.0 | 91.0 | 2.0 | 132.0 | 27.0 | 3.8 | 21.0 | 1.4 | 59.1 | 48.6 | 78.9 | 61.4 | 100.4 |
| 1 | 93.0 | 91.0 | 2.0 | 132.0 | 27.0 | 4.0 | 21.0 | 1.5 | 59.1 | 48.9 | 79.3 | 61.4 | 100.6 |
| 2 | 93.0 | 90.0 | 3.0 | 128.0 | 23.0 | 2.6 | 25.0 | 2.1 | 58.7 | 46.8 | 80.5 | 61.4 | 100.5 |
| 2 | 93.0 | 90.0 | 3.0 | 128.0 | 23.0 | 2.6 | 25.0 | 1.6 | 59.3 | 46.4 | 80.3 | 61.2 | 100.3 |
| 2 | 93.0 | 90.0 | 3.0 | 128.0 | 23.0 | 3.0 | 25.0 | 1.6 | 58.7 | 46.5 | 80.3 | 61.4 | 100.6 |
| 2 | 93.0 | 90.0 | 3.0 | 128.0 | 23.0 | 2.4 | 25.0 | 1.6 | 58.4 | 46.7 | 80.5 | 61.4 | 100.7 |
| 2 | 93.0 | 90.0 | 3.0 | 128.0 | 23.0 | 2.3 | 25.0 | 1.9 | 58.4 | 46.8 | 80.4 | 61.4 | 100.3 |
| 2 | 93.0 | 90.0 | 3.0 | 128.0 | 23.0 | 2.6 | 25.0 | 1.7 | 58.2 | 46.9 | 80.6 | 60.7 | 100.7 |
| 2 | 93.0 | 90.0 | 3.0 | 128.0 | 23.0 | 2.6 | 25.0 | 1.7 | 59.0 | 46.8 | 80.3 | 61.2 | 100.5 |
| 2 | 93.0 | 90.0 | 3.0 | 128.0 | 23.0 | 1.9 | 25.0 | 1.4 | 58.4 | 46.4 | 79.6 | 61.2 | 100.7 |
| 2 | 93.0 | 90.0 | 3.0 | 128.0 | 23.0 | 3.1 | 25.0 | 1.4 | 58.2 | 46.9 | 80.5 | 61.7 | 100.5 |
| 2 | 93.0 | 90.0 | 3.0 | 128.0 | 23.0 | 2.6 | 25.0 | 1.9 | 58.4 | 46.7 | 80.3 | 61.0 | 100.3 |
| 3 | 93.0 | 90.0 | 3.0 | 126.0 | 24.0 | 3.1 | 27.0 | 3.3 | 59.7 | 50.5 | 81.8 | 62.6 | 99.8 |
| 3 | 93.0 | 90.0 | 3.0 | 126.0 | 24.0 | 2.8 | 27.0 | 3.3 | 59.5 | 50.0 | 81.4 | 62.4 | 100.6 |
| 3 | 93.0 | 90.0 | 3.0 | 126.0 | 24.0 | 3.1 | 27.0 | 2.8 | 59.2 | 50.5 | 81.5 | 61.9 | 99.9 |
| 3 | 93.0 | 90.0 | 3.0 | 126.0 | 24.0 | 3.3 | 27.0 | 3.1 | 59.4 | 50.2 | 81.5 | 61.9 | 100.0 |
| 3 | 93.0 | 90.0 | 3.0 | 126.0 | 24.0 | 2.8 | 27.0 | 3.1 | 59.3 | 50.1 | 81.5 | 62.4 | 99.7 |
| 3 | 93.0 | 90.0 | 3.0 | 126.0 | 24.0 | 3.3 | 27.0 | 3.3 | 59.7 | 50.3 | 81.7 | 62.2 | 100.2 |
| 3 | 93.0 | 90.0 | 3.0 | 126.0 | 24.0 | 2.8 | 27.0 | 3.6 | 59.5 | 50.3 | 81.2 | 62.9 | 99.8 |
| 3 | 93.0 | 90.0 | 3.0 | 126.0 | 24.0 | 3.3 | 27.0 | 2.8 | 59.5 | 50.3 | 81.4 | 62.4 | 99.9 |
| 3 | 93.0 | 90.0 | 3.0 | 126.0 | 24.0 | 3.8 | 27.0 | 3.1 | 59.5 | 50.2 | 81.5 | 62.6 | 100.1 |
| 3 | 93.0 | 90.0 | 3.0 | 126.0 | 24.0 | 3.0 | 27.0 | 2.4 | 59.5 | 50.1 | 81.6 | 61.9 | 100.2 |

## E.2.8. Volunteer 3: MRI T1

| | SNA Angle | SNB Angle | ANB Angle | Interincisal Angle | 1-NA angle | 1-NA | 1-NB Angle | 1-NB | S-N | PNS-ANS | S-ANS | Me-ANS | N-Pog |
|---|---|---|---|---|---|---|---|---|---|---|---|---|---|
| 1 | 91.0 | 86.0 | 5.0 | 141.0 | 9.0 | 1.2 | 26.0 | 2.6 | 65.7 | 48.5 | 87.7 | 65.3 | 106.6 |
| 1 | 91.0 | 86.0 | 5.0 | 141.0 | 9.0 | 0.9 | 26.0 | 3.0 | 65.5 | 48.0 | 87.5 | 64.9 | 106.6 |
| 1 | 91.0 | 86.0 | 5.0 | 141.0 | 9.0 | 1.4 | 26.0 | 2.4 | 65.5 | 48.8 | 87.5 | 65.1 | 106.6 |
| 1 | 91.0 | 86.0 | 5.0 | 141.0 | 9.0 | 1.2 | 26.0 | 2.6 | 65.8 | 48.7 | 87.3 | 65.3 | 106.6 |
| 1 | 91.0 | 86.0 | 5.0 | 141.0 | 9.0 | 1.2 | 26.0 | 2.8 | 65.3 | 48.7 | 88.0 | 65.1 | 106.8 |
| 1 | 91.0 | 86.0 | 5.0 | 141.0 | 9.0 | 1.4 | 26.0 | 2.4 | 65.7 | 48.8 | 87.8 | 65.1 | 106.5 |
| 1 | 91.0 | 86.0 | 5.0 | 141.0 | 9.0 | 1.6 | 26.0 | 2.8 | 65.8 | 48.8 | 88.1 | 65.5 | 106.4 |
| 1 | 91.0 | 86.0 | 5.0 | 141.0 | 9.0 | 1.4 | 26.0 | 3.1 | 65.3 | 48.7 | 87.5 | 65.3 | 106.6 |
| 1 | 91.0 | 86.0 | 5.0 | 141.0 | 9.0 | 1.6 | 26.0 | 3.3 | 65.7 | 48.6 | 87.5 | 64.8 | 106.6 |
| 1 | 91.0 | 86.0 | 5.0 | 141.0 | 9.0 | 0.9 | 26.0 | 3.1 | 65.8 | 48.4 | 87.0 | 65.3 | 106.6 |
| 2 | 90.0 | 84.0 | 6.0 | 144.0 | 10.0 | 0.9 | 22.0 | 3.8 | 65.5 | 51.9 | 86.9 | 65.3 | 106.8 |
| 2 | 90.0 | 84.0 | 6.0 | 144.0 | 10.0 | 2.1 | 22.0 | 3.3 | 65.7 | 52.4 | 86.9 | 65.0 | 107.0 |
| 2 | 90.0 | 84.0 | 6.0 | 144.0 | 10.0 | 1.6 | 22.0 | 2.8 | 65.1 | 52.5 | 86.4 | 65.5 | 106.8 |
| 2 | 90.0 | 84.0 | 6.0 | 144.0 | 10.0 | 1.9 | 22.0 | 3.1 | 65.7 | 52.6 | 86.6 | 64.8 | 107.2 |
| 2 | 90.0 | 84.0 | 6.0 | 144.0 | 10.0 | 2.2 | 22.0 | 3.1 | 65.8 | 52.4 | 86.9 | 65.5 | 106.8 |
| 2 | 90.0 | 84.0 | 6.0 | 144.0 | 10.0 | 1.9 | 22.0 | 3.1 | 65.5 | 52.3 | 86.6 | 65.0 | 106.8 |
| 2 | 90.0 | 84.0 | 6.0 | 144.0 | 10.0 | 1.9 | 22.0 | 3.1 | 65.7 | 52.4 | 86.6 | 65.5 | 107.1 |
| 2 | 90.0 | 84.0 | 6.0 | 144.0 | 10.0 | 1.9 | 22.0 | 3.3 | 65.5 | 52.2 | 86.9 | 65.3 | 106.5 |
| 2 | 90.0 | 84.0 | 6.0 | 144.0 | 10.0 | 1.4 | 22.0 | 3.5 | 65.5 | 52.4 | 86.6 | 65.1 | 106.8 |
| 2 | 90.0 | 84.0 | 6.0 | 144.0 | 10.0 | 2.1 | 22.0 | 2.9 | 65.7 | 52.1 | 87.0 | 65.3 | 107.0 |
| 3 | 89.0 | 84.0 | 5.0 | 143.0 | 10.0 | 1.0 | 24.0 | 3.1 | 65.4 | 48.3 | 86.6 | 64.6 | 106.5 |
| 3 | 89.0 | 84.0 | 5.0 | 143.0 | 10.0 | 0.7 | 24.0 | 3.0 | 65.6 | 48.1 | 86.1 | 64.8 | 105.9 |
| 3 | 89.0 | 84.0 | 5.0 | 143.0 | 10.0 | 1.0 | 24.0 | 3.0 | 65.4 | 47.8 | 86.6 | 64.8 | 105.9 |
| 3 | 89.0 | 84.0 | 5.0 | 143.0 | 10.0 | 1.4 | 24.0 | 3.1 | 65.6 | 48.3 | 86.9 | 64.1 | 106.2 |
| 3 | 89.0 | 84.0 | 5.0 | 143.0 | 10.0 | 0.9 | 24.0 | 2.6 | 65.3 | 48.3 | 86.4 | 64.4 | 106.3 |
| 3 | 89.0 | 84.0 | 5.0 | 143.0 | 10.0 | 1.2 | 24.0 | 2.6 | 65.5 | 48.1 | 86.5 | 65.3 | 105.9 |
| 3 | 89.0 | 84.0 | 5.0 | 143.0 | 10.0 | 1.6 | 24.0 | 3.1 | 65.4 | 47.8 | 86.3 | 64.1 | 106.3 |
| 3 | 89.0 | 84.0 | 5.0 | 143.0 | 10.0 | 1.0 | 24.0 | 2.8 | 65.5 | 48.1 | 86.2 | 64.6 | 106.4 |
| 3 | 89.0 | 84.0 | 5.0 | 143.0 | 10.0 | 1.2 | 24.0 | 2.8 | 65.2 | 48.1 | 86.5 | 64.8 | 106.8 |
| 3 | 89.0 | 84.0 | 5.0 | 143.0 | 10.0 | 0.7 | 24.0 | 2.9 | 65.2 | 48.1 | 86.6 | 64.8 | 106.1 |

## E.2.9. Patient 1: Lateral Cephalogram

| | SNA Angle | SNB Angle | ANB Angle | S-N | PNS-ANS | S-PNS | S-ANS | Me-ANS | N -Pog | S-Gn | N-A | N-B |
|---|---|---|---|---|---|---|---|---|---|---|---|---|
| 1 | 80.0 | 88.0 | 8.0 | 66.8 | 50.6 | 46.5 | 84.1 | 70.7 | 118.0 | 137.3 | 53.9 | 102.3 |
| 1 | 80.0 | 88.0 | 8.0 | 67.2 | 50.8 | 46.4 | 84.4 | 70.9 | 117.6 | 137.0 | 53.8 | 102.0 |
| 1 | 80.0 | 88.0 | 8.0 | 67.4 | 50.8 | 47.1 | 84.1 | 70.9 | 118.0 | 136.8 | 53.5 | 102.0 |
| 1 | 80.0 | 88.0 | 8.0 | 67.4 | 50.8 | 47.0 | 84.2 | 71.3 | 117.3 | 137.5 | 53.9 | 101.6 |
| 1 | 80.0 | 88.0 | 8.0 | 67.0 | 50.8 | 46.6 | 84.2 | 71.3 | 117.8 | 137.0 | 54.2 | 101.9 |
| 1 | 80.0 | 88.0 | 8.0 | 67.2 | 50.8 | 47.0 | 84.4 | 70.7 | 117.8 | 137.0 | 53.4 | 102.0 |
| 1 | 80.0 | 88.0 | 8.0 | 67.0 | 50.8 | 46.8 | 84.0 | 70.9 | 117.8 | 137.0 | 53.9 | 102.0 |
| 1 | 80.0 | 88.0 | 8.0 | 67.2 | 50.7 | 46.7 | 84.2 | 70.9 | 117.8 | 137.1 | 53.5 | 102.0 |
| 1 | 80.0 | 88.0 | 8.0 | 67.6 | 50.8 | 46.9 | 84.1 | 70.7 | 117.8 | 137.0 | 53.9 | 102.0 |
| 1 | 80.0 | 88.0 | 8.0 | 67.4 | 50.7 | 47.0 | 84.4 | 70.5 | 117.8 | 137.0 | 54.1 | 102.0 |
| 2 | 78.0 | 87.0 | 9.0 | 68.5 | 45.8 | 49.3 | 82.3 | 70.0 | 118.4 | 137.0 | 53.8 | 103.8 |
| 2 | 78.0 | 87.0 | 9.0 | 68.5 | 45.7 | 49.5 | 82.6 | 70.2 | 118.4 | 136.8 | 53.7 | 103.4 |
| 2 | 78.0 | 87.0 | 9.0 | 68.4 | 45.7 | 49.4 | 82.4 | 70.0 | 118.4 | 137.1 | 53.8 | 103.8 |
| 2 | 78.0 | 87.0 | 9.0 | 68.5 | 45.8 | 49.3 | 82.5 | 69.8 | 118.4 | 137.1 | 53.6 | 103.6 |
| 2 | 78.0 | 87.0 | 9.0 | 68.4 | 46.1 | 49.4 | 82.0 | 70.0 | 118.4 | 137.2 | 53.5 | 103.6 |
| 2 | 78.0 | 87.0 | 9.0 | 68.7 | 45.9 | 49.4 | 82.6 | 70.4 | 118.2 | 137.2 | 53.9 | 103.8 |
| 2 | 78.0 | 87.0 | 9.0 | 68.7 | 45.7 | 49.6 | 82.4 | 70.0 | 118.4 | 137.2 | 53.8 | 103.5 |
| 2 | 78.0 | 87.0 | 9.0 | 68.5 | 46.1 | 49.2 | 82.4 | 70.4 | 118.1 | 137.3 | 54.1 | 104.0 |
| 2 | 78.0 | 87.0 | 9.0 | 68.5 | 45.9 | 49.4 | 82.2 | 70.2 | 118.5 | 137.0 | 53.5 | 103.6 |
| 2 | 78.0 | 87.0 | 9.0 | 68.5 | 45.9 | 49.5 | 82.3 | 70.4 | 118.4 | 137.0 | 53.6 | 103.8 |
| 3 | 79.0 | 88.0 | 9.0 | 59.9 | 45.3 | 48.4 | 80.7 | 71.2 | 118.5 | 137.3 | 54.4 | 103.4 |
| 3 | 79.0 | 88.0 | 9.0 | 68.2 | 45.1 | 48.6 | 80.4 | 71.2 | 118.3 | 137.5 | 54.8 | 103.0 |
| 3 | 79.0 | 88.0 | 9.0 | 68.0 | 45.1 | 48.7 | 80.8 | 71.2 | 118.1 | 137.2 | 54.3 | 103.2 |
| 3 | 79.0 | 88.0 | 9.0 | 67.7 | 45.3 | 48.7 | 80.8 | 71.3 | 118.3 | 136.5 | 54.5 | 103.4 |
| 3 | 79.0 | 88.0 | 9.0 | 67.9 | 45.0 | 48.8 | 80.7 | 71.5 | 118.1 | 136.8 | 54.4 | 103.4 |
| 3 | 79.0 | 88.0 | 9.0 | 68.2 | 44.9 | 48.8 | 80.7 | 71.3 | 118.1 | 137.3 | 54.1 | 103.2 |
| 3 | 79.0 | 88.0 | 9.0 | 68.2 | 45.1 | 49.0 | 80.3 | 71.2 | 118.5 | 136.8 | 54.3 | 103.0 |
| 3 | 79.0 | 88.0 | 9.0 | 68.2 | 44.8 | 49.0 | 80.6 | 71.2 | 118.1 | 137.1 | 54.2 | 103.0 |
| 3 | 79.0 | 88.0 | 9.0 | 68.2 | 45.6 | 49.1 | 80.5 | 71.2 | 118.5 | 137.2 | 54.6 | 103.4 |
| 3 | 79.0 | 88.0 | 9.0 | 67.9 | 45.1 | 48.8 | 80.4 | 71.0 | 118.1 | 137.1 | 54.5 | 103.2 |
| 4 | 80.0 | 88.0 | 8.0 | 68.4 | 46.9 | 48.8 | 82.9 | 70.7 | 116.7 | 138.1 | 53.5 | 103.6 |
| 4 | 80.0 | 88.0 | 8.0 | 68.4 | 46.5 | 49.5 | 83.1 | 70.7 | 116.7 | 138.2 | 53.3 | 103.5 |
| 4 | 80.0 | 88.0 | 8.0 | 68.4 | 46.5 | 48.8 | 83.3 | 71.5 | 117.2 | 138.1 | 53.7 | 103.7 |
| 4 | 80.0 | 88.0 | 8.0 | 68.8 | 46.5 | 48.9 | 82.9 | 71.3 | 117.0 | 138.6 | 53.5 | 103.7 |
| 4 | 80.0 | 88.0 | 8.0 | 68.4 | 46.5 | 48.8 | 83.1 | 71.2 | 117.2 | 138.3 | 53.3 | 103.6 |
| 4 | 80.0 | 88.0 | 8.0 | 68.2 | 46.5 | 49.2 | 82.9 | 71.3 | 116.7 | 138.3 | 53.5 | 103.5 |
| 4 | 80.0 | 88.0 | 8.0 | 68.4 | 46.5 | 48.8 | 83.1 | 70.9 | 116.7 | 138.3 | 53.5 | 103.3 |
| 4 | 80.0 | 88.0 | 8.0 | 68.4 | 46.5 | 49.3 | 83.1 | 71.1 | 116.7 | 138.9 | 53.5 | 103.3 |
| 4 | 80.0 | 88.0 | 8.0 | 68.4 | 46.7 | 49.1 | 83.0 | 70.9 | 116.7 | 138.4 | 53.5 | 103.5 |
| 4 | 80.0 | 88.0 | 8.0 | 68.2 | 46.5 | 49.1 | 82.8 | 70.9 | 117.0 | 138.3 | 53.5 | 103.3 |
| 5 | 80.0 | 87.0 | 7.0 | 68.2 | 46.3 | 48.2 | 81.8 | 70.7 | 118.0 | 137.3 | 55.4 | 105.9 |
| 5 | 80.0 | 87.0 | 7.0 | 68.5 | 46.3 | 48.1 | 81.6 | 70.9 | 118.1 | 137.1 | 55.4 | 106.4 |
| 5 | 80.0 | 87.0 | 7.0 | 68.7 | 46.2 | 48.4 | 81.9 | 71.3 | 118.0 | 137.5 | 55.7 | 106.4 |
| 5 | 80.0 | 87.0 | 7.0 | 68.2 | 46.3 | 48.0 | 81.8 | 70.9 | 118.0 | 137.4 | 55.2 | 106.1 |
| 5 | 80.0 | 87.0 | 7.0 | 68.2 | 46.5 | 48.2 | 81.7 | 70.9 | 118.0 | 137.0 | 55.7 | 106.1 |
| 5 | 80.0 | 87.0 | 7.0 | 68.1 | 46.1 | 48.0 | 81.5 | 70.9 | 117.8 | 137.6 | 55.4 | 106.1 |
| 5 | 80.0 | 87.0 | 7.0 | 68.2 | 46.3 | 48.3 | 81.5 | 70.9 | 118.1 | 136.9 | 55.8 | 106.4 |
| 5 | 80.0 | 87.0 | 7.0 | 67.9 | 46.0 | 47.9 | 81.7 | 71.3 | 118.1 | 137.3 | 55.2 | 106.4 |
| 5 | 80.0 | 87.0 | 7.0 | 68.1 | 46.0 | 48.0 | 81.9 | 70.7 | 118.0 | 137.4 | 55.6 | 106.1 |
| 5 | 80.0 | 87.0 | 7.0 | 68.5 | 46.0 | 48.0 | 81.7 | 70.3 | 117.8 | 137.0 | 55.4 | 106.1 |

## E.2.10. Patient 2: Lateral Cephalogram

| | SNA Angle | SNB Angle | ANB Angle | S-N | PNS-ANS | S-PNS | S-ANS | Me-ANS | N-Pog | S-Gn | N-A | N-B |
|---|---|---|---|---|---|---|---|---|---|---|---|---|
| 1 | 80.0 | 75.0 | 5.0 | 63.4 | 42.6 | 42.1 | 71.9 | 59.8 | 92.8 | 101.9 | 44.2 | 82.1 |
| 1 | 80.0 | 75.0 | 5.0 | 63.4 | 42.6 | 42.4 | 71.9 | 59.5 | 92.6 | 101.7 | 44.0 | 81.9 |
| 1 | 80.0 | 75.0 | 5.0 | 63.6 | 42.4 | 42.3 | 72.1 | 59.6 | 92.6 | 102.8 | 44.0 | 82.3 |
| 1 | 80.0 | 75.0 | 5.0 | 63.4 | 42.8 | 42.2 | 72.1 | 59.6 | 92.7 | 102.2 | 44.3 | 81.9 |
| 1 | 80.0 | 75.0 | 5.0 | 63.8 | 42.4 | 42.1 | 72.0 | 59.5 | 92.6 | 102.1 | 44.3 | 82.1 |
| 1 | 80.0 | 75.0 | 5.0 | 63.6 | 42.4 | 42.2 | 71.9 | 59.5 | 92.7 | 102.6 | 44.3 | 82.1 |
| 1 | 80.0 | 75.0 | 5.0 | 63.9 | 42.8 | 42.2 | 71.9 | 59.8 | 92.8 | 102.3 | 44.3 | 81.7 |
| 1 | 80.0 | 75.0 | 5.0 | 63.6 | 42.7 | 41.9 | 72.0 | 59.6 | 92.4 | 102.3 | 44.8 | 82.3 |
| 1 | 80.0 | 75.0 | 5.0 | 63.6 | 42.8 | 42.4 | 72.3 | 59.6 | 92.4 | 102.8 | 44.6 | 82.6 |
| 1 | 80.0 | 75.0 | 5.0 | 63.5 | 42.6 | 42.4 | 71.9 | 59.6 | 92.7 | 102.4 | 44.2 | 82.1 |
| 2 | 82.0 | 77.0 | 5.0 | 61.2 | 40.6 | 43.3 | 71.9 | 59.1 | 93.5 | 101.9 | 43.5 | 80.4 |
| 2 | 82.0 | 77.0 | 5.0 | 61.2 | 40.9 | 43.2 | 71.9 | 59.3 | 93.7 | 101.6 | 43.7 | 80.7 |
| 2 | 82.0 | 77.0 | 5.0 | 61.7 | 40.6 | 43.5 | 71.8 | 59.1 | 93.5 | 101.5 | 43.7 | 80.5 |
| 2 | 82.0 | 77.0 | 5.0 | 61.0 | 40.9 | 43.5 | 72.1 | 59.3 | 93.7 | 101.9 | 43.9 | 80.9 |
| 2 | 82.0 | 77.0 | 5.0 | 61.2 | 40.9 | 43.6 | 71.9 | 59.1 | 93.5 | 101.5 | 43.7 | 80.5 |
| 2 | 82.0 | 77.0 | 5.0 | 61.3 | 41.0 | 43.5 | 71.5 | 59.3 | 93.4 | 101.8 | 43.7 | 80.7 |
| 2 | 82.0 | 77.0 | 5.0 | 61.2 | 41.0 | 43.6 | 71.9 | 59.1 | 93.5 | 101.8 | 43.7 | 80.5 |
| 2 | 82.0 | 77.0 | 5.0 | 61.0 | 40.6 | 43.4 | 72.1 | 59.2 | 93.4 | 102.0 | 43.7 | 80.7 |
| 2 | 82.0 | 77.0 | 5.0 | 61.0 | 41.1 | 43.3 | 71.5 | 59.6 | 93.4 | 101.7 | 43.9 | 80.7 |
| 2 | 82.0 | 77.0 | 5.0 | 61.0 | 40.8 | 43.4 | 71.7 | 59.3 | 93.5 | 101.9 | 43.9 | 80.7 |
| 3 | 83.0 | 77.0 | 6.0 | 60.9 | 41.4 | 42.2 | 71.6 | 59.4 | 93.3 | 101.6 | 43.5 | 80.4 |
| 3 | 83.0 | 77.0 | 6.0 | 61.1 | 41.4 | 42.2 | 71.7 | 59.2 | 93.4 | 101.6 | 43.7 | 80.7 |
| 3 | 83.0 | 77.0 | 6.0 | 61.1 | 41.6 | 42.4 | 71.6 | 59.2 | 93.4 | 101.6 | 43.5 | 80.7 |
| 3 | 83.0 | 77.0 | 6.0 | 61.1 | 41.6 | 42.5 | 71.7 | 59.1 | 93.4 | 101.6 | 43.5 | 80.9 |
| 3 | 83.0 | 77.0 | 6.0 | 60.9 | 41.4 | 42.2 | 71.4 | 59.2 | 92.2 | 101.6 | 43.4 | 80.7 |
| 3 | 83.0 | 77.0 | 6.0 | 60.9 | 41.7 | 42.5 | 71.8 | 59.1 | 93.1 | 101.5 | 43.5 | 79.8 |
| 3 | 83.0 | 77.0 | 6.0 | 61.2 | 41.2 | 42.4 | 71.5 | 59.2 | 93.3 | 101.9 | 43.5 | 80.9 |
| 3 | 83.0 | 77.0 | 6.0 | 61.3 | 41.5 | 42.1 | 71.8 | 59.0 | 93.3 | 101.9 | 43.5 | 80.5 |
| 3 | 83.0 | 77.0 | 6.0 | 60.9 | 41.4 | 42.2 | 71.5 | 59.0 | 93.5 | 101.9 | 43.2 | 80.9 |
| 3 | 83.0 | 77.0 | 6.0 | 61.2 | 41.2 | 42.2 | 71.6 | 59.0 | 93.3 | 101.9 | 43.4 | 81.1 |
| 4 | 77.0 | 73.0 | 4.0 | 64.1 | 40.2 | 42.9 | 71.4 | 59.8 | 96.1 | 101.7 | 47.0 | 83.2 |
| 4 | 77.0 | 73.0 | 4.0 | 63.7 | 40.0 | 43.3 | 71.5 | 60.3 | 96.5 | 101.8 | 47.0 | 83.2 |
| 4 | 77.0 | 73.0 | 4.0 | 64.0 | 40.2 | 43.3 | 71.5 | 60.0 | 96.3 | 101.5 | 47.3 | 83.2 |
| 4 | 77.0 | 73.0 | 4.0 | 64.0 | 40.2 | 43.3 | 71.4 | 59.6 | 96.3 | 101.4 | 46.8 | 82.7 |
| 4 | 77.0 | 73.0 | 4.0 | 64.0 | 40.2 | 42.7 | 71.7 | 59.8 | 96.1 | 101.8 | 46.6 | 82.9 |
| 4 | 77.0 | 73.0 | 4.0 | 64.1 | 40.4 | 43.1 | 71.5 | 59.9 | 96.1 | 101.9 | 46.8 | 83.2 |
| 4 | 77.0 | 73.0 | 4.0 | 64.1 | 40.2 | 42.9 | 71.2 | 59.6 | 96.1 | 101.4 | 46.8 | 82.6 |
| 4 | 77.0 | 73.0 | 4.0 | 63.9 | 40.4 | 43.1 | 71.2 | 60.0 | 96.3 | 101.6 | 47.0 | 82.7 |
| 4 | 77.0 | 73.0 | 4.0 | 63.6 | 40.4 | 43.4 | 71.2 | 59.8 | 95.9 | 101.3 | 46.6 | 82.7 |
| 4 | 77.0 | 73.0 | 4.0 | 63.8 | 40.0 | 43.3 | 71.4 | 59.6 | 96.1 | 101.9 | 46.8 | 83.2 |
| 5 | 78.0 | 74.0 | 4.0 | 63.7 | 42.7 | 42.3 | 72.6 | 59.6 | 93.8 | 101.9 | 45.4 | 82.3 |
| 5 | 78.0 | 74.0 | 4.0 | 63.6 | 42.5 | 42.1 | 72.6 | 59.7 | 93.9 | 101.9 | 45.2 | 82.3 |
| 5 | 78.0 | 74.0 | 4.0 | 63.5 | 42.1 | 42.4 | 72.5 | 59.9 | 93.9 | 101.4 | 45.0 | 82.1 |
| 5 | 78.0 | 74.0 | 4.0 | 63.5 | 42.7 | 42.6 | 72.6 | 59.7 | 93.6 | 101.6 | 45.0 | 82.6 |
| 5 | 78.0 | 74.0 | 4.0 | 63.5 | 42.2 | 42.3 | 72.4 | 59.7 | 93.5 | 101.7 | 45.4 | 82.1 |
| 5 | 78.0 | 74.0 | 4.0 | 63.5 | 42.3 | 42.3 | 72.7 | 59.7 | 93.6 | 101.4 | 44.6 | 82.3 |
| 5 | 78.0 | 74.0 | 4.0 | 63.6 | 42.6 | 42.4 | 72.6 | 59.9 | 93.6 | 102.0 | 45.4 | 82.6 |
| 5 | 78.0 | 74.0 | 4.0 | 63.5 | 42.1 | 42.7 | 72.6 | 59.9 | 93.8 | 101.5 | 45.2 | 82.6 |
| 5 | 78.0 | 74.0 | 4.0 | 63.5 | 42.3 | 42.1 | 72.7 | 59.6 | 94.1 | 101.5 | 45.2 | 82.1 |
| 5 | 78.0 | 74.0 | 4.0 | 63.9 | 42.1 | 42.3 | 72.7 | 59.9 | 93.6 | 102.0 | 45.2 | 82.6 |

### E.2.11. Patient 3: Lateral Cephalogram

| | SNA | SNB | ANB | SN | PNS-ANS | S-PNS | S-ANS | Me-Ans | N-Pog | S-Gn | N-A | N-B |
|---|---|---|---|---|---|---|---|---|---|---|---|---|
| **1** | 92.0 | 85.0 | 7.0 | 69.9 | 52.8 | 51.5 | 89.1 | 66.4 | 106.7 | 124.4 | 52.0 | 113.1 |
| **2** | 92.0 | 85.0 | 7.0 | 69.7 | 52.6 | 51.5 | 89.1 | 66.5 | 106.5 | 124.8 | 53.0 | 112.8 |
| **3** | 92.0 | 85.0 | 7.0 | 69.7 | 52.8 | 51.5 | 89.1 | 66.4 | 106.5 | 124.4 | 53.0 | 112.7 |
| **4** | 92.0 | 85.0 | 7.0 | 69.9 | 52.6 | 51.4 | 89.1 | 66.4 | 106.5 | 124.5 | 53.0 | 112.5 |
| **5** | 93.0 | 85.0 | 7.0 | 69.7 | 52.8 | 51.3 | 89.3 | 66.5 | 106.5 | 124.6 | 52.8 | 112.7 |
| **6** | 93.0 | 85.0 | 7.0 | 69.9 | 52.8 | 51.3 | 89.1 | 66.4 | 106.5 | 124.4 | 53.0 | 112.7 |
| **7** | 92.0 | 85.0 | 7.0 | 69.9 | 52.8 | 51.5 | 88.8 | 66.5 | 106.6 | 124.4 | 53.0 | 112.9 |
| **8** | 91.0 | 85.0 | 7.0 | 69.9 | 52.8 | 51.5 | 88.7 | 66.5 | 106.5 | 124.7 | 53.0 | 113.0 |
| **9** | 92.0 | 84.0 | 7.0 | 69.5 | 53.0 | 51.4 | 89.1 | 66.4 | 106.5 | 124.9 | 53.0 | 112.8 |
| **10** | 92.0 | 85.0 | 7.0 | 69.9 | 52.8 | 51.5 | 88.7 | 66.7 | 106.5 | 124.3 | 53.0 | 112.8 |

### E.2.12. Patient 4: Lateral Cephalogram

| | SNA | SNB | ANB | S-N | PNS-ANS | S-PNS | S-ANS | Me-Ans | N-Pog | S-Gn | N-A | N-B |
|---|---|---|---|---|---|---|---|---|---|---|---|---|
| **1** | 81.0 | 73.0 | 8.0 | 72.9 | 56.5 | 47.3 | 87.9 | 64.0 | 112.0 | 117.1 | 56.4 | 95.2 |
| **2** | 82.0 | 73.0 | 8.0 | 73.4 | 56.4 | 47.1 | 88.0 | 63.8 | 111.9 | 117.3 | 56.5 | 95.2 |
| **3** | 81.0 | 73.0 | 8.0 | 73.2 | 56.4 | 47.1 | 88.5 | 64.1 | 112.1 | 117.3 | 56.4 | 95.2 |
| **4** | 82.0 | 73.0 | 8.0 | 73.4 | 56.4 | 46.9 | 88.1 | 63.9 | 111.9 | 117.8 | 56.5 | 95.2 |
| **5** | 81.0 | 73.0 | 8.0 | 73.2 | 56.7 | 47.0 | 88.2 | 63.7 | 111.9 | 117.3 | 56.5 | 95.4 |
| **6** | 81.0 | 73.0 | 8.0 | 73.4 | 56.4 | 46.9 | 88.1 | 64.0 | 111.8 | 117.5 | 56.5 | 95.4 |
| **7** | 81.0 | 73.0 | 8.0 | 73.2 | 56.4 | 47.1 | 88.1 | 63.9 | 111.9 | 117.3 | 56.5 | 95.5 |
| **8** | 81.0 | 73.0 | 8.0 | 73.2 | 56.4 | 47.0 | 88.0 | 63.8 | 111.9 | 117.5 | 56.4 | 95.4 |
| **9** | 81.0 | 73.0 | 8.0 | 73.4 | 56.1 | 46.9 | 88.1 | 63.9 | 111.9 | 117.5 | 56.5 | 95.5 |
| **10** | 81.0 | 73.0 | 8.0 | 73.4 | 56.4 | 47.1 | 88.3 | 64.1 | 111.9 | 117.3 | 56.5 | 95.5 |

### E.2.13. Patient 5: Lateral Cephalogram

| | SNA | SNB | ANB | SN | PNS-ANS | S-PNS | S-ANS | Me-Ans | N-Pog | S-Gn | N-A | N-B |
|---|---|---|---|---|---|---|---|---|---|---|---|---|
| **1** | 80.0 | 87.0 | 7.0 | 68.4 | 52.4 | 42.3 | 83.2 | 51.6 | 97.5 | 116.8 | 49.3 | 82.1 |
| **2** | 80.0 | 87.0 | 8.0 | 68.7 | 52.1 | 42.1 | 83.3 | 51.6 | 97.8 | 117.2 | 49.0 | 82.1 |
| **3** | 80.0 | 87.0 | 8.0 | 68.7 | 52.4 | 42.1 | 83.3 | 52.0 | 97.6 | 117.1 | 49.1 | 82.1 |
| **4** | 79.0 | 87.0 | 8.0 | 69.1 | 52.6 | 42.1 | 83.2 | 51.2 | 97.6 | 117.1 | 49.0 | 82.0 |
| **5** | 79.0 | 87.0 | 8.0 | 69.0 | 52.6 | 42.4 | 83.2 | 51.6 | 97.4 | 116.9 | 49.0 | 82.4 |
| **6** | 79.0 | 87.0 | 8.0 | 69.1 | 52.7 | 42.0 | 83.2 | 51.6 | 97.5 | 117.2 | 49.3 | 82.1 |
| **7** | 79.0 | 87.0 | 8.0 | 68.6 | 52.6 | 42.3 | 83.1 | 52.0 | 97.8 | 117.1 | 49.1 | 82.4 |
| **8** | 79.0 | 87.0 | 8.0 | 68.9 | 52.4 | 42.3 | 83.2 | 51.8 | 97.8 | 116.7 | 49.1 | 82.3 |
| **9** | 79.0 | 87.0 | 8.0 | 69.0 | 52.1 | 42.3 | 83.4 | 51.6 | 97.6 | 117.1 | 49.3 | 82.0 |
| **10** | 79.0 | 87.0 | 8.0 | 68.7 | 52.1 | 42.1 | 83.2 | 51.6 | 97.8 | 116.8 | 49.3 | 81.9 |

### E.2.14. Patient 1: "Black Bone"

| | SNA Angle | SNB Angle | ANB Angle | S-N | PNS-ANS | S-PNS | S-ANS | Me-ANS | N-Pog | S-Gn | N-A | N-B |
|---|---|---|---|---|---|---|---|---|---|---|---|---|
| 1 | 81.0 | 88.0 | 7.0 | 68.6 | 56.6 | 46.4 | 90.2 | 68.3 | 114.9 | 137.8 | 52.8 | 104.0 |
| 1 | 81.0 | 88.0 | 7.0 | 68.6 | 56.8 | 46.7 | 90.7 | 68.5 | 114.6 | 138.2 | 53.4 | 104.0 |
| 1 | 81.0 | 88.0 | 7.0 | 68.6 | 56.9 | 46.0 | 90.8 | 68.8 | 114.3 | 138.1 | 53.1 | 104.0 |
| 1 | 81.0 | 88.0 | 7.0 | 68.9 | 56.4 | 46.7 | 90.0 | 68.5 | 114.4 | 138.4 | 53.5 | 103.7 |
| 1 | 81.0 | 88.0 | 7.0 | 68.3 | 56.3 | 46.7 | 90.5 | 67.9 | 114.9 | 138.3 | 53.1 | 103.7 |
| 1 | 81.0 | 88.0 | 7.0 | 68.9 | 56.4 | 46.8 | 90.4 | 68.4 | 115.5 | 137.8 | 53.5 | 103.7 |
| 1 | 81.0 | 88.0 | 7.0 | 68.9 | 56.3 | 46.3 | 91.1 | 68.5 | 114.9 | 138.4 | 52.9 | 103.1 |
| 1 | 81.0 | 88.0 | 7.0 | 68.6 | 56.6 | 46.2 | 90.7 | 68.8 | 115.3 | 137.5 | 53.2 | 104.0 |
| 1 | 81.0 | 88.0 | 7.0 | 68.0 | 56.9 | 46.3 | 90.4 | 69.4 | 114.9 | 138.0 | 53.4 | 103.1 |
| 1 | 81.0 | 88.0 | 7.0 | 68.3 | 56.3 | 45.9 | 90.9 | 69.4 | 115.5 | 137.9 | 53.2 | 103.4 |
| 2 | 81.0 | 88.0 | 7.0 | 67.5 | 52.0 | 47.5 | 86.0 | 69.2 | 118.2 | 138.1 | 53.3 | 102.8 |
| 2 | 81.0 | 88.0 | 7.0 | 67.8 | 52.3 | 47.4 | 85.5 | 68.9 | 118.2 | 138.3 | 53.4 | 103.1 |
| 2 | 81.0 | 88.0 | 7.0 | 67.5 | 52.1 | 47.0 | 85.7 | 68.9 | 117.8 | 137.9 | 53.1 | 102.5 |
| 2 | 81.0 | 88.0 | 7.0 | 67.2 | 51.7 | 46.7 | 85.7 | 69.2 | 118.8 | 137.8 | 53.3 | 102.8 |
| 2 | 81.0 | 88.0 | 7.0 | 67.2 | 52.0 | 46.7 | 86.0 | 68.9 | 118.5 | 137.8 | 52.8 | 102.3 |
| 2 | 81.0 | 88.0 | 7.0 | 67.2 | 51.7 | 46.5 | 85.7 | 68.9 | 118.2 | 138.5 | 53.3 | 102.5 |
| 2 | 81.0 | 88.0 | 7.0 | 67.5 | 52.4 | 47.0 | 85.7 | 68.6 | 117.9 | 137.7 | 53.1 | 102.5 |
| 2 | 81.0 | 88.0 | 7.0 | 67.2 | 52.4 | 47.1 | 85.7 | 69.2 | 118.5 | 138.3 | 53.1 | 102.8 |
| 2 | 81.0 | 88.0 | 7.0 | 67.5 | 52.3 | 46.9 | 85.3 | 68.9 | 118.7 | 138.0 | 52.8 | 102.5 |
| 2 | 81.0 | 88.0 | 7.0 | 67.7 | 51.5 | 46.5 | 85.9 | 69.2 | 118.5 | 137.9 | 52.7 | 102.5 |
| 3 | 81.0 | 87.0 | 6.0 | 67.8 | 52.0 | 46.4 | 86.3 | 68.9 | 118.5 | 138.1 | 54.2 | 103.4 |
| 3 | 81.0 | 87.0 | 6.0 | 67.5 | 52.1 | 46.3 | 86.4 | 68.9 | 118.5 | 138.2 | 53.5 | 103.1 |
| 3 | 81.0 | 87.0 | 6.0 | 68.1 | 51.5 | 46.3 | 86.0 | 68.0 | 117.9 | 138.1 | 53.0 | 103.4 |
| 3 | 81.0 | 87.0 | 6.0 | 67.8 | 51.9 | 46.9 | 86.4 | 69.2 | 118.2 | 137.9 | 53.5 | 103.1 |
| 3 | 81.0 | 87.0 | 6.0 | 67.8 | 52.3 | 46.6 | 85.8 | 68.9 | 118.2 | 138.1 | 53.5 | 103.4 |
| 3 | 81.0 | 87.0 | 6.0 | 67.5 | 51.8 | 46.7 | 85.9 | 68.3 | 118.2 | 138.0 | 53.5 | 103.1 |
| 3 | 81.0 | 87.0 | 6.0 | 68.1 | 51.7 | 46.2 | 86.3 | 68.3 | 118.4 | 137.9 | 53.8 | 103.1 |
| 3 | 81.0 | 87.0 | 6.0 | 68.1 | 52.0 | 47.5 | 86.2 | 68.9 | 118.4 | 137.7 | 53.8 | 103.7 |
| 3 | 81.0 | 87.0 | 6.0 | 68.7 | 51.5 | 47.0 | 85.8 | 68.0 | 118.8 | 137.8 | 53.8 | 103.1 |
| 3 | 81.0 | 87.0 | 6.0 | 67.5 | 51.8 | 46.5 | 86.0 | 68.0 | 118.5 | 137.9 | 53.6 | 102.8 |
| 4 | 82.0 | 88.0 | 6.0 | 68.1 | 51.3 | 45.2 | 85.2 | 68.6 | 117.9 | 138.3 | 53.3 | 103.7 |
| 4 | 82.0 | 88.0 | 6.0 | 67.8 | 51.3 | 45.8 | 84.9 | 68.9 | 117.6 | 138.4 | 53.8 | 103.4 |
| 4 | 82.0 | 88.0 | 6.0 | 67.8 | 51.3 | 45.7 | 85.6 | 68.9 | 118.2 | 138.5 | 53.3 | 104.0 |
| 4 | 82.0 | 88.0 | 6.0 | 68.1 | 51.5 | 45.8 | 85.4 | 68.9 | 117.6 | 137.8 | 53.6 | 103.7 |
| 4 | 82.0 | 88.0 | 6.0 | 67.8 | 51.3 | 45.8 | 85.2 | 69.2 | 117.6 | 138.2 | 54.1 | 103.7 |
| 4 | 82.0 | 88.0 | 6.0 | 67.8 | 51.2 | 45.7 | 84.8 | 68.9 | 117.3 | 138.4 | 53.5 | 103.1 |
| 4 | 82.0 | 88.0 | 6.0 | 68.1 | 51.6 | 45.5 | 85.2 | 68.9 | 117.9 | 138.0 | 53.8 | 104.0 |
| 4 | 82.0 | 88.0 | 6.0 | 68.1 | 51.3 | 46.2 | 84.8 | 68.9 | 117.9 | 138.0 | 53.8 | 104.0 |
| 4 | 82.0 | 88.0 | 6.0 | 68.1 | 51.6 | 46.0 | 85.1 | 69.2 | 117.3 | 138.4 | 53.5 | 103.4 |
| 4 | 82.0 | 88.0 | 6.0 | 68.1 | 51.0 | 45.9 | 85.2 | 68.9 | 118.2 | 138.4 | 53.5 | 103.7 |
| 5 | 82.0 | 88.0 | 6.0 | 68.0 | 50.4 | 46.6 | 85.0 | 68.9 | 117.1 | 138.1 | 53.5 | 103.7 |
| 5 | 82.0 | 88.0 | 6.0 | 68.0 | 50.3 | 47.1 | 84.9 | 69.2 | 117.4 | 138.2 | 53.8 | 104.0 |
| 5 | 82.0 | 88.0 | 6.0 | 68.0 | 50.5 | 46.6 | 84.9 | 68.9 | 117.9 | 138.3 | 53.2 | 104.0 |
| 5 | 82.0 | 88.0 | 6.0 | 68.1 | 50.6 | 46.7 | 84.7 | 69.2 | 117.9 | 138.3 | 53.2 | 103.7 |
| 5 | 82.0 | 88.0 | 6.0 | 68.3 | 50.7 | 46.6 | 84.9 | 69.5 | 117.9 | 138.3 | 53.5 | 104.0 |
| 5 | 82.0 | 88.0 | 6.0 | 67.8 | 50.6 | 47.1 | 84.9 | 69.2 | 117.6 | 138.0 | 53.5 | 104.3 |
| 5 | 82.0 | 88.0 | 6.0 | 67.8 | 50.6 | 47.4 | 84.9 | 69.5 | 118.5 | 138.1 | 53.0 | 104.3 |
| 5 | 82.0 | 88.0 | 6.0 | 68.1 | 50.6 | 46.7 | 84.7 | 69.2 | 118.2 | 137.6 | 53.8 | 103.7 |
| 5 | 82.0 | 88.0 | 6.0 | 68.1 | 50.6 | 47.2 | 85.1 | 69.2 | 118.2 | 138.3 | 53.5 | 103.4 |
| 5 | 82.0 | 88.0 | 6.0 | 68.1 | 50.6 | 46.3 | 84.3 | 69.2 | 118.7 | 138.4 | 53.5 | 103.7 |

## E.2.15. Patient 2: "Black Bone"

| | SNA Angle | SNB Angle | ANB Angle | S-N | PNS-ANS | S-PNS | S-ANS | Me-ANS | N-Pog | S-Gn | N-A | N-B |
|---|---|---|---|---|---|---|---|---|---|---|---|---|
| 1 | 80.0 | 76.0 | 5.0 | 64.1 | 52.1 | 35.8 | 75.2 | 59.1 | 90.4 | 102.1 | 40.3 | 80.1 |
| 1 | 80.0 | 76.0 | 5.0 | 64.6 | 51.6 | 35.7 | 75.2 | 58.7 | 91.2 | 101.7 | 40.3 | 80.3 |
| 1 | 80.0 | 76.0 | 5.0 | 64.4 | 52.0 | 35.5 | 75.1 | 59.3 | 90.8 | 102.2 | 40.6 | 79.6 |
| 1 | 80.0 | 76.0 | 5.0 | 64.1 | 51.6 | 36.1 | 75.4 | 58.7 | 91.5 | 101.9 | 40.3 | 80.1 |
| 1 | 80.0 | 76.0 | 5.0 | 64.3 | 51.9 | 36.1 | 75.2 | 59.1 | 91.0 | 102.0 | 40.3 | 80.8 |
| 1 | 80.0 | 76.0 | 5.0 | 64.0 | 51.8 | 35.8 | 75.0 | 58.4 | 90.9 | 102.4 | 40.7 | 80.6 |
| 1 | 80.0 | 76.0 | 5.0 | 64.1 | 52.1 | 36.2 | 75.8 | 58.5 | 91.3 | 102.3 | 39.9 | 80.1 |
| 1 | 80.0 | 76.0 | 5.0 | 64.4 | 51.8 | 35.7 | 75.2 | 58.6 | 91.2 | 102.2 | 40.4 | 79.8 |
| 1 | 80.0 | 76.0 | 5.0 | 64.1 | 51.3 | 35.8 | 75.2 | 58.6 | 91.0 | 102.1 | 40.4 | 80.3 |
| 1 | 80.0 | 76.0 | 5.0 | 64.4 | 51.9 | 35.6 | 75.4 | 59.1 | 90.7 | 102.3 | 40.8 | 80.0 |
| 2 | 80.0 | 75.0 | 5.0 | 64.0 | 51.0 | 35.3 | 75.3 | 58.8 | 90.7 | 101.9 | 41.3 | 81.5 |
| 2 | 80.0 | 75.0 | 5.0 | 64.0 | 50.6 | 34.8 | 75.5 | 58.8 | 90.7 | 101.7 | 41.6 | 81.9 |
| 2 | 80.0 | 75.0 | 5.0 | 64.0 | 50.8 | 34.9 | 75.6 | 59.3 | 91.2 | 101.8 | 41.0 | 81.5 |
| 2 | 80.0 | 75.0 | 5.0 | 64.3 | 51.2 | 35.5 | 75.2 | 58.9 | 90.7 | 101.7 | 41.5 | 81.6 |
| 2 | 80.0 | 75.0 | 5.0 | 64.3 | 51.0 | 35.3 | 75.5 | 59.1 | 90.4 | 101.8 | 41.5 | 81.4 |
| 2 | 80.0 | 75.0 | 5.0 | 64.5 | 50.9 | 35.3 | 75.5 | 59.2 | 91.2 | 101.3 | 41.5 | 81.8 |
| 2 | 80.0 | 75.0 | 5.0 | 64.3 | 50.8 | 35.3 | 75.1 | 58.9 | 91.3 | 101.7 | 41.7 | 81.4 |
| 2 | 80.0 | 75.0 | 5.0 | 64.0 | 50.4 | 35.6 | 75.0 | 58.6 | 90.7 | 101.5 | 41.0 | 81.6 |
| 2 | 80.0 | 75.0 | 5.0 | 64.3 | 50.9 | 34.8 | 75.2 | 58.8 | 91.0 | 101.4 | 41.3 | 81.6 |
| 2 | 80.0 | 75.0 | 5.0 | 64.3 | 50.8 | 35.0 | 75.2 | 59.2 | 91.0 | 101.7 | 41.1 | 81.5 |
| 3 | 81.0 | 75.0 | 6.0 | 64.3 | 50.7 | 35.5 | 74.7 | 60.1 | 93.5 | 102.4 | 41.3 | 80.9 |
| 3 | 81.0 | 75.0 | 6.0 | 64.6 | 50.9 | 35.8 | 74.9 | 59.6 | 92.7 | 102.1 | 41.8 | 81.2 |
| 3 | 81.0 | 75.0 | 6.0 | 64.5 | 50.9 | 36.0 | 75.2 | 60.0 | 93.2 | 102.0 | 41.8 | 81.4 |
| 3 | 81.0 | 75.0 | 6.0 | 64.3 | 51.1 | 35.8 | 74.9 | 60.2 | 93.5 | 101.6 | 41.3 | 81.1 |
| 3 | 81.0 | 75.0 | 6.0 | 64.8 | 51.0 | 36.1 | 74.9 | 60.0 | 93.4 | 102.1 | 41.5 | 80.9 |
| 3 | 81.0 | 75.0 | 6.0 | 64.8 | 51.2 | 35.4 | 74.4 | 60.1 | 93.5 | 102.3 | 41.0 | 80.7 |
| 3 | 81.0 | 75.0 | 6.0 | 64.8 | 50.9 | 36.1 | 75.1 | 59.5 | 93.4 | 102.3 | 41.1 | 81.3 |
| 3 | 81.0 | 75.0 | 6.0 | 64.6 | 50.7 | 36.1 | 74.7 | 60.2 | 93.5 | 102.0 | 41.5 | 81.4 |
| 3 | 81.0 | 75.0 | 6.0 | 64.8 | 50.9 | 35.7 | 75.2 | 60.0 | 93.4 | 101.9 | 41.8 | 81.3 |
| 3 | 81.0 | 75.0 | 6.0 | 64.6 | 50.7 | 35.9 | 74.7 | 60.1 | 93.4 | 101.9 | 41.3 | 80.9 |
| 4 | 81.0 | 76.0 | 5.0 | 64.1 | 52.6 | 35.7 | 75.3 | 59.4 | 93.1 | 102.1 | 40.9 | 81.7 |
| 4 | 81.0 | 76.0 | 5.0 | 64.1 | 52.8 | 35.8 | 75.3 | 59.7 | 92.8 | 102.3 | 40.8 | 81.7 |
| 4 | 81.0 | 76.0 | 5.0 | 63.8 | 52.6 | 36.0 | 75.0 | 59.4 | 92.5 | 102.1 | 40.4 | 80.9 |
| 4 | 81.0 | 76.0 | 5.0 | 64.1 | 52.8 | 35.7 | 75.1 | 58.9 | 92.8 | 102.6 | 41.1 | 81.6 |
| 4 | 81.0 | 76.0 | 5.0 | 64.1 | 52.8 | 36.3 | 75.2 | 59.5 | 93.0 | 102.4 | 41.0 | 81.5 |
| 4 | 81.0 | 76.0 | 5.0 | 64.1 | 52.6 | 36.0 | 75.3 | 59.1 | 92.8 | 102.3 | 41.0 | 81.8 |
| 4 | 81.0 | 76.0 | 5.0 | 64.1 | 52.6 | 36.0 | 75.5 | 59.5 | 92.6 | 102.1 | 40.7 | 81.0 |
| 4 | 81.0 | 76.0 | 5.0 | 64.3 | 52.6 | 36.3 | 75.2 | 59.4 | 92.9 | 102.1 | 40.9 | 81.0 |
| 4 | 81.0 | 76.0 | 5.0 | 63.8 | 52.6 | 36.3 | 75.3 | 59.7 | 92.6 | 102.0 | 41.0 | 81.4 |
| 4 | 81.0 | 76.0 | 5.0 | 64.1 | 52.9 | 36.2 | 75.0 | 59.3 | 92.8 | 102.3 | 41.0 | 81.3 |
| 5 | 81.0 | 75.0 | 6.0 | 64.2 | 50.8 | 35.6 | 74.3 | 59.2 | 93.6 | 101.6 | 42.1 | 82.5 |
| 5 | 81.0 | 75.0 | 6.0 | 64.5 | 50.8 | 35.5 | 75.1 | 58.9 | 93.9 | 101.5 | 41.8 | 82.5 |
| 5 | 81.0 | 75.0 | 6.0 | 64.2 | 50.9 | 35.6 | 74.7 | 59.3 | 93.8 | 101.8 | 42.1 | 82.5 |
| 5 | 81.0 | 75.0 | 6.0 | 64.5 | 50.8 | 35.6 | 74.9 | 59.1 | 93.9 | 101.0 | 42.0 | 82.5 |
| 5 | 81.0 | 75.0 | 6.0 | 64.5 | 51.1 | 35.4 | 74.4 | 59.3 | 94.1 | 101.0 | 41.8 | 82.8 |
| 5 | 81.0 | 75.0 | 6.0 | 64.0 | 50.8 | 35.6 | 74.8 | 59.1 | 94.1 | 101.5 | 42.0 | 82.5 |
| 5 | 81.0 | 75.0 | 6.0 | 64.0 | 50.8 | 35.2 | 74.6 | 59.3 | 94.0 | 1014.0 | 42.1 | 82.7 |
| 5 | 81.0 | 75.0 | 6.0 | 64.5 | 51.3 | 35.3 | 74.4 | 59.3 | 94.1 | 101.2 | 42.0 | 82.5 |
| 5 | 81.0 | 75.0 | 6.0 | 64.2 | 51.1 | 35.3 | 74.4 | 59.2 | 93.4 | 101.1 | 41.7 | 81.9 |
| 5 | 81.0 | 75.0 | 6.0 | 64.0 | 50.9 | 35.2 | 74.7 | 59.6 | 94.1 | 101.7 | 42.0 | 82.2 |
| 6 | 80.0 | 74.0 | 6.0 | 64.2 | 50.2 | 36.8 | 74.6 | 59.1 | 94.4 | 102.5 | 43.8 | 83.4 |
| 6 | 80.0 | 74.0 | 6.0 | 64.5 | 50.2 | 36.5 | 75.0 | 58.8 | 94.3 | 102.5 | 43.6 | 83.3 |
| 6 | 80.0 | 74.0 | 6.0 | 64.2 | 50.1 | 36.9 | 74.7 | 58.8 | 94.4 | 102.7 | 44.0 | 83.2 |
| 6 | 80.0 | 74.0 | 6.0 | 64.7 | 50.5 | 36.9 | 74.6 | 59.3 | 94.6 | 102.3 | 43.8 | 83.4 |
| 6 | 80.0 | 74.0 | 6.0 | 64.2 | 50.3 | 36.8 | 75.0 | 59.3 | 94.6 | 102.5 | 44.1 | 83.8 |
| 6 | 80.0 | 74.0 | 6.0 | 64.2 | 50.3 | 36.8 | 74.8 | 59.3 | 94.4 | 102.4 | 43.8 | 83.5 |
| 6 | 80.0 | 74.0 | 6.0 | 64.5 | 50.3 | 36.7 | 75.5 | 59.1 | 94.4 | 102.7 | 43.9 | 83.2 |
| 6 | 80.0 | 74.0 | 6.0 | 64.5 | 50.0 | 36.4 | 74.8 | 59.1 | 94.6 | 102.7 | 43.9 | 83.4 |
| 6 | 80.0 | 74.0 | 6.0 | 64.5 | 50.2 | 37.1 | 74.8 | 58.9 | 94.4 | 102.7 | 43.9 | 83.7 |
| 6 | 80.0 | 74.0 | 6.0 | 64.5 | 50.4 | 37.1 | 74.8 | 59.2 | 94.4 | 102.4 | 43.8 | 83.2 |
| 7 | 81.0 | 75.0 | 5.0 | 64.3 | 50.6 | 36.4 | 74.1 | 59.0 | 92.8 | 101.6 | 42.9 | 83.2 |
| 7 | 81.0 | 75.0 | 5.0 | 64.0 | 50.3 | 36.1 | 74.7 | 59.1 | 92.6 | 101.8 | 43.0 | 83.0 |

| | SNA Angle | SNB Angle | ANB Angle | S-N | PNS-ANS | S-PNS | S-ANS | Me-ANS | N-Pog | S-Gn | N-A | N-B |
|---|---|---|---|---|---|---|---|---|---|---|---|---|
| 7 | 81.0 | 75.0 | 5.0 | 64.3 | 50.6 | 35.7 | 74.7 | 58.8 | 92.4 | 101.8 | 43.4 | 82.7 |
| 7 | 81.0 | 75.0 | 5.0 | 64.5 | 50.6 | 36.0 | 74.4 | 59.2 | 92.8 | 101.6 | 43.1 | 83.3 |
| 7 | 81.0 | 75.0 | 5.0 | 64.3 | 50.8 | 36.0 | 74.1 | 58.8 | 92.6 | 101.6 | 42.8 | 83.2 |
| 7 | 81.0 | 75.0 | 5.0 | 64.0 | 50.8 | 36.4 | 74.4 | 59.2 | 92.8 | 101.9 | 43.1 | 83.4 |
| 7 | 81.0 | 75.0 | 5.0 | 64.3 | 50.6 | 35.9 | 74.5 | 58.7 | 93.0 | 101.8 | 43.7 | 83.4 |
| 7 | 81.0 | 75.0 | 5.0 | 64.3 | 51.1 | 36.1 | 73.9 | 58.7 | 92.5 | 101.8 | 42.8 | 83.5 |
| 7 | 81.0 | 75.0 | 5.0 | 64.3 | 50.3 | 36.0 | 74.5 | 58.6 | 92.5 | 101.6 | 42.9 | 83.8 |
| 7 | 81.0 | 75.0 | 5.0 | 64.0 | 50.6 | 36.2 | 74.6 | 59.1 | 92.8 | 101.4 | 43.3 | 83.2 |
| 8 | 80.0 | 74.0 | 6.0 | 64.5 | 51.6 | 35.9 | 74.3 | 59.1 | 93.3 | 101.7 | 42.7 | 83.2 |
| 8 | 80.0 | 74.0 | 6.0 | 64.2 | 51.8 | 36.0 | 75.2 | 58.4 | 93.5 | 101.5 | 42.7 | 83.4 |
| 8 | 80.0 | 74.0 | 6.0 | 64.5 | 51.8 | 35.5 | 74.7 | 58.9 | 93.5 | 101.8 | 43.0 | 82.8 |
| 8 | 80.0 | 74.0 | 6.0 | 64.2 | 51.6 | 36.2 | 74.7 | 58.9 | 93.3 | 101.8 | 42.8 | 82.9 |
| 8 | 80.0 | 74.0 | 6.0 | 64.2 | 51.7 | 35.9 | 75.0 | 59.2 | 93.3 | 101.7 | 43.0 | 83.0 |
| 8 | 80.0 | 74.0 | 6.0 | 64.2 | 51.5 | 36.1 | 74.7 | 59.0 | 93.5 | 101.4 | 43.5 | 83.0 |
| 8 | 80.0 | 74.0 | 6.0 | 64.5 | 51.8 | 36.0 | 75.0 | 59.1 | 93.5 | 101.8 | 42.6 | 83.2 |
| 8 | 80.0 | 74.0 | 6.0 | 64.0 | 51.6 | 35.9 | 74.7 | 58.8 | 93.8 | 101.7 | 43.2 | 83.0 |
| 8 | 80.0 | 74.0 | 6.0 | 64.2 | 51.3 | 36.2 | 74.8 | 58.9 | 93.4 | 101.8 | 42.8 | 83.2 |
| 8 | 80.0 | 74.0 | 6.0 | 64.0 | 51.6 | 36.0 | 74.3 | 58.9 | 93.3 | 101.6 | 43.2 | 82.9 |
| 9 | 81.0 | 75.0 | 6.0 | 64.0 | 50.6 | 36.3 | 75.3 | 59.3 | 92.3 | 102.3 | 41.7 | 81.7 |
| 9 | 81.0 | 75.0 | 6.0 | 64.3 | 50.6 | 36.0 | 75.2 | 59.6 | 92.0 | 102.4 | 42.0 | 81.7 |
| 9 | 81.0 | 75.0 | 6.0 | 64.3 | 50.7 | 36.0 | 75.1 | 59.3 | 92.3 | 102.1 | 41.7 | 81.7 |
| 9 | 81.0 | 75.0 | 6.0 | 64.3 | 50.6 | 35.9 | 75.7 | 59.2 | 91.8 | 102.2 | 42.0 | 81.7 |
| 9 | 81.0 | 75.0 | 6.0 | 64.0 | 50.6 | 36.0 | 75.8 | 59.3 | 92.3 | 102.0 | 41.5 | 81.7 |
| 9 | 81.0 | 75.0 | 6.0 | 64.0 | 50.6 | 36.1 | 75.2 | 59.5 | 92.0 | 102.2 | 42.1 | 81.4 |
| 9 | 81.0 | 75.0 | 6.0 | 64.3 | 50.6 | 35.6 | 75.8 | 59.4 | 92.3 | 102.7 | 42.0 | 82.2 |
| 9 | 81.0 | 75.0 | 6.0 | 64.3 | 50.4 | 36.1 | 75.6 | 59.4 | 92.0 | 101.9 | 41.6 | 81.4 |
| 9 | 81.0 | 75.0 | 6.0 | 64.3 | 50.3 | 35.7 | 75.2 | 59.3 | 92.2 | 102.4 | 41.8 | 81.7 |
| 9 | 81.0 | 75.0 | 6.0 | 64.3 | 50.1 | 36.0 | 75.2 | 59.5 | 92.5 | 102.6 | 42.1 | 81.6 |
| 10 | 80.0 | 75.0 | 5.0 | 64.8 | 49.9 | 36.4 | 74.6 | 58.6 | 94.4 | 102.6 | 42.8 | 82.6 |
| 10 | 80.0 | 75.0 | 5.0 | 64.5 | 49.7 | 36.7 | 75.2 | 59.1 | 94.1 | 102.4 | 43.1 | 82.6 |
| 10 | 80.0 | 75.0 | 5.0 | 64.8 | 49.9 | 36.6 | 75.1 | 59.3 | 94.1 | 102.7 | 42.8 | 82.5 |
| 10 | 80.0 | 75.0 | 5.0 | 64.5 | 49.4 | 36.1 | 75.1 | 59.1 | 94.5 | 102.6 | 43.0 | 82.4 |
| 10 | 80.0 | 75.0 | 5.0 | 64.5 | 49.6 | 36.6 | 75.1 | 59.4 | 94.3 | 103.0 | 43.0 | 82.6 |
| 10 | 80.0 | 75.0 | 5.0 | 64.8 | 49.6 | 36.4 | 75.0 | 59.7 | 94.1 | 102.6 | 42.8 | 83.1 |
| 10 | 80.0 | 75.0 | 5.0 | 64.8 | 49.7 | 36.4 | 75.0 | 59.4 | 94.6 | 102.8 | 43.0 | 82.7 |
| 10 | 80.0 | 75.0 | 5.0 | 64.8 | 49.8 | 36.4 | 75.3 | 59.1 | 94.4 | 102.5 | 42.8 | 82.2 |
| 10 | 80.0 | 75.0 | 5.0 | 64.8 | 49.7 | 36.4 | 75.0 | 58.9 | 94.2 | 102.3 | 43.3 | 82.2 |
| 10 | 80.0 | 75.0 | 5.0 | 64.8 | 50.1 | 36.5 | 75.0 | 58.9 | 94.4 | 101.8 | 43.0 | 82.4 |

### E.2.16. Patient 3: "Black Bone"

| | SNA | SNB | ANB | SN | PNS-ANS | S-PNS | S-ANS | Me-Ans | N-Pog | S-Gn | N-A | N-B |
|---|---|---|---|---|---|---|---|---|---|---|---|---|
| 1 | 86.0 | 81.0 | 6.0 | 70.5 | 57.8 | 48.8 | 88.2 | 71.6 | 115.5 | 129.4 | 53.2 | 102.6 |
| 2 | 87.0 | 81.0 | 6.0 | 70.2 | 57.7 | 49.1 | 87.9 | 72.1 | 116.3 | 129.2 | 53.3 | 102.6 |
| 3 | 87.0 | 81.0 | 5.0 | 70.7 | 57.7 | 49.2 | 88.2 | 72.2 | 115.8 | 129.1 | 53.0 | 102.3 |
| 4 | 87.0 | 81.0 | 5.0 | 70.2 | 58.0 | 49.0 | 88.3 | 72.1 | 115.5 | 128.9 | 53.2 | 102.3 |
| 5 | 86.0 | 81.0 | 5.0 | 70.2 | 57.7 | 49.1 | 88.3 | 71.9 | 115.8 | 129.3 | 52.7 | 102.3 |
| 6 | 86.0 | 81.0 | 5.0 | 70.5 | 57.7 | 48.7 | 88.2 | 71.9 | 115.3 | 129.3 | 53.5 | 102.6 |
| 7 | 86.0 | 81.0 | 5.0 | 70.0 | 57.7 | 48.6 | 88.7 | 72.1 | 115.5 | 129.1 | 53.0 | 102.6 |
| 8 | 86.0 | 82.0 | 5.0 | 70.8 | 57.5 | 48.7 | 88.3 | 72.1 | 115.5 | 129.1 | 53.2 | 102.6 |
| 9 | 87.0 | 81.0 | 6.0 | 70.6 | 58.0 | 48.7 | 88.3 | 72.4 | 115.5 | 128.9 | 53.0 | 102.1 |
| 10 | 87.0 | 82.0 | 5.0 | 70.5 | 57.7 | 49.1 | 88.1 | 72.2 | 115.8 | 129.3 | 53.3 | 102.3 |

### E.2.17. Patient 4: "Black Bone"

| | SNA | SNB | ANB | SN | PNS-ANS | S-PNS | S-ANS | Me-Ans | N-Pog | S-Gn | N-A | N-B |
|---|---|---|---|---|---|---|---|---|---|---|---|---|
| 1 | 84.0 | 76.0 | 8.0 | 72.1 | 64.7 | 43.8 | 90.1 | 69.1 | 113.8 | 122.4 | 52.6 | 94.4 |
| 2 | 84.0 | 76.0 | 8.0 | 72.1 | 64.7 | 44.0 | 89.8 | 68.7 | 113.9 | 122.0 | 52.3 | 94.5 |
| 3 | 84.0 | 75.0 | 8.0 | 71.8 | 64.7 | 43.5 | 89.8 | 68.9 | 113.6 | 121.7 | 52.0 | 94.1 |
| 4 | 83.0 | 76.0 | 8.0 | 72.1 | 64.7 | 43.7 | 90.2 | 68.7 | 113.6 | 121.9 | 52.6 | 94.4 |
| 5 | 84.0 | 75.0 | 8.0 | 72.3 | 65.0 | 43.4 | 90.2 | 68.8 | 113.6 | 122.2 | 52.3 | 94.3 |
| 6 | 84.0 | 75.0 | 8.0 | 72.1 | 64.7 | 43.3 | 89.6 | 68.7 | 113.8 | 121.6 | 52.3 | 94.1 |
| 7 | 84.0 | 76.0 | 8.0 | 71.8 | 64.7 | 43.9 | 89.5 | 69.2 | 113.6 | 121.7 | 52.1 | 94.3 |
| 8 | 84.0 | 76.0 | 8.0 | 72.3 | 64.7 | 43.5 | 90.1 | 68.7 | 113.6 | 121.8 | 52.3 | 94.3 |
| 9 | 83.0 | 75.0 | 8.0 | 71.8 | 65.0 | 43.6 | 89.7 | 69.0 | 113.8 | 122.4 | 52.8 | 94.6 |
| 10 | 84.0 | 76.0 | 8.0 | 71.8 | 65.0 | 43.8 | 89.6 | 68.9 | 113.8 | 122.2 | 52.8 | 94.5 |

### E.2.18. Patient 5: "Black Bone"

| | SNA | SNB | ANB | SN | PNS-ANS | S-PNS | S-ANS | Me-Ans | N-Pog | S-Gn | N-A | N-B |
|---|---|---|---|---|---|---|---|---|---|---|---|---|
| **1** | 80.0 | 87.0 | 7.0 | 68.9 | 50.2 | 43.1 | 81.4 | 51.6 | 93.4 | 117.0 | 52.0 | 80.4 |
| **2** | 80.0 | 87.0 | 7.0 | 68.7 | 50.6 | 42.9 | 81.4 | 52.1 | 92.9 | 116.7 | 51.8 | 80.7 |
| **3** | 80.0 | 87.0 | 7.0 | 68.7 | 50.4 | 42.5 | 81.5 | 52.1 | 93.4 | 116.6 | 51.5 | 80.7 |
| **4** | 80.0 | 87.0 | 7.0 | 68.9 | 50.2 | 42.8 | 81.6 | 52.3 | 93.4 | 116.7 | 52.0 | 80.4 |
| **5** | 80.0 | 87.0 | 7.0 | 69.9 | 50.2 | 42.6 | 81.4 | 52.3 | 93.4 | 116.9 | 52.0 | 80.5 |
| **6** | 80.0 | 87.0 | 7.0 | 68.9 | 50.2 | 43.0 | 81.6 | 52.1 | 93.2 | 116.7 | 52.2 | 80.5 |
| **7** | 80.0 | 87.0 | 7.0 | 69.0 | 50.7 | 42.8 | 81.7 | 52.3 | 93.4 | 116.9 | 51.8 | 80.7 |
| **8** | 80.0 | 87.0 | 7.0 | 69.2 | 50.1 | 42.6 | 81.7 | 52.6 | 93.2 | 117.1 | 52.0 | 80.9 |
| **9** | 80.0 | 87.0 | 7.0 | 68.7 | 50.5 | 42.8 | 81.4 | 51.9 | 93.4 | 116.7 | 52.0 | 80.2 |
| **10** | 80.0 | 87.0 | 7.0 | 68.7 | 50.4 | 42.7 | 81.6 | 52.3 | 93.2 | 116.5 | 52.0 | 80.5 |

### E.2.19. Patient 3: MRI T1

| | SNA | SNB | ANB | SN | PNS-ANS | S-PNS | S-ANS | Me-Ans | N-Pog | S-Gn | N-A | N-B |
|---|---|---|---|---|---|---|---|---|---|---|---|---|
| **1** | 90.0 | 83.0 | 6.0 | 71.9 | 60.3 | 47.8 | 90.7 | 70.2 | 113.6 | 128.0 | 52.8 | 100.7 |
| **2** | 89.0 | 83.0 | 7.0 | 71.7 | 60.3 | 47.4 | 90.8 | 70.1 | 113.3 | 128.2 | 52.4 | 100.7 |
| **3** | 89.0 | 83.0 | 6.0 | 71.7 | 60.0 | 48.2 | 90.7 | 70.1 | 112.9 | 128.3 | 52.4 | 100.9 |
| **4** | 89.0 | 83.0 | 7.0 | 71.9 | 59.8 | 47.8 | 90.3 | 70.0 | 113.1 | 128.2 | 52.1 | 100.9 |
| **5** | 90.0 | 83.0 | 7.0 | 71.7 | 60.0 | 48.0 | 91.0 | 69.9 | 113.1 | 127.9 | 52.6 | 100.7 |
| **6** | 90.0 | 83.0 | 6.0 | 71.4 | 59.8 | 47.7 | 90.7 | 70.1 | 113.3 | 128.1 | 52.8 | 100.9 |
| **7** | 90.0 | 83.0 | 7.0 | 71.7 | 60.0 | 47.7 | 90.7 | 69.6 | 113.1 | 128.6 | 52.6 | 100.7 |
| **8** | 90.0 | 83.0 | 6.0 | 71.7 | 59.8 | 48.2 | 90.7 | 70.4 | 112.9 | 128.6 | 52.3 | 101.1 |
| **9** | 89.0 | 83.0 | 6.0 | 71.7 | 60.2 | 47.5 | 90.9 | 70.1 | 113.1 | 128.2 | 52.6 | 100.7 |
| **10** | 90.0 | 83.0 | 7.0 | 71.4 | 60.0 | 48.1 | 90.6 | 69.9 | 113.1 | 128.3 | 52.6 | 100.7 |

### E.2.20. Patient 4: MRI T1

| | SNA | SNB | ANB | SN | PNS-ANS | S-PNS | S-ANS | Me-Ans | N-Pog | S-Gn | N-A | N-B |
|---|---|---|---|---|---|---|---|---|---|---|---|---|
| **1** | 91.0 | 79.0 | 11.0 | 69.2 | 64.1 | 43.0 | 90.7 | 66.9 | 107.8 | 119.9 | 51.7 | 92.6 |
| **2** | 90.0 | 79.0 | 11.0 | 69.0 | 64.1 | 43.2 | 90.6 | 66.4 | 107.7 | 119.7 | 51.5 | 92.6 |
| **3** | 90.0 | 79.0 | 11.0 | 69.0 | 64.1 | 42.8 | 90.3 | 66.3 | 107.8 | 120.1 | 51.5 | 92.6 |
| **4** | 90.0 | 79.0 | 11.0 | 68.7 | 64.1 | 42.9 | 90.5 | 66.0 | 108.0 | 120.1 | 51.8 | 92.6 |
| **5** | 91.0 | 79.0 | 11.0 | 68.7 | 64.1 | 43.1 | 90.1 | 66.2 | 108.0 | 119.8 | 51.5 | 92.9 |
| **6** | 90.0 | 79.0 | 11.0 | 69.2 | 64.3 | 43.1 | 90.2 | 66.5 | 107.3 | 119.5 | 51.8 | 92.8 |
| **7** | 90.0 | 79.0 | 11.0 | 69.0 | 64.1 | 43.2 | 90.0 | 66.1 | 107.7 | 119.8 | 51.7 | 93.2 |
| **8** | 90.0 | 79.0 | 11.0 | 69.0 | 64.1 | 43.2 | 90.4 | 66.0 | 107.5 | 120.1 | 51.5 | 93.1 |
| **9** | 90.0 | 79.0 | 11.0 | 69.2 | 63.9 | 43.3 | 90.3 | 66.5 | 107.5 | 120.0 | 51.5 | 92.8 |
| **10** | 90.0 | 79.0 | 11.0 | 69.2 | 63.6 | 43.2 | 90.5 | 66.5 | 107.8 | 120.1 | 51.8 | 92.4 |

### E.2.21. Patient 5: MRI T1

| | SNA | SNB | ANB | SN | PNS-ANS | S-PNS | S-ANS | Me-Ans | N-Pog | S-Gn | N-A | N-B |
|---|---|---|---|---|---|---|---|---|---|---|---|---|
| **1** | 81.0 | 87.0 | 6.0 | 69.9 | 48.7 | 43.1 | 81.9 | 51.9 | 94.1 | 115.9 | 50.6 | 83.0 |
| **2** | 81.0 | 87.0 | 6.0 | 69.4 | 48.6 | 42.9 | 81.7 | 51.6 | 93.9 | 116.2 | 50.6 | 83.0 |
| **3** | 81.0 | 87.0 | 6.0 | 69.8 | 48.4 | 43.0 | 81.8 | 51.4 | 94.1 | 116.1 | 50.8 | 82.8 |
| **4** | 81.0 | 87.0 | 6.0 | 69.6 | 48.6 | 42.8 | 81.5 | 51.6 | 93.9 | 115.8 | 50.8 | 83.2 |
| **5** | 81.0 | 87.0 | 6.0 | 69.6 | 48.6 | 43.1 | 81.8 | 51.2 | 93.9 | 116.2 | 50.6 | 83.5 |
| **6** | 81.0 | 87.0 | 6.0 | 69.6 | 48.4 | 43.3 | 81.3 | 51.6 | 94.1 | 116.4 | 50.8 | 83.2 |
| **7** | 81.0 | 87.0 | 6.0 | 69.6 | 48.6 | 43.0 | 81.3 | 51.4 | 93.9 | 116.1 | 50.8 | 83.3 |
| **8** | 81.0 | 87.0 | 6.0 | 69.6 | 48.7 | 43.1 | 81.8 | 51.6 | 93.9 | 116.1 | 50.6 | 83.7 |
| **9** | 81.0 | 87.0 | 6.0 | 69.9 | 48.7 | 42.6 | 81.3 | 51.6 | 93.2 | 115.8 | 50.6 | 83.5 |
| **10** | 81.0 | 87.0 | 6.0 | 69.6 | 49.1 | 43.1 | 81.1 | 51.6 | 94.3 | 116.1 | 50.4 | 83.3 |

### E.2.22. Patient 3: MRI T2

| | SNA | SNB | ANB | SN | PNS-ANS | S-PNS | S-ANS | Me-Ans | N-Pog | S-Gn | N-A | N-B |
|---|---|---|---|---|---|---|---|---|---|---|---|---|
| **1** | 86.0 | 85.0 | 1.0 | 70.6 | 45.7 | 54.7 | 87.2 | 73.8 | 107.7 | 127.4 | 46.2 | 95.9 |
| **2** | 86.0 | 85.0 | 1.0 | 70.9 | 45.7 | 54.7 | 87.8 | 73.3 | 107.2 | 127.4 | 46.2 | 95.7 |
| **3** | 86.0 | 85.0 | 1.0 | 70.8 | 45.7 | 54.9 | 87.5 | 74.1 | 107.4 | 127.3 | 46.2 | 95.5 |
| **4** | 86.0 | 85.0 | 1.0 | 70.9 | 46.2 | 54.8 | 87.4 | 73.5 | 107.2 | 127.3 | 46.2 | 95.9 |
| **5** | 86.0 | 85.0 | 1.0 | 71.1 | 45.5 | 54.5 | 87.6 | 73.7 | 107.4 | 127.2 | 46.2 | 95.9 |
| **6** | 86.0 | 85.0 | 1.0 | 71.3 | 46.2 | 54.9 | 87.7 | 73.2 | 107.0 | 126.9 | 45.7 | 95.9 |
| **7** | 86.0 | 85.0 | 1.0 | 71.6 | 45.7 | 54.8 | 87.6 | 72.9 | 107.2 | 127.8 | 45.7 | 95.9 |
| **8** | 86.0 | 85.0 | 1.0 | 71.1 | 45.9 | 54.7 | 87.6 | 73.4 | 107.0 | 127.0 | 46.2 | 96.2 |
| **9** | 86.0 | 85.0 | 1.0 | 71.1 | 45.9 | 55.0 | 87.4 | 73.3 | 107.7 | 127.8 | 46.0 | 96.4 |
| **10** | 86.0 | 85.0 | 1.0 | 70.9 | 45.4 | 54.6 | 87.6 | 73.3 | 107.2 | 126.9 | 46.0 | 95.9 |

### E.2.23. Patient 4: MRI T2

| | SNA | SNB | ANB | SN | PNS-ANS | S-PNS | S-ANS | Me-Ans | N-Pog | S-Gn | N-A | N-B |
|---|---|---|---|---|---|---|---|---|---|---|---|---|
| **1** | 91.0 | 81.0 | 10.0 | 67.5 | 69.2 | 40.3 | 91.2 | 69.1 | 106.6 | 120.2 | 51.3 | 94.8 |
| **2** | 91.0 | 81.0 | 10.0 | 67.5 | 69.2 | 40.3 | 91.1 | 68.9 | 106.5 | 119.8 | 51.3 | 95.1 |
| **3** | 91.0 | 81.0 | 10.0 | 67.5 | 69.5 | 40.5 | 91.0 | 69.0 | 106.5 | 120.2 | 51.3 | 95.3 |
| **4** | 91.0 | 81.0 | 10.0 | 67.2 | 69.2 | 39.8 | 90.9 | 69.1 | 106.3 | 120.4 | 50.8 | 94.8 |
| **5** | 91.0 | 81.0 | 10.0 | 67.7 | 69.5 | 40.6 | 91.0 | 68.9 | 106.5 | 119.8 | 51.1 | 95.3 |
| **6** | 91.0 | 81.0 | 10.0 | 67.7 | 69.0 | 40.3 | 91.1 | 68.8 | 106.3 | 120.5 | 50.8 | 95.3 |
| **7** | 91.0 | 81.0 | 10.0 | 67.5 | 69.0 | 40.7 | 90.8 | 68.7 | 106.3 | 120.2 | 51.0 | 94.8 |
| **8** | 91.0 | 81.0 | 10.0 | 67.5 | 69.0 | 40.0 | 90.8 | 69.0 | 106.5 | 120.4 | 51.0 | 94.6 |
| **9** | 91.0 | 81.0 | 10.0 | 67.5 | 69.5 | 40.3 | 91.1 | 68.7 | 106.5 | 120.1 | 50.6 | 94.9 |
| **10** | 91.0 | 81.0 | 10.0 | 67.0 | 69.5 | 40.3 | 90.5 | 69.0 | 106.3 | 120.3 | 50.6 | 95.1 |

### E.2.24. Patient 5: MRI T2

| | SNA | SNB | ANB | SN | PNS-ANS | S-PNS | S-ANS | Me-Ans | S-Gn | N-Pog | N-A | N-B |
|---|---|---|---|---|---|---|---|---|---|---|---|---|
| **1** | 78.0 | 86.0 | 8.0 | 68.4 | 48.0 | 42.2 | 79.5 | 51.9 | 115.4 | 95.3 | 50.9 | 85.4 |
| **2** | 78.0 | 86.0 | 8.0 | 68.8 | 48.0 | 41.7 | 80.1 | 52.1 | 115.7 | 95.3 | 50.7 | 85.6 |
| **3** | 78.0 | 86.0 | 8.0 | 68.6 | 47.8 | 41.8 | 79.8 | 51.4 | 115.3 | 95.3 | 50.7 | 85.6 |
| **4** | 78.0 | 86.0 | 8.0 | 68.8 | 48.3 | 42.1 | 79.9 | 51.9 | 114.9 | 95.3 | 50.9 | 85.6 |
| **5** | 78.0 | 86.0 | 8.0 | 68.3 | 47.6 | 41.9 | 79.9 | 51.2 | 115.0 | 95.3 | 50.6 | 85.6 |
| **6** | 78.0 | 86.0 | 8.0 | 68.6 | 48.3 | 41.7 | 79.6 | 51.4 | 115.3 | 95.1 | 50.9 | 85.9 |
| **7** | 78.0 | 86.0 | 8.0 | 68.6 | 47.8 | 42.3 | 79.9 | 51.4 | 115.1 | 95.3 | 50.4 | 85.8 |
| **8** | 78.0 | 86.0 | 8.0 | 68.3 | 47.8 | 41.8 | 79.9 | 51.7 | 115.5 | 95.8 | 50.7 | 85.6 |
| **9** | 78.0 | 86.0 | 8.0 | 68.4 | 47.8 | 42.3 | 80.0 | 51.2 | 115.2 | 95.3 | 50.9 | 85.6 |
| **10** | 78.0 | 86.0 | 8.0 | 68.6 | 48.0 | 41.9 | 79.7 | 51.6 | 115.0 | 95.6 | 50.9 | 85.6 |

## E.3. Repeatability of Dolphin Measurements

| | SNA (º) | SNB (º) | ANB (º) | Interincisal Angle (U1-L1) (º) | U1 - NA (º) | U1 - NA (mm) | L1 - NB (º) | L1 - NB (mm) | Anterior Cranial Base (SN) (mm) | Maxillary length (ANS-PNS) (mm) | S - ANS (mm) | Anterior Facial Ht (ANS-Me)(mm) | N' - Pog' (mm) |
|---|---|---|---|---|---|---|---|---|---|---|---|---|---|
| **BB1** | 83.50 | 78.40 | 5.10 | 124.90 | 21.70 | 3.60 | 28.30 | 7.60 | 70.10 | 55.80 | 88.00 | 65.70 | 92.80 |
| **BB2** | 83.90 | 78.80 | 5.10 | 122.30 | 20.90 | 3.10 | 31.70 | 8.10 | 69.90 | 56.70 | 87.90 | 65.10 | 96.80 |
| **BB3** | 81.90 | 77.20 | 4.60 | 124.30 | 23.20 | 4.10 | 27.80 | 7.90 | 70.90 | 61.50 | 88.70 | 65.20 | 95.20 |
| **BB4** | 82.20 | 77.70 | 4.50 | 122.60 | 21.90 | 4.90 | 31.10 | 7.90 | 70.20 | 60.60 | 88.70 | 65.10 | 97.60 |
| **BB5** | 81.70 | 77.20 | 4.50 | 126.90 | 19.40 | 3.70 | 29.20 | 7.20 | 69.80 | 60.90 | 88.40 | 65.00 | 93.50 |
| **BB6** | 81.20 | 77.20 | 3.90 | 126.20 | 20.70 | 4.00 | 29.10 | 6.10 | 70.20 | 61.60 | 87.90 | 65.20 | 96.10 |
| **BB7** | 81.40 | 76.80 | 4.70 | 122.10 | 24.30 | 4.70 | 28.90 | 7.70 | 70.40 | 63.00 | 87.80 | 65.10 | 92.50 |
| **BB8** | 82.60 | 78.20 | 4.40 | 118.60 | 24.70 | 5.00 | 32.30 | 7.80 | 69.80 | 60.10 | 88.60 | 64.70 | 93.80 |
| **BB9** | 81.90 | 77.40 | 4.50 | 123.20 | 22.40 | 4.50 | 29.80 | 6.80 | 70.40 | 60.20 | 88.30 | 64.50 | 93.30 |
| **BB10** | 81.90 | 77.70 | 4.10 | 122.20 | 23.60 | 5.10 | 30.10 | 6.60 | 70.20 | 61.10 | 87.70 | 65.60 | 94.60 |
| **Mean** | 82.22 | 77.66 | 4.54 | 123.33 | 22.28 | 4.27 | 29.83 | 7.37 | 70.19 | 60.15 | 88.20 | 65.12 | 94.62 |
| **SD** | 0.88 | 0.63 | 0.38 | 2.38 | 1.69 | 0.68 | 1.47 | 0.67 | 0.33 | 2.22 | 0.39 | 0.36 | 1.75 |
| **CoV** | 1.06 | 0.81 | 8.32 | 1.93 | 7.59 | 15.81 | 4.94 | 9.05 | 0.47 | 3.70 | 0.44 | 0.55 | 1.85 |

## E.4. Co-ordinates of repeated digitisations of "Black Bone" using Dolphin with 1st digitisation as reference

| | 1 | | 2 | | | 3 | | | 4 | | | 5 | | | 6 | | | 7 | | | 8 | | | 9 | | | 10 | | |
|---|---|---|---|---|---|---|---|---|---|---|---|---|---|---|---|---|---|---|---|---|---|---|---|---|---|---|---|---|---|
| **Landmark Name** | X | Y | Dx | Dy | Dist | Dx | Dy | Dist | Dx | Dy | Dist | Dx | Dy | Dist | Dx | Dy | Dist | Dx | Dy | Dist | Dx | Dy | Dist | Dx | Dy | Dist | Dx | Dy | Dist |
| **A Point** | 72 | -36.3 | 0.2 | 0 | 0.2 | -0.5 | -1.8 | 1.9 | -0.9 | -1.9 | 2.1 | -1.7 | -3 | 3.5 | -1.8 | -2.7 | 3.3 | -1.4 | -2.2 | 2.6 | -1 | -1.2 | 1.6 | -0.9 | -2.1 | 2.3 | -1.2 | -2.4 | 2.7 |
| **ANS** | 81.4 | -33.3 | -0.1 | -0.2 | 0.2 | -0.2 | -2.3 | 2.3 | 0.2 | -1.5 | 1.5 | -0.8 | -3 | 3.2 | -0.9 | -1.9 | 2.1 | -1.1 | -2.1 | 2.4 | 0.3 | -1 | 1 | -0.6 | -2.2 | 2.3 | -0.9 | -1.5 | 1.7 |
| **B Point** | 66.6 | -75.2 | 0.5 | -0.2 | 0.5 | -1.1 | -1.4 | 1.8 | -0.9 | -0.1 | 0.9 | -2.2 | -1.7 | 2.8 | -1.8 | -2.3 | 3 | -2.3 | -1.8 | 2.9 | -0.6 | -0.5 | 0.7 | -1.2 | -0.9 | 1.5 | -1 | -0.9 | 1.3 |
| **Bridge of Nose** | 84.1 | -1.4 | 0.4 | 1.7 | 1.8 | 0.3 | -0.2 | 0.3 | 0.2 | 0.6 | 0.6 | -0.4 | -1 | 1.1 | -0.3 | -0.1 | 0.3 | 1.3 | -1.7 | 2.1 | 0.4 | 0 | 0.4 | 2.3 | -2.1 | 3.1 | 2.5 | -3.2 | 4.1 |
| **L1 Labial Gingival Border** | 71.4 | -63.6 | 0.9 | 0.6 | 1.1 | -0.6 | -1.5 | 1.6 | 0 | -0.2 | 0.2 | -1.6 | -2.7 | 3.2 | -3.7 | -5.4 | 6.6 | -1.2 | -1.6 | 2 | 0 | 0.3 | 0.3 | -1 | -3.1 | 3.3 | -1.1 | -2.1 | 2.3 |
| **L1 Lingual Gingival Border** | 69 | -61.7 | 1.5 | 0.6 | 1.6 | -1.1 | -2 | 2.3 | -1 | -1.8 | 2.1 | -3.8 | -2.9 | 4.7 | -3.4 | -3.7 | 5 | -1.7 | -0.7 | 1.8 | -1.1 | -0.5 | 1.2 | -1.3 | -2 | 2.4 | 0.3 | -0.7 | 0.8 |
| **L1 Root** | 64.4 | -74.1 | 0.5 | 1.4 | 1.5 | -1.3 | -2.2 | 2.5 | -1.7 | -1.1 | 2.1 | -2.5 | -2.2 | 3.3 | -3.4 | -2.8 | 4.4 | -2.5 | -1.2 | 2.8 | -0.6 | 0.9 | 1.1 | -1.1 | 0 | 1.1 | -2 | -1.4 | 2.5 |
| **L1 Tip** | 74.7 | -56.3 | 0.9 | 0.1 | 0.9 | -0.4 | -1 | 1.1 | -0.4 | -1.3 | 1.4 | -2.3 | -3.3 | 4 | -3 | -3.3 | 4.4 | -1.6 | -1.1 | 1.9 | -0.3 | -1.4 | 1.4 | -1.7 | -2.6 | 3.1 | -1.8 | -2.7 | 3.2 |
| **Lower Lip** | 83.1 | -61.7 | 0.6 | 0.2 | 0.7 | -0.8 | -2.3 | 2.4 | -0.5 | 0.2 | 0.5 | -1.6 | -3.9 | 4.2 | -1.7 | -2.2 | 2.8 | -1.1 | -1.3 | 1.8 | -0.1 | -0.8 | 0.8 | -0.2 | -3.6 | 3.6 | -1.1 | -2 | 2.3 |
| **Menton** | 62 | -96.1 | 0.4 | 0.3 | 0.5 | -0.7 | -1.6 | 1.7 | -0.7 | -0.6 | 0.9 | -2.8 | -1.6 | 3.2 | -1.8 | -1.1 | 2.1 | -2.2 | -1.1 | 2.5 | -0.1 | 0.2 | 0.2 | -1.2 | -0.8 | 1.4 | -1.5 | -1.1 | 1.9 |
| **Nasion** | 69 | 12.2 | -0.2 | 0 | 0.2 | 0.8 | 0.1 | 0.8 | 0.1 | 0 | 0.1 | -0.3 | 0 | 0.3 | 0.1 | 0 | 0.1 | 0.3 | 0.1 | 0.3 | -0.3 | 0 | 0.3 | 0.4 | 0.1 | 0.4 | 0.1 | 0 | 0.1 |
| **PNS** | 26 | -39.2 | -1.1 | 0 | 1.1 | -6 | -1.8 | 6.3 | -4.7 | -1.1 | 4.8 | -6 | -1.9 | 6.3 | -6.8 | -1.6 | 7 | -8.2 | -2.3 | 8.6 | -4 | -1.3 | 4.2 | -5.2 | -0.8 | 5.3 | -6.1 | -2.7 | 6.6 |
| **Pogonion** | 68.2 | -88.5 | 0.9 | 1.2 | 1.4 | -1.3 | -1.2 | 1.8 | -0.6 | 0.7 | 0.9 | -2.6 | -1 | 2.7 | -1.6 | -0.2 | 1.6 | -1.7 | 0.1 | 1.7 | -0.4 | -0.1 | 0.4 | -1.1 | 0.2 | 1.1 | -1.1 | 0.2 | 1.1 |
| **Ruler Point 1** | -133.7 | -129.1 | 1.1 | -1.4 | 1.8 | -2.2 | 2.3 | 3.2 | -1.2 | 2.4 | 2.7 | -3.4 | 3.9 | 5.2 | -3.2 | 4 | 5.1 | -2.9 | 2.8 | 4 | -0.4 | 0.3 | 0.5 | -1.4 | 1.5 | 2.1 | -1.8 | 2.2 | 2.8 |
| **Ruler Point 2** | 106.3 | -129.1 | 1.1 | 0.4 | 1.2 | -2.2 | -2.8 | 3.6 | -1.3 | -1.5 | 1.9 | -3.5 | -3.1 | 4.7 | -3.3 | -2.3 | 4 | -3 | -2.7 | 4 | -0.4 | -0.4 | 0.6 | -1.5 | -1.9 | 2.4 | -1.8 | -2.3 | 2.9 |
| **ST A-Point** | 83.9 | -41.1 | -0.1 | 0.4 | 0.4 | -1.2 | -3.4 | 3.6 | 0.4 | 0.4 | 0.5 | -1.6 | -2.5 | 3 | -0.8 | -0.9 | 1.3 | -1.8 | -2.7 | 3.2 | -1.6 | -0.9 | 1.9 | -1 | -1.4 | 1.7 | -0.2 | -1.2 | 1.2 |
| **ST B-Point** | 77.1 | -72 | -0.1 | -0.1 | 0.2 | -1.3 | -1.9 | 2.3 | -1.5 | -1.3 | 2 | -2.4 | -2.9 | 3.7 | -2.5 | -2.3 | 3.4 | -2.2 | -1.7 | 2.8 | -0.6 | -0.8 | 1 | -1.7 | -1.3 | 2.1 | -1.7 | -1.6 | 2.4 |
| **ST Nasion** | 77.7 | 8.9 | -0.7 | 2.7 | 2.8 | 0.5 | 0.2 | 0.5 | 0.1 | 2.6 | 2.6 | -0.6 | -0.8 | 1 | -0.3 | -0.5 | 0.6 | -0.6 | -0.4 | 0.7 | -0.3 | 0.7 | 0.8 | -0.2 | 0.2 | 0.3 | -0.2 | -0.9 | 0.9 |
| **ST Pogonion** | 78.2 | -83.9 | 1.1 | -1.2 | 1.6 | -1 | -2.2 | 2.4 | -0.8 | -2.2 | 2.3 | -1.9 | -1.5 | 2.5 | -1.5 | -3.7 | 4.1 | -1.9 | -0.1 | 1.9 | 0.7 | -0.2 | 0.7 | -0.5 | -0.2 | 0.5 | -1.1 | -2.7 | 2.9 |
| **Sella** | 0 | 0 | 0 | 0 | 0 | 0 | 0 | 0 | 0 | 0 | 0 | 0 | 0 | 0 | 0 | 0 | 0 | 0 | 0 | 0 | 0 | 0 | 0 | 0 | 0 | 0 | 0 | 0 | 0 |
| **Subnasale** | 87.4 | -36.5 | 0.2 | -0.4 | 0.4 | -2.5 | -3.4 | 4.2 | 1 | -1 | 1.4 | 0.2 | -1.6 | 1.6 | 0.1 | -1.6 | 1.6 | -0.9 | -2.5 | 2.7 | 0.3 | -0.4 | 0.5 | 0.5 | -0.7 | 0.8 | 0.7 | -1.3 | 1.5 |
| **Tip of Nose** | 105 | -25.4 | 0.6 | -0.2 | 0.7 | 0.3 | -2 | 2 | 0.6 | -1.6 | 1.7 | 0.5 | -3.2 | 3.2 | 0.1 | -3.4 | 3.4 | -0.6 | -3.2 | 3.3 | -0.3 | -2.4 | 2.5 | 0 | -1.8 | 1.8 | -0.3 | -2.4 | 2.4 |
| **U1 Labial Gingival Border** | 74.7 | -51.7 | 0 | 0.4 | 0.4 | -1.1 | 0 | 1.1 | -0.3 | 0 | 0.3 | -1.8 | -0.9 | 2 | -1.4 | -1.7 | 2.3 | -1.2 | -1.1 | 1.6 | -0.3 | -0.3 | 0.4 | 1 | -2.4 | 2.6 | -0.3 | -0.8 | 0.9 |
| **U1 Lingual Gingival Border** | 70.9 | -54.4 | 0.3 | 1.1 | 1.2 | -0.3 | 0.1 | 0.3 | -0.6 | 1.2 | 1.3 | -1.9 | -0.5 | 1.9 | -0.7 | -1.1 | 1.3 | -3.4 | 1.4 | 3.6 | 0 | 0.5 | 0.5 | 0.5 | -1.5 | 1.6 | -1.2 | 0.3 | 1.2 |
| **U1 Root** | 66.3 | -38.7 | 1 | -1.3 | 1.7 | -1.1 | 0 | 1.1 | 0.2 | 0.1 | 0.2 | 0.1 | -3.5 | 3.5 | -0.8 | -0.7 | 1.1 | -1.7 | -1.2 | 2.1 | 0.4 | -2 | 2 | -0.4 | -0.9 | 1 | -0.9 | 0.4 | 1 |
| **U1 Tip** | 77.1 | -61.7 | -0.2 | 0.9 | 0.9 | -0.8 | -0.8 | 1.1 | -0.2 | -0.3 | 0.4 | -2.4 | -2.1 | 3.1 | -2.5 | -0.4 | 2.5 | -1.2 | -1.7 | 2.1 | 0 | 0.8 | 0.8 | -0.7 | -1 | 1.3 | -0.5 | -0.3 | 0.6 |
| **Upper Lip** | 84.1 | -50.3 | 0.8 | -0.6 | 1.1 | -0.3 | -2.3 | 2.4 | -0.6 | -1.2 | 1.4 | -0.7 | -3.1 | 3.2 | -1.1 | -2.8 | 3 | -0.6 | -2.5 | 2.5 | -0.3 | -0.1 | 0.3 | -0.6 | -1.4 | 1.5 | -0.3 | -1.5 | 1.5 |

# Appendix F: Tumour Volume

# F.1 Staging of head & neck malignancy

The current staging system for head and neck malignancy is by the TNM classification of Malignant Tumours, by the International Union Against Cancer (UICC), Seventh Edition.

## Lip & Oral Cavity

The classification applies to carcinomas of the vermilion surfaces of the lips and of the oral cavity, including those of minor salivary glands.[207]

### *Anatomical Sites and Subsites*

**Lip (C00)**

1. External upper lip (vermilion border) (C00.0)
2. External lower lip (vermilion border) (C00.1)
3. Commissures (C00.6)

**Oral Cavity (C02-06)**

1. Buccal mucosa
    a. Mucosa of upper and lower lips (C0.3, 4)
    b. Cheek mucosa (C06.0)
    c. Retromolar areas (C06.2)
    d. Bucco-alveolar sulci, upper and lower (vestibule of mouth) (C06.1)
2. Upper alveolus and gingival (upper gum) (C03.0)
3. Lower alveolus and gingival (lower gum) (C03.1)
4. Hard palate (C05.0)
5. Tongue
    a. Dorsal surface and lateral borders anterior to vallate papillae (anterior two thirds) (C02.2)
    b. Inferior (ventral) surface (C02.2)
6. Floor of mouth (C04)

### *TNM Classification*

**T – Primary Tumour**

| | |
|---|---|
| T1 | ≤ 2cm |
| T2 | >2-4 cm |
| T3 | >4cm |
| T4a | **Oral Cavity:** through cortical bone, deep/extrinsic muscle of tongue, maxillary sinus, skin of face<br>**Lip:** through cortical bone, inferior alveolar nerve, floor of mouth, skin |
| T4b | Masticator space, pterygoid plates, skull base, internal carotid artery |

**N - Regional Lymph Nodes**

| | |
|---|---|
| N0 | No regional lymph node metastasis |
| N1 | Ipsilateral single ≤3cm |
| N2 | a. Ipsilateral single >3-6cm<br>b. Ipsilateral multiple ≤6cm<br>c. Bilateral, contralateral ≤6cm |
| N3 | >6cm |

**M – Distant Metastasis**

| | |
|---|---|
| M0 | No distant metastasis |
| M1 | Distant metastasis |

### *Stage Grouping*

| | | | |
|---|---|---|---|
| Stage 0 | Tis | N0 | M0 |
| Stage I | T1 | N0 | M0 |
| Stage II | T2 | N0 | M0 |
| Stage III | T3 | N0 | M0 |
| | T1, T2, T3 | N1 | M0 |
| Stage IVA | T4a | N0, N1 | M0 |
| | T1, T2, T3, T4a | N2 | M0 |
| Stage IVB | Any T | N3 | M0 |
| | T4b | Any N | M0 |
| Stage IVC | Any T | Any N | M1 |

# Nasal Cavity and Paranasal Sinuses

## *Anatomical Sites and Subsites*

**Nasal Cavity (C3.0)**
- Septum
- Floor
- Lateral wall
- Vestibule

**Maxillary Sinus (C31.0)**

**Ethmoid Sinus (C31.1)**

## *TNM Classification (Maxillary Sinus)*

**T – Primary Tumour**

| | |
|---|---|
| T1 | Mucosa |
| T2 | Bone erosion/destruction, hard palate, middle nasal meatus |
| T3 | Posterior bony wall maxillary sinus, subcutaneous tissues, floor/medial wall of orbit, pterygoid fossa, ethmoid sinus |
| T4a | Anterior orbit, cheek skin, pterygoid plates, infratemporal fossa, cribiform plate, sphenoid frontal sinus |
| T4b | Orbital apex, dura, brain, middle cranial fossa, cranial nerves other than V2, nasopharynx, clivus |

**N – Regional Lymph Nodes**

| | |
|---|---|
| N1 | Ipsilateral single ≤3cm |
| N2 | |
| | a. Ipsilateral single >3-6cm |
| | b. Ipsilateral multiple ≤6cm |
| | c. Bilateral, contralateral ≤6cm |
| N3 | >6cm |

## *Stage Grouping*

| | | | |
|---|---|---|---|
| Stage 0 | Tis | N0 | M0 |
| Stage I | T1 | N0 | M0 |
| Stage II | T2 | N0 | M0 |
| Stage III | T3 | N0 | M0 |
| | T1, T2, T3 | N1 | M0 |
| Stage IVA | T1, T2, T3 | N2 | M0 |
| | T4a | N0, N1, N2 | M0 |
| Stage IVB | T4b | Any N | M0 |
| | Any T | N3 | M0 |
| Stage IVC | Any T | Any N | M1 |

## F.2 ACE-27 Co-morbidity Scoring

### *Adult Comorbidity Evaluation-27*

Identify the important medical comorbidities and grade severity using the index.
Overall Comorbidity Score is defined according to the highest ranked single ailment, except in the case where two or more Grade 2 ailments occur in different organ systems. In this situation, the overall comorbidity score should be designated Grade 3.

| Cogent comorbid ailment | Grade 3<br>Severe Decompensation | Grade 2<br>Moderate Decompensation | Grade 1<br>Mild Decompensation |
|---|---|---|---|
| **Cardiovascular System** | | | |
| Myocardial Infarct | ☐ MI ≤ 6 months | ☐ MI > 6 months ago | ☐ MI by ECG only, age undetermined |
| Angina / Coronary Artery Disease | ☐ Unstable angina | ☐ Chronic exertional angina<br>☐ Recent (≤ 6 months) Coronary Artery Bypass Graft (CABG) or Percutaneous Transluminal Coronary Angioplasty (PTCA)<br>☐ Recent (≤ 6 months) coronary stent | ☐ ECG or stress test evidence or catheterization evidence of coronary disease without symptoms<br>☐ Angina pectoris not requiring hospitalization<br>☐ CABG or PTCA (>6 mos.)<br>☐ Coronary stent (>6 mos.) |
| Congestive Heart Failure (CHF) | ☐ Hospitalized for CHF within past 6 months<br>☐ Ejection fraction < 20% | ☐ Hospitalized for CHF >6 months prior<br>☐ CHF with dyspnea which limits activities | ☐ CHF with dyspnea which has responded to treatment<br>☐ Exertional dyspnea<br>☐ Paroxysmal Nocturnal Dyspnea (PND) |
| Arrhythmias | ☐ Ventricular arrhythmia ≤ 6 months | ☐ Ventricular arrhythmia > 6 months<br>☐ Chronic atrial fibrillation or flutter<br>☐ Pacemaker | ☐ Sick Sinus Syndrome<br>☐ Supraventricular tachycardia |
| Hypertension | ☐ DBP≥130 mm Hg<br>☐ Severe malignant papilledema or other eye changes<br>☐ Encephalopathy | ☐ DBP 115-129 mm Hg<br>☐ DBP 90-114 mm Hg while taking antihypertensive medications<br>☐ Secondary cardiovascular symptoms: vertigo, epistaxis, headaches | ☐ DBP 90-114 mm Hg while not taking antihypertensive medications<br>☐ DBP <90 mm Hg while taking antihypertensive medications<br>☐ Hypertension, not otherwise specified |
| Venous Disease | ☐ Recent PE (≤ 6 mos.)<br>☐ Use of venous filter for PE's | ☐ DVT controlled with Coumadin or heparin<br>☐ Old PE > 6 months | ☐ Old DVT no longer treated with Coumadin or Heparin |
| Peripheral Arterial Disease | ☐ Bypass or amputation for gangrene or arterial insufficiency < 6 months ago<br>☐ Untreated thoracic or abdominal aneurysm (≥6 cm) | ☐ Bypass or amputation for gangrene or arterial insufficiency > 6 months ago<br>☐ Chronic insufficiency | ☐ Intermittent claudication<br>☐ Untreated thoracic or abdominal aneurysm (< 6 cm)<br>☐ s/p abdominal or thoracic aortic aneurysm repair |
| **Respiratory System** | | | |
| | ☐ Marked pulmonary insufficiency<br>☐ Restrictive Lung Disease or COPD with dyspnea at rest despite treatment<br>☐ Chronic supplemental $O_2$<br>☐ $CO_2$ retention ($pCO_2$ > 50 torr)<br>☐ Baseline $pO_2$ < 50 torr<br>☐ FEV1 (< 50%) | ☐ Restrictive Lung Disease or COPD (chronic bronchitis, emphysema, or asthma) with dyspnea which limits activities<br>☐ FEV1 (51%-65%) | ☐ Restrictive Lung Disease or COPD (chronic bronchitis, emphysema, or asthma) with dyspnea which has responded to treatment<br>☐ FEV1 (66%-80%) |
| **Gastrointestinal System** | | | |
| Hepatic | ☐ Portal hypertension and/or esophageal bleeding ≤ 6 mos. (Encephalopathy, Ascites, Jaundice with Total Bilirubin > 2) | ☐ Chronic hepatitis, cirrhosis, portal hypertension with moderate symptoms "compensated hepatic failure" | ☐ Chronic hepatitis or cirrhosis without portal hypertension<br>☐ Acute hepatitis without cirrhosis<br>☐ Chronic liver disease manifested on biopsy or persistently elevated bilirubin (>3 mg/dl) |
| Stomach / Intestine | ☐ Recent ulcers( ≤ 6 months ago) requiring blood transfusion | ☐ Ulcers requiring surgery or transfusion > 6 months ago | ☐ Diagnosis of ulcers treated with meds<br>☐ Chronic malabsorption syndrome<br>☐ Inflammatory bowel disease (IBD) on meds or h/o with complications and/or surgery |
| Pancreas | ☐ Acute or chronic pancreatitis with major complications (phlegmon, abscess, or pseudocyst) | ☐ Uncomplicated acute pancreatitis<br>☐ Chronic pancreatitis with minor complications (malabsorption, impaired glucose tolerance, or GI bleeding) | ☐ Chronic pancreatitis w/o complications |

| Cogent comorbid ailment | Grade 3<br>Severe Decompensation | Grade 2<br>Moderate Decompensation | Grade 1<br>Mild Decompensation |
|---|---|---|---|
| **Renal System** | | | |
| End-stage renal disease | ☐ Creatinine > 3 mg% with multi-organ failure, shock, or sepsis<br>☐ Acute dialysis | ☐ Chronic Renal Insufficiency with creatinine >3 mg%<br>☐ Chronic dialysis | ☐ Chronic Renal Insufficiency with creatinine 2-3 mg%. |
| **Endocrine System** | **(Code the comorbid ailments with the (*) in both the Endocrine system and other organ systems if applicable)** | | |
| Diabetes Mellitus | ☐ Hospitalization ≤ 6 months for DKA<br>☐ Diabetes causing end-organ failure<br>☐ retinopathy<br>☐ neuropathy<br>☐ nephropathy*<br>☐ coronary disease*<br>☐ peripheral arterial disease* | ☐ IDDM without complications<br>☐ Poorly controlled AODM with oral agents | ☐ AODM controlled by oral agents only |
| **Neurological System** | | | |
| Stroke | ☐ Acute stroke with significant neurologic deficit | ☐ Old stroke with neurologic residual | ☐ Stroke with no residual<br>☐ Past or recent TIA |
| Dementia | ☐ Severe dementia requiring full support for activities of daily living | ☐ Moderate dementia (not completely self-sufficient, needs supervising) | ☐ Mild dementia (can take care of self) |
| Paralysis | ☐ Paraplegia or hemiplegia requiring full support for activities of daily living | ☐ Paraplegia or hemiplegia requiring wheelchair, able to do some self care | ☐ Paraplegia or hemiplegia, ambulatory and providing most of self care |
| Neuromuscular | ☐ MS, Parkinson's, Myasthenia Gravis, or other chronic neuromuscular disorder and requiring full support for activities of daily living | ☐ MS, Parkinson's, Myasthenia Gravis, or other chronic neuromuscular disorder, but able to do some self care | ☐ MS, Parkinson's, Myasthenia Gravis, or other chronic neuromuscular disorder, but ambulatory and providing most of self care |
| **Psychiatric** | | | |
| | ☐ Recent suicidal attempt<br>☐ Active schizophrenia | ☐ Depression or bipolar disorder uncontrolled<br>☐ Schizophrenia controlled w/ meds | ☐ Depression or bipolar disorder controlled w/ medication |
| **Rheumatologic** | **(Incl. Rheumatoid Arthritis, Systemic Lupus, Mixed Connective Tissue Disorder, Polymyositis, Rheumatic Polymyositis)** | | |
| | ☐ Connective Tissue Disorder with secondary end-organ failure (renal, cardiac, CNS) | ☐ Connective Tissue Disorder on steroids or immunosuppressant medications | ☐ Connective Tissue Disorder on NSAIDS or no treatment |
| **Immunological System** | **(AIDS should not be considered a comorbidity for Kaposi's Sarcoma or Non-Hodgkin's Lymphoma)** | | |
| AIDS | ☐ Fulminant AIDS w/KS, MAI, PCP (AIDS defining illness) | ☐ HIV+ with h/o defining illness. $CD4^+ < 200/\mu L$ | ☐ Asymptomatic HIV+ patient.<br>☐ $HIV^+$ w/o h/o AIDS defining illness. $CD4^+ > 200/\mu L$ |
| **Malignancy** | **(Excluding Cutaneous Basal Cell Ca., Cutaneous SCCA, Carcinoma in-situ, and Intraepithelial Neoplasm)** | | |
| Solid Tumor including melanoma | ☐ Uncontrolled cancer<br>☐ Newly diagnosed but not yet treated<br>☐ Metastatic solid tumor | ☐ Any controlled solid tumor without documented metastases, but initially diagnosed and treated within the last 5 years | ☐ Any controlled solid tumor without documented metastases, but initially diagnosed and treated > 5 years ago |
| Leukemia and Myeloma | ☐ Relapse<br>☐ Disease out of control | ☐ 1st remission or new dx <1yr<br>☐ Chronic suppressive therapy | ☐ H/o leukemia or myeloma with last Rx > 1 yr prior |
| Lymphoma | ☐ Relapse | ☐ 1st remission or new dx <1yr<br>☐ Chronic suppressive therapy | ☐ H/o lymphoma w/ last Rx >1 yr prior |
| **Substance Abuse** | **(Must be accompanied by social, behavioral, or medical complications)** | | |
| Alcohol | ☐ Delirium tremens | ☐ Active alcohol abuse with social, behavioral, or medical complications | ☐ H/o alcohol abuse but not presently drinking |
| Illicit Drugs | ☐ Acute Withdrawal Syndrome | ☐ Active substance abuse with social, behavioral, or medical complications | ☐ H/o substance abuse but not presently using |
| **Body Weight** | | | |
| Obesity | | ☐ Morbid (i.e., BMI ≥ 38) | |

**OVERALL COMORBIDITY SCORE (Circle one.)** **0** None **1** Mild **2** Moderate **3** Severe **9** Unknown

## F.3 Maxillary Tumour Volume: Patient Data Summary

| | | n |
|---|---|---|
| **Gender:** | Male | 20 |
| | Female | 19 |
| **Sub-site:** | Hard palate | 2 |
| | Upper alveolus/Maxilla | 37 |
| **Laterality:** | Right | 21 |
| | Left | 16 |
| | Midline | 1 |
| | Bilateral | 1 |
| **Brown Classification:** | 1a | 6 |
| | 1b | 1 |
| | 2a | 21 |
| | 2b | 5 |
| | 3a | 2 |
| | 3b | 1 |
| | 4a | 1 |
| | 4b | 1 |
| | 4c | 1 |
| **ACE-27 score:** | 0 | 10 |
| | 1 | 18 |
| | 2 | 11 |
| | 3 | 0 |
| **ASA Grade:** | I | 13 |
| | II | 15 |
| | III | 11 |
| | IV | 0 |
| **Smoking History:** | Current | 3 |
| | Non-smoker (including ex-smoker) | 36 |
| **Alcohol Abuse:** | Yes | 6 |
| | No | 21 |
| | Unknown | 12 |
| **Clinical Staging:** | cT1 | 4 |
| | cT2 | 10 |
| | cT3 | 2 |
| | cT4 | 12 |
| | Unknown | 11 |
| | cN0 | 24 |
| | cN1 | 4 |
| | cN2 | 11 |
| | Unknown | 0 |
| **Neck Dissection** | Unilateral: | 2 |
| | For access | 10 |
| | I-III | 4 |
| | I-IV | 5 |
| | I-V | 3 |
| | Bilateral: | 15 |
| | None | |
| **Reconstruction - Free Flap** | Radial Forearm | 20 |
| | Fibula | 18 |
| | Anterolateral thigh | 4 |
| | Scapular | 1 |
| | Fibula + Radial Forearm | 7 |
| | Fibula + Anterolateral thigh | 2 |
| | Other | 4 |
| - **Pedicled Flap** | Pectoralis Major | 4 |
| - **Pack /Grafts:** | Mucosal graft or proflavin pack | 2 |
| **Pathology - Differentiation** | Well | 9 |
| | Moderately | 28 |
| | Poorly | 2 |
| - **Invasive Front** | Cohesive | 13 |
| | Non-cohesive | 21 |
| | Unknown | 5 |
| - **Margin** | Clear | 12 |
| | Close | 14 |
| | Involved | 12 |
| | Unknown | 1 |

| | | | n |
|---|---|---|---|
| - **Neural Invasion** | Yes | | 8 |
| | No | | 30 |
| | Unknown | | 1 |
| - **Vascular Invasion** | Yes | | 3 |
| | No | | 35 |
| | Unknown | | 1 |
| - **Bone Invasion** | Yes | | 26 |
| | No | | 13 |
| - **Positive nodal disease** | Yes | | 9 |
| | | - With ECS | 4 |
| | | - Without ECS | 4 |
| | | - Unknown | 1 |
| | No | | 15 |
| **Pathological Staging** | pT1 | | 7 |
| | pT2 | | 2 |
| | pT3 | | 5 |
| | pT4a | | 24 |
| | pT4b | | 1 |
| | pN0 | | 30 |
| | pN1 | | 7 |
| | pN2a | | 1 |
| | pN2b | | 1 |
| **p Stage** | I | | 6 |
| | II | | 1 |
| | III | | 6 |
| | IVA | | 25 |
| | IVB | | 1 |
| **Adjuvant Therapy** | | | |
| - **Adjuvant chemotherapy** | Yes | | 1 |
| | For recurrence | | 1 |
| | No | | 30 |
| | Unknown | | 5 |
| - **Radiotherapy** | Yes | | 13 |
| | For recurrence | | 6 |
| | No | | 18 |
| | Unknown | | 2 |
| **Survival** | 1 year | | |
| | | - Yes | 32 |
| | | - No | 5 |
| | | - Not applicable | 2 |
| | 2 year | | |
| | | - Yes | 21 |
| | | - No | 11 |
| | | - Not applicable | 7 |
| | 5 year | | |
| | | - Yes | 8 |
| | | - No | 18 |
| | | - Not applicable | 13 |
| **Disease free survival** | 1 year | | |
| | | - Yes | 24 |
| | | - No | 13 |
| | | - Not applicable | 2 |
| | 2 year | | |
| | | - Yes | 19 |
| | | - No | 13 |
| | | - Not applicable | 7 |
| | 5 year | | |
| | | - Yes | 8 |
| | | - No | 15 |
| | | - Not applicable | 16 |

| | Mean | SD | 95% CI | Median | IQR |
|---|---|---|---|---|---|
| **Age** | 70.3 | 11.1 | 66.7-73.9 | 73 | 63 - 80 |
| **Pathological maximum depth of invasion** | 16.0 | 12.0 | 11.7 – 20.2 | 20.2 | 5 - 23 |
| **Tumour Volume** | 12.786 | 24.314 | 4.904-20.668 | 4.198 | 1.558 - 12.326 |
| **Time to death (n=18)** | 23.9 | 18.2 | 14.8-32.9 | 17.0 | 9.3-39.8 |
| **Length of follow-up (all)** | 36.1 | 30.8 | 26.1-46.0 | 27.0 | 15.0-55.0 |
| **Length of follow-up (alive patients n=21)** | 46.6 | 35.6 | 30.4-62.8 | 30.8 | 18.9-66.2 |

## F.4 Maxillary Tumour Volume MRI Parameters

| Pt | Plane | Sequence | Magnet | FOV (cm) | Matrix | NEX | ST | Spacing | ET | TR | TE | Flip angle |
|---|---|---|---|---|---|---|---|---|---|---|---|---|
| **1** | Coronal | T2 | 1.5 | 20 x 20 | 512 x 512 | 1 | 6 | 6.5 | 12 | 4640 | 73.3 | 90 |
| **2** | Coronal | T2 | 1.5 | 24 x 24 | 512 x 512 | 1 | 4 | 5 | 12 | 6160 | 69.2 | 90 |
| **3** | Coronal | STIR | 1.5 | 26 x 26 | 512 x 512 | 2 | 3 | 4 | 6 | 4900 | 15 | 90 |
| **4** | Axial | T2 | 1.5 | 26 x 26 | 512 x 512 | 4 | 5 | 5 | 14 | 5060 | 73.3 | 90 |
| **5** | Coronal | T2 | 1.5 | 20 x 20 | 512 x 512 | 1.5 | 6 | 7 | 10 | 4000 | 72.7 | 90 |
| **6** | - | | - | - | - | - | - | - | - | - | - | - |
| **7** | Coronal | T2 | 1.4 | 26 x 26 | 512 x 512 | 1 | 4 | 5 | 12 | 4380 | 69.1 | 90 |
| **8** | Coronal | T1 + contrast | 1.5 | 26 x 26 | 512 x 512 | 2 | 3.5 | 4.5 | 0 | 1008 | 12 | 90 |
| **9** | Coronal | T1 + contrast | 1.5 | 22 x 22 | 256 x 256 | 0.5 | 4 | 5 | 0 | 400 | 14 | 90 |
| **10** | Axial | T2 | 1.5 | 26 x 26 | 512 x 512 | 4 | 5 | 5 | 14 | 3500 | 74.9 | 90 |
| **11** | Axial | T2 | 1.5 | 30 x 30 | 512 x 512 | 4 | 5 | 5 | 14 | 5920 | 70.9 | 90 |
| **12** | Axial | T2 | 1.5 | 26 x 26 | 512 x 512 | 4 | 5 | 5 | 14 | 5040 | 74.9 | 90 |
| **13** | Axial | T2 | 1.5 | 26 x 26 | 512 x 512 | 4 | 5 | 5 | 14 | 5680 | 73.3 | 90 |
| **14** | - | | - | - | - | - | - | - | - | - | - | - |
| **15** | Axial | T2 | 1.5 | 26 x 26 | 512 x 512 | 3 | 5 | 5 | 14 | 3700 | 71.4 | 90 |
| **16** | Axial | T2 | 1.5 | 24 x 24 | 512 x 512 | 4 | 5 | 5 | 14 | 5080 | 73.7 | 90 |
| **17** | Coronal | T2 | 1.5 | 24 x 24 | 512 x 512 | 1 | 4 | 5 | 12 | 4840 | 69.2 | 90 |
| **18** | Coronal | T2 | 1.5 | 26 x 26 | 512 x 512 | 1 | 4 | 5 | 12 | 6600 | 68.8 | 90 |
| **19** | Axial | T2 | 1.5 | 26 x 26 | 512 x 512 | 4 | 5 | 5 | 14 | 4860 | 72.8 | 90 |
| **20** | Coronal | T2 | 1.5 | 26 x 26 | 512 x 512 | 1 | 4 | 5 | 12 | 4040 | 69.1 | 90 |
| **21** | Coronal | T2 | 1.5 | 26 x 26 | 512 x 512 | 1 | 4 | 5 | 12 | 4040 | 69.1 | 90 |
| **22** | Coronal | T2 | 1.5 | 26 x 26 | 512 x 512 | 1 | 4 | 5 | 12 | 4680 | 69.1 | 90 |
| **23** | Coronal | T2 | 1.5 | 24 x 24 | 512 x 512 | 1 | 4 | 5 | 12 | 5860 | 69.2 | 90 |
| **24** | Axial | T2 | 1.5 | 24 x 24 | 512 x 512 | 3 | 6 | 7 | 10 | 3000 | 75.3 | 90 |
| **25** | Coronal | T2 | 1.5 | 24 x 24 | 512 x 512 | 1 | 4 | 5 | 12 | 5120 | 69.2 | 90 |
| **26** | Coronal | T2 | 1.5 | 22 x 22 | 512 x 512 | 1 | 4 | 5 | 12 | 4080 | 70 | 90 |
| **27** | Coronal | T2 | 1.5 | 24 x 24 | 512 x 512 | 1 | 4 | 5 | 12 | 5860 | 69.2 | 90 |
| **28** | Axial | T2 | 1.5 | 26 x 26 | 512 x 512 | 4 | 5 | 5 | 14 | 5060 | 73.3 | 90 |
| **29** | Axial | T2 | 1.5 | 30 x 30 | 512 x 512 | 4 | 5 | 5 | 14 | 5640 | 70.9 | 90 |
| **30** | Coronal | T2 | 1.5 | 26 x 26 | 512 x 512 | 1 | 4 | 5 | 12 | 5820 | 68.8 | 90 |
| **31** | Coronal | T2 | 1.5 | 26 x 26 | 512 x 512 | 1 | 4 | 5 | 12 | 4040 | 69.1 | 90 |
| **32** | Axial | T2 | 1.5 | 24 x 24 | 512 x 512 | 4 | 5 | 5 | 14 | 4440 | 73.7 | 90 |
| **33** | - | - | - | - | - | - | - | - | - | - | - | - |
| **34** | Axial | T2 | 1.5 | 26 x 26 | 512 x 512 | 2 | 6 | 8 | 14 | 5700 | 71.7 | 90 |
| **35** | Coronal | T2 | 1.5 | 22 x 22 | 512 x 512 | 1 | 4 | 5 | 12 | 3680 | 73.7 | 90 |
| **36** | Coronal | T2 | 1.5 | 24 x 24 | 512 x 512 | 1 | 4 | 5 | 12 | 6100 | 69.2 | 90 |
| **37** | Coronal | T2 | 1.5 | 20 x 20 | 512 x 512 | 1 | 6 | 7 | 12 | 4400 | 73.3 | 90 |
| **38** | Axial | T1 + contrast | 1.5 | 23 x 23 | 480 x 480 | 3 | 4 | 5.5 | 3 | 467 | 18 | 90 |
| **39** | Axial | T2 | 3.0 | 24 x 24 | 512 x 512 | 3 | 4 | 4.5 | 17 | 5583 | 95.2 | 90 |

## F.5 Mandible Tumour Volume: Patient Data Summary

| | | n |
|---|---|---|
| **Gender** | Male | 32 |
| | Female | 30 |
| **Sub-site** | Retromolar | 22 |
| | Alveolus | 29 |
| | Floor of mouth | 11 |
| **Laterality** | Right | 23 |
| | Left | 35 |
| | Midline | 4 |
| **ACE-27 score** | 0 | 20 |
| | 1 | 26 |
| | 2 | 16 |
| | 3 | 0 |
| **ASA Grade** | I | 21 |
| | II | 30 |
| | III | 11 |
| | IV | 0 |
| **Dentate?** | Dentate | 8 |
| | Partially dentate | 36 |
| | Edentulous | 18 |
| **Smoking History** | Current | 16 |
| | Non-smoker (including ex-smoker) | 46 |
| **Alcohol Abuse** | Yes | 20 |
| | No | 42 |
| **Clinical Staging** | cT1 | 11 |
| | cT2 | 7 |
| | cT3 | 4 |
| | cT4 | 39 |
| | Unknown | 1 |
| | cN0 | 42 |
| | cN1 | 13 |
| | cN2 | 6 |
| | Unknown | 1 |
| **Surgical Resection** | Rim | 24 |
| | Hemimandible | |
| **Neck Dissection** | Unilateral: | 38 |
| | I-III | 3 |
| | I-IV | 12 |
| | I-V | 32 |
| | Bilateral: | 11 |
| | None | 4 |
| **Reconstruction - Free Flap:** | Radial Forearm | 20 |
| | Fibula | 18 |
| | Anterolateral thigh | 4 |
| | Scapular | 1 |
| | Fibula + Radial Forearm | 7 |
| | Fibula + Anterolateral thigh | 2 |
| | Fibula + Latissimus dorsi | 1 |
| | Rib + serratus + latissimus dorsi | 1 |
| | Rib + radial forearm | 1 |
| | Radial forearm + iliac bone graft | 1 |
| - **Pedicled Flap:** | Pectoralis Major | 4 |
| - **Pack or Grafts:** | Mucosal graft or proflavin pack | 2 |
| **Pathology - Teeth** | Contains teeth | 26 |
| | No teeth in specimen | 36 |
| - **Differentiation** | Well | 19 |
| | Moderately | 40 |
| | Poorly | 2 |
| | Unknown | 1 |
| - **Invasive front** | Cohesive | 37 |
| | Non-cohesive | 23 |
| | Unknown | 2 |
| - **Margin** | Clear | 26 |
| | Close | 21 |
| | Involved | 15 |
| - **Neural Invasion** | Yes | 19 |
| | No | 43 |
| - **Pedicled Flap:** | Pectoralis Major | 4 |
| - **Pack or Grafts:** | Mucosal graft or proflavin pack | 2 |
| **Pathology - Teeth** | Contains teeth | 26 |
| | No teeth in specimen | 36 |
| - **Differentiation** | Well | 19 |
| - **Vascular Invasion** | Yes | 18 |
| | No | 44 |
| | Unknown | 0 |

| | | | n |
|---|---|---|---|
| - | **Bone Invasion** | Yes | 50 |
| | | No | 12 |
| - | **Bone invasion** | None | 12 |
| | | Cortex | 35 |
| | | Cortex & Medullary | 15 |
| - | **Positive nodal disease** | Yes | |
| | | - With ECS | 20 |
| | | - Without ECS | 7 |
| | | - Unknown | 1 |
| | | No | 34 |
| **Staging** | | pT1 | 2 |
| | | pT2 | 11 |
| | | pT3 | 3 |
| | | pT4a | 46 |
| | | pT4b | 0 |
| | | pN0 | 35 |
| | | pN1 | 7 |
| | | pN2a | 4 |
| | | pN2b | 12 |
| | | pN2c | 4 |
| **pStage** | | I | 2 |
| | | II | 7 |
| | | III | 5 |
| | | IVA | 48 |
| | | IVB | 0 |
| **Radiotherapy at primary disease** | | Yes | 29 |
| | | No | 33 |
| **Survival** | | 1 year | |
| | | - Yes | 44 |
| | | - No | 13 |
| | | - Not applicable | 5 |
| | | 2 year | |
| | | - Yes | 38 |
| | | - No | 16 |
| | | - Not applicable | 8 |
| | | 5 year | |
| | | - Yes | 14 |
| | | - No | 21 |
| | | - Not applicable | 27 |
| **Disease free survival** | | 1 year | |
| | | - Yes | 42 |
| | | - No | 13 |
| | | - Not applicable | 7 |
| | | 2 year | |
| | | - Yes | 38 |
| | | - No | 13 |
| | | - Not applicable | 11 |
| | | 5 year | |
| | | - Yes | 11 |
| | | - No | 18 |
| | | - Not applicable | 33 |

| | Mean | SD | 95% CI | Median | IQR |
|---|---|---|---|---|---|
| **Age** | 66.8 | 13.7 | 63.4-70.3 | 68.5 | 56.0-77.5 |
| **Pathological maximum depth of invasion** | 13.2 | 8.6 | 11.0-15.4 | 10.5 | 7.0-15.0 |
| **Tumour Volume** | 5.725 | 7.303 | 3.870-7.580 | 3.594 | 1.530-6.502 |
| **Time to death (n=23)** | 20.7 | 22.9 | 10.7-30.6 | 11.0 | 5.0-32.0 |
| **Length of follow-up (all)** | 36.3 | 30.4 | 28.6-44.0 | 29.8 | 10.8-55.0 |
| **Length of follow-up (alive patients n=39)** | 45.5 | 30.7 | 35.6-55.5 | 40.9 | 25.2-61.6 |

## F.6 Mandible Tumour Volume MRI Parameters:

| Pt | Plane | Sequence | Magnet | FOV (cm) | Matrix | NEX | ST | Spacing | ET | TR | TE | Flip angle |
|---|---|---|---|---|---|---|---|---|---|---|---|---|
| **1** | - | - | - | - | - | - | - | - | - | - | - | - |
| **2** | Coronal | T2 | 1.5 | 200 | 512x512 | 1 | 6 | 7 | 12 | 4640 | 70.27 | 90 |
| **3** | Coronal | T2 | 1.5 | 240 | 512x512 | 1 | 4 | 5 | 12 | 5860 | 69.18 | 90 |
| **4** | Axial | T2 | 1.5 | 270 | 512x512 | 4 | 5 | 6 | 14 | 3900 | 73.25 | 90 |
| **5** | Coronal | T2 | 1.5 | 220 | 512x512 | 1 | 4 | 5 | 12 | 5120 | 69.69 | 90 |
| **6** | Coronal | STIR | 1.5 | 250 | 512x512 | 2 | 4 | 4.4 | 6 | 1600 | 23 | 90 |
| **7** | Axial | T2 | 1.5 | 260 | 512x512 | 4 | 5 | 5 | 14 | 5040 | 71.7 | 90 |
| **8** | Axial | STIR | 1.5 | 240 | 256x256 | 1 | 4 | 5 | 12 | 4420 | 21.85 | 90 |
| **9** | Coronal | T1+ contrast | 1.5 | 260 | 512x512 | 2 | 3 | 4 | 0 | 1260 | 12 | 90 |
| **10** | Axial | T2 | 1.5 | 260 | 512x512 | 4 | 5 | 5 | 14 | 4700 | 71.72 | 90 |
| **11** | Coronal | T2 | 1.5 | 260 | 512x512 | 1 | 4 | 5 | 12 | 4820 | 69.08 | 90 |
| **12** | Axial | T1 + contrast | 1.5 | 260 | 512x512 | 1 | 3.5 | 4.5 | 0 | 500 | 12 | 90 |
| **13** | Coronal | T2 | 1.5 | 220 | 512x512 | 1 | 4 | 5 | 12 | 6140 | 69.69 | 90 |
| **14** | Axial | T1 + contrast | 1.5 | 270 | 512x512 | 1 | 5 | 6 | 2 | 820 | 16.08 | 90 |
| **15** | Coronal | T2 | 1.5 | 200 | 512x512 | 1 | 6 | 7 | 12 | 4500 | 73.27 | 90 |
| **16** | Coronal | T2 | 1.5 |  | 256x256 | 1 | 5 | 6.5 |  | 4360 | 104.32 |  |
| **17** | Coronal | T2 | 1.5 | 280 | 512x512 | 1 | 4 | 5 | 12 | 5500 | 68.72 | 90 |
| **18** | Axial | T2 | 1.5 | 340 | 512x512 | 4 | 5 | 5 | 14 | 5420 | 70.52 | 90 |
| **19** | Coronal | STIR | 1.5 | 260 | 512x512 | 2 | 3 | 4 | 4 | 3027 | 15 | 90 |
| **20** | Coronal | T2 | 1.5 | 300 | 512x512 | 1 | 4 | 5 | 12 | 6800 | 68.06 | 90 |
| **21** | Coronal | T2 | 1.5 | 240 | 512x512 | 1 | 4 | 5 | 12 | 5900 | 69.18 | 90 |
| **22** | Coronal | T2 | 1.5 | 260 | 512x512 | 1 | 4 | 5 | 12 | 4040 | 69.08 | 90 |
| **23** | Coronal | STIR | 1.5 | 260 | 512x512 | 2 | 4 | 5 | 6 | 3400 | 15 | 90 |
| **24** | - | - | - | - | - | - | - | - | - | - | - | - |
| **25** | Axial | T2 | 1.5 |  | 256x256 | 1 | 6 | 7.5 |  | 3500 | 104.3 |  |
| **26** | Coronal | T2 | 1.5 | 280 | 512x512 | 1 | 4 | 5 | 12 | 5300 | 68.72 | 90 |
| **27** | Coronal | T2 | 1.5 | 200 | 512x512 | 1.5 | 3 | 4 | 12 | 5200 | 70.27 | 90 |
| **28** | Axial | T2 | 1.5 | 260 | 512x512 | 4 | 6 | 6 | 14 | 4940 | 71.72 | 90 |
| **29** | Axial | T2 | 1.5 | 240 | 512x512 | 4 | 5 | 5 | 14 | 5080 | 73.68 | 90 |
| **30** | Axial | T2 | 1.5 | 260 | 512x512 | 1.5 | 5 | 6 | 14 | 3800 | 71.76 | 90 |
| **31** | Axial | T2 | 1.5 | 260 | 512x512 | 4 | 5 | 6.5 | 14 | 4460 | 71.72 | 90 |
| **32** | Coronal | T2 | 1.5 | 280 | 512x512 | 1 | 5 | 6 | 12 | 4880 | 65.2 | 90 |
| **33** | Coronal | T2 | 1.5 | 260 | 512x512 | 1 | 4 | 5 | 12 | 4040 | 69.08 | 90 |
| **34** | Axial | T2 | 1.5 | 240 | 512x512 | 4 | 5 | 5 | 14 | 5080 | 73.68 | 90 |
| **35** | Coronal | T2 | 1.5 | 260 | 512x512 | 1 | 4 | 5 | 12 | 6000 | 68.76 | 90 |
| **36** | Coronal | T2 | 3.0 | 260 | 512x512 | 1.5 | 4 | 4.5 | 21 | 4744 | 91.2 | 90 |
| **37** | Axial | T2 | 1.5 | 260 | 512x512 | 4 | 3.5 | 7 | 14 | 5000 | 71.72 | 90 |
| **38** | Coronal | T2 | 1.5 | 260 | 512x512 | 1 | 4 | 5 | 12 | 4680 | 69.08 | 90 |
| **39** | Axial | T2 | 1.5 | 260 | 512x512 | 4 | 5 | 5 | 14 | 5720 | 71.4 | 90 |
| **40** | Axial | T2 | 1.5 | 260 | 512x512 | 4 | 3.5 | 8.5 | 14 | 5000 | 72.04 | 90 |
| **41** | Axial | T2 | 1.5 | 300 | 512x512 | 4 | 5 | 5 | 14 | 3940 | 70.92 | 90 |
| **42** | Axial | T2 | 1.5 | 260 | 512x512 | 4 | 6 | 8 | 14 | 4820 | 71.72 | 90 |
| **43** | Coronal | T2 | 1.5 | 220 | 512x512 | 1 | 4 | 5 | 12 | 5800 | 70 | 90 |
| **44** | Axial | T2 | 1.5 | 280 | 512x512 | 4 | 5 | 5 | 14 | 5720 | 71.12 | 90 |
| **45** | Coronal | STIR | 1.5 | 260 | 256x256 | 1 | 6 | 7 | 12 | 5960 | 28.42 | 90 |
| **46** | Coronal | T2 | 1.5 | 200 | 512x512 | 1 | 6 | 7 | 12 | 5300 | 75.9 | 90 |
| **47** | Coronal | T2 | 1.5 | 200 | 512x512 | 1 | 6 | 7 | 12 | 5300 | 75.90 | 90 |
| **48** | Coronal | T2 | 1.5 | 200 | 512x512 | 1 | 4 | 5 | 12 | 4140 | 70.64 | 90 |
| **49** | Axial | T2 | 1.5 | 260 | 512x512 | 4 | 5 | 5.5 | 14 | 6240 | 71.4 | 90 |
| **50** | Axial | STIR | 1.5 | 240 | 512x512 | 2 | 3.5 | 4.5 | 14 | 2454 | 20 |  |
| **51** | Axial | T2 | 1.5 | 260 | 512x512 | 4 | 5 | 5 | 14 | 5060 | 73.34 | 90 |
| **52** | Coronal | T2 | 1.5 | 260 | 512x512 | 1 | 4 | 5 | 12 | 4260 | 69.08 | 90 |
| **53** | Axial | Black Bone | 1.5 | 200 | 512x512 | 2 | 2.4 | 1.2 | 0 | 9.2 | 3.89 | 5 |
| **54** | Axial | STIR | 1.5 | 230 | 512x512 | 2 | 4 | 4.4 | 5 | 2000 | 15 | 90 |
| **55** | Coronal | T2 | 1.5 | 240 | 512x512 | 1 | 4 | 5 | 12 | 4580 | 69.18 | 90 |
| **56** | Axial | T2 | 1.5 | 270 | 512x512 | 4 | 5 | 5 | 14 | 5640 | 73.34 | 90 |
| **57** | Coronal | T2 | 1.5 | 220 | 512x512 | 1 | 4 | 5 | 12 | 6400 | 69.69 | 90 |
| **58** | Coronal | T2 | 1.5 | 240 | 512x512 | 1 | 4 | 5 | 12 | 3520 | 69.56 | 90 |
| **59** | Axial | T2 | 1.5 |  | 256x256 |  | 5 | 6 |  | 4000 | 104.32 |  |
| **60** | Coronal | T2 | 1.5 | 260 | 512x512 | 1 | 4 | 5 | 12 | 6160 | 69.08 | 90 |
| **61** | Coronal | T2 | 1.5 | 200 | 512x512 | 1 | 6 | 7 | 12 | 4800 | 70.27 | 90 |
| **62** | Axial | T2 | 1.5 |  | 256x256 | 2 | 4 | 4.4 | 10 | 6820 | 42 | 150 |

# Appendix G: “Black Bone” MRI & Pathology

## G.1 Reviewers' scoring sheet

| Pt | Pathology present? | | Side of pathology | | | Anatomical site of pathology | Process | | Bony erosion? | | Diagnosis | Comments |
|---|---|---|---|---|---|---|---|---|---|---|---|---|
| 1 | Yes | No | Right | Left | Bilateral | | Benign | Malignant | Yes | No | | |
| 2 | Yes | No | Right | Left | Bilateral | | Benign | Malignant | Yes | No | | |
| 3 | Yes | No | Right | Left | Bilateral | | Benign | Malignant | Yes | No | | |
| 4 | Yes | No | Right | Left | Bilateral | | Benign | Malignant | Yes | No | | |
| 5 | Yes | No | Right | Left | Bilateral | | Benign | Malignant | Yes | No | | |
| 6 | Yes | No | Right | Left | Bilateral | | Benign | Malignant | Yes | No | | |
| 7 | Yes | No | Right | Left | Bilateral | | Benign | Malignant | Yes | No | | |
| 8 | Yes | No | Right | Left | Bilateral | | Benign | Malignant | Yes | No | | |
| 9 | Yes | No | Right | Left | Bilateral | | Benign | Malignant | Yes | No | | |
| 10 | Yes | No | Right | Left | Bilateral | | Benign | Malignant | Yes | No | | |
| 11 | Yes | No | Right | Left | Bilateral | | Benign | Malignant | Yes | No | | |
| 12 | Yes | No | Right | Left | Bilateral | | Benign | Malignant | Yes | No | | |
| 13 | Yes | No | Right | Left | Bilateral | | Benign | Malignant | Yes | No | | |
| 14 | Yes | No | Right | Left | Bilateral | | Benign | Malignant | Yes | No | | |
| 15 | Yes | No | Right | Left | Bilateral | | Benign | Malignant | Yes | No | | |
| 16 | Yes | No | Right | Left | Bilateral | | Benign | Malignant | Yes | No | | |
| 17 | Yes | No | Right | Left | Bilateral | | Benign | Malignant | Yes | No | | |
| 18 | Yes | No | Right | Left | Bilateral | | Benign | Malignant | Yes | No | | |
| 19 | Yes | No | Right | Left | Bilateral | | Benign | Malignant | Yes | No | | |
| 20 | Yes | No | Right | Left | Bilateral | | Benign | Malignant | Yes | No | | |
| 21 | Yes | No | Right | Left | Bilateral | | Benign | Malignant | Yes | No | | |
| 22 | Yes | No | Right | Left | Bilateral | | Benign | Malignant | Yes | No | | |
| 23 | Yes | No | Right | Left | Bilateral | | Benign | Malignant | Yes | No | | |
| 24 | Yes | No | Right | Left | Bilateral | | Benign | Malignant | Yes | No | | |
| 25 | Yes | No | Right | Left | Bilateral | | Benign | Malignant | Yes | No | | |
| 26 | Yes | No | Right | Left | Bilateral | | Benign | Malignant | Yes | No | | |
| 27 | Yes | No | Right | Left | Bilateral | | Benign | Malignant | Yes | No | | |
| 28 | Yes | No | Right | Left | Bilateral | | Benign | Malignant | Yes | No | | |
| 29 | Yes | No | Right | Left | Bilateral | | Benign | Malignant | Yes | No | | |
| 30 | Yes | No | Right | Left | Bilateral | | Benign | Malignant | Yes | No | | |
| 31 | Yes | No | Right | Left | Bilateral | | Benign | Malignant | Yes | No | | |
| 32 | Yes | No | Right | Left | Bilateral | | Benign | Malignant | Yes | No | | |
| 43 | Yes | No | Right | Left | Bilateral | | Benign | Malignant | Yes | No | | |
| 44 | Yes | No | Right | Left | Bilateral | | Benign | Malignant | Yes | No | | |
| 45 | Yes | No | Right | Left | Bilateral | | Benign | Malignant | Yes | No | | |
| 46 | Yes | No | Right | Left | Bilateral | | Benign | Malignant | Yes | No | | |
| 47 | Yes | No | Right | Left | Bilateral | | Benign | Malignant | Yes | No | | |
| 48 | Yes | No | Right | Left | Bilateral | | Benign | Malignant | Yes | No | | |
| 49 | Yes | No | Right | Left | Bilateral | | Benign | Malignant | Yes | No | | |
| 50 | Yes | No | Right | Left | Bilateral | | Benign | Malignant | Yes | No | | |

## G.2 "Black Bone" Pathology Reviewers' Responses

| | Age | Sex | Side | Site | Process | Erosion | Indication | Pathology Present? | | | Side of pathology? | | | Anatomical site? | | | Process | | | Bony Erosion? | | |
|---|---|---|---|---|---|---|---|---|---|---|---|---|---|---|---|---|---|---|---|---|---|---|
| | | | | | | | | 1 | 2 | 3 | 1 | 2 | 3 | 1 | 2 | 3 | 1 | 2 | 3 | 1 | 2 | 3 |
| 1 | 61 | F | Left | Angle mandible | Malignant | | Osteosarcoma | Yes | Yes | Yes | Right | Left | Left | Maxilla /sinus | Ramus/body mandible | Post mandible | Benign | Benign | Malignant | No | No | Yes |
| 2 | 83 | F | Right | Superior alveolus | Malignant | Yes | SCC | Yes | Yes | Yes | Right | Right | Right | Maxilla /sinus | Maxillary alveolus | Maxillary sinus | Malignant | Malignant | Benign | Yes | Yes | No |
| 3 | 22 | F | Normal | | | | | No | No | No | - | - | - | - | - | - | - | - | - | - | - | - |
| 4 | 83 | M | Left | Inferior alveolus/FOM | Malignant | | SCC | Yes | Yes | No | Left | Left | - | Mandible | Inferior alveolus | - | Malignant | Malignant | - | Yes | Yes | - |
| 5 | 59 | M | Right | Inferior alveolus/lip | Malignant | Yes | SCC | Yes | Yes | Yes | Right | Right | Right | Mandible | Inferior alveolus | Premolar mandible | Malignant | Malignant | Malignant | Yes | Yes | Yes |
| 6 | 61 | M | Normal | | | | | No | No | No | - | - | - | - | - | - | - | - | - | - | - | - |
| 7 | 62 | M | Left | Mandible | Benign | Yes | Keratocyst | Yes | Yes | Yes | Left | Left | Left | Mandible/condyle | Neck mandible | Ascending ramus | Benign | Benign | Benign | No | No | Yes |
| 8 | 65 | F | Right | Mandible neck/FOM | Malignant | | Malignant Ameloblastoma | Yes | Yes | Yes | Right | Right | Right | Mandible | Ramus/body mandible | Mandible | Malignant | Malignant | Malignant | Yes | Yes | Yes |
| 9 | 48 | M | Right | FOM | Malignant | No | SCC | Yes | No | No | Left | - | - | Mandible | - | - | Malignant | - | - | Yes | - | - |
| 10 | 78 | F | Right | Mandible/ retromolar | Malignant | Yes | SCC | Yes | Yes | Yes | Left | Right | Left | Maxillary sinus | Retromolar | Maxillary sinus | Benign | Benign | Benign | - | Yes | No |
| 11 | 49 | M | Left | Mandible | Malignant | Yes | SCC | No | Yes | Yes | - | Left | Right | - | Lower left 7 | Oesophagus | - | Malignant | - | - | Yes | No |
| 12 | 52 | M | Left | Neck/ submandibular /retromolar | Malignant | Yes | SCC | Yes | Yes | Yes | Right | Left | Right | Maxilla /sinus | Lower left 8 | Maxillary sinus | Benign | Malignant | Benign | No | Yes | No |
| 13 | 20 | M | Left | Orbit | Benign | No | Orbital dystopia | Yes | Yes | Yes | Left | Left | Left | Orbit | maxillary antrum, ethmoid | Frontal sinus | Benign | Malignant | Benign | No | Yes | No |
| 14 | 67 | M | Right | Mandible | Malignant | Yes | SCC | Yes | Yes | Yes | Right | Right | Right | Mandible | Mandibular body | Mandible | Malignant | Malignant | Malignant | Yes | Yes | Yes |
| 15 | 42 | M | Normal | | | | | No | No | Yes | - | - | bilat eral | - | - | Big pterygoids | - | - | Benign | - | - | no |
| 16 | 76 | F | Right | Mandible | Malignant | Yes | SCC | Yes | Yes | No | Bilat eral | Right | | Mandible | Retromolar | | Malignant | Malignant | | Yes | Yes | |
| 17 | 64 | M | Left | Maxilla/ superior alveolus | Malignant | Yes | SCC | No | No | Yes | - | - | Left | - | - | Maxillary sinus | - | - | Benign | - | - | - |
| 18 | 57 | M | Right | UR5-6 | Benign | No | Periodontal inflammation | Yes | Yes | Yes | Right | Right | Right | Mandible/Alveolu s | Lower right 3,2 | Cyst mandible | Benign | Benign | Benign | No | Yes | No |
| 19 | 29 | M | Right | Maxilla | Benign | No | Giant cell granuloma | Yes | Yes | Yes | Right | Right | Right | Maxilla | Maxilla | Tumour maxilla | Malignant | Benign | Malignant | Yes | No | Yes |
| 20 | 70 | M | Right | Mandible retromolar | Malignant | Yes | SCC | Yes | Yes | Yes | Bilat eral | Right | Right | Anterior Maxilla | Angle/body mandible | Sinus | Benign | Malignant | Benign | No | Yes | No |
| 21 | 74 | M | Right | Mandible/ramus | Malignant | Yes | SCC | No | No | No | - | - | - | - | - | - | - | - | - | - | - | - |
| 22 | 81 | M | Left | Inferior buccal sulcus | Malignant | No | SCC | Yes | No | No | Left | - | - | Mandible | - | - | Benign | - | - | Yes | - | - |
| 23 | 50 | M | Left | Retromolar | Malignant | Yes | SCC | No | No | No | - | - | - | - | - | - | - | - | - | - | - | - |
| 24 | 44 | M | Right | FOM | Malignant | No | SCC | No | Yes | - | - | Right | - | - | Lower right 8 | - | - | Benign | - | - | No | - |
| 25 | 73 | F | Left | Maxilla | Benign | No | Cyst | Yes | Yes | Yes | Left | Left | Left | Maxilla | Superior alveolus | Post max sinus | Malignant | Malignant | Benign | Yes | Yes | Yes |
| 26 | 41 | M | Right | Inferior alveolus/LR8 | Malignant | No | SCC | Yes | Yes | Yes | Right | Right | Right | Retromolar | Lower right 8 | Lymph node | Malignant | Malignant | Malignant | Yes | Yes | - |
| 27 | 84 | F | Left | LL3-7 | Malignant | No | SCC | No | No | No | - | - | - | - | - | - | - | - | - | - | - | - |
| 28 | 68 | M | Right | Face/skull base/alveolus | Malignant | Yes | ?base of skull mass | Yes | Yes | Yes | Left | Right | Right | Maxilla | Superior alveolus | Sinus | Benign | Malignant | Benign | No | Yes | No |
| 29 | 84 | M | Right | Retromolar | Malignant | Yes | SCC | Yes | Yes | Yes | Right | Right | Right | Mandible | Retromolar | Jug vein | Malignant | Malignant | Benign | Yes | Yes | No |
| 30 | 75 | M | Left | Maxilla | Malignant | | SCC | No | Yes | Yes | - | Bilat eral | Left | - | Body mandible | Mandible | - | Malignant | Benign | = | Yes | No |
| 31 | 67 | M | Right | Superior alveolus | Malignant | | SCC | Yes | No | No | Right | - | - | Maxilla/Alveolus | - | - | Malignant | - | - | Yes | - | - |
| 32 | 64 | M | Midli ne | FOM | Malignant | No | SCC | Yes | No | No | Right | - | - | Mandible | - | - | Benign | - | - | No | - | - |
| 33 | 23 | M | Right | Sinus | Benign | No | Trauma ?blowout fracture | Yes | Yes | Yes | Bilat eral | Right | bilat eral | Maxillary Sinus | Superior alveolus | Sinus | Benign | Malignant | Benign | No | Yes | No |
| 34 | 65 | M | Right | Retromolar path# | Malignant | | Osteoradionecr osis | Yes | Yes | Yes | Right | Right | Right | Retromolar | Body mandible | Mandible | Malignant | Benign | Malignant | Yes | Yes | Yes |
| 35 | 69 | M | Right | LR5-7 | Malignant | Yes | SCC | Yes | Yes | Yes | Right | Right | Right | Mandible | Inferior alveolus | Mandible | Malignant | Malignant | Malignant | Yes | Yes | Yes |
| 36 | 67 | M | Left | Tongue | Malignant | No | SCC | Yes | Yes | Yes | Bilat eral | Bilat eral | Right | Maxillary Sinus | Mandible | Sinus | Benign | Benign | - | No | No | - |
| 37 | 89 | F | Left | FOM | Malignant | No | Pallatal follicular lymphoma | Yes | Yes | Yes | Left | Left | Left | Maxilla/Sinus | Antrum & nasoethmoid | Sinus | Malignant | Malignant | Malignant | Yes | Yes | Yes |
| 38 | 63 | F | Left | Maxilla | Malignant | Yes | SCC | Yes | Yes | No | Bilat eral | Bilat eral | - | Anterior Palate | Lower 8's | - | Benign | Benign | - | No | No | - |
| 39 | 67 | M | Right | Mandible | Benign | Yes | Giant cell granuloma | Yes | Yes | Yes | Right | Right | Right | Mandible | Body mandible | Mandible | Benign | Benign | Malignant | Yes | Yes | Yes |
| 40 | 64 | M | Right | Mandible | Benign | Yes | Osteoradionecr osis & Fracture | Yes | Yes | Yes | Right | Right | Right | Retromolar | Retromolar | Post mandible | Malignant | Malignant | Malignant | Yes | Yes | Yes |
| 41 | 58 | F | Left | Palate | Benign | No | Pleomorphic adenoma | Yes | Yes | Yes | Left | Left | Left | Maxilla | Retromolar | Palate | Malignant | Malignant | Benign | Yes | Yes | No |
| 42 | 26 | M | Normal | | | | | No | Yes | No | - | Right | - | - | Mandibular head | - | - | Benign | - | - | No | - |
| 43 | 68 | M | Right | Maxilla | Malignant | Yes | SCC | Yes | Yes | Yes | Right | Right | Right | Maxilla | Antrum & cheek | Cheek | Malignant | Malignant | Malignant | Yes | Yes | Yes |
| 44 | 3 | F | Right | Skull | Benign | Yes | LCH | Yes | Yes | Yes | Right | Right | Right | Skull | Petrous bone | Skull | Benign | Malignant | Malignant | Yes | Yes | Yes |
| 45 | 1 | F | Left | Cheek | Benign | No | Vascular malformation | Yes | No | Yes | Left | | Left | Cheek | - | Cheek | Benign | - | Benign | No | - | No |
| 46 | 79 | F | | ?Normal | | | SCC | No | Yes | No | - | Bilat eral | - | - | Mandible | - | - | Benign | - | - | No | - |
| 47 | 48 | M | Left | LL5-8 | Benign | No | Inflammation | Yes | Yes | Yes | Left | Left | Left | Mandible | Inferior alveolus | Mandible | Benign | Benign | Benign | Yes | Yes | Yes |
| 48 | 83 | F | Right | Maxilla | Benign | No | Giant cell granuloma | Yes | Yes | Yes | Right | Right | Right | Maxilla | Antrum, lower right 2-4 | Sinus | Benign | Benign | Malignant | No | Yes | Yes |
| 49 | 54 | F | Left | LL3-8 | Malignant | No | SCC | No | No | No | - | - | - | - | - | - | - | - | - | - | - | - |
| 50 | 64 | M | Right | Palate/alveouls | Malignant | Yes | SCC | Yes | Yes | Yes | Left | Left | Bilat eral | Maxillary sinus | Superior alveolus | Sinus | Benign | Malignant | Benign | No | Yes | No |

# Appendix H: 3D “Black Bone”

## H.1 Direct Phantom Cube Direct Measurements

| | a | b | c | d | e | f | g | h | i | j | hole |
|---|---|---|---|---|---|---|---|---|---|---|---|
| **1** | 60.11 | 60.07 | 20.10 | 20.05 | 60.07 | 60.09 | 19.90 | 19.94 | 49.96 | 19.97 | 5.82 |
| **2** | 60.16 | 60.08 | 20.00 | 20.03 | 60.14 | 60.09 | 19.84 | 19.94 | 49.89 | 19.98 | 5.84 |
| **3** | 60.09 | 60.06 | 20.08 | 20.07 | 60.12 | 60.11 | 19.87 | 19.97 | 49.87 | 19.97 | 5.81 |
| **4** | 60.13 | 60.12 | 20.09 | 20.07 | 60.11 | 60.12 | 19.88 | 19.87 | 49.89 | 20.01 | 5.85 |
| **5** | 60.17 | 60.09 | 20.04 | 20.15 | 60.16 | 60.90 | 19.87 | 19.89 | 49.87 | 20.01 | 5.85 |
| **6** | 60.10 | 60.07 | 20.07 | 20.09 | 60.09 | 60.08 | 19.89 | 19.90 | 49.88 | 19.99 | 5.87 |
| **7** | 60.11 | 60.10 | 20.07 | 20.12 | 60.12 | 60.10 | 19.93 | 19.89 | 49.86 | 19.98 | 5.86 |
| **8** | 60.09 | 60.08 | 20.06 | 20.06 | 60.08 | 60.08 | 19.87 | 19.90 | 49.92 | 19.98 | 5.87 |
| **9** | 60.10 | 60.09 | 20.07 | 20.09 | 60.08 | 60.12 | 19.92 | 19.91 | 49.85 | 20.00 | 5.73 |
| **10** | 60.11 | 60.10 | 20.09 | 20.07 | 60.09 | 60.11 | 19.87 | 19.91 | 49.91 | 20.00 | 5.87 |

## H.2 Phantom Cube Measurements on Software

| | a | b | c | d | e | f | g | h | i | j | hole |
|---|---|---|---|---|---|---|---|---|---|---|---|
| **Fovia – "Black Bone" 1.5T 0.8mm** | | | | | | | | | | | |
| **1** | 60.2 | 60.0 | 19.9 | 20.0 | 59.7 | 60.0 | 19.8 | 19.8 | 49.5 | 20.0 | 5.7 |
| **2** | 60.2 | 59.7 | 20.1 | 20.0 | 59.8 | 60.1 | 20.0 | 19.8 | 50.0 | 20.2 | 5.4 |
| **3** | 60.1 | 59.7 | 19.8 | 20.1 | 59.7 | 59.9 | 19.7 | 19.7 | 49.7 | 19.8 | 6.0 |
| **4** | 60.2 | 60.0 | 20.0 | 19.8 | 59.9 | 60.1 | 20.0 | 19.9 | 50.1 | 20.0 | 5.5 |
| **5** | 59.9 | 60.4 | 20.1 | 19.9 | 60.1 | 59.8 | 19.9 | 19.9 | 49.8 | 19.7 | 5.4 |
| **6** | 60.2 | 60.1 | 19.9 | 20.1 | 59.8 | 59.8 | 19.8 | 19.9 | 49.7 | 19.8 | 5.5 |
| **7** | 60.1 | 60.2 | 19.9 | 20.0 | 59.8 | 60.1 | 19.8 | 20.0 | 49.6 | 19.9 | 5.4 |
| **8** | 60.1 | 60.0 | 19.9 | 20.0 | 59.8 | 60.1 | 20.1 | 19.9 | 49.6 | 19.8 | 5.5 |
| **9** | 60.2 | 59.8 | 20.1 | 19.9 | 59.7 | 59.8 | 19.8 | 19.9 | 49.7 | 19.8 | 5.5 |
| **10** | 60.0 | 59.6 | 20.1 | 20.0 | 60.0 | 60.3 | 19.8 | 19.9 | 49.7 | 20.1 | 5.4 |
| **Fovia - "Black Bone" 1.5T 1.2mm** | | | | | | | | | | | |
| **1** | 60.1 | 59.6 | 19.5 | 20.1 | 59.6 | 59.8 | 19.5 | 20 | 48.8 | 20.1 | 5.6 |
| **2** | 59.9 | 59.7 | 19.7 | 19.9 | 59.6 | 59.9 | 19.7 | 19.9 | 49.2 | 20.0 | 5.6 |
| **3** | 59.9 | 59.7 | 19.8 | 20.0 | 59.8 | 59.7 | 19.8 | 19.7 | 48.7 | 19.9 | 5.6 |
| **4** | 60.0 | 59.9 | 19.9 | 20.1 | 59.6 | 59.7 | 19.7 | 19.7 | 49.0 | 20.0 | 5.8 |
| **5** | 59.8 | 59.8 | 19.9 | 20 | 59.7 | 59.8 | 19.8 | 19.8 | 49.1 | 20.1 | 5.6 |
| **6** | 60.0 | 59.8 | 19.9 | 20.1 | 59.8 | 59.8 | 19.7 | 19.9 | 49.1 | 20.0 | 5.8 |
| **7** | 60.0 | 59.9 | 20.0 | 20.1 | 59.5 | 60.1 | 19.7 | 20 | 49.2 | 19.9 | 5.7 |
| **8** | 60.0 | 59.9 | 19.9 | 20.0 | 59.6 | 59.9 | 19.7 | 19.6 | 49.1 | 20.1 | 5.6 |
| **9** | 60.0 | 59.7 | 20.1 | 20.1 | 59.5 | 59.9 | 19.7 | 19.9 | 49.4 | 20.1 | 5.7 |
| **10** | 60.0 | 59.6 | 20.0 | 20.0 | 59.8 | 60.0 | 19.9 | 19.9 | 49.0 | 20.0 | 5.8 |
| **Fovia – "Black Bone" 1.5T 2.0mm** | | | | | | | | | | | |
| **1** | 60.2 | 59.6 | 19.9 | 20.3 | 59.6 | 59.6 | 20.2 | 20.2 | 49.7 | 21.4 | 4.4 |
| **2** | 60.2 | 59.9 | 20.1 | 20.3 | 59.4 | 59.9 | 19.9 | 20 | 49.9 | 21 | 4.9 |
| **3** | 60.3 | 59.7 | 20 | 20.1 | 59.6 | 60.1 | 20.1 | 20 | 49.7 | 21 | 4.5 |
| **4** | 60.3 | 59.8 | 20.2 | 20.3 | 59.7 | 59.7 | 20.3 | 19.8 | 49.8 | 20.9 | 4.9 |
| **5** | 60.2 | 59.6 | 20.0 | 20.3 | 59.9 | 60.0 | 20.1 | 20.1 | 49.8 | 20.7 | 4.5 |
| **6** | 60.1 | 59.6 | 19.9 | 20.3 | 59.8 | 59.8 | 20.1 | 20.1 | 51.3 | 20.9 | 4.6 |
| **7** | 60.2 | 59.7 | 19.9 | 20.2 | 59.6 | 60.2 | 20.2 | 20.2 | 51.3 | 20.7 | 4.7 |
| **8** | 60.3 | 59.8 | 20.1 | 20.3 | 59.7 | 60.2 | 20.1 | 20.1 | 49.6 | 20.8 | 4.9 |
| **9** | 60.3 | 59.6 | 20.3 | 20.1 | 60.0 | 60.0 | 20.2 | 20.2 | 51.7 | 20.5 | 4.6 |
| **10** | 60.3 | 59.6 | 20.1 | 20.0 | 59.8 | 60.2 | 20.3 | 20.1 | 51.7 | 20.8 | 4.6 |
| **Fovia – "Black Bone" 1.5T 2.4mm** | | | | | | | | | | | |
| **1** | 60.3 | 60.2 | 20.0 | 20.1 | 59.7 | 60.0 | 20.0 | 20.0 | 49.2 | 21.1 | 4.4 |
| **2** | 60.3 | 59.0 | 20.2 | 20.2 | 59.9 | 60.2 | 20.0 | 20.0 | 49.6 | 21.1 | 4.4 |
| **3** | 60.3 | 59.8 | 20.1 | 20.2 | 59.8 | 59.9 | 19.9 | 19.8 | 49.6 | 21.1 | 4.5 |
| **4** | 60.3 | 60.2 | 20.2 | 20.2 | 59.9 | 59.9 | 19.7 | 20.0 | 49.5 | 21.2 | 4.4 |
| **5** | 60.2 | 60.4 | 20.2 | 20.3 | 59.9 | 60.2 | 20.1 | 20.0 | 49.5 | 21.2 | 4.5 |
| **6** | 60.3 | 60.4 | 20.3 | 20.0 | 59.7 | 59.8 | 20.1 | 19.9 | 49.5 | 21.1 | 4.5 |
| **7** | 60.2 | 60.1 | 20.1 | 20.1 | 59.8 | 59.8 | 19.7 | 19.9 | 49.7 | 21.0 | 4.4 |
| **8** | 60.2 | 60.4 | 20.2 | 20.0 | 59.9 | 60.0 | 19.9 | 19.9 | 49.6 | 21.3 | 4.4 |
| **9** | 60.2 | 60.1 | 20.2 | 19.9 | 60.0 | 60.0 | 19.8 | 20.0 | 49.7 | 21.2 | 4.4 |
| **10** | 60.1 | 60.4 | 20.1 | 20.1 | 59.9 | 60.0 | 20.0 | 19.8 | 49.6 | 21.2 | 4.5 |

| | a | b | c | d | e | f | g | h | i | j | hole |
|---|---|---|---|---|---|---|---|---|---|---|---|
| **Fovia – "Black Bone" 3T 0.8mm** | | | | | | | | | | | |
| **1** | 59.7 | 58.9 | 18.9 | 18.8 | 59.3 | 59.6 | 18.7 | 18.7 | 48.9 | 19.2 | 6.9 |
| **2** | 59 | 58.7 | 18.4 | 19 | 59.1 | 59.7 | 18.7 | 18.6 | 49.1 | 19.3 | 8.0 |
| **3** | 58.6 | 58.7 | 18.4 | 18.9 | 59.4 | 59.3 | 18.4 | 18.5 | 48.7 | 19.2 | 7.8 |
| **4** | 58.5 | 58.8 | 18.8 | 18.9 | 59.1 | 59.5 | 18.6 | 18.7 | 48.9 | 19.2 | 7.8 |
| **5** | 58.6 | 58.9 | 18.6 | 19.1 | 59.1 | 59.6 | 18.6 | 18.5 | 48.9 | 19.2 | 7.8 |
| **6** | 58.2 | 59.2 | 18.6 | 19.0 | 59.0 | 59.4 | 18.5 | 18.7 | 49.0 | 19.3 | 7.8 |
| **7** | 59.8 | 58.8 | 18.6 | 18.9 | 59.1 | 59.3 | 18.6 | 18.6 | 48.8 | 19.4 | 6.8 |
| **8** | 58.2 | 59.1 | 18.7 | 18.9 | 59.4 | 59.6 | 18.5 | 18.6 | 49.0 | 19.3 | 7.8 |
| **9** | 61.0 | 59.1 | 18.6 | 18.9 | 59.2 | 59.4 | 18.4 | 18.5 | 48.8 | 19.2 | 8.0 |
| **10** | 59.9 | 58.8 | 18.7 | 18.9 | 59.1 | 59.7 | 18.4 | 18.6 | 48.9 | 19.2 | 6.8 |
| **Fovia – "Black Bone" 3T 1.2mm** | | | | | | | | | | | |
| **1** | 58.1 | 59.2 | 18.5 | 19.1 | 58.7 | 58.1 | 18.3 | 19.3 | 48.4 | 18.0 | 7.0 |
| **2** | 58.9 | 58.4 | 18.6 | 18.7 | 58.7 | 58.1 | 18.5 | 18.5 | 48.2 | 18.0 | 7.1 |
| **3** | 58.0 | 58.5 | 18.8 | 18.7 | 58.7 | 58.3 | 18.4 | 18.1 | 48.5 | 18.2 | 7.0 |
| **4** | 58.2 | 58.6 | 18.7 | 18.8 | 58.6 | 58.1 | 18.5 | 18 | 48.2 | 18.6 | 6.9 |
| **5** | 58.0 | 58.6 | 18.6 | 18.8 | 58.6 | 58.2 | 19.1 | 18 | 48.4 | 18.4 | 6.8 |
| **6** | 60.3 | 58.5 | 18.5 | 19.0 | 58.6 | 58.1 | 18.3 | 18.3 | 48.9 | 18.3 | 7.8 |
| **7** | 58.2 | 59.2 | 18.8 | 19.0 | 58.6 | 58.2 | 18.7 | 18.3 | 48.8 | 18.3 | 7.7 |
| **8** | 58.1 | 58.5 | 18.6 | 18.9 | 58.8 | 58.4 | 18.4 | 18.2 | 48.3 | 18.3 | 6.8 |
| **9** | 59.1 | 58.5 | 18.6 | 18.8 | 58.8 | 58.2 | 18.6 | 18.1 | 49.2 | 18.5 | 6.9 |
| **10** | 57.8 | 59.3 | 18.6 | 18.7 | 58.7 | 58.2 | 18.3 | 18.4 | 49.2 | 18.4 | 6.9 |
| **Fovia – "Black Bone" 3T 2.0mm** | | | | | | | | | | | |
| **1** | 59.1 | 58.8 | 19.1 | 19.3 | 59.5 | 59.2 | 19.1 | 19.1 | 49.7 | 19.3 | 5.8 |
| **2** | 59 | 59 | 18.9 | 19.2 | 59.6 | 59.5 | 19 | 19.1 | 50.1 | 19.3 | 6.1 |
| **3** | 59.1 | 59.3 | 19.3 | 19.0 | 59 | 59.2 | 18.9 | 18.8 | 48.9 | 19.4 | 5.9 |
| **4** | 58.9 | 58.9 | 19.2 | 18.9 | 59.5 | 59.6 | 18.9 | 18.8 | 48.9 | 19.3 | 6.0 |
| **5** | 59.2 | 58.6 | 19.2 | 19.2 | 59.4 | 59.1 | 19.1 | 18.9 | 48.9 | 19.4 | 6.1 |
| **6** | 59.0 | 59.2 | 18.8 | 19.2 | 59.2 | 59.0 | 18.9 | 18.9 | 49.1 | 19.4 | 5.8 |
| **7** | 59.0 | 59.2 | 19.0 | 19.2 | 59.9 | 59.2 | 19.1 | 18.9 | 49.0 | 19.2 | 5.9 |
| **8** | 58.6 | 58.9 | 19.2 | 18.9 | 59.9 | 59.5 | 19 | 19.1 | 49.1 | 19.3 | 5.9 |
| **9** | 59.1 | 59.3 | 19 | 18.9 | 60.1 | 59.4 | 19.1 | 19.1 | 49.0 | 19.5 | 5.9 |
| **10** | 59 | 59 | 18.9 | 19.7 | 59.6 | 59.4 | 19.2 | 18.9 | 48.9 | 19.4 | 5.9 |
| **Fovia – "Black Bone" 3T 2.4mm** | | | | | | | | | | | |
| **1** | 59 | 58.2 | 18.8 | 19.3 | 59.1 | 59.1 | 19 | 18.7 | 48.3 | 18.3 | 6.3 |
| **2** | 59 | 58.2 | 19 | 19.2 | 59 | 58.8 | 18.7 | 18.9 | 48.4 | 18.2 | 7.1 |
| **3** | 59.3 | 58.3 | 18.8 | 19.1 | 58.8 | 58.9 | 18.7 | 18.9 | 48.4 | 18.2 | 6.3 |
| **4** | 59 | 58.6 | 18.9 | 19 | 58.9 | 60.6 | 18.7 | 19.1 | 48.3 | 18.3 | 7.7 |
| **5** | 59.4 | 58.1 | 18.8 | 19 | 58.6 | 59.4 | 18.9 | 18.6 | 48.4 | 18.4 | 6.2 |
| **6** | 59.2 | 58 | 18.9 | 19.1 | 58.6 | 60.5 | 19.1 | 18.8 | 48.3 | 18.5 | 6.7 |
| **7** | 59.4 | 58.3 | 19 | 19 | 58.8 | 59.6 | 19 | 18.7 | 48.1 | 18.6 | 6.6 |
| **8** | 59.2 | 58.3 | 19.3 | 19 | 58.8 | 59.6 | 18.9 | 19.1 | 48.1 | 18.4 | 6.6 |
| **9** | 59.3 | 58.1 | 19 | 18.9 | 58.8 | 59.7 | 19 | 18.5 | 48.1 | 18.2 | 6.5 |
| **10** | 59.2 | 58.6 | 19 | 19.2 | 58.9 | 59.7 | 18.9 | 18.7 | 48.4 | 18.5 | 6.5 |
| **Fovia - CT Face Protocol Soft Tissue Algorithm 0.625mm** | | | | | | | | | | | |
| **1** | 60.1 | 60.4 | 19.6 | 19.7 | 60 | 59.4 | 19.2 | 18.9 | 49.1 | 19 | 6.1 |
| **2** | 59.6 | 60.9 | 19.8 | 19.7 | 59.7 | 59.4 | 19.1 | 19.6 | 48.7 | 19.3 | 5.5 |
| **3** | 60.1 | 60.3 | 19.4 | 19.4 | 60.1 | 59.3 | 19.5 | 19.2 | 48.4 | 19.1 | 5.6 |
| **4** | 59.9 | 60.4 | 19.6 | 19.4 | 60.1 | 59.3 | 18.9 | 19.1 | 48.8 | 19.7 | 5.5 |
| **5** | 59.8 | 60.4 | 19.4 | 19.4 | 60.1 | 59 | 19.2 | 18.9 | 48.6 | 19.5 | 5.4 |
| **6** | 59.6 | 60.6 | 19.5 | 19.5 | 59.7 | 59.5 | 19.1 | 19.1 | 48.7 | 19.4 | 5.5 |
| **7** | 59.8 | 60.2 | 19.2 | 19.4 | 60.1 | 59.5 | 19.2 | 18.6 | 48.9 | 19.6 | 5.9 |
| **8** | 59.9 | 60.1 | 19.5 | 19.5 | 59.7 | 59.5 | 19.6 | 19.3 | 48.8 | 19.4 | 5.6 |
| **9** | 59.8 | 60.2 | 19.5 | 19.4 | 59.8 | 59.1 | 19.1 | 18.9 | 48.9 | 19.8 | 5.7 |
| **10** | 59.8 | 60.6 | 19.2 | 19.7 | 59.5 | 59.3 | 19.5 | 19.3 | 48.8 | 19.7 | 5.4 |
| **Fovia - CT Face Protocol Soft Tissue Algorithm 1.25mm** | | | | | | | | | | | |
| **1** | 59.9 | 60.5 | 19.2 | 19.4 | 59.9 | 59.9 | 19.4 | 19.3 | 49.1 | 19.4 | 5.2 |
| **2** | 59.7 | 60.7 | 19 | 19.4 | 60 | 60 | 19.3 | 19.3 | 48.8 | 20 | 5.7 |
| **3** | 60.2 | 60.7 | 19.3 | 20.1 | 59.9 | 59.5 | 20 | 19.7 | 50.1 | 20.3 | 5.8 |
| **4** | 60.3 | 60.2 | 19.3 | 19.6 | 59.6 | 59.7 | 19.4 | 20 | 49.1 | 19.4 | 5.7 |
| **5** | 59.6 | 60.6 | 19.3 | 19.3 | 59.3 | 59.7 | 19 | 19.6 | 48.8 | 19.5 | 5.8 |
| **6** | 59 | 60.8 | 20 | 19.4 | 59.2 | 59.7 | 19.3 | 19.8 | 48.8 | 20.2 | 6 |
| **7** | 59.4 | 60.6 | 19.4 | 20 | 59.7 | 59.4 | 18.9 | 19.6 | 49 | 19.5 | 5.6 |
| **8** | 59.9 | 60.4 | 19.7 | 19.6 | 60 | 59.4 | 19.6 | 19.9 | 48.6 | 19.8 | 5.8 |
| **9** | 59.6 | 60 | 19.3 | 19.7 | 59.9 | 60 | 19.4 | 19.4 | 49.6 | 19.8 | 5.7 |
| **10** | 59.6 | 60.2 | 19.1 | 20.1 | 60 | 60.2 | 19.3 | 19.5 | 49.7 | 19.8 | 5.9 |

| | a | b | c | d | e | f | g | h | i | j | hole |
|---|---|---|---|---|---|---|---|---|---|---|---|
| **Fovia - CT Face Protocol Soft Tissue Algorithm 2.5mm** | | | | | | | | | | | |
| **1** | 59.9 | 61.5 | 20.5 | 20.3 | 61 | 60.4 | 20.2 | 20.3 | 49.7 | 21.3 | 4.7 |
| **2** | 59.7 | 61.3 | 20.2 | 20.1 | 61.4 | 60.2 | 20.8 | 20.3 | 49.3 | 21.4 | 5.2 |
| **3** | 59.6 | 61.6 | 20.7 | 20.4 | 60.9 | 59.9 | 20.2 | 20 | 49.2 | 21.2 | 4.9 |
| **4** | 60.3 | 61.7 | 20.4 | 20.6 | 61.1 | 60.7 | 20.4 | 20.4 | 49.3 | 21.1 | 5.1 |
| **5** | 60.5 | 61.6 | 20.5 | 20.4 | 61.2 | 60.1 | 20.5 | 20.4 | 49.3 | 21.5 | 5.6 |
| **6** | 59.7 | 61.6 | 20.8 | 20.4 | 61.2 | 60.9 | 20.4 | 20.4 | 49.7 | 20.5 | 5.3 |
| **7** | 60.5 | 61.5 | 20.7 | 20.6 | 61.1 | 60.3 | 20.7 | 20.4 | 49.8 | 20.9 | 5.3 |
| **8** | 60 | 61.8 | 20.7 | 20.5 | 60.9 | 60.2 | 20.6 | 20.3 | 49.6 | 20.4 | 5.6 |
| **9** | 60.5 | 61.8 | 20.3 | 20.6 | 61.4 | 60.3 | 20.5 | 20.8 | 49.5 | 20.7 | 5.5 |
| **10** | 60.3 | 62.1 | 20.9 | 20.7 | 61.3 | 60.4 | 20.3 | 20.4 | 49.2 | 21.6 | 5.3 |
| **Fovia - CT Face Protocol Bone Algorithm 0.625m** | | | | | | | | | | | |
| **1** | 59.9 | 60.3 | 20 | 19.6 | 60.5 | 59.9 | 19.1 | 19.5 | 49.4 | 19.8 | 6.5 |
| **2** | 59.9 | 59.9 | 19.8 | 19.6 | 60.5 | 60.2 | 19.3 | 19.5 | 49.9 | 19.8 | 6.1 |
| **3** | 60.2 | 60.2 | 20.1 | 19.8 | 60.2 | 59.8 | 19.3 | 19.5 | 49.7 | 19.8 | 6 |
| **4** | 60.3 | 60.3 | 19.8 | 19.7 | 60.1 | 60 | 19.5 | 19.4 | 49.2 | 19.7 | 5.8 |
| **5** | 59.7 | 60.1 | 19.6 | 19.8 | 60 | 59.8 | 19.6 | 19.6 | 49.6 | 19.8 | 6.1 |
| **6** | 59.9 | 60.1 | 19.7 | 19.7 | 59.9 | 60 | 19.9 | 19.6 | 49.5 | 20 | 6.5 |
| **7** | 60.1 | 60.3 | 19.6 | 19.6 | 59.9 | 60.3 | 19.5 | 19.7 | 49.7 | 19.7 | 6.2 |
| **8** | 59.8 | 60.4 | 19.8 | 19.5 | 59.8 | 59.9 | 19.2 | 20.1 | 49.9 | 19.7 | 5.9 |
| **9** | 60.1 | 60.3 | 19.8 | 19.7 | 60.4 | 60.1 | 19.4 | 19.4 | 49.5 | 20 | 6 |
| **10** | 59.9 | 60.3 | 19.7 | 19.6 | 59.8 | 60 | 19.8 | 20.1 | 49.3 | 20.2 | 6.1 |
| **Fovia - CT Face Protocol Bone Algorithm 1.25mm** | | | | | | | | | | | |
| **1** | 59.7 | 60.4 | 19.6 | 19.5 | 60 | 59.3 | 19.8 | 19.7 | 49.7 | 21 | 5.7 |
| **2** | 59.6 | 60.6 | 19.7 | 19.5 | 59.9 | 59.9 | 19.7 | 19.6 | 50.1 | 20.6 | 5.8 |
| **3** | 59.7 | 60.4 | 19.6 | 19.8 | 60.2 | 59.7 | 19.7 | 19.5 | 49.5 | 21 | 6 |
| **4** | 59.7 | 60.5 | 19.9 | 19.5 | 59.9 | 59.9 | 19.6 | 19.6 | 50.1 | 20.3 | 5.9 |
| **5** | 59.5 | 60.7 | 19.9 | 19.7 | 60.3 | 59.6 | 19.9 | 19.7 | 49.3 | 21.2 | 6 |
| **6** | 59.7 | 60.4 | 19.8 | 19.6 | 59.8 | 59.7 | 20 | 19.5 | 49.4 | 20.3 | 5.7 |
| **7** | 59.7 | 60.3 | 20 | 19.6 | 60.2 | 59.7 | 9.6 | 20.1 | 49.7 | 20.2 | 5.9 |
| **8** | 59.7 | 60.4 | 19.8 | 19.7 | 60.2 | 59.3 | 19.4 | 19.9 | 49.7 | 21.2 | 6.3 |
| **9** | 59.6 | 60.3 | 19.7 | 19.6 | 60.1 | 59.9 | 19.6 | 19.4 | 49.7 | 20.9 | 6.1 |
| **10** | 59.6 | 60.3 | 19.8 | 19.8 | 60 | 59.4 | 19.5 | 19.8 | 49.5 | 20.5 | 5.7 |
| **Fovia - CT Face Protocol Bone Algorithm 2.5mm** | | | | | | | | | | | |
| **1** | 59.5 | 60.7 | 19.4 | 19.4 | 60.3 | 59.7 | 19.5 | 20.3 | 48.9 | 20.3 | 6.1 |
| **2** | 59.6 | 60.8 | 19.5 | 19.7 | 60.2 | 59.5 | 19.6 | 20.1 | 49.3 | 20.2 | 5.8 |
| **3** | 59.6 | 60.5 | 19.9 | 19.5 | 60.5 | 59.3 | 19.6 | 20 | 49.1 | 20.1 | 5.8 |
| **4** | 59.7 | 60.9 | 19.7 | 19.3 | 60.3 | 59.8 | 19.5 | 19.8 | 49.2 | 19.9 | 5.8 |
| **5** | 59.9 | 60.8 | 19.4 | 19.4 | 60 | 59.6 | 19.5 | 19.7 | 49.4 | 19.9 | 5.8 |
| **6** | 59.7 | 60.9 | 19.7 | 19.6 | 60.5 | 59.6 | 19.5 | 19.7 | 49.2 | 20.3 | 5.8 |
| **7** | 59.6 | 60.7 | 19.7 | 19.7 | 60.4 | 59.7 | 19.7 | 20.1 | 49.4 | 20.1 | 6 |
| **8** | 59.7 | 60.6 | 19.8 | 19.5 | 60.6 | 59.7 | 19.7 | 19.7 | 49.2 | 20.3 | 5.7 |
| **9** | 59.7 | 60.8 | 19.8 | 19.8 | 60.2 | 59.6 | 19.7 | 20 | 49.1 | 20 | 5.6 |
| **10** | 59.7 | 60.9 | 19.8 | 19.5 | 60 | 59.4 | 20 | 19.6 | 49.1 | 19.8 | 5.7 |
| **Fovia - CT Helical Head Soft Tissue Algorithm 0.625mm** | | | | | | | | | | | |
| **1** | 59.7 | 59.8 | 19.8 | 20.1 | 59.9 | 59.7 | 19.5 | 19.7 | 49.1 | 20.5 | 5.9 |
| **2** | 59.7 | 59.9 | 19.6 | 19.8 | 60 | 59.6 | 20.1 | 19.6 | 49.8 | 20.5 | 6.1 |
| **3** | 59.8 | 59.9 | 19.6 | 19.8 | 59.9 | 59.9 | 19.5 | 19.7 | 49.4 | 19.9 | 6 |
| **4** | 59.5 | 60 | 19.9 | 20 | 59.9 | 59.9 | 19.5 | 19.6 | 49.5 | 20.3 | 6 |
| **5** | 59.7 | 59.8 | 19.6 | 20.2 | 59.8 | 59.7 | 19.5 | 19.8 | 49.4 | 19.6 | 5.9 |
| **6** | 59.7 | 59.9 | 19.8 | 19.8 | 60 | 60 | 19.6 | 20.2 | 49.4 | 19.9 | 6 |
| **7** | 59.6 | 59.9 | 19.7 | 19.9 | 60 | 59.7 | 19.7 | 19.7 | 49.5 | 19.7 | 6 |
| **8** | 60 | 59.9 | 20.1 | 19.9 | 60.1 | 59.6 | 19.7 | 19.9 | 49.3 | 19.7 | 5.9 |
| **9** | 59.7 | 60.1 | 20 | 19.9 | 60 | 59.8 | 19.4 | 19.7 | 49.4 | 19.9 | 6 |
| **10** | 59.9 | 59.9 | 19.9 | 19.9 | 60.3 | 59.7 | 19.7 | 20.1 | 49.2 | 20 | 6 |
| **Fovia - CT Helical Head Soft Tissue Algorithm 1.25mm** | | | | | | | | | | | |
| **1** | 59.7 | 59.9 | 19.6 | 19.7 | 59.7 | 59.9 | 19.4 | 19.5 | 49.4 | 19.6 | 5.7 |
| **2** | 59.7 | 60 | 19.6 | 19.7 | 59.8 | 59.6 | 19.3 | 19.5 | 49.1 | 19.8 | 6.0 |
| **3** | 59.6 | 60.1 | 19.7 | 19.5 | 59.5 | 59.4 | 19.7 | 19.6 | 49.3 | 20.4 | 5.9 |
| **4** | 59.6 | 60.1 | 19.5 | 19.7 | 59.6 | 59.3 | 19.3 | 19.6 | 49.1 | 19.6 | 6.0 |
| **5** | 59.6 | 59.9 | 19.6 | 19.8 | 59.6 | 59.6 | 19.4 | 19.5 | 49.3 | 19.7 | 6.2 |
| **6** | 59.6 | 60.3 | 19.8 | 19.7 | 59.9 | 59.4 | 19.5 | 19.4 | 49.1 | 19.7 | 6.0 |
| **7** | 59.3 | 60.2 | 19.6 | 19.7 | 59.8 | 59.9 | 19.5 | 19.7 | 49.3 | 19.5 | 5.9 |
| **8** | 59.5 | 60.1 | 19.4 | 19.7 | 59.5 | 59.6 | 19.9 | 19.7 | 49.1 | 20.4 | 6.0 |
| **9** | 60.0 | 59.9 | 19.6 | 19.6 | 59.6 | 59.7 | 19.4 | 19.6 | 49.2 | 19.7 | 5.9 |
| **10** | 59.9 | 60.0 | 19.5 | 19.6 | 59.6 | 59.5 | 19.8 | 19.6 | 49.0 | 19.7 | 5.8 |

| | a | b | c | d | e | f | g | h | i | j | hole |
|---|---|---|---|---|---|---|---|---|---|---|---|
| **Fovia - CT Helical Head Soft Tissue Algorithm 2.5mm** | | | | | | | | | | | |
| **1** | 59.6 | 59.9 | 19.5 | 19.6 | 59.5 | 58.9 | 19.5 | 19.2 | 49.2 | 19.6 | 5.6 |
| **2** | 59.1 | 60.2 | 19.7 | 19.8 | 59.9 | 59.2 | 19.5 | 19.4 | 49.2 | 19.7 | 5.7 |
| **3** | 59.6 | 60.2 | 19.3 | 19.6 | 59.7 | 59 | 19 | 19.4 | 48.8 | 19.7 | 5.6 |
| **4** | 59.3 | 59.8 | 19.3 | 19.7 | 59.5 | 59.2 | 18.7 | 19.6 | 48.7 | 19.6 | 5.9 |
| **5** | 59.6 | 60.1 | 19.4 | 19.6 | 59.8 | 59.4 | 19.5 | 19.2 | 49 | 19.5 | 5.6 |
| **6** | 59.2 | 60 | 19.7 | 19.7 | 59.7 | 59.3 | 19.2 | 19.6 | 49.1 | 19.7 | 5.7 |
| **7** | 59.7 | 59.9 | 19.9 | 19.7 | 59.8 | 59.6 | 19.5 | 19.3 | 48.7 | 19.7 | 6.2 |
| **8** | 59.2 | 60.4 | 19.8 | 19.8 | 59.9 | 59.1 | 19.5 | 19.3 | 49 | 19.7 | 6.2 |
| **9** | 59.4 | 60 | 19.7 | 19.7 | 60 | 59.4 | 19.2 | 19 | 49 | 19.6 | 6 |
| **10** | 59.3 | 60.4 | 19.4 | 19.7 | 59.9 | 59.2 | 19.5 | 19.4 | 49.2 | 19.5 | 5.8 |
| **Fovia - CT Helical Head Bone Algorithm 0.625mm** | | | | | | | | | | | |
| **1** | 59.4 | 60.5 | 19.8 | 19.7 | 60.1 | 59.9 | 20 | 19.8 | 49.8 | 20 | 5.8 |
| **2** | 59.6 | 60.5 | 19.8 | 19.9 | 60.1 | 59.9 | 19.9 | 19.7 | 49.6 | 20.1 | 5.8 |
| **3** | 59.9 | 60.6 | 19.7 | 19.5 | 60.1 | 59.8 | 19.8 | 19.8 | 49.5 | 19.9 | 5.8 |
| **4** | 60.1 | 60.6 | 19.8 | 19.7 | 59.9 | 59.7 | 20 | 19.9 | 49.6 | 20 | 5.8 |
| **5** | 60.1 | 60.3 | 19.8 | 20.0 | 60.0 | 60.0 | 19.5 | 19.8 | 49.7 | 19.9 | 5.8 |
| **6** | 60.1 | 60.6 | 19.9 | 19.9 | 60.1 | 60.0 | 19.7 | 19.8 | 49.8 | 19.9 | 5.8 |
| **7** | 59.9 | 60.5 | 20 | 19.7 | 60.1 | 59.5 | 20.0 | 19.9 | 49.7 | 20.1 | 5.8 |
| **8** | 60.1 | 60.3 | 19.7 | 19.8 | 59.8 | 59.8 | 19.6 | 19.9 | 49.6 | 20.1 | 5.8 |
| **9** | 60.0 | 60.5 | 20.0 | 19.8 | 60.2 | 59.8 | 19.8 | 20.0 | 49.6 | 20.0 | 5.7 |
| **10** | 59.8 | 60.0 | 19.7 | 19.8 | 59.9 | 60.0 | 19.7 | 20.0 | 49.6 | 20.0 | 5.8 |
| **Fovia - CT Helical Head Bone Algorithm 1.25mm** | | | | | | | | | | | |
| **1** | 60.0 | 60.5 | 19.7 | 19.7 | 60.1 | 59.8 | 19.8 | 19.6 | 49.2 | 20.0 | 5.7 |
| **2** | 59.8 | 60.4 | 19.6 | 19.6 | 60.1 | 59.6 | 19.8 | 19.7 | 49.2 | 20.0 | 5.8 |
| **3** | 59.7 | 60.4 | 19.6 | 20.1 | 60.0 | 59.7 | 19.7 | 19.6 | 49.4 | 20.1 | 5.9 |
| **4** | 59.7 | 60.3 | 19.8 | 19.8 | 60.0 | 59.7 | 19.7 | 19.5 | 49.4 | 19.9 | 5.8 |
| **5** | 59.7 | 60.3 | 19.6 | 19.7 | 60.1 | 59.9 | 19.8 | 19.6 | 49.3 | 19.9 | 6.1 |
| **6** | 59.7 | 60.2 | 19.8 | 19.8 | 60.2 | 59.9 | 19.8 | 19.6 | 49.5 | 19.9 | 5.9 |
| **7** | 59.9 | 60.3 | 19.9 | 20.0 | 60.1 | 59.8 | 19.7 | 20.0 | 49.5 | 19.9 | 5.9 |
| **8** | 59.8 | 60.3 | 19.8 | 20 | 60.2 | 59.7 | 19.9 | 19.5 | 49.5 | 19.8 | 5.9 |
| **9** | 59.7 | 60.2 | 19.7 | 19.8 | 60.0 | 59.7 | 19.7 | 19.5 | 49.2 | 19.8 | 5.9 |
| **10** | 59.8 | 60.6 | 19.8 | 19.7 | 60.0 | 59.8 | 20.1 | 19.7 | 49.3 | 19.9 | 5.9 |
| **Fovia - CT Helical Head Bone Algorithm 2.5mm** | | | | | | | | | | | |
| **1** | 59.8 | 60.8 | 20.0 | 19.8 | 60.3 | 59.9 | 19.7 | 19.4 | 49.1 | 20.1 | 5.7 |
| **2** | 59.6 | 60.8 | 20.1 | 19.4 | 60.3 | 60.3 | 19.4 | 19.4 | 49.3 | 20.2 | 5.6 |
| **3** | 59.4 | 60.8 | 20.2 | 19.7 | 60.0 | 59.9 | 20.0 | 19.8 | 49.3 | 20.0 | 5.7 |
| **4** | 59.7 | 60.6 | 19.8 | 20.0 | 60.2 | 59.8 | 19.7 | 19.5 | 49.3 | 20.0 | 5.8 |
| **5** | 59.8 | 60.6 | 19.5 | 19.9 | 60.0 | 60.1 | 19.9 | 19.7 | 49.3 | 19.8 | 5.8 |
| **6** | 59.5 | 60.8 | 19.4 | 19.8 | 60.0 | 59.8 | 19.9 | 19.8 | 49.3 | 20.0 | 5.8 |
| **7** | 59.7 | 60.9 | 19.8 | 19.8 | 60.0 | 59.9 | 19.6 | 19.6 | 49.2 | 20.1 | 5.6 |
| **8** | 59.6 | 60.7 | 19.8 | 19.5 | 60.3 | 60 | 19.7 | 19.6 | 49.2 | 19.9 | 5.8 |
| **9** | 59.7 | 60.6 | 19.7 | 19.5 | 60.2 | 59.9 | 19.6 | 19.5 | 49.6 | 20.0 | 5.7 |
| **10** | 59.6 | 60.4 | 19.7 | 19.6 | 60.2 | 59.9 | 19.9 | 19.5 | 49.6 | 20.1 | 5.7 |
| **Mimics – "Black Bone" 1.5T 0.8mm** | | | | | | | | | | | |
| **1** | 60.00 | 59.19 | 19.85 | 19.95 | 59.75 | 59.74 | 19.73 | 19.78 | 50.19 | 19.65 | 5.71 |
| **2** | 59.83 | 59.20 | 19.96 | 19.98 | 59.59 | 59.66 | 19.72 | 19.85 | 50.81 | 19.77 | 5.75 |
| **3** | 60.01 | 59.29 | 19.86 | 20.48 | 59.70 | 59.76 | 19.79 | 19.85 | 49.48 | 19.71 | 5.75 |
| **4** | 60.01 | 59.42 | 19.96 | 20.05 | 59.76 | 59.76 | 19.65 | 19.93 | 49.56 | 19.71 | 5.86 |
| **5** | 59.82 | 59.30 | 19.78 | 19.98 | 59.78 | 59.66 | 19.78 | 19.91 | 49.56 | 19.77 | 5.75 |
| **6** | 59.92 | 59.50 | 19.86 | 20.05 | 59.59 | 59.57 | 19.67 | 19.78 | 49.59 | 19.84 | 5.81 |
| **7** | 59.83 | 59.54 | 19.94 | 19.99 | 59.67 | 59.66 | 19.72 | 19.91 | 49.40 | 19.71 | 5.73 |
| **8** | 60.03 | 59.72 | 19.85 | 20.11 | 59.77 | 59.65 | 19.78 | 19.92 | 49.56 | 19.84 | 5.79 |
| **9** | 59.83 | 59.54 | 19.86 | 19.97 | 59.67 | 59.65 | 19.72 | 19.85 | 49.49 | 19.71 | 5.73 |
| **10** | 59.92 | 59.54 | 19.86 | 20.05 | 59.85 | 60.22 | 19.78 | 19.99 | 49.64 | 19.77 | 5.75 |
| **Mimics – "Black Bone" 1.5T 1.2mm** | | | | | | | | | | | |
| **1** | 60.17 | 60.32 | 20.11 | 20.18 | 59.70 | 60.29 | 19.71 | 20.02 | 49.52 | 19.62 | 5.55 |
| **2** | 60.25 | 60.28 | 20.11 | 20.27 | 59.62 | 60.38 | 19.63 | 19.94 | 49.65 | 19.95 | 5.82 |
| **3** | 60.18 | 60.14 | 20.02 | 20.35 | 59.96 | 60.00 | 19.79 | 19.79 | 49.52 | 19.72 | 6.59 |
| **4** | 60.23 | 59.89 | 20.11 | 20.18 | 59.78 | 59.93 | 19.79 | 20.04 | 49.61 | 19.65 | 5.64 |
| **5** | 60.08 | 59.89 | 20.02 | 20.35 | 59.94 | 59.92 | 19.81 | 19.95 | 49.61 | 19.59 | 5.87 |
| **6** | 60.17 | 59.89 | 20.19 | 20.11 | 59.78 | 59.92 | 19.87 | 19.86 | 49.55 | 19.59 | 5.51 |
| **7** | 60.16 | 59.65 | 20.26 | 20.19 | 59.71 | 60.16 | 19.87 | 19.95 | 49.37 | 19.75 | 5.73 |
| **8** | 60.16 | 59.81 | 20.11 | 20.19 | 59.79 | 60.08 | 19.94 | 20.03 | 49.60 | 19.77 | 5.76 |
| **9** | 60.24 | 59.65 | 20.11 | 20.27 | 59.94 | 60.35 | 19.87 | 19.90 | 49.68 | 19.77 | 5.54 |
| **10** | 60.16 | 59.65 | 20.34 | 20.27 | 59.78 | 59.93 | 19.71 | 20.04 | 49.63 | 19.73 | 6.84 |

| | a | b | c | d | e | f | g | h | i | j | hole |
|---|---|---|---|---|---|---|---|---|---|---|---|
| **Mimics – "Black Bone" 1.5T 2.0mm** | | | | | | | | | | | |
| **1** | 60.37 | 60.29 | 20.26 | 20.35 | 60.11 | 59.82 | 19.87 | 19.87 | 49.45 | 19.80 | 4.99 |
| **2** | 60.22 | 59.95 | 20.02 | 20.11 | 60.01 | 60.22 | 19.86 | 20.07 | 49.71 | 19.89 | 5.08 |
| **3** | 60.22 | 60.70 | 20.26 | 20.26 | 60.19 | 60.15 | 19.86 | 20.01 | 49.88 | 19.74 | 4.86 |
| **4** | 60.22 | 60.01 | 20.18 | 20.34 | 60.02 | 60.15 | 19.94 | 20.07 | 49.66 | 20.09 | 4.87 |
| **5** | 60.14 | 60.31 | 20.10 | 20.34 | 60.02 | 60.05 | 10.94 | 19.88 | 49.62 | 20.03 | 4.86 |
| **6** | 60.21 | 60.02 | 20.10 | 20.34 | 60.10 | 60.05 | 19.78 | 19.94 | 49.79 | 20.25 | 4.90 |
| **7** | 60.30 | 60.06 | 20.26 | 20.26 | 60.01 | 59.98 | 19.86 | 20.01 | 49.62 | 20.04 | 4.86 |
| **8** | 60.15 | 60.03 | 20.26 | 20.25 | 59.93 | 59.99 | 19.86 | 20.03 | 49.71 | 20.02 | 4.85 |
| **9** | 60.09 | 59.95 | 20.18 | 20.33 | 60.20 | 60.05 | 19.94 | 19.95 | 49.52 | 20.21 | 4.82 |
| **10** | 60.37 | 60.11 | 20.02 | 20.26 | 60.12 | 60.14 | 19.70 | 20.01 | 49.61 | 20.11 | 4.85 |
| **Mimics – "Black Bone" 1.5T 2.4mm** | | | | | | | | | | | |
| **1** | 59.96 | 59.33 | 19.73 | 20.02 | 59.41 | 59.48 | 19.60 | 19.66 | 49.11 | 19.58 | 5.27 |
| **2** | 60.10 | 59.49 | 19.80 | 19.83 | 59.58 | 59.64 | 19.65 | 19.66 | 49.32 | 19.14 | 5.19 |
| **3** | 60.20 | 59.61 | 19.89 | 19.67 | 59.67 | 59.71 | 19.46 | 19.76 | 49.40 | 19.94 | 5.23 |
| **4** | 60.11 | 59.72 | 19.81 | 19.91 | 59.58 | 59.43 | 19.50 | 19.70 | 49.37 | 19.11 | 5.22 |
| **5** | 59.96 | 59.24 | 19.73 | 19.85 | 59.76 | 59.72 | 19.55 | 19.68 | 49.57 | 18.96 | 5.23 |
| **6** | 59.88 | 59.54 | 20.03 | 19.84 | 59.76 | 59.59 | 19.65 | 19.59 | 49.37 | 19.30 | 5.23 |
| **7** | 60.05 | 59.66 | 19.83 | 19.92 | 59.67 | 59.80 | 19.59 | 19.73 | 49.19 | 19.11 | 5.16 |
| **8** | 59.96 | 59.72 | 19.74 | 19.86 | 59.58 | 59.49 | 19.41 | 19.73 | 49.28 | 18.93 | 5.19 |
| **9** | 59.87 | 59.32 | 19.89 | 19.80 | 59.58 | 59.64 | 19.58 | 19.60 | 49.37 | 19.06 | 5.20 |
| **10** | 59.96 | 59.69 | 19.83 | 19.84 | 60.04 | 59.57 | 19.59 | 19.67 | 49.37 | 19.01 | 5.26 |
| **Mimics – "Black Bone" 3T 0.8mm** | | | | | | | | | | | |
| **1** | 59.65 | 59.29 | 19.47 | 19.34 | 59.84 | 59.75 | 19.04 | 19.37 | 49.79 | 19.80 | 6.52 |
| **2** | 59.04 | 59.29 | 19.25 | 19.26 | 59.68 | 59.26 | 19.05 | 19.04 | 49.62 | 19.81 | 6.44 |
| **3** | 59.10 | 59.29 | 19.12 | 19.43 | 60.22 | 59.44 | 19.31 | 19.03 | 49.62 | 19.88 | 6.62 |
| **4** | 59.76 | 59.22 | 19.88 | 19.42 | 59.77 | 59.84 | 19.19 | 19.11 | 49.79 | 19.74 | 6.34 |
| **5** | 59.09 | 59.29 | 19.03 | 19.20 | 59.76 | 59.55 | 19.64 | 19.19 | 49.62 | 19.88 | 6.57 |
| **6** | 59.01 | 59.14 | 19.20 | 19.45 | 59.76 | 59.25 | 19.99 | 19.36 | 49.79 | 19.90 | 6.43 |
| **7** | 59.10 | 59.29 | 19.22 | 19.79 | 59.59 | 59.55 | 19.27 | 19.12 | 49.98 | 19.78 | 6.38 |
| **8** | 59.16 | 59.38 | 19.04 | 19.34 | 59.85 | 59.48 | 19.37 | 19.27 | 49.62 | 19.92 | 6.37 |
| **9** | 59.09 | 59.22 | 19.19 | 19.42 | 59.98 | 59.32 | 19.71 | 19.26 | 49.70 | 19.85 | 6.56 |
| **10** | 59.02 | 59.23 | 19.04 | 19.34 | 59.85 | 59.32 | 19.26 | 19.19 | 49.62 | 19.89 | 6.44 |
| **Mimics – "Black Bone" 3T 1.2mm** | | | | | | | | | | | |
| **1** | 59.65 | 59.75 | 19.94 | 20.01 | 59.64 | 60.23 | 19.78 | 19.85 | 49.59 | 19.92 | 5.61 |
| **2** | 59.93 | 59.74 | 19.94 | 19.92 | 59.87 | 60.07 | 19.78 | 20.09 | 49.50 | 20.25 | 5.43 |
| **3** | 59.95 | 59.81 | 19.93 | 20.08 | 59.79 | 59.99 | 19.84 | 19.94 | 49.76 | 20.08 | 5.59 |
| **4** | 59.84 | 59.66 | 20.00 | 20.09 | 59.72 | 60.15 | 19.85 | 19.92 | 49.75 | 20.15 | 5.58 |
| **5** | 59.84 | 59.71 | 20.03 | 19.92 | 59.54 | 59.99 | 20.00 | 19.69 | 49.82 | 19.76 | 5.47 |
| **6** | 59.84 | 59.82 | 19.77 | 20.10 | 59.72 | 60.16 | 19.86 | 19.77 | 49.51 | 19.93 | 5.75 |
| **7** | 59.84 | 59.82 | 19.92 | 19.85 | 59.87 | 60.08 | 19.79 | 19.76 | 49.50 | 19.75 | 5.59 |
| **8** | 59.68 | 59.66 | 19.92 | 20.01 | 60.04 | 59.99 | 19.77 | 19.84 | 49.58 | 20.02 | 5.50 |
| **9** | 59.94 | 59.82 | 19.93 | 19.92 | 59.71 | 60.00 | 20.13 | 19.77 | 49.59 | 19.85 | 5.66 |
| **10** | 59.76 | 60.00 | 20.08 | 19.94 | 59.97 | 60.16 | 19.93 | 19.77 | 49.66 | 19.84 | 5.71 |
| **Mimics –"Black Bone" 3T 2.0mm** | | | | | | | | | | | |
| **1** | 59.87 | 60.30 | 19.78 | 19.95 | 59.78 | 60.19 | 19.76 | 19.69 | 49.70 | 19.95 | 6.52 |
| **2** | 59.62 | 59.78 | 19.78 | 19.77 | 59.87 | 60.29 | 19.60 | 19.80 | 49.59 | 20.11 | 5.42 |
| **3** | 59.63 | 60.18 | 19.96 | 19.85 | 59.89 | 60.37 | 19.85 | 19.72 | 49.68 | 20.09 | 5.30 |
| **4** | 59.64 | 60.17 | 19.76 | 19.84 | 59.70 | 60.20 | 19.86 | 19.70 | 49.66 | 20.09 | 5.24 |
| **5** | 59.94 | 60.14 | 19.86 | 20.09 | 59.96 | 60.45 | 19.68 | 19.83 | 49.54 | 20.09 | 6.56 |
| **6** | 59.97 | 60.28 | 19.86 | 19.86 | 59.99 | 60.03 | 19.85 | 19.62 | 49.56 | 20.08 | 5.17 |
| **7** | 60.19 | 59.91 | 19.94 | 20.09 | 59.79 | 60.37 | 19.81 | 19.68 | 49.47 | 20.09 | 5.22 |
| **8** | 59.71 | 59.94 | 19.68 | 19.77 | 59.87 | 60.29 | 19.77 | 19.63 | 49.82 | 19.95 | 5.31 |
| **9** | 59.79 | 59.76 | 19.77 | 20.02 | 59.87 | 60.28 | 19.87 | 19.78 | 49.62 | 20.09 | 5.18 |
| **10** | 60.23 | 59.97 | 19.94 | 19.93 | 59.88 | 60.12 | 19.77 | 19.77 | 49.61 | 20.02 | 5.28 |
| **Mimics – "Black Bone" 3T 2.4mm** | | | | | | | | | | | |
| **1** | 60.04 | 60.09 | 19.89 | 19.88 | 59.94 | 59.96 | 19.71 | 19.63 | 49.46 | 20.34 | 6.47 |
| **2** | 60.04 | 60.00 | 19.83 | 19.79 | 59.87 | 60.12 | 19.56 | 19.71 | 49.17 | 20.45 | 5.25 |
| **3** | 59.87 | 60.19 | 19.80 | 19.80 | 59.68 | 59.86 | 19.79 | 19.80 | 49.15 | 20.34 | 5.52 |
| **4** | 60.13 | 60.24 | 19.79 | 19.95 | 59.92 | 59.95 | 19.87 | 19.63 | 49.15 | 20.37 | 5.35 |
| **5** | 59.97 | 59.99 | 19.63 | 19.95 | 59.93 | 59.96 | 19.79 | 19.87 | 49.07 | 20.28 | 6.08 |
| **6** | 59.98 | 59.93 | 19.73 | 19.88 | 59.92 | 59.94 | 19.80 | 19.63 | 49.67 | 20.34 | 5.36 |
| **7** | 59.89 | 60.01 | 19.72 | 20.03 | 59.93 | 59.78 | 19.79 | 19.71 | 49.49 | 20.29 | 5.49 |
| **8** | 59.92 | 59.96 | 19.80 | 19.87 | 59.75 | 59.78 | 19.63 | 19.63 | 49.22 | 20.27 | 5.28 |
| **9** | 60.19 | 60.14 | 19.99 | 20.03 | 59.69 | 59.78 | 19.79 | 19.71 | 49.43 | 20.36 | 5.33 |
| **10** | 60.11 | 60.01 | 19.79 | 20.03 | 59.60 | 59.94 | 19.71 | 19.83 | 49.38 | 20.18 | 5.33 |

| | a | b | c | d | e | f | g | h | i | j | hole |
|---|---|---|---|---|---|---|---|---|---|---|---|
| **Mimics - CT Face Protocol Bone Algorithm 0.625mm** | | | | | | | | | | | |
| **1** | 60.18 | 60.19 | 20.19 | 21.00 | 60.38 | 60.42 | 19.87 | 20.16 | 50.20 | 20.70 | 5.52 |
| **2** | 60.49 | 59.94 | 20.06 | 21.12 | 60.06 | 60.58 | 19.86 | 19.77 | 50.32 | 19.53 | 5.57 |
| **3** | 60.27 | 59.94 | 20.43 | 20.90 | 60.62 | 60.48 | 19.85 | 19.85 | 50.59 | 19.74 | 5.63 |
| **4** | 60.18 | 61.49 | 20.60 | 20.17 | 60.15 | 60.48 | 19.96 | 19.86 | 51.35 | 19.81 | 5.59 |
| **5** | 60.27 | 61.06 | 20.50 | 20.37 | 60.14 | 60.38 | 19.96 | 20.07 | 49.90 | 19.77 | 5.75 |
| **6** | 60.33 | 59.84 | 20.63 | 20.98 | 60.22 | 60.38 | 20.31 | 19.98 | 50.54 | 19.78 | 6.68 |
| **7** | 60.33 | 60.26 | 20.41 | 21.47 | 60.14 | 60.38 | 19.85 | 19.85 | 50.58 | 19.76 | 5.58 |
| **8** | 60.27 | 60.31 | 20.27 | 21.02 | 60.22 | 60.17 | 20.20 | 19.96 | 51.45 | 20.18 | 5.57 |
| **9** | 60.20 | 59.90 | 20.17 | 20.90 | 59.98 | 60.08 | 20.21 | 19.98 | 50.41 | 19.99 | 5.59 |
| **10** | 60.29 | 59.73 | 20.27 | 21.01 | 60.40 | 60.19 | 20.13 | 20.06 | 49.98 | 20.19 | 5.96 |
| **Mimics - CT Face Protocol Bone Algorithm 1.25mm** | | | | | | | | | | | |
| **1** | 60.14 | 59.75 | 20.17 | 21.31 | 59.96 | 60.18 | 19.55 | 19.37 | 49.68 | 18.72 | 6.54 |
| **2** | 60.32 | 59.70 | 20.34 | 20.20 | 61.80 | 60.11 | 19.48 | 19.74 | 49.61 | 19.06 | 5.57 |
| **3** | 59.95 | 59.67 | 19.96 | 19.88 | 59.90 | 60.03 | 19.62 | 19.99 | 49.94 | 18.72 | 5.68 |
| **4** | 59.97 | 60.40 | 21.46 | 19.72 | 60.13 | 59.85 | 19.80 | 19.64 | 50.31 | 18.92 | 6.31 |
| **5** | 60.23 | 60.40 | 20.17 | 21.95 | 60.56 | 59.94 | 19.80 | 20.01 | 49.77 | 19.21 | 5.75 |
| **6** | 60.02 | 60.38 | 20.15 | 19.80 | 60.35 | 60.12 | 19.63 | 19.82 | 49.61 | 19.10 | 6.54 |
| **7** | 60.13 | 60.38 | 20.03 | 20.31 | 59.92 | 59.86 | 19.63 | 19.99 | 49.70 | 19.05 | 5.89 |
| **8** | 59.75 | 59.76 | 21.45 | 20.35 | 59.90 | 60.03 | 19.46 | 19.94 | 49.78 | 19.27 | 5.82 |
| **9** | 60.03 | 60.20 | 20.23 | 20.38 | 60.26 | 60.30 | 19.82 | 19.72 | 49.80 | 18.93 | 5.76 |
| **10** | 59.86 | 60.44 | 20.27 | 20.36 | 59.82 | 60.22 | 19.80 | 19.71 | 49.61 | 18.89 | 6.01 |
| **Mimics - CT Face Protocol Bone Algorithm 2.5mm** | | | | | | | | | | | |
| **1** | 59.86 | 59.80 | 19.65 | 19.83 | 60.18 | 59.69 | 19.62 | 19.69 | 49.55 | 18.99 | 5.73 |
| **2** | 59.87 | 59.95 | 19.82 | 19.82 | 59.94 | 60.01 | 19.59 | 19.53 | 49.79 | 19.30 | 5.70 |
| **3** | 59.77 | 60.05 | 19.94 | 19.72 | 59.88 | 59.85 | 19.58 | 19.47 | 51.22 | 19.15 | 5.92 |
| **4** | 59.78 | 61.28 | 20.30 | 19.91 | 59.82 | 59.68 | 19.66 | 19.56 | 49.58 | 19.07 | 5.55 |
| **5** | 59.93 | 59.91 | 19.82 | 19.93 | 60.14 | 59.76 | 19.97 | 19.60 | 49.76 | 19.05 | 5.64 |
| **6** | 59.79 | 60.45 | 20.34 | 19.84 | 59.67 | 59.68 | 19.51 | 19.75 | 49.79 | 19.23 | 5.73 |
| **7** | 59.78 | 60.30 | 19.85 | 19.84 | 59.98 | 59.68 | 19.76 | 19.68 | 49.84 | 19.15 | 5.68 |
| **8** | 59.94 | 60.00 | 20.25 | 19.77 | 60.08 | 59.68 | 19.66 | 19.62 | 49.73 | 19.41 | 5.86 |
| **9** | 59.77 | 60.07 | 19.92 | 20.00 | 59.83 | 59.79 | 19.85 | 19.56 | 49.65 | 19.16 | 5.56 |
| **10** | 59.76 | 60.16 | 20.34 | 19.67 | 59.83 | 59.76 | 19.65 | 19.40 | 50.57 | 19.14 | 5.70 |
| **Mimics - CT Face Protocol Soft Tissue Algorithm 0.625mm** | | | | | | | | | | | |
| **1** | 60.61 | 60.67 | 20.42 | 20.90 | 60.42 | 60.61 | 20.36 | 20.06 | 50.22 | 20.24 | 5.90 |
| **2** | 60.53 | 60.67 | 20.42 | 20.61 | 60.51 | 60.78 | 20.15 | 19.84 | 20.21 | 20.24 | 5.33 |
| **3** | 60.61 | 60.68 | 20.33 | 20.37 | 60.50 | 60.61 | 19.84 | 20.15 | 50.40 | 20.34 | 5.26 |
| **4** | 60.69 | 60.68 | 20.40 | 20.71 | 60.50 | 60.61 | 19.96 | 20.25 | 50.39 | 20.24 | 5.46 |
| **5** | 60.44 | 60.67 | 20.40 | 20.59 | 60.33 | 60.53 | 19.94 | 20.26 | 50.05 | 20.43 | 5.27 |
| **6** | 60.53 | 60.77 | 20.82 | 20.45 | 60.50 | 60.70 | 20.46 | 20.47 | 50.06 | 20.14 | 5.82 |
| **7** | 60.61 | 60.67 | 20.59 | 20.63 | 60.50 | 60.98 | 20.28 | 20.26 | 50.48 | 20.35 | 5.22 |
| **8** | 60.61 | 60.76 | 20.16 | 20.67 | 60.68 | 60.61 | 20.31 | 20.82 | 50.48 | 20.24 | 5.50 |
| **9** | 60.28 | 60.58 | 20.46 | 20.36 | 60.50 | 60.69 | 19.84 | 20.15 | 50.32 | 20.46 | 5.38 |
| **10** | 60.44 | 60.67 | 20.36 | 20.61 | 60.42 | 60.53 | 19.94 | 20.15 | 50.32 | 20.40 | 5.44 |
| **Mimics - CT Face Protocol Soft Tissue Algorithm 1.25mm** | | | | | | | | | | | |
| **1** | 60.51 | 60.73 | 20.40 | 20.65 | 60.46 | 60.66 | 20.04 | 20.19 | 50.22 | 20.27 | 4.83 |
| **2** | 60.42 | 60.80 | 20.74 | 20.53 | 60.46 | 60.75 | 20.21 | 20.53 | 50.29 | 20.49 | 5.48 |
| **3** | 60.67 | 60.72 | 20.53 | 20.53 | 60.47 | 60.85 | 20.03 | 19.95 | 50.13 | 20.27 | 5.48 |
| **4** | 60.66 | 60.72 | 20.53 | 20.46 | 60.21 | 60.67 | 20.28 | 20.11 | 50.05 | 20.18 | 4.89 |
| **5** | 6.50 | 60.74 | 20.57 | 20.45 | 60.38 | 60.50 | 20.04 | 20.36 | 49.88 | 20.36 | 4.88 |
| **6** | 60.60 | 60.90 | 20.37 | 20.46 | 60.30 | 60.75 | 20.17 | 20.11 | 50.17 | 20.19 | 4.93 |
| **7** | 60.59 | 60.81 | 20.45 | 20.62 | 60.62 | 60.74 | 20.12 | 20.20 | 50.16 | 20.46 | 5.51 |
| **8** | 60.50 | 60.88 | 20.37 | 20.36 | 60.46 | 60.58 | 20.22 | 20.12 | 50.14 | 20.44 | 5.56 |
| **9** | 60.51 | 60.64 | 20.28 | 20.45 | 60.54 | 60.41 | 20.20 | 20.20 | 50.13 | 20.27 | 4.83 |
| **10** | 60.67 | 60.67 | 20.45 | 20.36 | 60.63 | 60.58 | 19.87 | 20.11 | 50.13 | 20.27 | 4.93 |
| **Mimics - CT Face Protocol Soft Tissue Algorithm 2.5mm** | | | | | | | | | | | |
| **1** | 60.12 | 60.15 | 19.97 | 20.33 | 60.04 | 59.55 | 19.61 | 20.04 | 49.61 | 20.06 | 5.82 |
| **2** | 60.10 | 60.26 | 19.98 | 19.98 | 60.04 | 59.73 | 19.98 | 19.79 | 49.75 | 20.07 | 5.40 |
| **3** | 59.73 | 59.97 | 19.81 | 20.07 | 59.97 | 59.64 | 19.98 | 19.79 | 49.75 | 20.19 | 4.99 |
| **4** | 59.83 | 59.96 | 19.97 | 19.97 | 60.06 | 59.82 | 19.72 | 19.79 | 49.68 | 20.09 | 5.51 |
| **5** | 59.82 | 59.98 | 19.79 | 19.98 | 59.97 | 59.82 | 19.70 | 19.70 | 49.60 | 19.98 | 5.38 |
| **6** | 59.82 | 60.25 | 20.08 | 20.07 | 59.97 | 59.73 | 19.95 | 20.24 | 49.69 | 20.10 | 5.16 |
| **7** | 60.21 | 59.98 | 19.97 | 20.13 | 60.05 | 59.91 | 19.71 | 19.61 | 49.67 | 20.03 | 5.43 |
| **8** | 59.92 | 60.34 | 19.79 | 19.98 | 59.90 | 59.74 | 19.80 | 19.52 | 49.62 | 20.01 | 5.24 |
| **9** | 59.73 | 60.07 | 19.97 | 20.20 | 59.97 | 59.82 | 19.88 | 20.18 | 49.60 | 20.02 | 5.18 |
| **10** | 59.73 | 60.25 | 20.03 | 19.98 | 59.97 | 59.73 | 19.96 | 19.70 | 49.76 | 20.23 | 5.39 |

| | a | b | c | d | e | f | g | h | i | j | hole |
|---|---|---|---|---|---|---|---|---|---|---|---|
| **Mimics - CT Helical Head Bone Algorithm 0.625mm** | | | | | | | | | | | |
| **1** | 59.67 | 59.67 | 19.83 | 19.87 | 59.62 | 60.43 | 19.59 | 19.47 | 49.91 | 19.75 | 6.49 |
| **2** | 59.62 | 59.73 | 19.80 | 20.34 | 59.80 | 60.30 | 19.47 | 19.63 | 49.81 | 19.48 | 6.50 |
| **3** | 60.12 | 59.67 | 19.88 | 20.17 | 59.78 | 60.02 | 19.63 | 19.55 | 49.40 | 19.64 | 6.40 |
| **4** | 59.92 | 59.90 | 19.91 | 19.87 | 59.70 | 59.94 | 19.61 | 19.71 | 49.46 | 19.78 | 6.36 |
| **5** | 60.00 | 59.67 | 19.79 | 20.06 | 59.99 | 60.02 | 19.39 | 19.48 | 49.47 | 19.75 | 6.48 |
| **6** | 59.78 | 59.82 | 19.79 | 19.86 | 59.79 | 60.31 | 19.55 | 19.72 | 49.46 | 19.79 | 6.37 |
| **7** | 59.86 | 59.96 | 19.80 | 19.86 | 59.87 | 60.56 | 19.55 | 19.39 | 49.39 | 19.74 | 6.35 |
| **8** | 59.84 | 60.16 | 19.96 | 19.87 | 59.87 | 60.23 | 19.49 | 19.73 | 49.55 | 19.86 | 6.48 |
| **9** | 59.92 | 59.65 | 19.87 | 19.94 | 59.69 | 59.61 | 19.48 | 19.75 | 49.48 | 19.90 | 6.41 |
| **10** | 59.84 | 59.66 | 19.88 | 19.93 | 59.88 | 60.07 | 19.56 | 19.71 | 49.85 | 19.67 | 6.20 |
| **Mimics - CT Helical Head Bone Algorithm 1.25mm** | | | | | | | | | | | |
| **1** | 59.66 | 59.72 | 20.08 | 19.70 | 59.88 | 60.02 | 19.76 | 19.49 | 49.65 | 20.23 | 5.58 |
| **2** | 59.93 | 60.08 | 19.88 | 20.12 | 60.11 | 60.10 | 19.77 | 19.77 | 49.59 | 20.10 | 5.57 |
| **3** | 59.85 | 59.99 | 20.03 | 19.76 | 60.05 | 60.01 | 19.52 | 19.76 | 49.73 | 19.79 | 5.63 |
| **4** | 59.93 | 60.22 | 19.76 | 20.13 | 59.75 | 59.91 | 19.94 | 19.76 | 49.57 | 19.93 | 5.35 |
| **5** | 60.01 | 60.69 | 19.86 | 19.94 | 59.87 | 60.01 | 19.77 | 19.68 | 49.57 | 20.11 | 5.53 |
| **6** | 60.02 | 59.90 | 20.06 | 19.94 | 60.11 | 60.09 | 19.58 | 19.76 | 49.65 | 19.84 | 5.96 |
| **7** | 60.11 | 59.99 | 19.76 | 19.94 | 59.95 | 60.01 | 19.70 | 19.76 | 49.57 | 19.85 | 5.88 |
| **8** | 59.75 | 60.26 | 20.11 | 19.94 | 60.19 | 59.90 | 19.58 | 19.67 | 49.57 | 19.94 | 5.83 |
| **9** | 60.02 | 60.32 | 19.85 | 19.85 | 60.07 | 60.09 | 19.95 | 19.67 | 49.73 | 19.93 | 5.75 |
| **10** | 59.84 | 60.07 | 20.33 | 19.96 | 59.87 | 59.99 | 20.00 | 19.67 | 49.58 | 19.95 | 5.56 |
| **Mimics - CT Helical Head Bone Algorithm 2.5mm** | | | | | | | | | | | |
| **1** | 59.88 | 60.00 | 20.01 | 19.81 | 59.96 | 59.71 | 19.72 | 19.53 | 49.34 | 19.53 | 5.59 |
| **2** | 59.87 | 60.46 | 20.00 | 19.95 | 59.87 | 59.87 | 20.00 | 19.61 | 49.52 | 19.66 | 5.17 |
| **3** | 60.15 | 59.87 | 19.84 | 19.70 | 59.95 | 59.77 | 19.69 | 19.61 | 49.59 | 20.23 | 5.16 |
| **4** | 59.93 | 59.99 | 20.01 | 19.85 | 60.14 | 60.02 | 20.07 | 19.62 | 49.43 | 19.63 | 5.40 |
| **5** | 59.86 | 60.02 | 20.02 | 20.08 | 60.31 | 59.69 | 19.70 | 19.46 | 49.44 | 19.44 | 5.25 |
| **6** | 60.14 | 59.95 | 20.01 | 20.01 | 59.98 | 59.70 | 19.69 | 19.45 | 49.60 | 19.61 | 5.26 |
| **7** | 59.69 | 60.02 | 20.02 | 19.93 | 59.86 | 59.93 | 20.16 | 19.62 | 49.54 | 19.60 | 6.31 |
| **8** | 59.78 | 60.06 | 19.93 | 19.87 | 59.96 | 59.69 | 19.62 | 19.54 | 49.36 | 19.70 | 5.74 |
| **9** | 59.80 | 59.94 | 19.86 | 19.77 | 59.79 | 59.79 | 20.05 | 19.47 | 49.62 | 19.53 | 5.44 |
| **10** | 59.87 | 59.92 | 19.85 | 19.94 | 60.23 | 59.61 | 19.61 | 19.78 | 49.43 | 19.63 | 5.40 |
| **Mimics - CT Helical Head Soft Tissue Algorithm 0.625mm** | | | | | | | | | | | |
| **1** | 60.37 | 60.26 | 20.13 | 20.36 | 60.26 | 60.21 | 19.81 | 20.21 | 50.12 | 19.98 | 5.24 |
| **2** | 60.54 | 60.11 | 20.29 | 20.36 | 60.15 | 60.05 | 19.81 | 20.65 | 50.01 | 20.03 | 5.42 |
| **3** | 60.37 | 60.42 | 20.12 | 20.44 | 60.05 | 60.29 | 20.05 | 20.10 | 49.82 | 20.09 | 5.49 |
| **4** | 60.53 | 60.26 | 20.36 | 20.22 | 60.35 | 60.13 | 19.97 | 20.05 | 50.11 | 20.09 | 5.48 |
| **5** | 60.21 | 60.10 | 20.12 | 20.46 | 60.15 | 60.37 | 19.89 | 20.16 | 49.91 | 20.09 | 5.48 |
| **6** | 60.21 | 60.34 | 20.28 | 20.31 | 60.35 | 60.37 | 19.97 | 20.04 | 50.21 | 19.97 | 5.43 |
| **7** | 60.44 | 60.34 | 20.13 | 20.30 | 60.36 | 60.05 | 19.89 | 20.17 | 49.80 | 20.03 | 5.43 |
| **8** | 60.29 | 60.18 | 20.44 | 20.28 | 60.15 | 60.45 | 19.89 | 20.68 | 50.02 | 20.03 | 5.56 |
| **9** | 60.29 | 60.42 | 20.21 | 20.21 | 60.15 | 60.29 | 19.89 | 20.18 | 50.03 | 20.09 | 5.66 |
| **10** | 60.44 | 60.34 | 20.20 | 20.31 | 60.25 | 60.29 | 19.97 | 20.17 | 50.11 | 20.15 | 5.40 |
| **Mimics - CT Helical Head Soft Tissue Algorithm 1.25mm** | | | | | | | | | | | |
| **1** | 60.48 | 60.24 | 19.86 | 20.25 | 60.17 | 60.19 | 19.61 | 19.87 | 49.99 | 19.84 | 5.87 |
| **2** | 60.39 | 60.47 | 20.01 | 20.09 | 60.18 | 60.19 | 19.86 | 19.69 | 49.99 | 19.85 | 6.85 |
| **3** | 60.10 | 60.32 | 20.01 | 20.17 | 60.01 | 59.96 | 19.70 | 19.69 | 49.83 | 19.77 | 5.35 |
| **4** | 59.95 | 60.23 | 20.09 | 19.94 | 60.16 | 60.07 | 19.77 | 19.93 | 49.83 | 19.76 | 5.94 |
| **5** | 60.39 | 60.41 | 20.09 | 20.10 | 60.08 | 59.97 | 19.77 | 19.93 | 49.82 | 19.68 | 5.70 |
| **6** | 60.03 | 60.16 | 20.09 | 20.02 | 60.33 | 60.12 | 19.85 | 19.69 | 49.91 | 19.61 | 5.93 |
| **7** | 60.18 | 60.27 | 20.01 | 20.10 | 59.93 | 60.14 | 19.86 | 19.94 | 49.83 | 19.85 | 6.95 |
| **8** | 60.03 | 60.31 | 20.02 | 20.09 | 60.01 | 59.89 | 19.85 | 19.94 | 49.91 | 19.61 | 5.82 |
| **9** | 60.38 | 60.23 | 20.09 | 19.93 | 60.17 | 59.97 | 19.69 | 19.85 | 49.84 | 19.85 | 5.63 |
| **10** | 60.33 | 60.32 | 20.09 | 20.09 | 60.16 | 60.05 | 19.69 | 20.01 | 49.83 | 19.85 | 5.96 |
| **Mimics - CT Helical Head Soft Tissue Algorithm 2.5mm** | | | | | | | | | | | |
| **1** | 59.97 | 60.13 | 20.02 | 19.86 | 60.23 | 59.80 | 20.26 | 19.75 | 49.56 | 19.85 | 5.01 |
| **2** | 60.07 | 60.10 | 19.83 | 19.93 | 60.39 | 59.77 | 19.47 | 19.73 | 49.55 | 19.89 | 5.33 |
| **3** | 59.87 | 60.25 | 19.74 | 19.84 | 59.99 | 59.87 | 19.57 | 20.44 | 49.73 | 19.84 | 4.84 |
| **4** | 59.97 | 60.32 | 19.75 | 19.75 | 59.96 | 59.77 | 19.81 | 19.85 | 49.65 | 19.86 | 5.62 |
| **5** | 59.86 | 60.28 | 19.93 | 19.94 | 59.97 | 59.97 | 19.74 | 19.92 | 49.55 | 19.94 | 5.39 |
| **6** | 60.07 | 60.35 | 19.95 | 19.85 | 59.96 | 60.05 | 19.77 | 19.72 | 49.38 | 19.82 | 5.47 |
| **7** | 59.86 | 60.19 | 19.84 | 19.77 | 59.78 | 59.97 | 19.89 | 19.85 | 49.47 | 19.82 | 5.21 |
| **8** | 59.68 | 60.09 | 19.92 | 19.85 | 59.88 | 59.99 | 19.66 | 19.67 | 49.65 | 19.84 | 4.82 |
| **9** | 59.68 | 60.08 | 19.92 | 19.77 | 59.96 | 59.68 | 19.66 | 20.05 | 49.54 | 19.87 | 5.35 |
| **10** | 59.96 | 60.27 | 19.83 | 19.74 | 59.96 | 59.78 | 19.74 | 20.00 | 49.51 | 20.03 | 5.13 |

| | a | b | c | d | e | f | g | h | i | j | hole |
|---|---|---|---|---|---|---|---|---|---|---|---|
| **Osirix – "Black Bone" 1.5T 0.8mm** | | | | | | | | | | | |
| **1** | 60.40 | 60.10 | 20.70 | 20.20 | 60.00 | 60.00 | 20.20 | 20.20 | 49.50 | 20.10 | 4.20 |
| **2** | 60.10 | 60.10 | 20.30 | 20.30 | 60.20 | 60.10 | 20.30 | 20.20 | 49.50 | 20.00 | 4.30 |
| **3** | 60.40 | 59.90 | 20.40 | 20.20 | 60.30 | 60.10 | 20.10 | 20.00 | 49.40 | 19.80 | 4.20 |
| **4** | 60.10 | 60.30 | 20.50 | 20.30 | 60.30 | 59.90 | 20.10 | 20.20 | 49.80 | 20.00 | 4.10 |
| **5** | 60.00 | 60.10 | 20.20 | 20.10 | 60.00 | 60.00 | 20.10 | 20.00 | 49.40 | 20.00 | 4.30 |
| **6** | 60.40 | 60.00 | 20.50 | 20.00 | 60.20 | 59.90 | 20.30 | 20.10 | 49.50 | 20.10 | 4.20 |
| **7** | 60.30 | 60.10 | 20.20 | 20.50 | 60.30 | 60.00 | 20.20 | 20.00 | 49.60 | 20.10 | 4.40 |
| **8** | 60.00 | 60.30 | 20.50 | 20.30 | 60.20 | 60.00 | 20.00 | 20.00 | 49.40 | 20.20 | 4.30 |
| **9** | 60.10 | 60.10 | 20.20 | 20.10 | 60.40 | 59.90 | 20.20 | 20.00 | 49.60 | 20.00 | 4.40 |
| **10** | 60.30 | 60.10 | 20.40 | 20.00 | 60.30 | 59.90 | 20.00 | 20.10 | 49.60 | 20.00 | 4.30 |
| **Osirix – "Black Bone" 1.5T 1.2mm** | | | | | | | | | | | |
| **1** | 60.40 | 60.20 | 20.10 | 20.20 | 60.40 | 60.00 | 20.00 | 20.40 | 49.70 | 20.00 | 5.50 |
| **2** | 60.40 | 60.20 | 20.20 | 20.20 | 60.20 | 60.20 | 19.80 | 20.00 | 49.70 | 20.10 | 5.50 |
| **3** | 60.30 | 60.40 | 20.40 | 20.40 | 60.10 | 60.10 | 19.70 | 20.20 | 49.40 | 20.20 | 5.10 |
| **4** | 59.90 | 60.20 | 20.00 | 20.20 | 60.20 | 59.90 | 20.00 | 20.20 | 50.00 | 20.20 | 5.00 |
| **5** | 60.50 | 60.00 | 20.20 | 20.10 | 60.40 | 60.20 | 20.00 | 20.10 | 49.90 | 20.20 | 4.90 |
| **6** | 60.20 | 60.30 | 20.10 | 20.40 | 60.00 | 59.90 | 19.70 | 20.10 | 49.40 | 20.30 | 5.20 |
| **7** | 60.20 | 60.20 | 20.20 | 20.10 | 59.80 | 60.40 | 20.00 | 20.00 | 49.50 | 20.00 | 5.10 |
| **8** | 60.40 | 60.30 | 20.00 | 20.10 | 59.90 | 60.00 | 20.00 | 20.00 | 49.50 | 20.20 | 5.20 |
| **9** | 60.00 | 60.40 | 20.20 | 20.00 | 60.00 | 60.40 | 20.00 | 20.40 | 49.50 | 20.00 | 5.20 |
| **10** | 60.20 | 60.30 | 20.10 | 20.40 | 60.00 | 60.20 | 20.00 | 20.10 | 49.70 | 19.80 | 5.10 |
| **Osirix – "Black Bone" 1.5T 2.0mm** | | | | | | | | | | | |
| **1** | 60.50 | 60.70 | 20.30 | 20.50 | 59.80 | 60.70 | 20.10 | 2.10 | 49.40 | 20.40 | 4.60 |
| **2** | 60.40 | 60.70 | 20.00 | 20.60 | 60.20 | 60.50 | 20.10 | 20.10 | 49.80 | 20.40 | 4.90 |
| **3** | 60.50 | 60.50 | 20.50 | 20.70 | 60.40 | 60.70 | 20.10 | 20.30 | 49.70 | 20.70 | 4.50 |
| **4** | 60.70 | 60.50 | 20.50 | 20.50 | 60.50 | 60.10 | 20.20 | 20.30 | 50.10 | 20.40 | 4.60 |
| **5** | 60.30 | 60.70 | 20.40 | 20.10 | 60.30 | 60.50 | 20.00 | 20.40 | 49.80 | 20.50 | 4.70 |
| **6** | 60.40 | 60.80 | 20.40 | 20.40 | 60.00 | 60.30 | 20.00 | 20.40 | 49.70 | 20.50 | 4.90 |
| **7** | 60.40 | 60.80 | 20.50 | 20.50 | 60.50 | 60.50 | 2.04 | 20.40 | 50.10 | 20.60 | 4.70 |
| **8** | 60.40 | 60.80 | 20.40 | 20.40 | 60.20 | 60.40 | 20.50 | 20.30 | 49.70 | 20.50 | 4.80 |
| **9** | 60.50 | 60.50 | 20.70 | 20.50 | 60.40 | 60.70 | 20.40 | 20.30 | 49.40 | 20.70 | 4.80 |
| **10** | 60.50 | 60.70 | 20.10 | 20.50 | 60.20 | 60.40 | 20.10 | 20.30 | 49.70 | 20.40 | 4.90 |
| **Osirix – "Black Bone" 1.5T 2.4mm** | | | | | | | | | | | |
| **1** | 60.80 | 60.50 | 21.00 | 20.60 | 60.30 | 60.20 | 20.30 | 20.40 | 49.70 | 20.90 | 4.60 |
| **2** | 60.80 | 60.40 | 20.80 | 20.40 | 60.30 | 60.50 | 20.30 | 20.40 | 50.00 | 20.90 | 4.60 |
| **3** | 60.80 | 60.80 | 20.50 | 20.40 | 60.70 | 60.70 | 20.30 | 20.00 | 49.80 | 20.70 | 4.70 |
| **4** | 60.50 | 60.10 | 20.60 | 20.30 | 60.40 | 60.40 | 20.60 | 20.30 | 49.50 | 21.00 | 4.80 |
| **5** | 60.70 | 60.90 | 20.90 | 20.10 | 60.70 | 60.70 | 20.10 | 20.30 | 49.90 | 20.90 | 4.90 |
| **6** | 60.90 | 60.50 | 20.70 | 20.40 | 60.70 | 60.50 | 20.30 | 20.40 | 49.60 | 20.90 | 4.90 |
| **7** | 61.00 | 60.60 | 20.70 | 20.40 | 60.40 | 60.00 | 20.60 | 20.40 | 49.40 | 21.00 | 4.90 |
| **8** | 60.50 | 60.20 | 20.60 | 20.30 | 60.40 | 60.40 | 20.30 | 19.80 | 49.60 | 21.00 | 4.90 |
| **9** | 60.80 | 60.80 | 21.00 | 20.40 | 60.30 | 60.40 | 20.70 | 20.10 | 49.50 | 21.00 | 4.70 |
| **10** | 60.80 | 60.50 | 20.60 | 20.30 | 60.20 | 60.10 | 20.40 | 20.00 | 49.90 | 20.80 | 4.70 |
| **Osirix – "Black Bone" 3.0T 0.8mm** | | | | | | | | | | | |
| **1** | 59.60 | 59.70 | 19.60 | 19.80 | 59.90 | 60.20 | 19.80 | 19.90 | 49.80 | 20.20 | 5.60 |
| **2** | 60.00 | 59.80 | 19.80 | 20.10 | 60.10 | 60.10 | 19.80 | 19.80 | 49.60 | 20.10 | 5.70 |
| **3** | 60.00 | 59.60 | 20.00 | 19.70 | 60.10 | 60.10 | 19.80 | 19.80 | 49.80 | 20.20 | 5.80 |
| **4** | 60.00 | 59.70 | 19.50 | 20.20 | 59.90 | 60.20 | 19.60 | 19.70 | 49.80 | 20.10 | 5.70 |
| **5** | 60.10 | 59.80 | 19.80 | 19.80 | 60.10 | 60.20 | 19.70 | 19.70 | 49.90 | 19.90 | 5.70 |
| **6** | 60.00 | 59.80 | 20.10 | 19.80 | 59.70 | 60.10 | 19.80 | 19.60 | 49.40 | 20.10 | 5.70 |
| **7** | 59.70 | 59.80 | 19.70 | 19.80 | 60.10 | 60.00 | 19.80 | 20.00 | 49.60 | 20.10 | 5.70 |
| **8** | 59.90 | 59.80 | 19.60 | 20.10 | 60.10 | 60.20 | 19.90 | 20.00 | 49.60 | 20.10 | 5.60 |
| **9** | 60.00 | 59.60 | 20.10 | 19.90 | 60.00 | 60.10 | 20.00 | 19.60 | 49.70 | 20.10 | 5.60 |
| **10** | 59.70 | 59.70 | 19.90 | 20.20 | 60.00 | 59.70 | 19.80 | 19.60 | 49.70 | 20.10 | 5.60 |
| **Osirix – "Black Bone" 3.0T 1.2mm** | | | | | | | | | | | |
| **1** | 60.00 | 60.10 | 21.00 | 21.10 | 60.00 | 60.40 | 20.30 | 20.70 | 49.80 | 20.50 | 3.50 |
| **2** | 60.00 | 60.30 | 20.70 | 21.00 | 60.40 | 60.00 | 20.40 | 20.20 | 49.80 | 20.10 | 3.90 |
| **3** | 59.90 | 60.20 | 20.90 | 21.00 | 60.00 | 60.40 | 20.50 | 20.70 | 49.50 | 20.40 | 4.00 |
| **4** | 60.00 | 60.00 | 21.00 | 20.90 | 60.30 | 60.30 | 20.50 | 20.40 | 49.80 | 19.90 | 3.80 |
| **5** | 59.80 | 60.00 | 21.20 | 20.90 | 60.20 | 60.00 | 20.80 | 20.40 | 49.80 | 20.10 | 3.70 |
| **6** | 60.00 | 60.20 | 21.10 | 21.00 | 60.40 | 60.30 | 20.80 | 20.50 | 49.40 | 19.90 | 3.50 |
| **7** | 59.90 | 59.90 | 20.70 | 21.10 | 59.80 | 60.50 | 20.50 | 20.40 | 49.80 | 20.10 | 3.70 |
| **8** | 59.80 | 60.10 | 20.70 | 20.90 | 60.00 | 60.40 | 20.50 | 20.20 | 49.50 | 19.90 | 3.80 |
| **9** | 60.20 | 59.90 | 20.80 | 20.60 | 60.00 | 60.20 | 20.70 | 20.40 | 49.70 | 20.10 | 3.70 |
| **10** | 60.00 | 60.00 | 20.80 | 21.10 | 60.00 | 60.40 | 20.50 | 20.20 | 49.80 | 20.20 | 3.60 |

| | a | b | c | d | e | f | g | h | i | j | hole |
|---|---|---|---|---|---|---|---|---|---|---|---|
| **Osirix – "Black Bone" 3.0T 2.0mm** | | | | | | | | | | | |
| **1** | 60.00 | 60.10 | 19.70 | 20.20 | 60.00 | 60.10 | 19.70 | 20.00 | 49.50 | 19.80 | 5.10 |
| **2** | 59.90 | 6.50 | 20.10 | 20.10 | 60.20 | 60.20 | 19.80 | 20.00 | 49.90 | 19.80 | 5.20 |
| **3** | 60.10 | 60.40 | 19.60 | 20.00 | 60.20 | 60.10 | 19.80 | 20.10 | 49.90 | 20.20 | 5.10 |
| **4** | 59.80 | 60.30 | 20.00 | 20.00 | 60.10 | 60.00 | 20.00 | 20.00 | 50.00 | 20.00 | 5.10 |
| **5** | 59.80 | 60.50 | 20.10 | 20.10 | 60.00 | 60.40 | 19.80 | 20.00 | 49.40 | 19.70 | 5.10 |
| **6** | 60.20 | 60.40 | 20.10 | 20.10 | 60.10 | 60.30 | 20.10 | 20.00 | 49.70 | 20.10 | 5.10 |
| **7** | 59.90 | 59.90 | 19.70 | 20.20 | 60.00 | 60.40 | 20.10 | 20.00 | 49.80 | 20.10 | 5.10 |
| **8** | 60.20 | 60.20 | 20.00 | 20.20 | 59.80 | 60.30 | 20.10 | 20.10 | 49.60 | 20.20 | 5.20 |
| **9** | 59.90 | 60.40 | 20.00 | 20.10 | 60.00 | 60.10 | 20.10 | 20.00 | 49.60 | 20.20 | 5.20 |
| **10** | 60.10 | 60.10 | 20.10 | 19.80 | 60.00 | 60.00 | 20.00 | 20.00 | 49.70 | 20.10 | 5.10 |
| **Osirix – "Black Bone" 3.0T 2.4mm** | | | | | | | | | | | |
| **1** | 59.70 | 59.70 | 19.50 | 19.90 | 59.80 | 59.60 | 19.70 | 19.70 | 49.20 | 20.10 | 5.70 |
| **2** | 59.70 | 59.80 | 19.80 | 20.00 | 59.80 | 59.90 | 19.80 | 19.60 | 49.40 | 19.90 | 5.60 |
| **3** | 59.60 | 59.60 | 19.90 | 20.00 | 59.70 | 59.70 | 19.80 | 20.00 | 49.50 | 19.70 | 5.70 |
| **4** | 59.90 | 59.50 | 19.90 | 19.90 | 59.80 | 59.90 | 19.70 | 19.90 | 49.40 | 20.00 | 5.70 |
| **5** | 59.80 | 59.70 | 19.90 | 19.80 | 59.90 | 60.00 | 19.70 | 19.60 | 49.30 | 19.90 | 5.70 |
| **6** | 59.90 | 60.00 | 19.80 | 19.80 | 59.70 | 59.80 | 19.70 | 19.60 | 49.30 | 19.80 | 5.70 |
| **7** | 59.70 | 60.10 | 19.90 | 19.80 | 59.70 | 59.60 | 19.90 | 19.80 | 49.20 | 19.80 | 5.70 |
| **8** | 60.00 | 60.00 | 20.00 | 20.00 | 60.00 | 59.60 | 19.90 | 19.80 | 49.70 | 20.00 | 5.80 |
| **9** | 60.00 | 60.00 | 19.80 | 20.10 | 59.70 | 59.90 | 19.80 | 19.60 | 49.40 | 19.90 | 5.80 |
| **10** | 59.90 | 59.90 | 20.00 | 19.90 | 59.80 | 59.80 | 19.60 | 19.60 | 49.40 | 20.00 | 5.90 |
| **Osirix - CT Face Protocol Bone Algorithm 0.625mm** | | | | | | | | | | | |
| **1** | 60.00 | 59.90 | 20.50 | 20.30 | 60.00 | 59.80 | 19.80 | 19.80 | 4.80 | 20.00 | 5.80 |
| **2** | 60.10 | 59.80 | 20.20 | 19.80 | 60.10 | 59.90 | 19.70 | 19.70 | 49.80 | 20.20 | 5.80 |
| **3** | 60.00 | 60.00 | 20.00 | 20.00 | 60.00 | 60.00 | 19.70 | 19.80 | 49.70 | 20.20 | 5.70 |
| **4** | 60.30 | 60.10 | 20.20 | 20.20 | 60.10 | 59.90 | 19.70 | 19.80 | 49.60 | 20.30 | 5.90 |
| **5** | 60.10 | 59.90 | 20.30 | 20.20 | 60.20 | 59.80 | 19.90 | 19.90 | 49.80 | 20.30 | 5.70 |
| **6** | 60.20 | 60.10 | 20.20 | 19.90 | 60.00 | 59.90 | 19.80 | 19.70 | 49.70 | 20.00 | 5.90 |
| **7** | 60.00 | 60.00 | 20.20 | 20.30 | 60.00 | 60.00 | 19.90 | 19.80 | 49.80 | 20.10 | 6.00 |
| **8** | 60.10 | 60.10 | 20.30 | 20.20 | 59.90 | 59.80 | 19.70 | 20.00 | 49.70 | 20.20 | 5.80 |
| **9** | 60.10 | 59.90 | 20.30 | 20.20 | 59.90 | 59.80 | 19.70 | 19.80 | 49.60 | 20.20 | 5.90 |
| **10** | 60.00 | 59.80 | 20.30 | 20.10 | 59.80 | 59.90 | 19.80 | 19.80 | 49.70 | 20.20 | 5.90 |
| **Osirix - CT Face Protocol Bone Algorithm 1.25mm** | | | | | | | | | | | |
| **1** | 60.10 | 59.90 | 20.10 | 20.20 | 59.90 | 59.90 | 19.90 | 19.70 | 49.60 | 19.70 | 5.00 |
| **2** | 60.00 | 59.70 | 19.90 | 19.90 | 59.90 | 60.00 | 19.80 | 20.10 | 49.50 | 20.00 | 5.40 |
| **3** | 60.20 | 59.90 | 20.10 | 20.20 | 59.90 | 59.90 | 19.80 | 19.80 | 49.60 | 19.80 | 5.40 |
| **4** | 60.40 | 59.80 | 20.20 | 20.10 | 59.90 | 59.90 | 19.90 | 20.00 | 49.70 | 20.00 | 5.30 |
| **5** | 60.00 | 60.00 | 20.10 | 20.10 | 60.00 | 59.70 | 20.10 | 20.10 | 49.70 | 20.00 | 5.20 |
| **6** | 60.10 | 59.80 | 20.10 | 20.20 | 60.10 | 59.70 | 19.90 | 19.80 | 49.80 | 19.90 | 5.30 |
| **7** | 60.30 | 60.10 | 20.10 | 19.90 | 60.10 | 60.00 | 19.90 | 20.10 | 49.70 | 20.00 | 5.20 |
| **8** | 60.10 | 60.00 | 20.10 | 20.10 | 60.00 | 60.10 | 19.80 | 20.10 | 49.80 | 20.00 | 5.30 |
| **9** | 60.00 | 60.10 | 20.30 | 20.30 | 60.00 | 60.10 | 19.80 | 20.10 | 49.90 | 20.00 | 5.40 |
| **10** | 60.10 | 59.80 | 20.20 | 20.10 | 60.00 | 59.90 | 19.90 | 20.10 | 49.70 | 20.00 | 5.20 |
| **Osirix - CT Face Protocol Bone Algorithm 2.5mm** | | | | | | | | | | | |
| **1** | 60.20 | 60.30 | 20.00 | 20.10 | 60.10 | 59.90 | 20.00 | 19.70 | 49.30 | 20.10 | 4.90 |
| **2** | 60.10 | 60.10 | 20.00 | 19.80 | 60.50 | 60.10 | 19.90 | 19.80 | 49.40 | 19.70 | 4.60 |
| **3** | 60.20 | 60.10 | 19.90 | 19.90 | 60.10 | 59.90 | 19.60 | 20.10 | 49.80 | 20.40 | 5.00 |
| **4** | 60.20 | 60.10 | 19.90 | 20.00 | 59.80 | 60.10 | 19.70 | 19.80 | 50.00 | 20.20 | 4.90 |
| **5** | 59.90 | 60.30 | 20.00 | 20.10 | 60.30 | 60.00 | 20.00 | 19.90 | 49.80 | 20.20 | 4.40 |
| **6** | 60.10 | 59.90 | 19.90 | 20.20 | 60.30 | 60.30 | 20.00 | 20.00 | 49.60 | 20.00 | 5.00 |
| **7** | 60.20 | 59.80 | 20.30 | 20.30 | 60.10 | 60.20 | 20.00 | 20.20 | 49.40 | 20.30 | 4.80 |
| **8** | 59.90 | 59.60 | 20.00 | 20.00 | 60.10 | 60.00 | 19.70 | 20.10 | 49.40 | 20.30 | 4.90 |
| **9** | 60.10 | 59.60 | 20.30 | 19.70 | 60.00 | 60.40 | 20.00 | 20.00 | 49.60 | 19.90 | 5.00 |
| **10** | 59.80 | 60.10 | 19.80 | 20.20 | 60.40 | 60.20 | 19.70 | 19.70 | 49.80 | 20.30 | 5.10 |
| **Osirix - CT Face Protocol Soft Tissue Algorithm 0.625mm** | | | | | | | | | | | |
| **1** | 59.70 | 59.70 | 20.20 | 20.20 | 59.90 | 60.00 | 19.90 | 20.00 | 49.80 | 19.80 | 5.40 |
| **2** | 59.40 | 59.80 | 20.30 | 19.80 | 60.00 | 59.80 | 20.00 | 20.20 | 49.50 | 20.30 | 5.50 |
| **3** | 59.70 | 60.00 | 20.00 | 20.10 | 59.90 | 59.90 | 19.80 | 20.20 | 49.60 | 19.90 | 5.40 |
| **4** | 59.60 | 60.00 | 20.10 | 19.90 | 59.70 | 59.90 | 19.70 | 20.20 | 49.50 | 19.80 | 5.30 |
| **5** | 59.70 | 59.70 | 19.80 | 20.10 | 60.10 | 59.70 | 19.80 | 19.80 | 49.70 | 19.90 | 5.30 |
| **6** | 60.30 | 59.90 | 19.90 | 20.20 | 60.10 | 59.70 | 19.80 | 20.10 | 49.60 | 19.70 | 5.20 |
| **7** | 60.10 | 59.90 | 20.10 | 19.90 | 60.00 | 59.80 | 19.60 | 20.20 | 49.80 | 19.70 | 5.40 |
| **8** | 60.00 | 59.80 | 20.20 | 19.90 | 60.00 | 59.80 | 19.60 | 19.80 | 49.80 | 19.70 | 5.30 |
| **9** | 60.00 | 60.00 | 19.90 | 19.90 | 60.00 | 59.80 | 19.60 | 19.80 | 49.60 | 20.10 | 5.20 |
| **10** | 60.20 | 60.00 | 20.00 | 20.10 | 60.00 | 59.90 | 19.70 | 20.00 | 49.60 | 20.20 | 5.30 |

| | a | b | c | d | e | f | g | h | i | j | hole |
|---|---|---|---|---|---|---|---|---|---|---|---|
| **Osirix - CT Face Protocol Soft Tissue Algorithm 1.25mm** | | | | | | | | | | | |
| **1** | 59.90 | 59.90 | 20.10 | 20.10 | 59.80 | 59.90 | 20.10 | 19.50 | 49.60 | 19.40 | 5.00 |
| **2** | 59.70 | 60.20 | 19.80 | 19.90 | 59.60 | 60.10 | 19.70 | 19.50 | 49.70 | 20.10 | 4.60 |
| **3** | 59.70 | 59.90 | 19.90 | 19.70 | 59.60 | 59.90 | 19.90 | 19.50 | 49.20 | 19.80 | 4.70 |
| **4** | 59.60 | 60.00 | 19.60 | 19.70 | 59.90 | 60.10 | 19.70 | 19.70 | 49.30 | 19.80 | 5.10 |
| **5** | 59.90 | 60.30 | 19.70 | 19.80 | 59.90 | 59.90 | 20.00 | 19.60 | 49.50 | 19.80 | 5.20 |
| **6** | 59.80 | 59.90 | 20.20 | 20.00 | 59.70 | 59.80 | 19.60 | 19.50 | 49.40 | 20.20 | 5.00 |
| **7** | 60.00 | 59.90 | 20.20 | 20.10 | 59.80 | 59.90 | 19.60 | 19.70 | 49.50 | 20.20 | 5.00 |
| **8** | 60.10 | 59.90 | 10.80 | 20.10 | 59.80 | 59.90 | 19.90 | 19.60 | 49.70 | 19.60 | 5.00 |
| **9** | 60.00 | 60.10 | 20.00 | 19.80 | 60.00 | 60.10 | 19.70 | 19.60 | 49.70 | 19.90 | 5.20 |
| **10** | 59.60 | 60.00 | 19.90 | 19.90 | 59.60 | 59.80 | 19.50 | 19.60 | 49.80 | 19.90 | 5.10 |
| **Osirix - CT Face Protocol Soft Tissue Algorithm 2.5mm** | | | | | | | | | | | |
| **1** | 59.90 | 60.40 | 20.80 | 20.30 | 59.30 | 60.10 | 19.30 | 19.60 | 49.30 | 19.30 | 3.80 |
| **2** | 60.00 | 59.60 | 20.30 | 20.00 | 59.40 | 59.70 | 19.30 | 19.90 | 49.20 | 19.70 | 4.90 |
| **3** | 59.90 | 60.20 | 20.00 | 20.40 | 59.90 | 59.80 | 19.20 | 19.90 | 49.30 | 19.90 | 5.80 |
| **4** | 60.00 | 60.80 | 20.30 | 20.10 | 59.70 | 60.00 | 19.60 | 19.90 | 49.20 | 20.30 | 5.20 |
| **5** | 60.20 | 60.80 | 19.99 | 19.70 | 60.30 | 60.00 | 19.00 | 19.70 | 49.30 | 19.20 | 4.50 |
| **6** | 60.00 | 60.50 | 20.40 | 19.70 | 59.60 | 60.00 | 19.40 | 19.60 | 49.40 | 20.00 | 5.10 |
| **7** | 60.10 | 60.50 | 19.90 | 20.00 | 60.10 | 59.70 | 19.50 | 19.60 | 49.60 | 20.00 | 5.70 |
| **8** | 60.00 | 60.60 | 20.70 | 19.90 | 59.70 | 59.70 | 19.00 | 20.10 | 49.50 | 20.20 | 5.10 |
| **9** | 59.80 | 59.70 | 20.10 | 19.60 | 60.10 | 59.60 | 19.30 | 19.50 | 49.70 | 19.90 | 5.00 |
| **10** | 59.60 | 59.80 | 20.30 | 20.00 | 59.80 | 60.10 | 19.90 | 19.60 | 49.50 | 19.60 | 5.10 |
| **Osirix - CT Helical Head Bone Algorithm 0.625mm** | | | | | | | | | | | |
| **1** | 60.00 | 60.00 | 20.30 | 20.30 | 59.90 | 60.10 | 19.70 | 19.80 | 49.80 | 19.60 | 5.40 |
| **2** | 60.00 | 60.00 | 20.10 | 20.10 | 59.80 | 60.10 | 19.90 | 19.80 | 49.30 | 19.90 | 5.40 |
| **3** | 59.90 | 60.00 | 20.30 | 20.10 | 60.00 | 60.00 | 19.60 | 19.70 | 49.40 | 19.80 | 5.50 |
| **4** | 59.90 | 59.80 | 20.30 | 20.20 | 59.60 | 60.00 | 19.80 | 20.00 | 49.50 | 19.60 | 5.50 |
| **5** | 59.60 | 59.80 | 19.90 | 20.20 | 59.80 | 60.00 | 19.70 | 20.00 | 49.70 | 19.60 | 5.50 |
| **6** | 60.20 | 60.00 | 20.10 | 20.20 | 60.20 | 60.10 | 19.60 | 19.90 | 49.20 | 19.60 | 5.60 |
| **7** | 59.80 | 59.80 | 20.10 | 20.20 | 60.30 | 59.90 | 19.70 | 19.70 | 49.60 | 19.70 | 5.50 |
| **8** | 59.80 | 60.00 | 20.30 | 20.30 | 60.00 | 60.10 | 19.70 | 19.70 | 49.30 | 19.70 | 5.50 |
| **9** | 59.70 | 60.00 | 20.20 | 20.10 | 60.00 | 59.80 | 19.90 | 19.80 | 49.80 | 19.80 | 5.50 |
| **10** | 60.00 | 59.70 | 19.90 | 20.30 | 60.10 | 59.80 | 19.80 | 19.80 | 49.20 | 19.60 | 5.50 |
| **Osirix - CT Helical Head Bone Algorithm 1.25mm** | | | | | | | | | | | |
| **1** | 60.10 | 60.10 | 20.10 | 20.10 | 60.20 | 60.00 | 20.00 | 20.10 | 49.80 | 20.00 | 5.30 |
| **2** | 60.20 | 60.10 | 20.20 | 20.20 | 60.10 | 60.30 | 19.90 | 20.00 | 49.90 | 19.90 | 5.30 |
| **3** | 60.10 | 60.20 | 20.20 | 20.00 | 60.20 | 60.20 | 20.00 | 20.00 | 50.00 | 20.00 | 5.40 |
| **4** | 60.10 | 60.00 | 20.10 | 20.20 | 59.90 | 60.30 | 19.90 | 19.80 | 49.80 | 19.90 | 5.40 |
| **5** | 60.20 | 60.00 | 20.10 | 20.00 | 60.20 | 60.10 | 19.90 | 19.60 | 50.00 | 20.00 | 5.60 |
| **6** | 60.10 | 60.20 | 20.10 | 20.10 | 60.20 | 60.20 | 20.00 | 19.80 | 49.70 | 20.00 | 5.30 |
| **7** | 60.20 | 60.00 | 20.20 | 20.20 | 60.20 | 60.20 | 19.90 | 19.90 | 50.10 | 20.00 | 5.20 |
| **8** | 60.10 | 60.20 | 20.00 | 20.10 | 60.10 | 60.30 | 19.80 | 19.90 | 49.70 | 19.90 | 5.40 |
| **9** | 60.10 | 59.80 | 20.10 | 20.10 | 60.00 | 60.00 | 19.90 | 19.90 | 49.80 | 20.00 | 5.40 |
| **10** | 60.00 | 60.00 | 20.20 | 20.00 | 60.20 | 60.00 | 20.00 | 19.90 | 49.60 | 19.90 | 5.40 |
| **Osirix - CT Helical Head Bone Algorithm 2.5mm** | | | | | | | | | | | |
| **1** | 60.20 | 60.60 | 20.10 | 20.20 | 60.20 | 60.10 | 19.50 | 20.00 | 49.70 | 20.10 | 4.70 |
| **2** | 60.00 | 60.20 | 19.70 | 20.20 | 60.30 | 60.10 | 20.10 | 19.80 | 49.30 | 20.10 | 5.00 |
| **3** | 60.10 | 60.50 | 19.80 | 20.20 | 59.90 | 60.30 | 20.00 | 19.70 | 49.60 | 20.10 | 4.80 |
| **4** | 59.90 | 60.50 | 19.80 | 20.20 | 59.90 | 60.30 | 19.80 | 20.00 | 49.80 | 20.20 | 4.70 |
| **5** | 60.00 | 60.30 | 19.80 | 19.70 | 59.80 | 60.10 | 19.70 | 20.10 | 49.60 | 20.10 | 4.80 |
| **6** | 60.00 | 60.60 | 20.10 | 19.70 | 60.10 | 59.70 | 20.00 | 19.70 | 49.80 | 20.10 | 4.90 |
| **7** | 59.90 | 60.40 | 20.10 | 19.60 | 60.20 | 60.10 | 20.00 | 19.70 | 49.40 | 20.30 | 5.10 |
| **8** | 60.00 | 60.30 | 20.10 | 20.00 | 60.30 | 59.90 | 19.70 | 19.80 | 49.70 | 20.00 | 4.70 |
| **9** | 60.00 | 60.70 | 20.20 | 20.00 | 60.10 | 60.10 | 19.70 | 20.00 | 49.80 | 20.00 | 5.10 |
| **10** | 60.10 | 60.40 | 20.20 | 20.20 | 60.20 | 60.20 | 20.00 | 20.00 | 49.90 | 20.20 | 4.70 |
| **Osirix - CT Helical Head Soft Tissue Algorithm 0.625mm** | | | | | | | | | | | |
| **1** | 59.80 | 59.90 | 20.00 | 20.20 | 60.00 | 59.70 | 19.50 | 19.80 | 49.50 | 19.80 | 4.90 |
| **2** | 60.10 | 60.10 | 19.80 | 20.00 | 60.00 | 59.80 | 19.90 | 20.00 | 49.60 | 19.80 | 5.30 |
| **3** | 59.90 | 60.00 | 19.80 | 20.40 | 60.00 | 59.90 | 19.60 | 19.80 | 49.70 | 20.00 | 5.40 |
| **4** | 59.80 | 59.80 | 20.30 | 20.20 | 60.10 | 60.10 | 19.90 | 20.00 | 49.40 | 19.80 | 5.40 |
| **5** | 60.10 | 60.10 | 20.00 | 20.20 | 60.00 | 59.80 | 19.80 | 20.00 | 49.60 | 19.60 | 5.20 |
| **6** | 59.90 | 60.10 | 20.00 | 20.40 | 59.90 | 60.00 | 19.90 | 19.60 | 49.60 | 19.00 | 5.20 |
| **7** | 59.90 | 60.10 | 20.20 | 20.30 | 59.90 | 59.80 | 19.90 | 19.80 | 49.60 | 19.60 | 5.10 |
| **8** | 59.70 | 59.90 | 20.40 | 19.90 | 59.80 | 59.80 | 19.80 | 19.80 | 49.90 | 19.80 | 5.30 |
| **9** | 59.90 | 60.00 | 20.00 | 20.40 | 59.90 | 60.10 | 19.80 | 20.00 | 49.60 | 19.80 | 5.30 |
| **10** | 59.70 | 60.00 | 20.20 | 20.20 | 59.90 | 60.00 | 19.60 | 19.90 | 49.60 | 19.60 | 5.20 |

| | a | b | c | d | e | f | g | h | i | j | hole |
|---|---|---|---|---|---|---|---|---|---|---|---|
| **Osirix - CT Helical Head Soft Tissue Algorithm 1.25mm** | | | | | | | | | | | |
| **1** | 59.80 | 59.90 | 19.80 | 20.10 | 59.90 | 60.00 | 19.60 | 20.10 | 49.70 | 19.60 | 4.90 |
| **2** | 59.80 | 59.80 | 19.80 | 19.70 | 59.80 | 59.80 | 19.60 | 19.70 | 49.40 | 19.80 | 5.20 |
| **3** | 60.10 | 60.00 | 19.80 | 20.00 | 60.00 | 59.80 | 19.50 | 19.50 | 49.60 | 20.00 | 5.10 |
| **4** | 60.00 | 59.60 | 20.00 | 20.30 | 59.90 | 59.70 | 19.70 | 19.90 | 49.60 | 19.40 | 5.00 |
| **5** | 60.10 | 60.00 | 19.90 | 20.20 | 60.10 | 60.00 | 19.60 | 19.70 | 49.40 | 19.90 | 5.10 |
| **6** | 60.10 | 60.00 | 19.60 | 19.90 | 59.70 | 59.70 | 19.90 | 19.70 | 49.60 | 20.00 | 5.20 |
| **7** | 60.00 | 59.70 | 20.10 | 20.00 | 60.10 | 60.00 | 19.50 | 19.60 | 49.40 | 19.90 | 5.20 |
| **8** | 59.80 | 60.00 | 19.90 | 20.10 | 60.00 | 60.00 | 19.90 | 20.10 | 49.70 | 19.60 | 5.20 |
| **9** | 59.70 | 60.00 | 20.00 | 20.00 | 60.10 | 59.70 | 19.60 | 20.00 | 49.40 | 19.60 | 5.20 |
| **10** | 60.20 | 59.80 | 20.00 | 20.20 | 59.80 | 60.00 | 19.50 | 19.90 | 49.60 | 20.10 | 5.20 |
| **Osirix - CT Helical Head Soft Tissue Algorithm 2.5mm** | | | | | | | | | | | |
| **1** | 60.00 | 60.30 | 20.10 | 20.30 | 59.70 | 59.70 | 19.80 | 19.80 | 49.80 | 19.60 | 4.20 |
| **2** | 59.80 | 60.20 | 20.30 | 20.30 | 59.90 | 59.90 | 19.90 | 19.80 | 49.90 | 19.60 | 4.30 |
| **3** | 59.90 | 60.40 | 20.30 | 20.30 | 59.60 | 59.70 | 19.30 | 19.80 | 49.90 | 19.20 | 4.40 |
| **4** | 59.90 | 60.30 | 20.70 | 20.40 | 59.90 | 59.80 | 19.70 | 19.80 | 49.70 | 19.80 | 4.50 |
| **5** | 60.20 | 60.40 | 20.10 | 20.00 | 59.80 | 60.20 | 19.30 | 19.50 | 49.80 | 19.80 | 4.60 |
| **6** | 59.90 | 60.40 | 20.00 | 20.30 | 60.10 | 60.00 | 19.30 | 19.90 | 49.70 | 19.70 | 4.60 |
| **7** | 60.20 | 59.80 | 20.10 | 20.00 | 59.90 | 59.90 | 19.70 | 19.90 | 49.50 | 19.90 | 4.60 |
| **8** | 59.80 | 60.30 | 20.30 | 20.10 | 60.20 | 59.80 | 19.30 | 19.70 | 49.80 | 19.80 | 4.10 |
| **9** | 59.80 | 60.00 | 20.00 | 20.40 | 60.00 | 59.80 | 19.30 | 19.80 | 49.50 | 20.10 | 4.50 |
| **10** | 59.90 | 60.10 | 20.00 | 19.90 | 59.70 | 59.70 | 19.40 | 20.10 | 49.90 | 19.50 | 4.40 |

## H.2.1. Statistical Analysis Phantom Cube Measurements on Software

## H.4.1. Fovia

### *Direct Phantom v BB 1.5T 0.8mm*

| | Object | N | Mean | Std. Deviation | Std. Error Mean |
|---|---|---|---|---|---|
| a | Direct Phantom Cube | 10 | 60.1170 | .02791 | .00883 |
| | Fovia BB 1.5T 0.8mm | 10 | 60.1200 | .10328 | .03266 |
| b | Direct Phantom Cube | 10 | 60.0860 | .01776 | .00562 |
| | Fovia BB 1.5T 0.8mm | 10 | 59.9500 | .25055 | .07923 |
| c | Direct Phantom Cube | 10 | 20.0670 | .02908 | .00920 |
| | Fovia BB 1.5T 0.8mm | 10 | 19.9800 | .11353 | .03590 |
| d | Direct Phantom Cube | 10 | 20.0800 | .03464 | .01095 |
| | Fovia BB 1.5T 0.8mm | 10 | 19.9800 | .09189 | .02906 |
| e | Direct Phantom Cube | 10 | 60.1060 | .02914 | .00921 |
| | Fovia BB 1.5T 0.8mm | 10 | 59.8300 | .13375 | .04230 |
| f | Direct Phantom Cube | 10 | 60.1800 | .25342 | .08014 |
| | Fovia BB 1.5T 0.8mm | 10 | 60.0000 | .16997 | .05375 |
| g | Direct Phantom Cube | 10 | 19.8840 | .02675 | .00846 |
| | Fovia BB 1.5T 0.8mm | 10 | 19.8700 | .12517 | .03958 |
| h | Direct Phantom Cube | 10 | 19.9120 | .02974 | .00940 |
| | Fovia BB 1.5T 0.8mm | 10 | 19.8700 | .08233 | .02603 |
| i | Direct Phantom Cube | 10 | 49.8900 | .03266 | .01033 |
| | Fovia BB 1.5T 0.8mm | 10 | 49.7400 | .18379 | .05812 |
| j | Direct Phantom Cube | 10 | 19.9890 | .01524 | .00482 |
| | Fovia BB 1.5T 0.8mm | 10 | 19.9100 | .15951 | .05044 |
| hole | Direct Phantom Cube | 10 | 5.8370 | .04296 | .01359 |
| | Fovia BB 1.5T 0.8mm | 10 | 5.5300 | .18886 | .05972 |

| | Sig. (2-tailed) | Mean Difference | Std. Error Difference | 95% Confidence Interval of the Difference | |
|---|---|---|---|---|---|
| | | | | Lower | Upper |
| a | .930 | -.00300 | .03383 | -.07408 | .06808 |
| b | .104 | .13600 | .07943 | -.03088 | .30288 |
| c | .031 | .08700 | .03706 | .00914 | .16486 |
| d | .005 | .10000 | .03106 | .03475 | .16525 |
| e | .000 | .27600 | .04329 | .18506 | .36694 |
| f | .079 | .18000 | .09649 | -.02273 | .38273 |
| g | .733 | .01400 | .04047 | -.07103 | .09903 |
| h | .147 | .04200 | .02768 | -.01616 | .10016 |
| i | .020 | .15000 | .05903 | .02598 | .27402 |
| j | .136 | .07900 | .05067 | -.02746 | .18546 |
| hole | .000 | .30700 | .06125 | .17832 | .43568 |

## *Direct Phantom v BB 1.5T 1.2mm*

| | Object | N | Mean | Std. Deviation | Std. Error Mean |
|---|---|---|---|---|---|
| a | Direct Phantom Cube | 10 | 60.1170 | .02791 | .00883 |
| | Fovia BB 1.5T 1.2mm | 10 | 59.9700 | .08233 | .02603 |
| b | Direct Phantom Cube | 10 | 60.0860 | .01776 | .00562 |
| | Fovia BB 1.5T 1.2mm | 10 | 59.7600 | .11738 | .03712 |
| c | Direct Phantom Cube | 10 | 20.0670 | .02908 | .00920 |
| | Fovia BB 1.5T 1.2mm | 10 | 19.8700 | .17029 | .05385 |
| d | Direct Phantom Cube | 10 | 20.0800 | .03464 | .01095 |
| | Fovia BB 1.5T 1.2mm | 10 | 20.0400 | .06992 | .02211 |
| e | Direct Phantom Cube | 10 | 60.1060 | .02914 | .00921 |
| | Fovia BB 1.5T 1.2mm | 10 | 59.6500 | .11785 | .03727 |
| f | Direct Phantom Cube | 10 | 60.1800 | .25342 | .08014 |
| | Fovia BB 1.5T 1.2mm | 10 | 59.8600 | .12649 | .04000 |
| g | Direct Phantom Cube | 10 | 19.8840 | .02675 | .00846 |
| | Fovia BB 1.5T 1.2mm | 10 | 19.7200 | .10328 | .03266 |
| h | Direct Phantom Cube | 10 | 19.9120 | .02974 | .00940 |
| | Fovia BB 1.5T 1.2mm | 10 | 19.8400 | .13499 | .04269 |
| i | Direct Phantom Cube | 10 | 49.8900 | .03266 | .01033 |
| | Fovia BB 1.5T 1.2mm | 10 | 49.0600 | .20111 | .06360 |
| j | Direct Phantom Cube | 10 | 19.9890 | .01524 | .00482 |
| | Fovia BB 1.5T 1.2mm | 10 | 20.0200 | .07888 | .02494 |
| hole | Direct Phantom Cube | 10 | 5.8370 | .04296 | .01359 |
| | Fovia BB 1.5T 1.2mm | 10 | 5.6800 | .09189 | .02906 |

| | Sig. (2-tailed) | Mean Difference | Std. Error Difference | 95% Confidence Interval of the Difference | |
|---|---|---|---|---|---|
| | | | | Lower | Upper |
| a | .000 | .14700 | .02749 | .08925 | .20475 |
| b | .000 | .32600 | .03754 | .24713 | .40487 |
| c | .002 | .19700 | .05463 | .08222 | .31178 |
| d | .122 | .04000 | .02468 | -.01184 | .09184 |
| e | .000 | .45600 | .03839 | .37535 | .53665 |
| f | .002 | .32000 | .08957 | .13183 | .50817 |
| g | .000 | .16400 | .03374 | .09312 | .23488 |
| h | .117 | .07200 | .04371 | -.01983 | .16383 |
| i | .000 | .83000 | .06443 | .69464 | .96536 |
| j | .238 | -.03100 | .02541 | -.08438 | .02238 |
| hole | .000 | .15700 | .03208 | .08961 | .22439 |

## *Direct Phantom v BB 1.5T 2.0mm*

| | Object | N | Mean | Std. Deviation | Std. Error Mean |
|---|---|---|---|---|---|
| a | Direct Phantom Cube | 10 | 60.1170 | .02791 | .00883 |
| | Fovia BB 1.5T 2.0mm | 10 | 60.2400 | .06992 | .02211 |
| b | Direct Phantom Cube | 10 | 60.0860 | .01776 | .00562 |
| | Fovia BB 1.5T 2.0mm | 10 | 59.6900 | .11005 | .03480 |
| c | Direct Phantom Cube | 10 | 20.0670 | .02908 | .00920 |
| | Fovia BB 1.5T 2.0mm | 10 | 20.0500 | .13540 | .04282 |
| d | Direct Phantom Cube | 10 | 20.0800 | .03464 | .01095 |
| | Fovia BB 1.5T 2.0mm | 10 | 20.2200 | .11353 | .03590 |
| e | Direct Phantom Cube | 10 | 60.1060 | .02914 | .00921 |
| | Fovia BB 1.5T 2.0mm | 10 | 59.7100 | .17288 | .05467 |
| f | Direct Phantom Cube | 10 | 60.1800 | .25342 | .08014 |
| | Fovia BB 1.5T 2.0mm | 10 | 59.9700 | .21628 | .06839 |
| g | Direct Phantom Cube | 10 | 19.8840 | .02675 | .00846 |
| | Fovia BB 1.5T 2.0mm | 10 | 20.1500 | .11785 | .03727 |
| h | Direct Phantom Cube | 10 | 19.9120 | .02974 | .00940 |
| | Fovia BB 1.5T 2.0mm | 10 | 20.0800 | .12293 | .03887 |
| i | Direct Phantom Cube | 10 | 49.8900 | .03266 | .01033 |
| | Fovia BB 1.5T 2.0mm | 10 | 50.4500 | .91682 | .28992 |
| j | Direct Phantom Cube | 10 | 19.9890 | .01524 | .00482 |
| | Fovia BB 1.5T 2.0mm | 10 | 20.8700 | .24060 | .07608 |
| hole | Direct Phantom Cube | 10 | 5.8370 | .04296 | .01359 |
| | Fovia BB 1.5T 2.0mm | 10 | 4.6600 | .18379 | .05812 |

| | Sig. (2-tailed) | Mean Difference | Std. Error Difference | 95% Confidence Interval of the Difference | |
|---|---|---|---|---|---|
| | | | | Lower | Upper |
| A | .000 | -.12300 | .02381 | -.17302 | -.07298 |
| B | .000 | .39600 | .03525 | .32194 | .47006 |
| C | .702 | .01700 | .04379 | -.07501 | .10901 |
| D | .002 | -.14000 | .03754 | -.21886 | -.06114 |
| E | .000 | .39600 | .05544 | .27952 | .51248 |
| F | .062 | .21000 | .10536 | -.01135 | .43135 |
| G | .000 | -.26600 | .03822 | -.34629 | -.18571 |
| H | .001 | -.16800 | .03999 | -.25203 | -.08397 |
| I | .069 | -.56000 | .29011 | -1.16949 | .04949 |
| J | .000 | -.88100 | .07624 | -1.04117 | -.72083 |
| hole | .000 | 1.17700 | .05969 | 1.05161 | 1.30239 |

## *Direct phantom v BB 1.5T 2.4mm*

| | Object | N | Mean | Std. Deviation | Std. Error Mean |
|---|---|---|---|---|---|
| A | Direct Phantom Cube | 10 | 60.1170 | .02791 | .00883 |
| | Fovia BB 1.5T 2.4mm | 10 | 60.2400 | .06992 | .02211 |
| B | Direct Phantom Cube | 10 | 60.0860 | .01776 | .00562 |
| | Fovia BB 1.5T 2.4mm | 10 | 60.1000 | .43205 | .13663 |
| C | Direct Phantom Cube | 10 | 20.0670 | .02908 | .00920 |
| | Fovia BB 1.5T 2.4mm | 10 | 20.1600 | .08433 | .02667 |
| D | Direct Phantom Cube | 10 | 20.0800 | .03464 | .01095 |
| | Fovia BB 1.5T 2.4mm | 10 | 20.1100 | .11972 | .03786 |
| E | Direct Phantom Cube | 10 | 60.1060 | .02914 | .00921 |
| | Fovia BB 1.5T 2.4mm | 10 | 59.8500 | .09718 | .03073 |
| F | Direct Phantom Cube | 10 | 60.1800 | .25342 | .08014 |
| | Fovia BB 1.5T 2.4mm | 10 | 59.9800 | .13984 | .04422 |
| G | Direct Phantom Cube | 10 | 19.8840 | .02675 | .00846 |
| | Fovia BB 1.5T 2.4mm | 10 | 19.9200 | .14757 | .04667 |
| H | Direct Phantom Cube | 10 | 19.9120 | .02974 | .00940 |
| | Fovia BB 1.5T 2.4mm | 10 | 19.9300 | .08233 | .02603 |
| I | Direct Phantom Cube | 10 | 49.8900 | .03266 | .01033 |
| | Fovia BB 1.5T 2.4mm | 10 | 49.5500 | .14337 | .04534 |
| J | Direct Phantom Cube | 10 | 19.9890 | .01524 | .00482 |
| | Fovia BB 1.5T 2.4mm | 10 | 21.1500 | .08498 | .02687 |
| hole | Direct Phantom Cube | 10 | 5.8370 | .04296 | .01359 |
| | Fovia BB 1.5T 2.4mm | 10 | 4.4400 | .05164 | .01633 |

| | Sig. (2-tailed) | Mean Difference | Std. Error Difference | 95% Confidence Interval of the Difference | |
|---|---|---|---|---|---|
| | | | | Lower | Upper |
| a | .000 | -.12300 | .02381 | -.17302 | -.07298 |
| b | .920 | -.01400 | .13674 | -.30128 | .27328 |
| c | .004 | -.09300 | .02821 | -.15226 | -.03374 |
| d | .456 | -.03000 | .03941 | -.11280 | .05280 |
| e | .000 | .25600 | .03208 | .18860 | .32340 |
| f | .042 | .20000 | .09153 | .00770 | .39230 |
| g | .458 | -.03600 | .04743 | -.13564 | .06364 |
| h | .524 | -.01800 | .02768 | -.07616 | .04016 |
| i | .000 | .34000 | .04650 | .24231 | .43769 |
| j | .000 | -1.16100 | .02730 | -1.21836 | -1.10364 |
| hole | .000 | 1.39700 | .02124 | 1.35237 | 1.44163 |

## *Direct Phantom v BB 3T 0.8mm*

| | Object | N | Mean | Std. Deviation | Std. Error Mean |
|---|---|---|---|---|---|
| a | Direct Phantom Cube | 10 | 60.1170 | .02791 | .00883 |
| | Fovia BB 3.0T 0.8mm | 10 | 59.1500 | .91682 | .28992 |
| b | Direct Phantom Cube | 10 | 60.0860 | .01776 | .00562 |
| | Fovia BB 3.0T 0.8mm | 10 | 58.9000 | .17638 | .05578 |
| c | Direct Phantom Cube | 10 | 20.0670 | .02908 | .00920 |
| | Fovia BB 3.0T 0.8mm | 10 | 18.6300 | .15670 | .04955 |
| d | Direct Phantom Cube | 10 | 20.0800 | .03464 | .01095 |
| | Fovia BB 3.0T 0.8mm | 10 | 18.9300 | .08233 | .02603 |
| e | Direct Phantom Cube | 10 | 60.1060 | .02914 | .00921 |
| | Fovia BB 3.0T 0.8mm | 10 | 59.1800 | .13984 | .04422 |
| f | Direct Phantom Cube | 10 | 60.1800 | .25342 | .08014 |
| | Fovia BB 3.0T 0.8mm | 10 | 59.5100 | .15239 | .04819 |
| g | Direct Phantom Cube | 10 | 19.8840 | .02675 | .00846 |
| | Fovia BB 3.0T 0.8mm | 10 | 18.5400 | .11738 | .03712 |
| h | Direct Phantom Cube | 10 | 19.9120 | .02974 | .00940 |
| | Fovia BB 3.0T 0.8mm | 10 | 18.6000 | .08165 | .02582 |
| i | Direct Phantom Cube | 10 | 49.8900 | .03266 | .01033 |
| | Fovia BB 3.0T 0.8mm | 10 | 48.9000 | .11547 | .03651 |
| j | Direct Phantom Cube | 10 | 19.9890 | .01524 | .00482 |
| | Fovia BB 3.0T 0.8mm | 10 | 19.2500 | .07071 | .02236 |
| hole | Direct Phantom Cube | 10 | 5.8370 | .04296 | .01359 |
| | Fovia BB 3.0T 0.8mm | 10 | 7.5500 | .50166 | .15864 |

| | Sig. (2-tailed) | Mean Difference | Std. Error Difference | 95% Confidence Interval of the Difference | |
|---|---|---|---|---|---|
| | | | | Lower | Upper |
| a | .004 | .96700 | .29006 | .35761 | 1.57639 |
| b | .000 | 1.18600 | .05606 | 1.06822 | 1.30378 |
| c | .000 | 1.43700 | .05040 | 1.33111 | 1.54289 |
| d | .000 | 1.15000 | .02824 | 1.09066 | 1.20934 |
| e | .000 | .92600 | .04517 | .83110 | 1.02090 |
| f | .000 | .67000 | .09351 | .47354 | .86646 |
| g | .000 | 1.34400 | .03807 | 1.26402 | 1.42398 |
| h | .000 | 1.31200 | .02748 | 1.25427 | 1.36973 |
| i | .000 | .99000 | .03795 | .91028 | 1.06972 |
| j | .000 | .73900 | .02287 | .69094 | .78706 |
| hole | .000 | -1.71300 | .15922 | -2.04751 | -1.37849 |

## *Direct phantom v BB 3T 1.2*

| | Object | N | Mean | Std. Deviation | Std. Error Mean |
|---|---|---|---|---|---|
| a | Direct Phantom Cube | 10 | 60.1170 | .02791 | .00883 |
| | Fovia BB 3.0T 1.2mm | 10 | 58.4700 | .76311 | .24132 |
| b | Direct Phantom Cube | 10 | 60.0860 | .01776 | .00562 |
| | Fovia BB 3.0T 1.2mm | 10 | 58.7300 | .35292 | .11160 |
| c | Direct Phantom Cube | 10 | 20.0670 | .02908 | .00920 |
| | Fovia BB 3.0T 1.2mm | 10 | 18.6300 | .10593 | .03350 |
| d | Direct Phantom Cube | 10 | 20.0800 | .03464 | .01095 |
| | Fovia BB 3.0T 1.2mm | 10 | 18.8500 | .14337 | .04534 |
| e | Direct Phantom Cube | 10 | 60.1060 | .02914 | .00921 |
| | Fovia BB 3.0T 1.2mm | 10 | 58.6800 | .07888 | .02494 |
| f | Direct Phantom Cube | 10 | 60.1800 | .25342 | .08014 |
| | Fovia BB 3.0T 1.2mm | 10 | 58.1900 | .09944 | .03145 |
| g | Direct Phantom Cube | 10 | 19.8840 | .02675 | .00846 |
| | Fovia BB 3.0T 1.2mm | 10 | 18.5100 | .24698 | .07810 |
| h | Direct Phantom Cube | 10 | 19.9120 | .02974 | .00940 |
| | Fovia BB 3.0T 1.2mm | 10 | 18.3200 | .38239 | .12092 |
| i | Direct Phantom Cube | 10 | 49.8900 | .03266 | .01033 |
| | Fovia BB 3.0T 1.2mm | 10 | 48.6100 | .38715 | .12243 |
| j | Direct Phantom Cube | 10 | 19.9890 | .01524 | .00482 |
| | Fovia BB 3.0T 1.2mm | 10 | 18.3000 | .19437 | .06146 |
| hole | Direct Phantom Cube | 10 | 5.8370 | .04296 | .01359 |
| | Fovia BB 3.0T 1.2mm | 10 | 7.0900 | .36040 | .11397 |

| | Sig. (2-tailed) | Mean Difference | Std. Error Difference | 95% Confidence Interval of the Difference | |
|---|---|---|---|---|---|
| | | | | Lower | Upper |
| a | .000 | 1.64700 | .24148 | 1.13968 | 2.15432 |
| b | .000 | 1.35600 | .11175 | 1.12123 | 1.59077 |
| c | .000 | 1.43700 | .03474 | 1.36402 | 1.50998 |
| d | .000 | 1.23000 | .04664 | 1.13201 | 1.32799 |
| e | .000 | 1.42600 | .02659 | 1.37013 | 1.48187 |
| f | .000 | 1.99000 | .08609 | 1.80914 | 2.17086 |
| g | .000 | 1.37400 | .07856 | 1.20895 | 1.53905 |
| h | .000 | 1.59200 | .12129 | 1.33718 | 1.84682 |
| i | .000 | 1.28000 | .12286 | 1.02187 | 1.53813 |
| j | .000 | 1.68900 | .06165 | 1.55947 | 1.81853 |
| hole | .000 | -1.25300 | .11478 | -1.49413 | -1.01187 |

### *Direct Phantom v BB 3T 2.0mm*

| | Object | N | Mean | Std. Deviation | Std. Error Mean |
|---|---|---|---|---|---|
| a | Direct Phantom Cube | 10 | 60.1170 | .02791 | .00883 |
| | Fovia BB 3.0T 2.0mm | 10 | 59.0000 | .16330 | .05164 |
| b | Direct Phantom Cube | 10 | 60.0860 | .01776 | .00562 |
| | Fovia BB 3.0T 2.0mm | 10 | 59.0200 | .22998 | .07272 |
| c | Direct Phantom Cube | 10 | 20.0670 | .02908 | .00920 |
| | Fovia BB 3.0T 2.0mm | 10 | 19.0600 | .16465 | .05207 |
| d | Direct Phantom Cube | 10 | 20.0800 | .03464 | .01095 |
| | Fovia BB 3.0T 2.0mm | 10 | 19.1500 | .24608 | .07782 |
| e | Direct Phantom Cube | 10 | 60.1060 | .02914 | .00921 |
| | Fovia BB 3.0T 2.0mm | 10 | 59.5700 | .33350 | .10546 |
| f | Direct Phantom Cube | 10 | 60.1800 | .25342 | .08014 |
| | Fovia BB 3.0T 2.0mm | 10 | 59.3100 | .19692 | .06227 |
| g | Direct Phantom Cube | 10 | 19.8840 | .02675 | .00846 |
| | Fovia BB 3.0T 2.0mm | 10 | 19.0300 | .10593 | .03350 |
| h | Direct Phantom Cube | 10 | 19.9120 | .02974 | .00940 |
| | Fovia BB 3.0T 2.0mm | 10 | 18.9600 | .12649 | .04000 |
| i | Direct Phantom Cube | 10 | 49.8900 | .03266 | .01033 |
| | Fovia BB 3.0T 2.0mm | 10 | 49.1600 | .40879 | .12927 |
| j | Direct Phantom Cube | 10 | 19.9890 | .01524 | .00482 |
| | Fovia BB 3.0T 2.0mm | 10 | 19.3500 | .08498 | .02687 |
| hole | Direct Phantom Cube | 10 | 5.8370 | .04296 | .01359 |
| | Fovia BB 3.0T 2.0mm | 10 | 5.9300 | .10593 | .03350 |

| | Sig. (2-tailed) | Mean Difference | Std. Error Difference | 95% Confidence Interval of the Difference | |
|---|---|---|---|---|---|
| | | | | Lower | Upper |
| a | .000 | 1.11700 | .05239 | 1.00694 | 1.22706 |
| b | .000 | 1.06600 | .07294 | .91276 | 1.21924 |
| c | .000 | 1.00700 | .05287 | .89592 | 1.11808 |
| d | .000 | .93000 | .07858 | .76490 | 1.09510 |
| e | .000 | .53600 | .10586 | .31359 | .75841 |
| f | .000 | .87000 | .10149 | .65678 | 1.08322 |
| g | .000 | .85400 | .03455 | .78141 | .92659 |
| h | .000 | .95200 | .04109 | .86567 | 1.03833 |
| i | .000 | .73000 | .12968 | .45755 | 1.00245 |
| j | .000 | .63900 | .02730 | .58164 | .69636 |
| hole | .019 | -.09300 | .03615 | -.16895 | -.01705 |

## *Direct phantom v BB 3T 2.4mm*

| | Object | N | Mean | Std. Deviation | Std. Error Mean |
|---|---|---|---|---|---|
| a | Direct Phantom Cube | 10 | 60.1170 | .02791 | .00883 |
| | Fovia BB 3.0T 2.4mm | 10 | 59.2000 | .15635 | .04944 |
| b | Direct Phantom Cube | 10 | 60.0860 | .01776 | .00562 |
| | Fovia BB 3.0T 2.4mm | 10 | 58.2700 | .20028 | .06333 |
| c | Direct Phantom Cube | 10 | 20.0670 | .02908 | .00920 |
| | Fovia BB 3.0T 2.4mm | 10 | 18.9500 | .15092 | .04773 |
| d | Direct Phantom Cube | 10 | 20.0800 | .03464 | .01095 |
| | Fovia BB 3.0T 2.4mm | 10 | 19.0800 | .12293 | .03887 |
| e | Direct Phantom Cube | 10 | 60.1060 | .02914 | .00921 |
| | Fovia BB 3.0T 2.4mm | 10 | 58.8300 | .15670 | .04955 |
| f | Direct Phantom Cube | 10 | 60.1800 | .25342 | .08014 |
| | Fovia BB 3.0T 2.4mm | 10 | 59.5900 | .60083 | .19000 |
| g | Direct Phantom Cube | 10 | 19.8840 | .02675 | .00846 |
| | Fovia BB 3.0T 2.4mm | 10 | 18.8900 | .14491 | .04583 |
| h | Direct Phantom Cube | 10 | 19.9120 | .02974 | .00940 |
| | Fovia BB 3.0T 2.4mm | 10 | 18.8000 | .20000 | .06325 |
| i | Direct Phantom Cube | 10 | 49.8900 | .03266 | .01033 |
| | Fovia BB 3.0T 2.4mm | 10 | 48.2800 | .13166 | .04163 |
| j | Direct Phantom Cube | 10 | 19.9890 | .01524 | .00482 |
| | Fovia BB 3.0T 2.4mm | 10 | 18.3600 | .14298 | .04522 |
| hole | Direct Phantom Cube | 10 | 5.8370 | .04296 | .01359 |
| | Fovia BB 3.0T 2.4mm | 10 | 6.6500 | .44783 | .14162 |

| | Sig. (2-tailed) | Mean Difference | Std. Error Difference | 95% Confidence Interval of the Difference | |
|---|---|---|---|---|---|
| | | | | Lower | Upper |
| a | .000 | .91700 | .05022 | .81149 | 1.02251 |
| b | .000 | 1.81600 | .06358 | 1.68242 | 1.94958 |
| c | .000 | 1.11700 | .04860 | 1.01489 | 1.21911 |
| d | .000 | 1.00000 | .04039 | .91515 | 1.08485 |
| e | .000 | 1.27600 | .05040 | 1.17011 | 1.38189 |
| f | .010 | .59000 | .20621 | .15677 | 1.02323 |
| g | .000 | .99400 | .04660 | .89610 | 1.09190 |
| h | .000 | 1.11200 | .06394 | .97767 | 1.24633 |
| i | .000 | 1.61000 | .04290 | 1.51988 | 1.70012 |
| j | .000 | 1.62900 | .04547 | 1.53347 | 1.72453 |
| hole | .000 | -.81300 | .14227 | -1.11189 | -.51411 |

## *Direct phantom v CT face ST 0.625mm*

| | Object | N | Mean | Std. Deviation | Std. Error Mean |
|---|---|---|---|---|---|
| a | Direct Phantom Cube | 10 | 60.1170 | .02791 | .00883 |
| | Fovia CT Face ST 0.625mm | 10 | 59.8400 | .17127 | .05416 |
| b | Direct Phantom Cube | 10 | 60.0860 | .01776 | .00562 |
| | Fovia CT Face ST 0.625mm | 10 | 60.4100 | .23781 | .07520 |
| c | Direct Phantom Cube | 10 | 20.0670 | .02908 | .00920 |
| | Fovia CT Face ST 0.625mm | 10 | 19.4700 | .18288 | .05783 |
| d | Direct Phantom Cube | 10 | 20.0800 | .03464 | .01095 |
| | Fovia CT Face ST 0.625mm | 10 | 19.5100 | .13703 | .04333 |
| e | Direct Phantom Cube | 10 | 60.1060 | .02914 | .00921 |
| | Fovia CT Face ST 0.625mm | 10 | 59.8800 | .22509 | .07118 |
| f | Direct Phantom Cube | 10 | 60.1800 | .25342 | .08014 |
| | Fovia CT Face ST 0.625mm | 10 | 59.3300 | .17029 | .05385 |
| g | Direct Phantom Cube | 10 | 19.8840 | .02675 | .00846 |
| | Fovia CT Face ST 0.625mm | 10 | 19.2400 | .22211 | .07024 |
| h | Direct Phantom Cube | 10 | 19.9120 | .02974 | .00940 |
| | Fovia CT Face ST 0.625mm | 10 | 19.0900 | .28067 | .08876 |
| i | Direct Phantom Cube | 10 | 49.8900 | .03266 | .01033 |
| | Fovia CT Face ST 0.625mm | 10 | 48.7700 | .18886 | .05972 |
| j | Direct Phantom Cube | 10 | 19.9890 | .01524 | .00482 |
| | Fovia CT Face ST 0.625mm | 10 | 19.4500 | .26352 | .08333 |
| hole | Direct Phantom Cube | 10 | 5.8370 | .04296 | .01359 |
| | Fovia CT Face ST 0.625mm | 10 | 5.6200 | .22509 | .07118 |

| | Sig. (2-tailed) | Mean Difference | Std. Error Difference | 95% Confidence Interval of the Difference | |
|---|---|---|---|---|---|
| | | | | Lower | Upper |
| a | .000 | .27700 | .05487 | .16171 | .39229 |
| b | .000 | -.32400 | .07541 | -.48244 | -.16556 |
| c | .000 | .59700 | .05856 | .47397 | .72003 |
| d | .000 | .57000 | .04470 | .47610 | .66390 |
| e | .006 | .22600 | .07177 | .07521 | .37679 |
| f | .000 | .85000 | .09655 | .64715 | 1.05285 |
| g | .000 | .64400 | .07075 | .49537 | .79263 |
| h | .000 | .82200 | .08925 | .63448 | 1.00952 |
| i | .000 | 1.12000 | .06061 | .99267 | 1.24733 |
| j | .000 | .53900 | .08347 | .36363 | .71437 |
| hole | .008 | .21700 | .07247 | .06476 | .36924 |

### *Direct phantom v CT Face ST 1.25mm*

| Object | | N | Mean | Std. Deviation | Std. Error Mean |
|---|---|---|---|---|---|
| a | Direct Phantom Cube | 10 | 60.1170 | .02791 | .00883 |
| | Fovia CT Face ST 1.25mm | 10 | 59.7200 | .37947 | .12000 |
| b | Direct Phantom Cube | 10 | 60.0860 | .01776 | .00562 |
| | Fovia CT Face ST 1.25mm | 10 | 60.4700 | .26268 | .08307 |
| c | Direct Phantom Cube | 10 | 20.0670 | .02908 | .00920 |
| | Fovia CT Face ST 1.25mm | 10 | 19.3600 | .29136 | .09214 |
| d | Direct Phantom Cube | 10 | 20.0800 | .03464 | .01095 |
| | Fovia CT Face ST 1.25mm | 10 | 19.6600 | .30623 | .09684 |
| e | Direct Phantom Cube | 10 | 60.1060 | .02914 | .00921 |
| | Fovia CT Face ST 1.25mm | 10 | 59.7500 | .29533 | .09339 |
| f | Direct Phantom Cube | 10 | 60.1800 | .25342 | .08014 |
| | Fovia CT Face ST 1.25mm | 10 | 59.7500 | .27183 | .08596 |
| g | Direct Phantom Cube | 10 | 19.8840 | .02675 | .00846 |
| | Fovia CT Face ST 1.25mm | 10 | 19.3600 | .30258 | .09568 |
| h | Direct Phantom Cube | 10 | 19.9120 | .02974 | .00940 |
| | Fovia CT Face ST 1.25mm | 10 | 19.6100 | .24244 | .07667 |
| i | Direct Phantom Cube | 10 | 49.8900 | .03266 | .01033 |
| | Fovia CT Face ST 1.25mm | 10 | 49.1600 | .48351 | .15290 |
| j | Direct Phantom Cube | 10 | 19.9890 | .01524 | .00482 |
| | Fovia CT Face ST 1.25mm | 10 | 19.7700 | .32335 | .10225 |
| hole | Direct Phantom Cube | 10 | 5.8370 | .04296 | .01359 |
| | Fovia CT Face ST 1.25mm | 10 | 5.7200 | .21499 | .06799 |

| | Sig. (2-tailed) | Mean Difference | Std. Error Difference | 95% Confidence Interval of the Difference | |
|---|---|---|---|---|---|
| | | | | Lower | Upper |
| a | .004 | .39700 | .12032 | .14421 | .64979 |
| b | .000 | -.38400 | .08326 | -.55891 | -.20909 |
| c | .000 | .70700 | .09259 | .51247 | .90153 |
| d | .000 | .42000 | .09746 | .21525 | .62475 |
| e | .001 | .35600 | .09385 | .15884 | .55316 |
| f | .002 | .43000 | .11752 | .18310 | .67690 |
| g | .000 | .52400 | .09606 | .32219 | .72581 |
| h | .001 | .30200 | .07724 | .13972 | .46428 |
| i | .000 | .73000 | .15325 | .40804 | 1.05196 |
| j | .046 | .21900 | .10237 | .00394 | .43406 |
| hole | .109 | .11700 | .06933 | -.02866 | .26266 |

## *Direct phantom v CT face ST 2.5mm*

| | Object | N | Mean | Std. Deviation | Std. Error Mean |
|---|---|---|---|---|---|
| a | Direct Phantom Cube | 10 | 60.1170 | .02791 | .00883 |
| | Fovia CT Face ST 2.5mm | 10 | 60.1000 | .36209 | .11450 |
| b | Direct Phantom Cube | 10 | 60.0860 | .01776 | .00562 |
| | Fovia CT Face ST 2.5mm | 10 | 61.6500 | .21731 | .06872 |
| c | Direct Phantom Cube | 10 | 20.0670 | .02908 | .00920 |
| | Fovia CT Face ST 2.5mm | 10 | 20.5700 | .22632 | .07157 |
| d | Direct Phantom Cube | 10 | 20.0800 | .03464 | .01095 |
| | Fovia CT Face ST 2.5mm | 10 | 20.4600 | .17764 | .05617 |
| e | Direct Phantom Cube | 10 | 60.1060 | .02914 | .00921 |
| | Fovia CT Face ST 2.5mm | 10 | 61.1500 | .18409 | .05821 |
| f | Direct Phantom Cube | 10 | 60.1800 | .25342 | .08014 |
| | Fovia CT Face ST 2.5mm | 10 | 60.3400 | .28752 | .09092 |
| g | Direct Phantom Cube | 10 | 19.8840 | .02675 | .00846 |
| | Fovia CT Face ST 2.5mm | 10 | 20.4600 | .20111 | .06360 |
| h | Direct Phantom Cube | 10 | 19.9120 | .02974 | .00940 |
| | Fovia CT Face ST 2.5mm | 10 | 20.3700 | .19465 | .06155 |
| i | Direct Phantom Cube | 10 | 49.8900 | .03266 | .01033 |
| | Fovia CT Face ST 2.5mm | 10 | 49.4600 | .22706 | .07180 |
| j | Direct Phantom Cube | 10 | 19.9890 | .01524 | .00482 |
| | Fovia CT Face ST 2.5mm | 10 | 21.0600 | .41952 | .13266 |
| hole | Direct Phantom Cube | 10 | 5.8370 | .04296 | .01359 |
| | Fovia CT Face ST 2.5mm | 10 | 5.2500 | .29155 | .09220 |

| | Sig. (2-tailed) | Mean Difference | Std. Error Difference | 95% Confidence Interval of the Difference | |
|---|---|---|---|---|---|
| | | | | Lower | Upper |
| a | .884 | .01700 | .11484 | -.22428 | .25828 |
| b | .000 | -1.56400 | .06895 | -1.70885 | -1.41915 |
| c | .000 | -.50300 | .07216 | -.65460 | -.35140 |
| d | .000 | -.38000 | .05723 | -.50024 | -.25976 |
| e | .000 | -1.04400 | .05894 | -1.16783 | -.92017 |
| f | .203 | -.16000 | .12120 | -.41463 | .09463 |
| g | .000 | -.57600 | .06416 | -.71079 | -.44121 |
| h | .000 | -.45800 | .06227 | -.58882 | -.32718 |
| i | .000 | .43000 | .07254 | .27760 | .58240 |
| j | .000 | -1.07100 | .13275 | -1.34990 | -.79210 |
| hole | .000 | .58700 | .09319 | .39121 | .78279 |

## *Direct phantom v CT Face Bone 0.625mm*

| | Object | N | Mean | Std. Deviation | Std. Error Mean |
|---|---|---|---|---|---|
| a | Direct Phantom Cube | 10 | 60.1170 | .02791 | .00883 |
| | Fovia CT Face Bone 0.625mm | 10 | 59.9800 | .18738 | .05925 |
| b | Direct Phantom Cube | 10 | 60.0860 | .01776 | .00562 |
| | Fovia CT Face Bone 0.625mm | 10 | 60.2200 | .14757 | .04667 |
| c | Direct Phantom Cube | 10 | 20.0670 | .02908 | .00920 |
| | Fovia CT Face Bone 0.625mm | 10 | 19.7900 | .15951 | .05044 |
| d | Direct Phantom Cube | 10 | 20.0800 | .03464 | .01095 |
| | Fovia CT Face Bone 0.625mm | 10 | 19.6600 | .09661 | .03055 |
| e | Direct Phantom Cube | 10 | 60.1060 | .02914 | .00921 |
| | Fovia CT Face Bone 0.625mm | 10 | 60.1100 | .27669 | .08750 |
| f | Direct Phantom Cube | 10 | 60.1800 | .25342 | .08014 |
| | Fovia CT Face Bone 0.625mm | 10 | 60.0000 | .16330 | .05164 |
| g | Direct Phantom Cube | 10 | 19.8840 | .02675 | .00846 |
| | Fovia CT Face Bone 0.625mm | 10 | 19.4600 | .25473 | .08055 |
| h | Direct Phantom Cube | 10 | 19.9120 | .02974 | .00940 |
| | Fovia CT Face Bone 0.625mm | 10 | 19.6400 | .25906 | .08192 |
| i | Direct Phantom Cube | 10 | 49.8900 | .03266 | .01033 |
| | Fovia CT Face Bone 0.625mm | 10 | 49.5700 | .23594 | .07461 |
| j | Direct Phantom Cube | 10 | 19.9890 | .01524 | .00482 |
| | Fovia CT Face Bone 0.625mm | 10 | 19.8500 | .16499 | .05217 |
| hole | Direct Phantom Cube | 10 | 5.8370 | .04296 | .01359 |
| | Fovia CT Face Bone 0.625mm | 10 | 6.1200 | .22998 | .07272 |

| | Sig. (2-tailed) | Mean Difference | Std. Error Difference | 95% Confidence Interval of the Difference | |
|---|---|---|---|---|---|
| | | | | Lower | Upper |
| a | .035 | .13700 | .05991 | .01114 | .26286 |
| b | .011 | -.13400 | .04700 | -.23275 | -.03525 |
| c | .000 | .27700 | .05127 | .16928 | .38472 |
| d | .000 | .42000 | .03246 | .35181 | .48819 |
| e | .964 | -.00400 | .08798 | -.18884 | .18084 |
| f | .075 | .18000 | .09534 | -.02029 | .38029 |
| g | .000 | .42400 | .08100 | .25383 | .59417 |
| h | .004 | .27200 | .08246 | .09876 | .44524 |
| i | .000 | .32000 | .07532 | .16176 | .47824 |
| j | .016 | .13900 | .05240 | .02892 | .24908 |
| hole | .001 | -.28300 | .07398 | -.43843 | -.12757 |

### *Direct phantom v CT face bone 1.25mm*

| | Object | N | Mean | Std. Deviation | Std. Error Mean |
|---|---|---|---|---|---|
| a | Direct Phantom Cube | 10 | 60.1170 | .02791 | .00883 |
| | Fovia CT Face Bone 1.25mm | 10 | 59.6500 | .07071 | .02236 |
| b | Direct Phantom Cube | 10 | 60.0860 | .01776 | .00562 |
| | Fovia CT Face Bone 1.25mm | 10 | 60.4300 | .13375 | .04230 |
| c | Direct Phantom Cube | 10 | 20.0670 | .02908 | .00920 |
| | Fovia CT Face Bone 1.25mm | 10 | 19.7800 | .13166 | .04163 |
| d | Direct Phantom Cube | 10 | 20.0800 | .03464 | .01095 |
| | Fovia CT Face Bone 1.25mm | 10 | 19.6300 | .11595 | .03667 |
| e | Direct Phantom Cube | 10 | 60.1060 | .02914 | .00921 |
| | Fovia CT Face Bone 1.25mm | 10 | 60.0600 | .16465 | .05207 |
| f | Direct Phantom Cube | 10 | 60.1800 | .25342 | .08014 |
| | Fovia CT Face Bone 1.25mm | 10 | 59.6400 | .23664 | .07483 |
| g | Direct Phantom Cube | 10 | 19.8840 | .02675 | .00846 |
| | Fovia CT Face Bone 1.25mm | 10 | 18.6800 | 3.19541 | 1.01048 |
| h | Direct Phantom Cube | 10 | 19.9120 | .02974 | .00940 |
| | Fovia CT Face Bone 1.25mm | 10 | 19.6800 | .20976 | .06633 |
| i | Direct Phantom Cube | 10 | 49.8900 | .03266 | .01033 |
| | Fovia CT Face Bone 1.25mm | 10 | 49.6700 | .26687 | .08439 |
| j | Direct Phantom Cube | 10 | 19.9890 | .01524 | .00482 |
| | Fovia CT Face Bone 1.25mm | 10 | 20.7200 | .38528 | .12184 |
| hole | Direct Phantom Cube | 10 | 5.8370 | .04296 | .01359 |
| | Fovia CT Face Bone 1.25mm | 10 | 5.9100 | .19692 | .06227 |

| | Sig. (2-tailed) | Mean Difference | Std. Error Difference | 95% Confidence Interval of the Difference | |
|---|---|---|---|---|---|
| | | | | Lower | Upper |
| a | .000 | .46700 | .02404 | .41650 | .51750 |
| b | .000 | -.34400 | .04267 | -.43364 | -.25436 |
| c | .000 | .28700 | .04264 | .19742 | .37658 |
| d | .000 | .45000 | .03827 | .36960 | .53040 |
| e | .396 | .04600 | .05288 | -.06509 | .15709 |
| f | .000 | .54000 | .10965 | .30964 | .77036 |
| g | .249 | 1.20400 | 1.01051 | -.91901 | 3.32701 |
| h | .003 | .23200 | .06700 | .09125 | .37275 |
| i | .019 | .22000 | .08502 | .04137 | .39863 |
| j | .000 | -.73100 | .12193 | -.98717 | -.47483 |
| hole | .267 | -.07300 | .06374 | -.20691 | .06091 |

## *Direct phantom v CT face bone 2.5mm*

| | Object | N | Mean | Std. Deviation | Std. Error Mean |
|---|---|---|---|---|---|
| a | Direct Phantom Cube | 10 | 60.1170 | .02791 | .00883 |
| | Fovia CT Face Bone 2.5mm | 10 | 59.6700 | .10593 | .03350 |
| b | Direct Phantom Cube | 10 | 60.0860 | .01776 | .00562 |
| | Fovia CT Face Bone 2.5mm | 10 | 60.7600 | .13499 | .04269 |
| c | Direct Phantom Cube | 10 | 20.0670 | .02908 | .00920 |
| | Fovia CT Face Bone 2.5mm | 10 | 19.6700 | .17670 | .05588 |
| d | Direct Phantom Cube | 10 | 20.0800 | .03464 | .01095 |
| | Fovia CT Face Bone 2.5mm | 10 | 19.5400 | .15776 | .04989 |
| e | Direct Phantom Cube | 10 | 60.1060 | .02914 | .00921 |
| | Fovia CT Face Bone 2.5mm | 10 | 60.3000 | .20548 | .06498 |
| f | Direct Phantom Cube | 10 | 60.1800 | .25342 | .08014 |
| | Fovia CT Face Bone 2.5mm | 10 | 59.5900 | .15239 | .04819 |
| g | Direct Phantom Cube | 10 | 19.8840 | .02675 | .00846 |
| | Fovia CT Face Bone 2.5mm | 10 | 19.6300 | .15670 | .04955 |
| h | Direct Phantom Cube | 10 | 19.9120 | .02974 | .00940 |
| | Fovia CT Face Bone 2.5mm | 10 | 19.9000 | .23094 | .07303 |
| i | Direct Phantom Cube | 10 | 49.8900 | .03266 | .01033 |
| | Fovia CT Face Bone 2.5mm | 10 | 49.1900 | .15239 | .04819 |
| j | Direct Phantom Cube | 10 | 19.9890 | .01524 | .00482 |
| | Fovia CT Face Bone 2.5mm | 10 | 20.0900 | .18529 | .05859 |
| hole | Direct Phantom Cube | 10 | 5.8370 | .04296 | .01359 |
| | Fovia CT Face Bone 2.5mm | 10 | 5.8100 | .14491 | .04583 |

| | Sig. (2-tailed) | Mean Difference | Std. Error Difference | 95% Confidence Interval of the Difference | |
|---|---|---|---|---|---|
| | | | | Lower | Upper |
| a | .000 | .44700 | .03464 | .37422 | .51978 |
| b | .000 | -.67400 | .04306 | -.76446 | -.58354 |
| c | .000 | .39700 | .05663 | .27803 | .51597 |
| d | .000 | .54000 | .05108 | .43269 | .64731 |
| e | .008 | -.19400 | .06563 | -.33188 | -.05612 |
| f | .000 | .59000 | .09351 | .39354 | .78646 |
| g | .000 | .25400 | .05027 | .14839 | .35961 |
| h | .872 | .01200 | .07363 | -.14270 | .16670 |
| i | .000 | .70000 | .04928 | .59646 | .80354 |
| j | .103 | -.10100 | .05879 | -.22452 | .02252 |
| hole | .579 | .02700 | .04780 | -.07342 | .12742 |

## *Direct phantom v CT helical ST 0.625*

| | Object | N | Mean | Std. Deviation | Std. Error Mean |
|---|---|---|---|---|---|
| a | Direct Phantom Cube | 10 | 60.1170 | .02791 | .00883 |
| | Fovia CT Helical ST 0.625mm | 10 | 59.7300 | .14181 | .04485 |
| b | Direct Phantom Cube | 10 | 60.0860 | .01776 | .00562 |
| | Fovia CT Helical ST 0.625mm | 10 | 59.9100 | .08756 | .02769 |
| c | Direct Phantom Cube | 10 | 20.0670 | .02908 | .00920 |
| | Fovia CT Helical ST 0.625mm | 10 | 19.8000 | .17638 | .05578 |
| d | Direct Phantom Cube | 10 | 20.0800 | .03464 | .01095 |
| | Fovia CT Helical ST 0.625mm | 10 | 19.9300 | .13375 | .04230 |
| e | Direct Phantom Cube | 10 | 60.1060 | .02914 | .00921 |
| | Fovia CT Helical ST 0.625mm | 10 | 59.9900 | .13703 | .04333 |
| f | Direct Phantom Cube | 10 | 60.1800 | .25342 | .08014 |
| | Fovia CT Helical ST 0.625mm | 10 | 59.7600 | .13499 | .04269 |
| g | Direct Phantom Cube | 10 | 19.8840 | .02675 | .00846 |
| | Fovia CT Helical ST 0.625mm | 10 | 19.6200 | .19889 | .06289 |
| h | Direct Phantom Cube | 10 | 19.9120 | .02974 | .00940 |
| | Fovia CT Helical ST 0.625mm | 10 | 19.8000 | .20548 | .06498 |
| i | Direct Phantom Cube | 10 | 49.8900 | .03266 | .01033 |
| | Fovia CT Helical ST 0.625mm | 10 | 49.4000 | .18856 | .05963 |
| j | Direct Phantom Cube | 10 | 19.9890 | .01524 | .00482 |
| | Fovia CT Helical ST 0.625mm | 10 | 20.0000 | .32660 | .10328 |
| hole | Direct Phantom Cube | 10 | 5.8370 | .04296 | .01359 |
| | Fovia CT Helical ST 0.625mm | 10 | 5.9800 | .06325 | .02000 |

| | Sig. (2-tailed) | Mean Difference | Std. Error Difference | 95% Confidence Interval of the Difference | |
|---|---|---|---|---|---|
| | | | | Lower | Upper |
| a | .000 | .38700 | .04571 | .29098 | .48302 |
| b | .000 | .17600 | .02825 | .11664 | .23536 |
| c | .000 | .26700 | .05653 | .14823 | .38577 |
| d | .003 | .15000 | .04369 | .05821 | .24179 |
| e | .017 | .11600 | .04430 | .02292 | .20908 |
| f | .000 | .42000 | .09080 | .22924 | .61076 |
| g | .001 | .26400 | .06346 | .13068 | .39732 |
| h | .105 | .11200 | .06566 | -.02594 | .24994 |
| i | .000 | .49000 | .06052 | .36286 | .61714 |
| j | .916 | -.01100 | .10339 | -.22822 | .20622 |
| hole | .000 | -.14300 | .02418 | -.19380 | -.09220 |

### *Direct phantom v CT Helical ST 1.25mm*

| | Object | N | Mean | Std. Deviation | Std. Error Mean |
|---|---|---|---|---|---|
| a | Direct Phantom Cube | 10 | 60.1170 | .02791 | .00883 |
| | Fovia CT Helical ST 1.25mm | 10 | 59.6500 | .19579 | .06191 |
| b | Direct Phantom Cube | 10 | 60.0860 | .01776 | .00562 |
| | Fovia CT Helical ST 1.25mm | 10 | 60.0500 | .13540 | .04282 |
| c | Direct Phantom Cube | 10 | 20.0670 | .02908 | .00920 |
| | Fovia CT Helical ST 1.25mm | 10 | 19.5900 | .11005 | .03480 |
| d | Direct Phantom Cube | 10 | 20.0800 | .03464 | .01095 |
| | Fovia CT Helical ST 1.25mm | 10 | 19.6700 | .08233 | .02603 |
| e | Direct Phantom Cube | 10 | 60.1060 | .02914 | .00921 |
| | Fovia CT Helical ST 1.25mm | 10 | 59.6600 | .13499 | .04269 |
| f | Direct Phantom Cube | 10 | 60.1800 | .25342 | .08014 |
| | Fovia CT Helical ST 1.25mm | 10 | 59.5900 | .20248 | .06403 |
| g | Direct Phantom Cube | 10 | 19.8840 | .02675 | .00846 |
| | Fovia CT Helical ST 1.25mm | 10 | 19.5200 | .20976 | .06633 |
| h | Direct Phantom Cube | 10 | 19.9120 | .02974 | .00940 |
| | Fovia CT Helical ST 1.25mm | 10 | 19.5700 | .09487 | .03000 |
| i | Direct Phantom Cube | 10 | 49.8900 | .03266 | .01033 |
| | Fovia CT Helical ST 1.25mm | 10 | 49.1900 | .12867 | .04069 |
| j | Direct Phantom Cube | 10 | 19.9890 | .01524 | .00482 |
| | Fovia CT Helical ST 1.25mm | 10 | 19.8100 | .32128 | .10160 |
| hole | Direct Phantom Cube | 10 | 5.8370 | .04296 | .01359 |
| | Fovia CT Helical ST 1.25mm | 10 | 5.9400 | .13499 | .04269 |

| | Sig. (2-tailed) | Mean Difference | Std. Error Difference | 95% Confidence Interval of the Difference | |
|---|---|---|---|---|---|
| | | | | Lower | Upper |
| a | .000 | .46700 | .06254 | .33561 | .59839 |
| b | .415 | .03600 | .04318 | -.05473 | .12673 |
| c | .000 | .47700 | .03600 | .40138 | .55262 |
| d | .000 | .41000 | .02824 | .35066 | .46934 |
| e | .000 | .44600 | .04367 | .35425 | .53775 |
| f | .000 | .59000 | .10258 | .37449 | .80551 |
| g | .000 | .36400 | .06687 | .22351 | .50449 |
| h | .000 | .34200 | .03144 | .27595 | .40805 |
| i | .000 | .70000 | .04198 | .61181 | .78819 |
| j | .095 | .17900 | .10171 | -.03469 | .39269 |
| hole | .034 | -.10300 | .04480 | -.19712 | -.00888 |

## *Direct phantom v CT helical ST 2.5mm*

| | Object | N | Mean | Std. Deviation | Std. Error Mean |
|---|---|---|---|---|---|
| a | Direct Phantom Cube | 10 | 60.1170 | .02791 | .00883 |
| | Fovia CT Helical ST 2.5mm | 10 | 59.4000 | .21082 | .06667 |
| b | Direct Phantom Cube | 10 | 60.0860 | .01776 | .00562 |
| | Fovia CT Helical ST 2.5mm | 10 | 60.0900 | .20790 | .06574 |
| c | Direct Phantom Cube | 10 | 20.0670 | .02908 | .00920 |
| | Fovia CT Helical ST 2.5mm | 10 | 19.5700 | .21628 | .06839 |
| d | Direct Phantom Cube | 10 | 20.0800 | .03464 | .01095 |
| | Fovia CT Helical ST 2.5mm | 10 | 19.6900 | .07379 | .02333 |
| e | Direct Phantom Cube | 10 | 60.1060 | .02914 | .00921 |
| | Fovia CT Helical ST 2.5mm | 10 | 59.7700 | .17029 | .05385 |
| f | Direct Phantom Cube | 10 | 60.1800 | .25342 | .08014 |
| | Fovia CT Helical ST 2.5mm | 10 | 59.2300 | .20575 | .06506 |
| g | Direct Phantom Cube | 10 | 19.8840 | .02675 | .00846 |
| | Fovia CT Helical ST 2.5mm | 10 | 19.3100 | .28067 | .08876 |
| h | Direct Phantom Cube | 10 | 19.9120 | .02974 | .00940 |
| | Fovia CT Helical ST 2.5mm | 10 | 19.3400 | .18379 | .05812 |
| i | Direct Phantom Cube | 10 | 49.8900 | .03266 | .01033 |
| | Fovia CT Helical ST 2.5mm | 10 | 48.9900 | .19692 | .06227 |
| j | Direct Phantom Cube | 10 | 19.9890 | .01524 | .00482 |
| | Fovia CT Helical ST 2.5mm | 10 | 19.6300 | .08233 | .02603 |
| hole | Direct Phantom Cube | 10 | 5.8370 | .04296 | .01359 |
| | Fovia CT Helical ST 2.5mm | 10 | 5.8300 | .23594 | .07461 |

| | Sig. (2-tailed) | Mean Difference | Std. Error Difference | 95% Confidence Interval of the Difference | |
|---|---|---|---|---|---|
| | | | | Lower | Upper |
| a | .000 | .71700 | .06725 | .57572 | .85828 |
| b | .952 | -.00400 | .06598 | -.14263 | .13463 |
| c | .000 | .49700 | .06901 | .35202 | .64198 |
| d | .000 | .39000 | .02578 | .33584 | .44416 |
| e | .000 | .33600 | .05463 | .22122 | .45078 |
| f | .000 | .95000 | .10323 | .73313 | 1.16687 |
| g | .000 | .57400 | .08916 | .38668 | .76132 |
| h | .000 | .57200 | .05887 | .44831 | .69569 |
| i | .000 | .90000 | .06312 | .76738 | 1.03262 |
| j | .000 | .35900 | .02648 | .30338 | .41462 |
| hole | .927 | .00700 | .07584 | -.15233 | .16633 |

## *Direct phantom v CT helical bone 0.625*

| | Object | N | Mean | Std. Deviation | Std. Error Mean |
|---|---|---|---|---|---|
| a | Direct Phantom Cube | 10 | 60.1170 | .02791 | .00883 |
| | Fovia CT Helical Bone 0.625mm | 10 | 59.9000 | .24037 | .07601 |
| b | Direct Phantom Cube | 10 | 60.0860 | .01776 | .00562 |
| | Fovia CT Helical Bone 0.625mm | 10 | 60.4400 | .18974 | .06000 |
| c | Direct Phantom Cube | 10 | 20.0670 | .02908 | .00920 |
| | Fovia CT Helical Bone 0.625mm | 10 | 19.8200 | .11353 | .03590 |
| d | Direct Phantom Cube | 10 | 20.0800 | .03464 | .01095 |
| | Fovia CT Helical Bone 0.625mm | 10 | 19.7800 | .13984 | .04422 |
| e | Direct Phantom Cube | 10 | 60.1060 | .02914 | .00921 |
| | Fovia CT Helical Bone 0.625mm | 10 | 60.0300 | .12517 | .03958 |
| f | Direct Phantom Cube | 10 | 60.1800 | .25342 | .08014 |
| | Fovia CT Helical Bone 0.625mm | 10 | 59.8400 | .15776 | .04989 |
| g | Direct Phantom Cube | 10 | 19.8840 | .02675 | .00846 |
| | Fovia CT Helical Bone 0.625mm | 10 | 19.8000 | .17638 | .05578 |
| h | Direct Phantom Cube | 10 | 19.9120 | .02974 | .00940 |
| | Fovia CT Helical Bone 0.625mm | 10 | 19.8600 | .09661 | .03055 |
| i | Direct Phantom Cube | 10 | 49.8900 | .03266 | .01033 |
| | Fovia CT Helical Bone 0.625mm | 10 | 49.6500 | .09718 | .03073 |
| j | Direct Phantom Cube | 10 | 19.9890 | .01524 | .00482 |
| | Fovia CT Helical Bone 0.625mm | 10 | 20.0000 | .08165 | .02582 |
| hole | Direct Phantom Cube | 10 | 5.8370 | .04296 | .01359 |
| | Fovia CT Helical Bone 0.625mm | 10 | 5.7900 | .03162 | .01000 |

| | Sig. (2-tailed) | Mean Difference | Std. Error Difference | 95% Confidence Interval of the Difference | |
|---|---|---|---|---|---|
| | | | | Lower | Upper |
| a | .011 | .21700 | .07652 | .05623 | .37777 |
| b | .000 | -.35400 | .06026 | -.48061 | -.22739 |
| c | .000 | .24700 | .03706 | .16914 | .32486 |
| d | .000 | .30000 | .04556 | .20429 | .39571 |
| e | .078 | .07600 | .04064 | -.00938 | .16138 |
| f | .002 | .34000 | .09440 | .14168 | .53832 |
| g | .154 | .08400 | .05642 | -.03452 | .20252 |
| h | .121 | .05200 | .03197 | -.01516 | .11916 |
| i | .000 | .24000 | .03242 | .17189 | .30811 |
| j | .680 | -.01100 | .02627 | -.06618 | .04418 |
| hole | .012 | .04700 | .01687 | .01156 | .08244 |

### *Direct phantom v CT helical bone 1.25mm*

| | Object | N | Mean | Std. Deviation | Std. Error Mean |
|---|---|---|---|---|---|
| a | Direct Phantom Cube | 10 | 60.1170 | .02791 | .00883 |
| | Fovia CT Helical Bone 1.25mm | 10 | 59.7800 | .10328 | .03266 |
| b | Direct Phantom Cube | 10 | 60.0860 | .01776 | .00562 |
| | Fovia CT Helical Bone 1.25mm | 10 | 60.3500 | .12693 | .04014 |
| c | Direct Phantom Cube | 10 | 20.0670 | .02908 | .00920 |
| | Fovia CT Helical Bone 1.25mm | 10 | 19.7300 | .10593 | .03350 |
| d | Direct Phantom Cube | 10 | 20.0800 | .03464 | .01095 |
| | Fovia CT Helical Bone 1.25mm | 10 | 19.8200 | .16193 | .05121 |
| e | Direct Phantom Cube | 10 | 60.1060 | .02914 | .00921 |
| | Fovia CT Helical Bone 1.25mm | 10 | 60.0800 | .07888 | .02494 |
| f | Direct Phantom Cube | 10 | 60.1800 | .25342 | .08014 |
| | Fovia CT Helical Bone 1.25mm | 10 | 59.7600 | .09661 | .03055 |
| g | Direct Phantom Cube | 10 | 19.8840 | .02675 | .00846 |
| | Fovia CT Helical Bone 1.25mm | 10 | 19.8000 | .12472 | .03944 |
| h | Direct Phantom Cube | 10 | 19.9120 | .02974 | .00940 |
| | Fovia CT Helical Bone 1.25mm | 10 | 19.6300 | .14944 | .04726 |
| i | Direct Phantom Cube | 10 | 49.8900 | .03266 | .01033 |
| | Fovia CT Helical Bone 1.25mm | 10 | 49.3500 | .12693 | .04014 |
| j | Direct Phantom Cube | 10 | 19.9890 | .01524 | .00482 |
| | Fovia CT Helical Bone 1.25mm | 10 | 19.9200 | .09189 | .02906 |
| hole | Direct Phantom Cube | 10 | 5.8370 | .04296 | .01359 |
| | Fovia CT Helical Bone 1.25mm | 10 | 5.8800 | .10328 | .03266 |

| | Sig. (2-tailed) | Mean Difference | Std. Error Difference | 95% Confidence Interval of the Difference | |
|---|---|---|---|---|---|
| | | | | Lower | Upper |
| a | .000 | .33700 | .03383 | .26592 | .40808 |
| b | .000 | -.26400 | .04053 | -.34915 | -.17885 |
| c | .000 | .33700 | .03474 | .26402 | .40998 |
| d | .000 | .26000 | .05237 | .14998 | .37002 |
| e | .341 | .02600 | .02659 | -.02987 | .08187 |
| f | .000 | .42000 | .08576 | .23982 | .60018 |
| g | .052 | .08400 | .04034 | -.00075 | .16875 |
| h | .000 | .28200 | .04818 | .18077 | .38323 |
| i | .000 | .54000 | .04145 | .45293 | .62707 |
| j | .031 | .06900 | .02946 | .00711 | .13089 |
| hole | .240 | -.04300 | .03537 | -.11732 | .03132 |

### *Direct phantom v CT helical bone 2.5mm*

| | Object | N | Mean | Std. Deviation | Std. Error Mean |
|---|---|---|---|---|---|
| a | Direct Phantom Cube | 10 | 60.1170 | .02791 | .00883 |
| | Fovia CT Helical Bone 2.5mm | 10 | 59.6400 | .12649 | .04000 |
| b | Direct Phantom Cube | 10 | 60.0860 | .01776 | .00562 |
| | Fovia CT Helical Bone 2.5mm | 10 | 60.7000 | .14907 | .04714 |
| c | Direct Phantom Cube | 10 | 20.0670 | .02908 | .00920 |
| | Fovia CT Helical Bone 2.5mm | 10 | 19.8000 | .24944 | .07888 |
| d | Direct Phantom Cube | 10 | 20.0800 | .03464 | .01095 |
| | Fovia CT Helical Bone 2.5mm | 10 | 19.7000 | .19437 | .06146 |
| e | Direct Phantom Cube | 10 | 60.1060 | .02914 | .00921 |
| | Fovia CT Helical Bone 2.5mm | 10 | 60.1500 | .13540 | .04282 |
| f | Direct Phantom Cube | 10 | 60.1800 | .25342 | .08014 |
| | Fovia CT Helical Bone 2.5mm | 10 | 59.9500 | .15092 | .04773 |
| g | Direct Phantom Cube | 10 | 19.8840 | .02675 | .00846 |
| | Fovia CT Helical Bone 2.5mm | 10 | 19.7400 | .18379 | .05812 |
| h | Direct Phantom Cube | 10 | 19.9120 | .02974 | .00940 |
| | Fovia CT Helical Bone 2.5mm | 10 | 19.5800 | .14757 | .04667 |
| i | Direct Phantom Cube | 10 | 49.8900 | .03266 | .01033 |
| | Fovia CT Helical Bone 2.5mm | 10 | 49.3200 | .16193 | .05121 |
| j | Direct Phantom Cube | 10 | 19.9890 | .01524 | .00482 |
| | Fovia CT Helical Bone 2.5mm | 10 | 20.0200 | .11353 | .03590 |
| hole | Direct Phantom Cube | 10 | 5.8370 | .04296 | .01359 |
| | Fovia CT Helical Bone 2.5mm | 10 | 5.7200 | .07888 | .02494 |

| | Sig. (2-tailed) | Mean Difference | Std. Error Difference | 95% Confidence Interval of the Difference | |
|---|---|---|---|---|---|
| | | | | Lower | Upper |
| a | .000 | .47700 | .04096 | .39094 | .56306 |
| b | .000 | -.61400 | .04747 | -.71374 | -.51426 |
| c | .003 | .26700 | .07942 | .10015 | .43385 |
| d | .000 | .38000 | .06243 | .24883 | .51117 |
| e | .328 | -.04400 | .04380 | -.13602 | .04802 |
| f | .024 | .23000 | .09327 | .03404 | .42596 |
| g | .025 | .14400 | .05873 | .02061 | .26739 |
| h | .000 | .33200 | .04760 | .23199 | .43201 |
| i | .000 | .57000 | .05224 | .46025 | .67975 |
| j | .403 | -.03100 | .03622 | -.10710 | .04510 |
| hole | .001 | .11700 | .02840 | .05733 | .17667 |

### *BB 1.5T 0.8mm v CT Helical ST 2.5mm*

| | Object | N | Mean | Std. Deviation | Std. Error Mean |
|---|---|---|---|---|---|
| a | Fovia BB 1.5T 0.8mm | 10 | 60.1200 | .10328 | .03266 |
| | Fovia CT Helical Bone 0.625mm | 10 | 59.9000 | .24037 | .07601 |
| b | Fovia BB 1.5T 0.8mm | 10 | 59.9500 | .25055 | .07923 |
| | Fovia CT Helical Bone 0.625mm | 10 | 60.4400 | .18974 | .06000 |
| c | Fovia BB 1.5T 0.8mm | 10 | 19.9800 | .11353 | .03590 |
| | Fovia CT Helical Bone 0.625mm | 10 | 19.8200 | .11353 | .03590 |
| d | Fovia BB 1.5T 0.8mm | 10 | 19.9800 | .09189 | .02906 |
| | Fovia CT Helical Bone 0.625mm | 10 | 19.7800 | .13984 | .04422 |
| e | Fovia BB 1.5T 0.8mm | 10 | 59.8300 | .13375 | .04230 |
| | Fovia CT Helical Bone 0.625mm | 10 | 60.0300 | .12517 | .03958 |
| f | Fovia BB 1.5T 0.8mm | 10 | 60.0000 | .16997 | .05375 |
| | Fovia CT Helical Bone 0.625mm | 10 | 59.8400 | .15776 | .04989 |
| g | Fovia BB 1.5T 0.8mm | 10 | 19.8700 | .12517 | .03958 |
| | Fovia CT Helical Bone 0.625mm | 10 | 19.8000 | .17638 | .05578 |
| h | Fovia BB 1.5T 0.8mm | 10 | 19.8700 | .08233 | .02603 |
| | Fovia CT Helical Bone 0.625mm | 10 | 19.8600 | .09661 | .03055 |
| i | Fovia BB 1.5T 0.8mm | 10 | 49.7400 | .18379 | .05812 |
| | Fovia CT Helical Bone 0.625mm | 10 | 49.6500 | .09718 | .03073 |
| j | Fovia BB 1.5T 0.8mm | 10 | 19.9100 | .15951 | .05044 |
| | Fovia CT Helical Bone 0.625mm | 10 | 20.0000 | .08165 | .02582 |
| hole | Fovia BB 1.5T 0.8mm | 10 | 5.5300 | .18886 | .05972 |
| | Fovia CT Helical Bone 0.625mm | 10 | 5.7900 | .03162 | .01000 |

| | Sig. (2-tailed) | Mean Difference | Std. Error Difference | 95% Confidence Interval of the Difference | |
|---|---|---|---|---|---|
| | | | | Lower | Upper |
| A | .016 | .22000 | .08273 | .04619 | .39381 |
| B | .000 | -.49000 | .09939 | -.69880 | -.28120 |
| C | .006 | .16000 | .05077 | .05333 | .26667 |
| D | .001 | .20000 | .05292 | .08883 | .31117 |
| E | .003 | -.20000 | .05793 | -.32170 | -.07830 |
| F | .043 | .16000 | .07333 | .00593 | .31407 |
| G | .320 | .07000 | .06839 | -.07369 | .21369 |
| H | .806 | .01000 | .04014 | -.07433 | .09433 |
| I | .188 | .09000 | .06574 | -.04812 | .22812 |
| J | .130 | -.09000 | .05667 | -.20905 | .02905 |
| Hole | .000 | -.26000 | .06055 | -.38722 | -.13278 |

## H.4.2. Mimics

### *Direct Phantom v BB 1.5T 0.8mm*

| | Object | N | Mean | Std. Deviation | Std. Error Mean |
|---|---|---|---|---|---|
| A | Direct Phantom Cube | 10 | 60.1170 | .02791 | .00883 |
| | Mimics BB 1.5T 0.8mm | 10 | 59.9200 | .08756 | .02769 |
| B | Direct Phantom Cube | 10 | 60.0860 | .01776 | .00562 |
| | Mimics BB 1.5T 0.8mm | 10 | 59.4240 | .17386 | .05498 |
| C | Direct Phantom Cube | 10 | 20.0670 | .02908 | .00920 |
| | Mimics BB 1.5T 0.8mm | 10 | 19.8780 | .05750 | .01818 |
| D | Direct Phantom Cube | 10 | 20.0800 | .03464 | .01095 |
| | Mimics BB 1.5T 0.8mm | 10 | 20.0610 | .15531 | .04911 |
| E | Direct Phantom Cube | 10 | 60.1060 | .02914 | .00921 |
| | Mimics BB 1.5T 0.8mm | 10 | 59.7130 | .08447 | .02671 |
| F | Direct Phantom Cube | 10 | 60.1800 | .25342 | .08014 |
| | Mimics BB 1.5T 0.8mm | 10 | 59.7330 | .18105 | .05725 |
| G | Direct Phantom Cube | 10 | 19.8840 | .02675 | .00846 |
| | Mimics BB 1.5T 0.8mm | 10 | 19.7340 | .04858 | .01536 |
| H | Direct Phantom Cube | 10 | 19.9120 | .02974 | .00940 |
| | Mimics BB 1.5T 0.8mm | 10 | 19.8770 | .06717 | .02124 |
| I | Direct Phantom Cube | 10 | 49.8900 | .03266 | .01033 |
| | Mimics BB 1.5T 0.8mm | 10 | 49.7280 | .43734 | .13830 |
| J | Direct Phantom Cube | 10 | 19.9890 | .01524 | .00482 |
| | Mimics BB 1.5T 0.8mm | 10 | 19.7480 | .06125 | .01937 |
| Hole | Direct Phantom Cube | 10 | 5.8370 | .04296 | .01359 |
| | Mimics BB 1.5T 0.8mm | 10 | 5.7630 | .04473 | .01415 |

| | Sig. (2-tailed) | Mean Difference | Std. Error Difference | 95% Confidence Interval of the Difference | |
|---|---|---|---|---|---|
| | | | | Lower | Upper |
| A | .000 | .19700 | .02906 | .13594 | .25806 |
| B | .000 | .66200 | .05527 | .54589 | .77811 |
| C | .000 | .18900 | .02038 | .14619 | .23181 |
| D | .710 | .01900 | .05032 | -.08672 | .12472 |
| E | .000 | .39300 | .02825 | .33364 | .45236 |
| F | .000 | .44700 | .09849 | .24008 | .65392 |
| G | .000 | .15000 | .01754 | .11316 | .18684 |
| H | .149 | .03500 | .02323 | -.01381 | .08381 |
| I | .258 | .16200 | .13868 | -.12936 | .45336 |
| J | .000 | .24100 | .01996 | .19907 | .28293 |
| Hole | .001 | .07400 | .01961 | .03279 | .11521 |

## *Direct Phantom v BB 1.5T 1.2mm*

| | Object | N | Mean | Std. Deviation | Std. Error Mean |
|---|---|---|---|---|---|
| a | Direct Phantom Cube | 10 | 60.1170 | .02791 | .00883 |
| | Mimics BB 1.5T 1.2mm | 10 | 60.1800 | .04989 | .01578 |
| b | Direct Phantom Cube | 10 | 60.0860 | .01776 | .00562 |
| | Mimics BB 1.5T 1.2mm | 10 | 59.9170 | .25197 | .07968 |
| c | Direct Phantom Cube | 10 | 20.0670 | .02908 | .00920 |
| | Mimics BB 1.5T 1.2mm | 10 | 20.1380 | .10009 | .03165 |
| d | Direct Phantom Cube | 10 | 20.0800 | .03464 | .01095 |
| | Mimics BB 1.5T 1.2mm | 10 | 20.2360 | .07877 | .02491 |
| e | Direct Phantom Cube | 10 | 60.1060 | .02914 | .00921 |
| | Mimics BB 1.5T 1.2mm | 10 | 59.8000 | .11382 | .03599 |
| f | Direct Phantom Cube | 10 | 60.1800 | .25342 | .08014 |
| | Mimics BB 1.5T 1.2mm | 10 | 60.0960 | .18662 | .05901 |
| g | Direct Phantom Cube | 10 | 19.8840 | .02675 | .00846 |
| | Mimics BB 1.5T 1.2mm | 10 | 19.7990 | .09410 | .02976 |
| h | Direct Phantom Cube | 10 | 19.9120 | .02974 | .00940 |
| | Mimics BB 1.5T 1.2mm | 10 | 19.9520 | .08417 | .02662 |
| i | Direct Phantom Cube | 10 | 49.8900 | .03266 | .01033 |
| | Mimics BB 1.5T 1.2mm | 10 | 49.5740 | .08909 | .02817 |
| j | Direct Phantom Cube | 10 | 19.9890 | .01524 | .00482 |
| | Mimics BB 1.5T 1.2mm | 10 | 19.7140 | .10916 | .03452 |
| hole | Direct Phantom Cube | 10 | 5.8370 | .04296 | .01359 |
| | Mimics BB 1.5T 1.2mm | 10 | 5.8850 | .45766 | .14472 |

| | Sig. (2-tailed) | Mean Difference | Std. Error Difference | 95% Confidence Interval of the Difference | |
|---|---|---|---|---|---|
| | | | | Lower | Upper |
| A | .003 | -.06300 | .01808 | -.10098 | -.02502 |
| B | .049 | .16900 | .07988 | .00118 | .33682 |
| C | .045 | -.07100 | .03296 | -.14025 | -.00175 |
| D | .000 | -.15600 | .02721 | -.21317 | -.09883 |
| E | .000 | .30600 | .03715 | .22794 | .38406 |
| F | .410 | .08400 | .09952 | -.12509 | .29309 |
| G | .013 | .08500 | .03094 | .02001 | .14999 |
| H | .174 | -.04000 | .02823 | -.09931 | .01931 |
| I | .000 | .31600 | .03001 | .25296 | .37904 |
| J | .000 | .27500 | .03485 | .20178 | .34822 |
| Hole | .745 | -.04800 | .14536 | -.35339 | .25739 |

## *Direct Phantom v BB 1.5T 2.0mm*

| | Object | N | Mean | Std. Deviation | Std. Error Mean |
|---|---|---|---|---|---|
| a | Direct Phantom Cube | 10 | 60.1170 | .02791 | .00883 |
| | Mimics BB 1.5T 2.0mm | 10 | 60.2290 | .09362 | .02961 |
| b | Direct Phantom Cube | 10 | 60.0860 | .01776 | .00562 |
| | Mimics BB 1.5T 2.0mm | 10 | 60.1430 | .23281 | .07362 |
| c | Direct Phantom Cube | 10 | 20.0670 | .02908 | .00920 |
| | Mimics BB 1.5T 2.0mm | 10 | 20.1640 | .09834 | .03110 |
| d | Direct Phantom Cube | 10 | 20.0800 | .03464 | .01095 |
| | Mimics BB 1.5T 2.0mm | 10 | 20.2840 | .07382 | .02334 |
| e | Direct Phantom Cube | 10 | 60.1060 | .02914 | .00921 |
| | Mimics BB 1.5T 2.0mm | 10 | 60.0710 | .08698 | .02751 |
| f | Direct Phantom Cube | 10 | 60.1800 | .25342 | .08014 |
| | Mimics BB 1.5T 2.0mm | 10 | 60.0600 | .11421 | .03612 |
| g | Direct Phantom Cube | 10 | 19.8840 | .02675 | .00846 |
| | Mimics BB 1.5T 2.0mm | 10 | 18.9610 | 2.81917 | .89150 |
| h | Direct Phantom Cube | 10 | 19.9120 | .02974 | .00940 |
| | Mimics BB 1.5T 2.0mm | 10 | 19.9840 | .07137 | .02257 |
| i | Direct Phantom Cube | 10 | 49.8900 | .03266 | .01033 |
| | Mimics BB 1.5T 2.0mm | 10 | 49.6570 | .12455 | .03939 |
| j | Direct Phantom Cube | 10 | 19.9890 | .01524 | .00482 |
| | Mimics BB 1.5T 2.0mm | 10 | 20.0180 | .16538 | .05230 |
| hole | Direct Phantom Cube | 10 | 5.8370 | .04296 | .01359 |
| | Mimics BB 1.5T 2.0mm | 10 | 4.8940 | .07975 | .02522 |

| | Sig. (2-tailed) | Mean Difference | Std. Error Difference | 95% Confidence Interval of the Difference | |
|---|---|---|---|---|---|
| | | | | Lower | Upper |
| A | .002 | -.11200 | .03089 | -.17691 | -.04709 |
| B | .450 | -.05700 | .07384 | -.21212 | .09812 |
| C | .008 | -.09700 | .03243 | -.16513 | -.02887 |
| D | .000 | -.20400 | .02579 | -.25817 | -.14983 |
| E | .243 | .03500 | .02901 | -.02594 | .09594 |
| F | .189 | .12000 | .08790 | -.06467 | .30467 |
| G | .314 | .92300 | .89154 | -.95005 | 2.79605 |
| H | .009 | -.07200 | .02445 | -.12337 | -.02063 |
| I | .000 | .23300 | .04072 | .14746 | .31854 |
| J | .588 | -.02900 | .05252 | -.13934 | .08134 |
| Hole | .000 | .94300 | .02865 | .88282 | 1.00318 |

### *Direct Phantom v BB 1.5T 2.4mm*

| | Object | N | Mean | Std. Deviation | Std. Error Mean |
|---|---|---|---|---|---|
| a | Direct Phantom Cube | 10 | 60.1170 | .02791 | .00883 |
| | Mimics BB 1.5T 2.4mm | 10 | 60.0050 | .10648 | .03367 |
| b | Direct Phantom Cube | 10 | 60.0860 | .01776 | .00562 |
| | Mimics BB 1.5T 2.4mm | 10 | 59.5320 | .17980 | .05686 |
| c | Direct Phantom Cube | 10 | 20.0670 | .02908 | .00920 |
| | Mimics BB 1.5T 2.4mm | 10 | 19.8280 | .09223 | .02917 |
| d | Direct Phantom Cube | 10 | 20.0800 | .03464 | .01095 |
| | Mimics BB 1.5T 2.4mm | 10 | 19.8540 | .08996 | .02845 |
| e | Direct Phantom Cube | 10 | 60.1060 | .02914 | .00921 |
| | Mimics BB 1.5T 2.4mm | 10 | 59.6630 | .16753 | .05298 |
| f | Direct Phantom Cube | 10 | 60.1800 | .25342 | .08014 |
| | Mimics BB 1.5T 2.4mm | 10 | 59.6070 | .11814 | .03736 |
| g | Direct Phantom Cube | 10 | 19.8840 | .02675 | .00846 |
| | Mimics BB 1.5T 2.4mm | 10 | 19.5580 | .07899 | .02498 |
| h | Direct Phantom Cube | 10 | 19.9120 | .02974 | .00940 |
| | Mimics BB 1.5T 2.4mm | 10 | 19.6780 | .05493 | .01737 |
| i | Direct Phantom Cube | 10 | 49.8900 | .03266 | .01033 |
| | Mimics BB 1.5T 2.4mm | 10 | 49.3350 | .12439 | .03933 |
| j | Direct Phantom Cube | 10 | 19.9890 | .01524 | .00482 |
| | Mimics BB 1.5T 2.4mm | 10 | 19.2140 | .31729 | .10033 |
| hole | Direct Phantom Cube | 10 | 5.8370 | .04296 | .01359 |
| | Mimics BB 1.5T 2.4mm | 10 | 5.2180 | .03360 | .01062 |

| | Sig. (2-tailed) | Mean Difference | Std. Error Difference | 95% Confidence Interval of the Difference | |
|---|---|---|---|---|---|
| | | | | Lower | Upper |
| a | .005 | .11200 | .03481 | .03887 | .18513 |
| b | .000 | .55400 | .05714 | .43396 | .67404 |
| c | .000 | .23900 | .03058 | .17475 | .30325 |
| d | .000 | .22600 | .03048 | .16195 | .29005 |
| e | .000 | .44300 | .05377 | .33002 | .55598 |
| f | .000 | .57300 | .08842 | .38724 | .75876 |
| g | .000 | .32600 | .02637 | .27059 | .38141 |
| h | .000 | .23400 | .01975 | .19250 | .27550 |
| i | .000 | .55500 | .04067 | .46956 | .64044 |
| j | .000 | .77500 | .10045 | .56396 | .98604 |
| hole | .000 | .61900 | .01725 | .58277 | .65523 |

## *Direct Phantom v BB 3.0T 0.8mm*

| | Object | N | Mean | Std. Deviation | Std. Error Mean |
|---|---|---|---|---|---|
| a | Direct Phantom Cube | 10 | 60.1170 | .02791 | .00883 |
| | Mimics BB 3.0T 0.8mm | 10 | 59.2020 | .26997 | .08537 |
| b | Direct Phantom Cube | 10 | 60.0860 | .01776 | .00562 |
| | Mimics BB 3.0T 0.8mm | 10 | 59.2640 | .06433 | .02034 |
| c | Direct Phantom Cube | 10 | 20.0670 | .02908 | .00920 |
| | Mimics BB 3.0T 0.8mm | 10 | 19.2440 | .25937 | .08202 |
| d | Direct Phantom Cube | 10 | 20.0800 | .03464 | .01095 |
| | Mimics BB 3.0T 0.8mm | 10 | 19.3990 | .15871 | .05019 |
| e | Direct Phantom Cube | 10 | 60.1060 | .02914 | .00921 |
| | Mimics BB 3.0T 0.8mm | 10 | 59.8300 | .17288 | .05467 |
| f | Direct Phantom Cube | 10 | 60.1800 | .25342 | .08014 |
| | Mimics BB 3.0T 0.8mm | 10 | 59.4760 | .20173 | .06379 |
| g | Direct Phantom Cube | 10 | 19.8840 | .02675 | .00846 |
| | Mimics BB 3.0T 0.8mm | 10 | 19.3830 | .30562 | .09664 |
| h | Direct Phantom Cube | 10 | 19.9120 | .02974 | .00940 |
| | Mimics BB 3.0T 0.8mm | 10 | 19.1940 | .12103 | .03827 |
| i | Direct Phantom Cube | 10 | 49.8900 | .03266 | .01033 |
| | Mimics BB 3.0T 0.8mm | 10 | 49.7150 | .12131 | .03836 |
| j | Direct Phantom Cube | 10 | 19.9890 | .01524 | .00482 |
| | Mimics BB 3.0T 0.8mm | 10 | 19.8450 | .05930 | .01875 |
| hole | Direct Phantom Cube | 10 | 5.8370 | .04296 | .01359 |
| | Mimics BB 3.0T 0.8mm | 10 | 6.4670 | .09511 | .03008 |

| | Sig. (2-tailed) | Mean Difference | Std. Error Difference | 95% Confidence Interval of the Difference | |
|---|---|---|---|---|---|
| | | | | Lower | Upper |
| a | .000 | .91500 | .08583 | .73468 | 1.09532 |
| b | .000 | .82200 | .02110 | .77766 | .86634 |
| c | .000 | .82300 | .08253 | .64960 | .99640 |
| d | .000 | .68100 | .05137 | .57308 | .78892 |
| e | .000 | .27600 | .05544 | .15952 | .39248 |
| f | .000 | .70400 | .10243 | .48881 | .91919 |
| g | .000 | .50100 | .09701 | .29718 | .70482 |
| h | .000 | .71800 | .03941 | .63520 | .80080 |
| i | .000 | .17500 | .03973 | .09153 | .25847 |
| j | .000 | .14400 | .01936 | .10332 | .18468 |
| hole | .000 | -.63000 | .03300 | -.69933 | -.56067 |

## *Direct Phantom v BB 3.0T 1.2mm*

| | Object | N | Mean | Std. Deviation | Std. Error Mean |
|---|---|---|---|---|---|
| a | Direct Phantom Cube | 10 | 60.1170 | .02791 | .00883 |
| | Mimics BB 3.0T 1.2mm | 10 | 59.8270 | .10361 | .03276 |
| b | Direct Phantom Cube | 10 | 60.0860 | .01776 | .00562 |
| | Mimics BB 3.0T 1.2mm | 10 | 59.7790 | .10016 | .03167 |
| c | Direct Phantom Cube | 10 | 20.0670 | .02908 | .00920 |
| | Mimics BB 3.0T 1.2mm | 10 | 19.9460 | .08222 | .02600 |
| d | Direct Phantom Cube | 10 | 20.0800 | .03464 | .01095 |
| | Mimics BB 3.0T 1.2mm | 10 | 19.9840 | .08656 | .02737 |
| e | Direct Phantom Cube | 10 | 60.1060 | .02914 | .00921 |
| | Mimics BB 3.0T 1.2mm | 10 | 59.7870 | .15232 | .04817 |
| f | Direct Phantom Cube | 10 | 60.1800 | .25342 | .08014 |
| | Mimics BB 3.0T 1.2mm | 10 | 60.0820 | .08879 | .02808 |
| g | Direct Phantom Cube | 10 | 19.8840 | .02675 | .00846 |
| | Mimics BB 3.0T 1.2mm | 10 | 19.8730 | .11643 | .03682 |
| h | Direct Phantom Cube | 10 | 19.9120 | .02974 | .00940 |
| | Mimics BB 3.0T 1.2mm | 10 | 19.8400 | .11671 | .03691 |
| i | Direct Phantom Cube | 10 | 49.8900 | .03266 | .01033 |
| | Mimics BB 3.0T 1.2mm | 10 | 49.6260 | .11645 | .03682 |
| j | Direct Phantom Cube | 10 | 19.9890 | .01524 | .00482 |
| | Mimics BB 3.0T 1.2mm | 10 | 19.9550 | .16702 | .05282 |
| hole | Direct Phantom Cube | 10 | 5.8370 | .04296 | .01359 |
| | Mimics BB 3.0T 1.2mm | 10 | 5.5890 | .10192 | .03223 |

| | Sig. (2-tailed) | Mean Difference | Std. Error Difference | 95% Confidence Interval of the Difference | |
|---|---|---|---|---|---|
| | | | | Lower | Upper |
| a | .000 | .29000 | .03393 | .21871 | .36129 |
| b | .000 | .30700 | .03217 | .23942 | .37458 |
| c | .000 | .12100 | .02758 | .06306 | .17894 |
| d | .004 | .09600 | .02948 | .03406 | .15794 |
| e | .000 | .31900 | .04904 | .21597 | .42203 |
| f | .264 | .09800 | .08492 | -.08040 | .27640 |
| g | .774 | .01100 | .03778 | -.06837 | .09037 |
| h | .075 | .07200 | .03809 | -.00802 | .15202 |
| i | .000 | .26400 | .03824 | .18365 | .34435 |
| j | .530 | .03400 | .05303 | -.07742 | .14542 |
| hole | .000 | .24800 | .03498 | .17452 | .32148 |

### *Direct Phantom v BB 3.0T 2.0mm*

| | Object | N | Mean | Std. Deviation | Std. Error Mean |
|---|---|---|---|---|---|
| a | Direct Phantom Cube | 10 | 60.1170 | .02791 | .00883 |
| | Mimics BB 3.0T 2.0mm | 10 | 59.8590 | .22378 | .07076 |
| b | Direct Phantom Cube | 10 | 60.0860 | .01776 | .00562 |
| | Mimics BB 3.0T 2.0mm | 10 | 60.0430 | .19704 | .06231 |
| c | Direct Phantom Cube | 10 | 20.0670 | .02908 | .00920 |
| | Mimics BB 3.0T 2.0mm | 10 | 19.8330 | .09358 | .02959 |
| d | Direct Phantom Cube | 10 | 20.0800 | .03464 | .01095 |
| | Mimics BB 3.0T 2.0mm | 10 | 19.9170 | .11954 | .03780 |
| e | Direct Phantom Cube | 10 | 60.1060 | .02914 | .00921 |
| | Mimics BB 3.0T 2.0mm | 10 | 59.8600 | .08524 | .02696 |
| f | Direct Phantom Cube | 10 | 60.1800 | .25342 | .08014 |
| | Mimics BB 3.0T 2.0mm | 10 | 60.2590 | .12627 | .03993 |
| g | Direct Phantom Cube | 10 | 19.8840 | .02675 | .00846 |
| | Mimics BB 3.0T 2.0mm | 10 | 19.7820 | .08702 | .02752 |
| h | Direct Phantom Cube | 10 | 19.9120 | .02974 | .00940 |
| | Mimics BB 3.0T 2.0mm | 10 | 19.7220 | .07115 | .02250 |
| i | Direct Phantom Cube | 10 | 49.8900 | .03266 | .01033 |
| | Mimics BB 3.0T 2.0mm | 10 | 49.6250 | .09710 | .03070 |
| j | Direct Phantom Cube | 10 | 19.9890 | .01524 | .00482 |
| | Mimics BB 3.0T 2.0mm | 10 | 20.0560 | .06059 | .01916 |
| hole | Direct Phantom Cube | 10 | 5.8370 | .04296 | .01359 |
| | Mimics BB 3.0T 2.0mm | 10 | 5.5200 | .54244 | .17154 |

| | Sig. (2-tailed) | Mean Difference | Std. Error Difference | 95% Confidence Interval of the Difference | |
|---|---|---|---|---|---|
| | | | | Lower | Upper |
| a | .002 | .25800 | .07131 | .10818 | .40782 |
| b | .501 | .04300 | .06256 | -.08844 | .17444 |
| c | .000 | .23400 | .03099 | .16890 | .29910 |
| d | .001 | .16300 | .03936 | .08031 | .24569 |
| e | .000 | .24600 | .02849 | .18615 | .30585 |
| f | .389 | -.07900 | .08954 | -.26711 | .10911 |
| g | .002 | .10200 | .02879 | .04151 | .16249 |
| h | .000 | .19000 | .02439 | .13877 | .24123 |
| i | .000 | .26500 | .03240 | .19694 | .33306 |
| j | .003 | -.06700 | .01976 | -.10851 | -.02549 |
| hole | .082 | .31700 | .17207 | -.04451 | .67851 |

## *Direct Phantom v BB 3.0T 2.4mm*

| | Object | N | Mean | Std. Deviation | Std. Error Mean |
|---|---|---|---|---|---|
| a | Direct Phantom Cube | 10 | 60.1170 | .02791 | .00883 |
| | Mimics 3.0T 2.4mm | 10 | 60.0140 | .10700 | .03384 |
| b | Direct Phantom Cube | 10 | 60.0860 | .01776 | .00562 |
| | Mimics 3.0T 2.4mm | 10 | 60.0560 | .10373 | .03280 |
| c | Direct Phantom Cube | 10 | 20.0670 | .02908 | .00920 |
| | Mimics 3.0T 2.4mm | 10 | 19.7970 | .09742 | .03081 |
| d | Direct Phantom Cube | 10 | 20.0800 | .03464 | .01095 |
| | Mimics 3.0T 2.4mm | 10 | 19.9210 | .09134 | .02888 |
| e | Direct Phantom Cube | 10 | 60.1060 | .02914 | .00921 |
| | Mimics 3.0T 2.4mm | 10 | 59.8230 | .12945 | .04093 |
| f | Direct Phantom Cube | 10 | 60.1800 | .25342 | .08014 |
| | Mimics 3.0T 2.4mm | 10 | 59.9070 | .10833 | .03426 |
| g | Direct Phantom Cube | 10 | 19.8840 | .02675 | .00846 |
| | Mimics 3.0T 2.4mm | 10 | 19.7440 | .09228 | .02918 |
| h | Direct Phantom Cube | 10 | 19.9120 | .02974 | .00940 |
| | Mimics 3.0T 2.4mm | 10 | 19.7150 | .09034 | .02857 |
| i | Direct Phantom Cube | 10 | 49.8900 | .03266 | .01033 |
| | Mimics 3.0T 2.4mm | 10 | 49.3190 | .19422 | .06142 |
| j | Direct Phantom Cube | 10 | 19.9890 | .01524 | .00482 |
| | Mimics 3.0T 2.4mm | 10 | 20.3220 | .07208 | .02279 |
| hole | Direct Phantom Cube | 10 | 5.8370 | .04296 | .01359 |
| | Mimics 3.0T 2.4mm | 10 | 5.5460 | .40379 | .12769 |

| | Sig. (2-tailed) | Mean Difference | Std. Error Difference | 95% Confidence Interval of the Difference | |
|---|---|---|---|---|---|
| | | | | Lower | Upper |
| a | .009 | .10300 | .03497 | .02953 | .17647 |
| b | .379 | .03000 | .03328 | -.03992 | .09992 |
| c | .000 | .27000 | .03215 | .20246 | .33754 |
| d | .000 | .15900 | .03089 | .09410 | .22390 |
| e | .000 | .28300 | .04196 | .19485 | .37115 |
| f | .006 | .27300 | .08715 | .08990 | .45610 |
| g | .000 | .14000 | .03038 | .07617 | .20383 |
| h | .000 | .19700 | .03008 | .13381 | .26019 |
| i | .000 | .57100 | .06228 | .44015 | .70185 |
| j | .000 | -.33300 | .02330 | -.38195 | -.28405 |
| hole | .036 | .29100 | .12841 | .02122 | .56078 |

## *Direct Phantom v CT Face Bone 0.625mm*

| | Object | N | Mean | Std. Deviation | Std. Error Mean |
|---|---|---|---|---|---|
| a | Direct Phantom Cube | 10 | 60.1170 | .02791 | .00883 |
| | Mimics CT Face Bone 0.625mm | 10 | 60.2810 | .09183 | .02904 |
| b | Direct Phantom Cube | 10 | 60.0860 | .01776 | .00562 |
| | Mimics CT Face Bone 0.625mm | 10 | 60.2660 | .57268 | .18110 |
| c | Direct Phantom Cube | 10 | 20.0670 | .02908 | .00920 |
| | Mimics CT Face Bone 0.625mm | 10 | 20.3530 | .19097 | .06039 |
| d | Direct Phantom Cube | 10 | 20.0800 | .03464 | .01095 |
| | Mimics CT Face Bone 0.625mm | 10 | 20.8940 | .36963 | .11689 |
| e | Direct Phantom Cube | 10 | 60.1060 | .02914 | .00921 |
| | Mimics CT Face Bone 0.625mm | 10 | 60.2310 | .18788 | .05941 |
| f | Direct Phantom Cube | 10 | 60.1800 | .25342 | .08014 |
| | Mimics CT Face Bone 0.625mm | 10 | 60.3540 | .15813 | .05000 |
| g | Direct Phantom Cube | 10 | 19.8840 | .02675 | .00846 |
| | Mimics CT Face Bone 0.625mm | 10 | 20.0200 | .17569 | .05556 |
| h | Direct Phantom Cube | 10 | 19.9120 | .02974 | .00940 |
| | Mimics CT Face Bone 0.625mm | 10 | 19.9540 | .12149 | .03842 |
| i | Direct Phantom Cube | 10 | 49.8900 | .03266 | .01033 |
| | Mimics CT Face Bone 0.625mm | 10 | 50.5320 | .51551 | .16302 |
| j | Direct Phantom Cube | 10 | 19.9890 | .01524 | .00482 |
| | Mimics CT Face Bone 0.625mm | 10 | 19.9450 | .33530 | .10603 |
| hole | Direct Phantom Cube | 10 | 5.8370 | .04296 | .01359 |
| | Mimics CT Face Bone 0.625mm | 10 | 5.7440 | .35290 | .11160 |

| | Sig. (2-tailed) | Mean Difference | Std. Error Difference | 95% Confidence Interval of the Difference | |
|---|---|---|---|---|---|
| | | | | Lower | Upper |
| a | .000 | -.16400 | .03035 | -.22776 | -.10024 |
| b | .334 | -.18000 | .18118 | -.56065 | .20065 |
| c | .000 | -.28600 | .06108 | -.41433 | -.15767 |
| d | .000 | -.81400 | .11740 | -1.06065 | -.56735 |
| e | .052 | -.12500 | .06012 | -.25131 | .00131 |
| f | .082 | -.17400 | .09446 | -.37245 | .02445 |
| g | .026 | -.13600 | .05620 | -.25407 | -.01793 |
| h | .302 | -.04200 | .03955 | -.12510 | .04110 |
| i | .001 | -.64200 | .16335 | -.98518 | -.29882 |
| j | .683 | .04400 | .10614 | -.17899 | .26699 |
| hole | .419 | .09300 | .11242 | -.14319 | .32919 |

### *Direct Phantom v CT Face Bone 1.25mm*

| | Object | N | Mean | Std. Deviation | Std. Error Mean |
|---|---|---|---|---|---|
| a | Direct Phantom Cube | 10 | 60.1170 | .02791 | .00883 |
| | Mimics CT Face Bone 1.25mm | 10 | 60.0400 | .17082 | .05402 |
| b | Direct Phantom Cube | 10 | 60.0860 | .01776 | .00562 |
| | Mimics CT Face Bone 1.25mm | 10 | 60.1080 | .34071 | .10774 |
| c | Direct Phantom Cube | 10 | 20.0670 | .02908 | .00920 |
| | Mimics CT Face Bone 1.25mm | 10 | 20.4230 | .55468 | .17540 |
| d | Direct Phantom Cube | 10 | 20.0800 | .03464 | .01095 |
| | Mimics CT Face Bone 1.25mm | 10 | 20.4260 | .69676 | .22033 |
| e | Direct Phantom Cube | 10 | 60.1060 | .02914 | .00921 |
| | Mimics CT Face Bone 1.25mm | 10 | 60.2600 | .59114 | .18693 |
| f | Direct Phantom Cube | 10 | 60.1800 | .25342 | .08014 |
| | Mimics CT Face Bone 1.25mm | 10 | 60.0640 | .15050 | .04759 |
| g | Direct Phantom Cube | 10 | 19.8840 | .02675 | .00846 |
| | Mimics CT Face Bone 1.25mm | 10 | 19.6590 | .13836 | .04375 |
| h | Direct Phantom Cube | 10 | 19.9120 | .02974 | .00940 |
| | Mimics CT Face Bone 1.25mm | 10 | 19.7930 | .20122 | .06363 |
| i | Direct Phantom Cube | 10 | 49.8900 | .03266 | .01033 |
| | Mimics CT Face Bone 1.25mm | 10 | 49.7810 | .21346 | .06750 |
| j | Direct Phantom Cube | 10 | 19.9890 | .01524 | .00482 |
| | Mimics CT Face Bone 1.25mm | 10 | 18.9870 | .18607 | .05884 |
| hole | Direct Phantom Cube | 10 | 5.8370 | .04296 | .01359 |
| | Mimics CT Face Bone 1.25mm | 10 | 5.9870 | .35428 | .11203 |

| | Sig. (2-tailed) | Mean Difference | Std. Error Difference | 95% Confidence Interval of the Difference | |
|---|---|---|---|---|---|
| | | | | Lower | Upper |
| a | .177 | .07700 | .05473 | -.03799 | .19199 |
| b | .841 | -.02200 | .10789 | -.24867 | .20467 |
| c | .058 | -.35600 | .17565 | -.72502 | .01302 |
| d | .134 | -.34600 | .22061 | -.80948 | .11748 |
| e | .421 | -.15400 | .18716 | -.54721 | .23921 |
| f | .229 | .11600 | .09320 | -.07982 | .31182 |
| g | .000 | .22500 | .04456 | .13138 | .31862 |
| h | .081 | .11900 | .06432 | -.01614 | .25414 |
| i | .128 | .10900 | .06829 | -.03447 | .25247 |
| j | .000 | 1.00200 | .05904 | .87796 | 1.12604 |
| hole | .200 | -.15000 | .11285 | -.38710 | .08710 |

## *Direct Phantom v CT Face Bone 2.5mm*

| | Object | N | Mean | Std. Deviation | Std. Error Mean |
|---|---|---|---|---|---|
| a | Direct Phantom Cube | 10 | 60.1170 | .02791 | .00883 |
| | Mimics CT Face Bone 2.5mm | 10 | 59.8250 | .06916 | .02187 |
| b | Direct Phantom Cube | 10 | 60.0860 | .01776 | .00562 |
| | Mimics CT Face Bone 2.5mm | 10 | 60.1970 | .42510 | .13443 |
| c | Direct Phantom Cube | 10 | 20.0670 | .02908 | .00920 |
| | Mimics CT Face Bone 2.5mm | 10 | 20.0230 | .25781 | .08153 |
| d | Direct Phantom Cube | 10 | 20.0800 | .03464 | .01095 |
| | Mimics CT Face Bone 2.5mm | 10 | 19.8330 | .09821 | .03106 |
| e | Direct Phantom Cube | 10 | 60.1060 | .02914 | .00921 |
| | Mimics CT Face Bone 2.5mm | 10 | 59.9350 | .16112 | .05095 |
| f | Direct Phantom Cube | 10 | 60.1800 | .25342 | .08014 |
| | Mimics CT Face Bone 2.5mm | 10 | 59.7580 | .10644 | .03366 |
| g | Direct Phantom Cube | 10 | 19.8840 | .02675 | .00846 |
| | Mimics CT Face Bone 2.5mm | 10 | 19.6850 | .13802 | .04365 |
| h | Direct Phantom Cube | 10 | 19.9120 | .02974 | .00940 |
| | Mimics CT Face Bone 2.5mm | 10 | 19.5860 | .10564 | .03341 |
| i | Direct Phantom Cube | 10 | 49.8900 | .03266 | .01033 |
| | Mimics CT Face Bone 2.5mm | 10 | 49.9480 | .53040 | .16773 |
| j | Direct Phantom Cube | 10 | 19.9890 | .01524 | .00482 |
| | Mimics CT Face Bone 2.5mm | 10 | 19.1650 | .12313 | .03894 |
| hole | Direct Phantom Cube | 10 | 5.8370 | .04296 | .01359 |
| | Mimics CT Face Bone 2.5mm | 10 | 5.7070 | .11615 | .03673 |

| | Sig. (2-tailed) | Mean Difference | Std. Error Difference | 95% Confidence Interval of the Difference | |
|---|---|---|---|---|---|
| | | | | Lower | Upper |
| a | .000 | .29200 | .02358 | .24245 | .34155 |
| b | .420 | -.11100 | .13455 | -.39367 | .17167 |
| c | .598 | .04400 | .08204 | -.12837 | .21637 |
| d | .000 | .24700 | .03293 | .17781 | .31619 |
| e | .004 | .17100 | .05178 | .06222 | .27978 |
| f | .000 | .42200 | .08692 | .23939 | .60461 |
| g | .000 | .19900 | .04446 | .10560 | .29240 |
| h | .000 | .32600 | .03471 | .25309 | .39891 |
| i | .734 | -.05800 | .16805 | -.41105 | .29505 |
| j | .000 | .82400 | .03923 | .74157 | .90643 |
| hole | .004 | .13000 | .03916 | .04773 | .21227 |

## *Direct Phantom v CT Face ST 0.625mm*

| | Object | N | Mean | Std. Deviation | Std. Error Mean |
|---|---|---|---|---|---|
| a | Direct Phantom Cube | 10 | 60.1170 | .02791 | .00883 |
| | Mimics CT Face ST 0.625mm | 10 | 60.5350 | .12002 | .03795 |
| b | Direct Phantom Cube | 10 | 60.0860 | .01776 | .00562 |
| | Mimics CT Face ST 0.625mm | 10 | 60.6820 | .05266 | .01665 |
| c | Direct Phantom Cube | 10 | 20.0670 | .02908 | .00920 |
| | Mimics CT Face ST 0.625mm | 10 | 20.4360 | .17258 | .05457 |
| d | Direct Phantom Cube | 10 | 20.0800 | .03464 | .01095 |
| | Mimics CT Face ST 0.625mm | 10 | 20.5900 | .16337 | .05166 |
| e | Direct Phantom Cube | 10 | 60.1060 | .02914 | .00921 |
| | Mimics CT Face ST 0.625mm | 10 | 60.4860 | .08959 | .02833 |
| f | Direct Phantom Cube | 10 | 60.1800 | .25342 | .08014 |
| | Mimics CT Face ST 0.625mm | 10 | 60.6650 | .13452 | .04254 |
| g | Direct Phantom Cube | 10 | 19.8840 | .02675 | .00846 |
| | Mimics CT Face ST 0.625mm | 10 | 20.1080 | .23132 | .07315 |
| h | Direct Phantom Cube | 10 | 19.9120 | .02974 | .00940 |
| | Mimics CT Face ST 0.625mm | 10 | 20.2410 | .25968 | .08212 |
| i | Direct Phantom Cube | 10 | 49.8900 | .03266 | .01033 |
| | Mimics CT Face ST 0.625mm | 10 | 47.2930 | 9.51722 | 3.00961 |
| j | Direct Phantom Cube | 10 | 19.9890 | .01524 | .00482 |
| | Mimics CT Face ST 0.625mm | 10 | 20.3080 | .10326 | .03265 |
| hole | Direct Phantom Cube | 10 | 5.8370 | .04296 | .01359 |
| | Mimics CT Face ST 0.625mm | 10 | 5.4580 | .23146 | .07319 |

| | Sig. (2-tailed) | Mean Difference | Std. Error Difference | 95% Confidence Interval of the Difference | |
|---|---|---|---|---|---|
| | | | | Lower | Upper |
| a | .000 | -.41800 | .03897 | -.49987 | -.33613 |
| b | .000 | -.59600 | .01758 | -.63292 | -.55908 |
| c | .000 | -.36900 | .05534 | -.48527 | -.25273 |
| d | .000 | -.51000 | .05281 | -.62095 | -.39905 |
| e | .000 | -.38000 | .02979 | -.44259 | -.31741 |
| f | .000 | -.48500 | .09073 | -.67561 | -.29439 |
| g | .007 | -.22400 | .07364 | -.37870 | -.06930 |
| h | .001 | -.32900 | .08265 | -.50265 | -.15535 |
| i | .400 | 2.59700 | 3.00963 | -3.72599 | 8.91999 |
| j | .000 | -.31900 | .03301 | -.38834 | -.24966 |
| hole | .000 | .37900 | .07444 | .22260 | .53540 |

### *Direct Phantom v CT Face ST 1.25mm*

| | Object | N | Mean | Std. Deviation | Std. Error Mean |
|---|---|---|---|---|---|
| a | Direct Phantom Cube | 10 | 60.1170 | .02791 | .00883 |
| | Mimics CT Face ST 1.25mm | 10 | 60.5630 | .08718 | .02757 |
| b | Direct Phantom Cube | 10 | 60.0860 | .01776 | .00562 |
| | Mimics CT Face ST 1.25mm | 10 | 60.7610 | .08504 | .02689 |
| c | Direct Phantom Cube | 10 | 20.0670 | .02908 | .00920 |
| | Mimics CT Face ST 1.25mm | 10 | 20.4690 | .12991 | .04108 |
| d | Direct Phantom Cube | 10 | 20.0800 | .03464 | .01095 |
| | Mimics CT Face ST 1.25mm | 10 | 20.4870 | .09684 | .03062 |
| e | Direct Phantom Cube | 10 | 60.1060 | .02914 | .00921 |
| | Mimics CT Face ST 1.25mm | 10 | 60.4530 | .13124 | .04150 |
| f | Direct Phantom Cube | 10 | 60.1800 | .25342 | .08014 |
| | Mimics CT Face ST 1.25mm | 10 | 60.6490 | .13270 | .04196 |
| g | Direct Phantom Cube | 10 | 19.8840 | .02675 | .00846 |
| | Mimics CT Face ST 1.25mm | 10 | 20.1180 | .12291 | .03887 |
| h | Direct Phantom Cube | 10 | 19.9120 | .02974 | .00940 |
| | Mimics CT Face ST 1.25mm | 10 | 20.1880 | .15859 | .05015 |
| i | Direct Phantom Cube | 10 | 49.8900 | .03266 | .01033 |
| | Mimics CT Face ST 1.25mm | 10 | 50.1300 | .10812 | .03419 |
| j | Direct Phantom Cube | 10 | 19.9890 | .01524 | .00482 |
| | Mimics CT Face ST 1.25mm | 10 | 20.3200 | .11106 | .03512 |
| hole | Direct Phantom Cube | 10 | 5.8370 | .04296 | .01359 |
| | Mimics CT Face ST 1.25mm | 10 | 5.1320 | .32564 | .10298 |

| | Sig. (2-tailed) | Mean Difference | Std. Error Difference | 95% Confidence Interval of the Difference | |
|---|---|---|---|---|---|
| | | | | Lower | Upper |
| a | .000 | -.44600 | .02895 | -.50682 | -.38518 |
| b | .000 | -.67500 | .02747 | -.73272 | -.61728 |
| c | .000 | -.40200 | .04210 | -.49044 | -.31356 |
| d | .000 | -.40700 | .03253 | -.47533 | -.33867 |
| e | .000 | -.34700 | .04251 | -.43631 | -.25769 |
| f | .000 | -.46900 | .09046 | -.65905 | -.27895 |
| g | .000 | -.23400 | .03978 | -.31757 | -.15043 |
| h | .000 | -.27600 | .05103 | -.38320 | -.16880 |
| i | .000 | -.24000 | .03571 | -.31503 | -.16497 |
| j | .000 | -.33100 | .03545 | -.40547 | -.25653 |
| hole | .000 | .70500 | .10387 | .48678 | .92322 |

## *Direct Phantom v CT face ST 2.5mm*

| | Object | N | Mean | Std. Deviation | Std. Error Mean |
|---|---|---|---|---|---|
| a | Direct Phantom Cube | 10 | 60.1170 | .02791 | .00883 |
| | Mimics CT Face ST 2.5mm | 10 | 59.9010 | .17929 | .05670 |
| b | Direct Phantom Cube | 10 | 60.0860 | .01776 | .00562 |
| | Mimics CT Face ST 2.5mm | 10 | 60.1210 | .14625 | .04625 |
| c | Direct Phantom Cube | 10 | 20.0670 | .02908 | .00920 |
| | Mimics CT Face ST 2.5mm | 10 | 19.9360 | .10255 | .03243 |
| d | Direct Phantom Cube | 10 | 20.0800 | .03464 | .01095 |
| | Mimics CT Face ST 2.5mm | 10 | 20.0690 | .12041 | .03808 |
| e | Direct Phantom Cube | 10 | 60.1060 | .02914 | .00921 |
| | Mimics CT Face ST 2.5mm | 10 | 59.9940 | .05103 | .01614 |
| f | Direct Phantom Cube | 10 | 60.1800 | .25342 | .08014 |
| | Mimics CT Face ST 2.5mm | 10 | 59.7490 | .10203 | .03226 |
| g | Direct Phantom Cube | 10 | 19.8840 | .02675 | .00846 |
| | Mimics CT Face ST 2.5mm | 10 | 19.8290 | .13804 | .04365 |
| h | Direct Phantom Cube | 10 | 19.9120 | .02974 | .00940 |
| | Mimics CT Face ST 2.5mm | 10 | 19.8360 | .23978 | .07582 |
| i | Direct Phantom Cube | 10 | 49.8900 | .03266 | .01033 |
| | Mimics CT Face ST 2.5mm | 10 | 49.6730 | .06430 | .02033 |
| j | Direct Phantom Cube | 10 | 19.9890 | .01524 | .00482 |
| | Mimics CT Face ST 2.5mm | 10 | 20.0780 | .07927 | .02507 |
| hole | Direct Phantom Cube | 10 | 5.8370 | .04296 | .01359 |
| | Mimics CT Face ST 2.5mm | 10 | 5.3500 | .22721 | .07185 |

| | Sig. (2-tailed) | Mean Difference | Std. Error Difference | 95% Confidence Interval of the Difference | |
|---|---|---|---|---|---|
| | | | | Lower | Upper |
| a | .001 | .21600 | .05738 | .09545 | .33655 |
| b | .462 | -.03500 | .04659 | -.13288 | .06288 |
| c | .001 | .13100 | .03371 | .06019 | .20181 |
| d | .784 | .01100 | .03962 | -.07224 | .09424 |
| e | .000 | .11200 | .01858 | .07296 | .15104 |
| f | .000 | .43100 | .08639 | .24950 | .61250 |
| g | .232 | .05500 | .04446 | -.03841 | .14841 |
| h | .333 | .07600 | .07641 | -.08452 | .23652 |
| i | .000 | .21700 | .02281 | .16909 | .26491 |
| j | .003 | -.08900 | .02553 | -.14263 | -.03537 |
| hole | .000 | .48700 | .07312 | .33338 | .64062 |

## *Direct Phantom v CT Helical Bone 0.625*

| | Object | N | Mean | Std. Deviation | Std. Error Mean |
|---|---|---|---|---|---|
| a | Direct Phantom Cube | 10 | 60.1170 | .02791 | .00883 |
| | Mimics CT Helical Bone 0.625mm | 10 | 59.8570 | .14728 | .04657 |
| b | Direct Phantom Cube | 10 | 60.0860 | .01776 | .00562 |
| | Mimics CT Helical Bone 0.625mm | 10 | 59.7890 | .17065 | .05396 |
| c | Direct Phantom Cube | 10 | 20.0670 | .02908 | .00920 |
| | Mimics CT Helical Bone 0.625mm | 10 | 19.8510 | .05820 | .01841 |
| d | Direct Phantom Cube | 10 | 20.0800 | .03464 | .01095 |
| | Mimics CT Helical Bone 0.625mm | 10 | 19.9770 | .16371 | .05177 |
| e | Direct Phantom Cube | 10 | 60.1060 | .02914 | .00921 |
| | Mimics CT Helical Bone 0.625mm | 10 | 59.7990 | .10918 | .03453 |
| f | Direct Phantom Cube | 10 | 60.1800 | .25342 | .08014 |
| | Mimics CT Helical Bone 0.625mm | 10 | 60.1490 | .27424 | .08672 |
| g | Direct Phantom Cube | 10 | 19.8840 | .02675 | .00846 |
| | Mimics CT Helical Bone 0.625mm | 10 | 19.5320 | .07376 | .02332 |
| h | Direct Phantom Cube | 10 | 19.9120 | .02974 | .00940 |
| | Mimics CT Helical Bone 0.625mm | 10 | 19.6140 | .13117 | .04148 |
| i | Direct Phantom Cube | 10 | 49.8900 | .03266 | .01033 |
| | Mimics CT Helical Bone 0.625mm | 10 | 49.5780 | .19860 | .06280 |
| j | Direct Phantom Cube | 10 | 19.9890 | .01524 | .00482 |
| | Mimics CT Helical Bone 0.625mm | 10 | 19.7360 | .11862 | .03751 |
| hole | Direct Phantom Cube | 10 | 5.8370 | .04296 | .01359 |
| | Mimics CT Helical Bone 0.625mm | 10 | 6.4040 | .09180 | .02903 |

| | Sig. (2-tailed) | Mean Difference | Std. Error Difference | 95% Confidence Interval of the Difference | |
|---|---|---|---|---|---|
| | | | | Lower | Upper |
| a | .000 | .26000 | .04740 | .16041 | .35959 |
| b | .000 | .29700 | .05426 | .18301 | .41099 |
| c | .000 | .21600 | .02058 | .17277 | .25923 |
| d | .067 | .10300 | .05292 | -.00817 | .21417 |
| e | .000 | .30700 | .03574 | .23192 | .38208 |
| f | .796 | .03100 | .11808 | -.21708 | .27908 |
| g | .000 | .35200 | .02481 | .29988 | .40412 |
| h | .000 | .29800 | .04253 | .20865 | .38735 |
| i | .000 | .31200 | .06364 | .17829 | .44571 |
| j | .000 | .25300 | .03782 | .17354 | .33246 |
| hole | .000 | -.56700 | .03205 | -.63434 | -.49966 |

### *Direct Phantom v CT Helical Bone 1.25mm*

| Object | | N | Mean | Std. Deviation | Std. Error Mean |
|---|---|---|---|---|---|
| a | Direct Phantom Cube | 10 | 60.1170 | .02791 | .00883 |
| | Mimics CT Helical Bone 1.25mm | 10 | 59.9120 | .13807 | .04366 |
| b | Direct Phantom Cube | 10 | 60.0860 | .01776 | .00562 |
| | Mimics CT Helical Bone 1.25mm | 10 | 60.1240 | .26680 | .08437 |
| c | Direct Phantom Cube | 10 | 20.0670 | .02908 | .00920 |
| | Mimics CT Helical Bone 1.25mm | 10 | 19.9720 | .18128 | .05733 |
| d | Direct Phantom Cube | 10 | 20.0800 | .03464 | .01095 |
| | Mimics CT Helical Bone 1.25mm | 10 | 19.9280 | .13563 | .04289 |
| e | Direct Phantom Cube | 10 | 60.1060 | .02914 | .00921 |
| | Mimics CT Helical Bone 1.25mm | 10 | 59.9850 | .14089 | .04455 |
| f | Direct Phantom Cube | 10 | 60.1800 | .25342 | .08014 |
| | Mimics CT Helical Bone 1.25mm | 10 | 60.0130 | .06945 | .02196 |
| g | Direct Phantom Cube | 10 | 19.8840 | .02675 | .00846 |
| | Mimics CT Helical Bone 1.25mm | 10 | 19.7570 | .16740 | .05294 |
| h | Direct Phantom Cube | 10 | 19.9120 | .02974 | .00940 |
| | Mimics CT Helical Bone 1.25mm | 10 | 19.6990 | .08595 | .02718 |
| i | Direct Phantom Cube | 10 | 49.8900 | .03266 | .01033 |
| | Mimics CT Helical Bone 1.25mm | 10 | 49.6210 | .06540 | .02068 |
| j | Direct Phantom Cube | 10 | 19.9890 | .01524 | .00482 |
| | Mimics CT Helical Bone 1.25mm | 10 | 19.9670 | .13833 | .04374 |
| hole | Direct Phantom Cube | 10 | 5.8370 | .04296 | .01359 |
| | Mimics CT Helical Bone 1.25mm | 10 | 5.6640 | .18668 | .05903 |

| | Sig. (2-tailed) | Mean Difference | Std. Error Difference | 95% Confidence Interval of the Difference | |
|---|---|---|---|---|---|
| | | | | Lower | Upper |
| a | .000 | .20500 | .04454 | .11142 | .29858 |
| b | .659 | -.03800 | .08456 | -.21565 | .13965 |
| c | .119 | .09500 | .05806 | -.02698 | .21698 |
| d | .003 | .15200 | .04427 | .05900 | .24500 |
| e | .016 | .12100 | .04550 | .02542 | .21658 |
| f | .060 | .16700 | .08309 | -.00757 | .34157 |
| g | .029 | .12700 | .05361 | .01437 | .23963 |
| h | .000 | .21300 | .02876 | .15257 | .27343 |
| i | .000 | .26900 | .02312 | .22044 | .31756 |
| j | .623 | .02200 | .04401 | -.07046 | .11446 |
| hole | .010 | .17300 | .06058 | .04573 | .30027 |

## *Direct Phantom v CT Helical Bone 2.5mm*

| | Object | N | Mean | Std. Deviation | Std. Error Mean |
|---|---|---|---|---|---|
| a | Direct Phantom Cube | 10 | 60.1170 | .02791 | .00883 |
| | Mimics CT Helical Bone 2.5mm | 10 | 59.8970 | .14652 | .04633 |
| b | Direct Phantom Cube | 10 | 60.0860 | .01776 | .00562 |
| | Mimics CT Helical Bone 2.5mm | 10 | 60.0230 | .16337 | .05166 |
| c | Direct Phantom Cube | 10 | 20.0670 | .02908 | .00920 |
| | Mimics CT Helical Bone 2.5mm | 10 | 19.9550 | .07706 | .02437 |
| d | Direct Phantom Cube | 10 | 20.0800 | .03464 | .01095 |
| | Mimics CT Helical Bone 2.5mm | 10 | 19.8910 | .11406 | .03607 |
| e | Direct Phantom Cube | 10 | 60.1060 | .02914 | .00921 |
| | Mimics CT Helical Bone 2.5mm | 10 | 60.0050 | .16834 | .05323 |
| f | Direct Phantom Cube | 10 | 60.1800 | .25342 | .08014 |
| | Mimics CT Helical Bone 2.5mm | 10 | 59.7780 | .12682 | .04011 |
| g | Direct Phantom Cube | 10 | 19.8840 | .02675 | .00846 |
| | Mimics CT Helical Bone 2.5mm | 10 | 19.8310 | .21200 | .06704 |
| h | Direct Phantom Cube | 10 | 19.9120 | .02974 | .00940 |
| | Mimics CT Helical Bone 2.5mm | 10 | 19.5690 | .10071 | .03185 |
| i | Direct Phantom Cube | 10 | 49.8900 | .03266 | .01033 |
| | Mimics CT Helical Bone 2.5mm | 10 | 49.4870 | .10078 | .03187 |
| j | Direct Phantom Cube | 10 | 19.9890 | .01524 | .00482 |
| | Mimics CT Helical Bone 2.5mm | 10 | 19.6560 | .21511 | .06802 |
| hole | Direct Phantom Cube | 10 | 5.8370 | .04296 | .01359 |
| | Mimics CT Helical Bone 2.5mm | 10 | 5.4720 | .34676 | .10965 |

| | Sig. (2-tailed) | Mean Difference | Std. Error Difference | 95% Confidence Interval of the Difference | |
|---|---|---|---|---|---|
| | | | | Lower | Upper |
| a | .000 | .22000 | .04717 | .12091 | .31909 |
| b | .241 | .06300 | .05197 | -.04618 | .17218 |
| c | .000 | .11200 | .02605 | .05728 | .16672 |
| d | .000 | .18900 | .03770 | .10980 | .26820 |
| e | .078 | .10100 | .05403 | -.01250 | .21450 |
| f | .000 | .40200 | .08961 | .21373 | .59027 |
| g | .443 | .05300 | .06757 | -.08896 | .19496 |
| h | .000 | .34300 | .03321 | .27323 | .41277 |
| i | .000 | .40300 | .03350 | .33262 | .47338 |
| j | .000 | .33300 | .06819 | .18973 | .47627 |
| hole | .004 | .36500 | .11049 | .13286 | .59714 |

## *Direct Phantom v CT Helical ST 0.625*

| | Object | N | Mean | Std. Deviation | Std. Error Mean |
|---|---|---|---|---|---|
| a | Direct Phantom Cube | 10 | 60.1170 | .02791 | .00883 |
| | Mimics CT Helical ST 0.625mm | 10 | 60.3690 | .11939 | .03776 |
| b | Direct Phantom Cube | 10 | 60.0860 | .01776 | .00562 |
| | Mimics CT Helical ST 0.625mm | 10 | 60.2770 | .11643 | .03682 |
| c | Direct Phantom Cube | 10 | 20.0670 | .02908 | .00920 |
| | Mimics CT Helical ST 0.625mm | 10 | 20.2280 | .11183 | .03536 |
| d | Direct Phantom Cube | 10 | 20.0800 | .03464 | .01095 |
| | Mimics CT Helical ST 0.625mm | 10 | 20.3250 | .08250 | .02609 |
| e | Direct Phantom Cube | 10 | 60.1060 | .02914 | .00921 |
| | Mimics CT Helical ST 0.625mm | 10 | 60.2220 | .10768 | .03405 |
| f | Direct Phantom Cube | 10 | 60.1800 | .25342 | .08014 |
| | Mimics CT Helical ST 0.625mm | 10 | 60.2500 | .13728 | .04341 |
| g | Direct Phantom Cube | 10 | 19.8840 | .02675 | .00846 |
| | Mimics CT Helical ST 0.625mm | 10 | 19.9140 | .07589 | .02400 |
| h | Direct Phantom Cube | 10 | 19.9120 | .02974 | .00940 |
| | Mimics CT Helical ST 0.625mm | 10 | 20.2410 | .23048 | .07288 |
| i | Direct Phantom Cube | 10 | 49.8900 | .03266 | .01033 |
| | Mimics CT Helical ST 0.625mm | 10 | 50.0140 | .13443 | .04251 |
| j | Direct Phantom Cube | 10 | 19.9890 | .01524 | .00482 |
| | Mimics CT Helical ST 0.625mm | 10 | 20.0550 | .05642 | .01784 |
| hole | Direct Phantom Cube | 10 | 5.8370 | .04296 | .01359 |
| | Mimics CT Helical ST 0.625mm | 10 | 5.4590 | .10908 | .03449 |

| | Sig. (2-tailed) | Mean Difference | Std. Error Difference | 95% Confidence Interval of the Difference | |
|---|---|---|---|---|---|
| | | | | Lower | Upper |
| a | .000 | -.25200 | .03877 | -.33346 | -.17054 |
| b | .000 | -.19100 | .03725 | -.26925 | -.11275 |
| c | .000 | -.16100 | .03654 | -.23777 | -.08423 |
| d | .000 | -.24500 | .02829 | -.30444 | -.18556 |
| e | .004 | -.11600 | .03528 | -.19011 | -.04189 |
| f | .452 | -.07000 | .09114 | -.26148 | .12148 |
| g | .254 | -.03000 | .02545 | -.08346 | .02346 |
| h | .000 | -.32900 | .07349 | -.48339 | -.17461 |
| i | .011 | -.12400 | .04375 | -.21591 | -.03209 |
| j | .002 | -.06600 | .01848 | -.10483 | -.02717 |
| hole | .000 | .37800 | .03707 | .30011 | .45589 |

### *Direct Phantom v CT Helical ST 1.25mm*

| Object | | N | Mean | Std. Deviation | Std. Error Mean |
|---|---|---|---|---|---|
| a | Direct Phantom Cube | 10 | 60.1170 | .02791 | .00883 |
| | Mimics CT Helical ST 1.25mm | 10 | 60.2260 | .18969 | .05999 |
| b | Direct Phantom Cube | 10 | 60.0860 | .01776 | .00562 |
| | Mimics CT Helical ST 1.25mm | 10 | 60.2960 | .09168 | .02899 |
| c | Direct Phantom Cube | 10 | 20.0670 | .02908 | .00920 |
| | Mimics CT Helical ST 1.25mm | 10 | 20.0360 | .07291 | .02306 |
| d | Direct Phantom Cube | 10 | 20.0800 | .03464 | .01095 |
| | Mimics CT Helical ST 1.25mm | 10 | 20.0780 | .09647 | .03051 |
| e | Direct Phantom Cube | 10 | 60.1060 | .02914 | .00921 |
| | Mimics CT Helical ST 1.25mm | 10 | 60.1200 | .11441 | .03618 |
| f | Direct Phantom Cube | 10 | 60.1800 | .25342 | .08014 |
| | Mimics CT Helical ST 1.25mm | 10 | 60.0550 | .10480 | .03314 |
| g | Direct Phantom Cube | 10 | 19.8840 | .02675 | .00846 |
| | Mimics CT Helical ST 1.25mm | 10 | 19.7650 | .08947 | .02829 |
| h | Direct Phantom Cube | 10 | 19.9120 | .02974 | .00940 |
| | Mimics CT Helical ST 1.25mm | 10 | 19.8540 | .12094 | .03824 |
| i | Direct Phantom Cube | 10 | 49.8900 | .03266 | .01033 |
| | Mimics CT Helical ST 1.25mm | 10 | 49.8780 | .06763 | .02139 |
| j | Direct Phantom Cube | 10 | 19.9890 | .01524 | .00482 |
| | Mimics CT Helical ST 1.25mm | 10 | 19.7670 | .09989 | .03159 |
| hole | Direct Phantom Cube | 10 | 5.8370 | .04296 | .01359 |
| | Mimics CT Helical ST 1.25mm | 10 | 6.0000 | .50923 | .16103 |

| | Sig. (2-tailed) | Mean Difference | Std. Error Difference | 95% Confidence Interval of the Difference | |
|---|---|---|---|---|---|
| | | | | Lower | Upper |
| a | .089 | -.10900 | .06063 | -.23638 | .01838 |
| b | .000 | -.21000 | .02953 | -.27204 | -.14796 |
| c | .228 | .03100 | .02482 | -.02115 | .08315 |
| d | .951 | .00200 | .03241 | -.06610 | .07010 |
| e | .712 | -.01400 | .03733 | -.09243 | .06443 |
| f | .167 | .12500 | .08672 | -.05719 | .30719 |
| g | .001 | .11900 | .02953 | .05696 | .18104 |
| h | .158 | .05800 | .03938 | -.02474 | .14074 |
| i | .619 | .01200 | .02375 | -.03789 | .06189 |
| j | .000 | .22200 | .03195 | .15487 | .28913 |
| hole | .327 | -.16300 | .16160 | -.50252 | .17652 |

### *Direct Phantom v CT Helical ST 2.5mm*

| | Object | N | Mean | Std. Deviation | Std. Error Mean |
|---|---|---|---|---|---|
| a | Direct Phantom Cube | 10 | 60.1170 | .02791 | .00883 |
| | Mimics CT Helical ST 2.5mm | 10 | 59.8990 | .13828 | .04373 |
| b | Direct Phantom Cube | 10 | 60.0860 | .01776 | .00562 |
| | Mimics CT Helical ST 2.5mm | 10 | 60.2060 | .10102 | .03194 |
| c | Direct Phantom Cube | 10 | 20.0670 | .02908 | .00920 |
| | Mimics CT Helical ST 2.5mm | 10 | 19.8730 | .08994 | .02844 |
| d | Direct Phantom Cube | 10 | 20.0800 | .03464 | .01095 |
| | Mimics CT Helical ST 2.5mm | 10 | 19.8300 | .07118 | .02251 |
| e | Direct Phantom Cube | 10 | 60.1060 | .02914 | .00921 |
| | Mimics CT Helical ST 2.5mm | 10 | 60.0080 | .17466 | .05523 |
| f | Direct Phantom Cube | 10 | 60.1800 | .25342 | .08014 |
| | Mimics CT Helical ST 2.5mm | 10 | 59.8650 | .12277 | .03882 |
| g | Direct Phantom Cube | 10 | 19.8840 | .02675 | .00846 |
| | Mimics CT Helical ST 2.5mm | 10 | 19.7570 | .21354 | .06753 |
| h | Direct Phantom Cube | 10 | 19.9120 | .02974 | .00940 |
| | Mimics CT Helical ST 2.5mm | 10 | 19.8980 | .22759 | .07197 |
| i | Direct Phantom Cube | 10 | 49.8900 | .03266 | .01033 |
| | Mimics CT Helical ST 2.5mm | 10 | 49.5590 | .09927 | .03139 |
| j | Direct Phantom Cube | 10 | 19.9890 | .01524 | .00482 |
| | Mimics CT Helical ST 2.5mm | 10 | 19.8760 | .06484 | .02050 |
| hole | Direct Phantom Cube | 10 | 5.8370 | .04296 | .01359 |
| | Mimics CT Helical ST 2.5mm | 10 | 5.2170 | .26604 | .08413 |

| | Sig. (2-tailed) | Mean Difference | Std. Error Difference | 95% Confidence Interval of the Difference | |
|---|---|---|---|---|---|
| | | | | Lower | Upper |
| a | .000 | .21800 | .04461 | .12428 | .31172 |
| b | .002 | -.12000 | .03243 | -.18814 | -.05186 |
| c | .000 | .19400 | .02989 | .13120 | .25680 |
| d | .000 | .25000 | .02503 | .19741 | .30259 |
| e | .097 | .09800 | .05600 | -.01964 | .21564 |
| f | .002 | .31500 | .08905 | .12792 | .50208 |
| g | .078 | .12700 | .06806 | -.01598 | .26998 |
| h | .849 | .01400 | .07258 | -.13849 | .16649 |
| i | .000 | .33100 | .03305 | .26157 | .40043 |
| j | .000 | .11300 | .02106 | .06875 | .15725 |
| hole | .000 | .62000 | .08522 | .44096 | .79904 |

### *BB 1.5T 0.8mm v CT Helical Bone 0.625mm*

| | Object | N | Mean | Std. Deviation | Std. Error Mean |
|---|---|---|---|---|---|
| a | Mimics BB 1.5T 0.8mm | 10 | 59.9200 | .08756 | .02769 |
| | Mimics CT Helical Bone 0.625mm | 10 | 59.8570 | .14728 | .04657 |
| b | Mimics BB 1.5T 0.8mm | 10 | 59.4240 | .17386 | .05498 |
| | Mimics CT Helical Bone 0.625mm | 10 | 59.7890 | .17065 | .05396 |
| c | Mimics BB 1.5T 0.8mm | 10 | 19.8780 | .05750 | .01818 |
| | Mimics CT Helical Bone 0.625mm | 10 | 19.8510 | .05820 | .01841 |
| d | Mimics BB 1.5T 0.8mm | 10 | 20.0610 | .15531 | .04911 |
| | Mimics CT Helical Bone 0.625mm | 10 | 19.9770 | .16371 | .05177 |
| e | Mimics BB 1.5T 0.8mm | 10 | 59.7130 | .08447 | .02671 |
| | Mimics CT Helical Bone 0.625mm | 10 | 59.7990 | .10918 | .03453 |
| f | Mimics BB 1.5T 0.8mm | 10 | 59.7330 | .18105 | .05725 |
| | Mimics CT Helical Bone 0.625mm | 10 | 60.1490 | .27424 | .08672 |
| g | Mimics BB 1.5T 0.8mm | 10 | 19.7340 | .04858 | .01536 |
| | Mimics CT Helical Bone 0.625mm | 10 | 19.5320 | .07376 | .02332 |
| h | Mimics BB 1.5T 0.8mm | 10 | 19.8770 | .06717 | .02124 |
| | Mimics CT Helical Bone 0.625mm | 10 | 19.6140 | .13117 | .04148 |
| i | Mimics BB 1.5T 0.8mm | 10 | 49.7280 | .43734 | .13830 |
| | Mimics CT Helical Bone 0.625mm | 10 | 49.5780 | .19860 | .06280 |
| j | Mimics BB 1.5T 0.8mm | 10 | 19.7480 | .06125 | .01937 |
| | Mimics CT Helical Bone 0.625mm | 10 | 19.7360 | .11862 | .03751 |
| hole | Mimics BB 1.5T 0.8mm | 10 | 5.7630 | .04473 | .01415 |
| | Mimics CT Helical Bone 0.625mm | 10 | 6.4040 | .09180 | .02903 |

| | Sig. (2-tailed) | Mean Difference | Std. Error Difference | 95% Confidence Interval of the Difference | |
|---|---|---|---|---|---|
| | | | | Lower | Upper |
| a | .260 | .06300 | .05418 | -.05083 | .17683 |
| b | .000 | -.36500 | .07704 | -.52685 | -.20315 |
| c | .311 | .02700 | .02587 | -.02736 | .08136 |
| d | .254 | .08400 | .07136 | -.06592 | .23392 |
| e | .064 | -.08600 | .04365 | -.17771 | .00571 |
| f | .001 | -.41600 | .10392 | -.63432 | -.19768 |
| g | .000 | .20200 | .02793 | .14332 | .26068 |
| h | .000 | .26300 | .04660 | .16509 | .36091 |
| i | .336 | .15000 | .15189 | -.16911 | .46911 |
| j | .779 | .01200 | .04222 | -.07669 | .10069 |
| hole | .000 | -.64100 | .03229 | -.70884 | -.57316 |

## H.4.3. Osirix

### *Direct Phantom v BB 1.5T 0.8mm*

| | Object | N | Mean | Std. Deviation | Std. Error Mean |
|---|---|---|---|---|---|
| a | Direct Phantom Cube | 10 | 60.1170 | .02791 | .00883 |
| | Osirix BB 1.5T 0.8mm | 10 | 60.2100 | .16633 | .05260 |
| b | Direct Phantom Cube | 10 | 60.0860 | .01776 | .00562 |
| | Osirix BB 1.5T 0.8mm | 10 | 60.1100 | .11972 | .03786 |
| c | Direct Phantom Cube | 10 | 20.0670 | .02908 | .00920 |
| | Osirix BB 1.5T 0.8mm | 10 | 20.3900 | .16633 | .05260 |
| d | Direct Phantom Cube | 10 | 20.0800 | .03464 | .01095 |
| | Osirix BB 1.5T 0.8mm | 10 | 20.2000 | .15635 | .04944 |
| e | Direct Phantom Cube | 10 | 60.1060 | .02914 | .00921 |
| | Osirix BB 1.5T 0.8mm | 10 | 60.2200 | .13166 | .04163 |
| f | Direct Phantom Cube | 10 | 60.1800 | .25342 | .08014 |
| | Osirix BB 1.5T 0.8mm | 10 | 59.9800 | .07888 | .02494 |
| g | Direct Phantom Cube | 10 | 19.8840 | .02675 | .00846 |
| | Osirix BB 1.5T 0.8mm | 10 | 20.1500 | .10801 | .03416 |
| h | Direct Phantom Cube | 10 | 19.9120 | .02974 | .00940 |
| | Osirix BB 1.5T 0.8mm | 10 | 20.0800 | .09189 | .02906 |
| i | Direct Phantom Cube | 10 | 49.8900 | .03266 | .01033 |
| | Osirix BB 1.5T 0.8mm | 10 | 49.5300 | .12517 | .03958 |
| j | Direct Phantom Cube | 10 | 19.9890 | .01524 | .00482 |
| | Osirix BB 1.5T 0.8mm | 10 | 20.0300 | .10593 | .03350 |
| hole | Direct Phantom Cube | 10 | 5.8370 | .04296 | .01359 |
| | Osirix BB 1.5T 0.8mm | 10 | 4.2700 | .09487 | .03000 |

| | Sig. (2-tailed) | Mean Difference | Std. Error Difference | 95% Confidence Interval of the Difference | |
|---|---|---|---|---|---|
| | | | | Lower | Upper |
| a | .098 | -.09300 | .05333 | -.20505 | .01905 |
| b | .538 | -.02400 | .03827 | -.10441 | .05641 |
| c | .000 | -.32300 | .05340 | -.43518 | -.21082 |
| d | .029 | -.12000 | .05064 | -.22639 | -.01361 |
| e | .015 | -.11400 | .04264 | -.20358 | -.02442 |
| f | .028 | .20000 | .08393 | .02367 | .37633 |
| g | .000 | -.26600 | .03519 | -.33993 | -.19207 |
| h | .000 | -.16800 | .03054 | -.23217 | -.10383 |
| i | .000 | .36000 | .04091 | .27406 | .44594 |
| j | .241 | -.04100 | .03384 | -.11210 | .03010 |
| hole | .000 | 1.56700 | .03293 | 1.49781 | 1.63619 |

## *Direct phantom v BB 1.5T 1.2mm*

| | Object | N | Mean | Std. Deviation | Std. Error Mean |
|---|---|---|---|---|---|
| a | Direct Phantom Cube | 10 | 60.1170 | .02791 | .00883 |
| | Osirix BB 1.5T 1.2mm | 10 | 60.2500 | .19003 | .06009 |
| b | Direct Phantom Cube | 10 | 60.0860 | .01776 | .00562 |
| | Osirix BB 1.5T 1.2mm | 10 | 60.2500 | .11785 | .03727 |
| c | Direct Phantom Cube | 10 | 20.0670 | .02908 | .00920 |
| | Osirix BB 1.5T 1.2mm | 10 | 20.1500 | .11785 | .03727 |
| d | Direct Phantom Cube | 10 | 20.0800 | .03464 | .01095 |
| | Osirix BB 1.5T 1.2mm | 10 | 20.2100 | .14491 | .04583 |
| e | Direct Phantom Cube | 10 | 60.1060 | .02914 | .00921 |
| | Osirix BB 1.5T 1.2mm | 10 | 60.1000 | .20000 | .06325 |
| f | Direct Phantom Cube | 10 | 60.1800 | .25342 | .08014 |
| | Osirix BB 1.5T 1.2mm | 10 | 60.1300 | .18288 | .05783 |
| g | Direct Phantom Cube | 10 | 19.8840 | .02675 | .00846 |
| | Osirix BB 1.5T 1.2mm | 10 | 19.9200 | .13166 | .04163 |
| h | Direct Phantom Cube | 10 | 19.9120 | .02974 | .00940 |
| | Osirix BB 1.5T 1.2mm | 10 | 20.1500 | .15092 | .04773 |
| i | Direct Phantom Cube | 10 | 49.8900 | .03266 | .01033 |
| | Osirix BB 1.5T 1.2mm | 10 | 49.6300 | .20575 | .06506 |
| j | Direct Phantom Cube | 10 | 19.9890 | .01524 | .00482 |
| | Osirix BB 1.5T 1.2mm | 10 | 20.1000 | .14907 | .04714 |
| hole | Direct Phantom Cube | 10 | 5.8370 | .04296 | .01359 |
| | Osirix BB 1.5T 1.2mm | 10 | 5.1800 | .19322 | .06110 |

| | Sig. (2-tailed) | Mean Difference | Std. Error Difference | 95% Confidence Interval of the Difference | |
|---|---|---|---|---|---|
| | | | | Lower | Upper |
| a | .042 | -.13300 | .06074 | -.26060 | -.00540 |
| b | .000 | -.16400 | .03769 | -.24318 | -.08482 |
| c | .044 | -.08300 | .03839 | -.16364 | -.00236 |
| d | .013 | -.13000 | .04712 | -.22899 | -.03101 |
| e | .926 | .00600 | .06391 | -.12828 | .14028 |
| f | .619 | .05000 | .09883 | -.15763 | .25763 |
| g | .408 | -.03600 | .04248 | -.12526 | .05326 |
| h | .000 | -.23800 | .04864 | -.34020 | -.13580 |
| i | .001 | .26000 | .06588 | .12159 | .39841 |
| j | .031 | -.11100 | .04739 | -.21055 | -.01145 |
| hole | .000 | .65700 | .06259 | .52550 | .78850 |

## *Direct Phantom v BB 1.5T 2.0mm*

| | Object | N | Mean | Std. Deviation | Std. Error Mean |
|---|---|---|---|---|---|
| a | Direct Phantom Cube | 10 | 60.1170 | .02791 | .00883 |
| | Osirix BB 1.5T 2.0mm | 10 | 60.4600 | .10750 | .03399 |
| b | Direct Phantom Cube | 10 | 60.0860 | .01776 | .00562 |
| | Osirix BB 1.5T 2.0mm | 10 | 60.6700 | .12517 | .03958 |
| c | Direct Phantom Cube | 10 | 20.0670 | .02908 | .00920 |
| | Osirix BB 1.5T 2.0mm | 10 | 20.3800 | .20440 | .06464 |
| d | Direct Phantom Cube | 10 | 20.0800 | .03464 | .01095 |
| | Osirix BB 1.5T 2.0mm | 10 | 20.4700 | .15670 | .04955 |
| e | Direct Phantom Cube | 10 | 60.1060 | .02914 | .00921 |
| | Osirix BB 1.5T 2.0mm | 10 | 60.2500 | .22236 | .07032 |
| f | Direct Phantom Cube | 10 | 60.1800 | .25342 | .08014 |
| | Osirix BB 1.5T 2.0mm | 10 | 60.4800 | .19322 | .06110 |
| g | Direct Phantom Cube | 10 | 19.8840 | .02675 | .00846 |
| | Osirix BB 1.5T 2.0mm | 10 | 18.3540 | 5.73448 | 1.81340 |
| h | Direct Phantom Cube | 10 | 19.9120 | .02974 | .00940 |
| | Osirix BB 1.5T 2.0mm | 10 | 18.4900 | 5.75952 | 1.82132 |
| i | Direct Phantom Cube | 10 | 49.8900 | .03266 | .01033 |
| | Osirix BB 1.5T 2.0mm | 10 | 49.7400 | .23664 | .07483 |
| j | Direct Phantom Cube | 10 | 19.9890 | .01524 | .00482 |
| | Osirix BB 1.5T 2.0mm | 10 | 20.5100 | .11972 | .03786 |
| hole | Direct Phantom Cube | 10 | 5.8370 | .04296 | .01359 |
| | Osirix BB 1.5T 2.0mm | 10 | 4.7400 | .14298 | .04522 |

| | Sig. (2-tailed) | Mean Difference | Std. Error Difference | 95% Confidence Interval of the Difference | |
|---|---|---|---|---|---|
| | | | | Lower | Upper |
| a | .000 | -.34300 | .03512 | -.41679 | -.26921 |
| b | .000 | -.58400 | .03998 | -.66799 | -.50001 |
| c | .000 | -.31300 | .06529 | -.45016 | -.17584 |
| d | .000 | -.39000 | .05075 | -.49662 | -.28338 |
| e | .057 | -.14400 | .07092 | -.29299 | .00499 |
| f | .008 | -.30000 | .10077 | -.51172 | -.08828 |
| g | .410 | 1.53000 | 1.81342 | -2.27986 | 5.33986 |
| h | .445 | 1.42200 | 1.82135 | -2.40450 | 5.24850 |
| i | .063 | .15000 | .07554 | -.00871 | .30871 |
| j | .000 | -.52100 | .03816 | -.60118 | -.44082 |
| hole | .000 | 1.09700 | .04721 | .99781 | 1.19619 |

### *Direct Phantom v BB 1.5T 2.4mm*

| | Object | N | Mean | Std. Deviation | Std. Error Mean |
|---|---|---|---|---|---|
| a | Direct Phantom Cube | 10 | 60.1170 | .02791 | .00883 |
| | Osirix BB 1.5T 2.4mm | 10 | 60.7600 | .15776 | .04989 |
| b | Direct Phantom Cube | 10 | 60.0860 | .01776 | .00562 |
| | Osirix BB 1.5T 2.4mm | 10 | 60.5300 | .25841 | .08172 |
| c | Direct Phantom Cube | 10 | 20.0670 | .02908 | .00920 |
| | Osirix BB 1.5T 2.4mm | 10 | 20.7400 | .17764 | .05617 |
| d | Direct Phantom Cube | 10 | 20.0800 | .03464 | .01095 |
| | Osirix BB 1.5T 2.4mm | 10 | 20.3600 | .12649 | .04000 |
| e | Direct Phantom Cube | 10 | 60.1060 | .02914 | .00921 |
| | Osirix BB 1.5T 2.4mm | 10 | 60.4400 | .18974 | .06000 |
| f | Direct Phantom Cube | 10 | 60.1800 | .25342 | .08014 |
| | Osirix BB 1.5T 2.4mm | 10 | 60.3900 | .23310 | .07371 |
| g | Direct Phantom Cube | 10 | 19.8840 | .02675 | .00846 |
| | Osirix BB 1.5T 2.4mm | 10 | 20.3900 | .18529 | .05859 |
| h | Direct Phantom Cube | 10 | 19.9120 | .02974 | .00940 |
| | Osirix BB 1.5T 2.4mm | 10 | 20.2100 | .21833 | .06904 |
| i | Direct Phantom Cube | 10 | 49.8900 | .03266 | .01033 |
| | Osirix BB 1.5T 2.4mm | 10 | 49.6900 | .20248 | .06403 |
| j | Direct Phantom Cube | 10 | 19.9890 | .01524 | .00482 |
| | Osirix BB 1.5T 2.4mm | 10 | 20.9100 | .09944 | .03145 |
| hole | Direct Phantom Cube | 10 | 5.8370 | .04296 | .01359 |
| | Osirix BB 1.5T 2.4mm | 10 | 4.7700 | .12517 | .03958 |

| | Sig. (2-tailed) | Mean Difference | Std. Error Difference | 95% Confidence Interval of the Difference | |
|---|---|---|---|---|---|
| | | | | Lower | Upper |
| a | .000 | -.64300 | .05066 | -.74944 | -.53656 |
| b | .000 | -.44400 | .08191 | -.61609 | -.27191 |
| c | .000 | -.67300 | .05692 | -.79259 | -.55341 |
| d | .000 | -.28000 | .04147 | -.36713 | -.19287 |
| e | .000 | -.33400 | .06070 | -.46153 | -.20647 |
| f | .070 | -.21000 | .10888 | -.43876 | .01876 |
| g | .000 | -.50600 | .05920 | -.63038 | -.38162 |
| h | .000 | -.29800 | .06968 | -.44439 | -.15161 |
| i | .006 | .20000 | .06486 | .06374 | .33626 |
| j | .000 | -.92100 | .03181 | -.98784 | -.85416 |
| hole | .000 | 1.06700 | .04185 | .97908 | 1.15492 |

## *Direct Phantom v BB 3.0T 0.8mm*

| | Object | N | Mean | Std. Deviation | Std. Error Mean |
|---|---|---|---|---|---|
| a | Direct Phantom Cube | 10 | 60.1170 | .02791 | .00883 |
| | Osirix BB 3.0T 0.8mm | 10 | 59.9000 | .16997 | .05375 |
| b | Direct Phantom Cube | 10 | 60.0860 | .01776 | .00562 |
| | Osirix BB 3.0T 0.8mm | 10 | 59.7300 | .08233 | .02603 |
| c | Direct Phantom Cube | 10 | 20.0670 | .02908 | .00920 |
| | Osirix BB 3.0T 0.8mm | 10 | 19.8100 | .21318 | .06741 |
| d | Direct Phantom Cube | 10 | 20.0800 | .03464 | .01095 |
| | Osirix BB 3.0T 0.8mm | 10 | 19.9400 | .18974 | .06000 |
| e | Direct Phantom Cube | 10 | 60.1060 | .02914 | .00921 |
| | Osirix BB 3.0T 0.8mm | 10 | 60.0000 | .13333 | .04216 |
| f | Direct Phantom Cube | 10 | 60.1800 | .25342 | .08014 |
| | Osirix BB 3.0T 0.8mm | 10 | 60.0900 | .15239 | .04819 |
| g | Direct Phantom Cube | 10 | 19.8840 | .02675 | .00846 |
| | Osirix BB 3.0T 0.8mm | 10 | 19.8000 | .10541 | .03333 |
| h | Direct Phantom Cube | 10 | 19.9120 | .02974 | .00940 |
| | Osirix BB 3.0T 0.8mm | 10 | 19.7700 | .15670 | .04955 |
| i | Direct Phantom Cube | 10 | 49.8900 | .03266 | .01033 |
| | Osirix BB 3.0T 0.8mm | 10 | 49.6900 | .14491 | .04583 |
| j | Direct Phantom Cube | 10 | 19.9890 | .01524 | .00482 |
| | Osirix BB 3.0T 0.8mm | 10 | 20.1000 | .08165 | .02582 |
| hole | Direct Phantom Cube | 10 | 5.8370 | .04296 | .01359 |
| | Osirix BB 3.0T 0.8mm | 10 | 5.6700 | .06749 | .02134 |

| | Sig. (2-tailed) | Mean Difference | Std. Error Difference | 95% Confidence Interval of the Difference | |
|---|---|---|---|---|---|
| | | | | Lower | Upper |
| a | .001 | .21700 | .05447 | .10257 | .33143 |
| b | .000 | .35600 | .02663 | .30005 | .41195 |
| c | .001 | .25700 | .06804 | .11406 | .39994 |
| d | .034 | .14000 | .06099 | .01186 | .26814 |
| e | .024 | .10600 | .04316 | .01533 | .19667 |
| f | .349 | .09000 | .09351 | -.10646 | .28646 |
| g | .025 | .08400 | .03439 | .01175 | .15625 |
| h | .011 | .14200 | .05044 | .03603 | .24797 |
| i | .000 | .20000 | .04698 | .10131 | .29869 |
| j | .001 | -.11100 | .02627 | -.16618 | -.05582 |
| hole | .000 | .16700 | .02530 | .11385 | .22015 |

## *Direct Phantom v BB 3.0T 1.2mm*

| | Object | N | Mean | Std. Deviation | Std. Error Mean |
|---|---|---|---|---|---|
| a | Direct Phantom Cube | 10 | 60.1170 | .02791 | .00883 |
| | Osirix BB 3.0T 1.2mm | 10 | 59.9600 | .11738 | .03712 |
| b | Direct Phantom Cube | 10 | 60.0860 | .01776 | .00562 |
| | Osirix BB 3.0T 1.2mm | 10 | 60.0700 | .13375 | .04230 |
| c | Direct Phantom Cube | 10 | 20.0670 | .02908 | .00920 |
| | Osirix BB 3.0T 1.2mm | 10 | 20.8900 | .17920 | .05667 |
| d | Direct Phantom Cube | 10 | 20.0800 | .03464 | .01095 |
| | Osirix BB 3.0T 1.2mm | 10 | 20.9600 | .15055 | .04761 |
| e | Direct Phantom Cube | 10 | 60.1060 | .02914 | .00921 |
| | Osirix BB 3.0T 1.2mm | 10 | 60.1100 | .20248 | .06403 |
| f | Direct Phantom Cube | 10 | 60.1800 | .25342 | .08014 |
| | Osirix BB 3.0T 1.2mm | 10 | 60.2900 | .17288 | .05467 |
| g | Direct Phantom Cube | 10 | 19.8840 | .02675 | .00846 |
| | Osirix BB 3.0T 1.2mm | 10 | 20.5500 | .16499 | .05217 |
| h | Direct Phantom Cube | 10 | 19.9120 | .02974 | .00940 |
| | Osirix BB 3.0T 1.2mm | 10 | 20.4100 | .18529 | .05859 |
| i | Direct Phantom Cube | 10 | 49.8900 | .03266 | .01033 |
| | Osirix BB 3.0T 1.2mm | 10 | 49.6900 | .15951 | .05044 |
| j | Direct Phantom Cube | 10 | 19.9890 | .01524 | .00482 |
| | Osirix BB 3.0T 1.2mm | 10 | 20.1200 | .20440 | .06464 |
| hole | Direct Phantom Cube | 10 | 5.8370 | .04296 | .01359 |
| | Osirix BB 3.0T 1.2mm | 10 | 3.7200 | .16193 | .05121 |

| | Sig. (2-tailed) | Mean Difference | Std. Error Difference | 95% Confidence Interval of the Difference | |
|---|---|---|---|---|---|
| | | | | Lower | Upper |
| a | .001 | .15700 | .03815 | .07684 | .23716 |
| b | .712 | .01600 | .04267 | -.07364 | .10564 |
| c | .000 | -.82300 | .05741 | -.94361 | -.70239 |
| d | .000 | -.88000 | .04885 | -.98264 | -.77736 |
| e | .951 | -.00400 | .06469 | -.13991 | .13191 |
| f | .272 | -.11000 | .09701 | -.31381 | .09381 |
| g | .000 | -.66600 | .05286 | -.77705 | -.55495 |
| h | .000 | -.49800 | .05934 | -.62268 | -.37332 |
| i | .001 | .20000 | .05149 | .09183 | .30817 |
| j | .058 | -.13100 | .06482 | -.26717 | .00517 |
| hole | .000 | 2.11700 | .05298 | 2.00570 | 2.22830 |

### *Direct Phantom v BB 3.0T 2.0mm*

| | Object | N | Mean | Std. Deviation | Std. Error Mean |
|---|---|---|---|---|---|
| a | Direct Phantom Cube | 10 | 60.1170 | .02791 | .00883 |
| | Osirix BB 3.0T 2.0mm | 10 | 59.9900 | .15239 | .04819 |
| b | Direct Phantom Cube | 10 | 60.0860 | .01776 | .00562 |
| | Osirix BB 3.0T 2.0mm | 10 | 54.8800 | 16.99999 | 5.37587 |
| c | Direct Phantom Cube | 10 | 20.0670 | .02908 | .00920 |
| | Osirix BB 3.0T 2.0mm | 10 | 19.9400 | .19551 | .06182 |
| d | Direct Phantom Cube | 10 | 20.0800 | .03464 | .01095 |
| | Osirix BB 3.0T 2.0mm | 10 | 20.0800 | .12293 | .03887 |
| e | Direct Phantom Cube | 10 | 60.1060 | .02914 | .00921 |
| | Osirix BB 3.0T 2.0mm | 10 | 60.0400 | .11738 | .03712 |
| f | Direct Phantom Cube | 10 | 60.1800 | .25342 | .08014 |
| | Osirix BB 3.0T 2.0mm | 10 | 60.1900 | .15239 | .04819 |
| g | Direct Phantom Cube | 10 | 19.8840 | .02675 | .00846 |
| | Osirix BB 3.0T 2.0mm | 10 | 19.9500 | .15811 | .05000 |
| h | Direct Phantom Cube | 10 | 19.9120 | .02974 | .00940 |
| | Osirix BB 3.0T 2.0mm | 10 | 20.0200 | .04216 | .01333 |
| i | Direct Phantom Cube | 10 | 49.8900 | .03266 | .01033 |
| | Osirix BB 3.0T 2.0mm | 10 | 49.7100 | .19120 | .06046 |
| j | Direct Phantom Cube | 10 | 19.9890 | .01524 | .00482 |
| | Osirix BB 3.0T 2.0mm | 10 | 20.0200 | .18738 | .05925 |
| hole | Direct Phantom Cube | 10 | 5.8370 | .04296 | .01359 |
| | Osirix BB 3.0T 2.0mm | 10 | 5.1300 | .04830 | .01528 |

| | Sig. (2-tailed) | Mean Difference | Std. Error Difference | 95% Confidence Interval of the Difference | |
|---|---|---|---|---|---|
| | | | | Lower | Upper |
| A | .018 | .12700 | .04899 | .02407 | .22993 |
| B | .346 | 5.20600 | 5.37587 | -6.08829 | 16.50029 |
| C | .057 | .12700 | .06250 | -.00432 | .25832 |
| D | 1.000 | .00000 | .04039 | -.08485 | .08485 |
| E | .102 | .06600 | .03824 | -.01435 | .14635 |
| F | .916 | -.01000 | .09351 | -.20646 | .18646 |
| G | .209 | -.06600 | .05071 | -.17254 | .04054 |
| H | .000 | -.10800 | .01632 | -.14228 | -.07372 |
| I | .009 | .18000 | .06134 | .05114 | .30886 |
| J | .608 | -.03100 | .05945 | -.15590 | .09390 |
| hole | .000 | .70700 | .02044 | .66405 | .74995 |

## *Direct Phantom v BB 3.0T 2.4mm*

| | Object | N | Mean | Std. Deviation | Std. Error Mean |
|---|---|---|---|---|---|
| a | Direct Phantom Cube | 10 | 60.1170 | .02791 | .00883 |
| | Osirix BB 3.0T 2.4mm | 10 | 59.8200 | .13984 | .04422 |
| b | Direct Phantom Cube | 10 | 60.0860 | .01776 | .00562 |
| | Osirix BB 3.0T 2.4mm | 10 | 59.8300 | .20028 | .06333 |
| c | Direct Phantom Cube | 10 | 20.0670 | .02908 | .00920 |
| | Osirix BB 3.0T 2.4mm | 10 | 19.8500 | .14337 | .04534 |
| d | Direct Phantom Cube | 10 | 20.0800 | .03464 | .01095 |
| | Osirix BB 3.0T 2.4mm | 10 | 19.9200 | .10328 | .03266 |
| e | Direct Phantom Cube | 10 | 60.1060 | .02914 | .00921 |
| | Osirix BB 3.0T 2.4mm | 10 | 59.7900 | .09944 | .03145 |
| f | Direct Phantom Cube | 10 | 60.1800 | .25342 | .08014 |
| | Osirix BB 3.0T 2.4mm | 10 | 59.7800 | .14757 | .04667 |
| g | Direct Phantom Cube | 10 | 19.8840 | .02675 | .00846 |
| | Osirix BB 3.0T 2.4mm | 10 | 19.7600 | .09661 | .03055 |
| h | Direct Phantom Cube | 10 | 19.9120 | .02974 | .00940 |
| | Osirix BB 3.0T 2.4mm | 10 | 19.7200 | .14757 | .04667 |
| i | Direct Phantom Cube | 10 | 49.8900 | .03266 | .01033 |
| | Osirix BB 3.0T 2.4mm | 10 | 49.3800 | .14757 | .04667 |
| j | Direct Phantom Cube | 10 | 19.9890 | .01524 | .00482 |
| | Osirix BB 3.0T 2.4mm | 10 | 19.9100 | .11972 | .03786 |
| hole | Direct Phantom Cube | 10 | 5.8370 | .04296 | .01359 |
| | Osirix BB 3.0T 2.4mm | 10 | 5.7300 | .08233 | .02603 |

| | Sig. (2-tailed) | Mean Difference | Std. Error Difference | 95% Confidence Interval of the Difference | |
|---|---|---|---|---|---|
| | | | | Lower | Upper |
| a | .000 | .29700 | .04509 | .20226 | .39174 |
| b | .001 | .25600 | .06358 | .12242 | .38958 |
| c | .000 | .21700 | .04626 | .11981 | .31419 |
| d | .000 | .16000 | .03445 | .08763 | .23237 |
| e | .000 | .31600 | .03277 | .24716 | .38484 |
| f | .000 | .40000 | .09274 | .20517 | .59483 |
| g | .001 | .12400 | .03170 | .05740 | .19060 |
| h | .001 | .19200 | .04760 | .09199 | .29201 |
| i | .000 | .51000 | .04780 | .40958 | .61042 |
| j | .053 | .07900 | .03816 | -.00118 | .15918 |
| hole | .002 | .10700 | .02937 | .04531 | .16869 |

## *Direct Phantom CT Face Bone 0.625mm*

| | Object | N | Mean | Std. Deviation | Std. Error Mean |
|---|---|---|---|---|---|
| a | Direct Phantom Cube | 10 | 60.1170 | .02791 | .00883 |
| | Osirix CT Face Bone 0.625mm | 10 | 60.0900 | .09944 | .03145 |
| b | Direct Phantom Cube | 10 | 60.0860 | .01776 | .00562 |
| | Osirix CT Face Bone 0.625mm | 10 | 59.9600 | .11738 | .03712 |
| c | Direct Phantom Cube | 10 | 20.0670 | .02908 | .00920 |
| | Osirix CT Face Bone 0.625mm | 10 | 20.2500 | .12693 | .04014 |
| d | Direct Phantom Cube | 10 | 20.0800 | .03464 | .01095 |
| | Osirix CT Face Bone 0.625mm | 10 | 20.1200 | .16865 | .05333 |
| e | Direct Phantom Cube | 10 | 60.1060 | .02914 | .00921 |
| | Osirix CT Face Bone 0.625mm | 10 | 60.0000 | .11547 | .03651 |
| f | Direct Phantom Cube | 10 | 60.1800 | .25342 | .08014 |
| | Osirix CT Face Bone 0.625mm | 10 | 59.8800 | .07888 | .02494 |
| g | Direct Phantom Cube | 10 | 19.8840 | .02675 | .00846 |
| | Osirix CT Face Bone 0.625mm | 10 | 19.7700 | .08233 | .02603 |
| h | Direct Phantom Cube | 10 | 19.9120 | .02974 | .00940 |
| | Osirix CT Face Bone 0.625mm | 10 | 19.8100 | .08756 | .02769 |
| i | Direct Phantom Cube | 10 | 49.8900 | .03266 | .01033 |
| | Osirix CT Face Bone 0.625mm | 10 | 45.2200 | 14.20233 | 4.49117 |
| j | Direct Phantom Cube | 10 | 19.9890 | .01524 | .00482 |
| | Osirix CT Face Bone 0.625mm | 10 | 20.1700 | .10593 | .03350 |
| hole | Direct Phantom Cube | 10 | 5.8370 | .04296 | .01359 |
| | Osirix CT Face Bone 0.625mm | 10 | 5.8400 | .09661 | .03055 |

| | Sig. (2-tailed) | Mean Difference | Std. Error Difference | 95% Confidence Interval of the Difference | |
|---|---|---|---|---|---|
| | | | | Lower | Upper |
| a | .419 | .02700 | .03266 | -.04162 | .09562 |
| b | .004 | .12600 | .03754 | .04713 | .20487 |
| c | .000 | -.18300 | .04118 | -.26951 | -.09649 |
| d | .472 | -.04000 | .05445 | -.15439 | .07439 |
| e | .011 | .10600 | .03766 | .02688 | .18512 |
| f | .002 | .30000 | .08393 | .12367 | .47633 |
| g | .001 | .11400 | .02737 | .05649 | .17151 |
| h | .003 | .10200 | .02924 | .04056 | .16344 |
| i | .312 | 4.67000 | 4.49118 | -4.76563 | 14.10563 |
| j | .000 | -.18100 | .03384 | -.25210 | -.10990 |
| hole | .929 | -.00300 | .03343 | -.07324 | .06724 |

### *Direct Phantom v CT Face Bone 1.25mm*

| | Object | N | Mean | Std. Deviation | Std. Error Mean |
|---|---|---|---|---|---|
| a | Direct Phantom Cube | 10 | 60.1170 | .02791 | .00883 |
| | Osirix CT Face Bone 1.25mm | 10 | 60.1300 | .13375 | .04230 |
| b | Direct Phantom Cube | 10 | 60.0860 | .01776 | .00562 |
| | Osirix CT Face Bone 1.25mm | 10 | 59.9100 | .13703 | .04333 |
| c | Direct Phantom Cube | 10 | 20.0670 | .02908 | .00920 |
| | Osirix CT Face Bone 1.25mm | 10 | 20.1200 | .10328 | .03266 |
| d | Direct Phantom Cube | 10 | 20.0800 | .03464 | .01095 |
| | Osirix CT Face Bone 1.25mm | 10 | 20.1100 | .12867 | .04069 |
| e | Direct Phantom Cube | 10 | 60.1060 | .02914 | .00921 |
| | Osirix CT Face Bone 1.25mm | 10 | 59.9800 | .07888 | .02494 |
| f | Direct Phantom Cube | 10 | 60.1800 | .25342 | .08014 |
| | Osirix CT Face Bone 1.25mm | 10 | 59.9200 | .13984 | .04422 |
| g | Direct Phantom Cube | 10 | 19.8840 | .02675 | .00846 |
| | Osirix CT Face Bone 1.25mm | 10 | 19.8800 | .09189 | .02906 |
| h | Direct Phantom Cube | 10 | 19.9120 | .02974 | .00940 |
| | Osirix CT Face Bone 1.25mm | 10 | 19.9900 | .15951 | .05044 |
| i | Direct Phantom Cube | 10 | 49.8900 | .03266 | .01033 |
| | Osirix CT Face Bone 1.25mm | 10 | 49.7000 | .11547 | .03651 |
| j | Direct Phantom Cube | 10 | 19.9890 | .01524 | .00482 |
| | Osirix CT Face Bone 1.25mm | 10 | 19.9400 | .10750 | .03399 |
| hole | Direct Phantom Cube | 10 | 5.8370 | .04296 | .01359 |
| | Osirix CT Face Bone 1.25mm | 10 | 5.2700 | .12517 | .03958 |

| | Sig. (2-tailed) | Mean Difference | Std. Error Difference | 95% Confidence Interval of the Difference | |
|---|---|---|---|---|---|
| | | | | Lower | Upper |
| a | .767 | -.01300 | .04321 | -.10377 | .07777 |
| b | .001 | .17600 | .04370 | .08420 | .26780 |
| c | .136 | -.05300 | .03393 | -.12428 | .01828 |
| d | .486 | -.03000 | .04214 | -.11853 | .05853 |
| e | .000 | .12600 | .02659 | .07013 | .18187 |
| f | .011 | .26000 | .09153 | .06770 | .45230 |
| g | .896 | .00400 | .03027 | -.05959 | .06759 |
| h | .146 | -.07800 | .05131 | -.18580 | .02980 |
| i | .000 | .19000 | .03795 | .11028 | .26972 |
| j | .171 | .04900 | .03433 | -.02313 | .12113 |
| hole | .000 | .56700 | .04185 | .47908 | .65492 |

## *Direct Phantom v CT Face Bone 2.5mm*

| | Object | N | Mean | Std. Deviation | Std. Error Mean |
|---|---|---|---|---|---|
| a | Direct Phantom Cube | 10 | 60.1170 | .02791 | .00883 |
| | Osirix CT Face Bone 2.5mm | 10 | 60.0700 | .14944 | .04726 |
| b | Direct Phantom Cube | 10 | 60.0860 | .01776 | .00562 |
| | Osirix CT Face Bone 2.5mm | 10 | 59.9900 | .25582 | .08090 |
| c | Direct Phantom Cube | 10 | 20.0670 | .02908 | .00920 |
| | Osirix CT Face Bone 2.5mm | 10 | 20.0100 | .16633 | .05260 |
| d | Direct Phantom Cube | 10 | 20.0800 | .03464 | .01095 |
| | Osirix CT Face Bone 2.5mm | 10 | 20.0300 | .18886 | .05972 |
| e | Direct Phantom Cube | 10 | 60.1060 | .02914 | .00921 |
| | Osirix CT Face Bone 2.5mm | 10 | 60.1700 | .20575 | .06506 |
| f | Direct Phantom Cube | 10 | 60.1800 | .25342 | .08014 |
| | Osirix CT Face Bone 2.5mm | 10 | 60.1100 | .16633 | .05260 |
| g | Direct Phantom Cube | 10 | 19.8840 | .02675 | .00846 |
| | Osirix CT Face Bone 2.5mm | 10 | 19.8600 | .16465 | .05207 |
| h | Direct Phantom Cube | 10 | 19.9120 | .02974 | .00940 |
| | Osirix CT Face Bone 2.5mm | 10 | 19.9300 | .17670 | .05588 |
| i | Direct Phantom Cube | 10 | 49.8900 | .03266 | .01033 |
| | Osirix CT Face Bone 2.5mm | 10 | 49.6100 | .23310 | .07371 |
| j | Direct Phantom Cube | 10 | 19.9890 | .01524 | .00482 |
| | Osirix CT Face Bone 2.5mm | 10 | 20.1400 | .21705 | .06864 |
| hole | Direct Phantom Cube | 10 | 5.8370 | .04296 | .01359 |
| | Osirix CT Face Bone 2.5mm | 10 | 4.8600 | .21187 | .06700 |

| | Sig. (2-tailed) | Mean Difference | Std. Error Difference | 95% Confidence Interval of the Difference | |
|---|---|---|---|---|---|
| | | | | Lower | Upper |
| a | .341 | .04700 | .04808 | -.05400 | .14800 |
| b | .252 | .09600 | .08109 | -.07437 | .26637 |
| c | .300 | .05700 | .05340 | -.05518 | .16918 |
| d | .421 | .05000 | .06072 | -.07756 | .17756 |
| e | .343 | -.06400 | .06571 | -.20206 | .07406 |
| f | .475 | .07000 | .09586 | -.13139 | .27139 |
| g | .655 | .02400 | .05275 | -.08683 | .13483 |
| h | .754 | -.01800 | .05666 | -.13704 | .10104 |
| i | .001 | .28000 | .07443 | .12363 | .43637 |
| j | .042 | -.15100 | .06881 | -.29556 | -.00644 |
| hole | .000 | .97700 | .06836 | .83338 | 1.12062 |

## *Direct Phantom v CT Face ST 0.625mm*

| | Object | N | Mean | Std. Deviation | Std. Error Mean |
|---|---|---|---|---|---|
| a | Direct Phantom Cube | 10 | 60.1170 | .02791 | .00883 |
| | Osirix CT Face ST 0.625mm | 10 | 59.8700 | .29078 | .09195 |
| b | Direct Phantom Cube | 10 | 60.0860 | .01776 | .00562 |
| | Osirix CT Face ST 0.625mm | 10 | 59.8800 | .12293 | .03887 |
| c | Direct Phantom Cube | 10 | 20.0670 | .02908 | .00920 |
| | Osirix CT Face ST 0.625mm | 10 | 20.0500 | .15811 | .05000 |
| d | Direct Phantom Cube | 10 | 20.0800 | .03464 | .01095 |
| | Osirix CT Face ST 0.625mm | 10 | 20.0100 | .14491 | .04583 |
| e | Direct Phantom Cube | 10 | 60.1060 | .02914 | .00921 |
| | Osirix CT Face ST 0.625mm | 10 | 59.9700 | .11595 | .03667 |
| f | Direct Phantom Cube | 10 | 60.1800 | .25342 | .08014 |
| | Osirix CT Face ST 0.625mm | 10 | 59.8300 | .09487 | .03000 |
| g | Direct Phantom Cube | 10 | 19.8840 | .02675 | .00846 |
| | Osirix CT Face ST 0.625mm | 10 | 19.7500 | .13540 | .04282 |
| h | Direct Phantom Cube | 10 | 19.9120 | .02974 | .00940 |
| | Osirix CT Face ST 0.625mm | 10 | 20.0300 | .17670 | .05588 |
| i | Direct Phantom Cube | 10 | 49.8900 | .03266 | .01033 |
| | Osirix CT Face ST 0.625mm | 10 | 49.6500 | .11785 | .03727 |
| j | Direct Phantom Cube | 10 | 19.9890 | .01524 | .00482 |
| | Osirix CT Face ST 0.625mm | 10 | 19.9100 | .21833 | .06904 |
| hole | Direct Phantom Cube | 10 | 5.8370 | .04296 | .01359 |
| | Osirix CT Face ST 0.625mm | 10 | 5.3300 | .09487 | .03000 |

| | Sig. (2-tailed) | Mean Difference | Std. Error Difference | 95% Confidence Interval of the Difference | |
|---|---|---|---|---|---|
| | | | | Lower | Upper |
| a | .015 | .24700 | .09238 | .05292 | .44108 |
| b | .000 | .20600 | .03928 | .12348 | .28852 |
| c | .742 | .01700 | .05084 | -.08981 | .12381 |
| d | .155 | .07000 | .04712 | -.02899 | .16899 |
| e | .002 | .13600 | .03781 | .05657 | .21543 |
| f | .001 | .35000 | .08557 | .17022 | .52978 |
| g | .007 | .13400 | .04365 | .04231 | .22569 |
| h | .052 | -.11800 | .05666 | -.23704 | .00104 |
| i | .000 | .24000 | .03867 | .15875 | .32125 |
| j | .269 | .07900 | .06921 | -.06640 | .22440 |
| hole | .000 | .50700 | .03293 | .43781 | .57619 |

### *Direct Phantom v CT Face ST 1.25mm*

| | Object | N | Mean | Std. Deviation | Std. Error Mean |
|---|---|---|---|---|---|
| a | Direct Phantom Cube | 10 | 60.1170 | .02791 | .00883 |
| | Osirix CT Face ST 1.25mm | 10 | 59.8300 | .17670 | .05588 |
| b | Direct Phantom Cube | 10 | 60.0860 | .01776 | .00562 |
| | Osirix CT Face ST 1.25mm | 10 | 60.0100 | .14491 | .04583 |
| c | Direct Phantom Cube | 10 | 20.0670 | .02908 | .00920 |
| | Osirix CT Face ST 1.25mm | 10 | 19.0200 | 2.89513 | .91552 |
| d | Direct Phantom Cube | 10 | 20.0800 | .03464 | .01095 |
| | Osirix CT Face ST 1.25mm | 10 | 19.9100 | .15951 | .05044 |
| e | Direct Phantom Cube | 10 | 60.1060 | .02914 | .00921 |
| | Osirix CT Face ST 1.25mm | 10 | 59.7700 | .14181 | .04485 |
| f | Direct Phantom Cube | 10 | 60.1800 | .25342 | .08014 |
| | Osirix CT Face ST 1.25mm | 10 | 59.9400 | .11738 | .03712 |
| g | Direct Phantom Cube | 10 | 19.8840 | .02675 | .00846 |
| | Osirix CT Face ST 1.25mm | 10 | 19.7700 | .19465 | .06155 |
| h | Direct Phantom Cube | 10 | 19.9120 | .02974 | .00940 |
| | Osirix CT Face ST 1.25mm | 10 | 19.5800 | .07888 | .02494 |
| i | Direct Phantom Cube | 10 | 49.8900 | .03266 | .01033 |
| | Osirix CT Face ST 1.25mm | 10 | 49.5400 | .19551 | .06182 |
| j | Direct Phantom Cube | 10 | 19.9890 | .01524 | .00482 |
| | Osirix CT Face ST 1.25mm | 10 | 19.8700 | .25408 | .08035 |
| hole | Direct Phantom Cube | 10 | 5.8370 | .04296 | .01359 |
| | Osirix CT Face ST 1.25mm | 10 | 4.9900 | .19692 | .06227 |

| | Sig. (2-tailed) | Mean Difference | Std. Error Difference | 95% Confidence Interval of the Difference | |
|---|---|---|---|---|---|
| | | | | Lower | Upper |
| a | .000 | .28700 | .05657 | .16815 | .40585 |
| b | .117 | .07600 | .04617 | -.02100 | .17300 |
| c | .268 | 1.04700 | .91557 | -.87653 | 2.97053 |
| d | .004 | .17000 | .05162 | .06155 | .27845 |
| e | .000 | .33600 | .04578 | .23982 | .43218 |
| f | .014 | .24000 | .08832 | .05445 | .42555 |
| g | .083 | .11400 | .06213 | -.01654 | .24454 |
| h | .000 | .33200 | .02666 | .27599 | .38801 |
| i | .000 | .35000 | .06268 | .21831 | .48169 |
| j | .157 | .11900 | .08049 | -.05011 | .28811 |
| hole | .000 | .84700 | .06374 | .71309 | .98091 |

## *Direct Phantom v CT Face 2.5mm*

| | Object | N | Mean | Std. Deviation | Std. Error Mean |
|---|---|---|---|---|---|
| a | Direct Phantom Cube | 10 | 60.1170 | .02791 | .00883 |
| | Osirix CT Face ST 2.5mm | 10 | 59.9500 | .16499 | .05217 |
| b | Direct Phantom Cube | 10 | 60.0860 | .01776 | .00562 |
| | Osirix CT Face ST 2.5mm | 10 | 60.2900 | .44585 | .14099 |
| c | Direct Phantom Cube | 10 | 20.0670 | .02908 | .00920 |
| | Osirix CT Face ST 2.5mm | 10 | 20.2790 | .29846 | .09438 |
| d | Direct Phantom Cube | 10 | 20.0800 | .03464 | .01095 |
| | Osirix CT Face ST 2.5mm | 10 | 19.9700 | .25841 | .08172 |
| e | Direct Phantom Cube | 10 | 60.1060 | .02914 | .00921 |
| | Osirix CT Face ST 2.5mm | 10 | 59.7900 | .31780 | .10050 |
| f | Direct Phantom Cube | 10 | 60.1800 | .25342 | .08014 |
| | Osirix CT Face ST 2.5mm | 10 | 59.8700 | .18886 | .05972 |
| g | Direct Phantom Cube | 10 | 19.8840 | .02675 | .00846 |
| | Osirix CT Face ST 2.5mm | 10 | 19.3500 | .27183 | .08596 |
| h | Direct Phantom Cube | 10 | 19.9120 | .02974 | .00940 |
| | Osirix CT Face ST 2.5mm | 10 | 19.7400 | .19551 | .06182 |
| i | Direct Phantom Cube | 10 | 49.8900 | .03266 | .01033 |
| | Osirix CT Face ST 2.5mm | 10 | 49.4000 | .16997 | .05375 |
| j | Direct Phantom Cube | 10 | 19.9890 | .01524 | .00482 |
| | Osirix CT Face ST 2.5mm | 10 | 19.8100 | .36040 | .11397 |
| hole | Direct Phantom Cube | 10 | 5.8370 | .04296 | .01359 |
| | Osirix CT Face ST 2.5mm | 10 | 5.0200 | .56725 | .17938 |

| | Sig. (2-tailed) | Mean Difference | Std. Error Difference | 95% Confidence Interval of the Difference | |
|---|---|---|---|---|---|
| | | | | Lower | Upper |
| a | .005 | .16700 | .05292 | .05583 | .27817 |
| b | .165 | -.20400 | .14110 | -.50044 | .09244 |
| c | .038 | -.21200 | .09483 | -.41122 | -.01278 |
| d | .199 | .11000 | .08245 | -.06322 | .28322 |
| e | .006 | .31600 | .10092 | .10397 | .52803 |
| f | .006 | .31000 | .09994 | .10002 | .51998 |
| g | .000 | .53400 | .08637 | .35254 | .71546 |
| h | .013 | .17200 | .06254 | .04062 | .30338 |
| i | .000 | .49000 | .05473 | .37501 | .60499 |
| j | .134 | .17900 | .11407 | -.06065 | .41865 |
| hole | .000 | .81700 | .17990 | .43905 | 1.19495 |

## *Direct Phantom v CT Helical Bone 0.625mm*

| | Object | N | Mean | Std. Deviation | Std. Error Mean |
|---|---|---|---|---|---|
| a | Direct Phantom Cube | 10 | 60.1170 | .02791 | .00883 |
| | Osirix CT Helical Bone 0.625mm | 10 | 59.8900 | .17288 | .05467 |
| b | Direct Phantom Cube | 10 | 60.0860 | .01776 | .00562 |
| | Osirix CT Helical Bone 0.625mm | 10 | 59.9100 | .11972 | .03786 |
| c | Direct Phantom Cube | 10 | 20.0670 | .02908 | .00920 |
| | Osirix CT Helical Bone 0.625mm | 10 | 20.1500 | .15811 | .05000 |
| d | Direct Phantom Cube | 10 | 20.0800 | .03464 | .01095 |
| | Osirix CT Helical Bone 0.625mm | 10 | 20.2000 | .08165 | .02582 |
| e | Direct Phantom Cube | 10 | 60.1060 | .02914 | .00921 |
| | Osirix CT Helical Bone 0.625mm | 10 | 59.9700 | .20575 | .06506 |
| f | Direct Phantom Cube | 10 | 60.1800 | .25342 | .08014 |
| | Osirix CT Helical Bone 0.625mm | 10 | 59.9900 | .11972 | .03786 |
| g | Direct Phantom Cube | 10 | 19.8840 | .02675 | .00846 |
| | Osirix CT Helical Bone 0.625mm | 10 | 19.7400 | .10750 | .03399 |
| h | Direct Phantom Cube | 10 | 19.9120 | .02974 | .00940 |
| | Osirix CT Helical Bone 0.625mm | 10 | 19.8200 | .11353 | .03590 |
| i | Direct Phantom Cube | 10 | 49.8900 | .03266 | .01033 |
| | Osirix CT Helical Bone 0.625mm | 10 | 49.4800 | .23476 | .07424 |
| j | Direct Phantom Cube | 10 | 19.9890 | .01524 | .00482 |
| | Osirix CT Helical Bone 0.625mm | 10 | 19.6900 | .11005 | .03480 |
| hole | Direct Phantom Cube | 10 | 5.8370 | .04296 | .01359 |
| | Osirix CT Helical Bone 0.625mm | 10 | 5.4900 | .05676 | .01795 |

| | Sig. (2-tailed) | Mean Difference | Std. Error Difference | 95% Confidence Interval of the Difference | |
|---|---|---|---|---|---|
| | | | | Lower | Upper |
| a | .001 | .22700 | .05538 | .11065 | .34335 |
| b | .000 | .17600 | .03827 | .09559 | .25641 |
| c | .120 | -.08300 | .05084 | -.18981 | .02381 |
| d | .000 | -.12000 | .02805 | -.17893 | -.06107 |
| e | .053 | .13600 | .06571 | -.00206 | .27406 |
| f | .046 | .19000 | .08863 | .00379 | .37621 |
| g | .001 | .14400 | .03503 | .07040 | .21760 |
| h | .023 | .09200 | .03711 | .01403 | .16997 |
| i | .000 | .41000 | .07495 | .25253 | .56747 |
| j | .000 | .29900 | .03513 | .22519 | .37281 |
| hole | .000 | .34700 | .02251 | .29970 | .39430 |

### *Direct Phantom v CT Helical Bone 1.25mm*

| | Object | N | Mean | Std. Deviation | Std. Error Mean |
|---|---|---|---|---|---|
| a | Direct Phantom Cube | 10 | 60.1170 | .02791 | .00883 |
| | Osirix CT Helical Bone 1.25mm | 10 | 60.1200 | .06325 | .02000 |
| b | Direct Phantom Cube | 10 | 60.0860 | .01776 | .00562 |
| | Osirix CT Helical Bone 1.25mm | 10 | 60.0600 | .12649 | .04000 |
| c | Direct Phantom Cube | 10 | 20.0670 | .02908 | .00920 |
| | Osirix CT Helical Bone 1.25mm | 10 | 20.1300 | .06749 | .02134 |
| d | Direct Phantom Cube | 10 | 20.0800 | .03464 | .01095 |
| | Osirix CT Helical Bone 1.25mm | 10 | 20.1000 | .08165 | .02582 |
| e | Direct Phantom Cube | 10 | 60.1060 | .02914 | .00921 |
| | Osirix CT Helical Bone 1.25mm | 10 | 60.1300 | .10593 | .03350 |
| f | Direct Phantom Cube | 10 | 60.1800 | .25342 | .08014 |
| | Osirix CT Helical Bone 1.25mm | 10 | 60.1600 | .12649 | .04000 |
| g | Direct Phantom Cube | 10 | 19.8840 | .02675 | .00846 |
| | Osirix CT Helical Bone 1.25mm | 10 | 19.9300 | .06749 | .02134 |
| h | Direct Phantom Cube | 10 | 19.9120 | .02974 | .00940 |
| | Osirix CT Helical Bone 1.25mm | 10 | 19.8900 | .13703 | .04333 |
| i | Direct Phantom Cube | 10 | 49.8900 | .03266 | .01033 |
| | Osirix CT Helical Bone 1.25mm | 10 | 49.8400 | .15776 | .04989 |
| j | Direct Phantom Cube | 10 | 19.9890 | .01524 | .00482 |
| | Osirix CT Helical Bone 1.25mm | 10 | 19.9600 | .05164 | .01633 |
| hole | Direct Phantom Cube | 10 | 5.8370 | .04296 | .01359 |
| | Osirix CT Helical Bone 1.25mm | 10 | 5.3700 | .10593 | .03350 |

| | Sig. (2-tailed) | Mean Difference | Std. Error Difference | 95% Confidence Interval of the Difference | |
|---|---|---|---|---|---|
| | | | | Lower | Upper |
| a | .892 | -.00300 | .02186 | -.04893 | .04293 |
| b | .528 | .02600 | .04039 | -.05886 | .11086 |
| c | .014 | -.06300 | .02324 | -.11183 | -.01417 |
| d | .485 | -.02000 | .02805 | -.07893 | .03893 |
| e | .499 | -.02400 | .03474 | -.09699 | .04899 |
| f | .826 | .02000 | .08957 | -.16817 | .20817 |
| g | .060 | -.04600 | .02296 | -.09423 | .00223 |
| h | .626 | .02200 | .04434 | -.07116 | .11516 |
| i | .339 | .05000 | .05095 | -.05703 | .15703 |
| j | .106 | .02900 | .01703 | -.00677 | .06477 |
| hole | .000 | .46700 | .03615 | .39105 | .54295 |

## *Direct Phantom v CT Helical Bone 2.5mm*

| | Object | N | Mean | Std. Deviation | Std. Error Mean |
|---|---|---|---|---|---|
| a | Direct Phantom Cube | 10 | 60.1170 | .02791 | .00883 |
| | Osirix CT Helical Bone 2.5mm | 10 | 60.0200 | .09189 | .02906 |
| b | Direct Phantom Cube | 10 | 60.0860 | .01776 | .00562 |
| | Osirix CT Helical Bone 2.5mm | 10 | 60.4500 | .15811 | .05000 |
| c | Direct Phantom Cube | 10 | 20.0670 | .02908 | .00920 |
| | Osirix CT Helical Bone 2.5mm | 10 | 19.9900 | .19120 | .06046 |
| d | Direct Phantom Cube | 10 | 20.0800 | .03464 | .01095 |
| | Osirix CT Helical Bone 2.5mm | 10 | 20.0000 | .24495 | .07746 |
| e | Direct Phantom Cube | 10 | 60.1060 | .02914 | .00921 |
| | Osirix CT Helical Bone 2.5mm | 10 | 60.1000 | .17638 | .05578 |
| f | Direct Phantom Cube | 10 | 60.1800 | .25342 | .08014 |
| | Osirix CT Helical Bone 2.5mm | 10 | 60.0900 | .17920 | .05667 |
| g | Direct Phantom Cube | 10 | 19.8840 | .02675 | .00846 |
| | Osirix CT Helical Bone 2.5mm | 10 | 19.8500 | .19579 | .06191 |
| h | Direct Phantom Cube | 10 | 19.9120 | .02974 | .00940 |
| | Osirix CT Helical Bone 2.5mm | 10 | 19.8800 | .15492 | .04899 |
| i | Direct Phantom Cube | 10 | 49.8900 | .03266 | .01033 |
| | Osirix CT Helical Bone 2.5mm | 10 | 49.6600 | .18974 | .06000 |
| j | Direct Phantom Cube | 10 | 19.9890 | .01524 | .00482 |
| | Osirix CT Helical Bone 2.5mm | 10 | 20.1200 | .09189 | .02906 |
| hole | Direct Phantom Cube | 10 | 5.8370 | .04296 | .01359 |
| | Osirix CT Helical Bone 2.5mm | 10 | 4.8500 | .16499 | .05217 |

| | Sig. (2-tailed) | Mean Difference | Std. Error Difference | 95% Confidence Interval of the Difference | |
|---|---|---|---|---|---|
| | | | | Lower | Upper |
| a | .005 | .09700 | .03037 | .03320 | .16080 |
| b | .000 | -.36400 | .05031 | -.46971 | -.25829 |
| c | .224 | .07700 | .06116 | -.05148 | .20548 |
| d | .320 | .08000 | .07823 | -.08436 | .24436 |
| e | .917 | .00600 | .05653 | -.11277 | .12477 |
| f | .371 | .09000 | .09815 | -.11620 | .29620 |
| g | .593 | .03400 | .06249 | -.09728 | .16528 |
| h | .529 | .03200 | .04988 | -.07280 | .13680 |
| i | .001 | .23000 | .06088 | .10209 | .35791 |
| j | .000 | -.13100 | .02946 | -.19289 | -.06911 |
| hole | .000 | .98700 | .05391 | .87373 | 1.10027 |

## *Direct Phantom v CT Helical ST 0.625mm*

| | Object | N | Mean | Std. Deviation | Std. Error Mean |
|---|---|---|---|---|---|
| a | Direct Phantom Cube | 10 | 60.1170 | .02791 | .00883 |
| | Osirix CT Helical ST 0.625mm | 10 | 59.8800 | .13984 | .04422 |
| b | Direct Phantom Cube | 10 | 60.0860 | .01776 | .00562 |
| | Osirix CT Helical ST 0.625mm | 10 | 60.0000 | .10541 | .03333 |
| c | Direct Phantom Cube | 10 | 20.0670 | .02908 | .00920 |
| | Osirix CT Helical ST 0.625mm | 10 | 20.0700 | .20028 | .06333 |
| d | Direct Phantom Cube | 10 | 20.0800 | .03464 | .01095 |
| | Osirix CT Helical ST 0.625mm | 10 | 20.2200 | .16865 | .05333 |
| e | Direct Phantom Cube | 10 | 60.1060 | .02914 | .00921 |
| | Osirix CT Helical ST 0.625mm | 10 | 59.9500 | .08498 | .02687 |
| f | Direct Phantom Cube | 10 | 60.1800 | .25342 | .08014 |
| | Osirix CT Helical ST 0.625mm | 10 | 59.9000 | .14142 | .04472 |
| g | Direct Phantom Cube | 10 | 19.8840 | .02675 | .00846 |
| | Osirix CT Helical ST 0.625mm | 10 | 19.7700 | .14944 | .04726 |
| h | Direct Phantom Cube | 10 | 19.9120 | .02974 | .00940 |
| | Osirix CT Helical ST 0.625mm | 10 | 19.8700 | .13375 | .04230 |
| i | Direct Phantom Cube | 10 | 49.8900 | .03266 | .01033 |
| | Osirix CT Helical ST 0.625mm | 10 | 49.6100 | .12867 | .04069 |
| j | Direct Phantom Cube | 10 | 19.9890 | .01524 | .00482 |
| | Osirix CT Helical ST 0.625mm | 10 | 19.6800 | .26998 | .08537 |
| hole | Direct Phantom Cube | 10 | 5.8370 | .04296 | .01359 |
| | Osirix CT Helical ST 0.625mm | 10 | 5.2300 | .14944 | .04726 |

| | Sig. (2-tailed) | Mean Difference | Std. Error Difference | 95% Confidence Interval of the Difference | |
|---|---|---|---|---|---|
| | | | | Lower | Upper |
| a | .000 | .23700 | .04509 | .14226 | .33174 |
| b | .020 | .08600 | .03380 | .01498 | .15702 |
| c | .963 | -.00300 | .06400 | -.13745 | .13145 |
| d | .019 | -.14000 | .05445 | -.25439 | -.02561 |
| e | .000 | .15600 | .02841 | .09631 | .21569 |
| f | .007 | .28000 | .09177 | .08719 | .47281 |
| g | .029 | .11400 | .04801 | .01314 | .21486 |
| h | .345 | .04200 | .04333 | -.04903 | .13303 |
| i | .000 | .28000 | .04198 | .19181 | .36819 |
| j | .002 | .30900 | .08551 | .12935 | .48865 |
| hole | .000 | .60700 | .04917 | .50369 | .71031 |

### *Direct Phantom v CT Helical ST 1.25mm*

| | Object | N | Mean | Std. Deviation | Std. Error Mean |
|---|---|---|---|---|---|
| a | Direct Phantom Cube | 10 | 60.1170 | .02791 | .00883 |
| | Osirix CT Helical ST 1.25mm | 10 | 59.9600 | .17127 | .05416 |
| b | Direct Phantom Cube | 10 | 60.0860 | .01776 | .00562 |
| | Osirix CT Helical ST 1.25mm | 10 | 59.8800 | .14757 | .04667 |
| c | Direct Phantom Cube | 10 | 20.0670 | .02908 | .00920 |
| | Osirix CT Helical ST 1.25mm | 10 | 19.8900 | .14491 | .04583 |
| d | Direct Phantom Cube | 10 | 20.0800 | .03464 | .01095 |
| | Osirix CT Helical ST 1.25mm | 10 | 20.0500 | .17159 | .05426 |
| e | Direct Phantom Cube | 10 | 60.1060 | .02914 | .00921 |
| | Osirix CT Helical ST 1.25mm | 10 | 59.9400 | .14298 | .04522 |
| f | Direct Phantom Cube | 10 | 60.1800 | .25342 | .08014 |
| | Osirix CT Helical ST 1.25mm | 10 | 59.8700 | .14181 | .04485 |
| g | Direct Phantom Cube | 10 | 19.8840 | .02675 | .00846 |
| | Osirix CT Helical ST 1.25mm | 10 | 19.6400 | .15055 | .04761 |
| h | Direct Phantom Cube | 10 | 19.9120 | .02974 | .00940 |
| | Osirix CT Helical ST 1.25mm | 10 | 19.8200 | .20976 | .06633 |
| i | Direct Phantom Cube | 10 | 49.8900 | .03266 | .01033 |
| | Osirix CT Helical ST 1.25mm | 10 | 49.5400 | .12649 | .04000 |
| j | Direct Phantom Cube | 10 | 19.9890 | .01524 | .00482 |
| | Osirix CT Helical ST 1.25mm | 10 | 19.7900 | .22828 | .07219 |
| hole | Direct Phantom Cube | 10 | 5.8370 | .04296 | .01359 |
| | Osirix CT Helical ST 1.25mm | 10 | 5.1300 | .10593 | .03350 |

| | Sig. (2-tailed) | Mean Difference | Std. Error Difference | 95% Confidence Interval of the Difference | |
|---|---|---|---|---|---|
| | | | | Lower | Upper |
| a | .010 | .15700 | .05487 | .04171 | .27229 |
| b | .000 | .20600 | .04700 | .10725 | .30475 |
| c | .001 | .17700 | .04674 | .07880 | .27520 |
| d | .595 | .03000 | .05536 | -.08630 | .14630 |
| e | .002 | .16600 | .04614 | .06905 | .26295 |
| f | .003 | .31000 | .09183 | .11707 | .50293 |
| g | .000 | .24400 | .04836 | .14241 | .34559 |
| h | .187 | .09200 | .06700 | -.04875 | .23275 |
| i | .000 | .35000 | .04131 | .26321 | .43679 |
| j | .013 | .19900 | .07235 | .04700 | .35100 |
| hole | .000 | .70700 | .03615 | .63105 | .78295 |

### *Direct Phantom v CT Helical ST 2.5mm*

| | Object | N | Mean | Std. Deviation | Std. Error Mean |
|---|---|---|---|---|---|
| a | Direct Phantom Cube | 10 | 60.1170 | .02791 | .00883 |
| | Osirix CT Helical ST 2.5mm | 10 | 59.9400 | .15055 | .04761 |
| b | Direct Phantom Cube | 10 | 60.0860 | .01776 | .00562 |
| | Osirix CT Helical ST 2.5mm | 10 | 60.2200 | .19889 | .06289 |
| c | Direct Phantom Cube | 10 | 20.0670 | .02908 | .00920 |
| | Osirix CT Helical ST 2.5mm | 10 | 20.1900 | .21833 | .06904 |
| d | Direct Phantom Cube | 10 | 20.0800 | .03464 | .01095 |
| | Osirix CT Helical ST 2.5mm | 10 | 20.2000 | .18257 | .05774 |
| e | Direct Phantom Cube | 10 | 60.1060 | .02914 | .00921 |
| | Osirix CT Helical ST 2.5mm | 10 | 59.8800 | .18738 | .05925 |
| f | Direct Phantom Cube | 10 | 60.1800 | .25342 | .08014 |
| | Osirix CT Helical ST 2.5mm | 10 | 59.8500 | .15811 | .05000 |
| g | Direct Phantom Cube | 10 | 19.8840 | .02675 | .00846 |
| | Osirix CT Helical ST 2.5mm | 10 | 19.5000 | .24495 | .07746 |
| h | Direct Phantom Cube | 10 | 19.9120 | .02974 | .00940 |
| | Osirix CT Helical ST 2.5mm | 10 | 19.8100 | .15239 | .04819 |
| i | Direct Phantom Cube | 10 | 49.8900 | .03266 | .01033 |
| | Osirix CT Helical ST 2.5mm | 10 | 49.7500 | .15092 | .04773 |
| j | Direct Phantom Cube | 10 | 19.9890 | .01524 | .00482 |
| | Osirix CT Helical ST 2.5mm | 10 | 19.7000 | .24495 | .07746 |
| hole | Direct Phantom Cube | 10 | 5.8370 | .04296 | .01359 |
| | Osirix CT Helical ST 2.5mm | 10 | 4.4200 | .17512 | .05538 |

| | Sig. (2-tailed) | Mean Difference | Std. Error Difference | 95% Confidence Interval of the Difference | |
|---|---|---|---|---|---|
| | | | | Lower | Upper |
| a | .002 | .17700 | .04842 | .07527 | .27873 |
| b | .048 | -.13400 | .06314 | -.26666 | -.00134 |
| c | .094 | -.12300 | .06965 | -.26933 | .02333 |
| d | .056 | -.12000 | .05877 | -.24346 | .00346 |
| e | .001 | .22600 | .05997 | .10001 | .35199 |
| f | .003 | .33000 | .09446 | .13155 | .52845 |
| g | .000 | .38400 | .07792 | .22030 | .54770 |
| h | .052 | .10200 | .04910 | -.00115 | .20515 |
| i | .010 | .14000 | .04883 | .03741 | .24259 |
| j | .002 | .28900 | .07761 | .12595 | .45205 |
| hole | .000 | 1.41700 | .05702 | 1.29721 | 1.53679 |

### *BB 1.5T 0.8mm v CT Helical Bone 0.625mm*

| | Object | N | Mean | Std. Deviation | Std. Error Mean |
|---|---|---|---|---|---|
| a | Osirix BB 1.5T 0.8mm | 10 | 60.2100 | .16633 | .05260 |
| | Osirix CT Helical Bone 0.625mm | 10 | 59.8900 | .17288 | .05467 |
| b | Osirix BB 1.5T 0.8mm | 10 | 60.1100 | .11972 | .03786 |
| | Osirix CT Helical Bone 0.625mm | 10 | 59.9100 | .11972 | .03786 |
| c | Osirix BB 1.5T 0.8mm | 10 | 20.3900 | .16633 | .05260 |
| | Osirix CT Helical Bone 0.625mm | 10 | 20.1500 | .15811 | .05000 |
| d | Osirix BB 1.5T 0.8mm | 10 | 20.2000 | .15635 | .04944 |
| | Osirix CT Helical Bone 0.625mm | 10 | 20.2000 | .08165 | .02582 |
| e | Osirix BB 1.5T 0.8mm | 10 | 60.2200 | .13166 | .04163 |
| | Osirix CT Helical Bone 0.625mm | 10 | 59.9700 | .20575 | .06506 |
| f | Osirix BB 1.5T 0.8mm | 10 | 59.9800 | .07888 | .02494 |
| | Osirix CT Helical Bone 0.625mm | 10 | 59.9900 | .11972 | .03786 |
| g | Osirix BB 1.5T 0.8mm | 10 | 20.1500 | .10801 | .03416 |
| | Osirix CT Helical Bone 0.625mm | 10 | 19.7400 | .10750 | .03399 |
| h | Osirix BB 1.5T 0.8mm | 10 | 20.0800 | .09189 | .02906 |
| | Osirix CT Helical Bone 0.625mm | 10 | 19.8200 | .11353 | .03590 |
| i | Osirix BB 1.5T 0.8mm | 10 | 49.5300 | .12517 | .03958 |
| | Osirix CT Helical Bone 0.625mm | 10 | 49.4800 | .23476 | .07424 |
| j | Osirix BB 1.5T 0.8mm | 10 | 20.0300 | .10593 | .03350 |
| | Osirix CT Helical Bone 0.625mm | 10 | 19.6900 | .11005 | .03480 |
| hole | Osirix BB 1.5T 0.8mm | 10 | 4.2700 | .09487 | .03000 |
| | Osirix CT Helical Bone 0.625mm | 10 | 5.4900 | .05676 | .01795 |

| | Sig. (2-tailed) | Mean Difference | Std. Error Difference | 95% Confidence Interval of the Difference | |
|---|---|---|---|---|---|
| | | | | Lower | Upper |
| a | .001 | .32000 | .07587 | .16061 | .47939 |
| b | .002 | .20000 | .05354 | .08751 | .31249 |
| c | .004 | .24000 | .07257 | .08753 | .39247 |
| d | 1.000 | .00000 | .05578 | -.11718 | .11718 |
| e | .005 | .25000 | .07724 | .08772 | .41228 |
| f | .828 | -.01000 | .04534 | -.10525 | .08525 |
| g | .000 | .41000 | .04819 | .30876 | .51124 |
| h | .000 | .26000 | .04619 | .16296 | .35704 |
| i | .560 | .05000 | .08413 | -.12675 | .22675 |
| j | .000 | .34000 | .04830 | .23852 | .44148 |
| hole | .000 | -1.22000 | .03496 | -1.29345 | -1.14655 |

## H.3 Mathematical Modelling

*Report from the University of Swansea*

**A Comparison of 3D Reconstructions from MR and CT Scans of a Phantom Box**

Kewei Zhang, Elaine Crooks and Antonio Orlando

### 1. Introduction

In this report, we present a procedure for a quantitative assessment of the accuracy of MR and CT scans of a phantom box. The assessment is pursued by comparing set of points retrieved from cross section images obtained by each imaging modality. Such set of points can represent either the whole reconstructed volume or the whole reconstructed surface or some of their subset. The comparison can have different level of detail. Such level can vary from a qualitative description such as to query whether the reconstructed model contains the feature of interest of the real object, which in turn depends on the scope of the examination, to a quantitative one, such as to give a measure of how much a set resembles the other. It follows, therefore, that to perform a comparison between imaging modalities one must first describe the process that reconstructs the object from its slice representation. Given a real object (which in our case is the phantom box), we have a geometrical representation of the object and of its surrounding in terms of slices. Slices orientation in the space might be the same or might change one from the other one. The slices contain in general 2d gray scale images that represent cross-sections of the object. The gray scale intensity is associated with a property that depends on the medical imaging modality, and on the behaviour of the object and its surrounding with respect to the physical process used by the medical imaging technique. It follows that for the reconstruction of the object of interest, one must in each slice locate the points belonging to the object. This step is called segmentation and represents a basic step for the object reconstruction in the procedure we are following.

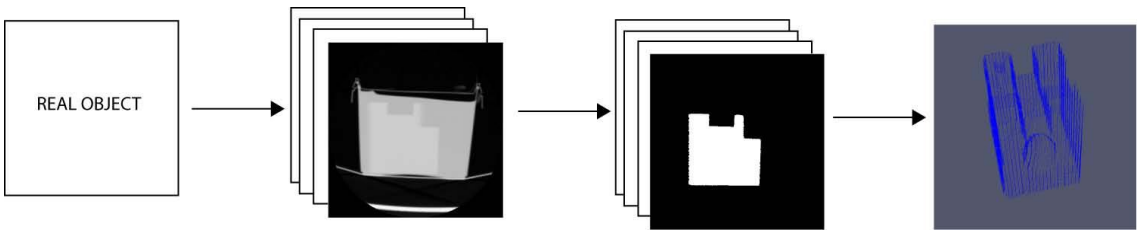



**Figure 1: Pipeline for the Vectorization of a Real Object Starting from Its Slice Representation**

The segmentation can aim at identifying either the solid region occupied by the object or only its boundary through the definition of an edge map. Metric information, such as pixel size, slice spacing, orientation and other, is stored in the overhead of each image file with the DICOM format

[1]. Such information can be then accessed and used to position each slice in the reference space, followed by segmentation and vectorization (that is, extraction of the coordinates) of the segmented object. With this data at hand, one can then perform surface and/or volume reconstruction following, for example, one of the methods surveyed in [2]. By this we actually mean that one is able to retrieve a digitized or vectorized representation of the shape of the object or of its boundary. Figure 1 sketches these steps. The geometric representation of the object in general will be different from the real object. Reasons for such differences can be ascribed to the physics of the imaging modality, to the reconstruction algorithm used to produce the slice representation, and to the methods used for the object reconstruction starting from the slices. We are interested here in providing a quantitative measure of the resemblance of the reconstructed objects, given that no geometric feature of the real object was known. Such measure must have preferably metric properties, that is, must be positive and have the properties of identity, symmetry and triangle inequality. Various distance functions have been used in literature [4], in particular much work has been based on the so-called Hausdorff distance [4]. Given two compact subset Ω1 and Ω2 of the Euclidean space $R^3$, the onesided Hausdorff distance H(Ω1, Ω2) from Ω1 to Ω2 is defined as

$$H(\Omega_1, \Omega_2) = \max_{x \in \Omega_1} \min_{y \in \Omega_2} ||x - y||, \qquad (1)$$

with ||x − y|| denoting the Euclidean distance between the points x and y. The Hausdorff distance between Ω1 and Ω2 is then given by:

$$dH(\Omega 1, \Omega 2) = \max \{ H(\Omega 1, \Omega 2), H(\Omega 2, \Omega 1)\}. \qquad (2)$$

This means that the two sets Ω1 and Ω2 are within the Hausdorff distance dH from each other if any point of the set Ω1 is within the distance dH from some point of the set Ω2. The function dH(Ω1, Ω2) is a metric but numerical experiments reported in [5] show that it is not robust with respect to small perturbation. The values of dH(Ω1, Ω2) can be large even in presence of small amounts of noise. In the context of object comparison, this can be a real problem since few outliers, which can inevitably occur as a result of a not clean segmentation, can perturb the value of dH(Ω1, Ω2) greatly, even though the two objects might be very similar. In order to alleviate such problem, in [5] it is proposed to consider the following measure

$$dMH(\Omega 1, \Omega 2) = \max \{ MH(\Omega 1, \Omega 2), MH(\Omega 2, \Omega 1)\}. \qquad (3)$$

where MH(Ω1, Ω2) is the average of the distances of the points of Ω2 to the set Ω2, that is,

$$MH(\Omega_1, \Omega_2) = \frac{1}{N_1} \sum_{x \in \Omega_1} \min_{y \in \Omega_2} ||x - y||. \qquad (4)$$

with N1 denoting the number of points in the set Ω1. The distance dMH(Ω1, Ω2) is positive and

meets the identity and symmetry property but not the triangular inequality. This means that one could not conclude that if two shapes are highly dissimilar to each other, then they will not be both similar to a some third shape. Another issue related to the measure of the mismatch between Ω1 and Ω2 is the so called pose estimation problem: The reconstructed geometries Ω1 and Ω2 can have arbitrary location, hence the problem of comparing the two objects should be formulated as to find a transformation from an allowed set (which in our case, being representation of the same real object, will be the group of the rigid body motion) that minimizes the distance between Ω1 and Ω2. Rather than solving such optimization problem, we split the problem into two separated ones. The first one, referred to as pose estimation problem, consists in using a criteria to properly position and align the two objects. The second one is the comparison measurement of the two objects by means of a Hausdorff type distance, such as the one given by equation (2) and equation (3). As for the solution of the pose estimation problem, we enquire whether there are intrinsic properties of the object that if taken to be coincident and the two objects were equal, then the two objects are in fact coincident. A partial answer to such question is obtained through the principal component analysis. Such analysis identifies the centre of mass and the principal axes of the secondorder central moment tensor as object intrinsic features that are not modified by rigid body motion. It follows that rather than taking all the rigid body motion, we will consider only those that take the barycentre and the principal axes of the object Ω1 to be coincident with the barycentre and the corresponding principal axes of the other object Ω2. Whether is taken Ω1 onto Ω2 or vice versa it is not relevant because by using the Hausdorff distance one would obtain the same result. Given the ambiguity on the sign of the principal directions for the positioning, we will have four rotations that make the principal axes of Ω1 and Ω2 coincident. As conclusion of this introduction, we recall the steps involved in the comparison of shapes reconstructed from slice representations. These are: i) segmentation ; ii) digitization/vectorization of the segmented region; iii) surface/volume reconstruction; iv) pose estimation; v) evaluation of the distance. Since the entire procedure is designed to be modular, this modularity should then facilitate the modification or replacement of the individual components with improved algorithms and identify the part of the procedure that eventually would produce major errors. The following sections are devoted to exemplify this procedure. Section 2 considers a special case where we take two sets of images corresponding to the same slice spacing and slice thickness but different resolution in the plane.

## 2. Comparison of CT Helical Head Protocol and Face Protocol

In this Section we describe the geometrical comparison of the object reconstructed from two different protocols of CT scan images with soft tissue algorithm reconstruction, the face central and the head helical protocol. Table 1 contains data taken from the image stacks stored in files with DICOM format. The voxel size is set equal to the pixel dimension and for the third dimension equal to the sum of Slice Thickness and Slice Spacing. The slices are assumed to be parallel to each other.

| Characteristics | CT Head Helical Protocol Soft Tissue | CT Face Protocol Soft Tissue |
|---|---|---|
| **Array Size** | **512 x 512** | **512 x 512** |
| **Density resolution** | **16 bits (65536 levels)** | **16 bits (65536 levels)** |
| **Pixel dimension** | **0.3066mm x 0. 3066mm** | **0.2930mm x 0.2930mm** |
| **Slice Thickness** | **2.5mm** | **2.5mm** |
| **Slice Spacing** | **0.65mm** | **0.65mm** |
| **Voxel dimension** | **0.3066mm x 0. 3066mm x 3.150mm** | **0.2930mm x 0.2930mm x 3.150mm** |
| **Number of slices** | **53** | **53** |

**Table 1: Characteristics of CT scans as they apply to the 3D reconstruction of image data**

**2.1 Segmentation**

We perform a manual segmentation of each slice, by identifying first the region of interest and then by setting a threshold, which is used to locate all the pixels with intensity value above such threshold. Both region of interest and threshold can change from slice to slice, with the threshold set by looking at the intensity profiles along scan lines drawn by the operator. The result of the segmentation is a binary image with value one at the pixels belonging to the object and zero otherwise. Since the images we are considering present a quite sharp contrast between the object and the background, a simple segmentation through setting a threshold can serve for the purpose. Figure 2 displays an instance of CT Scan image, together with the identification of the region of interest whereas Figure 3 displays the intensity value profile along the scan lines that are chosen by the user and used to set a lower and upper threshold for the segmentation. Figure 4 depicts the segmentation of the object whereas Figure 5 displays only the edges of the object of interest. The edges represent the contour lines of the boundary of the object. Whatever be the type of segmentation, the outcome is a binary image representing either cross section of the object or only the boundary of the object crosssections.

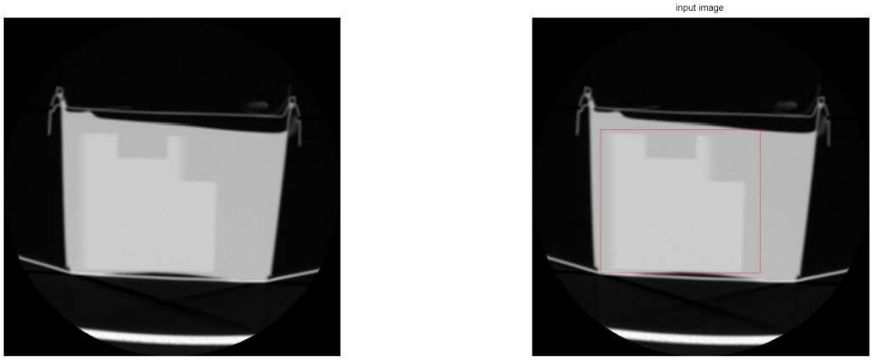



**Figure 2: CT scan image with identification of the region of interest**

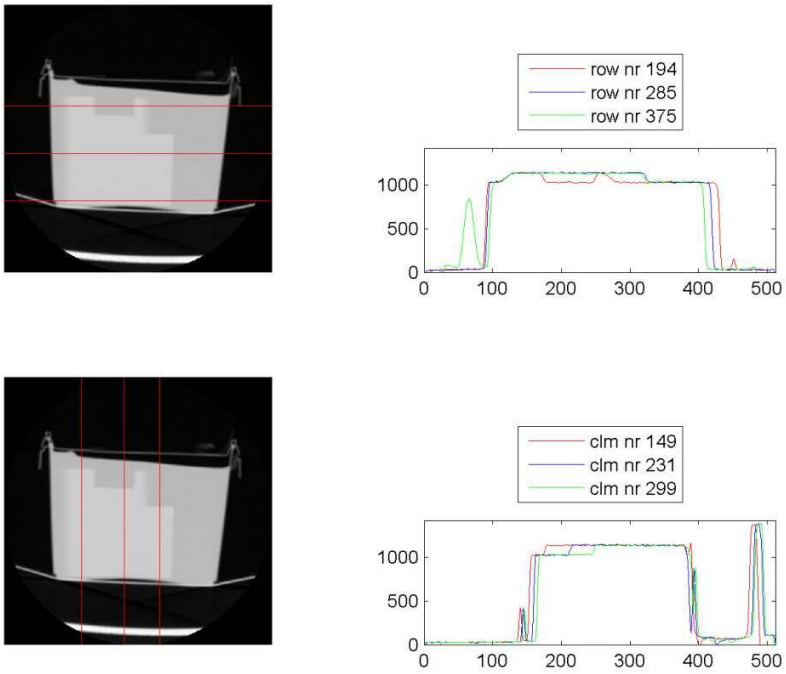



**Figure 3: Scan lines with intensity profile used to set lower and upper threshold for image segmentation.**




**Figure 4: Image Segmentation**




**Figure 5: Image Segmentation Through Edge Detection**

### 2.2. Vectorization

By vectorization here we mean the operation that maps the binary image contained in each slice into points of the Euclidean reference space. We assume here that the two stack of slices are parallel to each other and have the same orientation. This is a piece of information that should be retrieved from the overhead of the DICOM file. If the slices are not parallel to each other, their single orientation is anyway known in the field of observation and as such, this information can be used to compute the coordinates of the points. The Cartesian reference system is then set with one of its coordinate plane parallel to the common slice orientation and the other axis lying along the orthogonal direction. The outcome of the vectorization operation is the creation of a cloud of points representing the object of interest or its contours. Figure 6 displays the location of the cloud points obtained from the object segmentation of the two CT scan images stacks. Note that because of the no perfect clean segmentation, there are pots of points that do not belong to the object. Before any analysis these points should be cleaned out.

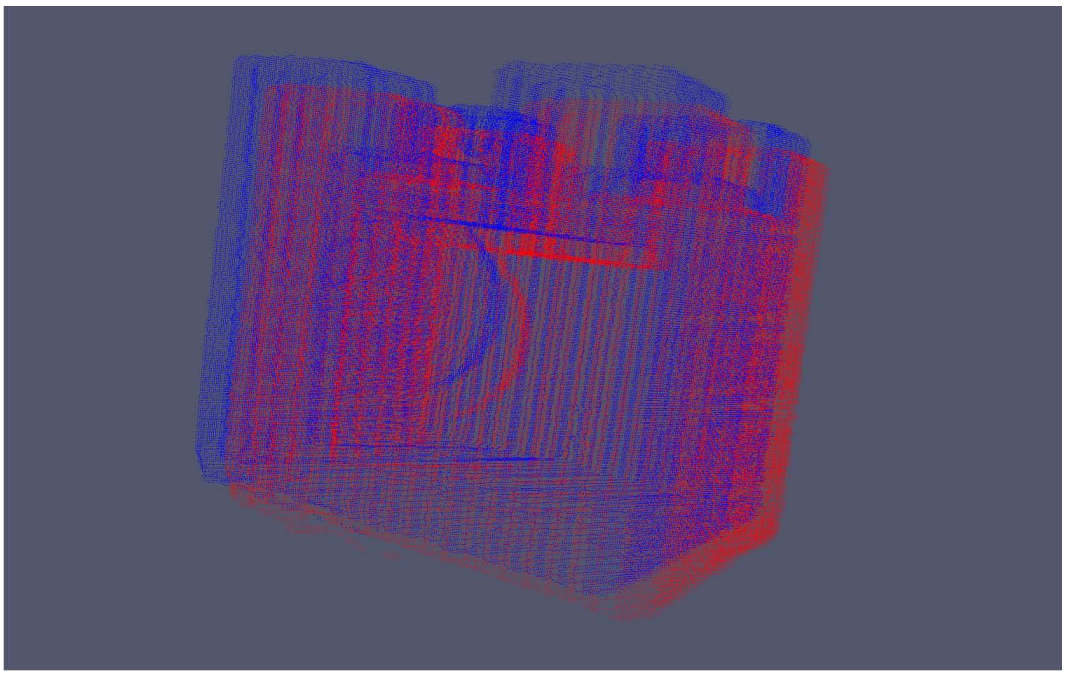


**Figure 6: Cloud points obtained from vectorization of the images segmentation. The one displayed in blue refers to the CT Face Protocol with the Soft Tissue Reconstruction algorithm whereas the one in red refers to the CT Helical Head Protocol with the Soft Tissue Reconstruction algorithm.**

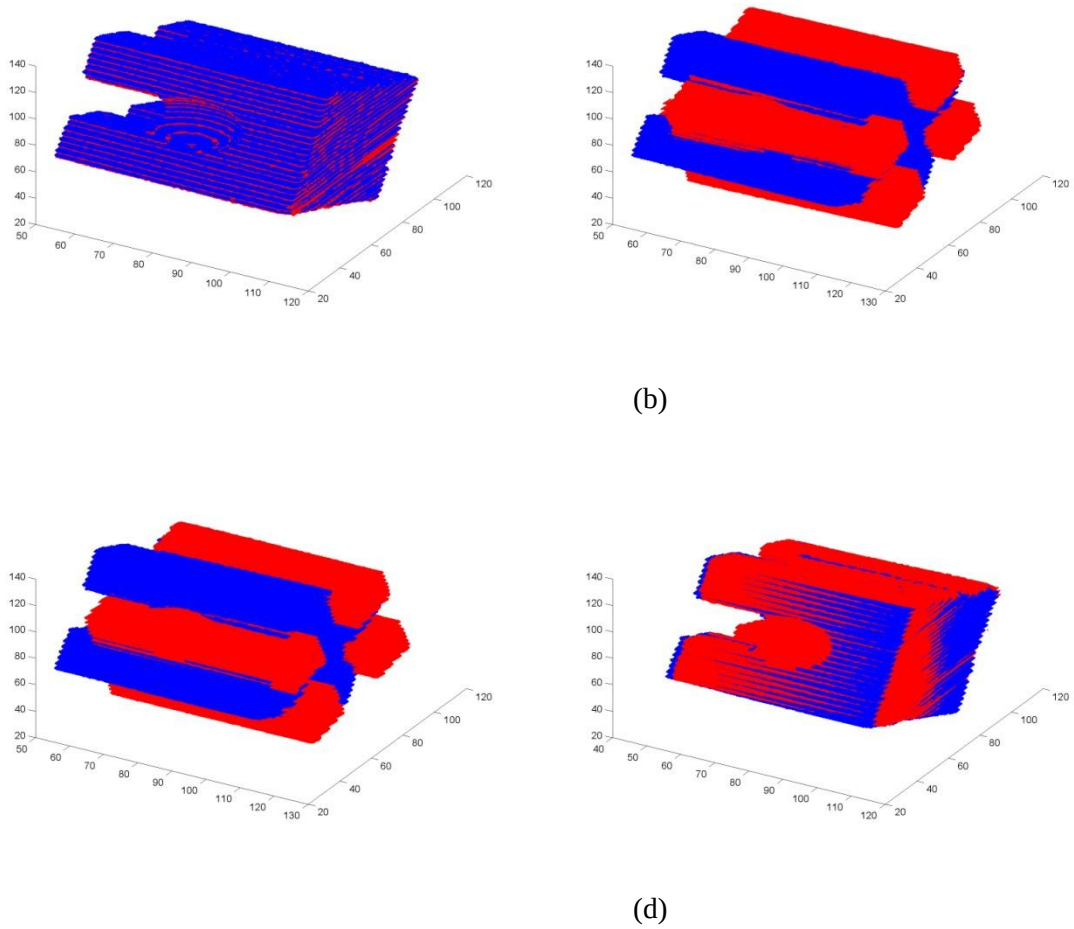
### 2.3. Surface/Volume Reconstruction

Given that the two CT scan image slices have the same slice thickness and slice spacing, and following the assumption that they have the same orientation with respect to the same reference system, we assume that up to a rigid body motion (translation and rotation) the slices of the two CT examinations can be made correspondent to each other. This means that we can then compare only the two cloud points representing the cross sections of the two objects, without need to reconstruct first either the surface or the volume. If that would not have been the case, then we would have had to perform surface or volume reconstruction and measure the distance between the resulting structures.

### 2.4 Pose Estimation

By inspecting Figure 6 we see that the slices of the two CT examinations, as positioned from the information retrieved by the corresponding DICOM, are not coincident one with each other. Before computing the distance between the two objects, we need therefore to bring the inspected objects into a standard pose. The problem is to find an affine transformation, representing a translation and rotation such that if the two objects were equal, in taking one object onto the other according such transformation and by evaluating then the distance, the distance is zero. As mentioned in the introduction, we carry out the principal component analysis as described in [6] which uses volume properties, such as the barycentre and the central principal axes, to position and align the objects.

Note that because of the ambiguity on the sign of the direction, we can find four rotations that can take the central axes of the inertia tensor of an object coincident with those of the other object. Figure 7 displays the result of the positioning according to these four rotations. The inspection of this Figure allows one already to identify the rotations that will yield the smallest values of the Hausdorff distance. In this example, these would be the rotations corresponding to Figure 7(a) and Figure 7(d).



(a) (b)

(c) (d)

**Figure 7: Effect of the Four Rotations Obtained from the Principal Component Analysis for the Pose estimation Problem**

### 2.5 Geometric similarity measurement

To assess how a cloud points representing one type of examination resembles the one representing the other type of examination, we use the Hausdorff distance and the modified Hausdorff distance as defined by the equation (2) and equation (3), respectively. For each examination, we then consider the following cloud points:

$\Omega i1$: denotes the cloud points obtained from object segmentation with small perturbation of the points, as a result of a noclean segmentation;

$\Omega i2$: denotes the cloud points obtained from object segmentation without points perturbation, i.e. as a result of a cleaned segmentation;

$\partial\Omega i1$: denotes the boundary/edges of $\Omega i1$;

$\partial\Omega i2$: denotes the boundary/edges of $\Omega i2$;

for i = 1,2 with i=1 denoting the CT Head Helical Protocol Soft Tissue and i=2 the CT Face Protocol Soft Tissue. Table 2 reports the values of the following distances of Hausdorff as given by equation (2): $dH(\Omega 11, \Omega 21)$ , $dH(\Omega 12, \Omega 22)$, $dH(\partial\Omega 11, \partial\Omega 21)$, $dH(\partial\Omega 12, \partial\Omega 22)$ and the corresponding values of the modified Hausdorff distance as given by equation (3). By referring to the clean segmentation, we have that the object reconstructed from the CT HH ST using the data in Table 1, has a volume equal to 240085.54 $mm^3$ whereas for the object reconstructed from the CT HH ST the volume is 237634.20$mm^3$ Note that the modified Hausdorff distance is more robust than the Hausdorff distance to the perturbation of the cloud points.

| CT HH ST | CT F ST | Hausdorff Distance | Modified Hausdorff Distance |
|---|---|---|---|
| $\Omega 1_1$ | $\Omega 2_1$ | 0.9326mm | 0.5484mm |
| $\Omega 1_2$ $Vol(\Omega_{12})$=240085.54 $mm_3$ | $\Omega 2_2$ $Vol(\Omega_{12})$=2376634.20 $mm_3$ | 0.7975mm | 0.5469mm |
| $\partial\Omega 1_1$ | $\partial\Omega 2_1$ | 0.9207mm | 0.2435mm |
| $\partial\Omega 1_2$ | $\partial\Omega 2_2$ | 0.7621mm | 0.2580mm |

**Table 2: Values of the Hausdorff Distance and of the Modified Hausdorff Distance for the point clouds corresponding to the CT Face Protocol with Soft Tissue and 2.5mm slice thickness, and to the CT Head Helical Protocol with Soft Tissue and 2.5mm slice thickness.**

**References**


[1] http://medical.nema.org/ (retrieved on March 2012)

[2] M. R. Stytz, G. Frieder, O. Frieder, Threedimensional medical imaging: Algorithms and computer systems, ACM Computing Surveys 23 (1991)

[3] C. Barillot, Surface and volume rendering techniques to display 3D data, IEEE Engineering in Medicine and Biology Magazine, 12 (1993) 111 – 119

[4] D. P. Huttenlocher, G. A. Klanderman, W. J. Rucklidge, Comparing images using the Hausdorff distance, IEEE Pattern Analysis and Machine Intelligence, 15 (1993) 850 863

[5] M. P. Dubuisson and A. K. Jain. A Modified Hausdorff distance for object matching. In Proc. of IAPR Int. Conf. on Pattern Recognition (1994) 566568

[6] M. Novotni, R. Klein, A geometric approach to 3D object comparison, SMI 2001 International Conference on Shape Modeling and Applications, 2001, 167 175

[7] K. Zhang, A. Orlando, E. Crooks, Image and Data Processing, Provisional application for patent in the European Union, PCT/EP2010/069815, December 15th, 2010

[8] J. Toriwaki, H. Yoshida, Fundamentals of Three Dimensional Digital Image Processing, Springer,

## H.4 Smoothing effects of Mimics on Phantom cube measurements

| | a | b | c | d | e | f | g | h | i | j | hole |
|---|---|---|---|---|---|---|---|---|---|---|---|
| **Phantom measurements without smoothing** | | | | | | | | | | | |
| **1** | 59.83 | 59.23 | 19.78 | 19.94 | 59.47 | 59.58 | 19.86 | 19.78 | 49.36 | 19.62 | 5.79 |
| **2** | 59.88 | 59.42 | 19.78 | 20.02 | 59.62 | 59.66 | 19.62 | 19.63 | 49.5 | 19.58 | 5.77 |
| **3** | 60.01 | 59.46 | 19.78 | 19.86 | 59.7 | 59.74 | 19.7 | 19.7 | 49.43 | 19.57 | 5.79 |
| **4** | 59.92 | 49.54 | 19.94 | 19.87 | 59.86 | 59.57 | 20.02 | 19.78 | 49.51 | 19.45 | 5.81 |
| **5** | 59.92 | 49.54 | 19.94 | 19.78 | 59.79 | 59.76 | 19.71 | 19.78 | 49.52 | 19.39 | 5.82 |
| **6** | 59.91 | 59.54 | 19.86 | 19.86 | 59.77 | 59.65 | 19.54 | 19.97 | 49.56 | 19.55 | 5.82 |
| **7** | 59.99 | 59.68 | 20.02 | 19.94 | 59.7 | 59.59 | 20 | 19.86 | 49.51 | 19.46 | 5.82 |
| **8** | 59.98 | 59.55 | 19.94 | 20.07 | 59.71 | 59.58 | 19.54 | 19.78 | 49.51 | 19.55 | 5.74 |
| **9** | 59.9 | 59.74 | 19.94 | 20.04 | 59.79 | 59.6 | 19.7 | 19.95 | 49.44 | 19.69 | 5.78 |
| **10** | 59.84 | 59.56 | 19.94 | 19.86 | 59.71 | 59.66 | 19.7 | 19.78 | 49.43 | 19.63 | 5.78 |
| **Iterations 2 smoothing 0.2** | | | | | | | | | | | |
| **1** | 60 | 59.7 | 19.9 | 19.81 | 59.69 | 59.72 | 19.79 | 19.82 | 49.34 | 19.58 | 5.8 |
| **2** | 59.75 | 59.74 | 19.95 | 20.06 | 59.84 | 59.6 | 19.8 | 19.75 | 49.47 | 19.81 | 5.77 |
| **3** | 59.92 | 59.64 | 19.89 | 20.09 | 59.83 | 59.69 | 19.59 | 19.74 | 49.95 | 19.66 | 5.79 |
| **4** | 59.9 | 59.64 | 19.82 | 19.89 | 59.69 | 59.61 | 19.59 | 19.82 | 49.33 | 19.58 | 5.78 |
| **5** | 59.98 | 59.64 | 19.96 | 20.05 | 59.83 | 59.6 | 19.66 | 19.81 | 49.26 | 19.58 | 5.78 |
| **6** | 59.83 | 59.64 | 19.75 | 19.82 | 59.69 | 59.6 | 19.45 | 19.9 | 49.48 | 19.6 | 5.73 |
| **7** | 59.82 | 59.64 | 19.67 | 20.04 | 59.69 | 59.52 | 19.53 | 19.66 | 49.55 | 19.73 | 5.77 |
| **8** | 59.82 | 59.56 | 19.74 | 19.9 | 59.77 | 59.6 | 19.82 | 19.66 | 49.47 | 19.94 | 5.79 |
| **9** | 59.9 | 59.64 | 19.83 | 19.89 | 59.62 | 59.7 | 19.58 | 19.74 | 49.4 | 19.73 | 5.73 |
| **10** | 59.97 | 59.41 | 19.97 | 19.74 | 59.7 | 59.6 | 19.51 | 19.59 | 49.33 | 19.65 | 5.79 |
| **Iterations 2 smooth 1** | | | | | | | | | | | |
| **1** | 60.04 | 59.42 | 19.72 | 19.81 | 59.59 | 59.59 | 19.66 | 19.73 | 49.5 | 19.71 | 5.82 |
| **2** | 59.97 | 59.64 | 19.5 | 19.72 | 59.44 | 59.61 | 19.84 | 19.58 | 49.42 | 19.56 | 5.78 |
| **3** | 59.81 | 59.81 | 19.73 | 19.59 | 59.59 | 59.52 | 19.5 | 19.58 | 49.5 | 19.56 | 5.82 |
| **4** | 59.96 | 59.57 | 19.58 | 19.66 | 59.66 | 59.59 | 19.64 | 19.57 | 49.27 | 19.56 | 5.76 |
| **5** | 59.97 | 59.57 | 19.57 | 19.72 | 59.66 | 59.46 | 19.57 | 19.79 | 49.35 | 19.56 | 5.8 |
| **6** | 59.96 | 59.74 | 19.83 | 19.72 | 59.52 | 59.52 | 19.72 | 19.87 | 49.5 | 19.5 | 5.8 |
| **7** | 59.89 | 59.57 | 19.57 | 19.79 | 59.59 | 59.61 | 19.72 | 19.72 | 49.5 | 19.27 | 5.8 |
| **8** | 59.89 | 59.59 | 19.42 | 19.73 | 59.52 | 59.52 | 19.5 | 19.57 | 49.42 | 19.39 | 5.86 |
| **9** | 59.9 | 59.81 | 19.57 | 19.64 | 59.66 | 59.67 | 19.57 | 19.73 | 49.42 | 19.14 | 5.7 |
| **10** | 59.89 | 59.5 | 19.57 | 19.65 | 59.51 | 59.52 | 19.5 | 19.64 | 49.35 | 19.22 | 5.91 |
| **Iterations 500 smooth 0.01** | | | | | | | | | | | |
| **1** | 60.03 | 59.64 | 19.68 | 19.78 | 59.64 | 59.68 | 19.41 | 19.5 | 49.33 | 19.49 | 5.78 |
| **2** | 59.85 | 59.73 | 19.68 | 19.86 | 59.67 | 59.5 | 19.5 | 19.41 | 49.23 | 19.4 | 5.7 |
| **3** | 59.96 | 59.73 | 19.77 | 19.86 | 59.67 | 59.68 | 19.32 | 19.5 | 49.31 | 19.41 | 5.78 |
| **4** | 59.96 | 59.64 | 19.77 | 19.68 | 59.57 | 59.67 | 19.42 | 19.59 | 49.4 | 19.41 | 5.75 |
| **5** | 59.97 | 60.18 | 19.69 | 19.77 | 59.65 | 59.49 | 19.5 | 19.59 | 49.47 | 19.56 | 5.78 |
| **6** | 59.9 | 60.27 | 19.88 | 19.77 | 59.57 | 59.58 | 19.41 | 19.5 | 49.32 | 19.23 | 5.78 |
| **7** | 59.99 | 59.74 | 19.68 | 19.86 | 59.72 | 59.59 | 19.59 | 19.5 | 49.4 | 19.86 | 5.8 |
| **8** | 59.87 | 59.81 | 19.59 | 19.98 | 59.57 | 59.6 | 19.32 | 19.32 | 49.25 | 19.51 | 5.76 |
| **9** | 60.04 | 59.66 | 19.77 | 19.86 | 59.33 | 59.58 | 19.51 | 19.41 | 49.32 | 19.4 | 5.77 |
| **10** | 59.94 | 60.19 | 19.88 | 19.77 | 59.57 | 59.67 | 19.51 | 19.41 | 49.4 | 19.33 | 5.69 |
| **Iterations 2 smooth 0.0001** | | | | | | | | | | | |
| **1** | 59.97 | 59.57 | 19.89 | 20.12 | 59.79 | 59.67 | 19.94 | 19.91 | 49.54 | 19.73 | 6.01 |
| **2** | 60.14 | 59.48 | 19.96 | 20.02 | 59.86 | 59.51 | 19.65 | 19.85 | 49.46 | 19.64 | 5.79 |
| **3** | 59.9 | 59.41 | 19.89 | 20.11 | 59.86 | 59.89 | 19.73 | 19.91 | 49.45 | 19.69 | 5.77 |
| **4** | 60.13 | 59.56 | 19.97 | 20.06 | 59.78 | 59.83 | 19.79 | 19.87 | 49.38 | 19.71 | 5.82 |
| **5** | 59.98 | 59.56 | 20.01 | 20.06 | 59.86 | 59.97 | 19.72 | 19.87 | 49.53 | 19.74 | 5.99 |
| **6** | 59.99 | 59.74 | 19.86 | 20.02 | 59.71 | 59.9 | 19.83 | 19.92 | 59.3 | 19.77 | 5.76 |
| **7** | 59.91 | 59.6 | 20.03 | 20.01 | 59.86 | 59.89 | 19.76 | 19.88 | 49.53 | 19.75 | 5.9 |
| **8** | 60.06 | 59.56 | 20.02 | 19.96 | 59.71 | 59.89 | 19.71 | 19.92 | 49.53 | 19.82 | 5.89 |
| **9** | 60.12 | 59.56 | 19.95 | 20.06 | 59.63 | 59.89 | 19.75 | 19.87 | 49.53 | 19.78 | 5.84 |
| **10** | 59.99 | 59.73 | 20.01 | 19.97 | 59.94 | 59.97 | 20.08 | 19.88 | 49.51 | 19.63 | 5.87 |
| **Iterations 2 smooth 0.01** | | | | | | | | | | | |
| **1** | 59.92 | 59.56 | 19.81 | 20.01 | 59.47 | 59.94 | 19.82 | 19.94 | 49.58 | 20.04 | 5.75 |
| **2** | 60.06 | 59.49 | 20.01 | 20.04 | 59.75 | 59.51 | 19.84 | 19.95 | 49.44 | 19.87 | 5.74 |
| **3** | 60.12 | 59.56 | 20.02 | 20.06 | 59.82 | 59.59 | 19.8 | 19.99 | 49.52 | 19.9 | 5.76 |
| **4** | 59.9 | 59.64 | 19.94 | 20 | 59.91 | 59.67 | 19.83 | 20.01 | 49.58 | 19.88 | 5.76 |
| **5** | 60.19 | 59.41 | 19.94 | 19.98 | 59.76 | 59.59 | 19.87 | 20.01 | 49.58 | 19.91 | 5.76 |
| **6** | 60.05 | 59.65 | 19.98 | 20.03 | 59.68 | 59.67 | 19.83 | 19.89 | 49.53 | 19.85 | 5.74 |
| **7** | 60.06 | 59.64 | 20.04 | 19.92 | 59.76 | 59.59 | 19.87 | 19.97 | 59.46 | 19.88 | 5.78 |
| **8** | 60.07 | 59.49 | 19.97 | 20.03 | 59.83 | 59.59 | 19.83 | 19.94 | 49.45 | 19.91 | 5.78 |
| **9** | 59.97 | 59.73 | 20.04 | 20.02 | 59.75 | 59.77 | 19.78 | 20.01 | 49.58 | 19.88 | 5.74 |
| **10** | 59.97 | 59.49 | 19.99 | 19.97 | 59.75 | 59.66 | 19.84 | 19.99 | 49.52 | 19.9 | 5.8 |

| | a | b | c | d | e | f | g | h | i | j | hole |
|---|---|---|---|---|---|---|---|---|---|---|---|
| **Iterations 5 smooth 0.0001** | | | | | | | | | | | |
| **1** | 59.92 | 59.28 | 19.96 | 20.06 | 59.73 | 59.49 | 19.68 | 19.87 | 49.41 | 19.71 | 5.84 |
| **2** | 59.98 | 59.56 | 19.9 | 20.1 | 59.58 | 59.73 | 19.72 | 19.83 | 49.41 | 19.72 | 5.76 |
| **3** | 60.06 | 59.36 | 20.01 | 20.1 | 59.73 | 59.73 | 19.77 | 19.72 | 49.41 | 19.9 | 5.76 |
| **4** | 60.06 | 59.45 | 19.91 | 20.06 | 59.84 | 59.82 | 19.77 | 19.96 | 50.01 | 19.85 | 5.73 |
| **5** | 60.06 | 59.45 | 19.96 | 20.01 | 59.52 | 59.74 | 19.77 | 19.87 | 49.34 | 19.81 | 5.77 |
| **6** | 60.06 | 59.45 | 19.96 | 20.01 | 59.73 | 59.81 | 19.86 | 19.82 | 49.45 | 19.86 | 5.78 |
| **7** | 59.98 | 59.45 | 20.01 | 20.01 | 59.66 | 59.73 | 19.77 | 19.82 | 49.56 | 19.79 | 5.76 |
| **8** | 59.98 | 59.39 | 19.97 | 20.1 | 59.56 | 59.73 | 19.77 | 19.77 | 49.33 | 19.56 | 5.75 |
| **9** | 60.06 | 59.38 | 19.92 | 19.97 | 59.73 | 59.64 | 19.72 | 19.72 | 49.41 | 19.54 | 5.79 |
| **10** | 59.9 | 59.45 | 20.06 | 20.06 | 59.66 | 59.74 | 19.91 | 19.81 | 49.49 | 19.63 | 5.78 |
| **Iterations 5 smooth 0.01** | | | | | | | | | | | |
| **1** | 60.02 | 59.39 | 19.94 | 20.1 | 59.79 | 59.55 | 19.76 | 19.86 | 49.56 | 19.79 | 5.78 |
| **2** | 59.94 | 59.39 | 19.88 | 19.88 | 59.7 | 59.82 | 19.71 | 19.82 | 49.61 | 19.87 | 5.76 |
| **3** | 59.94 | 59.39 | 19.88 | 20 | 59.94 | 59.62 | 19.88 | 19.82 | 49.58 | 19.87 | 5.75 |
| **4** | 59.86 | 59.47 | 19.82 | 20.09 | 59.7 | 59.7 | 19.81 | 19.98 | 49.58 | 19.87 | 5.73 |
| **5** | 59.86 | 59.39 | 19.93 | 20.04 | 59.63 | 59.54 | 19.91 | 19.86 | 49.52 | 19.79 | 5.77 |
| **6** | 60.03 | 59.39 | 19.82 | 19.98 | 59.7 | 59.54 | 19.85 | 19.85 | 49.48 | 19.91 | 5.73 |
| **7** | 59.95 | 60.04 | 19.83 | 19.98 | 59.86 | 59.62 | 19.74 | 19.81 | 49.66 | 19.87 | 5.75 |
| **8** | 59.86 | 59.39 | 19.79 | 20.1 | 59.86 | 59.7 | 19.82 | 19.89 | 49.56 | 19.79 | 5.74 |
| **9** | 60.02 | 59.55 | 19.83 | 19.94 | 59.79 | 59.55 | 19.74 | 19.86 | 49.41 | 19.91 | 5.78 |
| **10** | 59.94 | 59.64 | 19.88 | 19.99 | 59.78 | 59.46 | 19.77 | 19.85 | 49.56 | 19.87 | 5.75 |
| **Iterations 5 smooth 0.2** | | | | | | | | | | | |
| **1** | 59.87 | 59.43 | 19.99 | 20 | 59.69 | 59.59 | 19.66 | 19.76 | 49.57 | 19.79 | 5.76 |
| **2** | 60.01 | 59.43 | 19.88 | 19.93 | 59.77 | 59.58 | 19.73 | 19.8 | 49.47 | 19.64 | 5.77 |
| **3** | 60.02 | 59.68 | 19.9 | 20 | 59.7 | 59.68 | 19.83 | 19.8 | 49.49 | 19.61 | 5.78 |
| **4** | 60.01 | 59.51 | 19.88 | 20 | 59.84 | 59.51 | 19.84 | 19.9 | 49.4 | 19.61 | 5.74 |
| **5** | 60.01 | 59.6 | 19.81 | 20.03 | 59.92 | 59.65 | 19.76 | 19.83 | 49.31 | 19.64 | 5.77 |
| **6** | 60.01 | 59.51 | 19.91 | 20 | 59.77 | 59.65 | 19.76 | 19.83 | 49.56 | 19.61 | 5.74 |
| **7** | 60.01 | 59.58 | 19.91 | 19.96 | 59.69 | 59.65 | 19.7 | 19.86 | 49.39 | 19.54 | 5.75 |
| **8** | 60.01 | 59.51 | 19.93 | 19.93 | 59.76 | 59.5 | 19.76 | 19.83 | 49.4 | 19.79 | 5.74 |
| **9** | 59.87 | 59.58 | 19.95 | 20.03 | 59.85 | 59.58 | 19.7 | 19.86 | 49.4 | 19.64 | 5.76 |
| **10** | 59.94 | 59.67 | 19.87 | 19.97 | 59.77 | 59.5 | 19.73 | 19.9 | 49.56 | 19.82 | 5.72 |
| **Iterations 25 smooth 0.0001** | | | | | | | | | | | |
| **1** | 59.87 | 59.31 | 19.92 | 20.01 | 59.46 | 59.63 | 19.83 | 19.88 | 49.37 | 19.76 | 5.76 |
| **2** | 59.78 | 59.39 | 19.98 | 19.99 | 59.87 | 59.71 | 19.8 | 19.92 | 49.53 | 19.72 | 5.79 |
| **3** | 59.95 | 59.63 | 20.01 | 19.98 | 59.88 | 59.62 | 19.74 | 19.91 | 49.44 | 19.88 | 5.78 |
| **4** | 59.88 | 59.55 | 20.02 | 19.97 | 59.79 | 59.7 | 19.8 | 19.89 | 49.52 | 19.62 | 5.79 |
| **5** | 59.8 | 59.47 | 20.01 | 20.04 | 59.81 | 59.62 | 19.77 | 19.91 | 49.37 | 19.67 | 5.77 |
| **6** | 59.86 | 59.55 | 19.98 | 19.97 | 59.79 | 59.73 | 19.76 | 19.91 | 49.54 | 19.75 | 5.76 |
| **7** | 59.88 | 59.47 | 20.02 | 20.01 | 59.71 | 59.63 | 19.82 | 19.87 | 49.52 | 19.8 | 5.8 |
| **8** | 59.89 | 59.47 | 19.98 | 20.06 | 59.63 | 59.63 | 19.88 | 19.85 | 49.62 | 19.77 | 5.71 |
| **9** | 59.95 | 59.56 | 19.95 | 20.01 | 59.89 | 59.63 | 19.94 | 19.81 | 49.45 | 19.76 | 5.76 |
| **10** | 59.95 | 59.39 | 20.02 | 19.97 | 59.95 | 59.62 | 19.84 | 19.97 | 49.45 | 19.74 | 5.76 |
| **Iterations 25 smooth 0.01** | | | | | | | | | | | |
| **1** | 59.94 | 59.57 | 19.95 | 20.02 | 59.71 | 59.73 | 19.86 | 19.83 | 49.39 | 19.87 | 5.76 |
| **2** | 60.01 | 59.49 | 19.96 | 20.02 | 59.75 | 59.72 | 19.87 | 19.86 | 49.61 | 19.89 | 5.78 |
| **3** | 59.86 | 59.64 | 19.95 | 20.01 | 59.79 | 59.72 | 20.03 | 19.9 | 49.53 | 19.92 | 5.77 |
| **4** | 60 | 59.63 | 20 | 20 | 59.71 | 59.65 | 19.85 | 19.95 | 49.54 | 19.93 | 5.77 |
| **5** | 59.94 | 59.64 | 20 | 19.95 | 59.78 | 59.72 | 19.8 | 19.96 | 49.57 | 19.9 | 5.78 |
| **6** | 60 | 59.56 | 19.99 | 20.02 | 59.79 | 59.64 | 19.77 | 19.86 | 49.53 | 19.86 | 5.62 |
| **7** | 59.86 | 59.58 | 19.99 | 19.99 | 59.79 | 59.59 | 19.85 | 19.92 | 49.61 | 19.87 | 5.59 |
| **8** | 59.94 | 59.49 | 20.01 | 19.99 | 59.88 | 59.72 | 20 | 19.89 | 49.3 | 19.92 | 5.6 |
| **9** | 60 | 59.49 | 19.99 | 19.96 | 59.81 | 59.73 | 19.8 | 19.9 | 49.54 | 19.89 | 5.59 |
| **10** | 59.93 | 59.63 | 19.92 | 19.92 | 59.72 | 59.72 | 19.87 | 19.85 | 49.46 | 19.86 | 5.52 |
| **Iterations 50 smooth 0.0001** | | | | | | | | | | | |
| **1** | 59.96 | 59.48 | 19.92 | 19.94 | 59.66 | 59.62 | 19.84 | 19.85 | 49.55 | 19.96 | 5.84 |
| **2** | 59.81 | 59.55 | 20.02 | 20.04 | 59.89 | 59.64 | 19.84 | 19.9 | 49.44 | 19.91 | 5.77 |
| **3** | 59.88 | 59.42 | 20 | 20.02 | 59.88 | 59.56 | 19.83 | 19.95 | 49.5 | 19.91 | 5.85 |
| **4** | 59.97 | 59.57 | 19.96 | 19.97 | 59.74 | 59.75 | 19.87 | 19.83 | 49.51 | 19.84 | 5.75 |
| **5** | 60.03 | 59.55 | 19.97 | 20 | 59.66 | 59.91 | 19.82 | 19.97 | 49.41 | 19.88 | 5.83 |
| **6** | 60.06 | 59.5 | 19.91 | 19.96 | 59.89 | 59.71 | 19.88 | 19.9 | 49.42 | 19.91 | 5.8 |
| **7** | 60.05 | 59.64 | 19.99 | 19.98 | 59.74 | 59.73 | 19.85 | 19.85 | 49.4 | 19.84 | 5.84 |
| **8** | 59.96 | 59.56 | 19.96 | 19.98 | 59.82 | 59.65 | 19.86 | 19.91 | 49.57 | 19.84 | 5.77 |
| **9** | 59.97 | 59.54 | 19.99 | 19.96 | 59.82 | 59.65 | 19.84 | 19.87 | 49.49 | 19.89 | 5.84 |
| **10** | 60.03 | 59.49 | 19.98 | 19.99 | 59.74 | 59.56 | 19.79 | 19.84 | 49.43 | 19.91 | 5.79 |

| | a | b | c | d | e | f | g | h | i | j | hole |
|---|---|---|---|---|---|---|---|---|---|---|---|
| **Iterations 50 smooth 0.01** | | | | | | | | | | | |
| **1** | 60.02 | 59.94 | 19.93 | 20.02 | 59.72 | 59.48 | 19.95 | 19.89 | 49.53 | 19.86 | 5.83 |
| **2** | 59.78 | 59.94 | 19.97 | 19.96 | 59.79 | 59.67 | 19.8 | 19.82 | 49.47 | 19.86 | 5.84 |
| **3** | 60.02 | 59.47 | 20.01 | 19.99 | 59.71 | 59.7 | 19.89 | 19.96 | 49.62 | 19.79 | 5.81 |
| **4** | 59.94 | 59.55 | 19.99 | 19.92 | 59.64 | 59.63 | 19.82 | 19.86 | 49.48 | 19.83 | 5.83 |
| **5** | 59.95 | 59.62 | 19.99 | 20.02 | 59.87 | 59.48 | 19.78 | 19.89 | 49.46 | 19.75 | 5.81 |
| **6** | 59.85 | 59.54 | 19.9 | 19.99 | 59.79 | 59.56 | 19.87 | 19.95 | 49.33 | 19.83 | 5.84 |
| **7** | 59.94 | 59.46 | 20 | 19.99 | 59.79 | 59.57 | 19.8 | 19.92 | 49.38 | 19.91 | 5.85 |
| **8** | 59.86 | 59.54 | 19.96 | 20.03 | 59.89 | 59.84 | 19.87 | 19.92 | 49.61 | 19.76 | 5.77 |
| **9** | 59.86 | 59.9 | 19.96 | 20.03 | 59.87 | 59.64 | 19.82 | 19.82 | 49.54 | 19.87 | 5.83 |
| **10** | 59.94 | 59.71 | 19.96 | 20.03 | 59.56 | 59.68 | 19.82 | 19.84 | 49.53 | 19.86 | 5.83 |
| **Iterations 100 smooth 0.0001** | | | | | | | | | | | |
| **1** | 60.02 | 59.55 | 19.95 | 19.96 | 59.77 | 59.63 | 19.68 | 19.9 | 49.54 | 19.74 | 5.86 |
| **2** | 59.87 | 59.55 | 20.01 | 20 | 59.85 | 59.71 | 19.67 | 19.95 | 49.46 | 19.83 | 5.78 |
| **3** | 60.02 | 59.55 | 19.97 | 19.96 | 59.78 | 59.71 | 19.85 | 19.81 | 49.48 | 19.83 | 5.86 |
| **4** | 60.02 | 59.55 | 19.91 | 20.01 | 59.85 | 59.65 | 19.82 | 19.95 | 49.63 | 19.83 | 5.8 |
| **5** | 59.79 | 59.63 | 20.02 | 19.94 | 59.77 | 59.7 | 19.71 | 19.89 | 49.49 | 19.92 | 5.76 |
| **6** | 60.02 | 59.47 | 19.96 | 19.97 | 59.77 | 59.55 | 19.72 | 19.9 | 49.53 | 19.92 | 5.8 |
| **7** | 59.95 | 59.47 | 20.01 | 20 | 59.77 | 59.63 | 19.81 | 19.9 | 49.83 | 19.83 | 5.78 |
| **8** | 59.94 | 59.72 | 20.01 | 19.91 | 59.62 | 59.71 | 19.83 | 19.95 | 49.61 | 19.83 | 5.75 |
| **9** | 60.03 | 59.47 | 19.97 | 19.9 | 59.92 | 59.71 | 19.85 | 19.86 | 49.61 | 19.88 | 5.8 |
| **10** | 59.86 | 59.64 | 19.91 | 19.91 | 59.77 | 59.62 | 19.8 | 19.9 | 49.54 | 19.87 | 5.81 |
| **Iterations 100 smooth 0.01** | | | | | | | | | | | |
| **1** | 60.02 | 59.41 | 19.93 | 20 | 59.69 | 59.8 | 19.76 | 19.9 | 49.46 | 19.83 | 5.86 |
| **2** | 59.93 | 59.46 | 19.93 | 19.95 | 59.69 | 59.77 | 19.82 | 19.86 | 49.46 | 19.83 | 5.8 |
| **3** | 59.85 | 59.7 | 19.9 | 19.97 | 59.69 | 59.58 | 19.82 | 19.82 | 49.46 | 19.76 | 5.82 |
| **4** | 59.94 | 59.62 | 19.92 | 19.96 | 59.77 | 59.53 | 19.79 | 19.87 | 49.57 | 19.86 | 5.84 |
| **5** | 59.93 | 59.54 | 19.89 | 19.95 | 59.68 | 59.63 | 19.82 | 19.87 | 49.37 | 19.86 | 5.86 |
| **6** | 60.02 | 59.46 | 19.89 | 19.87 | 59.77 | 59.61 | 19.75 | 19.95 | 49.55 | 19.84 | 5.86 |
| **7** | 59.86 | 59.72 | 19.95 | 19.98 | 59.69 | 59.61 | 19.71 | 19.85 | 49.49 | 19.79 | 5.84 |
| **8** | 59.77 | 59.54 | 19.85 | 19.99 | 59.69 | 59.53 | 19.75 | 19.86 | 49.37 | 19.83 | 5.82 |
| **9** | 59.85 | 59.54 | 19.97 | 19.9 | 59.68 | 59.75 | 19.86 | 19.9 | 49.39 | 19.86 | 5.84 |
| **10** | 59.94 | 59.54 | 19.89 | 19.97 | 59.77 | 59.44 | 19.82 | 19.9 | 49.37 | 19.76 | 5.84 |
| **Iterations 250 smooth 0.0001** | | | | | | | | | | | |
| **1** | 59.79 | 59.55 | 20 | 19.97 | 59.75 | 59.54 | 20.03 | 19.97 | 49.5 | 19.97 | 5.78 |
| **2** | 59.78 | 59.55 | 19.99 | 20.03 | 59.6 | 59.46 | 19.83 | 19.97 | 49.34 | 19.94 | 5.86 |
| **3** | 59.86 | 59.56 | 19.97 | 19.87 | 59.68 | 59.62 | 19.76 | 19.9 | 49.56 | 19.77 | 5.82 |
| **4** | 59.94 | 59.64 | 19.94 | 20 | 59.68 | 59.62 | 19.82 | 19.87 | 49.42 | 19.84 | 5.82 |
| **5** | 59.87 | 59.76 | 19.9 | 20.04 | 59.75 | 59.7 | 19.8 | 19.9 | 49.57 | 19.87 | 5.88 |
| **6** | 59.87 | 59.65 | 19.98 | 19.95 | 59.75 | 59.79 | 19.96 | 19.87 | 49.42 | 19.87 | 5.86 |
| **7** | 59.7 | 59.65 | 20 | 19.9 | 59.83 | 59.62 | 19.79 | 19.93 | 49.41 | 19.87 | 5.86 |
| **8** | 59.86 | 59.55 | 19.87 | 19.93 | 59.83 | 59.63 | 19.8 | 19.8 | 49.36 | 19.87 | 5.86 |
| **9** | 59.86 | 59.47 | 19.93 | 19.98 | 59.83 | 59.54 | 19.83 | 19.87 | 49.47 | 19.84 | 5.8 |
| **10** | 59.94 | 59.55 | 19.98 | 19.97 | 59.75 | 59.78 | 19.86 | 19.83 | 49.63 | 19.91 | 5.84 |
| **Iterations 250 smooth 0.01** | | | | | | | | | | | |
| **1** | 59.98 | 59.78 | 19.93 | 19.96 | 59.58 | 59.59 | 19.79 | 19.8 | 49.45 | 19.74 | 5.81 |
| **2** | 59.97 | 59.65 | 19.9 | 19.97 | 59.66 | 59.6 | 19.82 | 19.79 | 49.46 | 19.83 | 5.79 |
| **3** | 59.97 | 59.78 | 19.91 | 20.03 | 59.58 | 59.67 | 19.83 | 19.83 | 49.44 | 19.87 | 5.84 |
| **4** | 59.97 | 59.77 | 19.83 | 20 | 59.9 | 59.67 | 19.72 | 19.79 | 49.44 | 19.83 | 5.83 |
| **5** | 59.98 | 59.7 | 19.87 | 19.97 | 59.89 | 59.67 | 19.83 | 19.89 | 49.44 | 19.77 | 5.83 |
| **6** | 59.96 | 59.65 | 19.91 | 20.03 | 59.82 | 59.66 | 19.83 | 19.8 | 49.5 | 19.77 | 5.83 |
| **7** | 59.97 | 59.68 | 19.91 | 19.96 | 59.89 | 59.74 | 19.8 | 19.84 | 49.44 | 19.77 | 5.86 |
| **8** | 59.96 | 59.56 | 19.92 | 20.04 | 59.82 | 59.97 | 19.84 | 19.79 | 49.44 | 19.84 | 5.81 |
| **9** | 59.97 | 59.65 | 19.98 | 20 | 59.74 | 60.03 | 19.83 | 19.79 | 49.44 | 19.83 | 5.82 |
| **10** | 59.97 | 59.64 | 19.89 | 19.97 | 59.89 | 59.86 | 19.83 | 19.82 | 49.44 | 19.87 | 5.83 |
| **Iterations 500 smooth 0.0001** | | | | | | | | | | | |
| **1** | 60.04 | 59.79 | 19.97 | 19.97 | 59.63 | 59.72 | 19.84 | 19.8 | 49.61 | 19.62 | 5.85 |
| **2** | 59.56 | 59.84 | 19.97 | 20.01 | 59.62 | 59.97 | 19.87 | 19.86 | 49.59 | 19.74 | 5.85 |
| **3** | 60.06 | 59.47 | 19.93 | 20.01 | 59.79 | 59.72 | 19.8 | 19.87 | 49.41 | 19.87 | 5.81 |
| **4** | 59.79 | 59.71 | 19.96 | 20.05 | 59.87 | 59.63 | 19.83 | 19.84 | 49.62 | 19.91 | 5.79 |
| **5** | 59.87 | 59.73 | 20 | 20.04 | 59.87 | 59.8 | 19.86 | 19.83 | 49.52 | 19.91 | 5.82 |
| **6** | 59.95 | 59.55 | 19.96 | 20.01 | 59.87 | 59.71 | 19.8 | 19.81 | 49.56 | 19.84 | 5.85 |
| **7** | 50.87 | 59.51 | 20.03 | 20.03 | 59.78 | 59.63 | 19.8 | 19.8 | 49.69 | 19.74 | 5.79 |
| **8** | 60.03 | 59.81 | 19.93 | 19.98 | 59.78 | 59.71 | 19.77 | 19.83 | 49.52 | 19.74 | 5.8 |
| **9** | 60.03 | 59.4 | 20.04 | 19.95 | 59.87 | 59.8 | 19.8 | 19.87 | 49.44 | 19.87 | 5.84 |
| **10** | 60.03 | 59.51 | 19.97 | 19.98 | 59.86 | 59.73 | 19.84 | 19.91 | 49.45 | 19.81 | 5.81 |

## H.4.1. Smoothing Effects: Statistical Analysis

### *Smoothing 0.0001, Iterations 2*

| | Group | N | Mean | Std. Deviation | Std. Error Mean |
|---|---|---|---|---|---|
| A | Original without smoothing | 10 | 59.9180 | .06070 | .01919 |
| | Iterations 2, Smoothing 0.0001 | 10 | 60.0190 | .08850 | .02799 |
| B | Original without smoothing | 10 | 57.5260 | 4.21129 | 1.33173 |
| | Iterations 2, Smoothing 0.0001 | 10 | 59.5770 | .09945 | .03145 |
| C | Original without smoothing | 10 | 19.8920 | .08600 | .02719 |
| | Iterations 2, Smoothing 0.0001 | 10 | 19.9590 | .06100 | .01929 |
| D | Original without smoothing | 10 | 19.9240 | .09454 | .02990 |
| | Iterations 2, Smoothing 0.0001 | 10 | 20.0390 | .05322 | .01683 |
| E | Original without smoothing | 10 | 59.7120 | .10789 | .03412 |
| | Iterations 2, Smoothing 0.0001 | 10 | 59.8000 | .09404 | .02974 |
| F | Original without smoothing | 10 | 59.6390 | .06790 | .02147 |
| | Iterations 2, Smoothing 0.0001 | 10 | 59.8410 | .14348 | .04537 |
| G | Original without smoothing | 10 | 19.7390 | .17013 | .05380 |
| | Iterations 2, Smoothing 0.0001 | 10 | 19.7960 | .12686 | .04012 |
| H | Original without smoothing | 10 | 19.8010 | .10322 | .03264 |
| | Iterations 2, Smoothing 0.0001 | 10 | 19.8880 | .02486 | .00786 |
| I | Original without smoothing | 10 | 49.4770 | .05964 | .01886 |
| | Iterations 2, Smoothing 0.0001 | 10 | 50.4760 | 3.10086 | .98058 |
| J | Original without smoothing | 10 | 19.5490 | .09183 | .02904 |
| | Iterations 2, Smoothing 0.0001 | 10 | 19.7260 | .06022 | .01904 |
| Hole | Original without smoothing | 10 | 5.7920 | .02616 | .00827 |
| | Iterations 2, Smoothing 0.0001 | 10 | 5.8640 | .08618 | .02725 |

| | Sig. (2-tailed) | Mean Difference | Std. Error Difference | 95% Confidence Interval of the Difference | |
|---|---|---|---|---|---|
| | | | | Lower | Upper |
| A | .008 | -.10100 | .03394 | -.17230 | -.02970 |
| B | .141 | -2.05100 | 1.33210 | -4.84964 | .74764 |
| C | .060 | -.06700 | .03334 | -.13705 | .00305 |
| D | .004 | -.11500 | .03431 | -.18708 | -.04292 |
| E | .068 | -.08800 | .04526 | -.18309 | .00709 |
| F | .001 | -.20200 | .05020 | -.30746 | -.09654 |
| G | .407 | -.05700 | .06711 | -.19799 | .08399 |
| H | .018 | -.08700 | .03357 | -.15754 | -.01646 |
| I | .322 | -.99900 | .98076 | -3.05950 | 1.06150 |
| J | .000 | -.17700 | .03473 | -.24996 | -.10404 |
| Hole | .021 | -.07200 | .02848 | -.13183 | -.01217 |

### *Smoothing 0.0001, Iterations 5*

| | Group | N | Mean | Std. Deviation | Std. Error Mean |
|---|---|---|---|---|---|
| A | Original without smoothing | 10 | 59.9180 | .06070 | .01919 |
| | Iterations 5, Smoothing 0.0001 | 10 | 60.0060 | .06257 | .01979 |
| B | Original without smoothing | 10 | 57.5260 | 4.21129 | 1.33173 |
| | Iterations 5, Smoothing 0.0001 | 10 | 59.4220 | .07436 | .02351 |
| C | Original without smoothing | 10 | 19.8920 | .08600 | .02719 |
| | Iterations 5, Smoothing 0.0001 | 10 | 19.9660 | .04993 | .01579 |
| D | Original without smoothing | 10 | 19.9240 | .09454 | .02990 |
| | Iterations 5, Smoothing 0.0001 | 10 | 20.0480 | .04590 | .01451 |
| E | Original without smoothing | 10 | 59.7120 | .10789 | .03412 |
| | Iterations 5, Smoothing 0.0001 | 10 | 59.6740 | .09778 | .03092 |
| F | Original without smoothing | 10 | 59.6390 | .06790 | .02147 |
| | Iterations 5, Smoothing 0.0001 | 10 | 59.7160 | .09336 | .02952 |
| G | Original without smoothing | 10 | 19.7390 | .17013 | .05380 |
| | Iterations 5, Smoothing 0.0001 | 10 | 19.7740 | .06720 | .02125 |
| H | Original without smoothing | 10 | 19.8010 | .10322 | .03264 |
| | Iterations 5, Smoothing 0.0001 | 10 | 19.8190 | .07249 | .02292 |
| I | Original without smoothing | 10 | 49.4770 | .05964 | .01886 |
| | Iterations 5, Smoothing 0.0001 | 10 | 49.4820 | .19719 | .06236 |
| J | Original without smoothing | 10 | 19.5490 | .09183 | .02904 |
| | Iterations 5, Smoothing 0.0001 | 10 | 19.7370 | .12702 | .04017 |
| Hole | Original without smoothing | 10 | 5.7920 | .02616 | .00827 |
| | Iterations 5, Smoothing 0.0001 | 10 | 5.7720 | .02936 | .00929 |

| | Sig. (2-tailed) | Mean Difference | Std. Error Difference | 95% Confidence Interval of the Difference | |
|---|---|---|---|---|---|
| | | | | Lower | Upper |
| A | .005 | -.08800 | .02757 | -.14592 | -.03008 |
| B | .172 | -1.89600 | 1.33194 | -4.69429 | .90229 |
| C | .030 | -.07400 | .03145 | -.14007 | -.00793 |
| D | .002 | -.12400 | .03323 | -.19382 | -.05418 |
| E | .420 | .03800 | .04604 | -.05873 | .13473 |
| F | .049 | -.07700 | .03650 | -.15369 | -.00031 |
| G | .553 | -.03500 | .05784 | -.15653 | .08653 |
| H | .657 | -.01800 | .03989 | -.10180 | .06580 |
| I | .940 | -.00500 | .06515 | -.14187 | .13187 |
| J | .001 | -.18800 | .04956 | -.29213 | -.08387 |
| Hole | .125 | .02000 | .01244 | -.00613 | .04613 |

### *Smoothing 0.0001, Iterations 25*

| | Group | N | Mean | Std. Deviation | Std. Error Mean |
|---|---|---|---|---|---|
| A | Original without smoothing | 10 | 59.9180 | .06070 | .01919 |
| | Iterations 25, Smoothing 0.0001 | 10 | 59.8810 | .05934 | .01876 |
| B | Original without smoothing | 10 | 57.5260 | 4.21129 | 1.33173 |
| | Iterations 25, Smoothing 0.0001 | 10 | 59.4790 | .09666 | .03057 |
| C | Original without smoothing | 10 | 19.8920 | .08600 | .02719 |
| | Iterations 25, Smoothing 0.0001 | 10 | 19.9890 | .03381 | .01069 |
| D | Original without smoothing | 10 | 19.9240 | .09454 | .02990 |
| | Iterations 25, Smoothing 0.0001 | 10 | 20.0010 | .03107 | .00983 |
| E | Original without smoothing | 10 | 59.7120 | .10789 | .03412 |
| | Iterations 25, Smoothing 0.0001 | 10 | 59.7780 | .14528 | .04594 |
| F | Original without smoothing | 10 | 59.6390 | .06790 | .02147 |
| | Iterations 25, Smoothing 0.0001 | 10 | 59.6520 | .04315 | .01365 |
| G | Original without smoothing | 10 | 19.7390 | .17013 | .05380 |
| | Iterations 25, Smoothing 0.0001 | 10 | 19.8180 | .05940 | .01879 |
| H | Original without smoothing | 10 | 19.8010 | .10322 | .03264 |
| | Iterations 25, Smoothing 0.0001 | 10 | 19.8920 | .04341 | .01373 |
| I | Original without smoothing | 10 | 49.4770 | .05964 | .01886 |
| | Iterations 25, Smoothing 0.0001 | 10 | 49.4810 | .07923 | .02505 |
| J | Original without smoothing | 10 | 19.5490 | .09183 | .02904 |
| | Iterations 25, Smoothing 0.0001 | 10 | 19.7470 | .07009 | .02216 |
| Hole | Original without smoothing | 10 | 5.7920 | .02616 | .00827 |
| | Iterations 25, Smoothing 0.0001 | 10 | 5.7680 | .02530 | .00800 |

| | Sig. (2-tailed) | Mean Difference | Std. Error Difference | 95% Confidence Interval of the Difference | |
|---|---|---|---|---|---|
| | | | | Lower | Upper |
| A | .185 | .03700 | .02684 | -.01940 | .09340 |
| B | .160 | -1.95300 | 1.33208 | -4.75159 | .84559 |
| C | .004 | -.09700 | .02922 | -.15839 | -.03561 |
| D | .025 | -.07700 | .03147 | -.14312 | -.01088 |
| E | .264 | -.06600 | .05722 | -.18622 | .05422 |
| F | .616 | -.01300 | .02544 | -.06645 | .04045 |
| G | .183 | -.07900 | .05698 | -.19872 | .04072 |
| H | .019 | -.09100 | .03541 | -.16539 | -.01661 |
| I | .900 | -.00400 | .03136 | -.06988 | .06188 |
| J | .000 | -.19800 | .03653 | -.27475 | -.12125 |
| Hole | .052 | .02400 | .01151 | -.00018 | .04818 |

### *Smoothing 0.0001, Iterations 50*

| | Group | N | Mean | Std. Deviation | Std. Error Mean |
|---|---|---|---|---|---|
| A | Original without smoothing | 10 | 59.9180 | .06070 | .01919 |
| | Iterations 50, Smoothing 0.0001 | 10 | 59.9720 | .07857 | .02485 |
| B | Original without smoothing | 10 | 57.5260 | 4.21129 | 1.33173 |
| | Iterations 50, Smoothing 0.0001 | 10 | 59.5300 | .06018 | .01903 |
| C | Original without smoothing | 10 | 19.8920 | .08600 | .02719 |
| | Iterations 50, Smoothing 0.0001 | 10 | 19.9700 | .03432 | .01085 |
| D | Original without smoothing | 10 | 19.9240 | .09454 | .02990 |
| | Iterations 50, Smoothing 0.0001 | 10 | 19.9840 | .02989 | .00945 |
| E | Original without smoothing | 10 | 59.7120 | .10789 | .03412 |
| | Iterations 50, Smoothing 0.0001 | 10 | 59.7840 | .08872 | .02806 |
| F | Original without smoothing | 10 | 59.6390 | .06790 | .02147 |
| | Iterations 50, Smoothing 0.0001 | 10 | 59.6780 | .10379 | .03282 |
| G | Original without smoothing | 10 | 19.7390 | .17013 | .05380 |
| | Iterations 50, Smoothing 0.0001 | 10 | 19.8420 | .02573 | .00814 |
| H | Original without smoothing | 10 | 19.8010 | .10322 | .03264 |
| | Iterations 50, Smoothing 0.0001 | 10 | 19.8870 | .04739 | .01499 |
| I | Original without smoothing | 10 | 49.4770 | .05964 | .01886 |
| | Iterations 50, Smoothing 0.0001 | 10 | 49.4720 | .06033 | .01908 |
| J | Original without smoothing | 10 | 19.5490 | .09183 | .02904 |
| | Iterations 50, Smoothing 0.0001 | 10 | 19.8890 | .03957 | .01251 |
| Hole | Original without smoothing | 10 | 5.7920 | .02616 | .00827 |
| | Iterations 50, Smoothing 0.0001 | 10 | 5.8080 | .03645 | .01153 |

| | Sig. (2-tailed) | Mean Difference | Std. Error Difference | 95% Confidence Interval of the Difference | |
|---|---|---|---|---|---|
| | | | | Lower | Upper |
| A | .103 | -.05400 | .03140 | -.11996 | .01196 |
| B | .150 | -2.00400 | 1.33186 | -4.80214 | .79414 |
| C | .016 | -.07800 | .02928 | -.13952 | -.01648 |
| D | .072 | -.06000 | .03135 | -.12587 | .00587 |
| E | .120 | -.07200 | .04417 | -.16480 | .02080 |
| F | .333 | -.03900 | .03922 | -.12140 | .04340 |
| G | .075 | -.10300 | .05441 | -.21731 | .01131 |
| H | .028 | -.08600 | .03592 | -.16146 | -.01054 |
| I | .854 | .00500 | .02683 | -.05136 | .06136 |
| J | .000 | -.34000 | .03162 | -.40643 | -.27357 |
| Hole | .274 | -.01600 | .01419 | -.04581 | .01381 |

### *Smoothing 0.0001, Iterations 100*

| | Group | N | Mean | Std. Deviation | Std. Error Mean |
|---|---|---|---|---|---|
| A | Original without smoothing | 10 | 59.9180 | .06070 | .01919 |
| | Iterations 100, Smoothing 0.0001 | 10 | 59.9520 | .08574 | .02711 |
| B | Original without smoothing | 10 | 57.5260 | 4.21129 | 1.33173 |
| | Iterations 100, Smoothing 0.0001 | 10 | 59.5600 | .08273 | .02616 |
| C | Original without smoothing | 10 | 19.8920 | .08600 | .02719 |
| | Iterations 100, Smoothing 0.0001 | 10 | 19.9720 | .04077 | .01289 |
| D | Original without smoothing | 10 | 19.9240 | .09454 | .02990 |
| | Iterations 100, Smoothing 0.0001 | 10 | 19.9560 | .04033 | .01275 |
| E | Original without smoothing | 10 | 59.7120 | .10789 | .03412 |
| | Iterations 100, Smoothing 0.0001 | 10 | 59.7870 | .07818 | .02472 |
| F | Original without smoothing | 10 | 59.6390 | .06790 | .02147 |
| | Iterations 100, Smoothing 0.0001 | 10 | 59.6620 | .05493 | .01737 |
| G | Original without smoothing | 10 | 19.7390 | .17013 | .05380 |
| | Iterations 100, Smoothing 0.0001 | 10 | 19.7740 | .07106 | .02247 |
| H | Original without smoothing | 10 | 19.8010 | .10322 | .03264 |
| | Iterations 100, Smoothing 0.0001 | 10 | 19.9010 | .04383 | .01386 |
| I | Original without smoothing | 10 | 49.4770 | .05964 | .01886 |
| | Iterations 100, Smoothing 0.0001 | 10 | 49.5720 | .10768 | .03405 |
| J | Original without smoothing | 10 | 19.5490 | .09183 | .02904 |
| | Iterations 100, Smoothing 0.0001 | 10 | 19.8480 | .05287 | .01672 |
| Hole | Original without smoothing | 10 | 5.7920 | .02616 | .00827 |
| | Iterations 100, Smoothing 0.0001 | 10 | 5.8000 | .03682 | .01164 |

| | Sig. (2-tailed) | Mean Difference | Std. Error Difference | 95% Confidence Interval of the Difference | |
|---|---|---|---|---|---|
| | | | | Lower | Upper |
| A | .320 | -.03400 | .03322 | -.10379 | .03579 |
| B | .144 | -2.03400 | 1.33199 | -4.83240 | .76440 |
| C | .016 | -.08000 | .03010 | -.14323 | -.01677 |
| D | .338 | -.03200 | .03250 | -.10029 | .03629 |
| E | .092 | -.07500 | .04213 | -.16352 | .01352 |
| F | .416 | -.02300 | .02762 | -.08102 | .03502 |
| G | .556 | -.03500 | .05830 | -.15749 | .08749 |
| H | .011 | -.10000 | .03546 | -.17450 | -.02550 |
| I | .025 | -.09500 | .03893 | -.17678 | -.01322 |
| J | .000 | -.29900 | .03351 | -.36940 | -.22860 |
| Hole | .582 | -.00800 | .01428 | -.03801 | .02201 |

### *Smoothing 0.0001, Iterations 250*

| | Group | N | Mean | Std. Deviation | Std. Error Mean |
|---|---|---|---|---|---|
| A | Original without smoothing | 10 | 59.9180 | .06070 | .01919 |
| | Iterations 250, Smoothing 0.0001 | 10 | 59.8470 | .07319 | .02314 |
| B | Original without smoothing | 10 | 57.5260 | 4.21129 | 1.33173 |
| | Iterations 250, Smoothing 0.0001 | 10 | 59.5930 | .08179 | .02587 |
| C | Original without smoothing | 10 | 19.8920 | .08600 | .02719 |
| | Iterations 250, Smoothing 0.0001 | 10 | 19.9560 | .04452 | .01408 |
| D | Original without smoothing | 10 | 19.9240 | .09454 | .02990 |
| | Iterations 250, Smoothing 0.0001 | 10 | 19.9640 | .05379 | .01701 |
| E | Original without smoothing | 10 | 59.7120 | .10789 | .03412 |
| | Iterations 250, Smoothing 0.0001 | 10 | 59.7450 | .07546 | .02386 |
| F | Original without smoothing | 10 | 59.6390 | .06790 | .02147 |
| | Iterations 250, Smoothing 0.0001 | 10 | 59.6300 | .10456 | .03307 |
| G | Original without smoothing | 10 | 19.7390 | .17013 | .05380 |
| | Iterations 250, Smoothing 0.0001 | 10 | 19.8480 | .08364 | .02645 |
| H | Original without smoothing | 10 | 19.8010 | .10322 | .03264 |
| | Iterations 250, Smoothing 0.0001 | 10 | 19.8910 | .05527 | .01748 |
| I | Original without smoothing | 10 | 49.4770 | .05964 | .01886 |
| | Iterations 250, Smoothing 0.0001 | 10 | 49.4680 | .09555 | .03021 |
| J | Original without smoothing | 10 | 19.5490 | .09183 | .02904 |
| | Iterations 250, Smoothing 0.0001 | 10 | 19.8750 | .05583 | .01765 |
| Hole | Original without smoothing | 10 | 5.7920 | .02616 | .00827 |
| | Iterations 250, Smoothing 0.0001 | 10 | 5.8380 | .03190 | .01009 |

| | Sig. (2-tailed) | Mean Difference | Std. Error Difference | 95% Confidence Interval of the Difference | |
|---|---|---|---|---|---|
| | | | | Lower | Upper |
| A | .030 | .07100 | .03007 | .00783 | .13417 |
| B | .138 | -2.06700 | 1.33198 | -4.86539 | .73139 |
| C | .051 | -.06400 | .03062 | -.12834 | .00034 |
| D | .260 | -.04000 | .03440 | -.11226 | .03226 |
| E | .438 | -.03300 | .04163 | -.12047 | .05447 |
| F | .822 | .00900 | .03943 | -.07383 | .09183 |
| G | .086 | -.10900 | .05995 | -.23495 | .01695 |
| H | .026 | -.09000 | .03703 | -.16779 | -.01221 |
| I | .803 | .00900 | .03562 | -.06583 | .08383 |
| J | .000 | -.32600 | .03398 | -.39740 | -.25460 |
| Hole | .002 | -.04600 | .01305 | -.07341 | -.01859 |

### *Smoothing 0.0001, Iterations 500*

| | Group | N | Mean | Std. Deviation | Std. Error Mean |
|---|---|---|---|---|---|
| A | Original without smoothing | 10 | 59.9180 | .06070 | .01919 |
| | Iterations 500, Smoothing 0.0001 | 10 | 59.0230 | 2.86893 | .90723 |
| B | Original without smoothing | 10 | 57.5260 | 4.21129 | 1.33173 |
| | Iterations 500, Smoothing 0.0001 | 10 | 59.6320 | .16061 | .05079 |
| C | Original without smoothing | 10 | 19.8920 | .08600 | .02719 |
| | Iterations 500, Smoothing 0.0001 | 10 | 19.9760 | .03718 | .01176 |
| D | Original without smoothing | 10 | 19.9240 | .09454 | .02990 |
| | Iterations 500, Smoothing 0.0001 | 10 | 20.0030 | .03234 | .01023 |
| E | Original without smoothing | 10 | 59.7120 | .10789 | .03412 |
| | Iterations 500, Smoothing 0.0001 | 10 | 59.7940 | .09721 | .03074 |
| F | Original without smoothing | 10 | 59.6390 | .06790 | .02147 |
| | Iterations 500, Smoothing 0.0001 | 10 | 59.7420 | .09830 | .03108 |
| G | Original without smoothing | 10 | 19.7390 | .17013 | .05380 |
| | Iterations 500, Smoothing 0.0001 | 10 | 19.8210 | .03178 | .01005 |
| H | Original without smoothing | 10 | 19.8010 | .10322 | .03264 |
| | Iterations 500, Smoothing 0.0001 | 10 | 19.8420 | .03553 | .01123 |
| I | Original without smoothing | 10 | 49.4770 | .05964 | .01886 |
| | Iterations 500, Smoothing 0.0001 | 10 | 49.5410 | .08975 | .02838 |
| J | Original without smoothing | 10 | 19.5490 | .09183 | .02904 |
| | Iterations 500, Smoothing 0.0001 | 10 | 19.8050 | .09348 | .02956 |
| Hole | Original without smoothing | 10 | 5.7920 | .02616 | .00827 |
| | Iterations 500, Smoothing 0.0001 | 10 | 5.8210 | .02470 | .00781 |

| | Sig. (2-tailed) | Mean Difference | Std. Error Difference | 95% Confidence Interval of the Difference | |
|---|---|---|---|---|---|
| | | | | Lower | Upper |
| A | .337 | .89500 | .90744 | -1.01145 | 2.80145 |
| B | .131 | -2.10600 | 1.33270 | -4.90589 | .69389 |
| C | .011 | -.08400 | .02963 | -.14624 | -.02176 |
| D | .022 | -.07900 | .03160 | -.14538 | -.01262 |
| E | .091 | -.08200 | .04592 | -.17848 | .01448 |
| F | .014 | -.10300 | .03778 | -.18237 | -.02363 |
| G | .151 | -.08200 | .05473 | -.19698 | .03298 |
| H | .250 | -.04100 | .03452 | -.11352 | .03152 |
| I | .077 | -.06400 | .03408 | -.13559 | .00759 |
| J | .000 | -.25600 | .04144 | -.34306 | -.16894 |
| Hole | .020 | -.02900 | .01138 | -.05290 | -.00510 |

### *Smoothing 0.01, Iterations 2*

| | Group | N | Mean | Std. Deviation | Std. Error Mean |
|---|---|---|---|---|---|
| A | Original without smoothing | 10 | 59.9180 | .06070 | .01919 |
| | Iterations 2, Smoothing 0.01 | 10 | 60.0310 | .09049 | .02861 |
| B | Original without smoothing | 10 | 57.5260 | 4.21129 | 1.33173 |
| | Iterations 2, Smoothing 0.01 | 10 | 59.5660 | .09812 | .03103 |
| C | Original without smoothing | 10 | 19.8920 | .08600 | .02719 |
| | Iterations 2, Smoothing 0.01 | 10 | 19.9740 | .06802 | .02151 |
| D | Original without smoothing | 10 | 19.9240 | .09454 | .02990 |
| | Iterations 2, Smoothing 0.01 | 10 | 20.0060 | .04061 | .01284 |
| E | Original without smoothing | 10 | 59.7120 | .10789 | .03412 |
| | Iterations 2, Smoothing 0.01 | 10 | 59.7480 | .11564 | .03657 |
| F | Original without smoothing | 10 | 59.6390 | .06790 | .02147 |
| | Iterations 2, Smoothing 0.01 | 10 | 59.6580 | .12145 | .03841 |
| G | Original without smoothing | 10 | 19.7390 | .17013 | .05380 |
| | Iterations 2, Smoothing 0.01 | 10 | 19.8310 | .02767 | .00875 |
| H | Original without smoothing | 10 | 19.8010 | .10322 | .03264 |
| | Iterations 2, Smoothing 0.01 | 10 | 19.9700 | .03972 | .01256 |
| I | Original without smoothing | 10 | 49.4770 | .05964 | .01886 |
| | Iterations 2, Smoothing 0.01 | 10 | 50.5240 | 3.14023 | .99303 |
| J | Original without smoothing | 10 | 19.5490 | .09183 | .02904 |
| | Iterations 2, Smoothing 0.01 | 10 | 19.9020 | .05203 | .01645 |
| Hole | Original without smoothing | 10 | 5.7920 | .02616 | .00827 |
| | Iterations 2, Smoothing 0.01 | 10 | 5.7610 | .02025 | .00640 |

| | Sig. (2-tailed) | Mean Difference | Std. Error Difference | 95% Confidence Interval of the Difference | |
|---|---|---|---|---|---|
| | | | | Lower | Upper |
| A | .004 | -.11300 | .03446 | -.18539 | -.04061 |
| B | .143 | -2.04000 | 1.33209 | -4.83862 | .75862 |
| C | .029 | -.08200 | .03467 | -.15485 | -.00915 |
| D | .021 | -.08200 | .03254 | -.15036 | -.01364 |
| E | .481 | -.03600 | .05001 | -.14107 | .06907 |
| F | .671 | -.01900 | .04400 | -.11144 | .07344 |
| G | .109 | -.09200 | .05451 | -.20651 | .02251 |
| H | .000 | -.16900 | .03497 | -.24248 | -.09552 |
| I | .306 | -1.04700 | .99321 | -3.13365 | 1.03965 |
| J | .000 | -.35300 | .03337 | -.42312 | -.28288 |
| Hole | .008 | .03100 | .01046 | .00902 | .05298 |

### *Smoothing 0.01, Iterations 5*

| Group | | N | Mean | Std. Deviation | Std. Error Mean |
|---|---|---|---|---|---|
| A | Original without smoothing | 10 | 59.9180 | .06070 | .01919 |
| | Iterations 5, Smoothing 0.01 | 10 | 59.9420 | .06680 | .02112 |
| B | Original without smoothing | 10 | 57.5260 | 4.21129 | 1.33173 |
| | Iterations 5, Smoothing 0.01 | 10 | 59.5040 | .20738 | .06558 |
| C | Original without smoothing | 10 | 19.8920 | .08600 | .02719 |
| | Iterations 5, Smoothing 0.01 | 10 | 19.8600 | .04989 | .01578 |
| D | Original without smoothing | 10 | 19.9240 | .09454 | .02990 |
| | Iterations 5, Smoothing 0.01 | 10 | 20.0100 | .07272 | .02300 |
| E | Original without smoothing | 10 | 59.7120 | .10789 | .03412 |
| | Iterations 5, Smoothing 0.01 | 10 | 59.7750 | .09431 | .02982 |
| F | Original without smoothing | 10 | 59.6390 | .06790 | .02147 |
| | Iterations 5, Smoothing 0.01 | 10 | 59.6100 | .10541 | .03333 |
| G | Original without smoothing | 10 | 19.7390 | .17013 | .05380 |
| | Iterations 5, Smoothing 0.01 | 10 | 19.7990 | .06607 | .02089 |
| H | Original without smoothing | 10 | 19.8010 | .10322 | .03264 |
| | Iterations 5, Smoothing 0.01 | 10 | 19.8600 | .04853 | .01535 |
| I | Original without smoothing | 10 | 49.4770 | .05964 | .01886 |
| | Iterations 5, Smoothing 0.01 | 10 | 49.5520 | .06925 | .02190 |
| J | Original without smoothing | 10 | 19.5490 | .09183 | .02904 |
| | Iterations 5, Smoothing 0.01 | 10 | 19.8540 | .04695 | .01485 |
| Hole | Original without smoothing | 10 | 5.7920 | .02616 | .00827 |
| | Iterations 5, Smoothing 0.01 | 10 | 5.7540 | .01838 | .00581 |

| | Sig. (2-tailed) | Mean Difference | Std. Error Difference | 95% Confidence Interval of the Difference | |
|---|---|---|---|---|---|
| | | | | Lower | Upper |
| A | .411 | -.02400 | .02854 | -.08397 | .03597 |
| B | .155 | -1.97800 | 1.33334 | -4.77925 | .82325 |
| C | .322 | .03200 | .03144 | -.03405 | .09805 |
| D | .035 | -.08600 | .03772 | -.16524 | -.00676 |
| E | .181 | -.06300 | .04531 | -.15820 | .03220 |
| F | .474 | .02900 | .03965 | -.05430 | .11230 |
| G | .312 | -.06000 | .05771 | -.18125 | .06125 |
| H | .119 | -.05900 | .03607 | -.13478 | .01678 |
| I | .018 | -.07500 | .02890 | -.13572 | -.01428 |
| J | .000 | -.30500 | .03261 | -.37352 | -.23648 |
| Hole | .001 | .03800 | .01011 | .01676 | .05924 |

### *Smoothing 0.01, Iterations 25*

| | Group | N | Mean | Std. Deviation | Std. Error Mean |
|---|---|---|---|---|---|
| A | Original without smoothing | 10 | 59.9180 | .06070 | .01919 |
| | Iterations 25, Smoothing 0.01 | 10 | 59.9480 | .05574 | .01763 |
| B | Original without smoothing | 10 | 57.5260 | 4.21129 | 1.33173 |
| | Iterations 25, Smoothing 0.01 | 10 | 59.5720 | .06356 | .02010 |
| C | Original without smoothing | 10 | 19.8920 | .08600 | .02719 |
| | Iterations 25, Smoothing 0.01 | 10 | 19.9760 | .02914 | .00921 |
| D | Original without smoothing | 10 | 19.9240 | .09454 | .02990 |
| | Iterations 25, Smoothing 0.01 | 10 | 19.9880 | .03425 | .01083 |
| E | Original without smoothing | 10 | 59.7120 | .10789 | .03412 |
| | Iterations 25, Smoothing 0.01 | 10 | 59.7730 | .05272 | .01667 |
| F | Original without smoothing | 10 | 59.6390 | .06790 | .02147 |
| | Iterations 25, Smoothing 0.01 | 10 | 59.6940 | .04904 | .01551 |
| G | Original without smoothing | 10 | 19.7390 | .17013 | .05380 |
| | Iterations 25, Smoothing 0.01 | 10 | 19.8700 | .08380 | .02650 |
| H | Original without smoothing | 10 | 19.8010 | .10322 | .03264 |
| | Iterations 25, Smoothing 0.01 | 10 | 19.8920 | .04290 | .01356 |
| I | Original without smoothing | 10 | 49.4770 | .05964 | .01886 |
| | Iterations 25, Smoothing 0.01 | 10 | 49.5080 | .09841 | .03112 |
| J | Original without smoothing | 10 | 19.5490 | .09183 | .02904 |
| | Iterations 25, Smoothing 0.01 | 10 | 19.8910 | .02601 | .00823 |
| Hole | Original without smoothing | 10 | 5.7920 | .02616 | .00827 |
| | Iterations 25, Smoothing 0.01 | 10 | 5.6780 | .10239 | .03238 |

| | Sig. (2-tailed) | Mean Difference | Std. Error Difference | 95% Confidence Interval of the Difference | |
|---|---|---|---|---|---|
| | | | | Lower | Upper |
| A | .265 | -.03000 | .02606 | -.08475 | .02475 |
| B | .142 | -2.04600 | 1.33188 | -4.84418 | .75218 |
| C | .009 | -.08400 | .02871 | -.14432 | -.02368 |
| D | .059 | -.06400 | .03180 | -.13081 | .00281 |
| E | .126 | -.06100 | .03797 | -.14078 | .01878 |
| F | .052 | -.05500 | .02648 | -.11064 | .00064 |
| G | .042 | -.13100 | .05997 | -.25700 | -.00500 |
| H | .019 | -.09100 | .03535 | -.16526 | -.01674 |
| I | .405 | -.03100 | .03639 | -.10745 | .04545 |
| J | .000 | -.34200 | .03018 | -.40541 | -.27859 |
| Hole | .003 | .11400 | .03342 | .04379 | .18421 |

### *Smoothing 0.01, Iterations 50*

| | Group | N | Mean | Std. Deviation | Std. Error Mean |
|---|---|---|---|---|---|
| A | Original without smoothing | 10 | 59.9180 | .06070 | .01919 |
| | Iterations 50, Smoothing 0.01 | 10 | 59.9160 | .07720 | .02441 |
| B | Original without smoothing | 10 | 57.5260 | 4.21129 | 1.33173 |
| | Iterations 50, Smoothing 0.01 | 10 | 59.6670 | .19293 | .06101 |
| C | Original without smoothing | 10 | 19.8920 | .08600 | .02719 |
| | Iterations 50, Smoothing 0.01 | 10 | 19.9670 | .03335 | .01055 |
| D | Original without smoothing | 10 | 19.9240 | .09454 | .02990 |
| | Iterations 50, Smoothing 0.01 | 10 | 19.9980 | .03615 | .01143 |
| E | Original without smoothing | 10 | 59.7120 | .10789 | .03412 |
| | Iterations 50, Smoothing 0.01 | 10 | 59.7630 | .10657 | .03370 |
| F | Original without smoothing | 10 | 59.6390 | .06790 | .02147 |
| | Iterations 50, Smoothing 0.01 | 10 | 59.6250 | .10876 | .03439 |
| G | Original without smoothing | 10 | 19.7390 | .17013 | .05380 |
| | Iterations 50, Smoothing 0.01 | 10 | 19.8420 | .05203 | .01645 |
| H | Original without smoothing | 10 | 19.8010 | .10322 | .03264 |
| | Iterations 50, Smoothing 0.01 | 10 | 19.8870 | .05100 | .01613 |
| I | Original without smoothing | 10 | 49.4770 | .05964 | .01886 |
| | Iterations 50, Smoothing 0.01 | 10 | 49.4950 | .09180 | .02903 |
| J | Original without smoothing | 10 | 19.5490 | .09183 | .02904 |
| | Iterations 50, Smoothing 0.01 | 10 | 19.8320 | .05116 | .01618 |
| Hole | Original without smoothing | 10 | 5.7920 | .02616 | .00827 |
| | Iterations 50, Smoothing 0.01 | 10 | 5.8240 | .02271 | .00718 |

| | Sig. (2-tailed) | Mean Difference | Std. Error Difference | 95% Confidence Interval of the Difference | |
|---|---|---|---|---|---|
| | | | | Lower | Upper |
| A | .949 | .00200 | .03106 | -.06325 | .06725 |
| B | .126 | -2.14100 | 1.33313 | -4.94179 | .65979 |
| C | .019 | -.07500 | .02917 | -.13628 | -.01372 |
| D | .033 | -.07400 | .03201 | -.14124 | -.00676 |
| E | .302 | -.05100 | .04795 | -.15175 | .04975 |
| F | .734 | .01400 | .04054 | -.07118 | .09918 |
| G | .084 | -.10300 | .05626 | -.22119 | .01519 |
| H | .030 | -.08600 | .03641 | -.16249 | -.00951 |
| I | .609 | -.01800 | .03462 | -.09073 | .05473 |
| J | .000 | -.28300 | .03324 | -.35284 | -.21316 |
| Hole | .009 | -.03200 | .01095 | -.05501 | -.00899 |

### *Smoothing 0.01, Iterations 100*

| | Group | N | Mean | Std. Deviation | Std. Error Mean |
|---|---|---|---|---|---|
| A | Original without smoothing | 10 | 59.9180 | .06070 | .01919 |
| | Iterations 100, Smoothing 0.01 | 10 | 59.9110 | .07894 | .02496 |
| B | Original without smoothing | 10 | 57.5260 | 4.21129 | 1.33173 |
| | Iterations 100, Smoothing 0.01 | 10 | 59.5530 | .10133 | .03204 |
| C | Original without smoothing | 10 | 19.8920 | .08600 | .02719 |
| | Iterations 100, Smoothing 0.01 | 10 | 19.9120 | .03490 | .01104 |
| D | Original without smoothing | 10 | 19.9240 | .09454 | .02990 |
| | Iterations 100, Smoothing 0.01 | 10 | 19.9540 | .04033 | .01275 |
| E | Original without smoothing | 10 | 59.7120 | .10789 | .03412 |
| | Iterations 100, Smoothing 0.01 | 10 | 59.7120 | .04022 | .01272 |
| F | Original without smoothing | 10 | 59.6390 | .06790 | .02147 |
| | Iterations 100, Smoothing 0.01 | 10 | 59.6250 | .11645 | .03683 |
| G | Original without smoothing | 10 | 19.7390 | .17013 | .05380 |
| | Iterations 100, Smoothing 0.01 | 10 | 19.7900 | .04595 | .01453 |
| H | Original without smoothing | 10 | 19.8010 | .10322 | .03264 |
| | Iterations 100, Smoothing 0.01 | 10 | 19.8780 | .03584 | .01133 |
| I | Original without smoothing | 10 | 49.4770 | .05964 | .01886 |
| | Iterations 100, Smoothing 0.01 | 10 | 49.4490 | .07385 | .02335 |
| J | Original without smoothing | 10 | 19.5490 | .09183 | .02904 |
| | Iterations 100, Smoothing 0.01 | 10 | 19.8220 | .03882 | .01227 |
| Hole | Original without smoothing | 10 | 5.7920 | .02616 | .00827 |
| | Iterations 100, Smoothing 0.01 | 10 | 5.8380 | .01989 | .00629 |

| | Sig. (2-tailed) | Mean Difference | Std. Error Difference | 95% Confidence Interval of the Difference | |
|---|---|---|---|---|---|
| | | | | Lower | Upper |
| A | .827 | .00700 | .03149 | -.05916 | .07316 |
| B | .145 | -2.02700 | 1.33211 | -4.82567 | .77167 |
| C | .504 | -.02000 | .02935 | -.08166 | .04166 |
| D | .368 | -.03000 | .03250 | -.09829 | .03829 |
| E | 1.000 | .00000 | .03641 | -.07650 | .07650 |
| F | .746 | .01400 | .04263 | -.07556 | .10356 |
| G | .372 | -.05100 | .05573 | -.16808 | .06608 |
| H | .039 | -.07700 | .03455 | -.14959 | -.00441 |
| I | .363 | .02800 | .03002 | -.03507 | .09107 |
| J | .000 | -.27300 | .03153 | -.33923 | -.20677 |
| Hole | .000 | -.04600 | .01039 | -.06783 | -.02417 |

### *Smoothing 0.01, Iterations 250*

| | Group | N | Mean | Std. Deviation | Std. Error Mean |
|---|---|---|---|---|---|
| A | Original without smoothing | 10 | 59.9180 | .06070 | .01919 |
| | Iterations 250, Smoothing 0.01 | 10 | 59.9700 | .00667 | .00211 |
| B | Original without smoothing | 10 | 57.5260 | 4.21129 | 1.33173 |
| | Iterations 250, Smoothing 0.01 | 10 | 59.6860 | .07214 | .02281 |
| C | Original without smoothing | 10 | 19.8920 | .08600 | .02719 |
| | Iterations 250, Smoothing 0.01 | 10 | 19.9050 | .03894 | .01232 |
| D | Original without smoothing | 10 | 19.9240 | .09454 | .02990 |
| | Iterations 250, Smoothing 0.01 | 10 | 19.9930 | .03129 | .00989 |
| E | Original without smoothing | 10 | 59.7120 | .10789 | .03412 |
| | Iterations 250, Smoothing 0.01 | 10 | 59.7770 | .12902 | .04080 |
| F | Original without smoothing | 10 | 59.6390 | .06790 | .02147 |
| | Iterations 250, Smoothing 0.01 | 10 | 59.7460 | .15429 | .04879 |
| G | Original without smoothing | 10 | 19.7390 | .17013 | .05380 |
| | Iterations 250, Smoothing 0.01 | 10 | 19.8120 | .03584 | .01133 |
| H | Original without smoothing | 10 | 19.8010 | .10322 | .03264 |
| | Iterations 250, Smoothing 0.01 | 10 | 19.8140 | .03239 | .01024 |
| I | Original without smoothing | 10 | 49.4770 | .05964 | .01886 |
| | Iterations 250, Smoothing 0.01 | 10 | 49.4490 | .01912 | .00605 |
| J | Original without smoothing | 10 | 19.5490 | .09183 | .02904 |
| | Iterations 250, Smoothing 0.01 | 10 | 19.8120 | .04590 | .01451 |
| Hole | Original without smoothing | 10 | 5.7920 | .02616 | .00827 |
| | Iterations 250, Smoothing 0.01 | 10 | 5.8250 | .01900 | .00601 |

| | Sig. (2-tailed) | Mean Difference | Std. Error Difference | 95% Confidence Interval of the Difference | |
|---|---|---|---|---|---|
| | | | | Lower | Upper |
| A | .015 | -.05200 | .01931 | -.09257 | -.01143 |
| B | .122 | -2.16000 | 1.33192 | -4.95827 | .63827 |
| C | .668 | -.01300 | .02985 | -.07572 | .04972 |
| D | .042 | -.06900 | .03149 | -.13516 | -.00284 |
| E | .237 | -.06500 | .05318 | -.17674 | .04674 |
| F | .060 | -.10700 | .05331 | -.21899 | .00499 |
| G | .201 | -.07300 | .05498 | -.18851 | .04251 |
| H | .708 | -.01300 | .03421 | -.08487 | .05887 |
| I | .174 | .02800 | .01980 | -.01361 | .06961 |
| J | .000 | -.26300 | .03246 | -.33120 | -.19480 |
| Hole | .005 | -.03300 | .01023 | -.05448 | -.01152 |

### *Smoothing 0.01, Iterations 500*

| | Group | N | Mean | Std. Deviation | Std. Error Mean |
|---|---|---|---|---|---|
| A | Original without smoothing | 10 | 59.9180 | .06070 | .01919 |
| | Iterations 500, Smoothing 0.01 | 10 | 59.9510 | .06297 | .01991 |
| B | Original without smoothing | 10 | 57.5260 | 4.21129 | 1.33173 |
| | Iterations 500, Smoothing 0.01 | 10 | 59.8590 | .25097 | .07936 |
| C | Original without smoothing | 10 | 19.8920 | .08600 | .02719 |
| | Iterations 500, Smoothing 0.01 | 10 | 19.7390 | .09291 | .02938 |
| D | Original without smoothing | 10 | 19.9240 | .09454 | .02990 |
| | Iterations 500, Smoothing 0.01 | 10 | 19.8190 | .08212 | .02597 |
| E | Original without smoothing | 10 | 59.7120 | .10789 | .03412 |
| | Iterations 500, Smoothing 0.01 | 10 | 59.5960 | .10783 | .03410 |
| F | Original without smoothing | 10 | 59.6390 | .06790 | .02147 |
| | Iterations 500, Smoothing 0.01 | 10 | 59.6040 | .07106 | .02247 |
| G | Original without smoothing | 10 | 19.7390 | .17013 | .05380 |
| | Iterations 500, Smoothing 0.01 | 10 | 19.4490 | .08800 | .02783 |
| H | Original without smoothing | 10 | 19.8010 | .10322 | .03264 |
| | Iterations 500, Smoothing 0.01 | 10 | 19.4730 | .08538 | .02700 |
| I | Original without smoothing | 10 | 49.4770 | .05964 | .01886 |
| | Iterations 500, Smoothing 0.01 | 10 | 49.3430 | .07424 | .02348 |
| J | Original without smoothing | 10 | 19.5490 | .09183 | .02904 |
| | Iterations 500, Smoothing 0.01 | 10 | 19.4600 | .16846 | .05327 |
| Hole | Original without smoothing | 10 | 5.7920 | .02616 | .00827 |
| | Iterations 500, Smoothing 0.01 | 10 | 5.7590 | .03635 | .01149 |

| | Sig. (2-tailed) | Mean Difference | Std. Error Difference | 95% Confidence Interval of the Difference | |
|---|---|---|---|---|---|
| | | | | Lower | Upper |
| A | .248 | -.03300 | .02766 | -.09111 | .02511 |
| B | .097 | -2.33300 | 1.33409 | -5.13582 | .46982 |
| C | .001 | .15300 | .04003 | .06889 | .23711 |
| D | .016 | .10500 | .03960 | .02180 | .18820 |
| E | .027 | .11600 | .04824 | .01466 | .21734 |
| F | .275 | .03500 | .03108 | -.03029 | .10029 |
| G | .000 | .29000 | .06057 | .16275 | .41725 |
| H | .000 | .32800 | .04236 | .23900 | .41700 |
| I | .000 | .13400 | .03011 | .07073 | .19727 |
| J | .160 | .08900 | .06067 | -.03847 | .21647 |
| Hole | .032 | .03300 | .01416 | .00325 | .06275 |

### *Smoothing 0.2, Iterations 2*

| | Group | N | Mean | Std. Deviation | Std. Error Mean |
|---|---|---|---|---|---|
| A | Original without smoothing | 10 | 59.9180 | .06070 | .01919 |
| | Iterations 2, Smoothing 0.2 | 10 | 59.8890 | .08212 | .02597 |
| B | Original without smoothing | 10 | 57.5260 | 4.21129 | 1.33173 |
| | Iterations 2, Smoothing 0.2 | 10 | 59.6250 | .08860 | .02802 |
| C | Original without smoothing | 10 | 19.8920 | .08600 | .02719 |
| | Iterations 2, Smoothing 0.2 | 10 | 19.8480 | .10347 | .03272 |
| D | Original without smoothing | 10 | 19.9240 | .09454 | .02990 |
| | Iterations 2, Smoothing 0.2 | 10 | 19.9290 | .12279 | .03883 |
| E | Original without smoothing | 10 | 59.7120 | .10789 | .03412 |
| | Iterations 2, Smoothing 0.2 | 10 | 59.7350 | .07663 | .02423 |
| F | Original without smoothing | 10 | 59.6390 | .06790 | .02147 |
| | Iterations 2, Smoothing 0.2 | 10 | 59.6240 | .06077 | .01922 |
| G | Original without smoothing | 10 | 19.7390 | .17013 | .05380 |
| | Iterations 2, Smoothing 0.2 | 10 | 19.6320 | .13079 | .04136 |
| H | Original without smoothing | 10 | 19.8010 | .10322 | .03264 |
| | Iterations 2, Smoothing 0.2 | 10 | 19.7490 | .09303 | .02942 |
| I | Original without smoothing | 10 | 49.4770 | .05964 | .01886 |
| | Iterations 2, Smoothing 0.2 | 10 | 49.4580 | .19453 | .06151 |
| J | Original without smoothing | 10 | 19.5490 | .09183 | .02904 |
| | Iterations 2, Smoothing 0.2 | 10 | 19.6860 | .11872 | .03754 |
| Hole | Original without smoothing | 10 | 5.7920 | .02616 | .00827 |
| | Iterations 2, Smoothing 0.2 | 10 | 5.7730 | .02452 | .00775 |

| | Sig. (2-tailed) | Mean Difference | Std. Error Difference | 95% Confidence Interval of the Difference | |
|---|---|---|---|---|---|
| | | | | Lower | Upper |
| A | .381 | .02900 | .03229 | -.03884 | .09684 |
| B | .132 | -2.09900 | 1.33202 | -4.89748 | .69948 |
| C | .315 | .04400 | .04255 | -.04539 | .13339 |
| D | .920 | -.00500 | .04900 | -.10795 | .09795 |
| E | .589 | -.02300 | .04185 | -.11092 | .06492 |
| F | .609 | .01500 | .02882 | -.04554 | .07554 |
| G | .132 | .10700 | .06786 | -.03557 | .24957 |
| H | .252 | .05200 | .04394 | -.04032 | .14432 |
| I | .771 | .01900 | .06434 | -.11617 | .15417 |
| J | .010 | -.13700 | .04746 | -.23671 | -.03729 |
| Hole | .111 | .01900 | .01134 | -.00482 | .04282 |

### *Smoothing 0.2, Iterations 5*

| | Group | N | Mean | Std. Deviation | Std. Error Mean |
|---|---|---|---|---|---|
| A | Original without smoothing | 10 | 59.9180 | .06070 | .01919 |
| | Iterations 5, Smoothing 0.2 | 10 | 59.9760 | .06022 | .01904 |
| B | Original without smoothing | 10 | 57.5260 | 4.21129 | 1.33173 |
| | Iterations 5, Smoothing 0.2 | 10 | 59.5500 | .08769 | .02773 |
| C | Original without smoothing | 10 | 19.8920 | .08600 | .02719 |
| | Iterations 5, Smoothing 0.2 | 10 | 19.9030 | .04877 | .01542 |
| D | Original without smoothing | 10 | 19.9240 | .09454 | .02990 |
| | Iterations 5, Smoothing 0.2 | 10 | 19.9850 | .03629 | .01147 |
| E | Original without smoothing | 10 | 59.7120 | .10789 | .03412 |
| | Iterations 5, Smoothing 0.2 | 10 | 59.7760 | .07545 | .02386 |
| F | Original without smoothing | 10 | 59.6390 | .06790 | .02147 |
| | Iterations 5, Smoothing 0.2 | 10 | 59.5890 | .06806 | .02152 |
| G | Original without smoothing | 10 | 19.7390 | .17013 | .05380 |
| | Iterations 5, Smoothing 0.2 | 10 | 19.7470 | .05638 | .01783 |
| H | Original without smoothing | 10 | 19.8010 | .10322 | .03264 |
| | Iterations 5, Smoothing 0.2 | 10 | 19.8370 | .04448 | .01407 |
| I | Original without smoothing | 10 | 49.4770 | .05964 | .01886 |
| | Iterations 5, Smoothing 0.2 | 10 | 49.4550 | .08885 | .02810 |
| J | Original without smoothing | 10 | 19.5490 | .09183 | .02904 |
| | Iterations 5, Smoothing 0.2 | 10 | 19.6690 | .09527 | .03013 |
| Hole | Original without smoothing | 10 | 5.7920 | .02616 | .00827 |
| | Iterations 5, Smoothing 0.2 | 10 | 5.7530 | .01829 | .00578 |

| | Sig. (2-tailed) | Mean Difference | Std. Error Difference | 95% Confidence Interval of the Difference | |
|---|---|---|---|---|---|
| | | | | Lower | Upper |
| A | .046 | -.05800 | .02704 | -.11481 | -.00119 |
| B | .146 | -2.02400 | 1.33202 | -4.82246 | .77446 |
| C | .729 | -.01100 | .03126 | -.07668 | .05468 |
| D | .073 | -.06100 | .03202 | -.12828 | .00628 |
| E | .142 | -.06400 | .04163 | -.15147 | .02347 |
| F | .117 | .05000 | .03040 | -.01387 | .11387 |
| G | .889 | -.00800 | .05668 | -.12707 | .11107 |
| H | .325 | -.03600 | .03554 | -.11067 | .03867 |
| I | .524 | .02200 | .03384 | -.04909 | .09309 |
| J | .010 | -.12000 | .04184 | -.20791 | -.03209 |
| Hole | .001 | .03900 | .01009 | .01779 | .06021 |

### *Smoothing 1, Iterations 2*

| | Group | N | Mean | Std. Deviation | Std. Error Mean |
|---|---|---|---|---|---|
| A | Original without smoothing | 10 | 59.9180 | .06070 | .01919 |
| | Iterations 2, Smoothing 1 | 10 | 59.9280 | .06426 | .02032 |
| B | Original without smoothing | 10 | 57.5260 | 4.21129 | 1.33173 |
| | Iterations 2, Smoothing 1 | 10 | 59.6220 | .12900 | .04079 |
| C | Original without smoothing | 10 | 19.8920 | .08600 | .02719 |
| | Iterations 2, Smoothing 1 | 10 | 19.6060 | .12030 | .03804 |
| D | Original without smoothing | 10 | 19.9240 | .09454 | .02990 |
| | Iterations 2, Smoothing 1 | 10 | 19.7030 | .06832 | .02161 |
| E | Original without smoothing | 10 | 59.7120 | .10789 | .03412 |
| | Iterations 2, Smoothing 1 | 10 | 59.5740 | .07516 | .02377 |
| F | Original without smoothing | 10 | 59.6390 | .06790 | .02147 |
| | Iterations 2, Smoothing 1 | 10 | 59.5610 | .06262 | .01980 |
| G | Original without smoothing | 10 | 19.7390 | .17013 | .05380 |
| | Iterations 2, Smoothing 1 | 10 | 19.6220 | .11478 | .03630 |
| H | Original without smoothing | 10 | 19.8010 | .10322 | .03264 |
| | Iterations 2, Smoothing 1 | 10 | 19.6780 | .10570 | .03343 |
| I | Original without smoothing | 10 | 49.4770 | .05964 | .01886 |
| | Iterations 2, Smoothing 1 | 10 | 49.4230 | .08015 | .02534 |
| J | Original without smoothing | 10 | 19.5490 | .09183 | .02904 |
| | Iterations 2, Smoothing 1 | 10 | 19.4470 | .18361 | .05806 |
| Hole | Original without smoothing | 10 | 5.7920 | .02616 | .00827 |
| | Iterations 2, Smoothing 1 | 10 | 5.8050 | .05603 | .01772 |

| | Sig. (2-tailed) | Mean Difference | Std. Error Difference | 95% Confidence Interval of the Difference | |
|---|---|---|---|---|---|
| | | | | Lower | Upper |
| A | .725 | -.01000 | .02795 | -.06873 | .04873 |
| B | .133 | -2.09600 | 1.33235 | -4.89517 | .70317 |
| C | .000 | .28600 | .04676 | .18776 | .38424 |
| D | .000 | .22100 | .03689 | .14351 | .29849 |
| E | .004 | .13800 | .04158 | .05064 | .22536 |
| F | .016 | .07800 | .02921 | .01664 | .13936 |
| G | .088 | .11700 | .06490 | -.01934 | .25334 |
| H | .017 | .12300 | .04672 | .02484 | .22116 |
| I | .105 | .05400 | .03159 | -.01237 | .12037 |
| J | .134 | .10200 | .06492 | -.03439 | .23839 |
| Hole | .515 | -.01300 | .01955 | -.05408 | .02808 |

# Appendix I: “Black Bone” & Anatomical Models

## I.1. Model Cube measurements

| | a | b | c | d | e | f | g | h | i | j | hole |
|---|---|---|---|---|---|---|---|---|---|---|---|
| **CT Mimics** | | | | | | | | | | | |
| **1** | 61.08 | 60.8 | 20.81 | 20.76 | 60.96 | 61.16 | 20.61 | 20.63 | 50.73 | 20.66 | 4.75 |
| **2** | 61.19 | 60.92 | 20.85 | 20.82 | 60.97 | 61.03 | 20.6 | 20.62 | 51.27 | 20.63 | 4.27 |
| **3** | 60.99 | 60.85 | 20.86 | 20.85 | 60.93 | 61 | 20.6 | 20.63 | 51.15 | 20.64 | 4.75 |
| **4** | 61.03 | 60.79 | 20.88 | 20.83 | 60.98 | 60.98 | 20.6 | 20.62 | 51.16 | 20.62 | 4.69 |
| **5** | 61.25 | 60.77 | 20.88 | 20.86 | 60.92 | 60.99 | 20.59 | 20.61 | 50.96 | 20.67 | 4.64 |
| **6** | 61.1 | 60.83 | 20.97 | 20.89 | 60.95 | 61.04 | 20.63 | 20.63 | 51.04 | 20.65 | 4.72 |
| **7** | 60.95 | 60.76 | 20.92 | 20.88 | 60.99 | 61.19 | 20.66 | 20.62 | 50.94 | 20.64 | 4.74 |
| **8** | 61.13 | 60.93 | 20.91 | 20.88 | 60.96 | 60.96 | 20.64 | 20.64 | 51.04 | 20.63 | 4.8 |
| **9** | 61.07 | 60.75 | 20.85 | 20.81 | 60.98 | 60.94 | 20.58 | 20.61 | 51.22 | 20.62 | 4.73 |
| **10** | 60.98 | 60.77 | 20.92 | 20.84 | 60.99 | 61.06 | 20.63 | 20.61 | 51.17 | 20.62 | 4.73 |
| **CT osirix** | | | | | | | | | | | |
| **1** | 60.95 | 60.72 | 20.11 | 20.11 | 60.06 | 60.76 | 19.64 | 19.79 | 50.73 | 19.8 | 5.55 |
| **2** | 60.95 | 60.27 | 19.93 | 20.28 | 60.1 | 60.86 | 19.84 | 19.73 | 51.22 | 19.82 | 5.3 |
| **3** | 60.94 | 60.32 | 19.9 | 20.07 | 60.09 | 60.79 | 19.64 | 19.75 | 50.75 | 19.87 | 5.51 |
| **4** | 60.94 | 60.45 | 19.85 | 20.02 | 60.1 | 60.78 | 19.83 | 19.71 | 50.78 | 19.89 | 5.66 |
| **5** | 60.97 | 60.61 | 19.86 | 20.13 | 60.1 | 60.79 | 19.76 | 19.77 | 50.77 | 19.9 | 5.68 |
| **6** | 60.98 | 60.64 | 19.93 | 20.21 | 60.07 | 60.75 | 19.78 | 19.78 | 50.72 | 19.87 | 5.09 |
| **7** | 61.01 | 60.62 | 19.93 | 20.09 | 60.08 | 60.74 | 19.73 | 19.71 | 50.69 | 19.86 | 5.62 |
| **8** | 61 | 60.64 | 19.84 | 20.03 | 60.06 | 60.84 | 19.82 | 19.76 | 50.83 | 19.84 | 5.69 |
| **9** | 60.99 | 60.66 | 19.82 | 20.06 | 60.07 | 60.83 | 19.77 | 19.65 | 50.69 | 19.86 | 5.61 |
| **10** | 60.97 | 60.59 | 19.82 | 20.15 | 60.11 | 60.76 | 19.76 | 19.75 | 50.78 | 19.84 | 5.73 |
| **BB 1.5T Mimics** | | | | | | | | | | | |
| **1** | 60.22 | 60.26 | 20.41 | 20.47 | 60.8 | 60.12 | 20.36 | 20.3 | 49.98 | 20.43 | 5.23 |
| **2** | 60.2 | 60.15 | 20.41 | 20.3 | 60.83 | 60.23 | 20.41 | 20.37 | 50.38 | 20.46 | 5.64 |
| **3** | 60.18 | 60.22 | 20.44 | 20.32 | 60.77 | 60.15 | 20.2 | 20.3 | 50.23 | 20.47 | 5.16 |
| **4** | 60.15 | 60.18 | 20.44 | 20.25 | 60.66 | 60.11 | 20.41 | 20.18 | 50.14 | 20.45 | 5.25 |
| **5** | 60.29 | 60.29 | 20.38 | 20.34 | 60.72 | 60.13 | 20.34 | 20.15 | 50.2 | 20.46 | 5.31 |
| **6** | 60.18 | 60.35 | 20.38 | 20.34 | 60.73 | 60.14 | 20.33 | 20.12 | 50.16 | 20.45 | 5.31 |
| **7** | 60.15 | 60.18 | 20.34 | 20.24 | 60.78 | 60.22 | 20.28 | 20.12 | 50.24 | 20.44 | 5.46 |
| **8** | 60.15 | 60.19 | 20.48 | 20.35 | 60.78 | 60.22 | 20.24 | 20.11 | 50.27 | 20.46 | 5.44 |
| **9** | 60.18 | 60.2 | 20.35 | 20.28 | 60.78 | 60.16 | 20.28 | 20.27 | 50.06 | 20.46 | 5.21 |
| **10** | 60.16 | 60.19 | 20.44 | 20.26 | 60.81 | 60.17 | 20.21 | 20.15 | 50.12 | 20.43 | 5.34 |
| **BB 1.5T Osirix** | | | | | | | | | | | |
| **1** | 60.02 | 59.73 | 20.06 | 19.74 | 59.96 | 60.11 | 19.65 | 19.65 | 50.09 | 19.73 | 5.95 |
| **2** | 60 | 59.89 | 19.87 | 19.76 | 60.06 | 60.05 | 19.69 | 19.76 | 49.88 | 19.75 | 5.65 |
| **3** | 60 | 59.73 | 20.08 | 19.79 | 59.98 | 60.1 | 19.86 | 19.63 | 49.87 | 19.74 | 5.95 |
| **4** | 60.02 | 59.83 | 19.86 | 19.76 | 59.84 | 60.15 | 19.95 | 19.77 | 50.12 | 19.75 | 5.95 |
| **5** | 60 | 59.81 | 19.83 | 19.81 | 59.95 | 60.15 | 19.84 | 19.8 | 49.97 | 19.73 | 5.6 |
| **6** | 60.09 | 59.73 | 19.72 | 19.91 | 59.97 | 60.24 | 19.91 | 19.82 | 50.02 | 19.72 | 5.82 |
| **7** | 60.2 | 59.83 | 19.62 | 19.84 | 59.83 | 60.12 | 19.64 | 19.77 | 49.78 | 19.75 | 5.61 |
| **8** | 60.14 | 59.88 | 19.73 | 19.94 | 59.84 | 60.12 | 19.91 | 19.69 | 49.81 | 19.73 | 5.69 |
| **9** | 60.22 | 59.96 | 19.77 | 19.83 | 59.97 | 60.06 | 19.69 | 19.79 | 49.94 | 19.72 | 5.75 |
| **10** | 60.03 | 59.86 | 19.74 | 19.78 | 59.95 | 60.11 | 19.86 | 19.66 | 49.84 | 19.71 | 5.64 |
| **BB 3T Mimics** | | | | | | | | | | | |
| **1** | 61.38 | 60.68 | 18.78 | 18.86 | 55.13 | 61.16 | 18.65 | 18.23 | 50.85 | 20.49 | 5.12 |
| **2** | 61.34 | 60.5 | 18.85 | 18.75 | 55.14 | 61.12 | 18.74 | 18.24 | 50.84 | 20.54 | 4.79 |
| **3** | 61.4 | 60.5 | 18.76 | 18.67 | 55.05 | 61.16 | 18.67 | 18.34 | 50.91 | 20.6 | 4.68 |
| **4** | 61.46 | 60.57 | 18.75 | 18.71 | 55.07 | 61.25 | 18.66 | 18.47 | 50.95 | 20.59 | 4.81 |
| **5** | 61.3 | 60.48 | 18.69 | 18.67 | 55.12 | 61.16 | 18.66 | 18.32 | 50.83 | 20.6 | 4.7 |
| **6** | 61.25 | 60.48 | 18.52 | 18.75 | 55.09 | 61.15 | 18.68 | 18.28 | 51.04 | 20.59 | 4.91 |
| **7** | 61.35 | 60.44 | 18.83 | 18.67 | 55.06 | 61.22 | 18.62 | 18.3 | 50.9 | 20.6 | 4.85 |
| **8** | 61.28 | 60.6 | 18.76 | 18.67 | 55.03 | 61.23 | 18.6 | 18.64 | 50.85 | 20.6 | 4.78 |
| **9** | 61.23 | 60.48 | 18.62 | 18.72 | 55.04 | 61.19 | 18.56 | 18.34 | 50.73 | 20.43 | 4.9 |
| **10** | 61.32 | 60.54 | 18.84 | 18.66 | 55.19 | 61.13 | 18.69 | 18.44 | 50.94 | 20.41 | 4.82 |
| **BB 3T Osirix** | | | | | | | | | | | |
| **1** | 60.27 | 60.08 | 19.67 | 19.79 | 59.45 | 60.5 | 19.44 | 19.27 | 49.84 | 20 | 6.12 |
| **2** | 60.42 | 60.16 | 19.66 | 19.79 | 59.29 | 60.41 | 19.3 | 19.21 | 49.93 | 20.07 | 6.09 |
| **3** | 60.32 | 60.13 | 19.62 | 19.8 | 59.72 | 60.33 | 19.32 | 19.19 | 49.72 | 19.97 | 5.9 |
| **4** | 60.35 | 60.14 | 19.66 | 19.77 | 59.3 | 60.4 | 19.34 | 19.26 | 49.65 | 20.02 | 5.93 |
| **5** | 60.47 | 60.1 | 19.62 | 19.82 | 59.29 | 60.37 | 19.31 | 19.23 | 49.87 | 19.98 | 5.95 |
| **6** | 60.4 | 60.22 | 19.6 | 19.73 | 59.4 | 60.36 | 19.36 | 19.26 | 49.78 | 19.98 | 5.85 |
| **7** | 60.51 | 60.16 | 19.66 | 19.75 | 59.23 | 60.22 | 19.33 | 19.26 | 49.81 | 20 | 5.55 |
| **8** | 60.55 | 60.23 | 19.68 | 19.77 | 59.33 | 60.41 | 19.29 | 19.21 | 50.08 | 19.99 | 5.62 |
| **9** | 60.42 | 60.22 | 19.69 | 19.77 | 59.38 | 60.35 | 19.34 | 19.21 | 50.04 | 20.01 | 6.08 |
| **10** | 60.5 | 60.25 | 19.71 | 19.76 | 59.38 | 60.3 | 19.32 | 19.25 | 49.86 | 19.97 | 5.64 |